Naval Ocean Research and Development Activity

August 1985 Report 111

Comprehensive Final Report for the Marine Seismic System Program

AD-A162 539



J.D. Ward
Engineering Laboratory
Computer Sciences Corporation

J.A. Ballard
Seafloor Geosciences Division
Ocean Sciences Directorate

DTIC FILE COPY

Approved for public release; distribution unlimited. Naval Ocean Research and Development Activity, NSTL, Mississippi 39529-5004.

Foreword

This document is a final comprehensive report for the Defense Advanced Research Projects Agency's Marine Seismic System developmental program. The Naval Ocean Research and Development Activity directed the program, with the cooperation and support of many industrial, academic, and governmental engineering and research organizations.

This report describes the equipment, procedures, operating techniques, problems encountered, and achievements recorded during three attempts to deploy experimental deep-ocean seismic systems. Material for this report in the areas of instrumentation, deployment equipment, and techniques was drawn from numerous studies and reports prepared by the participating individuals and organizations. Whereas condensation of the latter studies and reports was necessary, the reports of seismic data analyses are, to the maximum extent practical, quoted verbatim in this report. In this respect, data analyses are treated as separate entities within the final comprehensive report.

This report summarizes the developments and achievements of the Marine Seismic System program in a single document that would serve as a principal reference for transitioning marine seismic system techniques and results from the research and development arena to the operational community.



R.P. Onorati, Captain, USN
Commanding Officer, NORDA

BEST
AVAILABLE COPY

Naval Ocean Research and Development Activity

August 1985 Report 111

Comprehensive Final Report for the Marine Seismic System Program

Sponsored By:

Defense Advanced Research Projects Agency (DoD)
ARPA Order No. 4152
Monitored by NORDA

J.D. Ward
Engineering Laboratory
Computer Sciences Corporation

J.A. Ballard
Seafloor Geosciences Division
Ocean Sciences Directorate

Executive summary

From 1981 through 1983, the Defense Advanced Research Projects Agency funded the National Science Foundation to conduct three marine expeditions as part of a developmental program for a deep-ocean marine seismic station. Long-range plans called for installation of a seismic station at a site in the Northwest Pacific in 1982. A coalition of institutions, agencies, and private firms combined various aspects of marine technology for placing large seismic instrument packages in dedicated boreholes in the floor of the Atlantic and Pacific Oceans. The drillship GLOMAR CHALLENGER was used as the deployment vehicle for preparing boreholes and emplacing the seismometer in the borehole, and for positioning a companion ocean-floor data recording package.

During an expedition in the Atlantic Ocean in March 1981, a large instrument package was lowered, external to the drill string, and placed in a previously drilled borehole at a depth about 2000 ft below the ocean floor. Water depth at the site was 14,708 ft. The seismic instruments were monitored by shipboard recorders. Background noise levels were quite low, and refraction shooting by a second ship produced crisp, clean signals. The instrument package was recovered with a cable winch.

A full-scale Marine Seismic System installation was attempted near the Kurile Trench in the Northwest Pacific in August–September 1982. This expedition was plagued by drilling equipment failures and adverse weather and drill conditions. The cased reentry borehole, required for seismic instrument installation, was never completed. Seasonal weather deterioration, the GLOMAR CHALLENGER operating schedule, and logistical considerations forced abandonment of the operation. However, a simpler seismometer, owned by Hawaii Institute of Geophysics, not requiring a cased reentry borehole was installed and provided an outstanding data set.

Failure of the 1982 attempt led to a schedule for a priority test in the South Pacific in early 1983. The area selected was about 500 miles east of the Tonga Trench and is one of the most seismically active regions in the world. Water depth at the site was 18,417 ft. A seismic instrument package was implanted in igneous rock at about 340 ft below the sea floor. A large bottom-processing package for data formatting and recording was successfully deployed and later recovered. Although some technical and equipment problems were encountered, the operation was considered successful. An extensive set of noise, explosion, and earthquake data was collected by the borehole instrument package and an ocean-bottom seismometer array. Two-ship refraction experiments were carried out with explosion data recorded from distances up to 140 miles.

The Marine Seismic System program demonstrated that the technology exists to place large instrument packages, carried external to the drill string, in deep-ocean boreholes using a single deployment vessel. Operating depths

of 20,000 ft are feasible, with borehole depths to 2000 ft below the ocean floor. Large, heavy, long-term data recording packages may be deployed on the sea floor and recovered by vessels with adequate winch and navigation systems. Seismic data collected by the Marine Seismic System are generally superior to ocean-bottom seismometer data. Signal/noise ratios of borehole instruments exceed those of ocean bottom seismometers by more than 15 dB in the 1–15 Hz frequency band.

Subsequent to the 1983 expedition, the Marine Seismic System program was terminated. The borehole instrument package and a dummy bottom processing package remain at the 1983 experiment site. No existing programs are presently designed for continued development of a permanent marine seismic station.

Keywords: borehole seismometers; charts; Glomar Challenger drillship; ambient seismic noise; deep ocean; state of the art seismic stations.

Preface

This report documents the principal techniques, procedures, and equipment developed for the purpose of exploratory marine seismic system deployments. The report focuses in particular on those functions and parameters requisite to deploying a deep-ocean, state-of-the-art seismic station. However, the quality of the data acquired by the borehole seismic instrument serves as an overall measure of the success of the marine seismic system concept. Therefore, the report includes detailed analyses of data acquired during the 1981 and 1983 experiments. The 1982 data, considered proprietary by Hawaii Institute of Geophysics, will not be published before 1987.

The information included herein, other than seismic data analyses, was drawn from numerous studies, analyses, and operational reports prepared by the organizations that supported the Marine Seismic System program. Operational reports, development of specialized deployment equipment, planning factors, and procedures were provided to a large extent by Global Marine Development, Inc. Teledyne Geotech and Gould, Inc., were major contributors of specialized electronic control and recording equipment as well as seismic instrument packages. Other contributors to equipment design and feasibility studies included the Raytheon Corporation, Sierra Geophysics, Inc., and the Naval Civil Engineering Laboratory. The data analyses were provided by the Scripps Institution of Oceanography, NORDA, and Oregon State University.

Accesion For	
NTIS CRA&I	☑
DTIC TAB	☐
Unannounced	☐
Justification	
By	
Distribution /	
Availability Codes	
Dist	Avail and / or Special
A-1	

QUALITY INSPECTED 3

The drawings in this report are not proprietary information. They are the property of the U. S. Government.
Per Mr. J. A. Ballard, NORDA/Code 360

Acknowledgements

The authors wish to thank the Geophysical Sciences Division of the Defense Advanced Research Projects Agency for providing funding for the Marine Seismic System under ARPA Order 4152, program element 62714E, Drs. Ralph W. Alewine and Robert R. Blandford, program managers.

Contents

I. Introduction 1

II. Data reports 2

A. Background 2

B. MSS-81 data 3

1. Analysis of ambient seismic noise 3
2. Preliminary seismic refraction results 3

C. MSS-83 data 3

1. Preliminary analysis of MSS-83 data 3
2. Ocean bottom and subbottom ambient microseismic noise 4
3. Seismic refraction experiments for MSS-83 4
4. Anisotropy in the oceanic lithosphere—Ngendei expedition 4

III. Project status 102

A. Background 102

B. Progress to date 103

1. MSS-81 103
2. MSS-82 103
3. MSS-83 103

IV. Operations 103

A. MSS-81 operations 103

1. Summary 103
2. Reentry site 104
3. Downhole instrument system 104
4. Deployment equipment 107
5. Operations summary 108
6. Test data evaluation, BIP impact forces, and EM cable dynamics 109
7. Mobilization and demobilization 110
8. Test evaluations and recommendations 110

B. MSS-82 operations 111

1. Summary 111
2. Reentry site 112

3. Downhole instrument system 112
4. Deployment equipment 114
5. Operations summary 115
6. Test data evaluation (equipment) 115
7. Mobilization and demobilization 116
8. Test evaluations and recommendations 117

C. MSS-83 operations 117

1. Summary 117
2. Reentry site 118
3. Downhole instrument system 118
4. Deployment equipment 118
5. Operations summary 118
6. Test data evaluation (equipment) 123
7. Mobilization and demobilization 126
8. Test evaluations and recommendations 126

V. Instrumentation 127

A. Borehole instrument package 127

B. Shipboard test console 132

C. Bottom processing package 135

D. Test equipment rack 138

E. Ocean bottom seismometer 139

VI. Deployment equipment 140

A. Shipboard equipment 140

1. EM cable winch 140
2. A-frame 140
3. Heave compensator 141
4. Idler sheave 141
5. Work platform 141
6. IRR system mooring line box 142
7. Miscellaneous equipment 142

B. Subsea equipment 142

1. Reentry subassembly 142
2. EM cable 144
3. IRR system 144

VII. MSS program cost summary 148

A. Overall MSS program costs 148

B. Deployment costs 148

VIII. Extension of MSS technology 150

A. Current status 150

1. Studies and analyses 150

B. Future operational aspects of the MSS program 151

1. Alternate reentry concepts 151
2. Alternate drillships 151
3. Deep-ocean seismometers 152
4. Drill string characteristics 156
5. MSS data transmission systems 157
6. Projected MSS development tests 158
7. Deepwater operational program 162

IX. Conclusions 164

X. Recommendations 165

XI. References 166

Bibliography 167

Appendix A. Description of the D/V GLOMAR CHALLENGER 169

Appendix B. Marine Seismic System EM Cable Static and Dynamic Response Due to Current and GLOMAR CHALLENGER Motions 173

Appendix C. The Ocean Subbottom Seismometer 177

Appendix D. List of MSS equipment drawings 195

Appendix E. Additional Studies and Reports of Interest to a Future MSS Program 199

Report Documentation Page (DD Form 1473)

Illustrations

Figure 1.	Location of MSS-81 site.	105
Figure 2.	DSDP/MSS reentry cone.	106
Figure 3.	Location of MSS-82 site.	113
Figure 4.	Location of MSS-83 site.	119
Figure 5.	Sketch of deployed IRR system.	122
Figure 6.	MSS-81 BIP physical layout.	128
Figure 7.	Dynamic gain ranging format used for BIP.	129
Figure 8.	BIP normalized frequency response.	130
Figure 9.	MSS PCM data format.	131
Figure 10.	BIP data transceiver unit.	133
Figure 11.	MSS-81 BIP functional block diagram.	134
Figure 12.	Functional block diagram of STC and BIP.	135
Figure 13.	BPP configuration.	136
Figure 14.	Block diagram of BPP and DARS.	137
Figure 15.	TER block diagram.	138
Figure 16.	OBS frequency response.	139
Figure 17.	Layout of MSS equipment aboard GLOMAR CHALLENGER.	140
Figure 18.	Layout of EM cable winch, idler sheave, A-frame, etc.	141
Figure 19.	Reentry subassembly configuration.	142
Figure 20.	EM cable components.	145
Figure 21.	Deployed configuration of BPP and IRR system.	146
Figure 22.	Conceptual MSS fly-in platform.	152
Figure 23.	Mooring configuration for MSS satellite telemetry buoy.	159
Figure 24.	Projected multiple MSS site deployment schedule.	164

Tables

Table 1.	IRR system components.	147
Table 2.	MSS deployment program costs.	148
Table 3.	Costs for MSS-81 deployment.	149
Table 4.	Costs for MSS-82 deployment.	149
Table 5.	Costs for MSS-83 deployment.	149
Table 6.	Requirements for cable reentry deployment.	151
Table 7.	Program for cable reentry platform development.	152
Table 8.	U.S. Flag drilling ships.	153
Table 9.	Foreign built-U.S. owned drilling ships.	153
Table 10.	MSS operations cost projections.	154
Table 11.	Potential seismometer packages.	154
Table 12.	Seismometer deployment concepts.	155
Table 13.	MSS drill string comparison.	156
Table 14.	Shallow-water test recording packages.	160
Table 15.	Shallow-water test costs.	161
Table 16.	Deepwater test recording packages.	162
Table 17.	Deepwater test cost estimates.	163
Table 18.	Cost estimate for multiple sites.	163

Glossary

Term	Definition word or phrase
A/D	Analog-to-digital
ASK	Automatic station keeping
BIP	Borehole instrument package
BPP	Bottom processing package
D/A	Digital-to-analog
DARPA	Defense Advanced Research Projects Agency
DARS	Data Acquisition and Recording System
DIA	Data input assembly
DSA	Data storage assembly
DSC	Data storage controller
DSDP	Deep Sea Drilling Project
DTU	Data transceiver unit
D/V	Drilling vessel
EDME	Enhanced delta modulator encoder
EM	Electromechanical
FIR	Finite impulse response
FM	Frequency modulated
FSK	Frequency shift keyed
GSD	Geophysical Sciences Division (DARPA)
HIG	Hawaii Institute of Geophysics
IRR	Installation, recovery and reinstallation
MSS	Marine Seismic System
NORDA	Naval Ocean Research and Development Activity
NSF	National Science Foundation
OBS	Ocean bottom seismometer
OSS	Ocean subbottom seismometer
PCM	Pulse code modulated
R/V	Research vessel
SIO	Scripps Institution of Oceanography
SPS	Switching power supply
STC	Shipboard test console
TER	Test equipment rack

Comprehensive Final Report for the Marine Seismic System Program

I. Introduction

A primary mission of the Defense Advanced Research Project Agency's Geophysical Sciences Division (DARPA/GSD) is world-wide definition and characterization of regional seismicity for the purpose of monitoring compliance with nuclear test ban treaties.

Earthquake activity in the Northwest Pacific makes this area particularly critical for this purpose. The Kurile Island-Kamchatka region of the Northwest Pacific is characterized by a tabular block of earthquake foci that dips landward from the Kurile-Kamchatka Trench. Under Kamchatka, this block dips 50° to 60° for earthquakes with focal depths of about 136 miles or less and 75° for deeper ones. Thickness of the focal zone measures about 25 to 31 miles. A line of active volcanoes parallels the Kurile-Kamchatka Trench at an average distance of 124–161 miles northeast of the trench axis. Beneath the volcanic zone earthquake depths average 62 miles under Kamchatka and 74 miles under the Southern Kurile Islands [1].

The seismicity of the Northwest Pacific Plate between the Kurile-Kamchatka Trench and the Emperor Seamounts to the east is critical to understanding the causes and distribution of anomalous eastern Asian earthquakes. Therefore, the Panel for Seismic Improvement (Berkner Panel) recommended (June 1959) that marine seismograph stations be established in that area. Seismic stations located at regional distances from the Kamchatka-Kurile Island area of the Soviet Union should significantly increase signal detection capability and at the same time reduce by up to 50% the number of events that currently cannot be identified in this area [2]. A marine seismic station (MSS) in that portion of the Northwest Pacific would provide DARPA/GSD with a capability for accurately determining locations, focal depths, magnitudes, and other significant earthquake parameters at regional distances (MSS Program Plan, unpublished).

Future nuclear armorers will undoubtedly place increased emphasis on weapons of limited yield. Accordingly, an MSS capable of detecting low-magnitude earthquakes in a millimicron noise field would provide valuable background information if a complete nuclear test ban treaty were instituted. Detecting clandestine nuclear tests would be greatly hampered if testing should be conducted in remote areas of high natural seismicity. Thus, a high-quality seismic station seaward of the Kurile-Kamchatka Trench would be essential for differentiation of natural and nuclear seismic events in eastern Asia.

The ultimate objective of such an MSS is to discriminate man-made explosions from natural seismicity. In the early 1960s a DARPA sponsored project, in response to the Berkner Panel recommendations, developed the ocean bottom seismometer (OBS). This project was abandoned because noise levels on the ocean floor were significantly higher than expected. The marine seismic station concept is radically different in that sensors would be emplaced deep into the volcanic basement. Because microseismic noise, the principal component of 1.0–0.1 Hz ambient noise in the ocean, travels as Scholte waves (a type of Rayleigh wave) along the water-sediment interface, the deeply emplaced seismic sensor should incur reduced ambient noise. Thus, MSS data should have two significant advantages over OBS data. First, coupling of the downhole seismic sensor to the earth should be firm and predictable. Second, by situating the sensors below the sediment-basement interface, complexities in seismograms, caused by compressional to shear wave converted phases, should be minimized.

Such an ocean-based detection system would require an extensive program for developing and testing components of the seabed seismic sensor system, including seismometer and electronic packages, seabed-to-surface-to-shore facility communications, and implantation methods. Current developments (1979 time frame) in instrumentation design and fabrication, deep-water drilling, ocean-bottom recovery techniques, and ocean communications offered significant promise for successfully deploying an ocean-based seismic system that would overcome the deficiencies of ocean-bottom sensor packages developed in the past. (The equipment and expertise developed by the Deep Sea Drilling Project (DSDP) of the National Science Foundation (NSF) could accommodate the installation and operation of subseafloor borehole instrumentation.) Advanced seismic sensor technology should make deploying reliable, compact borehole seismometers possible. Existing communications capabilities could facilitate satellite relay of seismic data, if desired. However, substantial prototype field testing would be required before such a system could be integrated with existing operational systems.

DARPA sponsored NORDA to direct and coordinate the MSS program for developing, installing, and operating

a broadband, triaxial, ocean-bottom borehole seismometer station in the Northwest Pacific. The initial requirement of the project was to develop a borehole seismic instrument package along with borehole reentry and deployment equipment that was capable of installing the instrumentation package in the ocean-bottom basalt layer in water depths as great as 20,000 ft. Thus, an immediate goal of the project was to establish interfaces between pertinent seismological, communications, and deep-sea technologies, while most economically and expeditiously developing an MSS capable of satisfying both seismic research and operational monitoring requirements.

Operational objectives of the MSS included a quality of data output comparable to and compatible with both the National Seismic System and the Seismic Research Observatories. The system, designed for an operational life of 5 years, would operate by continuously collecting data from its subocean bottom sensor package, digitizing the data, and transferring it in a store-and-forward mode to a postprocessing and control station where it would be recovered for final processing and analysis at a land site.

The MSS offered numerous research objectives complementary to its operational objectives. No seismic observatories are located on the leading edge of a downgoing lithospheric plate, and no facilities exist for recording continental margin earthquakes from the converging side of such a plate. Wideband and wide dynamic range seismological data from a high-quality seismic observatory in a low ambient noise environment, located near an active continental margin, would provide heretofore unavailable information capable of contributing to numerous scientific objectives.

NORDA directed the MSS program through interaction with both government agencies and a number of civilian contractors. The MSS mission and schedule required concurrent design of subsidiary system components, such as buoys, sensor packages, and telemetry links. This concurrent mode of system development, combined with a somewhat compressed schedule, placed a heavy load on program managers for ensuring that all phases and subsystems were coordinated and integrated into the system. Specialized equipment to be acquired or developed included an encapsulated seismic instrument package for borehole insertion, a reentry subassembly for carrying the instrument package at the end of a drill string and inserting the seismometers in the borehole, an electromechanical (EM) cable for communications with the borehole instrument package (BIP), an assortment of handling equipment such as cable winches, support frames, etc., and a control facility for temporary shipboard monitoring of the borehole instrument package. Early plans also required developing a retrievable bottom processing package (BPP) for receiving and recording borehole seismic instrument data. Implantation techniques would be developed around procedures already demonstrated by the DSDP team.

In late 1980, an agreement was negotiated between DARPA and NSF for services of the DSDP drill ship, GLOMAR CHALLENGER, during a series of MSS experiments and deployments. The MSS operations were to be inserted into a previously developed DSDP schedule. The MSS deployment program was developed around three major operational elements. The initial operation was planned as an at-sea test demonstration in an existing borehole in the mid-Atlantic in early 1981 (MSS-81). MSS-82 and MSS-83 deployments were planned for Northwest and South Pacific sites, respectively.

Experience gained through the three deployments demonstrated both the technical feasibility of MSSs and the quality of data obtained from a seismic instrument implanted in a subocean-bottom borehole. The various aspects of the program's three major at-sea experiments had been documented separately by principal investigators from several organizations. Accordingly, the MSS research products and newly developed technology would not be readily available to the operational community in the event of MSS program reactivation, or if a decision were made to establish a hardened MSS site.

This document is a final comprehensive report of the MSS program. This report will inform the scientific and operational communities of the MSS system and its capabilities and will facilitate the system's transition to the operational community.

II. Data reports

A. Background

Significant difficulties exist in measuring the velocity structure in the uppermost ocean crust by seismic refraction methods. Efforts with OBSs during the 1960s encountered a number of problems, including poor sensitivity and high levels of instrument noise. Ambient ocean-bottom noise levels were comparable to or higher than land sites. Recent developments in semiconductor technology, hardware, and digital recording techniques have resulted in renewed interests in OBS usage. However, the OBS still suffers from such problems as poor coupling, signal "ringing" due to unconsolidated sediments, difficulty of observing converted shear phases, and in particular, high ambient noise levels at the ocean bottom.

A borehole seismograph, implanted in the more rigid material underlying the ocean bottom sediments, should reduce the ambient noise problem and offer an alternative to the OBS. Information on noise within the ocean crust is sparse, particularly for reliable, absolute noise levels at and beneath the seafloor. Accordingly, MSS data acquisition efforts focused on both ambient seismic noise and seismic refraction data.

The techniques and procedures used in studies and analyses of seismic data are well established. This report is concerned primarily with the research and development efforts, as well as operational procedures and techniques employed in establishing a deep-ocean subbottom seismic station, rather than data analysis. However, the quality of the seismic data obtained from the MSS sites represents a measure of the success of the entire project.

The data acquired during the MSS project was the subject of extensive analyses for publication in a continuing series of reports for the NSF's Deep Sea Drilling Project. Applicable studies from the latter source are reprinted essentially verbatim in this report. This results in some repetition in such areas as discussions of operations and MSS instrumentation; however, condensation or extensive editing of these studies was considered inappropriate.

Useful data was obtained from both the MSS-81 and MSS-83 experiments. The primary MSS-82 deployment attempt was abandoned due to drilling equipment problems, although a back-up seismometer from Hawaii Institute of Geophysics was successfully deployed. All MSS data, except that retained by Hawaii Institute of Geophysics, now reside at the Center for Seismic Studies for access by end users.

B. MSS-81 data

The preliminary results of the studies of MSS-81 ambient seismic noise and seismic refraction data were published in volume 78B of the *Initial Reports of the Deep Sea Drilling Project [3]*. The locations of the reprints of Chapter 12 (Analysis of Ambient Seismic Noise) and Chapter 13 (Preliminary Seismic Refraction Results) of the above DSDP report are indicated below.

1. Analysis of ambient seismic noise

The information for this section is found on pages 7 to 21.

2. Preliminary seismic refraction results

The information for this section is found on pages 25 to 34.

C. MSS-83 data

The scientific community, concerned with studies and analyses of the MSS-83 data, referred to the 1983 operation as the Ngendei Expedition (Ngendei was a Polynesian deity associated with volcanoes and earthquakes). An extensive set of noise, explosion, and earthquake data was collected by the borehole seismometer and an ocean-bottom seismometer array during the MSS-83 deployment. The MSS-83 data analysis program had four primary objectives:

- comparing noise levels and signals recorded by the borehole instrument package and ocean bottom seismometers to assess the signal-to-noise improvement attainable by burying seismometers below the sediments in a deep-ocean environment;
- using noise data to investigate the mode of noise propagation on the sea floor and to test physical models of noise generation in the deep ocean;
- analyzing refraction data to study the structure of the crust and upper mantle, in particular the anelastic and anisotropic structures of the ocean lithosphere;
- using earthquake data to examine the propagation of seismic signals to regional and teleseismic distance over purely oceanic paths and to constrain elastic and anelastic models of the sublithospheric mantle.

This section presents a study of the seismic refraction experiments conducted with the MSS-83 borehole seismometer and a preliminary analysis of ocean-bottom and subbottom ambient microseismic noise recorded by ocean bottom seismometers and the borehole instrument package.

1. Preliminary analysis of MSS-83 data

Reports of the various studies and data analyses pertinent to the MSS-83 experiment will be published in Volume 88/91 of the *Initial Reports of the Deep Sea Drilling Project* [4]. The preliminary analyses of MSS-83 data have been completed in draft form and forwarded for incorporation in the latter DSDP reports. For purposes of this report, the draft reports on ambient microseismic noise, and seismic refraction experiments for MSS-83 have been included in the following paragraphs.

2. Ocean bottom and subbottom ambient microseismic noise

The information for this section is found on pages 35 to 60.

3. Seismic refraction experiments for MSS-83

The information for this section is found on pages 61 to 72.

4. Anisotropy in the oceanic lithosphere—Ngendei expedition

MSS-83 studies prepared for the DSDP initial reports included a study of anisotropy in the oceanic lithosphere [4].

The report on this subject is found on pages 73 to 101.

Analysis of Ambient Seismic Noise Recorded by Downhole and Ocean-Bottom Seismometers on Deep Sea Drilling Project Leg 78B

Richard G. Adair, John A. Orcutt, and Thomas H. Jordan
Geological Research Division, Scripps Institution of Oceanography
University of California, La Jolla, California

12. ANALYSIS OF AMBIENT SEISMIC NOISE RECORDED BY DOWNHOLE AND OCEAN-BOTTOM SEISMOMETERS ON DEEP SEA DRILLING PROJECT LEG 78B[1]

Richard G. Adair, John A. Orcutt, and Thomas H. Jordan, Geological Research Division,
Scripps Institution of Oceanography[2]

ABSTRACT

Ambient seismic noise at depth in the ocean crust is characterized using data from the Marine Seismic System (MSS), a vertical-component, digitally recording, short-period seismograph system which was part of the borehole instrumentation deployed on Deep Sea Drilling Project Leg 78B. The instrument package rested unclamped in Hole 395A, 516 m sub-basement. Reliable estimates of microseismic noise levels were obtained between 0.16 and 2.2 Hz; instrument noise dominatcd outside this band. The observed microseismic noise was quasi-stationary on a time scale of 1 hr., but not 10. Although spectral shapes were stable, noise amplitudes grew with time over the 26-hr. observation period by 3 to 5 dB. The borehole noise levels increased concurrently with local swell height, suggesting a causal relationship. An estimate of displacement power densities obtained early in the experiment had a peak value of 4×10^6 nm^2/Hz at 0.21 Hz, and decreased at 80 dB/decade from 1×10^6 nm^2/Hz at 0.33 Hz to 1 nm^2/Hz at 1.9 Hz. Noise levels observed at the seafloor near Hole 395A were greater than those observed in the borehole by a factor which increased with frequency from 10 dB at 0.2 Hz to 28 dB at 2 Hz. This is consistent with noise propagating as a fundamental-mode Stoneley wave trapped near the sediment/seawater interface. If the relationship observed between noise at and below the seafloor during Leg 78B is a general one, ocean-bottom borehole noise levels could approach those at quiet continental sites.

INTRODUCTION

A knowledge of ambient seismic noise near the seafloor is needed in formulating optimal strategies for the deployment of marine seismometer systems. There are, however, no published studies of noise within the ocean crust and few of noise at the seafloor, especially of reliable, absolute noise levels. Most available measurements were made during the VELA Uniform Project sponsored by the Advanced Research Projects Agency in the 1960s. It was hoped that noise levels at the seafloor would be comparable to those on land (Prentiss and Ewing, 1963), but in fact they were found to be significantly higher (Bradner and Dodds, 1964; Schneider and Backus, 1964; Schneider et al., 1964; Latham and Sutton, 1966; Latham and Nowroozi, 1968). These studies suggest that the noise propagates as an evanescent wave (Stoneley wave) trapped near the ocean bottom/seafloor interface (Bradner et al., 1965; Latham and Sutton, 1966; Latham and Nowroozi, 1968), so reduced noise levels are expected within the ocean crust. The technology and expertise needed to implant instruments in the seafloor has only recently been developed, primarily by the Deep Sea Drilling Project (DSDP). Borehole seismometers have been used in oblique seismic experiments on several DSDP cruises (Stephen et al., 1980, Stephen et al., 1983), but the data are not suited for the quantitative analysis of seismic noise. A downhole seismometer system sponsored by the Defense Advanced Research Projects Agency, the Marine Seismic System (MSS), was deployed in Hole 395A (Fig. 1) during Leg 78B with the intent of recording high-quality noise and seismic data. This chapter presents the first quantitative characterization of ambient seismic noise within the ocean crust. In addition, noise characteristics at and below the seafloor are directly compared using data acquired with a nearby ocean-bottom seismograph (OBS) (See Fig. 1).

INSTRUMENTATION AND OPERATIONS

The borehole instrumentation of the MSS consisted of state-of-health sensors and two vertical-component, short-period seismometers (Teledyne Geotech model S-700'), one configured approximately 50 cm below the other. Each seismometer's output was split into three channels, and the gains of the resultant six channels were staggered with overlap to yield a dynamic range of 144 dB (Fig. 2). The data streams were filtered to prevent aliasing, digitized at 75 samples/s using a 10-bit digital word, and transmitted via cable to a shipboard recorder. The cable was also used to recover the borehole instrumentation package. The computed displacement response for the combined seismometer and filter stages is shown in Figure 3. The response is peaked near 11 Hz, and rolls off at 12 dB/octave toward lower frequencies and at 15 dB/octave to the Nyquist frequency.

The borchole package was lowered from the *Glomar Challenger* to a sub-bottom depth of 609 m in Hole 395A (516 m sub-basement), where cave-ins blocked access to the bottom 55 m. The package was in place for 29.5 hrs., but data were recorded only during the final 26 hrs., which included a refraction experiment (see Fig. 4). Although the seismometers were not clamped in the hole, the adjacent unfractured and massive wall rock doubtless promoted proper coupling. (The wall-rock character was inferred from caliper and acoustic reflection logs conducted earlier during Leg 78B.) Ship motions conveyed to the package were quelled with 0.7 km of slack cable payed out on the seafloor. Noise samples were recorded between refraction shots and during breaks in the refraction experiment, both intentional and unintentional (when explosives failed to detonate). The times of relevant operations and events are shown in Figure 4.

Four triaxial ocean-bottom seismographs (OBSs) were dropped from the *Lynch* by seismologists from the University of Texas (UT) Institute of Geophysics. Each OBS was programmed to record 40 s of digital data with a sampling interval of 8.352 ms during the refraction shots

[1] Hyndman, R. D., Salisbury, M. H., et al., *Init. Repts. DSDP*, 78B: Washington (U.S. Govt. Printing Office).

[2] Address: Geological Research Div., Scripps Institution of Oceanography, Univ. of California, San Diego, La Jolla, CA 92093.

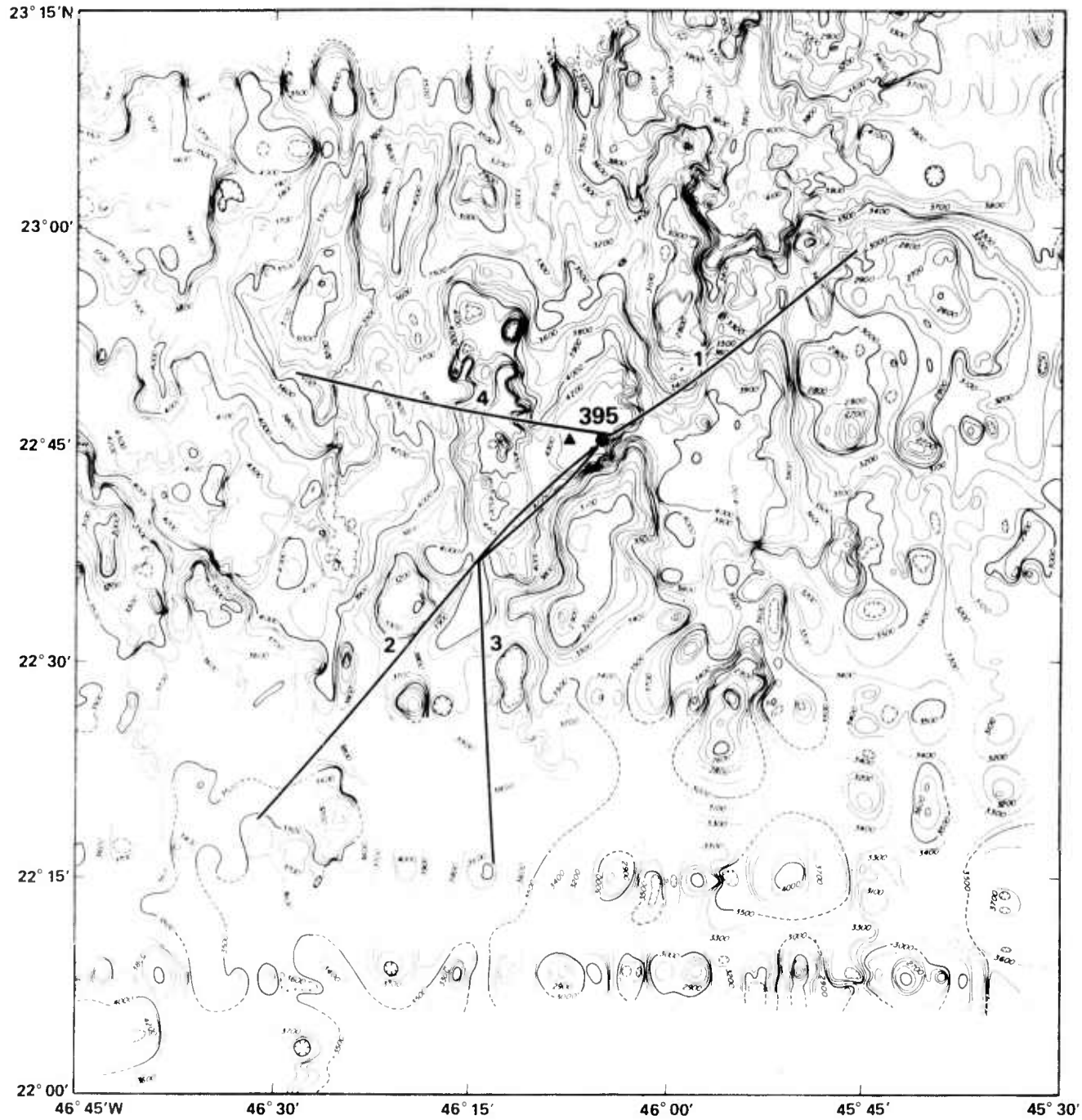


Figure 1. Location of the seismic instrumentation used in the Leg 78B noise experiment. The borehole instrumentation package of the Marine Seismic System (MSS) rested unclamped at the bottom of Hole 395A (22°45.35'N, 46°04.91'W), drilled five years earlier on Leg 45. The ocean-bottom seismometer (OBS) referred to here, one of four deployed during Leg 78B, was approximately 1 to 2 km west of Hole 395A. The OBS launch point (22°45.50'N, 46°05.43'W) is shown as a triangle. Depths shown in corrected meters.

and the intentional shooting hiatus. The OBS seismometers were 10-Hz Mark L6 geophones. The OBS displacement response (Fig. 3) increases with frequence at 18 dB/octave up to 10 Hz, and at 6 dB/octave thereafter. A variety of malfunctions prevented data acquisition except from the vertical component of an OBS located approximately 1 to 2 km west of the borehole (see Fig. 1 for launch point). A more precise location based on water-wave arrivals was not possible, because recordings of the shots (but not of the noise) were severely clipped by frame resonances above 10 Hz. Eleven 34-s samples of noise were obtained from the OBS data.

DATA QUALITY

Intrinsic earth noise was distinguished from instrument and ship noise on the basis of temporal and spectral characteristics. Spectral characteristics were determined from power densities and coherences computed in the manner described by Welch (1967). Time series were broken into segments which, after the mean was subtracted, were tapered with a normalized Hanning win-

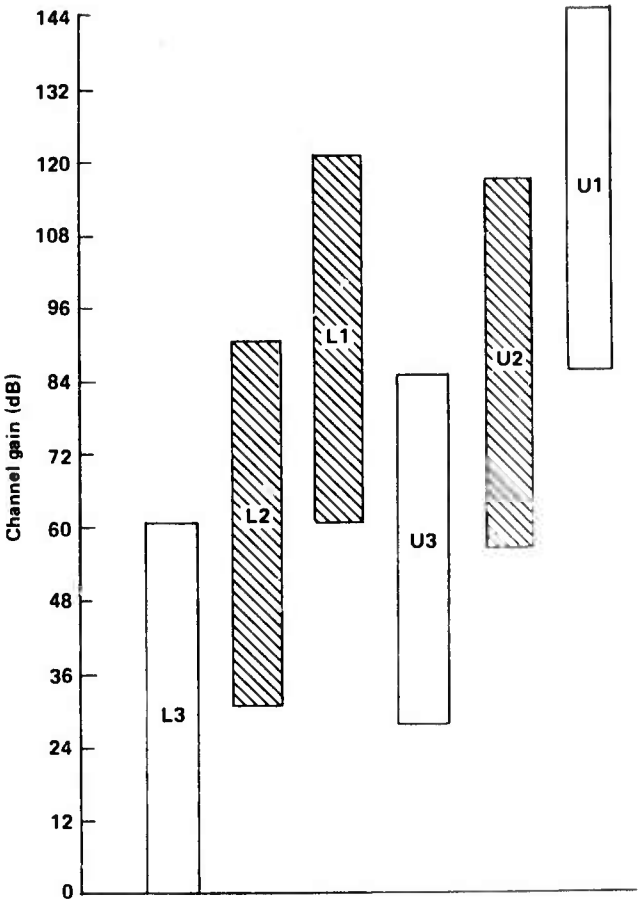


Figure 2. Schematic depiction of the MSS-data channel gains. The outputs of the two vertical-component seismometers, one configured 50 cm below the other, were split into 3 channels each, and the gains of the resultant 6 channels were staggered to yield 144 dB of dynamic range. "U" and "L" refer to the upper and lower seismometers, respectively. The use of a 10-bit unsigned digital word resulted in a range of 60 dB for each channel. Adjacent channels of a seismometer overlapped by 30 dB; the upper seismometer gains were offset from the lower seismometer gains by 24 dB. Because of noise and clipping, only the data from channels L1, L2, and U2 could be used in this study.

dow, and Fourier-transformed. Auto-(power) and cross-spectra were averaged (stacked) to reduce spectral estimate variance. Stable estimates were generally achieved with stacks of eight segments, although as many as 24 segments were used when available.

Of the six MSS data channels (Fig. 2), only three were usable for noise analysis (L1, U2, and L2); the highest-gain channel (U1) was always clipped, and the two with the lowest gain (U3 and L3) were dominated by least-count noise. An example of MSS data from channel L1 is shown in Figure 5. Typically, the data were dominated by monotonous, 1- to 4-s energy, whereas equally persistent high-frequency energy (>10 Hz) was of much lower amplitude. Features in Figure 5 attributed to instrument noise or not considered to represent ground motion are the dropped bit near 11 s; the frequent, random, unidirectional (sensor mass up) transients of variable magnitude (e.g., near 10.5 s); and the truncated, low-frequency peak centered at 6 s (a rare event). Single dropped bits, clearly resulting from instrument errors, were replaced with linearly interpolated values. The amplitudes and occurrence rates of the high-frequency transients generally decreased with time. Power densities of the MSS data and instrument noise are shown in Figure 6. The data were eight 13.65-s samples from channel L1 not corrected for instrument response. Electronics noise levels were estimated from RMS noise power values of one-half octave bandwidth provided by Teledyne Geotech. The least-count noise level is that expected from uniformly distributed errors resulting from the representation of a continuous variable by a finite, digital word (e.g., Otnes and Enochson, 1972). Neither of these sources of instrument noise dominated above 0.3 Hz. Least-count noise became increasingly important at frequencies where the instrument response rolled off and resulted in diminished coherence of energy between the two MSS seismometers. Power densities at frequencies below 0.16 Hz are inferred to be dominated by instrument noise, on the basis of low coherence (Fig. 7).

The transients shown in Figure 5 are assumed to result either from movement of the unclamped borehole package or from pressure impulses caused by the escape of the casing gas (helium). The transients strongly resemble the MSS response to a step in displacement (Figure 8), and are taken as such for the purpose of determining power densities. The transients were modeled as a compound Poisson process (Appendix), and their predicted power density $P(f)$ at frequency f is

$$P(f) = 2\lambda\langle\alpha^2\rangle |H(f)|^2 \qquad (1)$$

where λ is the mean rate of transient occurrence, $\langle\alpha^2\rangle$ is the mean squared amplitude, and $H(f)$ is the Fourier transform of a transient of unit amplitude. λ and $\langle\alpha^2\rangle$ were estimated for the data with the power densities shown in Figure 6, and the resulting $P(f)$ is plotted in the same figure as the curve labeled "Transient noise." The remarkably close agreement between the observed and predicted noise levels implies that energy beyond the break in power-density slope (near 2.2 Hz) is concentrated almost entirely in the transients.

System noise levels are not known for the OBS, nor can coherences be estimated, since only the vertical component of one instrument was functional. The frequencies at which instrument noise dominated were qualitatively determined from uncorrected power densities (Fig. 9). The OBS frame resonance is dominant between 10 and 25 Hz, and the essentially flat portions of the spectrum beyond 4 Hz and below 0.18 Hz imply instrumental sources of white noise. In addition, estimate stability could not be achieved below 0.18 Hz with the available time-series lengths.

Ship-generated acoustic signals undoubtedly contributed to local microseismic noise. Sources aboard the *Challenger* include machinery and the dynamic positioning system. The dynamic positioning system was silenced only once during the MSS deployment (0104–0120Z, 29 March), but since this was before the start of data recording, a quantitative assessment of its effects is not possible. Unpublished ocean-bottom noise spectra esti-

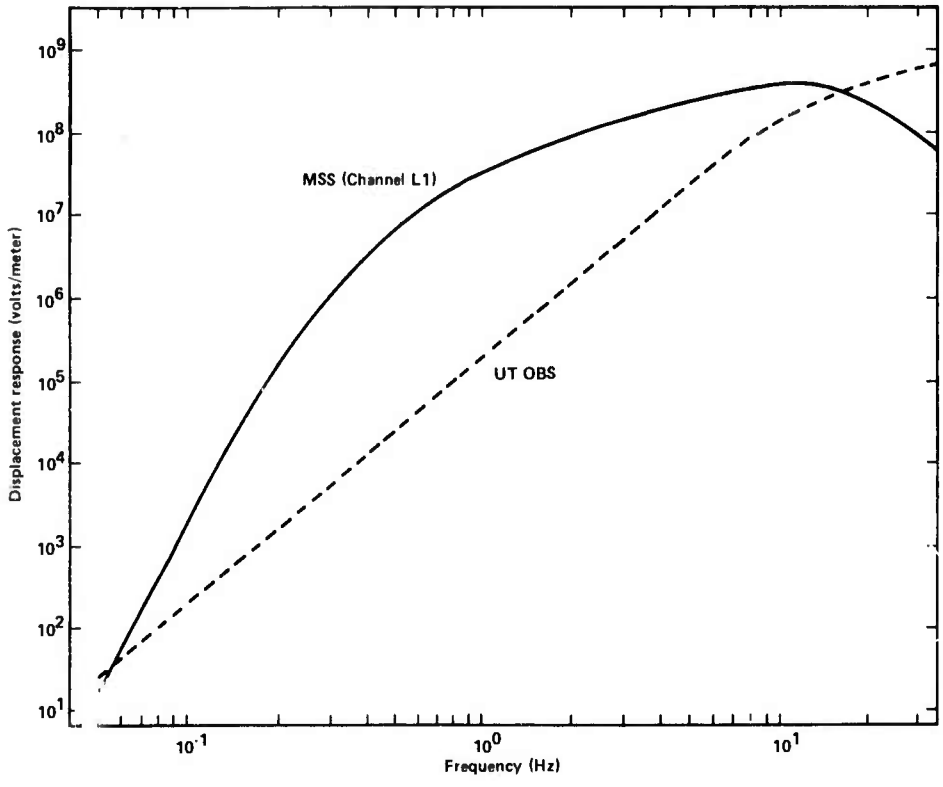


Figure 3. Displacement responses of Leg 78B seismic systems. The MSS employed two vertical-component, short-period, force-feedback, piezoelectric seismometers (Teledyne Geotech model S-700') whose outputs were filtered to prevent aliasing and then digitized at 75 samples/s. The MSS response is peaked near 11 Hz, and falls off at 12 dB/octave toward lower frequencies and at 15 dB/octave to the Nyquist frequency. The University of Texas (UT) ocean-bottom seismometer system consisted of a triaxial set of critically damped, 10-Hz Mark L6 geophones whose outputs were sampled with an 8.352-ms digitizing interval. The UT OBS response increases with frequency at 18 dB/octave up to 10 Hz, and at 6 dB/octave thereafter.

mated from the data collected by Scripps Institution of Oceanography OBSs suggest that noise caused by nearby ships is significant only above approximately 5 Hz and is typically manifested as sharp peaks at a few frequencies and several of their higher harmonics. The high noise levels above 10 Hz on the UT OBS may be attributed, at least in part, to ship noise amplified by frame resonances.

Another possible noise source is the flow of water past the instruments (Duennebier et al., 1981). This noise is thought to be generated when current speeds are in excess of 10 cm/s, but there is a complex dependence on body geometry. In the simple case of a cylinder, the frequency of the noise is inversely proportional to the diameter; the whip antenna on the OBS would have a flow-noise frequency of about 6 Hz for a current speed of 10 cm/s. Near-bottom current measurements (5 m above the seafloor) were made approximately 4 km north of the UT OBS during the period 28 March–1 April (Boyd, this volume). The average current speed was 4.4 cm/s and the maximum was 8.9 cm/s, so it is likely that current noise is not significant for the OBS noise observations. In the case of the MSS, temperature logs indicate that water was flowing down the hole at a rate of 25 m/hr. but disappeared into the basement within the upper 500 m of the hole, 100 m above the borehole instrument package (Becker et al., this volume). Also, there was no evidence for hydrothermal circulation anywhere in the hole. Water flow is not, therefore, a significant contribution to noise levels observed on the MSS. We feel the MSS data reliably represent intrinsic earth noise in the band 0.16 to 2.2 Hz; the OBS data probably do so between 0.18 and 4 Hz.

DISCUSSION

Although the stability of the noise estimates computed from 44 min. of MSS data implies that the microseismic noise was quasistationary on the time scale of 1 hr., the recorded amplitudes increased enough over one day to cause clipping on the channel of highest usable gain (L1). On the time scale of 10 hrs., the power densities, computed from channel U2 data, were stable in shape but increased by up to 5 dB (Fig. 10). Displacement spectra were peaked between 0.2 and 0.3 Hz, and decreased with frequency at 80 dB/decade. The earliest of the spectra in Figure 10 had a peak value of 4×10^6 nm^2/Hz at 0.21 Hz, and fell from 1×10^6 nm^2/Hz at 0.33 Hz to 1 nm^2/Hz at 1.9 Hz. A more detailed study of the temporal noise variation was conducted using integrated, uncorrected power densities from channel U2 (which was not clipped by noise) as a measure of level (Fig. 11A). The power densities were computed from

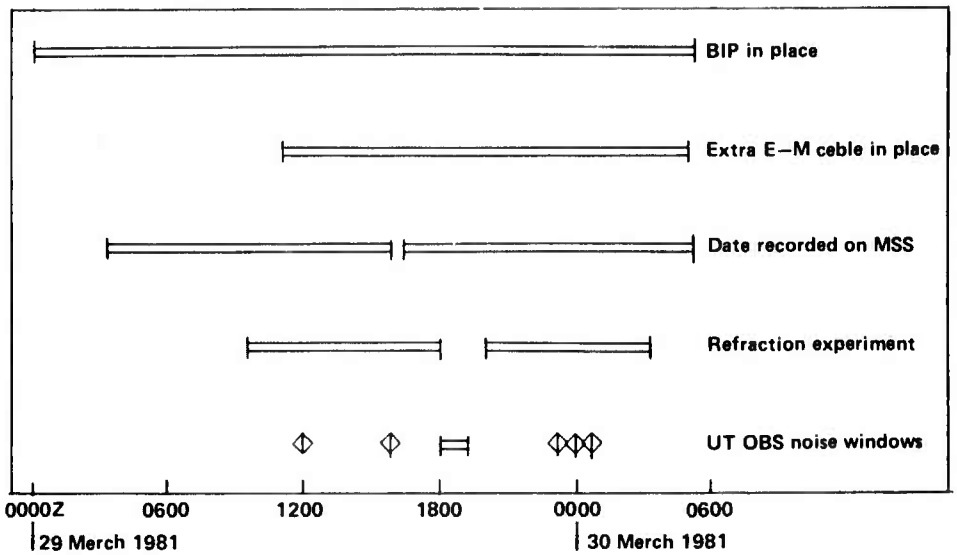


Figure 4. Times of important operations and events during the Leg 78B noise experiment. The borehole instrument package (BIP) first entered Hole 395A at 0257Z, 28 March 1981, but was not in place for the refraction and noise experiments until 0000Z, 29 March. The BIP was recovered at 0512Z, 30 March. The BIP was not clamped in the hole, but was isolated from ship motions by 0.7 km of electromechanical (E-M) cable payed out on the seafloor at 1100Z, 29 March. Twenty-six hrs. of data were recorded continuously by the MSS, except for a 35-min. gap beginning at 0545Z, 29 March. The refraction experiment began at 0925Z, 29 March, ended at 0220Z, 30 March, and was broken by a 2-hr. hiatus between 1800 and 2000Z, 29 March, during which the noise experiment was performed. The University of Texas ocean-bottom seismograph (UT OBS) recorded eleven 34-s noise samples, six during the noise experiment. The remaining five, denoted by diamonds, correspond to windows when refraction shots failed to explode.

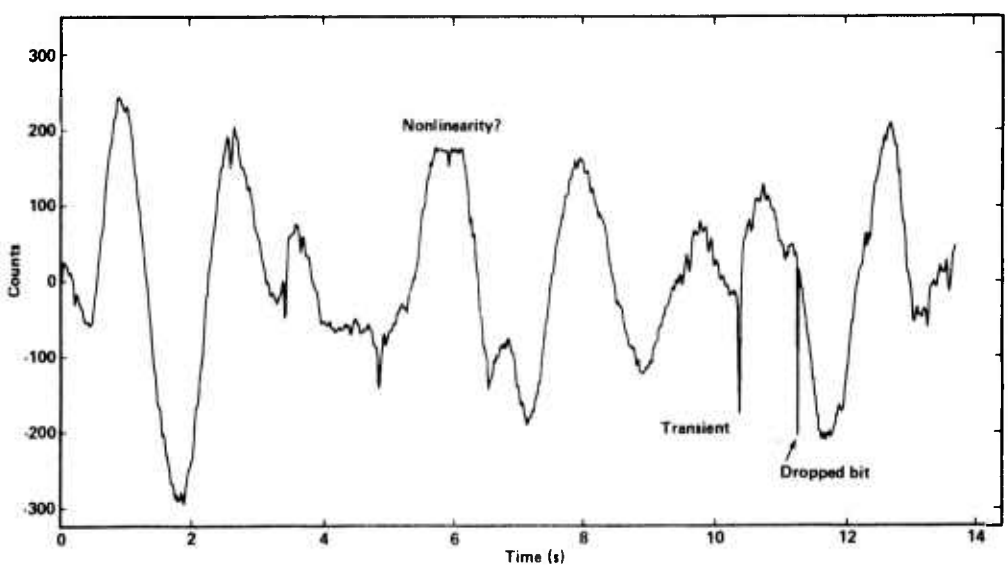


Figure 5. Record sample from channel L1, illustrating characteristics of MSS noise data. Low-frequency (0.2–0.3 Hz) energy dominates the time series. Features typical of those which contribute to noise are the dropped bit near 11 s; the frequent, random, unidirectional transients, such as the one labeled near 10.5 s; and the truncated low-frequency peak centered at 6 s. The last may result from an instrument nonlinearity. Units are digital counts, and positive amplitude corresponds to upward mass movement.

13.65 s of data sampled at approximately 15-min. intervals and smoothed with a three-point running mean. A trend of increasing noise levels is clearly discernible. This variability of ocean-bottom noise may be caused by changes in local sea state and/or weather (Latham and Sutton, 1966; Latham and Nowroozi, 1968). As can be seen in Figure 11B, bihourly observations of swell height recorded on the *Challenger*'s deck log strongly correlated with the noise level. The (nonlinear) interaction between opposing swell produces significant pressure fluctuations on the seafloor at half the swell period (Longuet-Higgins, 1950; Kadota and Labianca, 1981), and indeed, the reported swell period of 10 to 11 s is approximately twice that of the spectral peak between 3

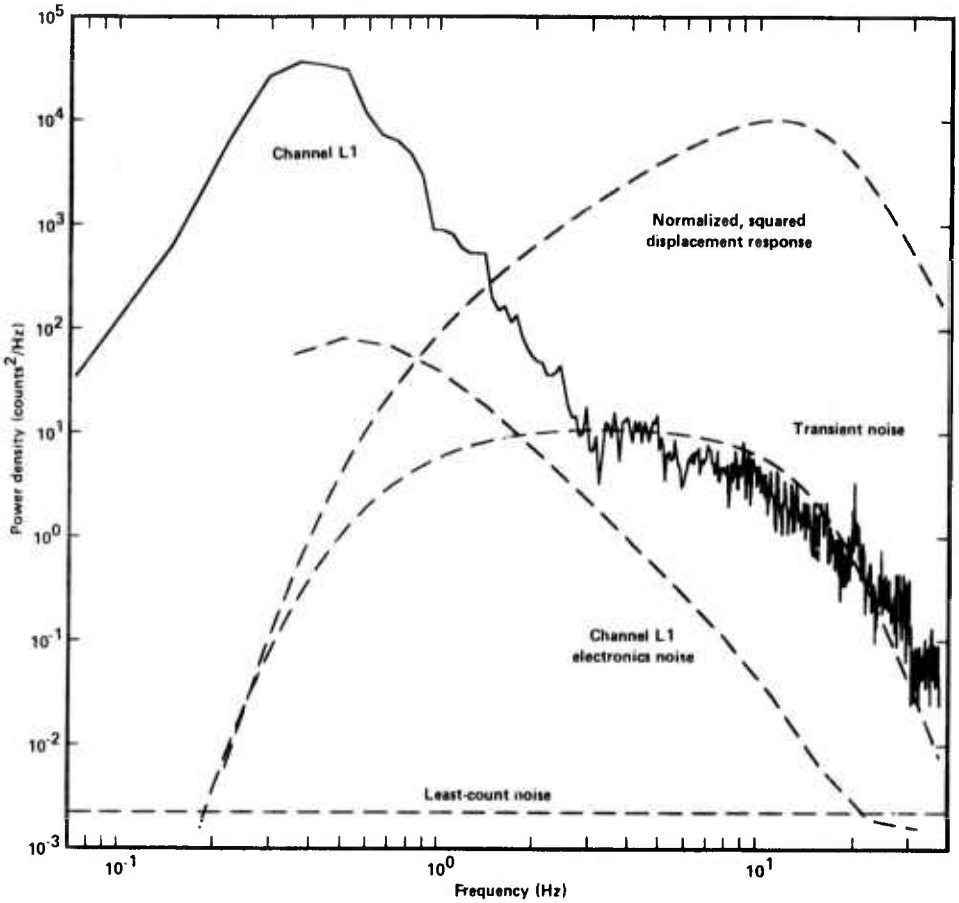


Figure 6. Power spectral densities of MSS data compared with estimates of instrument noise. The data (solid line) were computed from eight 13.65-s samples from channel L1, with no instrument correction applied. The electronics noise was estimated from RMS power values of ½-octave bandwidth provided by Teledyne Geotech. The least-count noise level is that expected from uniformly distributed errors owing to the representation of a continuous quantity by a finite digital word. The transient-noise spectrum, which is attributed to the frequent, impulsive features identified in Figure 5, was computed from equation A24 (see Appendix), and defines the high-frequency limit of reliable microseismic noise estimates. Also shown in this figure is the squared, normalized MSS displacement response.

and 5 s (Fig. 10). A more definite conclusion is not justified, however, by the limited data set used here. The period of the noise peak is within the range of the so-called "microseism peak" observed at the ocean bottom (Latham and Sutton, 1966; Latham and Nowroozi, 1968) and on continents (Melton, 1976), where, in the latter instance, there is ample evidence ascribing the microseism peak to the nonlinear swell interaction (Haubrich et al., 1963; Haubrich and McCamy, 1969).

The detailed, temporal behavior of noise at the seafloor during the MSS deployment cannot be reliably determined because of the paucity of appropriate OBS data. However, simultaneous noise observations were made by the two seismic systems on eleven occasions, nine of which may be used for comparison (Fig. 4). Six of these were recorded over a 75-min. period scheduled specifically for noise studies, and afford stable, high-resolution spectral estimates (Fig. 12). In the band of overlap (0.18–2 Hz), noise levels were higher at the seafloor than in the borehole by an amount which increased with frequency from 10 dB at 0.2 Hz to 28 dB at 2.2 Hz. This is consistent with the notion that, at these frequencies, microseismic noise propagates primarily as fundamental-mode Stoneley waves (Latham and Sutton, 1966; Latham and Nowroozi, 1968; Bradner and Dodds, 1964; Bradner et al., 1965; Tuthill et al., 1981). A large acoustic-wave/shear-wave impedance mismatch at a fluid/solid interface results in the severe exponential decay of this wave away from the interface, essentially trapping the seismic energy (Latham and Sutton, 1966; Tuthill et al., 1981). Site 395 is in a ponded depression amid rugged bathymetric relief (Fig. 1), which may affect seismic amplitudes in complex ways; but if the sediments are the dominating influence at this site, Stoneley-wave amplitudes at frequencies above the frequency of the microseismic peak should be significantly lower below the base of the sediments than at the seafloor.

The remaining five noise windows were widely spaced in time and were intended to be for explosion signals, but the shots failed to detonate; only three may be used for comparison, because of excessive instrument noise on the MSS. Seafloor noise levels were 10 to 30 dB higher than in the borehole for these samples as well. (The power densities shown in Fig. 13 were of similar resolu-

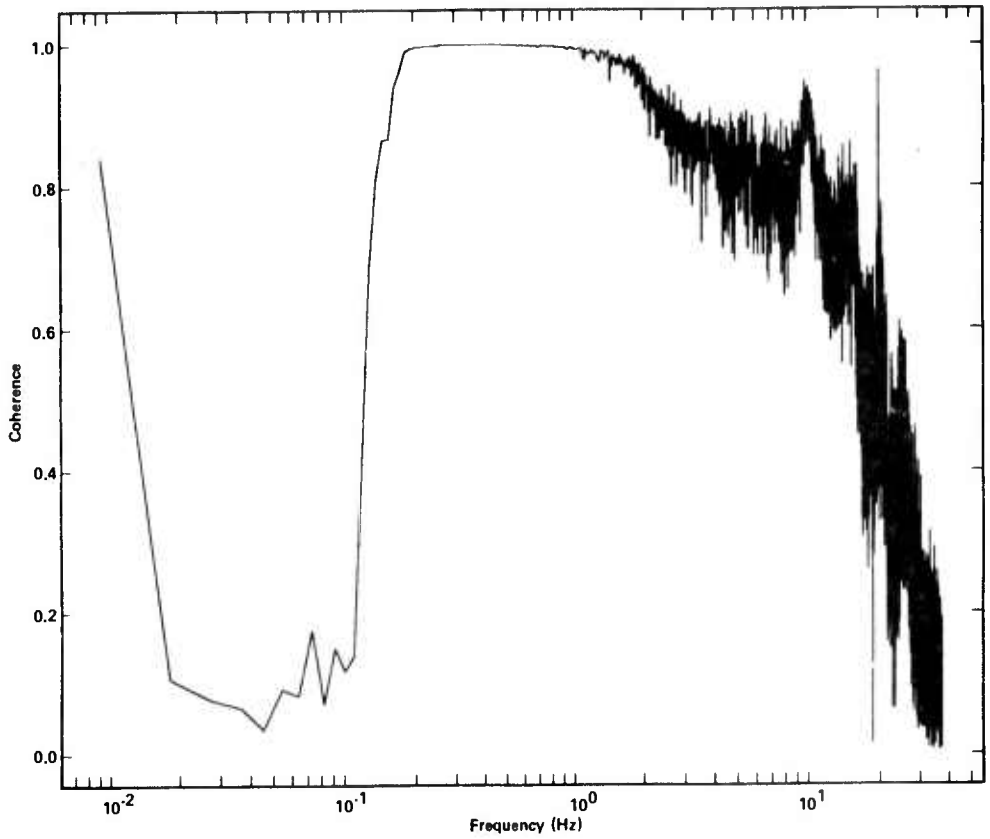


Figure 7. Coherence between the highest-usable-gain channels of each of the MSS seismometers (L1 and U2). The coherence spectrum was computed from twenty-four 109.2-s samples from each channel. The energy is highly incoherent below 0.16 Hz, where response roll-off causes instrument noise to dominate.

tion and variance: the MSS data were eight 6.83-s samples, and the UT OBS data were eight 4.28-s samples.)

Representative extrema of microseismic noise levels observed during the ten years of the Scripps Institution of Oceanography's OBS program are compared in Figure 14 with the lowest reliable levels observed during Leg 78B. The SIO OBSs employed 1-Hz digitally recorded seismometers (Prothero, 1974; Moore et al., 1981). Power densities were computed from the vertical-component output, which resided in semiconductor memory before being buffered to tape, and thus were not contaminated by the mechanical tape-recorder noise. Data for the "noisiest site" were fifty-one 8-s samples collected southeast of Hawaii, and those for the "quietest site" were thirty-four 4-s samples collected on the East Pacific Rise near 20°N. The extrema are separated by 20 to 30 dB. The UT OBS values are similar to the SIO OBS maxima; the MSS values are intermediate to low.

Continental noise observations are compared with the MSS spectrum in Figure 15. The Queen Creek data were recorded in a mine in Queen Creek, Arizona (Melton, 1976; Fix, 1972), and the Lajitas data were recorded at a site near Lajitas, Texas (Herrin, 1982). The Brune-Oliver curves represent average and high levels for continental stations, and were taken from Melton (1976), who reanalyzed Brune and Oliver's (1959) summary of published noise observations. MSS levels are 35 to 40 dB greater than the exceptionally low Queen Creek and Lajitas values, and fall between the Brune-Oliver curves.

CONCLUSIONS

The noise levels detected by the MSS in Hole 595A, approximately 600 m below the sediment/water interface, were 10 to 30 dB lower than those recorded by the University of Texas OBS over the frequency range 0.2 to 2.0 Hz (Figs. 12 and 13). This observation is consistent with the hypothesis that seismic noise at these frequencies propagates primarily as low-order Stoneley modes trapped at the seafloor interface (Bradner et al., 1965; Latham and Sutton, 1966; Latham and Nowroozi, 1968; Tuthill et al., 1981). The correlation of the noise levels with swell heights (Fig. 11) suggests that the generation of seafloor noise at this mid-Atlantic site is dominated by local nonlinear ocean-wave interactions. To within the accuracy of the deck-log observations, the swell period was approximately twice that of the microseismic noise peak, consistent with the Longuet-Higgins mechanism and previous ocean-bottom measurements (Latham and Nowroozi, 1968).

Seafloor noise levels at Site 395 were comparable to the highest values yet recorded by Scripps OBSs in the Pacific (Fig. 14), so, even with the reduction achieved by placing the sensor down a borehole, the MSS noise levels are on the order of 30 dB greater than these obtained

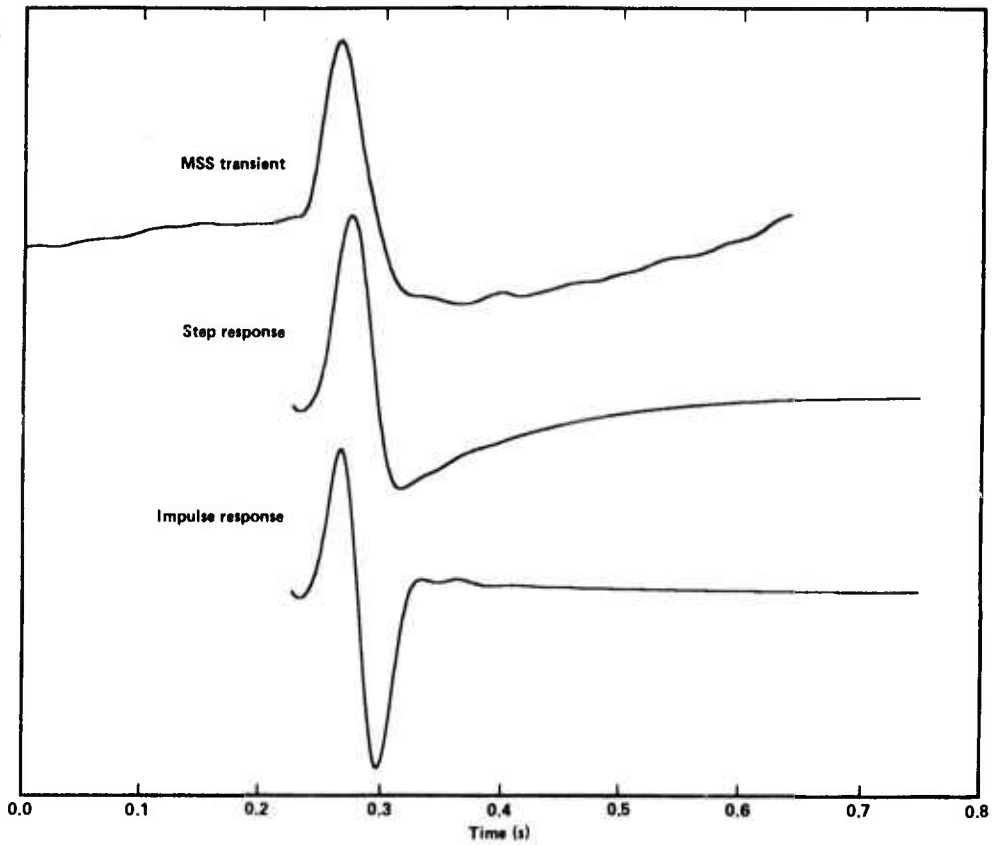


Figure 8. Transient shape compared with the MSS responses to a step and to an impulse in displacement. The transients observed in the MSS data resemble the step responses more closely than the impulse responses, and are taken as such for the purpose of computing the transient-noise spectrum shown in Figure 6.

at quiet continental sites (Fig. 15). If the relationship between seafloor and sub-bottom noise spectra in Figure 14 is maintained at quieter locations, however, then the noise levels may be reduced substantially downhole, and could compare favorably with typical continental sites.

Future deployments of the MSS are planned using a triaxial set of seismometers and a long-term ocean-bottom recording package. Such a system, complemented by an array of OBSs, should be able to answer definitively questions concerning the mode and generation mechanism of microseismic noise in the deep ocean.

ACKNOWLEDGMENTS

The authors thank Teledyne Geotech and the University of Texas for making available the data used in the noise analysis. In particular, Carl Mulcahy of Teledyne Geotech is to be thanked for his firsthand knowledge of the MSS and for his tireless assistance. Bill O'Brien was helpful with details of the OBS deployment.

REFERENCES

Bradner, H., and Dodds, J. G., 1964. Comparative seismic noise on the ocean bottom and on land. *J. Geophys. Res.*, 69:4339–4348.

Bradner, H., Dodds, J. G., and Foulks, R. E., 1965. Investigation of microseism sources with ocean-bottom seismometers. *Geophysics*, 30:511–526.

Brune, J. N., and Oliver, J., 1959. The seismic noise of the Earth's surface. *Seismol. Soc. Am. Bull.*, 49:349–353.

Darbyshire, J., 1960. Microseisms. *In* Hill, M. N. (Ed.), *The Sea* (Vol. 1): New York (Wiley-Interscience), 700–719.

Duennebier, F. K., Blackinton, G., and Sutton, G. H., 1981. Current-generated noise recorded on ocean bottom seismometers. *Mar. Geophys. Res.*, 5:109–115.

Fix, J. E., 1972. Ambient Earth motion in the period range from 0.1 to 2560 s. *Seismol. Soc. Am. Bull.*, 62:1753–1760.

Haubrich, R. A., and McCamy, K., 1969. Microseisms: coastal and pelagic sources. *Rev. Geophys.*, 7:539–571.

Haubrich, R. A., Munk, W. H., and Snodgrass, F. E., 1963. Comparative spectra of microseisms and swell. *Seismol. Soc. Am. Bull.*, 53:27–37.

Herrin, E., 1982. Seismic instruments used in treaty verification. *Seismol. Soc. Am. Bull.*, 72:S61–S67.

Kadota, T. T., and Labianca, F. M., 1981. Gravity-wave-induced pressure fluctuations in the deep ocean. *IEEE J. Oceanic Eng.*, OE-6: 50–58.

Latham, G. V., and Sutton, G. H., 1966. Seismic measurement on the ocean floor. 1. Bermuda area. *J. Geophys. Res.*, 71:2545–2573.

Latham, G. V., and Nowroozi, A. A., 1968. Waves, weather, and ocean bottom microseisms. *J. Geophys. Res.*, 73:3945–3956.

Longuet-Higgins, M., 1950. A theory of the origin of microseism. *Phil. Trans. Roy. Soc. London*, A243:1–35.

Melton, B. S., 1976. The sensitivity and dynamic range of inertial seismographs. *Rev. Geophys. Space Phys.*, 14:93–116.

Moore, R. D., Dorman, L. M., Huang, C.-Y., and Berliner, D. L., 1981. An ocean bottom, microprocessor based seismometer. *Mar. Geophys. Res.*, 4:451–477.

Otnes, R. K., and Enochson, L., 1982. *Digital Time Series Analysis:* New York (John Wiley).

Prentiss, D. D., and Ewing, J. I., 1963. The seismic motion of the deep ocean floor. *Seismol. Soc. Am. Bull.*, 53:765–781.

Prothero, W. A., 1974. Ocean bottom seismomete capsule. *Seismol. Soc. Am. Bull.*, 64:1251–1262.

Rice, S. O., 1944–1945. Mathematical analysis of random noise. *Bell Sys. Tech. J.*, Vol. 23–24. *Also in* Wax, N. (Ed.), 1954. *Selected Papers on Noise and Stochastic Processes:* New York (Dover).

Schneider, W. A., and Backus, M. M., 1964. Ocean bottom seismic measurements off the California coast. *J. Geophys. Res.*, 69: 1135–1143.

Schneider, W. A., Farrell, P. J., and Brannian, R. E., 1964. Collection and analysis of Pacific ocean-bottom seismic data. *Geophysics*, 29: 745–771.

Stephen, R. A., Johnson, S., and Lewis, B., 1983. The oblique seismic experiment on Deep Sea Drilling Project Leg 65. *In* Lewis, B. T. R., Robinson, P., et al., *Init. Repts. DSDP*, 65: Washington (U.S. Govt. Printing Office), 319–327.

Stephen, R. A., Louden, K. E., and Matthews, D. H., 1980. The oblique seismic experiment on Deep Sea Drilling Project Leg 52. *In* Donnelly, T., Francheteau, J., Bryan, W., Robinson, P., Flower, M., Salisbury, M., et al., *Init. Repts. DSDP*, 51, 52, 53, Pt. 1: Washington (U.S. Govt. Printing Office), 675–704.

Tuthill, J. D., Lewis, B. T. R., and Garmany, J. D., 1981. Stoneley waves, Lopez Island noise, and deep sea noise from 1 to 5 Hz. *Mar. Geophys. Res.*, 5:95–108.

Welch, P. D., 1967. The use of fast Fourier transform for the estimation of power spectra: A method based on time averaging over short, modified periodograms. *IEEE Trans. Audio Electro-Acoust.*, AU-15:70–73.

Date of Initial Receipt: January 12, 1983
Date of Acceptance: July 29, 1983

APPENDIX

In this appendix we model the transient noise observed in the MSS data as a compound, stationary Poisson process (Feller, 1968), and derive an expresson for its power spectral density function for the time interval $0 \le t \le T$. We define the process

$$S_N(t) = \sum_{k=1}^{N} X_k(t) \tag{A1}$$

where $\{X_k\}$ is a sequence of identically distributed, independent, stochastic variables, and N has a stationary Poisson probability distribution

$$P(N = n) = \frac{e^{-\lambda T}(\lambda T)^n}{n!} \tag{A2}$$

The expected value of N is

$$\langle N \rangle = \sum_{n=0}^{\infty} n\, P(N = n) \tag{A3}$$

$$= \lambda T \tag{A4}$$

so that the constant λ may be interpreted as the mean rate of event occurrence.

The $\{X_k\}$ are assumed to have the form

$$X_k(t) = \alpha_k h(t - t_k) \tag{A5}$$

where $h(t)$ is the transient shape and $\{\alpha_k\}$ and $\{t_k\}$ are the transient amplitude and occurrence times, respectively. N, $\{\alpha_k\}$, and $\{t_k\}$ are assumed to be mutually independent random variables; in particular, the $\{t_k\}$ are assumed to be uniformly distributed over the time of observation, T.

We wish to find the power spectral density function $P_S(f)$ of $S_N(t)$ at frequency f. P_S is the Fourier transform of the autocovariance function $R_{SS}(\tau)$ of S_N:

$$P_S(f) = 2 \int_{-\infty}^{\infty} R_{SS}(\tau) e^{-i2\pi f\tau} d\tau \tag{A6}$$

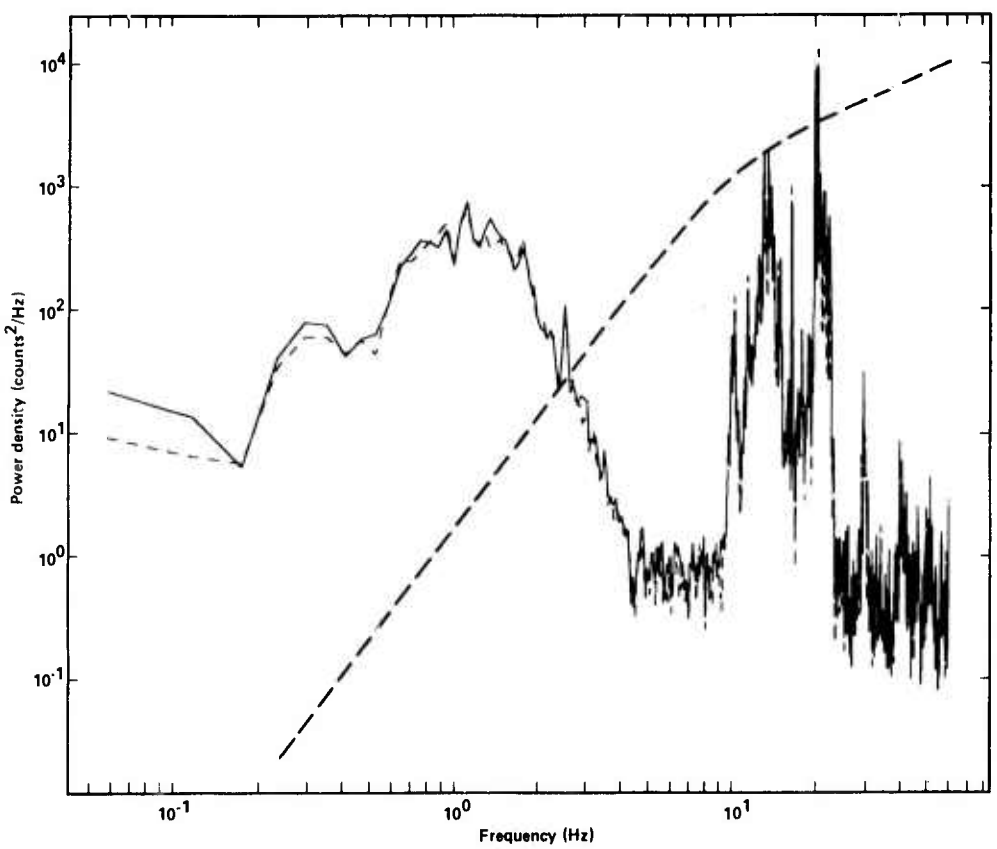


Figure 9. Uncorrected UT OBS power densities. Spectra were computed from eleven 17.1-s segments obtained from six 34.2-s noise samples recorded over a 75-min. period. The large amplitudes between 10 and 25 Hz may be the result of resonance of the OBS frame, and the flat portions above 4 Hz and below 0.18 Hz are probably imposed by instrument noise. Spectra between 0.18 and 4 Hz are thought to estimate reliably the ambient noise levels on the seafloor.

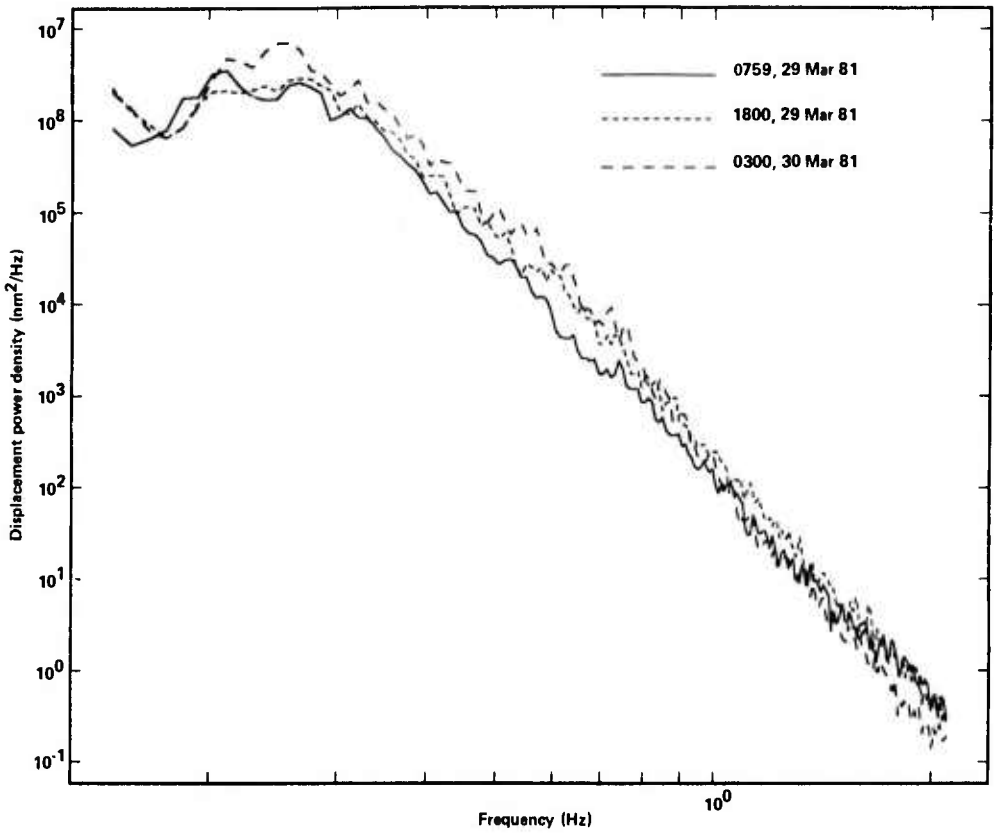


Figure 10. Displacement power densities (in nm^2/Hz) in Hole 395A at approximately 10-hr. intervals. Each curve was computed from twenty-four 109.2-s samples from channel U2. The spectral shape of the noise was stable over this period, but amplitudes increased with time. Power densities fall at approximately 80 dB/decade beyond the peak at 0.2–0.3 Hz (24 × 8192 points; corrected Channel U2).

$$R_{SS}(\tau) = \langle\ [S_N(t) - \langle S_N(t)\rangle]\ [S_N(t+\tau) - \langle S_N(t+\tau)\rangle]\ \rangle \quad \text{(A7)}$$

The factor of 2 in equation A6 is consequent to our normalization of $P_S(f)$, in which the total power per Nyquist bandwidth is equal to the variance of the time signal (the energy of the negative frequencies s folded into the positive).

Note that since S_N is stationary, $\langle S_N(t)\rangle$ is independent of t, and equation A7 is equivalent to

$$R_{SS}(\tau) = \langle S_N(t)S_N(t+\tau)\rangle - \langle S_N\rangle^2 \quad \text{(A8)}$$

We will evaluate the two terms of this equation separately. The mean value of S_N is

$$\langle S_N\rangle = \sum_{n=0}^{\infty} P(N=n)\langle \sum_{k=1}^{n} X_k\rangle = \sum_{n=0}^{\infty} P(N=n)n\langle X_k\rangle \quad \text{(A9)}$$

Since N, $\{\alpha_k\}$, and $\{t_k\}$ are mutually independent,

$$\langle S_k\rangle = \langle N\rangle\langle X_k\rangle \quad \text{(A10)}$$

where for each X_k,

$$\langle X_k\rangle = \langle \alpha_k h(t-t_k)\rangle = \langle\alpha\rangle \frac{1}{T}\int_0^T h(t-t_k)dt_k \quad \text{(A11)}$$

in which we have used the assumption that the $\{\alpha_k\}$ are identically distributed and therefore have the same mean $\langle\alpha\rangle$. We assume that the interval of observation T is much larger than the transient duration, so that, approximately,

$$\langle X_k\rangle = \langle\alpha\rangle \frac{1}{T}\int_0^{\infty} h(t)dt = \langle X\rangle \quad \text{(A12)}$$

and thus, using equation A4,

$$\langle S_N\rangle = \lambda\langle\alpha\rangle\int_0^{\infty} h(t)dt = \langle S\rangle \quad \text{(A13)}$$

We now consider the bivariate moment in equation A8:

$$\langle S_N(t)S_N(t+\tau)\rangle$$

$$= \sum_{n=0}^{\infty} P(N=n)\ \langle \sum_{k=1}^{n} X_k(t) \sum_{m=1}^{n} X_m(t+\tau)\rangle \quad \text{(A14)}$$

The mutual independence of the $\{X_k\}$ implies

$$\langle \sum_{k=1}^{n} X_k(t) \sum_{m=1}^{n} X_m(t-\tau)\rangle = n\langle X_k(t)X_k(t+\tau)\rangle + n(n-1)\langle X\rangle^2 \quad \text{(A15)}$$

The bivariate moment of X_k at lag τ is

$$\langle X_k(t)X_k(t+\tau)\rangle = \langle[\alpha_k h(t-t_k)][\alpha_k h(t-t_k+\tau)]\rangle \quad \text{(A16)}$$

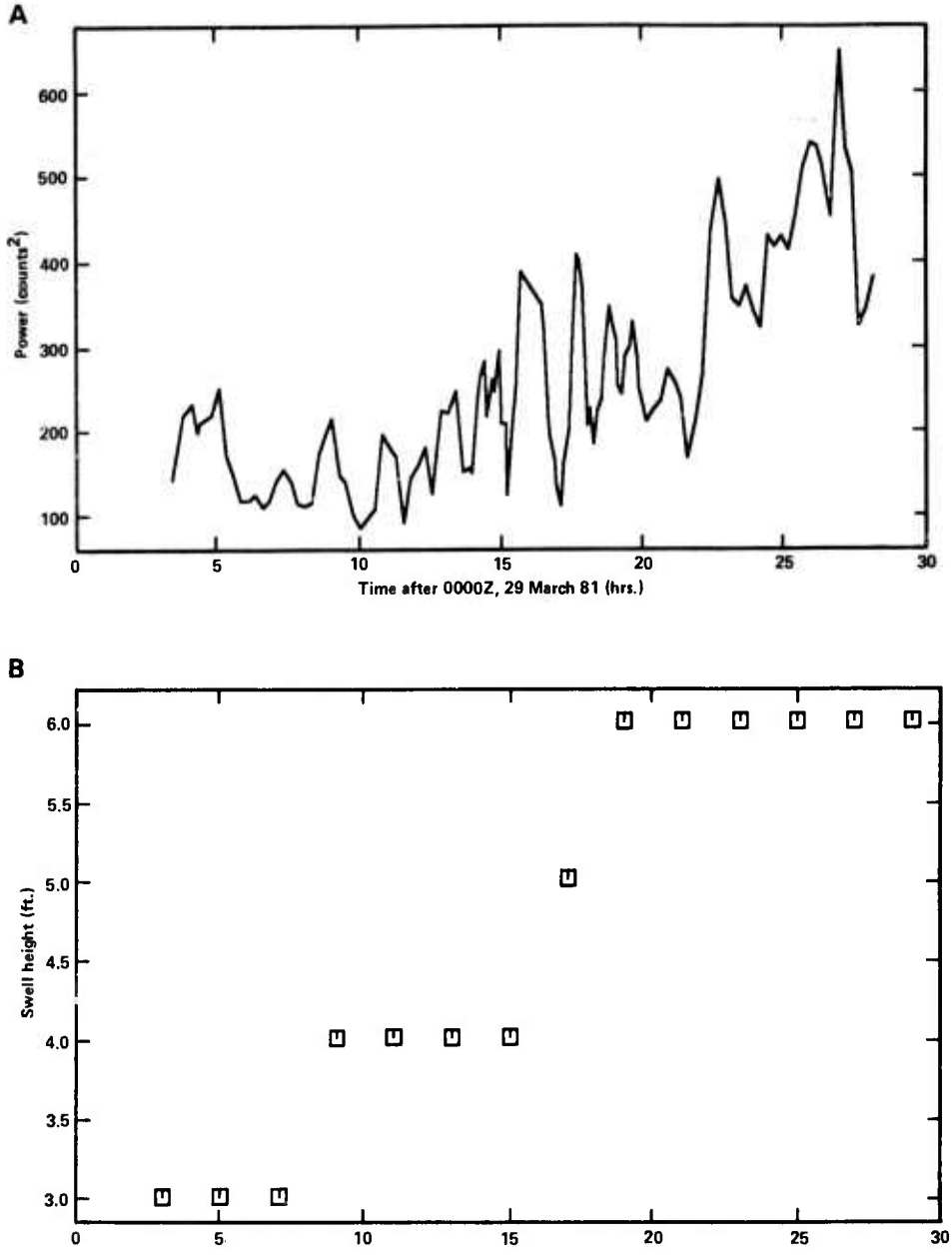


Figure 11. Temporal variations of (A) borehole noise levels and (B) local swell height. The noise level was estimated from integrated, smoothed power densities computed from 13.65 s of uncorrected channel U2 data sampled at approximately 15-min. intervals. A three-point running mean was applied to the integrated values. The swell height was recorded bihourly on the *Challenger*'s deck log.

$$= \langle \alpha^2 \rangle \frac{1}{T} \int_{t_k}^{T} h(t')h(t' + \tau)dt' \qquad \text{(A17)}$$

$$\approx \langle \alpha^2 \rangle \frac{1}{T} h * h(\tau) \qquad \text{(A18)}$$

where "*" denotes cross-correlation. Collecting these results,

$$\langle S_N(t)S_N(t + \tau) \rangle = \langle N \rangle \langle \alpha^2 \rangle \frac{1}{T} h * h(\tau)$$

$$+ \langle N(N - 1) \rangle \langle X \rangle^2 \qquad \text{(A19)}$$

From equation A2 we find that

$$\langle N(N - 1) \rangle = (\lambda T)^2 \qquad \text{(A20)}$$

Thus, from equations A12 and A13,

$$\langle S_N(t)S_N(t + \tau) \rangle = \lambda \langle \alpha^2 \rangle h * h(\tau) + \langle S \rangle^2 \qquad \text{(A21)}$$

so, finally,

$$R_{SS}(\tau) = \lambda \langle \alpha^2 \rangle h * h(\tau) \qquad \text{(A22)}$$

It is now a simple matter to determine $P_S(f)$ using equations A7 and A22. A well-known result from Fourier analysis (Bracewell, 1965) is that

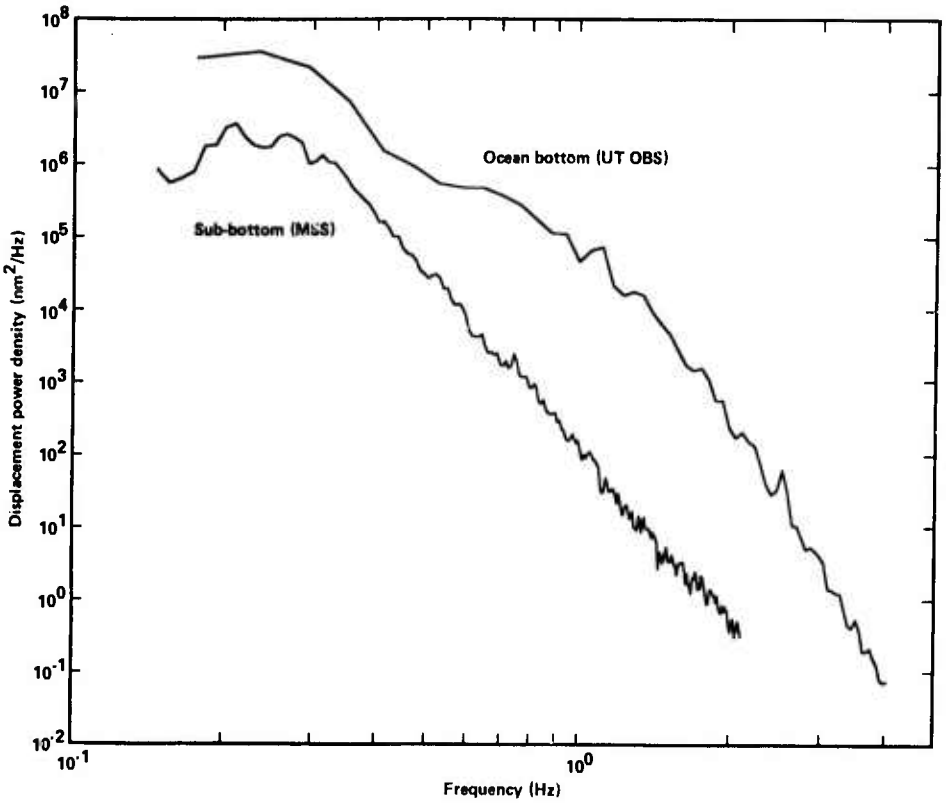


Figure 12. Comparison of ambient seismic noise at and below the seafloor near Hole 395A, using corrected UT OBS and MSS data recorded during the period 1800 to 1900Z, 29 March 1981. The UT OBS data were six 34.2-s samples, and the MSS data were six 109.2-s samples; the former were broken into eleven 17.1-s segments, the latter into eleven of 54.6-s duration.

$$\int_0^\infty h * h(\tau) e^{-i2\pi f\tau} d\tau = |H(f)|^2 \qquad \text{(A23)}$$

where $H(f)$ is the Fourier transform of $h(t)$. Hence,

$$P_S(f) = 2\lambda\langle\alpha^2\rangle\, |H(f)|^2 \qquad \text{(A24)}$$

REFERENCES

Bracewell, R., 1965. *The Fourier Transform and Its Application:* New York (NcGraw-Hill).

Feller, W., 1968. *An Introduction to Probability Theory and Its Application* (Vol. 1): New York (John Wiley).

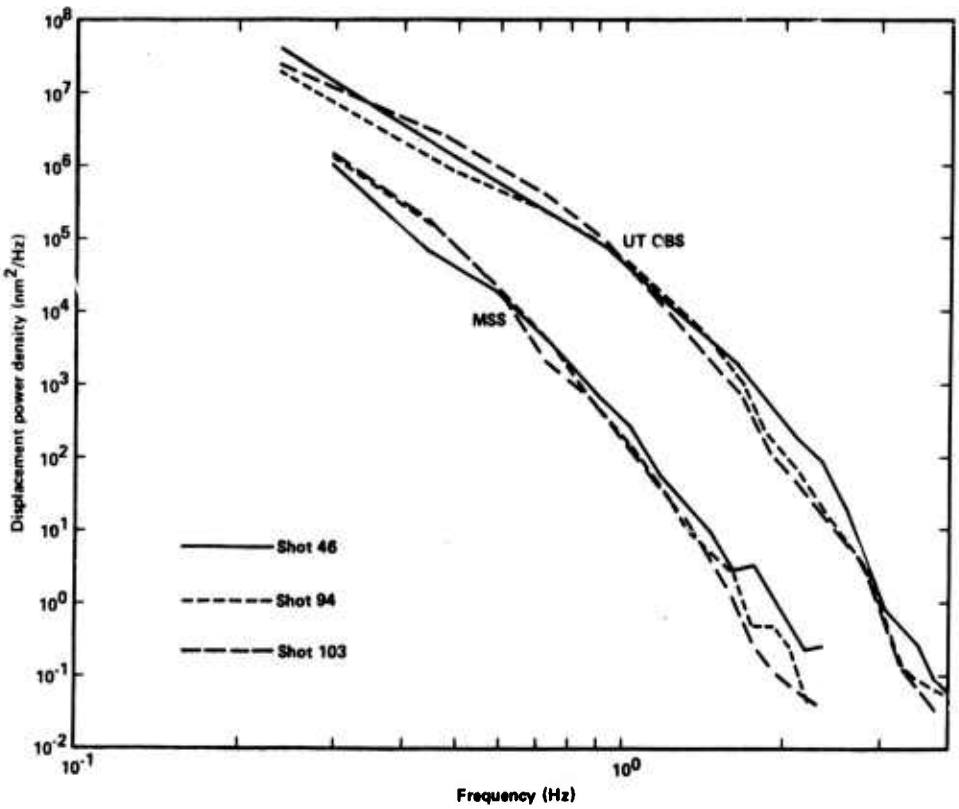


Figure 13. Comparison of corrected UT OBS and MSS noise observations recorded during refraction experiment windows when shots failed to explode. Curves in the upper set were computed from UT OBS data, those in the bottom set from MSS data. The UT OBS was programmed to record a maximum of 40 s per event, but in practice only 34.2 s of data (4096 samples) were available for analysis. Eight segments of 512 time points were used to calculate the estimates for both the UT OBS and MSS data.

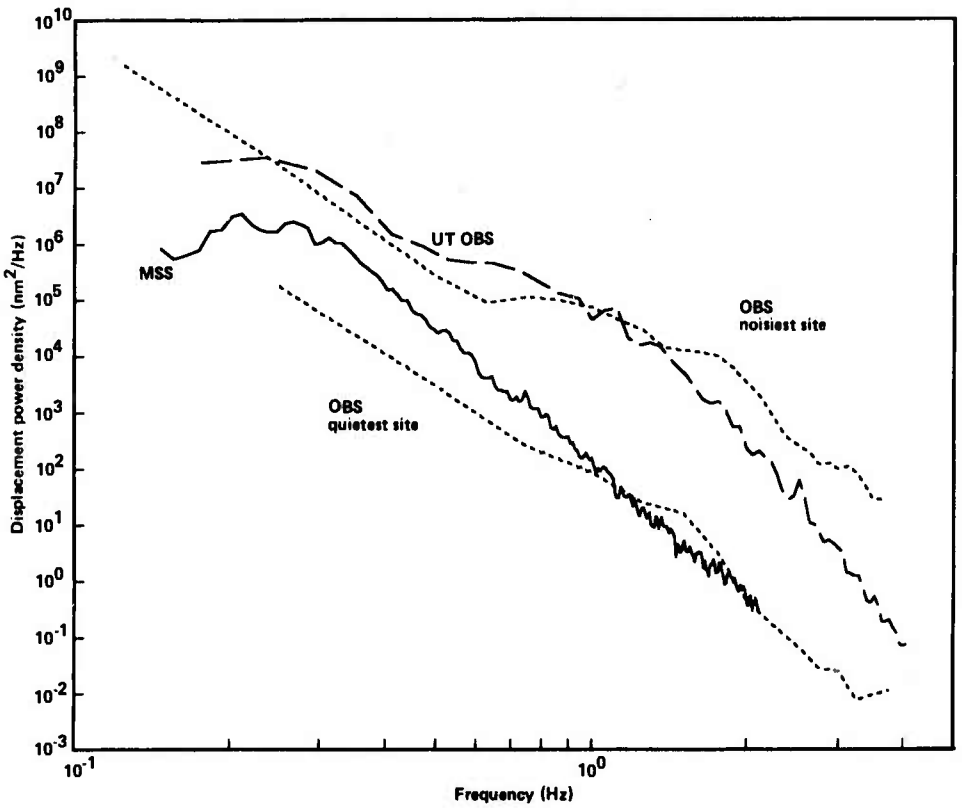


Figure 14. Comparison of Leg 78B noise spectra with OBS observations in the Pacific. The UT OBS data are the same as those in Figure 12; the MSS data are the earliest (and therefore lowest) of those in Figure 10. The two dashed curves are extrema of observations made with the Scripps Institution of Oceanography OBSs. The "noisiest site" was southeast of Hawaii, and the data were fifty-four 8-s samples; the "quietest site" was on the East Pacific Rise, and the data were thirty-one 4-s samples.

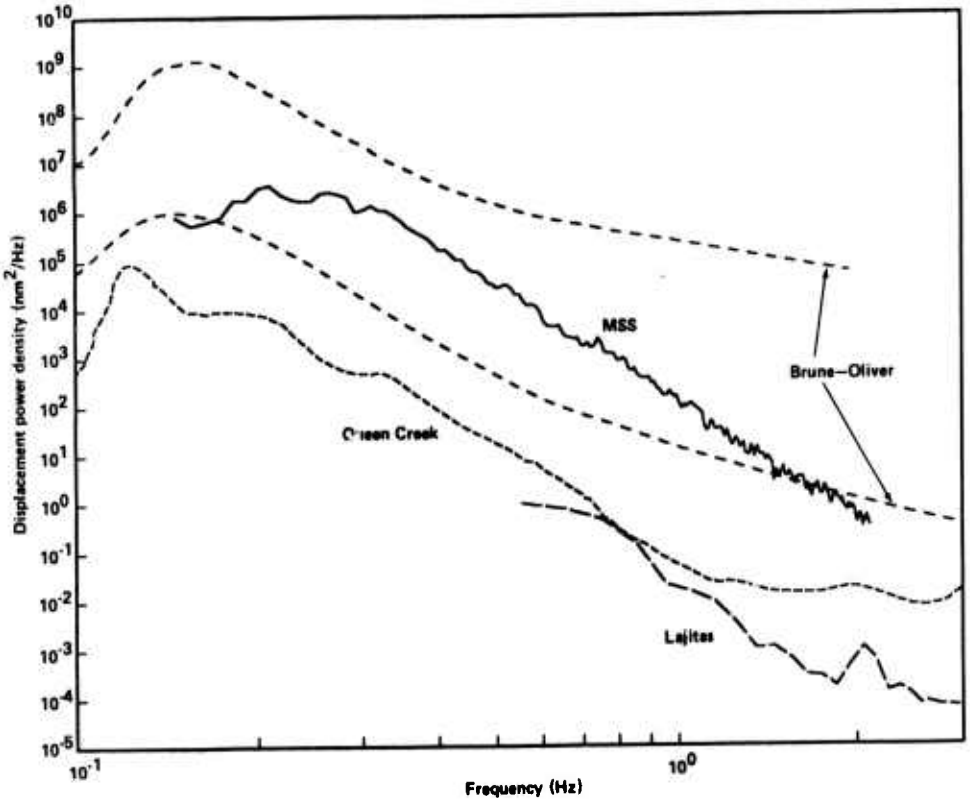


Figure 15. Comparison of the sub-bottom noise spectrum at Site 395 with spectra at two quiet continental sites. The Queen Creek, Arizona curve was taken from Melton (1976), who extracted it from Fix (1972). The Lajitas, Texas data were recorded at an extremely quiet surface site during a time of low winds (Herrin, 1982). Brune-Oliver (1959) curves are from Melton (1976).

Preliminary Seismic Refraction Results Using a Borehole Seismometer in Deep Sea Drilling Project Hole 395A

R.S. Jacobson,
College of Oceanography,
Oregon State University, Corvallis, Oregon

R. Adair and J. Orcutt,
Geological Research Division,
Scripps Institution of Oceanography, La Jolla, California.

13. PRELIMINARY SEISMIC REFRACTION RESULTS USING A BOREHOLE SEISMOMETER IN DEEP SEA DRILLING PROJECT HOLE 395A[1]

R. S. Jacobson, College of Oceanography, Oregon State University
R. Adair and J. Orcutt, Geological Research Division, Scripps Institution of Oceanography[2]

ABSTRACT

Three seismic refraction lines shot to the Marine Seismic System, a vertical-component borehole seismometer in DSDP Hole 395A at 609 m sub-bottom depth, have been analyzed. Despite inconsistencies between various velocity determinations in the upper crust, the velocity of the uppermost 600 m appears to be high, about 4.5 km/s. Between 600 m and 1.8 km sub-bottom, the crust yields an apparent velocity of 4.6 km/s. This value is somewhat lower than that determined near the base of the hole using acoustic logging tools (5.0–5.5 km/s), and is also lower than the average velocity of core samples from the same depth (5.7 km/s). The lower crust is unusually thin, only 1.8 to 2.4 km thick, and has compressional-wave velocities of 6.8 to 7.3 km/s. Mantle velocities range from 7.8 to 8.2 km/s. There is little or no velocity gradient in the uppermost kilometers of the crust, but our results indicate widespread lateral inhomogeneities, supporting the observations based on refraction profiles shot for the original site survey.

INTRODUCTION

For the past 30 years, seismic refraction results have described in general terms the oceanic crustal velocity structure, its variation with age, and its relation to the spreading rate at the time of formation (Raitt, 1963; Shor et al., 1971; Bibee and Shor, 1976; Spudich and Orcutt, 1980a). Until a few years ago, correlation of compressional-wave velocities with lithology has been determined primarily on the basis of measurements on rocks dredged from the sea floor (e.g., Christensen and Salisbury, 1975). Velocity measurements on dredge samples show a systematic bias toward higher velocities than may be expected on the basis of seismic refraction velocities. Since seismic refraction techniques are wavelength-limited (~200 m), they must also average such features as large-scale fractures, voids, vugs, and joints, all of which profoundly affect the porosity and velocity of the rock. Further, many different lithologies can be averaged together, making correlation of refraction velocities with lithology even more difficult.

With the advent of deep drilling into igneous ocean crust, it may be possible to resolve and quantify the differences between velocity determinations made by seismic refraction, laboratory studies on dredge or core samples, and downhole acoustic logs. A large portion of these differences must be related to the scale of measurement and the wavelengths over which velocity determinations are made, varying from less than a meter to many hundreds of meters (Salisbury et al., 1979). Important questions need to be addressed and answered. Under what conditions do laboratory and log velocities converge? Can seismic refraction velocities be predicted from acoustic logs? Is there a smooth velocity increase with depth in the uppermost crust, and if so, is it controlled by porosity changes or lithologic changes, or both?

There exist significant difficulties in measuring the velocity structure in the uppermost 500 m of ocean crust by seismic refraction methods (White and Matthews, 1980; Ewing and Purdy, 1982). These difficulties arise because of the geometry of the experiment, usually involving near-surface explosive charges as sources and either near-surface hydrophones or ocean-bottom seismometers as receivers. The thick water layer acts to mask refracted waves, which penetrate only through the uppermost crust, making identification of arrivals tenuous at best.

One possible way of improving the resolution of upper crustal velocity structure is to use a borehole seismometer as a receiver. The effective use of a borehole seismometer in seismic refraction studies has been demonstrated at DSDP Site 417 (Stephen, 1979; Stephen et al., 1980). Another borehole seismometer has been deployed in DSDP Holes 482C and 494A, but the results are not yet published. More recently, the Defense Advanced Research Projects Agency (DARPA) and the Naval Ocean Research and Development Activity (NORDA) cosponsored the development of a borehole seismometer called the Marine Seismic System (MSS). The long-range objective of this system is to monitor man-made and natural seismicity over long periods of time. Before Leg 78B, the system was untested in a borehole situation, and a series of engineering tests was needed to ensure operational capability. The Deep Sea Drilling Project had planned to re-enter Hole 395A (Fig. 1), in the central Atlantic, to measure geophysical properties—using downhole logging instruments—to a sub-bottom depth of 600 m in the igneous crust. Hole 395A was selected as an optimal location for testing the MSS, combining downhole geophysical logging with a series of seismic refraction profiles in a coherent geophysical investigation. This experiment would provide a

[1] Hyndman, R. D., Salisbury, M. H., et al., *Init. Repts. DSDP*, 78B: Washington (U.S. Govt. Printing Office).

[2] Present addresses: (Jacobson) College of Oceanography, Oregon State Univ., Corvallis, OR 97331; (Adair and Orcutt) Geological Research Div., A-015, Scripps Institution of Oceanography, La Jolla, CA 92093.

unique opportunity to answer some of the questions we have raised here.

DSDP Hole 395A was re-entered in March and April of 1981. This hole, at 22°45'N, 46°05'W, is near the Mid-Atlantic Ridge in 7.2-Ma-old crust formed at a half-spreading rate of 1.7 cm/y. (Hussong et al., 1979). Hussong et al. (1979) observed in their site survey of the area that the geology appears to be very complex. Their seismic refraction results show a diverse range of crustal structure and varying thicknesses and seismic velocities. It was hoped that these results could be improved upon by using the borehole seismometer (BHS) of the Marine Seismic System.

Since it was planned to monitor the BHS in real time aboard the *Challenger*, it was necessary to have an additional ship, the *USNS Lynch*, deploy the explosive charges. In addition, the *Lynch* deployed four University of Texas ocean-bottom seismometers (OBS's) around Hole 395A. Comparison of the OBS and borehole seismometer data would determine whether burial would reduce absolute noise levels, thus increasing the signal-to-noise ratio, and whether there are any advantages in using a sub-bottom instrument in inversion techniques and velocity determinations. Unfortunately, none of the data collected by the ocean-bottom seismometers was usable for travel-time inversion, owing to mechanical and electrical failures. A noise comparison between one of the OBS's and the MSS (Adair et al., this volume) demonstrated, however, that the ambient noise was lower at the bottom of the hole by almost two orders of magnitude.

This paper presents the velocity structure determined around Hole 395A using a variety of simple travel-time inversion techniques. We will compare the results presented here with those obtained from the original site survey using OBS's and sonobuoys (Hussong, et al., 1979), and with other regional surveys, core samples, and the acoustic log.

FIELD OPERATIONS

Four seismic refraction lines were shot to the borehole seismometer (Fig. 1). These lines were originally planned on the basis of previously published bathymetry (Hussong et al., 1979, their figure 3) to reduce the effects of topography. Topographic corrections to the refraction data were expected to be on the order of 0.5 s.

A shot calibration profile was performed to determine the shot size necessary to overcome ambient background noise. This was accomplished by monitoring the BHS in real time aboard the *Challenger* and relaying the results back to the shooting party aboard the *Lynch*. The real-time monitoring also made possible adjustment of charge sizes during the refraction profiles themselves.

Information necessary for reducing the refraction data was collected by the *Lynch* personnel. This information included shot detonation times as recorded by a shot-break streamer, time checks to WWV (a universal time code), depth under the shot, charge size, fuse length, sinking time, and the position, speed, and heading of the *Lynch*. Clock calibrations were also performed aboard the *Challenger*.

The topography under the four seismic lines was sufficiently rough to strain the assumptions made in using most travel-time inversion methods. A few sediment ponds were encountered, the thickest pond (apparently) being at Site 395. The seismic reflection system aboard the *Lynch* was inoperative, making sediment thickness corrections impossible.

The borehole seismometer data proved to be of exceptionally high quality. Background noise levels were comparable to the quietest OBS sites yet observed, and seismic signal-to-noise ratios were very high (Adair et al., this volume). A total of 112 shots were recorded at a sampling rate of 75 samples/second at six different gain settings. One shot, number 23, was located directly over the borehole, and will be used to calculate an interval velocity from the seabed to the instrument at 609 m sub-bottom.

DATA PROCESSING

Data recorded by the BHS instrument were digitized downhole at 75 samples/second and sent to the *Challenger* via a cable, where they were recorded on digital tape. Real-time playback was performed in order to ensure system operation. The raw data have been transcribed into ROSE format (Latraille et al., 1982) by Teledyne Geotech, but not without some problems. Pseudo-random timing errors on the order of 0.5 s were observed when comparing the transcribed digital data with the real-time playback recordings. A systematic process of comparing times of numerous peaks and troughs from both data sets has reconciled the timing inaccuracy to less than 0.05 s.

Shot detonation times were adjusted for distance offset to the shot-break streamer, and corrected to WWV, as were the borehole data. Shot depths were then corrected to the sea surface and shot-receiver ranges were computed on the basis of *Lynch* navigation. Topographic corrections were applied to a flat datum, defined by the depth of the seafloor at Hole 395A. The depth used for the topographic correction was measured at the point the waves entered the seafloor, although allowance was made for picking a nearby strong reflector on the echo sounder recording as the probable location for the signal to enter the seafloor. The topographic correction was designed to replace igneous crust of velocity 6.8 km/s above the datum level with water of velocity 1.5 km/s. It is thus assumed that the upper crust is of constant thickness, and that all topography is the result of undulations in the top of Layer 3. Topographic corrections were as much as 0.82 s. The use of dipping-bottom datum planes could reduce this amount considerably, but would have made it difficult to compare profiles. Finally, the data were filtered from 2 to 20 Hz, using a fourth-order Chebyshev filter, and plotted in reduced record sections.

Seven record sections have been prepared for travel-time analysis. For each of the three lines (Line 3 has not been corrected for timing discrepancies, and will not be discussed further), a true amplitude plot and an autoscaled plot have been prepared. For the true amplitude plot, signal levels have been adjusted for shot size and range, according to the formula

$$A = A_0 (R/R_0)^{Rexp} (W_0/W)^{Wexp}$$

where A is the true amplitude, A_0 is the measured amplitude, R and W are the shot range and weight, R_0 and W_0 are reference ranges and weights, and *Rexp* and *Wexp* are empirical constants equal to 1.75 and 0.65, respectively. A seventh record section, from range zero to 10 km, depicts the autoscaled combined short-range refracted arrivals from Lines 1, 2, and 4.

The autoscaled plots are of channel L1, which had sufficiently high gain to show clearly the first refracted arrivals. Unfortunately, the high gain on this channel clipped the later-arriving high-amplitude arrivals. Channel L2, with a gain about 0.02 that of channel L1, was used to produce the true amplitude plots. No clipping of signals is evident, but at large ranges, the amplitude only barely exceeded the system noise level. The autoscaled and the true amplitude plots for refraction lines 1, 2, and 4 are shown in Figures 2, 3, and 4, respectively. The autoscaled record section of the combined short-range shots is shown in Figure 5.

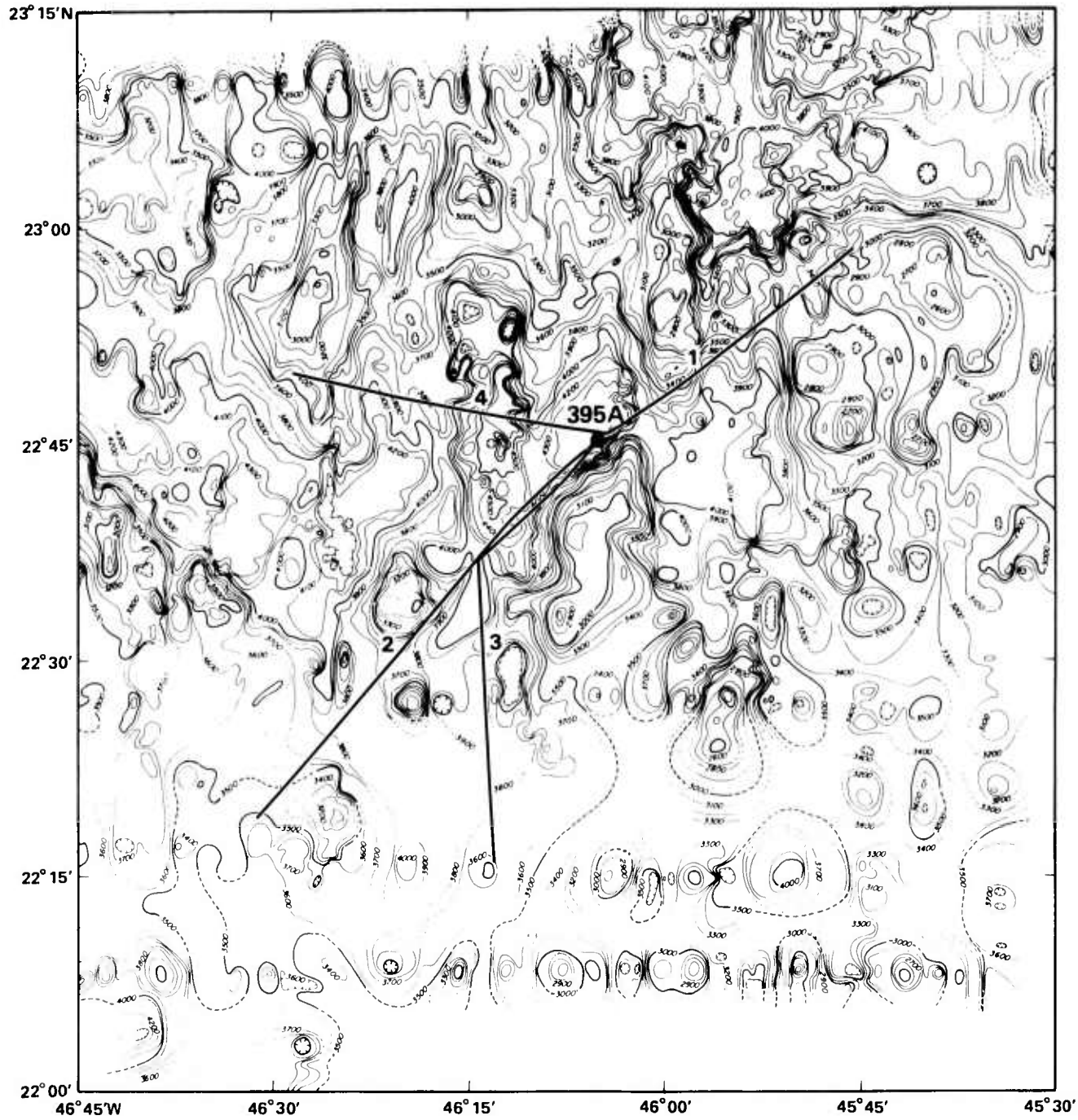


Figure 1. Bathymetric chart of the area surrounding DSDP Hole 395A (reprinted from Hussong et al., 1979), showing the locations of the seismic refraction profiles shot to the borehole seismometer. Depths shown in corrected meters.

The most prominent arrivals are the secondary arrivals, seen in the true-amplitude record sections. These arrivals are interpreted as vertically polarized converted shear waves. The coherence of the arrival times of these waves in the record sections is seriously degraded, since the topographic corrections were made assuming a high refraction velocity to correct the compressional-wave arrivals. The velocities of the shear-wave arrivals vary between 2.5 and 4.7 km/s.

The first refracted arrivals show a change of polarity at a range of 2.8 km (Fig. 5), corresponding to a change in propagation direction of the seismic energy at the instrument from above to just below the horizontal. The phase velocity of the seismic energy just beyond this range yields the seismic velocity (at low frequencies) at the depth of the instrument, since the seismic waves have just reached horizontal propagation. This will be discussed later in more detail. The first arrivals at all ranges show clear onset times, as recorded on channel L1.

TRAVEL-TIME ANALYSIS

The first attempt to analyze travel times was to visually fit straight-line segments to the first arrivals of the travel-time curve. This approach yields the classical plane-layer solution of Officer (1958) and Ewing (1963). Each record section has three distinct travel-time branches, corresponding to the classical Layer 2, Layer 3, and mantle arrivals. Breaks in the travel-time curve were de-

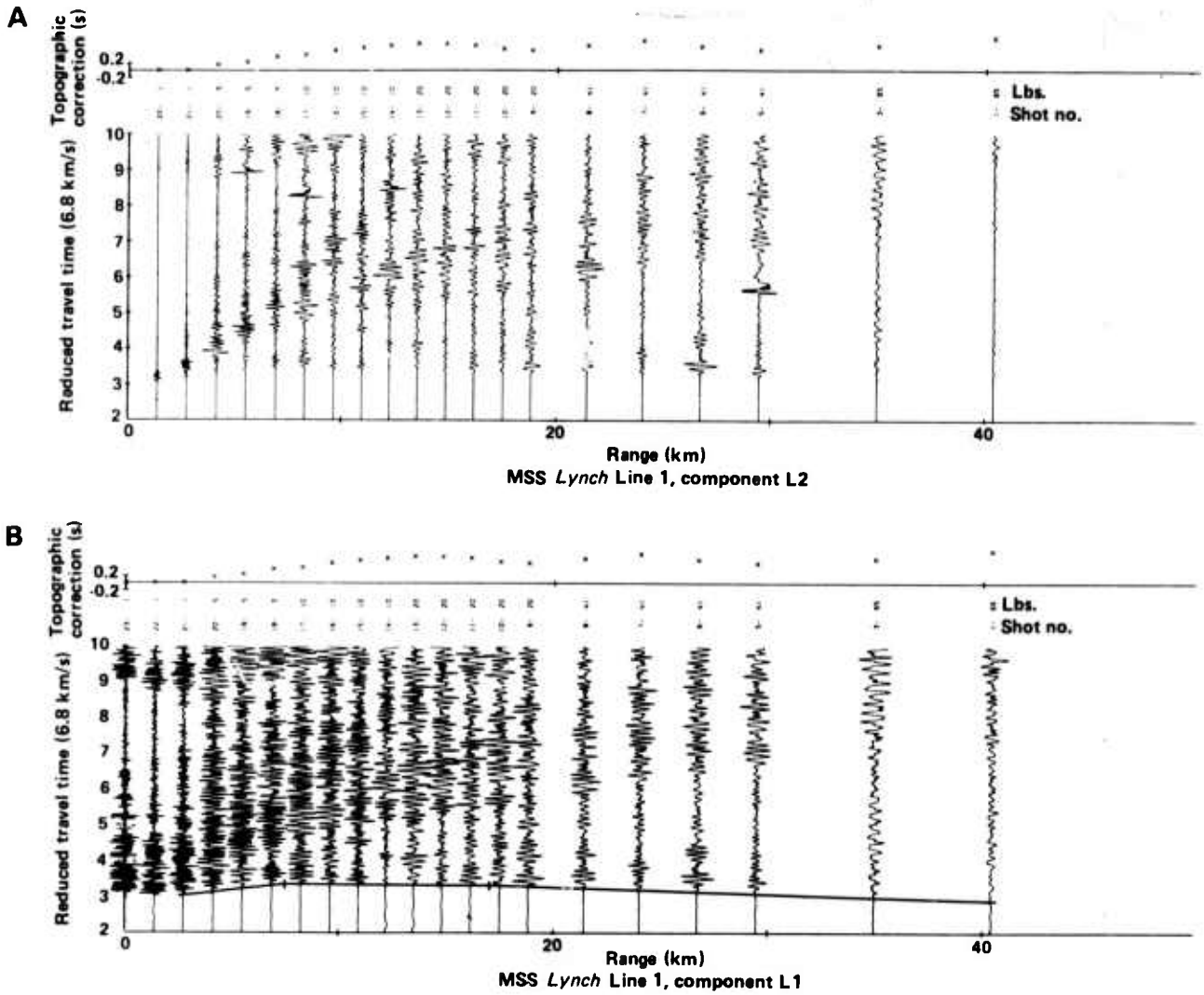


Figure 2. True amplitude (A) and autoscaled (B) record sections for Line 1, located in Figure 1. Both plots are reduced using a velocity of 6.8 km/s. The true amplitude plot, using component L2, has a weighting applied to each trace to adjust for charge size and receiver–source offset. The autoscaled plot, using component L1, has clipped signal levels beyond the first refracted arrival. Also shown are the straight-line segments used for the velocity analysis.

termined by slope changes and verified by amplitude increases corresponding to critical reflections. The increase of amplitudes in the range of 15 to 25 km corresponds to the critical reflections of the mantle. The location and character of the critical reflections differed among the record sections, reflecting lateral inhomogeneity in the crust surrounding Site 395.

Plane-layer solutions were calculated for each of the three available lines, assuming flat layers. The uppermost crustal structure was combined for all three profiles. The record section in Figure 5, combining all refracted arrivals available out to 10 km within the sediment pond, yields an apparent velocity of 4.62 km/s. Because of the geometry of the receiver and source locations, the polarity of the arrivals detected by the vertical-component seismometer is negative at near zero ranges, changing to positive just when the waves start to refract upward from the horizontal. The polarity change of the first arrivals serves to separate the "oblique refraction branch" of the travel-time curve from the standard head-wave refracted branch, the break occurring at an offset of 2.8 km. The refraction velocity of 4.62 km/s observed at the offset range of 3 to 10 km is inferred to be the average seismic velocity at the depth of the seismometer (609 m sub-bottom). No curvature of the travel-time branch just beyond the range of 3 km is readily apparent, indicating that upper crustal velocity gradients below 600 m are extremely low.

Before proceeding to a discussion of the deeper velocity structure, we must first describe the velocity structure in the uppermost 609 m. Shot 23, located directly above the borehole, enables us to determine an average interval velocity to the instrument. Our best determination of this interval velocity is 5.30 km/s. The velocity of 5.30 km/s averages 93 m of sediment and 516 m of igneous crust, implying that the uppermost crust has an even higher velocity. The value of the average interval velocity is inconsistent with the inferred velocity at 609 m depth of 4.62 km/s. The velocity inconsistency is probably caused by measurement error or lateral refraction of shot 23 into the surrounding hill of igneous crust near the borehole, bypassing the sedimen-

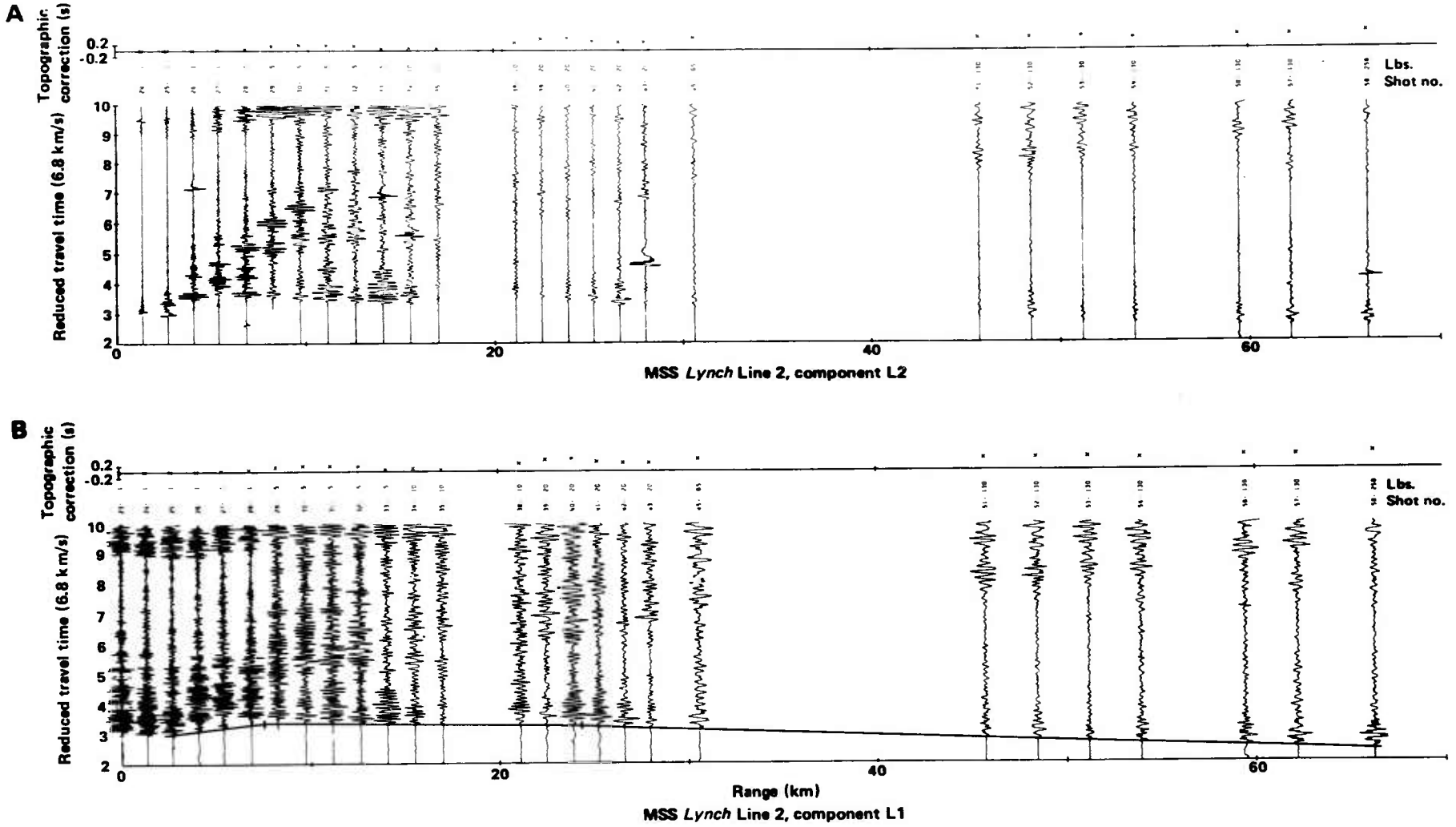


Figure 3. True amplitude (A) and autoscaled (B) record sections for Line 2.

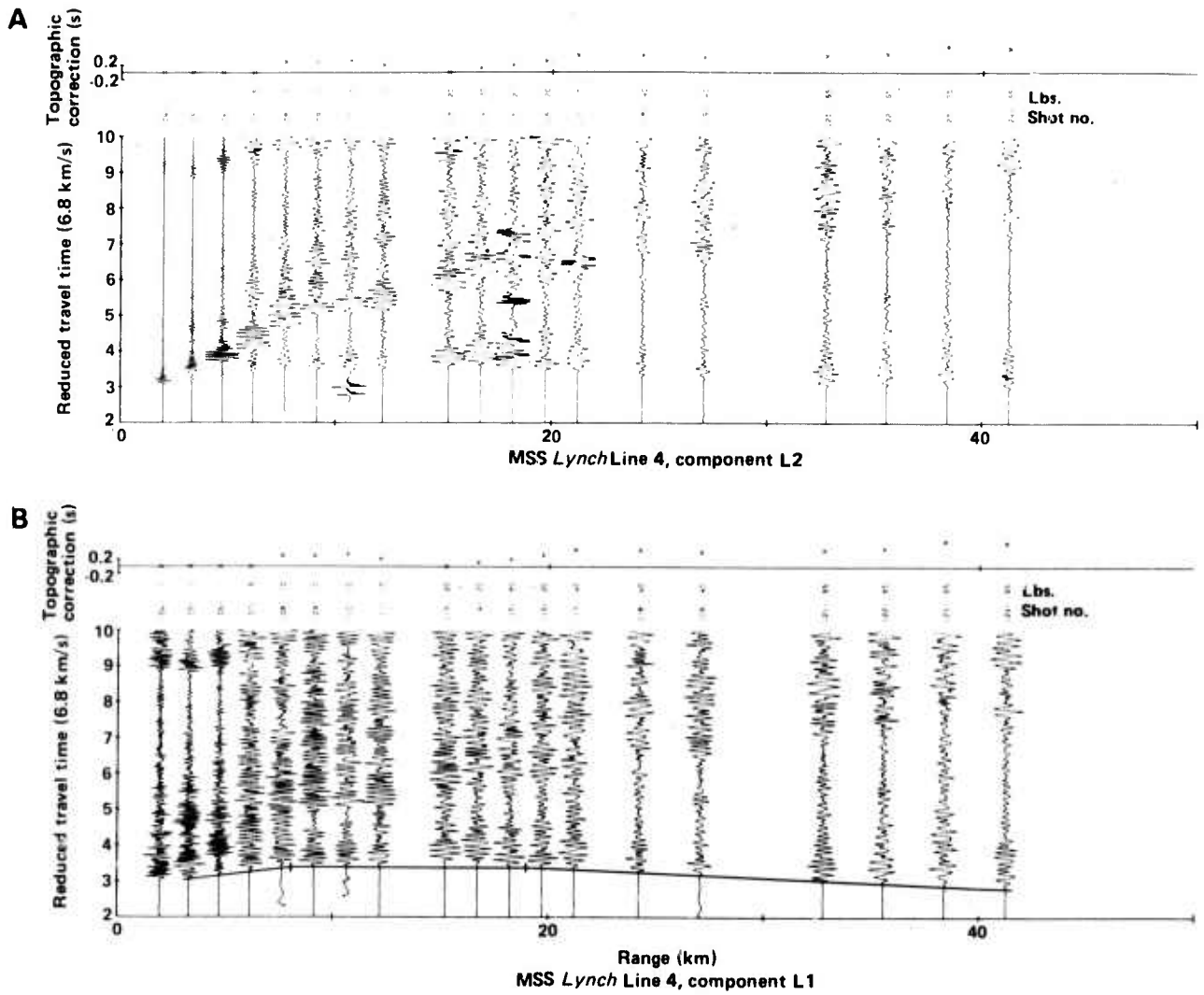


Figure 4. True amplitude (A) and autoscaled (B) record sections for Line 4.

tary layer. Further, our apparent velocity of 4.62 km/s may be low, since the sediment thickness increases away from Hole 395A along our shot lines. If we could correct for the sediment thickness along the shot lines, the apparent velocity at short ranges would be close to 5.0 km/s. That the compressional-wave velocity in the uppermost crust is quite high is indicated by the observed high amplitude of the converted shear-wave arrivals seen in Figures 2, 3, and 4. Spudich and Orcutt (1980b) have noted that *P*- to *S*-wave conversion is efficient across boundaries with a high velocity contrast, that is, when the uppermost crust displays a high compressional-wave velocity. They also infer that the shear-wave amplitude should decrease as the apparent velocity of the shear waves approaches the compressional-wave velocity at the top of the basement. A *P*-wave velocity of around 5.0 km/s near the seafloor, shear-wave velocities of 2.7 to 4.7 km/s, and the observed high amplitudes, are consistent with this hypothesis.

We still need to determine an appropriate velocity for the upper-most crust around Site 395. The shallow crustal structure at Hole 395A includes 93 m of sediment. Elsewhere in the sediment pond, the sediment thicknesses can exceed 0.3 s (Hussong et al., 1979). Outside the pond, little sediment cover was observed, suggesting that lateral inhomogeneity should be taken into consideration. We need to determine a refraction velocity for the upper crust outside the pond, such that the delay time to the 4.62-km/s layer is satisfied. Knowing the thickness of this layer (609 m), a velocity of 4.47 km/s was calculated. Figure 6 depicts the upper crustal structure used for the modified plane-layer solution.

The velocity structure inferred below the level of the seismometer differs between the three profiles, as outlined in Table 1. The thickness of Layer 2, of velocity 4.62 km/s, was rather uniform, varying between 1.14 and 1.25 km. Layer 3 velocities vary significantly, from 6.81 to 7.32 km/s, as did thicknesses, from 1.92 to 2.39 km. Total crustal thickness ranged from 3.67 to 4.25 km. Mantle velocities also showed a wide range of values, between 7.75 and 8.18 km/s, with V_p fast parallel to the spreading direction.

Much of the velocity variation could be the result of dipping layers. We applied the data to a dipping-layer model, solving for the dip and strike of plane layers. The solution indicated that the dips were severe enough

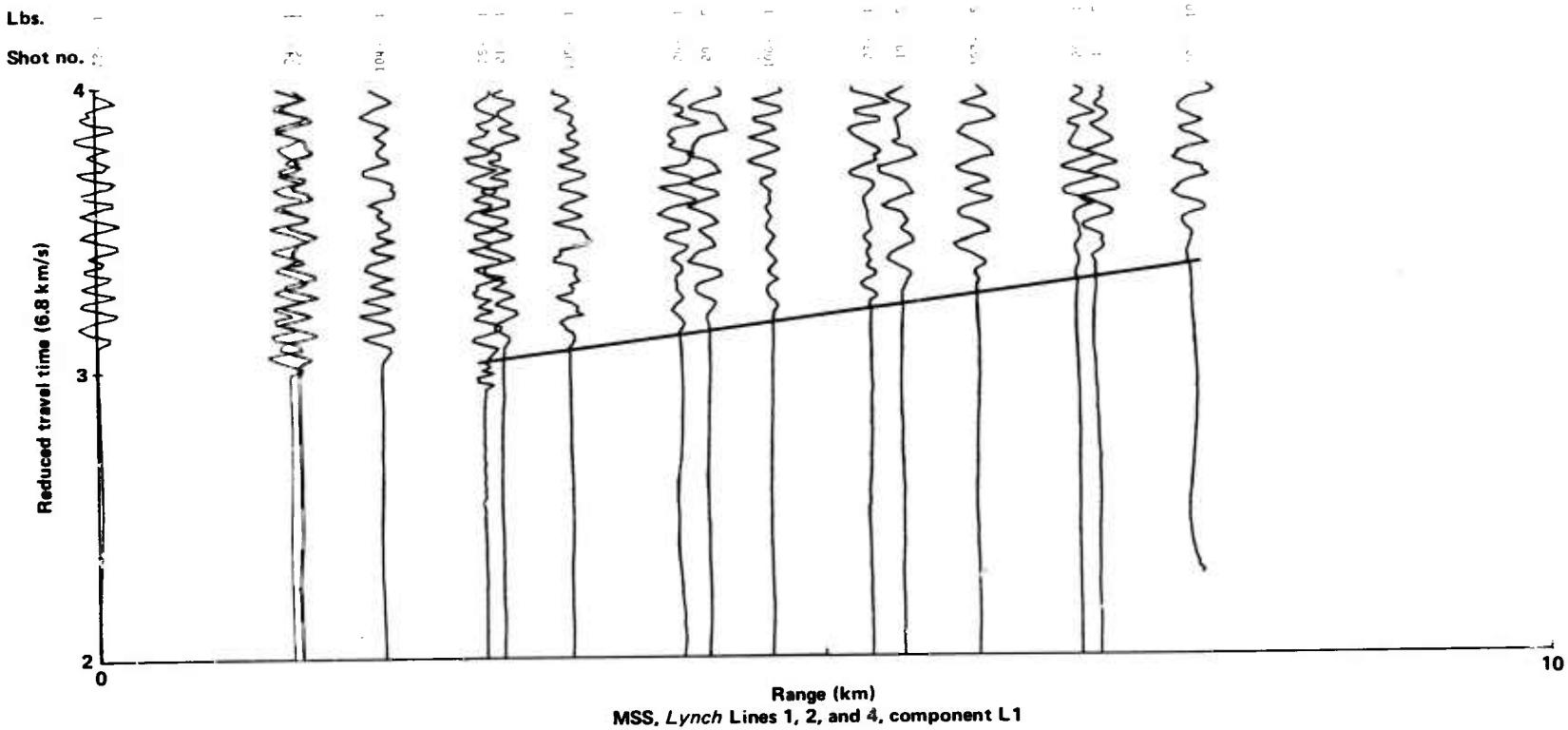


Figure 5. Combined autoscaled record section for all shots from Lines 1, 2, and 4 with an offset of less than 10 km.

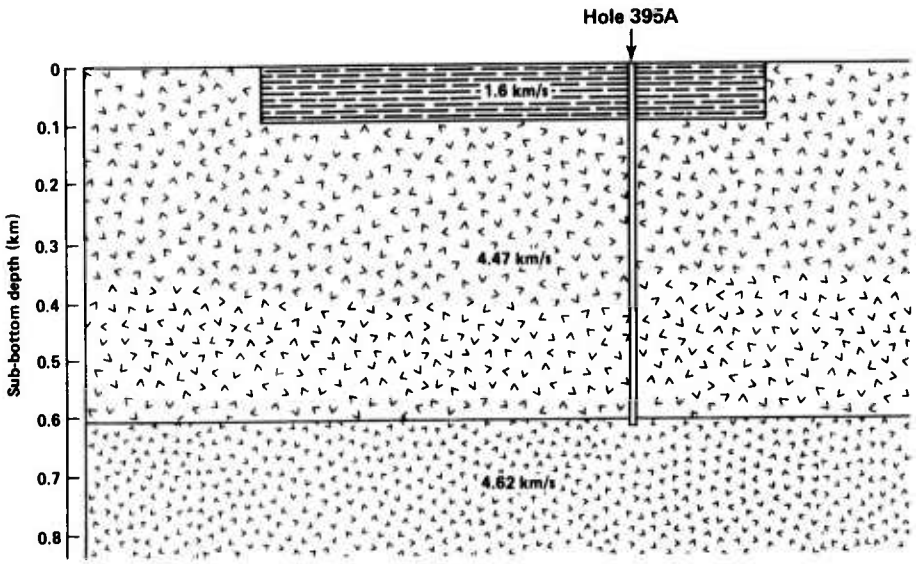


Figure 6. Model of upper crustal velocity structure immediate surrounding DSDP Hole 395A, as deduced from the seismic refraction data. Velocities not corrected for dip.

Table 1. Plane-layer regional solution assuming flat datums.

	Line 1			Line 2			Line 4		
Layer	V_p (km/s)	Thickness (km)	Total thickness (km)	V_p (km/s)	Thickness (km)	Total thickness (km)	V_p (km/s)	Thickness (km)	Total thickness (km)
0	1.509	4.483		1.509	4.483		1.509	4.483	
1	4.47[a]	0.609	0.609	4.47[a]	0.609	0.609	4.47[a]	0.609	0.609
2	4.62	1.140	1.749	4.62	1.247	1.858	4.62	1.178	1.787
3	7.04	1.921	3.670	7.32	2.393	4.251	6.81	2.368	4.155
4	7.75			7.81			8.18		

Note: Drilling results indicate that the uppermost 0.093 km consists of 1.6 km/s sediment.
[a] Assumed velocity.

that the refracting plane layers crossed each other, a physically unrealizable model. A more complex geometry for the refracting horizons would produce an even more unstable solution. However, a somewhat satisfactory model with flat, non-dipping layers is proposed, having velocities of 4.47 (assumed), 4.62, and 7.11 km/s, and a mantle velocity of 7.89 km/s, and thicknesses of 0.609, 1.24, and 1.85 km, respectively, for the three uppermost layers. Systematic residuals in travel times were evident for all layers, indicating either the presence of dipping layers or lateral variations in velocity.

Comparison with Earlier Refraction Studies

In the original site survey by Hussong et al. (1979), it was emphasized that the crustal velocity structure exhibited inhomogeneity which reflected the complex geology of the area. Our results certainly support this conclusion. The great variability in Layer 3 and mantle velocities and crustal thicknesses cannot be attributed solely to timing errors. The close-range arrivals, out to 10 km, show fairly good coherence and exhibit unusually well-behaved travel times (Fig. 5), considering the lack of sediment-thickness corrections. All shots within 10 km of Hole 395A were within the sediment pond, an obviously downfaulted piece of oceanic crust. The crust under the sediment pond at Site 395 may be laterally homogeneous, but it may also be anomalous when compared with the surrounding crust. The sediment pond is deeper than any other seafloor within a radius of 100 km, and also has the thickest sediment cover. The most important evidence of lateral inhomogeneities are the ranges where critical mantle reflections become most prominent. These ranges vary between 15 and 25 km, indicating major structural changes in the crust surrounding Site 395.

It is instructive to examine the differences between the results of this study and those of Hussong et al. (1979). Figure 7 shows a comparison of our lines with profiles of Hussong et al. having similar geographic placement. Very little agreement exists, either in velocities or crustal thicknesses. The exception is Layer 2: the profiles of Hussong et al. show a range in Layer 2 velocities of 3.9 to 4.8 km/and a fairly uniform thickness. It appears that Layer 2 is more homogeneous in this area than is the more deep-seated structure.

The results of this experiment, compared with the regional structure given by Hussong et al. (1979), are more encouraging (Fig. 8). The agreement between velocities and lower crustal layer thicknesses are good. Perhaps more surprising is the greater similarity between our three lines than between those of Hussong et al. This must be the result of our only having one seismometer location in an area of lateral complexity, whereas Hussong et al. had more than 10 receivers.

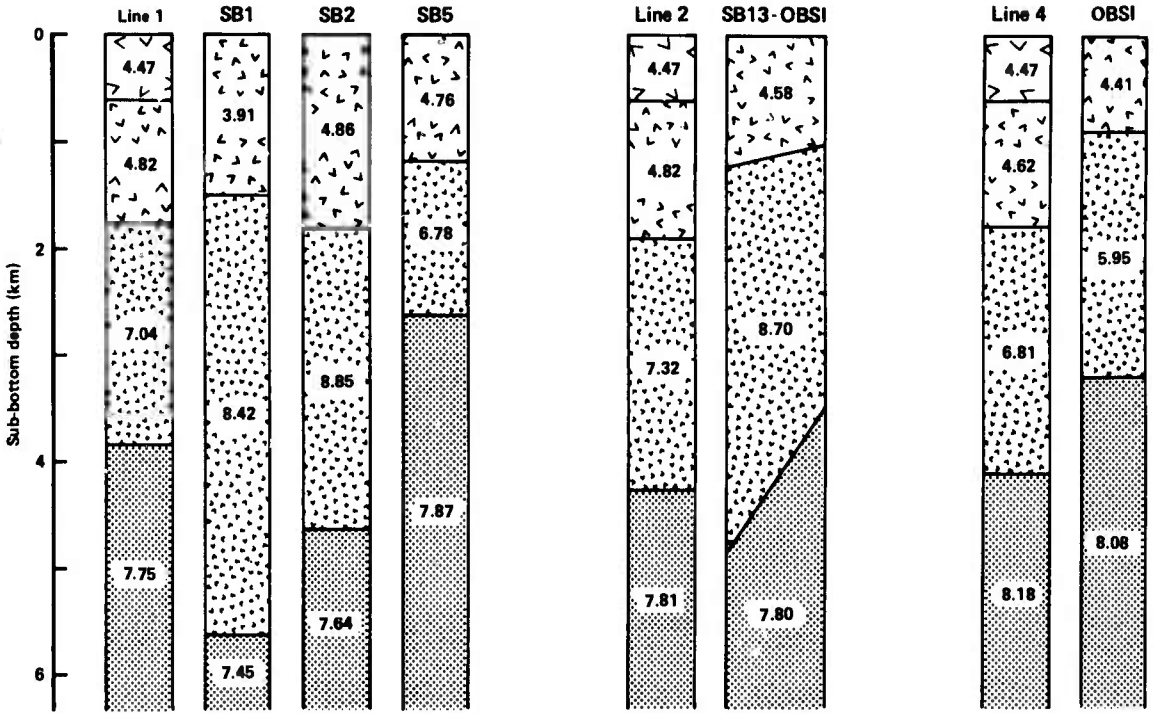


Figure 7. Comparison of crustal velocity structure near Site 395 determined from the DARPA borehole seismometer experiment (Lines 1, 2, and 4) with co-located seismic refraction profiles run by Hussong et al. (1979) using sonobuoys and OBS's. Layer velocities in km/s.

Other crustal velocity structure determinations have been made reasonably close to Site 395. Barrett and Purdy (1979) report on the seismic structure at Site 396, situated to the east of the same ridge crest at 23°50′N, 44°30′W. This site is on 10-Ma-old crust formed at a half-spreading rate of 1.5 cm/y. (Purdy, Rabinowitz, and Schouten, 1979). These authors determined a total crustal thickness of 6.8 km, with a 4.6-km-thick Layer 3 (Purdy, Schouten, et al., 1979), shown in Figure 8.

Detrick and Purdy (1980) have reported a series of crustal determinations across the Kane Fracture Zone at 44°W. The crust south of the fracture zone, created at the same ridge that created the crust at Site 395, is 7 Ma old, and formed at a half-spreading rate of 1.4 cm/y. Their results from OBH2, within 40 km of the fracture zone, are shown in Figure 8, and more closely resemble ours.

Detrick and Purdy (1980) also mention the possible existence of several small-scale fracture zones south of the Kane Fracture Zone which trend WNW. Hussong et al. (1979) also noted two possible fracture zones trending WNW which offset magnetic anomaly patterns around Site 395. The existence of fracture zones may explain the unusually thin crust under Hole 395A. The well-developed Kane Fracture Zone, just to the north, shows a complete absence of Layer 3 (Detrick and Purdy, 1980).

Comparison with Laboratory and Logging Velocities

Melson, Rabinowitz, et al. (1979) reported selected laboratory sonic velocity determinations for crustal rocks from Site 395. Their results, for samples from a depth of 609 m sub-bottom, indicate an average velocity of 5.69 km/s for doloritic basalt, greater than our 4.62 km/s determination of apparent velocity. It is well known that velocities determined on core samples represent maximum velocities because of a sampling bias toward coherent material. A better indication of *in situ* velocities may often be obtained by using downhole acoustic logs. The log for Hole 395A (Mathews et al., this volume) recorded reliable velocities only in the deepest part of the hole. The results indicate an interval velocity of 5.26 km/s. Unfortunately, the acoustic log was unreliable for the shallower structure, and could not be used to verify the lack of velocity gradients deduced above.

SUMMARY

The preliminary results from three out of four seismic refraction lines shot to the DARPA borehole seismometer implanted in DSDP Hole 395A support the results obtained by Hussong et al. (1979) using ocean-bottom seismometers and sonobuoys. Major lateral inhomogeneities are evident in the lower crustal velocity structure, whereas the Layer 2 velocities and thicknesses are more uniform from profile to profile. The gross features of the crust include a 1.85-km-thick Layer 2 overlying a 1.9-km-thick Layer 3 or lower oceanic crust. This crustal section is considerably thinner than that normally expected for Atlantic-type crust. There is little evidence to indicate the existence of velocity gradients within Layer 2, but if gradients do exist, they must be small. Velocity determinations from the sonic logs are considerably higher than the observed refraction velocities, and are somewhat lower than the sonic velocities of discrete samples from the borehole.

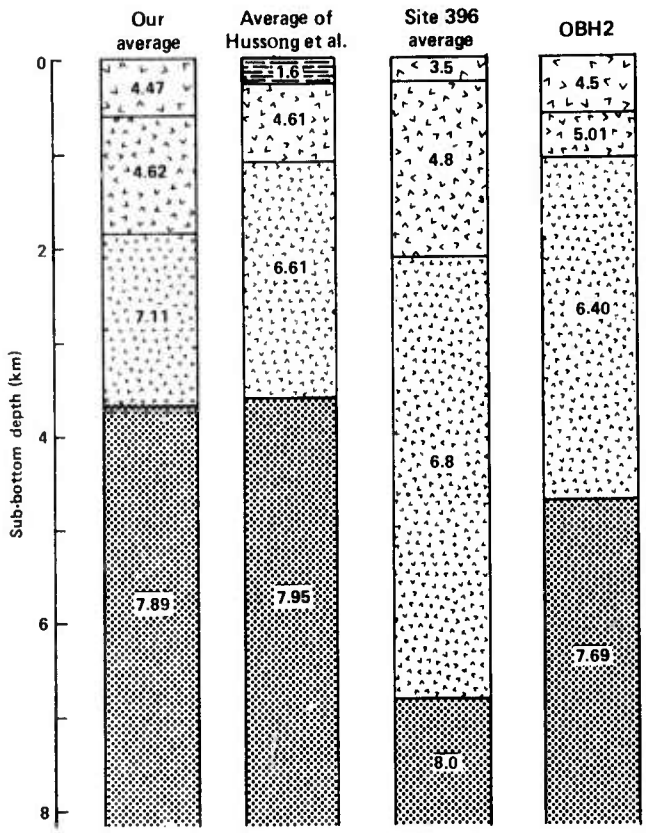


Figure 8. Comparison of the results presented here and the average velocity structure near Site 395 deduced by Hussong et al. (1979). Also shown are the crustal structure near Site 396 (Purdy, Schouten, et al., 1979) and the velocity structure near the Kane Fracture Zone (OBH2), determined by Detrick and Purdy (1980). Layer velocities in km/s.

The results of the data collected from the borehole seismometer are more self-consistent than those obtained using many OBS's, but this may be the result of having a single sensor in a geologically complicated structure. The use of a borehole seismometer offers considerable advantages in travel-time analysis, especially for determining the velocity at the depth of the sensor. Nonetheless, we expect that the conclusions reached in this chapter will change little with further analysis. Because amplitudes are strongly dependent on vertical and horizontal velocity gradients, the use of synthetic seismograms to refine the compressional- and shear-wave velocity structure any further will prove extremely difficult.

ACKNOWLEDGMENTS

We would like to thank the crew of the *USNS Lynch* for their cooperation and patience. We especially appreciate the fine effort put forth by the master, E. Maier, without whom many of our results could not have been obtained. We also thank the UT Galveston crew, headed by D. McGowan and P. Donoho, for their efforts in working with the OBS's. We also wish to thank the NORDA Code 360 personnel aboard the *Lynch* for making the cruise function smoothly. Finally, we with to express our thanks to L. Dorman, F. Duennebier, and M. Salisbury for reviewing this manuscript.

This work was supported by NORDA Code 543, ONR (N00014-79-C-0004), the School of Oceanography at Oregon State University, and by a grant from the Defense Advanced Research Projects Agency (F49620-79-C-0019).

REFERENCES

Barrett, D. L., and Purdy, G. M., 1979. IPOD survey area AT-6: Seismic refraction results. *In* Melson, W. G., Rabinowitz, P. D., et al., *Init. Repts. DSDP*, 45: Washington (U.S. Govt. Printing Office), 49–53.

Bibee, L. E., and Shor, B. B., Jr., 1976. Compressional wave anisotropy in the crust and upper mantle of the Pacific. *Geophys. Res. Lett.*, 3:639–642.

Christensen, N. I., and Salisbury, M. H., 1975. Structure and constitution of the lower oceanic crust. *Rev. Geophys. Space Phys.*, 13: 57–86.

Detrick, R. S., Jr., and Purdy, G. M., 1980. The crustal structure of the Kane Fracture Zone from seismic refraction studies. *J. Geophys. Res.*, 85:3759–3777.

Ewing, J. I., 1963. Elementary theory of seismic refraction and reflection measurements. *In* Hill, M. N. (Ed.), *The Sea* (Vol. 3): New York (Interscience), pp. 3–19.

Ewing, J. I., and Purdy, G. M., 1982. Upper crustal velocity structure in the ROSE area of the East Pacific Rise. *J. Geophys. Res.*, 87: 8397–8402.

Hussong, D. M., Fryer, P. B., Tuthill, J. D., and Wipperman, L. K., 1979. The geological and geophysical setting near DSDP Site 395, North Atlantic Ocean. *In* Melson, W. G., Rabinowitz, P. D., et al., *Init. Repts. DSDP*, 45: Washington (U.S. Govt. Printing Office), 23–37.

LaTraille, S. L., Gettrust, J. F., and Simpson, M. E., 1982. The ROSE seismic data storage and exchange facility. *J. Geophys. Res.*, 87: 8359–8363.

Melson, W. G., Rabinowitz, P. D., et al., 1979. Site 395: 23°N, Mid-Atlantic Ridge. *In* Melson, W. G., Rabinowitz, P. D., et al., *Init. Repts. DSDP*, 45: Washington (U.S. Govt. Printing Office), 131–264.

Officer, C. B., 1958. *Introduction to the Theory of Sound Transmission:* New York (McGraw-Hill).

Purdy, G. M., Rabinowitz, P. D., and Schouten, H., 1979. The Mid-Atlantic Ridge at 23°N: Bathymetry and magnetics. *In* Melson, W. G., Rabinowitz, P. D., et al., *Init. Repts. DSDP*, 45: Washington (U.S. Govt. Printing Office), 119–128.

Purdy, G. M., Schouten, H., Crowe, J., Barrett, D. L., Falconer, R. K. H., Udintsev, G. B., Marova, N. A., Litvin, V. M., Vlayashko, G. M., Markushevich, V. M., and Zdorovenin, V. V., 1979. IPOD survey area AT-6: A site survey. *In* Melson, W. G., Rabinowitz, P. D., et al., *Init. Repts. DSDP*, 45: Washington (U.S. Govt. Printing Office), 39–48.

Raitt, R. W., 1963. The crustal rocks. *In* Hill, M. N. (Ed.), *The Sea* (Vol. 3): New York, (Interscience), pp. 85–102.

Salisbury, M. H., Stephen, R., Christensen, N. I., Francheteau, J., Hamano, Y., Hobart, M., and Johnson, D., 1979. The physical state of the upper levels of Cretaceous oceanic crust from the results of logging, laboratory studies and the oblique seismic experiment at DSDP Sites 417 and 418. *In* Talwani, M., Harrison, C. G., and Hayes, D. E., (Eds.) *Deep Drilling Results in the Atlantic Ocean: Ocean Crust*, Am. Geophys. Union, p. 113–134.

Shor, G. G., Jr., Menard, H. W., and Raitt, R. W., 1971. Structure of the Pacific basin. *In* Maxwell, E. (Ed.), *The Sea* (Vol. 4): New York (Wiley), pp. 3–27.

Spudich, P., and Orcutt, J., 1980a. A new look at the seismic velocity structure of the oceanic crust. *Rev. Geophys. Space Phys.*, 18: 627–645.

———, 1980b. Petrology and porosity of an oceanic crustal site: results from wave form modeling of seismic refraction data. *J. Geophys. Res.*, 85:1409–1433.

Stephen, R. A., 1979. The oblique seismic experiment in oceanic crust—equipment and technique. *Mar. Geophys. Res.*, 4:213–226.

Stephen, R. A., Louden, K. E., and Matthews, D. H., 1980. The oblique seismic experiment on Deep Sea Drilling Project Leg 52. *In* Donnelly, T. Francheteau, J., Bryan, W., Robinson, P., Flower, M., Salisbury, M., et al., *Init. Repts. DSDP*, 51, 52, 53, Pt. 1: Washington (U.S. Govt. Printing Office), 675–704.

White, R. S., and Matthews, D. H., 1980. Variations in oceanic upper crustal structure in a small area of the north-eastern Atlantic. *Geophys. J. R. Astron. Soc.*, 61:401–435.

Date of Initial Receipt: January 5, 1983
Date of Acceptance: June 24, 1983

Preliminary Analysis of Ocean Bottom and Subbottom Ambient Microseismic Noise During the Ngendei Experiment

Richard G. Adair and John A. Orcutt,
Institute of Geophysics and Planetary Physics
Scripps Institution of Oceanography, La Jolla, California

Thomas H. Jordan, Department of Earth, Atmospheric, and Planetary Sciences,
Massachusetts Institute of Technology, Cambridge, Massachusetts.

Abstract

Simultaneous measurements of ambient microseismic noise at and below the seafloor are compared over the band 0.2–7.0 Hz. The MSS sensors rested unclamped at 124 m subbottom, 54 m within basement rock, while six 4-component OBSs, variously configured, ranged between 0.5–30 km from the borehole. Vertical-component noise spectra of displacement power density at both borehole and ocean-bottom sites typically displayed the microseism peak between 0.1–0.3 Hz, and fell as (frequency)$^{-9}$ at higher frequencies with various peaks superposed. Vertical ocean-bottom and borehole noise levels are nearly identical at the microseism peak, on the order of 10^8 nanometer^2/Hz, but OBS values exceed MSS values by 20 dB or more at frequencies between approximately 0.5 and 7 Hz. Horizontal-component noise levels in the borehole were essentially the same as the vertical-component levels. At the ocean bottom, horizontal noise spectra were similar in shape to and 15–20 dB higher than vertical spectra between 0.4 and 7 Hz, but had comparable values at the microseism peak, which extended to approximately 0.4 Hz on the horizontal components. Ocean-bottom pressure measurements of ambient noise are comparable to other published measurements, having a value on the order of 10^4 Pascals^2/Hz at the microseism peak and falling at higher frequencies as (frequency)$^{-7}$. Vertical-component noise levels at the quietest land sites are between 10–30 dB lower than those measured in the borehole during Leg 91, with the difference diminishing towards higher frequencies. Leg 91 vertical-component noise measurements contrast those from the prototype MSS deployment during DSDP Leg 78B in which microseism-peak levels at the proximate seafloor site exceeded borehole levels by 10 dB. However, relative ocean-bottom and seafloor noise levels at higher frequencies during Leg 78B were similar to those observed during Leg 91. Absolute borehole levels measured in these two deployments are comparable. Persistent peaks at 0.5, 0.75 and 1 Hz, observed in both the borehole and seafloor data, appear to be genuine features of earth noise. Leg 78B spectra were relatively featureless. High vertical-component coherence was seen at the microseism peak between pairs of OBSs separated by distances on the order of 1 km.

Introduction

The current revitalization of ocean bottom seismograph usage is due primarily to recent developments in semiconductor technology and hardware, particularly in digital recording techniques, and they have been used primarily to investigate seafloor structure through refraction experiments. Several problems still arise, however, from the nearly ubiquitous blanket of sediments in the world's waters. The OBS must contend with poor coupling and signal "ringing" due to unconsolidated sediments (see Sutton et al., 1981), as well as the inherent difficulty of observing important converted shear phases (see Spudich and Orcutt, 1980). A final difficulty, which is the primary interest of this paper, is the high ambient noise levels at the ocean bottom, thought to be due to noise propagation as low-order Stoneley wave modes trapped near the ocean-bottom-seafloor interface.

DSDP Leg 91 was designed to specifically answer some outstanding questions regarding the generation and propagation of ambient microseismic noise in the deep ocean, as well as the relative characteristics of seismic signals at and below the seafloor employing an array of six OBSs at various distances from the MSS site. This paper discusses some preliminary analysis of the Leg 91 seismic data regarding the relative character and values of ambient microseismic noise at and below the seafloor.

Instrumentation and Operations, Marine Seismic System

When operationally deployed, the MSS comprises a borehole instrumentation package (BIP) containing the seismic sensors connected by coaxial cable to an ocean bottom recording system, the Bottom Processing Package (BPP) (Adair et al., 1983). Following BIP emplacement, data are recorded on two shipboard consoles, each distinguished by different digitization methods and post-digitization processing (described below). One of the consoles, referred to here as the Gould system, emulates most of the BPP functions. The other, referred to as the Teledyne system, monitors the BIP and provides redundant data logging. After a satisfactory checkout of the BIP and a period of shipboard data recording, the coaxial cable link to the BIP is connected to the BPP, which is then lowered to the seafloor to record up to 45 days of data.

A triaxial set of Teledyne Model S-750's (orthogonal horizontals, X and Y, and one vertical Z) and a backup vertical component (B) compose the MSS seismic sensors. Output from each of the three primary sensors is split into a mid-period (MP) and short-period (SP) passband between approximately 0.1–2.0 Hz and 0.5–20.0 Hz, respectively, while the redundant vertical is passed through the SP band only. The resultant seven data streams, labeled MX, MY, MZ, SX, SY, SZ, and SB, are then digitized and transmitted to logging devices over the coaxial cable. Output destined for the shipboard Teledyne system is sampled, gain-ranged, and digitally-represented to yield a 21-bit dynamic range with 14-bit resolution. MP data are digitized at the rate of 4 samples/second (s/sec), and SP data at 40 s/sec. Either of the SP vertical channels may be sampled 80 s/sec to the exclusion of the other. Data transmitted to the BPP and its shipboard counterpart are oversampled 256 times and their amplitudes represented

by means of an enhanced delta modulator encoding (EDME) technique. These encoded, oversampled streams are then sent to the recording unit, digitally convolved with an anti-aliasing, finite-impulse response (FIR) filter, resampled at their proper rates (4 and 40 s/sec for the MP and SP data, respectively), and decoded as a 24-bit integer with 24-bit resolution.

The low-ripple, zero phase-shift FIR filter is nearly flat to 75% of the Nyquist frequency, and thereafter falls 160 dB by 125% of the Nyquist frequency, a decline of approximately 720 dB/decade. Figure 1 illustrates the net MSS displacement responses for the MP and SP passbands; the dashed lines at their high frequency ends depict the augmentation due to the FIR filter. At the Nyquist frequencies and in the absence of this filter, the MP response is down 29 dB from its peak, while the SP response is down only 1.5 dB from its peak. In the case of the 80 s/sec SP vertical data recorded on the Teledyne system, the response is down 11.5 dB by 40 Hz from the peak value.

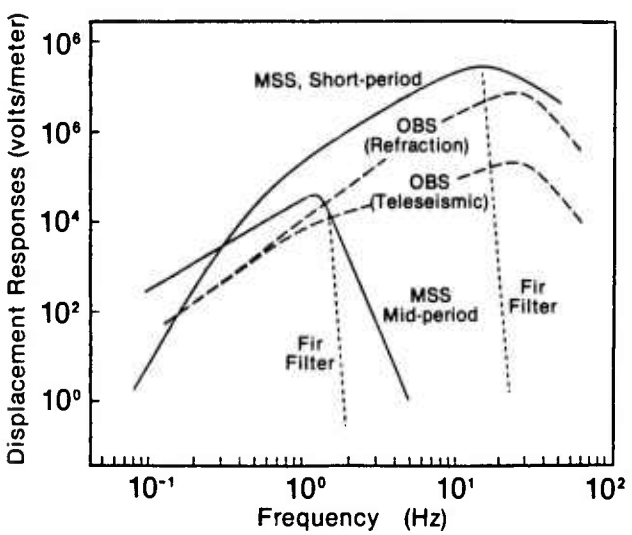


Figure 1. Ocean bottom seismometer selectable frequency responses.

Ocean Bottom Seismographs

The six OBSs are four-component (one vertical and two horizontal seismometers, and a hydrophone), digital, event recorders (Moore et al., 1981). Sensor outputs are amplified at successive factors of 2 from 1 to 512, bandpassed, and digitized with a 12-bit word at 128 s/sec. The gain of each channel is modified only when the long-term average of its digital output falls outside pre-defined limits of a few least significant bits. Semiconductor memory continuously accumulates four-channel data, time code, and gain information in a cyclically-overwritten buffer in order to avoid mechanical and electric contamination due to recorder operation. The length of this "pre-event" buffer is normally approximately 13 sec, but was extended to approximately 58 sec in several of the capsules; see Tables 1 and 2 for specific OBS characteristics during the experiment. An OBS buffers an event to tape when scheduled and/or when triggered by a comparison criterion of long term and short term averages of the vertical-component's digital output. Two OBS responses (see Fig. 1) are selectable prior to capsule deployment by the exchange of a filter board. One of these, designated "Teleseismic," emphasizes lower frequencies more than the other, designated "Refraction", in order to make the OBS event-triggering alogrithm more sensitive to moderate-amplitude, high-frequency depleted teleseismic signals. An acoustic transducer permits capsule ranging, release control, and exchange of diagnostic information.

Operations

Leg 91 events may be broken into three phases, a refraction experiment, a teleseismic experiment, and instrument recovery, during all of which noise measurements were made. Figures 2 and 3 show the OBS locations during the refraction and teleseismic experiments, respectively. Tables 1 and 2 give identification name, location, deployment period, range to the BIP, response type and pre-event buffer length of each capsule for the refraction and teleseismic experiments, respectively. Figure 4 summarizes events pertinent to the noise experiment. Events which occurred during the refraction experiment include:

- the deployment from MELVILLE of four OBSs within 0.5 km of the MSS site (Hole 595B) and two at approximately 25 and 30 km (Fig. 2 and Table 1),
- the aborted deployment of the primary BIP (BIP-1) and the subsequent successful deployment of the backup BIP (BIP-2),
- commencement of recording on the Teledyne and Gould shipboard recording consoles, and
- shooting of five distinct refraction lines.

The four OBSs nearest Hole 595B [see Fig. 2(a)] recorded with the "refraction" response in scheduled mode, and the other two [see Fig. 2(b)] with the "teleseismic" response in both triggered and scheduled mode. The deployment attempt of BIP-1 was aborted because of coaxial cable damage caused by its hole-lock mechanism, which was dismantled in BIP-2. BIP-2 was therefore not locked in the hole, but coupling with the basement rock was accomplished by resting it at the hole

Table 1. OBS Locations and Characteristics During Refraction Experiment

Name	Location		Deployed		Range* (km)	Response** Type	Buffer Length
	Lat.	Long.	From:	To:			
Janice	23 56.2	165.47.5	0626Z, 24 Jan 83	0715Z, 31 Jan 83	29.51212	TEL	59 sec
Juan	23.82204	165.53114	1104Z, 29 Jan 83	0535Z, 9 Feb 83	0.43929	REF	13 sec
Karen	23.81823	165.52695	0102Z, 29 Jan 83	0807Z, 9 Feb 83	0.45643	REF	13 sec
Lynn	23.82238	165.53031	1123Z, 30 Jan 83	0817Z, 10 Feb 83	0.35369	REF	13 sec
Phred	23.56.5	165.46.2	0610Z, 30 Jan 83	0850Z 7 Feb 83	28.05962	TEL	59 sec
Suzy	23.81864	165.52679	0038Z, 30 Jan 83	0556Z, 10 Feb 83	0.410705	REF	13 sec

*Reference site is MSS location: Lat., 23 49.34; Long., 165 31.61

**TEL = Teleseismic, REF = Refraction

Table 2. OBS Locations and Characteristics During Teleseismic Experiment

Name	Location		Deployed		Range* (km)	Response** Type	Buffer Length
	Lat.	Long.	From:	To:			
Janice	23.48.98	165.31.58	1432Z, 5 Feb 83	1520Z, 22 Mar 83	0.669107	TEL	59 sec
Juan	24.02.66	165.31.91	1124Z, 11 Feb 83	1100Z, 22 Mar 83	24.690504	TEL	13 sec
Karen	23.48.4	165.32.5	2142Z, 11 Feb 83	0600Z, 23 Mar 83	2.304714	TEL	59 sec
Lynn	23.48.74	165.33.07	1356Z, 9 Feb 83	1040Z, 23 Mar 83	2.713599	TEL	13 sec
Phred	23.49.06	165.32.74	2045Z, 9 Feb 83	0900Z, 23 Mar 83	1.9848196	TEL	13 sec
Suzy	23.51.48	165.17.83	2246Z, 10 Feb 83	0531Z, 22 Mar 83	23.7246575	TEL	59 sec

*Reference site is MSS location: Lat., 23 49.34; Long., 165 31.61

**TEL = Teleseismic, REF= Refraction

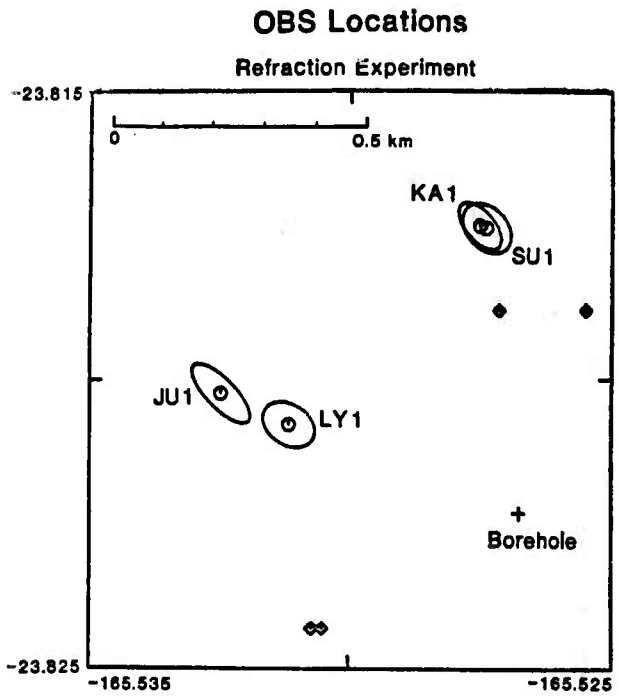


Figure 2(a). Ocean bottom seismometer locations for refraction experiments (Karen, Suzy, Juan and Lynn).

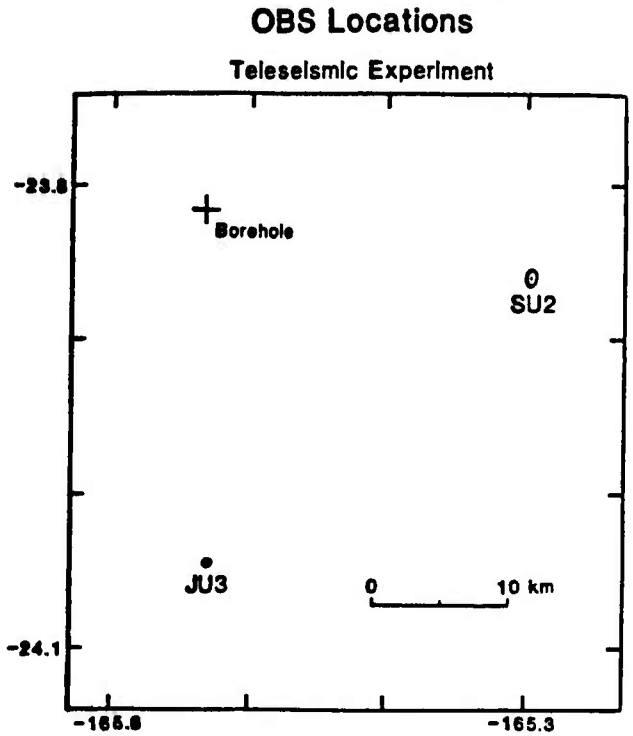


Figure 3(a). Ocean bottom seismometer locations for teleseismic experiment (Suzy-2 and Juan-3).

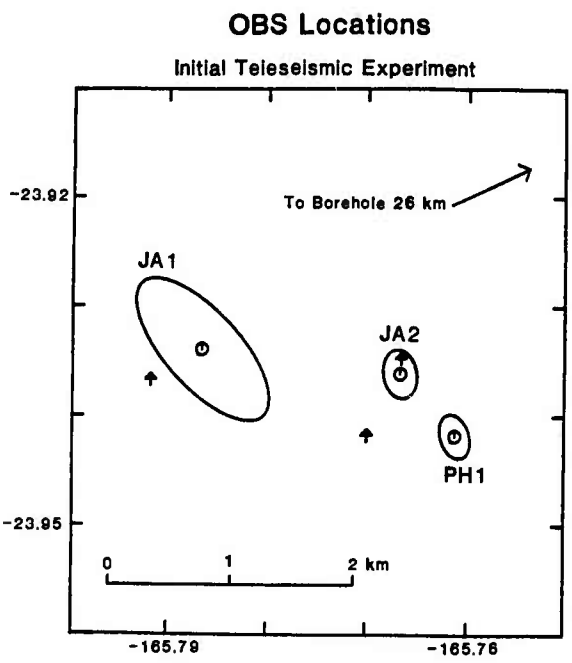


Figure 2(b). Ocean bottom seismometer locations for initial teleseismic experiment (Janice-1, Janice-2, and Phred).

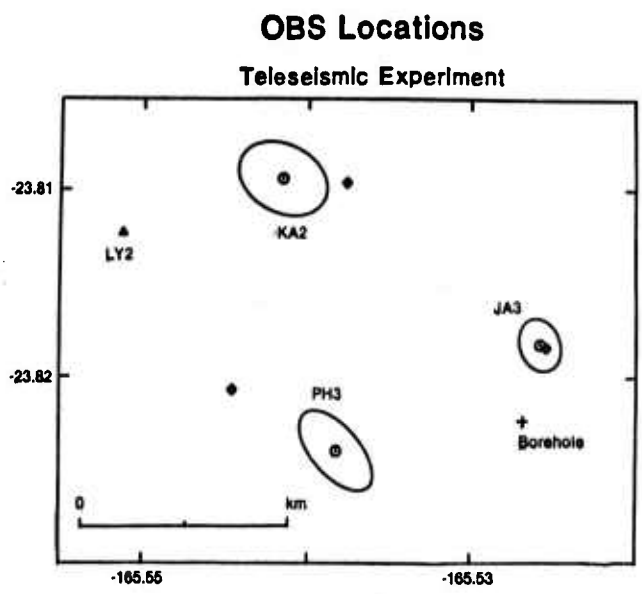


Figure 3(b). Ocean bottom seismometer locations for teleseismic experiment (Lynn-2, Karen-2, Janice-3, and Phred-3).

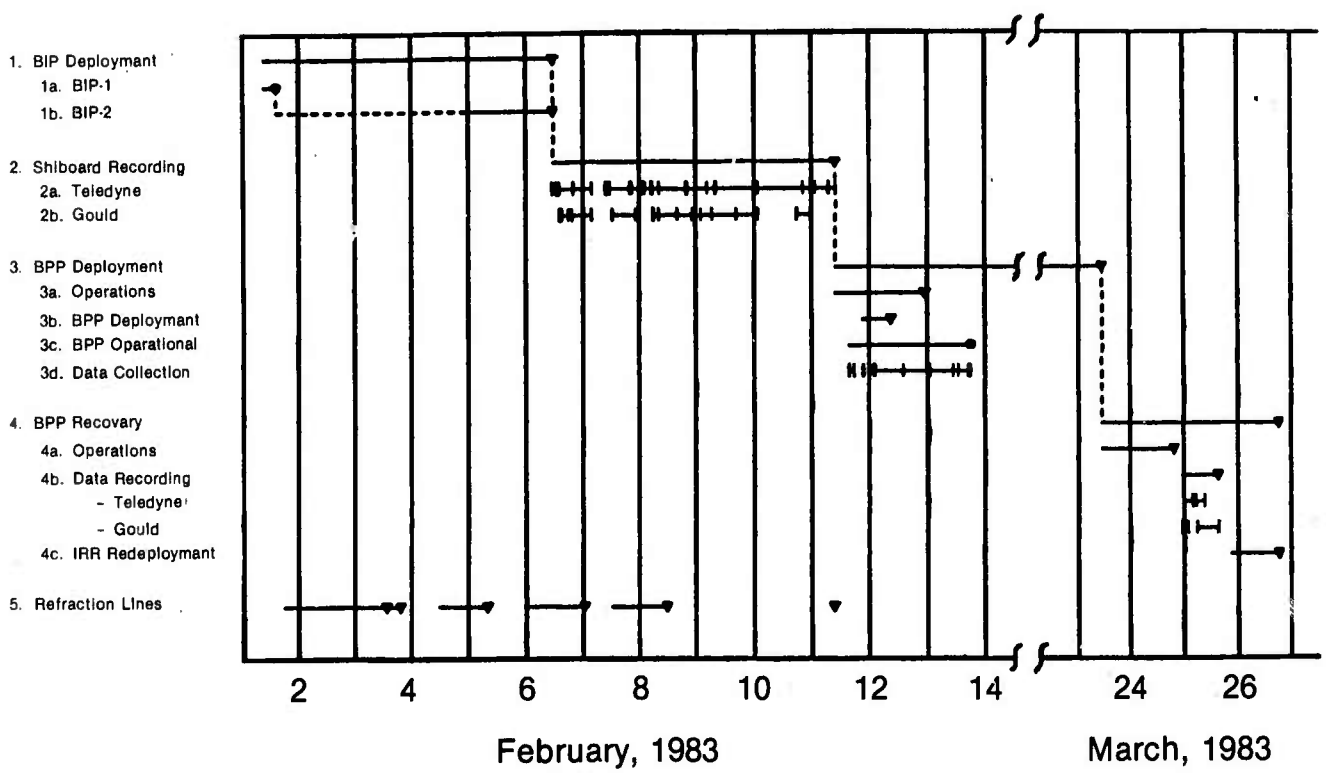


Figure 4. MSS operational chronology.

bottom. Adequate cable isolation was achieved with a length of coaxial cable coiled on the seafloor.

During the teleseismic experiments:

- The six OBSs, all employing the "teleseismic" response, were redeployed in a roughly linear array extending WNW from Hole 595B towards the Tonga-Kermadec Trench (Fig. 3 and Table 2).
- Shipboard recording on CHALLENGER concluded with fill-in shooting of the first portion of the fourth refraction line's outbound leg, and
- The BPP was deployed.

Finally, during recovery operations 45 days after BPP deployment:

- The BPP and all OBSs were all successfully recovered,
- The BPP was discovered to have ceased operations approximately two days after its deployment because of a water leak in one of its two power pressure vessels,
- Further MSS data were recorded aboard MELVILLE on both Teledyne and Gould consoles over a 16-hr period, and
- The BPP was replaced with a dummy load and its recovery mooring reinstalled, leaving the BIP in Hole 595B.

Noise Data

Figures 5–7 chart data available for noise analysis during the Ngendei Expedition prior to the teleseismic experiment of each OBS. Such data were obtained from OBSs either at specifically-scheduled times or at times when refraction shots detonated late or not at all. In particular, a refraction line abandoned on February 8, 1983, because of BIP deployment delays, provided a large number of noise samples. During the teleseismic experiment, all OBSs recorded daily noise samples at CUT midnight. A total of nearly 1400 noise samples are available, over half of which were recorded simultaneously with MSS data.

Also shown in Figures 5–7 are MELVILLE's ranges from the MSS site during the refraction experiment, delineating the times of the refraction lines. During the

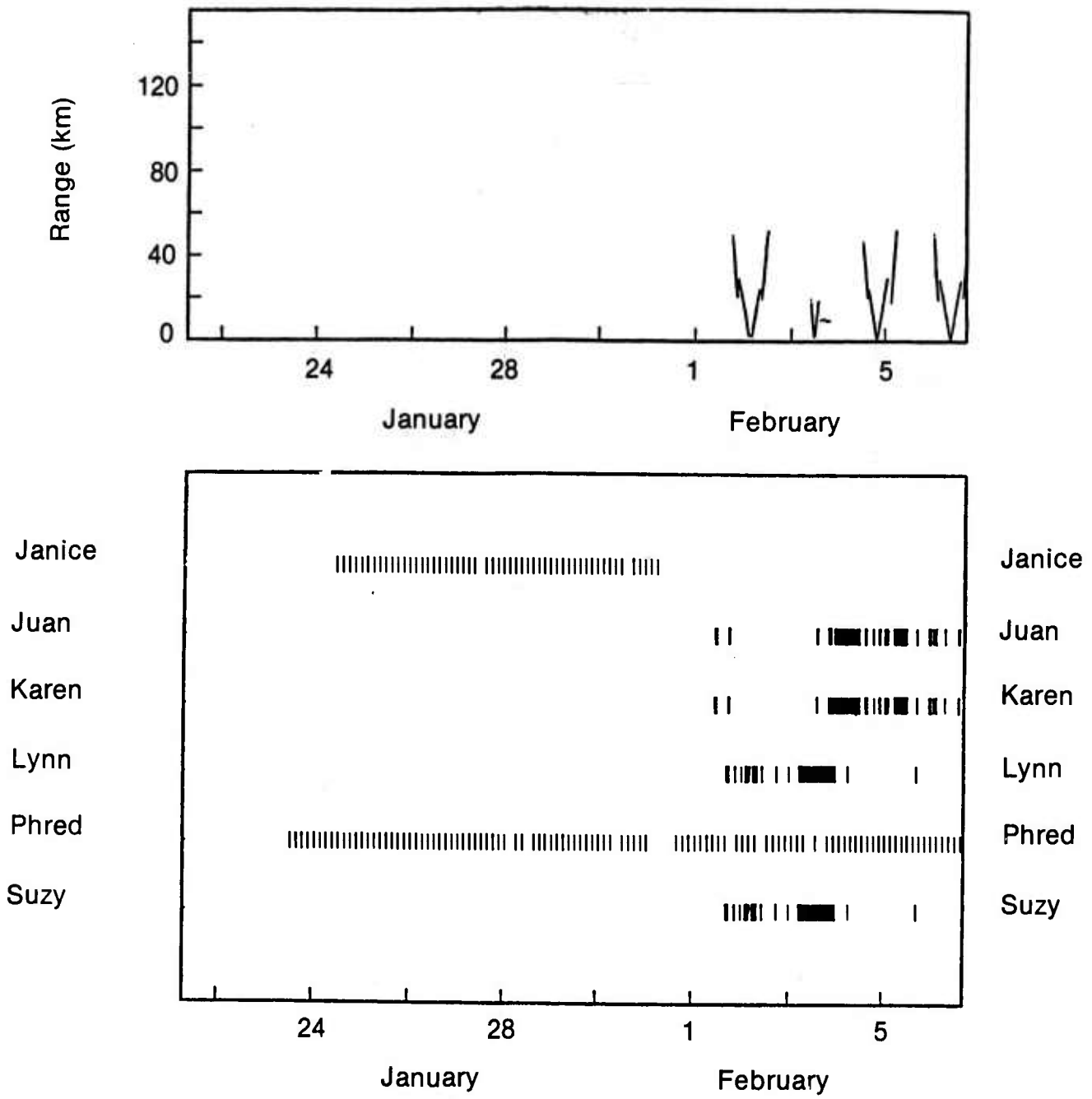


Figure 5. RV Melville ranges from MSS site and times of refraction lines for OBSs.

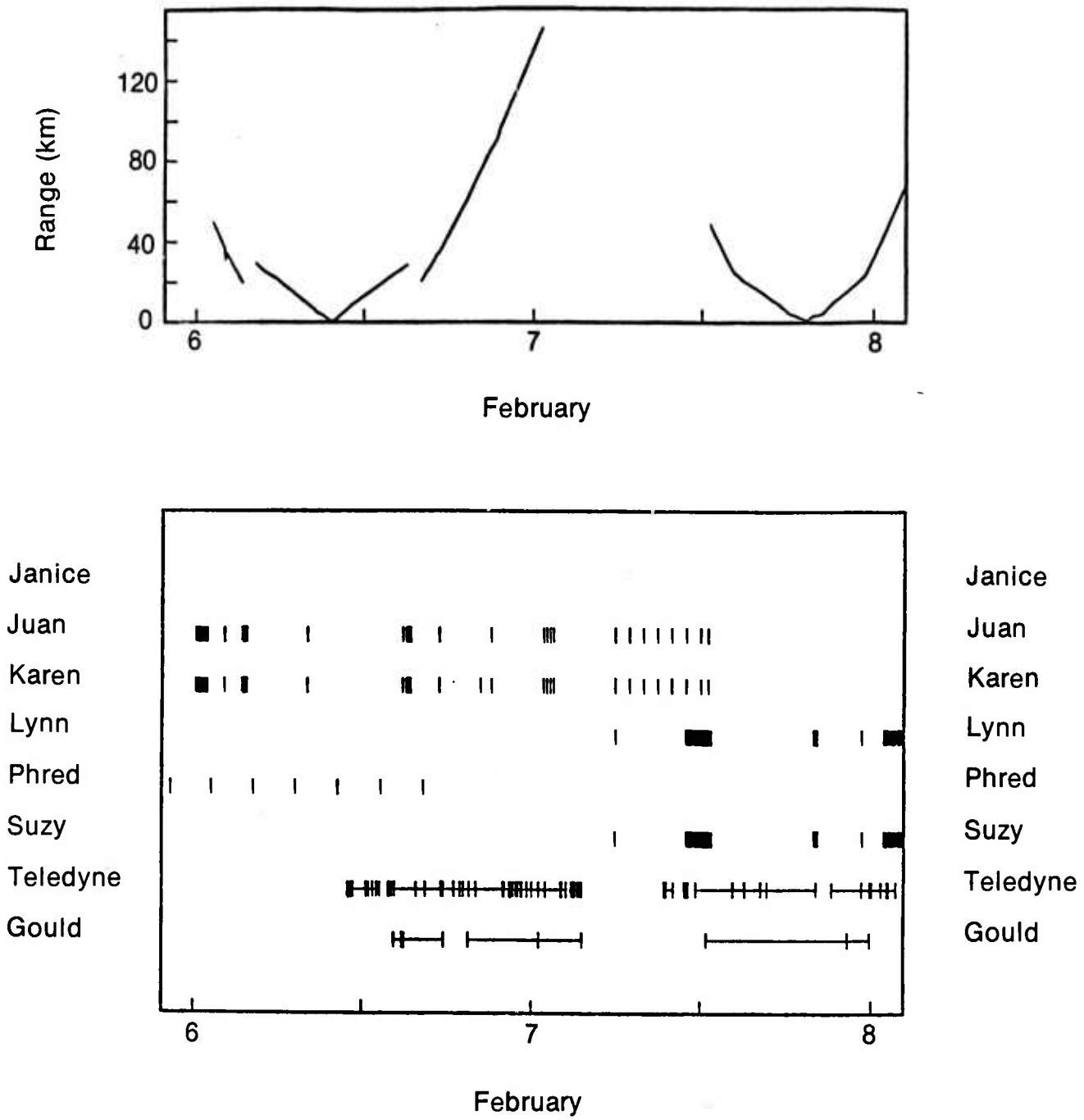


Figure 6. RV Melville ranges from MSS site and recording periods for Gould and Teledyne systems (Feb. 6–8).

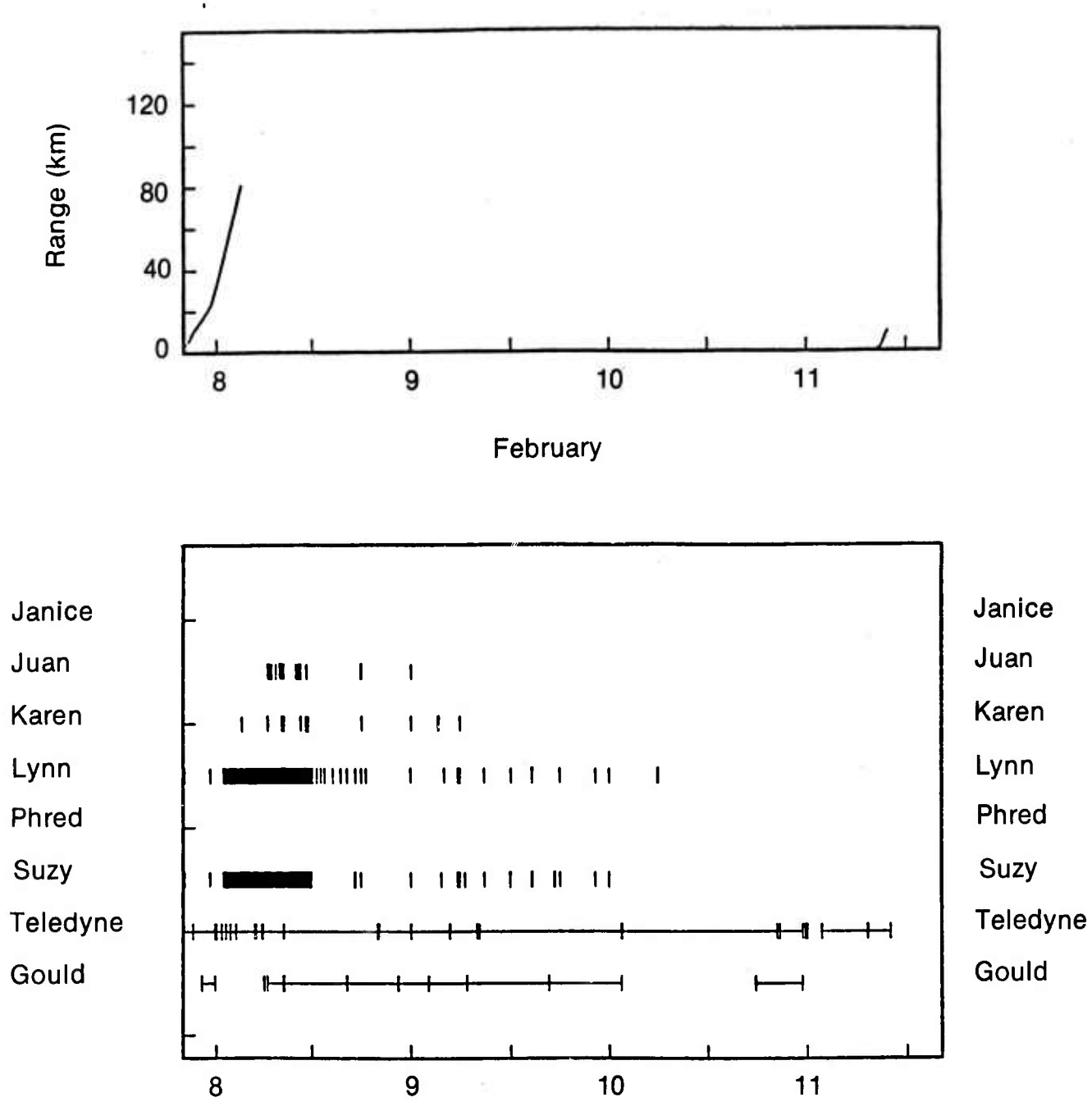


Figure 7. RV Melville ranges from MSS site and recording periods for Gould and Teledyne systems (Feb. 8–11).

refraction experiment, capsule Juan's hydrophone channel improperly gain-ranged, resulting in frequently-clipped digital data. During the teleseismic experiment, the digitizer of Janice's vertical channel malfunctioned, and progressive tape head misalignment in Juan rendered data recorded beyond 25 February inaccessible.

MSS recording was continuous except during maintenance or intermittent system malfunction. A total of 119.5 hrs of Teledyne data and 126.5 hrs of Gould data were recovered. Water leakage into the battery sphere caused system shutdown approximately two days after BPP deployment, with the last datum recorded at 1805Z, 13 February 1983. No further borehole data were collected until shipboard recording during recovery operations. The recovered MSS data may be obtained from the DARPA-funded Center for Seismic Studies (CSS) on 9-track tape. The Teledyne data are corrected for gain-range, and both Teledyne and Gould data are represented as 32-bit integers. These tapes identify sensors X and Y as East (E) and North (N), respectively, but, in fact, their orientations are unknown. Brief gaps of approximately 18 sec due to establishment of playback synchronization pepper the retrieved, reformatted Teleydyne data. Certain of the MSS data channels malfunctioned or were not recorded at various times. The horizontal MSS sensor Y malfunctioned for unknown reasons throughout the experiment. An unknown shipboard source of radio frequency radiation interfered with the Gould console's channel SZ, so it was disabled and only the SP vertical backup SB was recorded. During BPP deployment, channel SZ was recorded, and channel SB replaced by hydrophone data (channel SH). The Gould electronics bay in the BIP which initiates calibrations and processes channel MZ output malfunctioned just prior to BPP deployment and never resumed operation. One or the other of the Teledyne short-period vertical channels was not available when SP vertical-component data were digitized at 80 s/sec, as described above.

Data Quality

Data quality and valid frequencies of microseismic noise measurement were assessed with both time and spectral-domain criteria. In particular, power density and coherence estimates were computed in the manner described by Welch (1967). Spectra were obtained from de-meaned, non-overlapping data segments tapered with a normalized Hanning window, using a mixed-radix Fast Fourier Transform algorithm which obviates the restrictive requirement of power-of-two data lengths. Stable spectral estimates are then formed from averages of cross- and auto-spectra. Spectra are normalized so that the total power per Nyquist bandwidth is equal to the time-domain variance, which essentially folds the energy of the negative frequencies into that of the positive.

Figures 8 and 9 show a typical example of multi-channel MSS data from the Teledyne and Gould systems, respectively, recorded during the shipboard recording period. Y sensor malfunction is evident from both figures. Note that Gould channel SZ (Fig. 9) is disabled, as explained above. The high-frequency content of Teledyne and Gould SP signals is mostly ship-generated by CHALLENGER.

Proper representation of the data was investigated by computing relative amplitudes and timing between the two recording systems with cross-correlations and linear regressions of corresponding channels (Fig. 10). Typically, both SP and MP Gould data led Teledyne data by 15 or 16 samples and were approximately 5 times greater in amplitude rather than 8 times as we would expect from the difference in digital word length (24 and 21 bits, respectively), a consequent 4 dB uncertainty in spectral estimates. Comparisons of data timing with independent time code (WWV) written adjacent to Teledyne data on strip-charts indicate that Gould's timing is in error. Teledyne calibrations (Fig. 11) of properly-functioning channels are within their expected norms by less than 4 dB, suggesting that Gould amplitudes are skewed, although since the calibration loop excludes portions of the total seismograph circuitry this cannot be verified. The departure of the MX and SY calibrations from the norms further demonstrate sensor malfunction. Note that the other MP channels depart drastically from the norm below approximately 0.2 Hz.

Figure 12 compares power spectral density estimates of simultaneous vertical-component Teledyne and Gould data with instrument noise spectra; the data are not corrected for instrument response. The peaks above 8 Hz in the SB spectra [Fig. 12(b) and (c)] are ship-generated. Peaks in the SB Teledyne spectrum [Fig. 12(c)] which are absent in the SP Gould spectrum [Fig. 12(a)] are manifestations of Teledyne aliasing. However, both Gould and Teledyne spectra have comparable values near the Nyquist frequency, implying improper functioning of Gould's SB FIR filter.

Also shown in Figure 12 are estimates of system noise, provided by H.B. Durham of Sandia Laboratories. The system noise is not significant over the entire SP passband for either Teledyne or Gould data. A white spectrum of least count noise, applicable to the Teledyne data, is that expected from uniformly-distributed round-off errors due to the discrete representation of data.

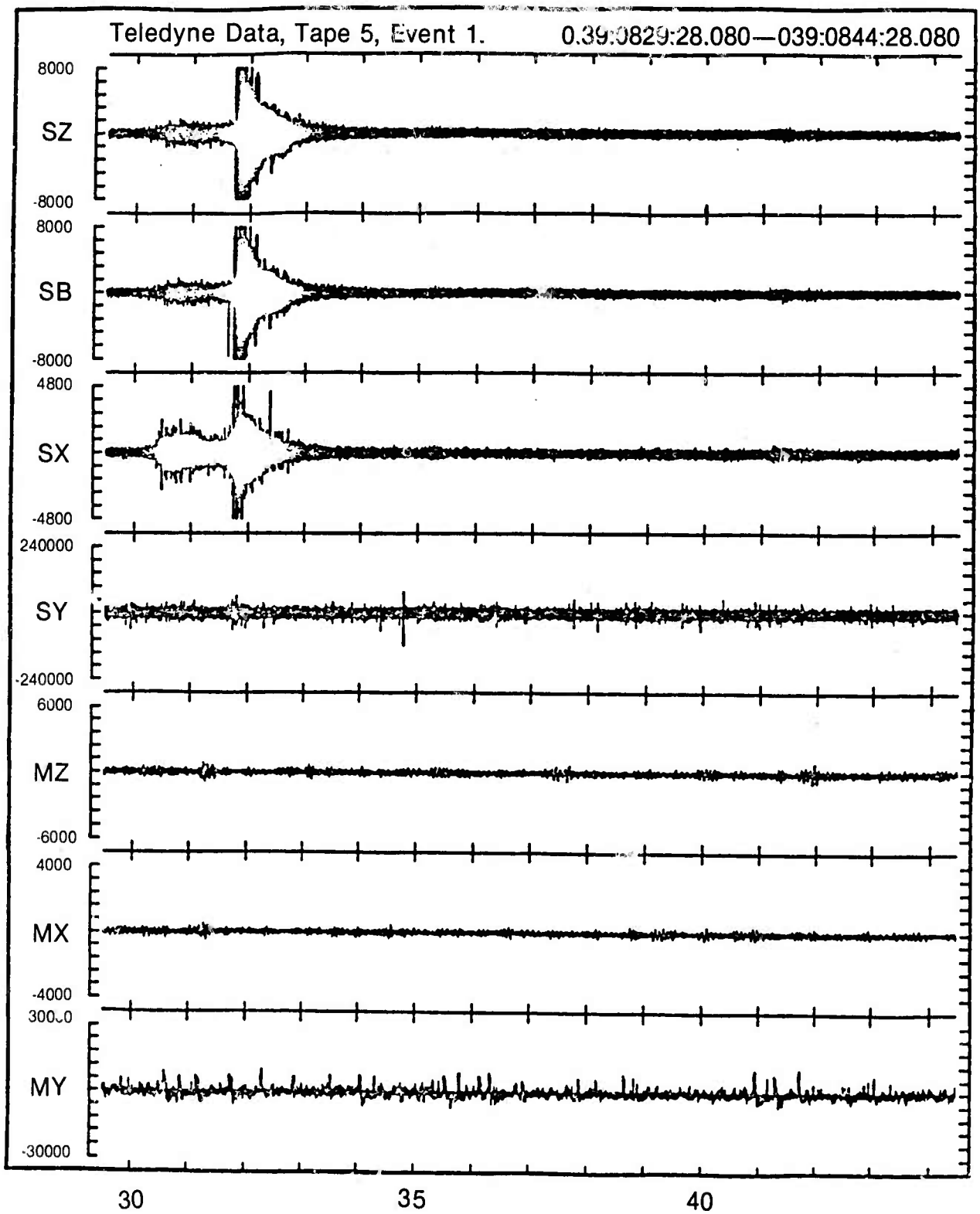


Figure 8. Teledyne data, tape 5, event 1. Example of multi-channel MSS data from the Teledyne system. (039:0829:28.080-039:0844:28.080).

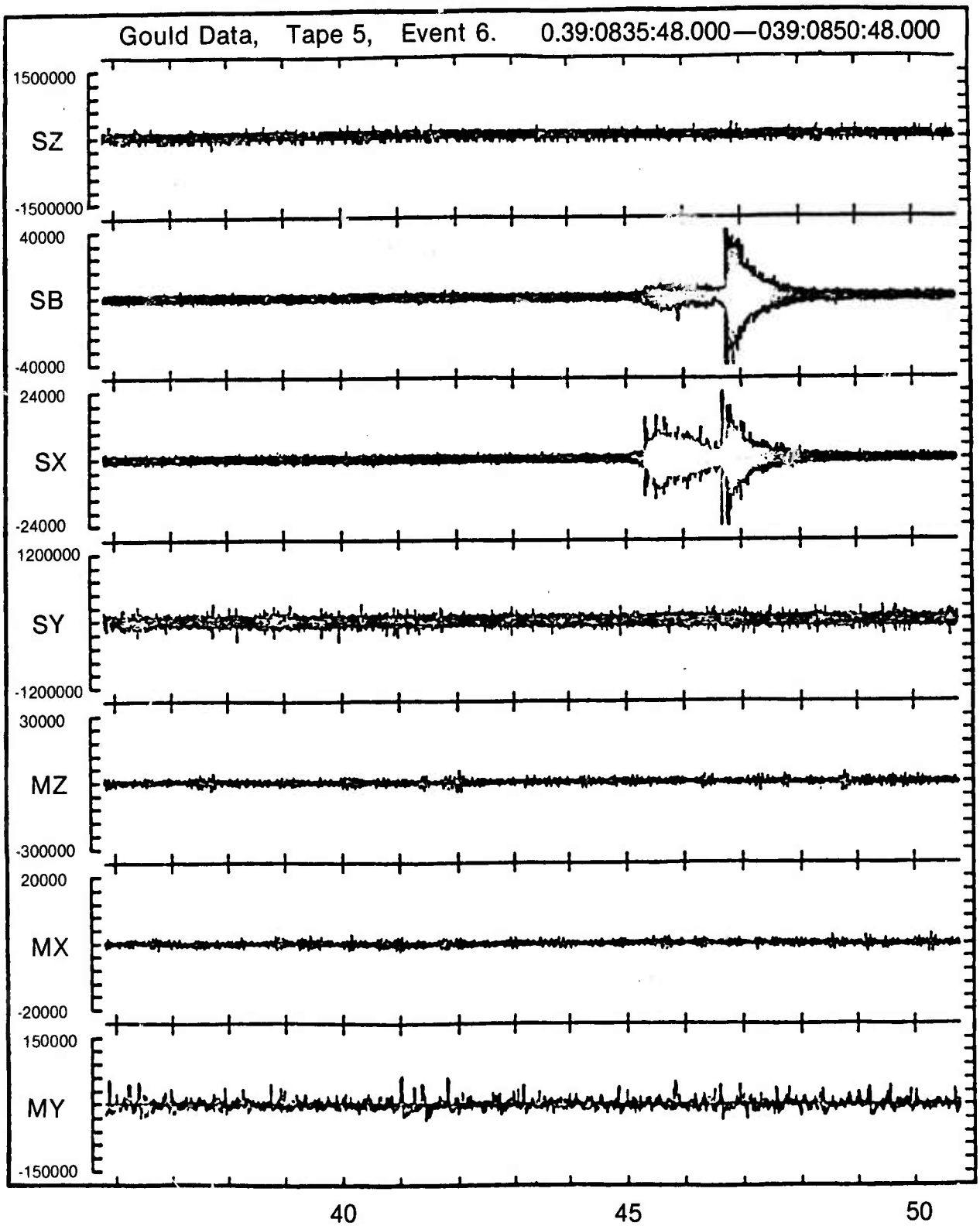


Figure 9. Gould data, tape 5, event 6. Example of multi-channel MSS data from the Gould system. (039:0835:48.000–039:0850:48.000).

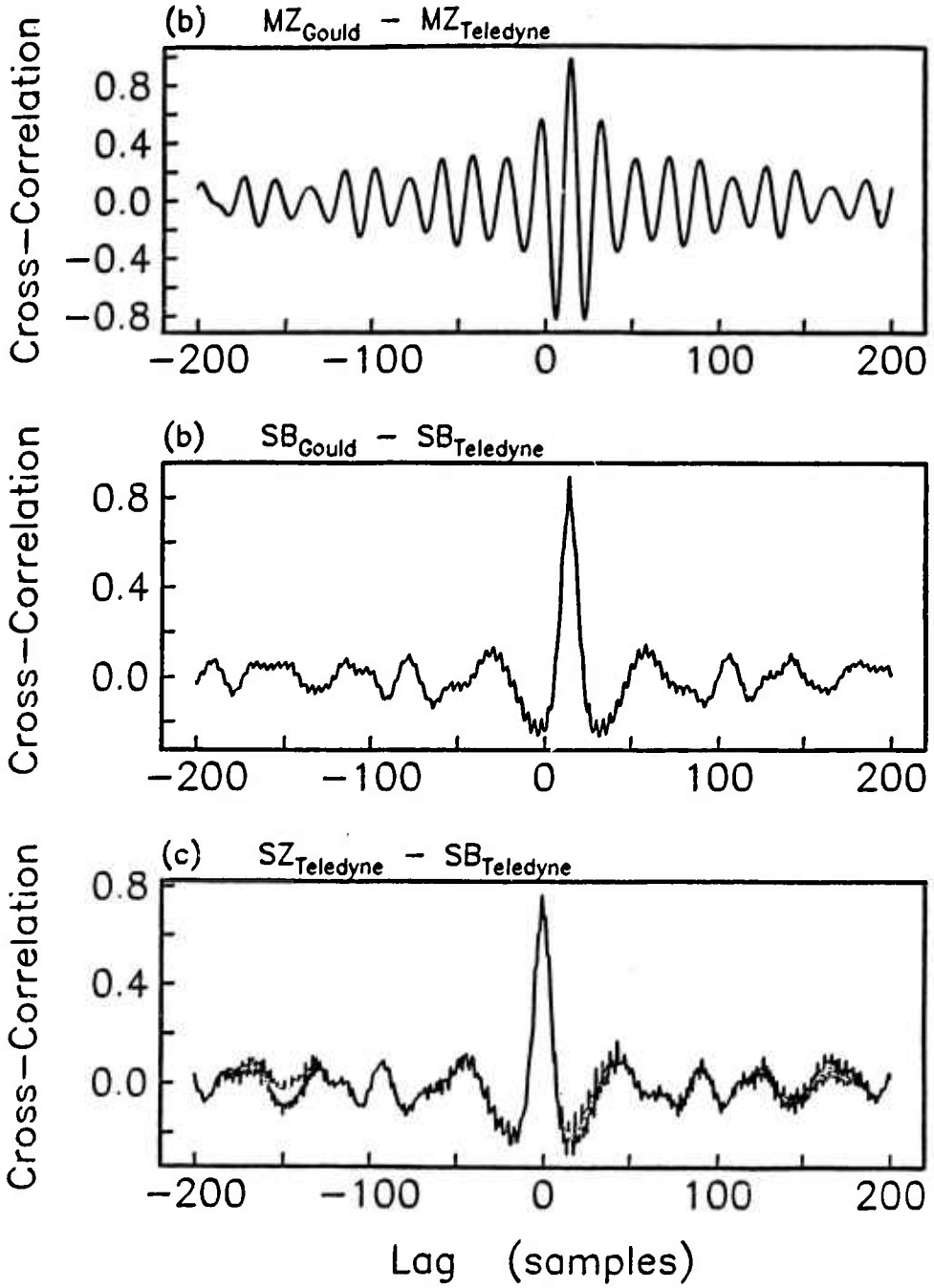


Figure 10. Relative amplitudes and timing between Gould and Teledyne recording systems with cross-correlations and linear regressions of corresponding channels.

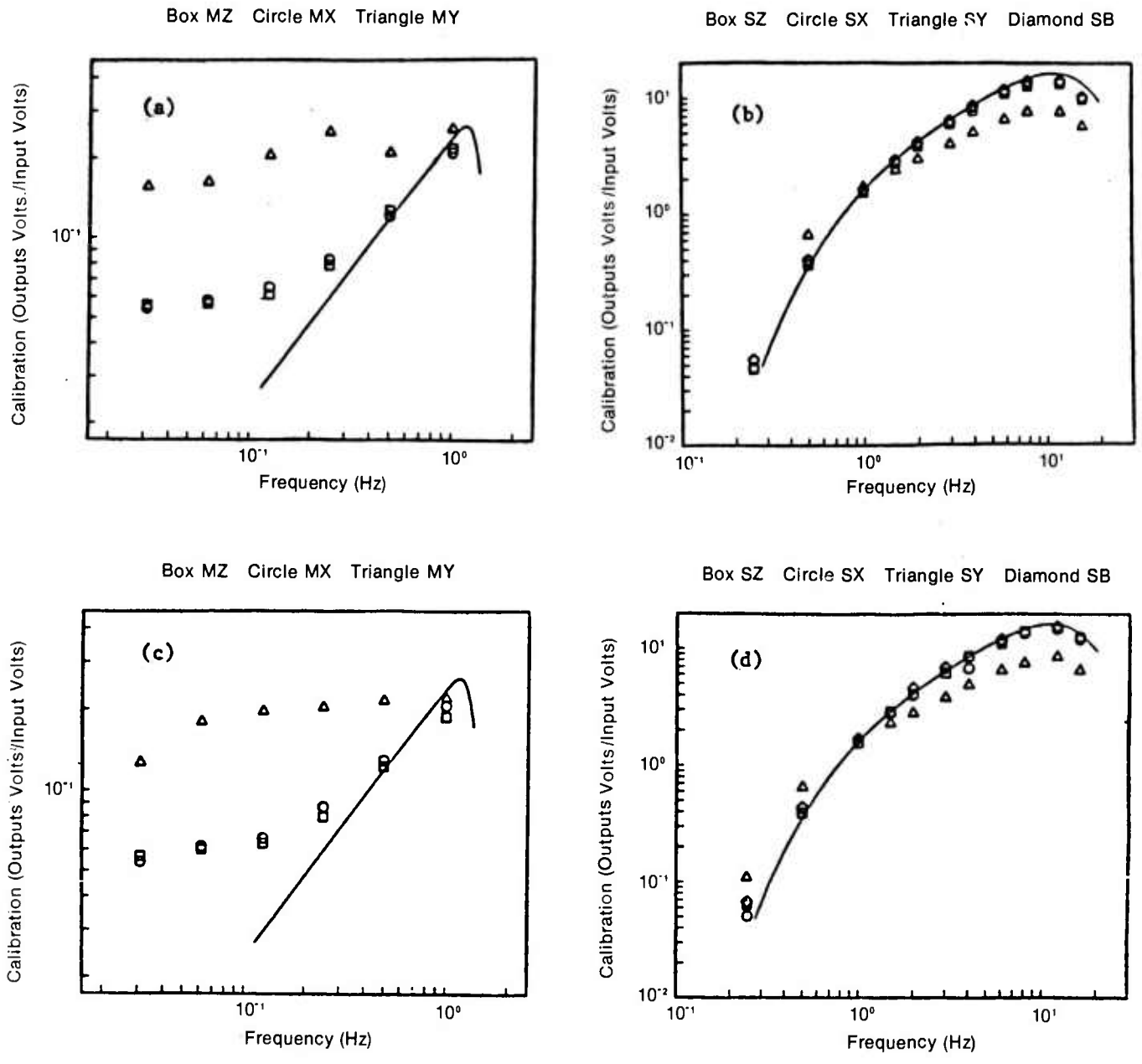


Figure 11. Teledyne calibrations of properly functioning channels.

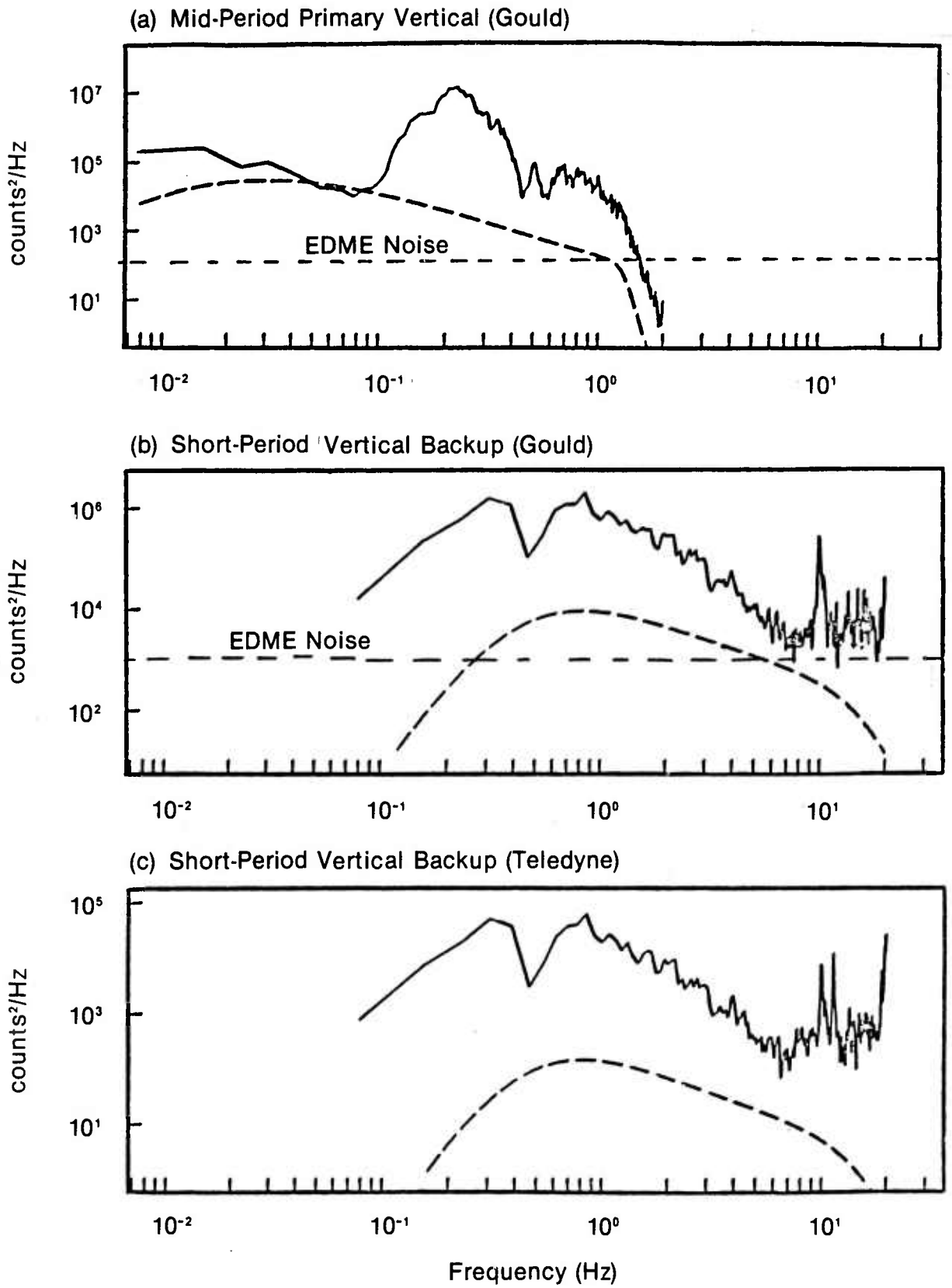


Figure 12. Comparison of power spectral density estimates of simultaneous vertical component Teledyne and Gould data with instrument noise spectra (not corrected for instrument response).

Empirical estimates of Gould's EDME noise threshold, labeled "EDME Noise" in Figure 12 was also provided by Durham. This, too, is an apparently inconsequential source of data contamination. Spectra for simultaneous SB and SZ Teledyne data are compared in Figure 14. Differences at frequencies greater than 4 Hz are probably due to the combined effects of aliasing and actual signal differences over the 175.5-cm sensor separation. The MZ spectra [Fig. 12(a)] are similarly untainted by system and sampling noise, and, furthermore, have sufficient frequency response rolloff at the high end to avoid aliasing.

Spectral coherences further delineate frequencies usable for earth noise estimates. Gould and Teledyne SB coherence (Fig. 13) exceeds 0.9 between approximately 0.2 and 4.0 Hz. The coherence at higher frequencies declines midst peaks due to ship-generated signals. The sharp drop at approximately 4 Hz is due to energy present in the Gould data but not the Teledyne, and may be related to the Gould digitizing scheme. The bounding frequencies of the SP band of high coherence varied a great deal during the MSS deployment, but generally were those shown in Figure 13. Coherence estimates between SB and SZ Teledyne data (Fig. 14) were similar but high only up to 2 or 3 Hz. MP coherences (Fig. 15), on the other hand, typically exceed 0.95 below the FIR filter knee at 1.5 Hz except at 1 Hz, where it drops sharply over a very narrow band of frequencies; this feature is similar to that observed at 4 Hz in the SB coherences of Figure 13.

Since the OBSs have no redundant sensors, valid frequencies can be assumed from time-domain and power density spectra, but no from channel coherences.

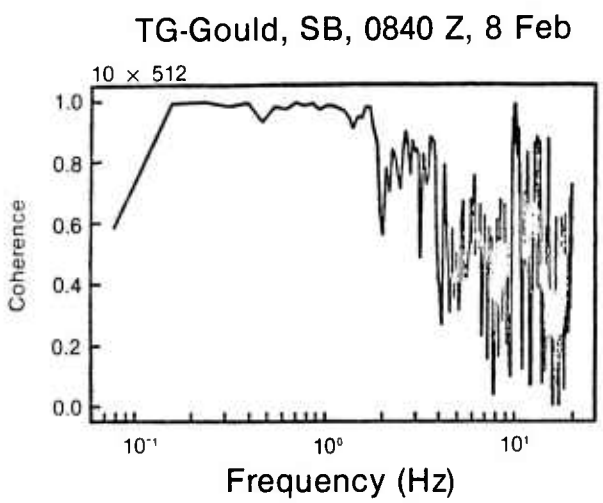


Figure 13. Decline of SB data stream coherence at high frequencies due to ship generated noise. (SB, 0840Z, 8 Feb.).

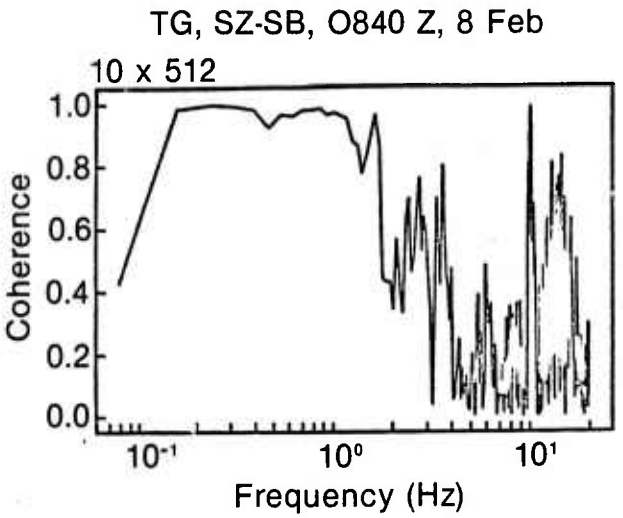


Figure 14. Coherence between SB and SZ Teledyne data streams (0840Z 8 Feb.).

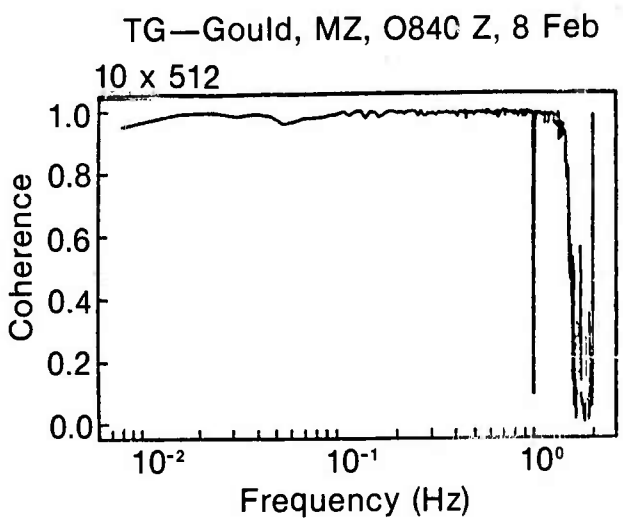


Figure 15. Mid-period coherence, SB data stream, (0840Z, 8 Feb.).

Figure 16 shows typical 4-channel OBS noise data collected from a capsule employed to record refraction signals. Ship-generated energy dominates high frequency features on all channels. The large-amplitude signal commencing at approximately 13 sec is due to recorder operation, as explained above in the instrumentation section. Data amplitudes on the seismometer channels are all comparable, the largest, in general, being on the vertical channel.

An uncorrected power density spectrum of vertical-component OBS Suzy data is shown in Figure 17(a). Least-count noise dominates the data above approximately 35 Hz.

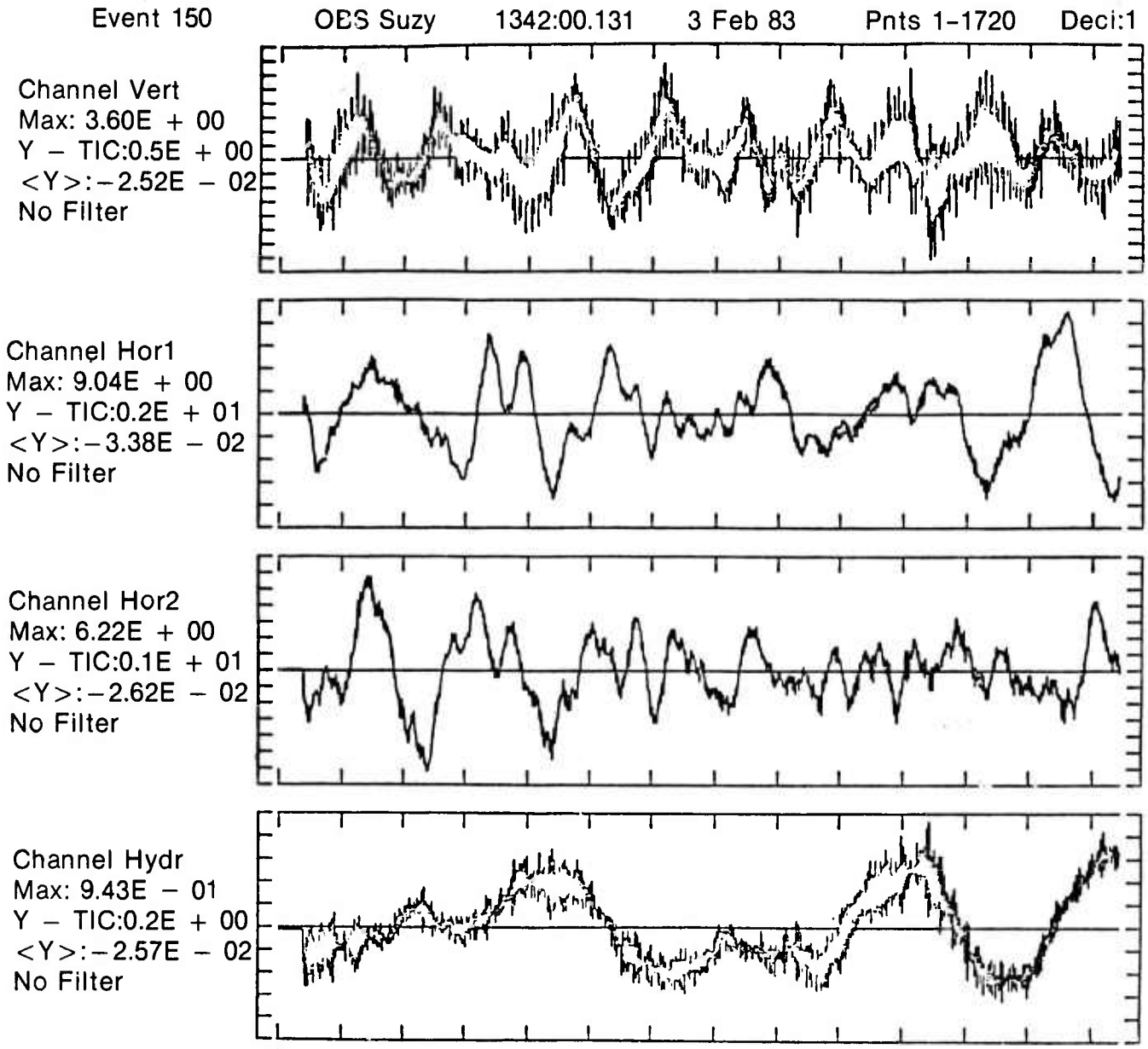


Figure 16. Typical 4-channel OBS noise data (OBS Suzy, event 150, 1342:00.131, 3 Feb., pnts 1–1720).

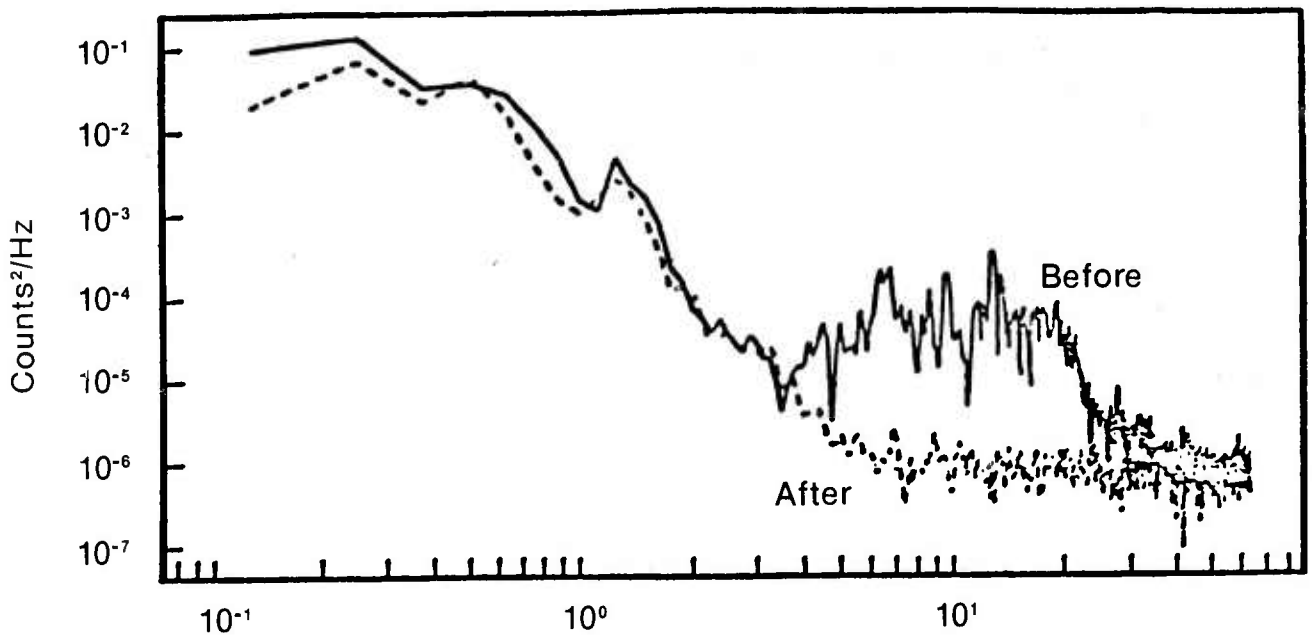


Figure 17(a). Uncorrected power density spectrum of vertical component OBS Suzy data; comparison of OBS spectra recorded before and after ship departure.

Ship noise is an obvious feature of this spectrum at lower frequencies. Figure 17(a) compares OBS spectra recorded before and after ship departure. After ship departure, the least-count noise dominates above approximately 7 Hz. Ship noise, when CHALLENGER was on station, therefore dominated between 4 and 35 Hz. Some variation of the upper frequency at which least-count noise dominates the spectrum occurs because of OBS gain-ranging, but in general the gain did not vary more than 12 dB, which is equivalent to a variation of 1 Hz given the spectral slope of the OBS data.

Some ambiguity exists concerning ship noise in the MSS data. Because the BPP failed within 2 days of its deployment, at which time CHALLENGER was 30 km away drilling Hole 595 and MELVILLE was en route to Tahiti, no MSS noise data is available at any time when no ships were nearby. However, CHALLENGER was briefly silent at 0510Z, 13 Feb., while monitoring an ocean-bottom navigational transponder, providing a sample of low ship noise for the MSS, the spectrum of which is compared in Figure 17(b) with that of data observed shortly after CHALLENGER began using its dynamic positioning system. This comparison demonstrates that, in this instance, ship noise dominated MSS noise data at all frequencies above 6 Hz. While CHALLENGER was at the MSS site, ship noise probably dominated frequencies beginning one or two Hz lower.

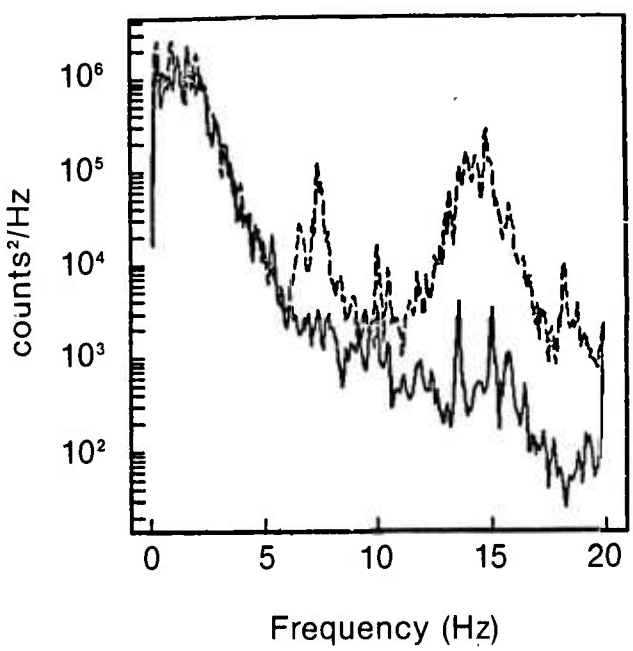


Figure 17(b). Sampling of low ship noise from the MSS in comparison with data observed with CHALLENGER dynamic positioning system in operation.

The lower bound of valid OBS frequencies are estimated from averages of various numbers of spectra; stability of values is indicative of reliable estimation. On this basis, 0.1 Hz is taken as the lowest valid frequency of spectral estimates.

Thus, in summary, reliable spectral estimates are available from MSS MP data between 0.2 and 1.5 Hz; from MSS SP data between 0.2 and 7.0 Hz; and from OBS data between 0.1 and 7.0 Hz. These bands are subject to the variability described above due to ship proximity, and OBS gain range.

Discussion

Figures 18-21 show typical, simultaneous displacement power density estimates over the band representation of earth noise. Stable estimates, unless otherwise noted, were computed from averages of ten individual spectra. Each MSS spectrum is a composite of MP and SP spectra joined at approximately 1.4 Hz. Of the horizontal MSS sensors, only the X component had usable data. MSS spectra were formed from 128 and 12.8 sec of MP and SP data, respectively, while OBS spectra were formed from 13.02 and 59.09 sec (1666 and 7436 time points, respectively) depending on the length of each capsule's pre-event buffer (see Table 1). Displacement power densities are given in units of nanometers^2/Hz (nm^2/Hz).

MSS and OBS vertical-component spectra are compared in Figure 18. The most striking feature here is that while the noise levels are comparable at the microseism peak (near 0.2 Hz), they are quite different at higher frequencies. MSS levels are approximately 15 dB lower than OBS levels above 0.5 Hz. The horizontal ocean-bottom and borehole noise levels are similarly related (Fig. 19). The fall-off at high frequencies for all these spectra is approximately (frequency)$^{-9}$.

MSS vertical and horizontal (X-sensor) noise levels are similar over the entire band (Fig. 20), whereas vertical OBS levels are less than the horizontal levels by 10-20 dB at the frequencies greater than that of the microseism peak (Fig. 21). In Figure 21, the spectral estimates are averages

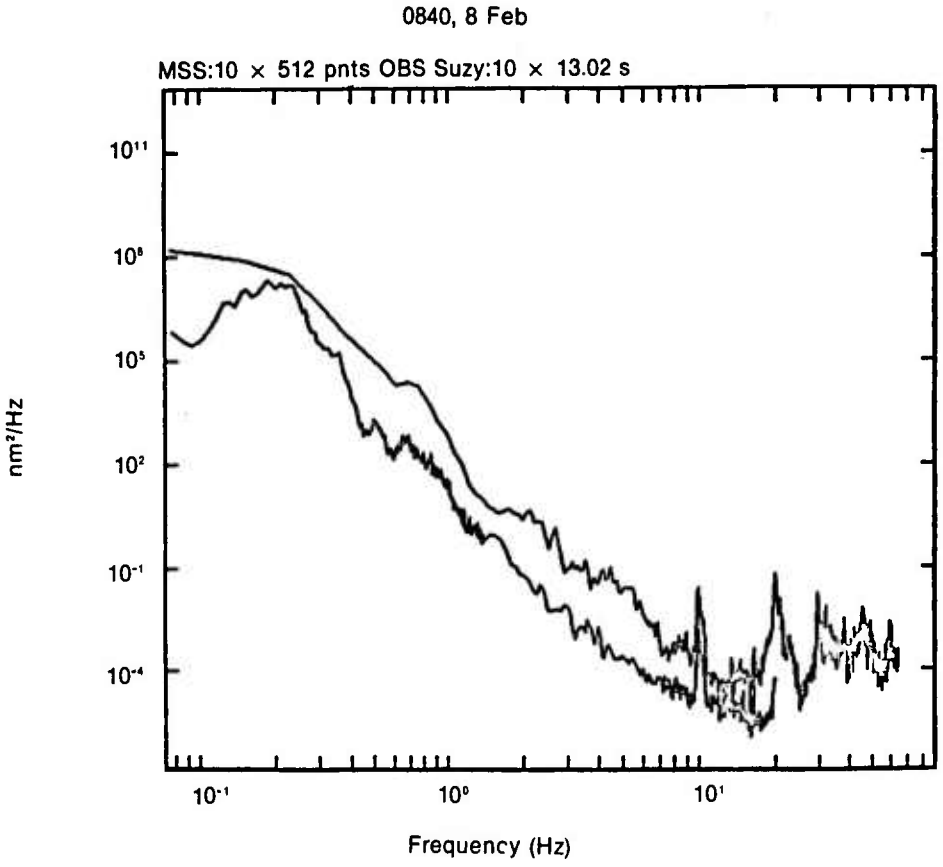


Figure 18. Comparison of MSS and OBS vertical component spectra. MSS levels are about 15 dB lower than OBS levels above 0.3 Hz. (MSS: 10 × 512 pnts, OBS Suzy: 10 × 13.02 ×, 0840Z, 8 Feb.).

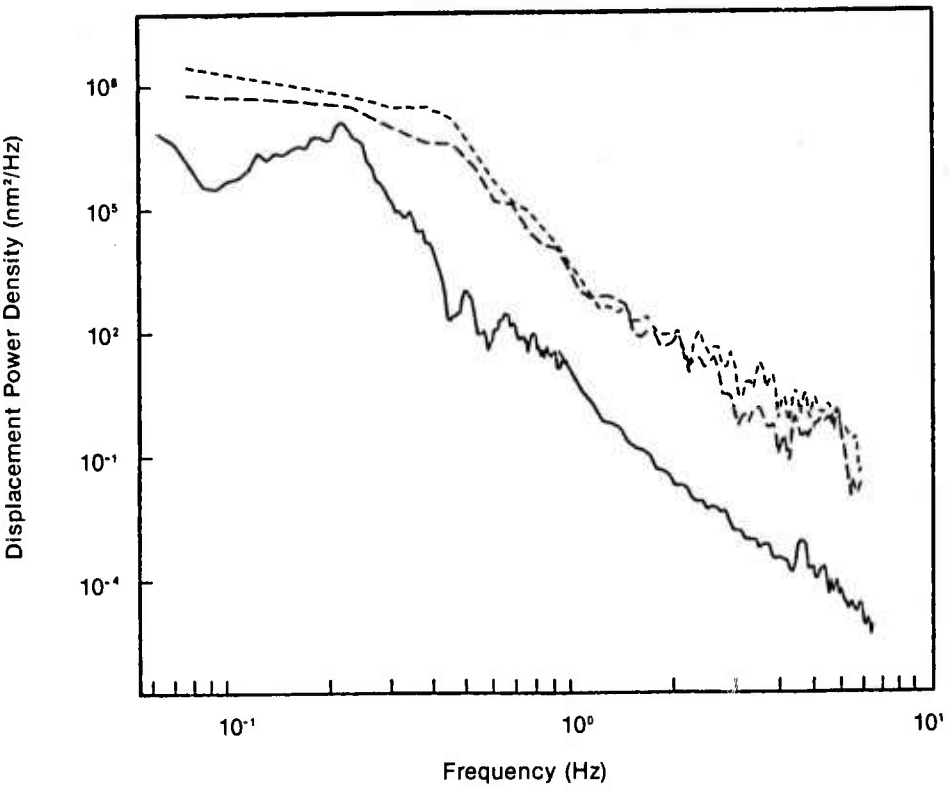


Figure 19. Comparison of horizontal ocean-bottom and borehole noise levels (lower noise level is from borehole).

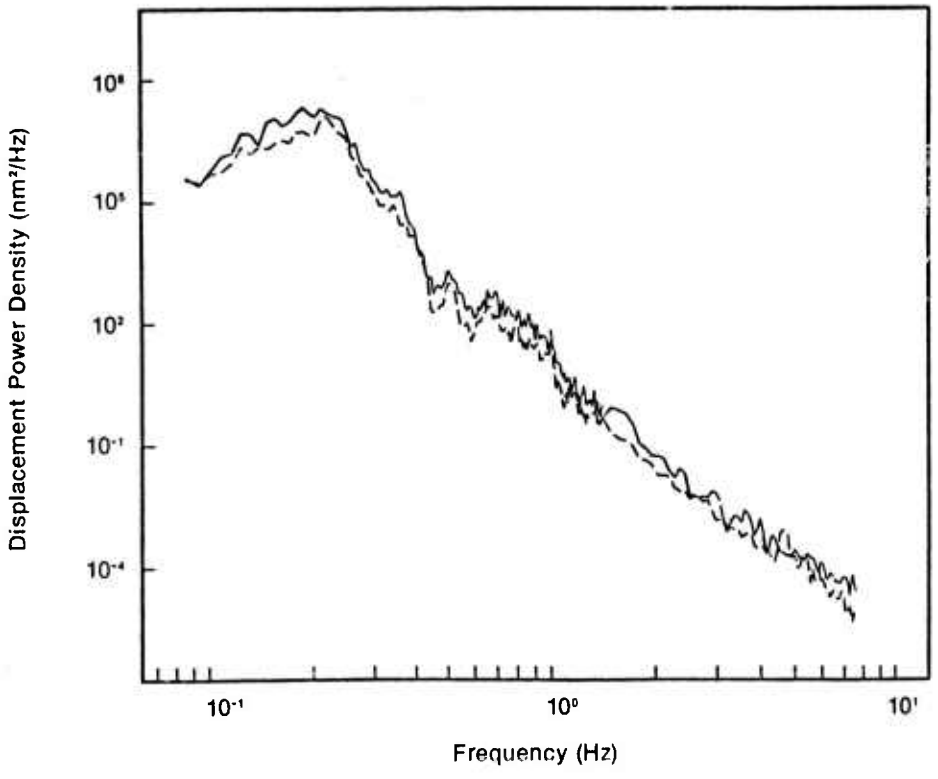


Figure 20. Similarity of MSS vertical and horizontal (X-sensor) noise levels.

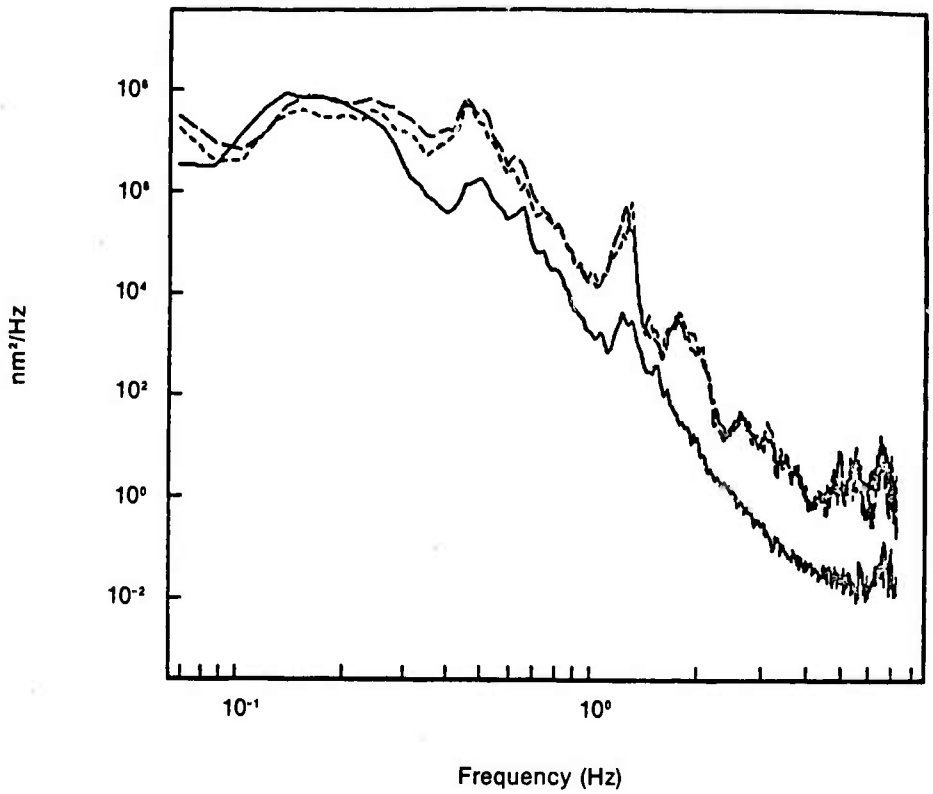


Figure 21. OBS vertical and horizontal noise levels (lesser noise levels are from vertical sensor).

of 39 59.09-sec samples separated by 24 hr each. The similarity of the two horizontal OBS spectra suggest that, for these data at least, the noise field was isotropic.

Of interest are the numerous peaks present in both MSS and OBS spectra, in particular, near 0.5, 0.75, and 1.0 Hz. Their persistence throughout the deployment period implies that these are, in fact, genuine features of earth noise, a situation that would otherwise be extraordinarily fortuitous. In contrast, vertical-component spectra obtained from the prototype MSS, deployed in the mid-Atlantic during DSDP Leg 78B, while of comparable value near the microseism peak, are relatively featureless (Fig. 22). Also different is the spectral slope at frequencies greater than 1 Hz. Spectra from Leg 78B fall off at approximately (frequency)$^{-8}$.

Figure 23 shows ocean-bottom pressure spectra of ambient noise as measured by Suzy's hydrophone during its teleseismic deployment. As with the seismic sensors, the microseism peak is the most prominent feature, lying between 0.1 and 0.3 Hz at a value of approximately 10^4 Pascals^2/Hz. The spectrum falls of as (frequency)$^{-7}$ at higher frequencies. Also shown for comparison are comparable noise values measured by Webb and others (Webb, 1984) off the California coast in deep water with a pressure transducer. The high frequency fall off of Webb's spectrum was successfully modeled with local forcing by unattenuated pressure fluctuations of surface wind waves. Peaks at frequencies above that of the microseism peak were attributed by Webb to resonate forcing of interface waves trapped at the ocean bottom-seafloor interface or to other suites of surface wind waves.

High-resolution, low-variance estimates of vertical-component, ocean-bottom noise from OBS Suzy are compared in Figure 24 with extrema of similar measurements from Scripps Institution of Oceanography (SIO) OBSs. Also displayed are the previously-shown MSS values. Above about 1.5 Hz, the Leg 91 measurements are comparable to the lower extrema, with amplitudes falling at a similar rate. The extrema are not well-defined at lower frequencies due to the short data sample lengths from which the spectra were obtained.

Subbottom noise levels during Leg 91 are 10-20 dB greater than those at the quietest land sites (Fig. 25). The Lajitas spectrum (Herrin, 1982) is representative of the quietest-known land site, which is near the village of Lajitas, Texas, on the Rio Grande River. At frequencies less than 2 Hz, ambient noise levels at Lajitas differ little from the Queen Creek levels (Fix, 1982; Melton, 1976) measured at a quiet site in a mine shaft near Queen Creek, Arizona.

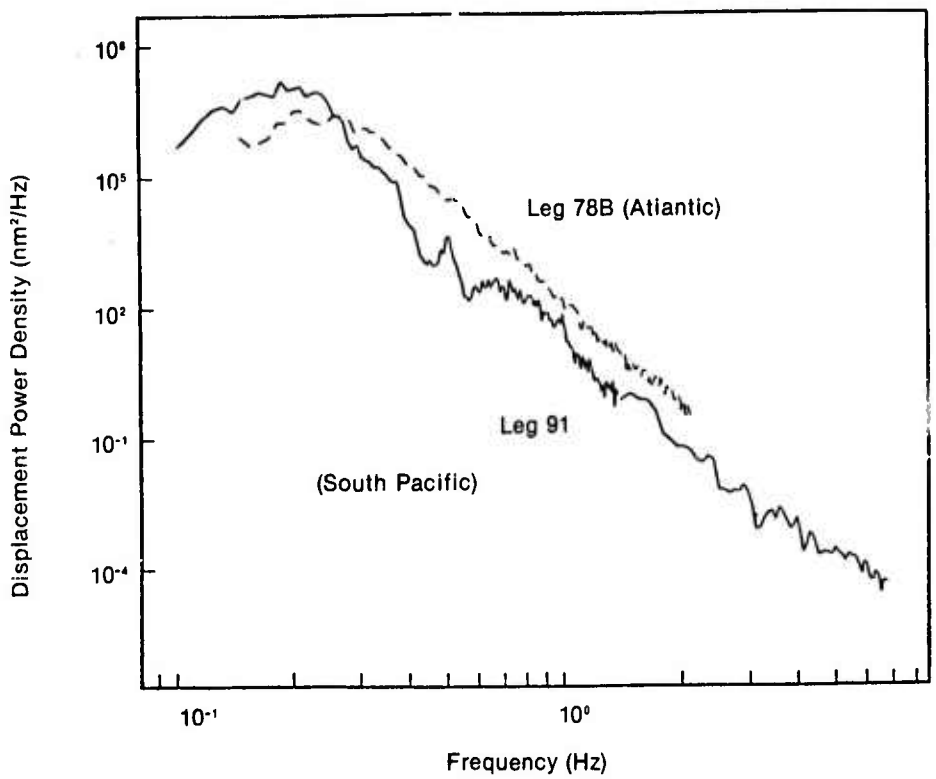


Figure 22. Comparison of MSS vertical-component spectra from DSDP Leg 78B (mid-Atlantic) and DSDP Leg 91.

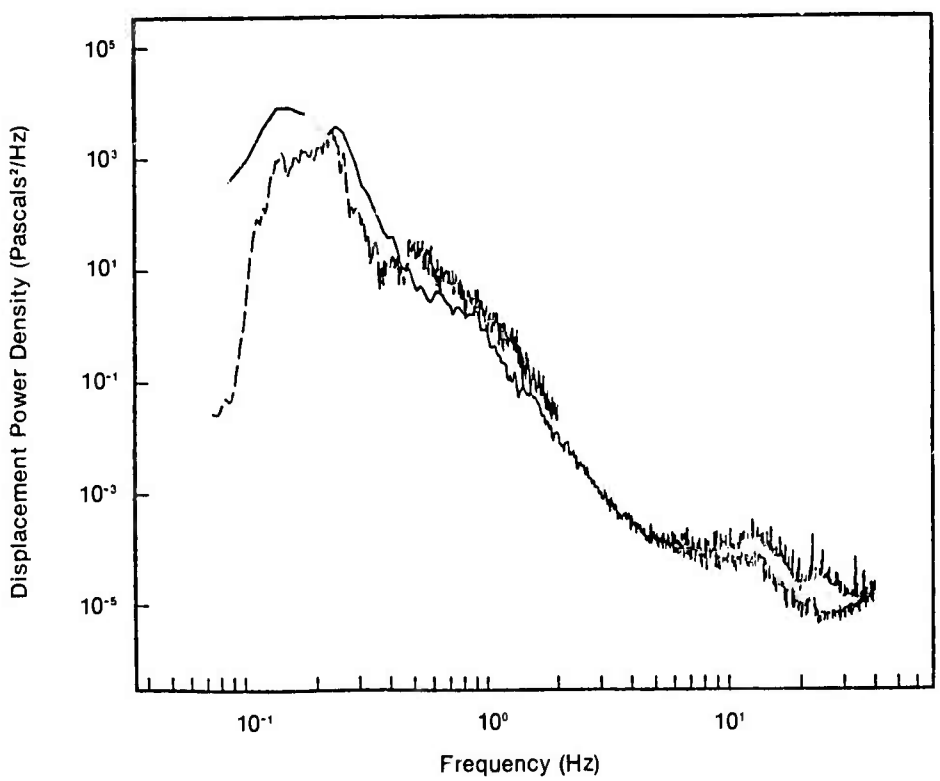


Figure 23. Ocean-bottom pressure spectra of ambient noise from OBS Suzy.

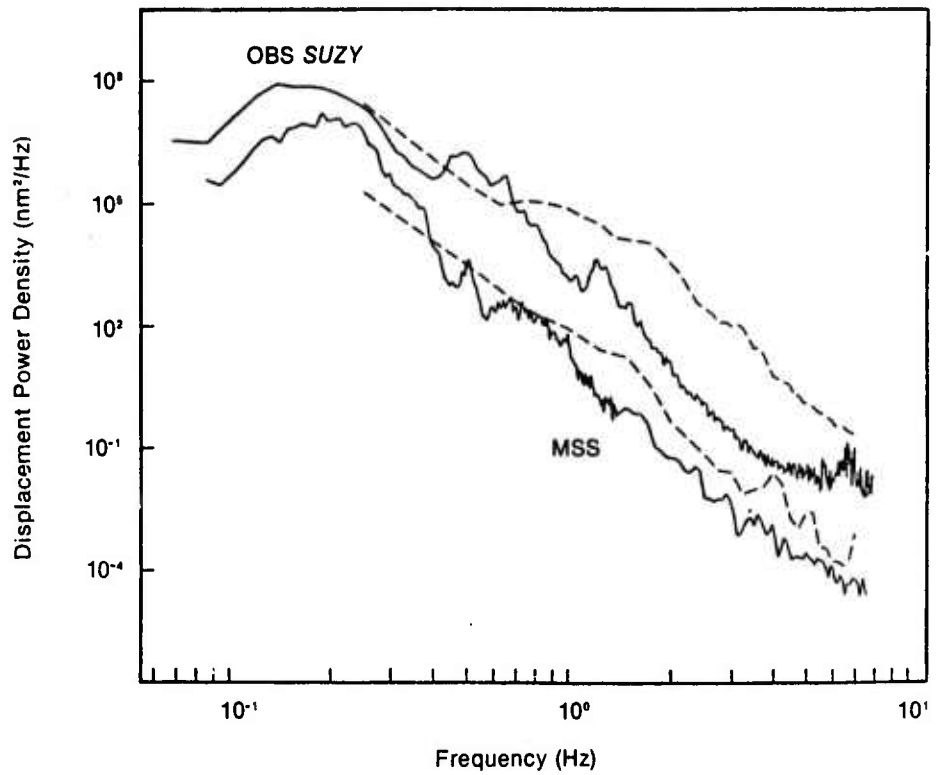


Figure 24. OBS Suzy and MSS high-resolution low-variance estimates of vertical-component ocean-bottom noise.

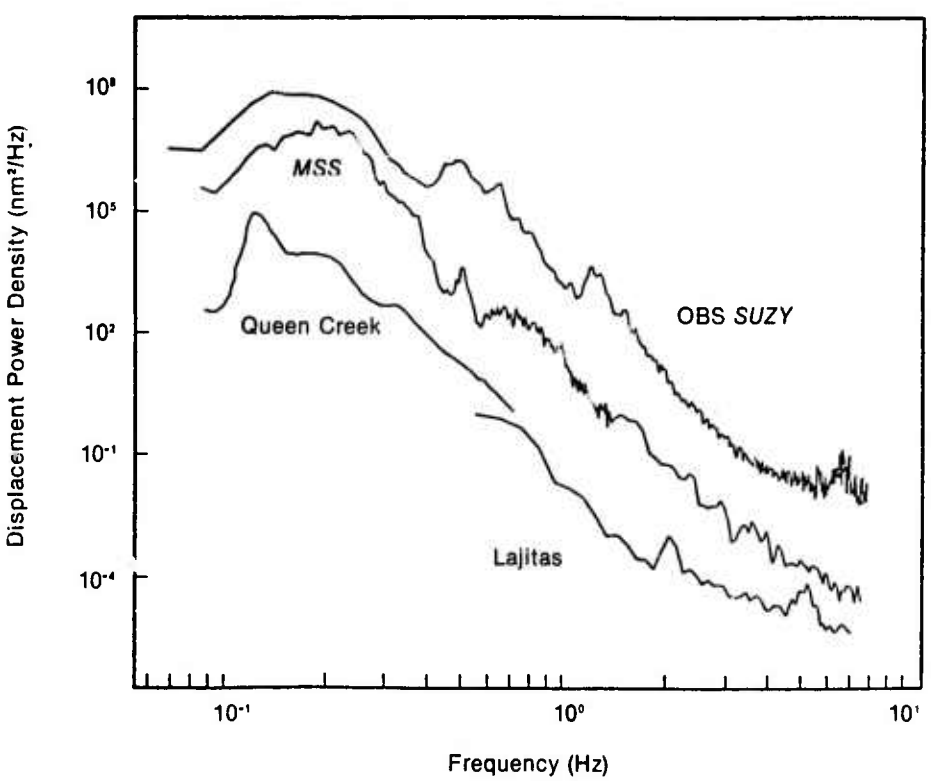


Figure 25. Comparison of subbottom noise levels from OBS Suzy, the MSS, and two land sites (Lajitas, Texas and Queen Creek, Arizona).

Coherence between OBS capsule pairs were compared to investigate propagation of the noise field. To reduce possible bias due to misalignment of coincident features, the two series were aligned, after first correcting OBS clocks for drift and fiducial offsets, at the leg of their cross-correlation's maximum values. Figures 26 and 27 show coherences between Suzy and Lynn (Fig. 26) and between Karen and Juan (Fig. 27) using data from the first and third of February, respectively. Power spectra are superimposed on these plots to aid in identifying coherence features. Each member of the capsule pairs were within a kilometer of each other. Their coherence is high at the microseismic peak in both spectra, as well as those frequencies dominated by ship noise. The alignment lags for the more southwestern pair of OBSs (Juan and Lynn) were consistently late with respect to their partner capsules to the northeast [see Fig. 2(a)], suggesting that energy in the microseism peak was sweeping across the array towards the more southwestern pair of OBSs.

References

Adair, Richard G., Orcutt, John A., and Jordan, Thomas H. 1983. *Analysis of ambient seismic noise recorded downhole and ocean bottom seismometers on Deep Sea Drilling Project Leg 78B.* In Hyndman, R.D., Salisbury, M.H. et al., Init. Repts. DSDP. 78: Washington (US Govt. Printing Office), 767-781.

Fix, J.E., 1972. *Ambient earth noise in the period range from 0.1 to 2560 sec.* Bull. Seism. Soc. Am., 62: 1753-1760.

Herrin, Eugene, 1982. *The resolution of seismic instruments used in treaty verification research.* Bull. Seism. Soc. Am., 72: S31-S67.

Melton, Ben S., 1976. *The sensitivity and dynamic range of inertial seismographs.* Rev. Geophys. Space Phys., 14:93-116.

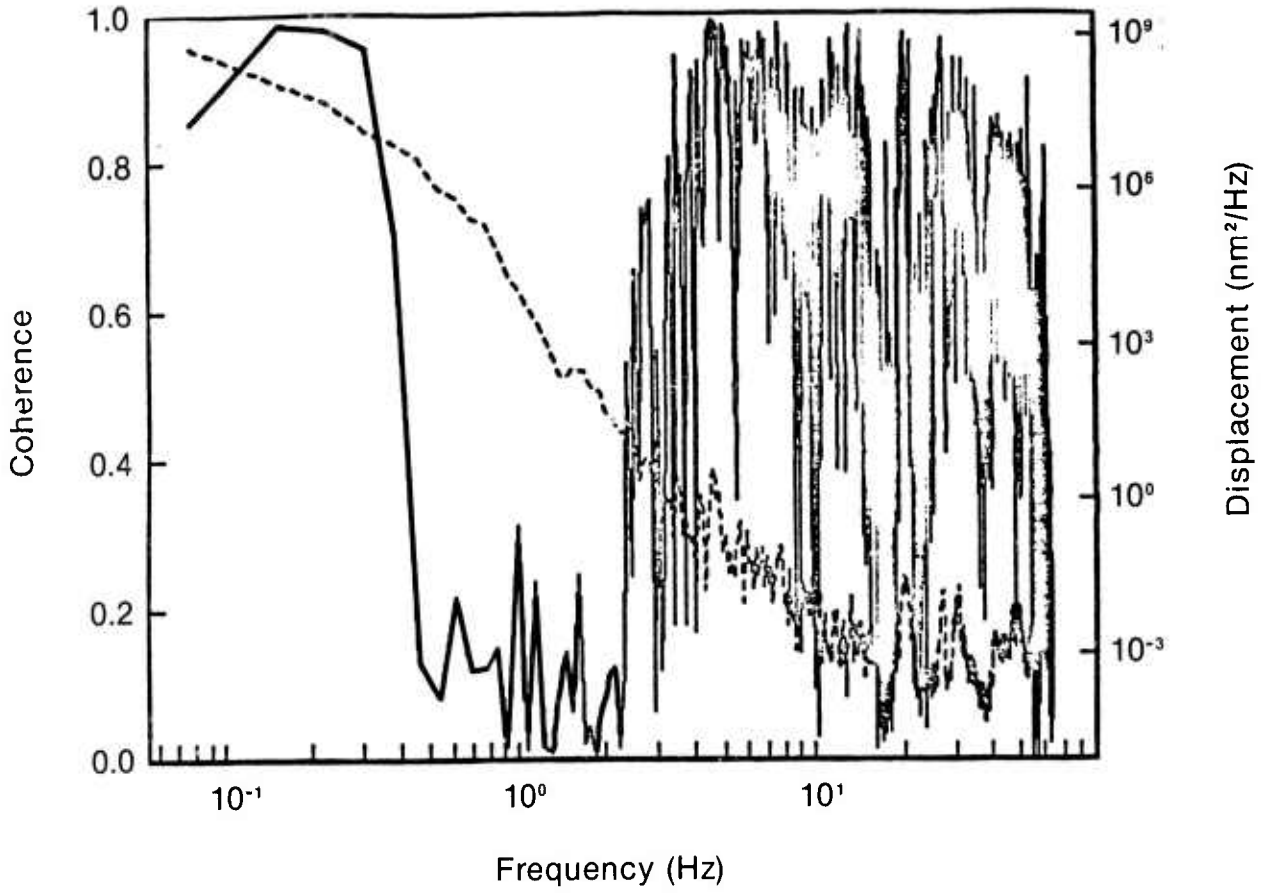


Figure 26. Coherences between OBSs Suzy and Lynn (1 Feb.).

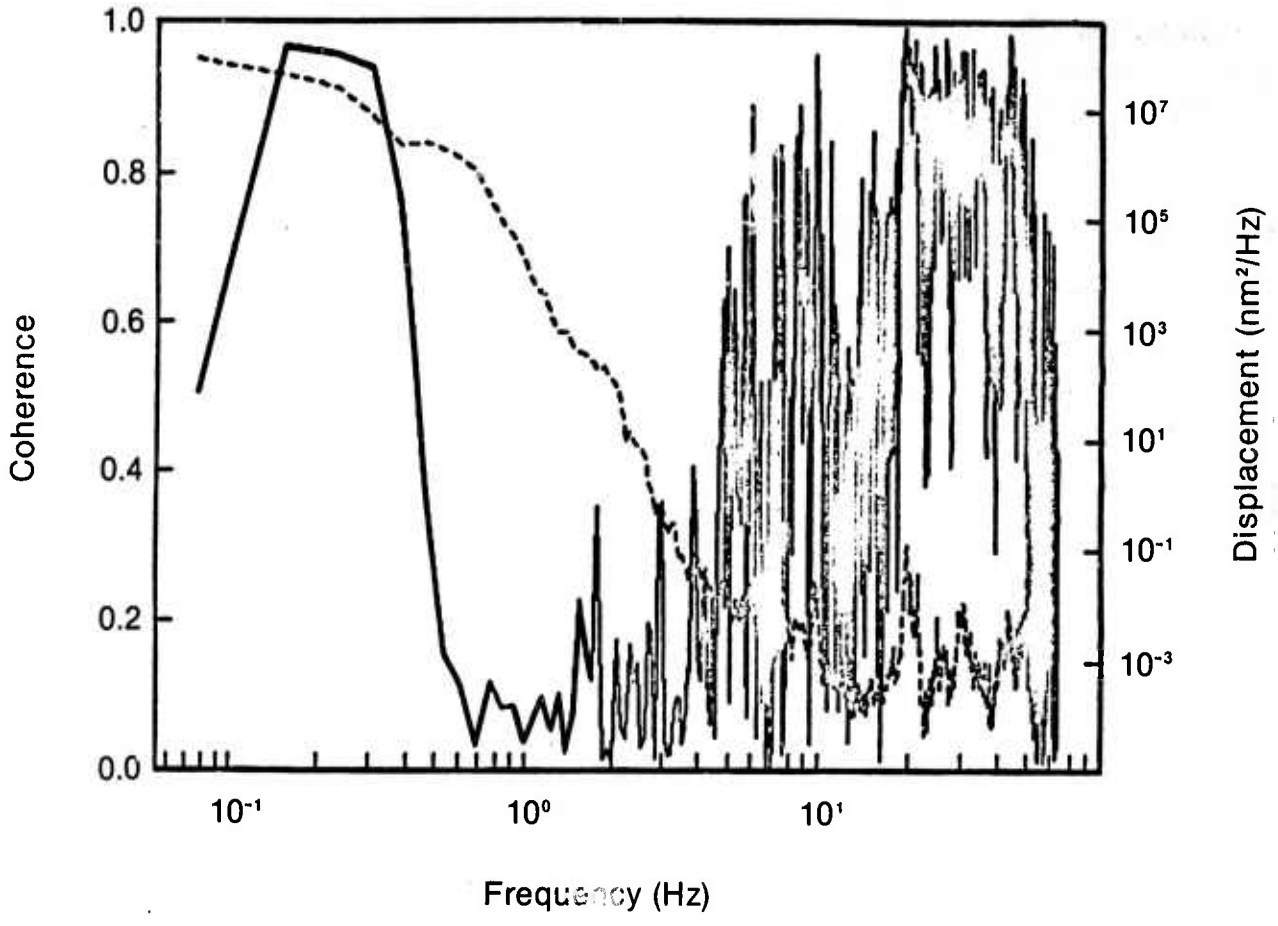


Figure 27. Coherence between OBSs Karen and Jean (3 Feb.).

Moore, R.D., Dorman, L., Huang, C.Y., and Berliner, D.L., 1981. *An ocean bottom, processor based seismometer.* Mar. Geophys. Res., 4:451-477.

Spudich, Paul, and Orcutt, John, 1980. *Petrology and porosity of an oceanic coastal site: Results from wave form modeling of seismic refraction data.* J.G.R., 85: 1409-1433.

Sutton, G.H., Duennebier, F.K., and Iwatake, B., 1981. *Coupling of ocean bottom seismometers to soft bottom.* Mar. Geophys. Res., 5: 35-51.

Welch, F.D., 1967. *The use of Fast Fourier transform for the estimation of power spectra.* A method based on time averaging over short, modified periodograms. IEEE Trans. Audio Electro-acoust., AU-15: 70-73.

Velocity Bounds on the Seismic Structure of Late Jurassic (157 Ma Old) Crust and Upper Mantle in the Southwest Pacific Basin from Downhole Observations at Deep-Sea Drilling Project Hole 595B

R.B. Whitmarsh, J.A. Orcutt, T.H. Jordan, R.G. Adair, and P.M. Shearer,
Geological Research Division, Scripps Institution of Oceanography, La Jolla, California

Introduction

The recent advent of digitally recording ocean-bottom seismographs (OBS) has allowed data sets with high signal-to-noise and relatively broad bandwidths to be collected. However, an OBS is normally susceptible to the uncertainties of imperfect coupling via unlithified sediments of low shear strength to the solid earth (Sutton et al., 1981; Trehu, in press) and to the multiply converted and reflected phases generated at the boundaries of the sediment layer (Lewis and McClain, 1977). These problems, which can distort and complicate the signals, are largely avoided by emplacing sensors down holes drilled into igneous basement (Layer 2) beneath the sediments. This paper describes the analysis of two orthogonal unreversed refraction profiles, which exhibit an unusually good signal-to-noise ratio, obtained by recording signals from a set of downhole seismometers emplaced in Deep Sea Drilling Project Hole 595B. The preliminary results of these profiles are reported here.

Regional Setting

The experiment was conducted in the Southwest Pacific Basin about 1000 km east of the Tonga Trench and 1800 km west-south-west of Tahiti (Fig. 1., inset). This is a remote, poorly surveyed and little known region. At the time of the experiment, no clear indication of the direction of spreading centers and fracture zones was available from magnetic anomalies. From a knowledge of the regional depth (about 5600 m) and of the history of adjacent portions of the Pacific Ocean, it was inferred only that the lithosphere at Site 595 had been produced as a fast-spreading ridge at high southern latitude sometime during the Mesozoic. The geoid calculated from satellite altimetry suggested that there were no substantial bathymetric or tectonic features in the immediate area (Sandwell, 1984; Dixon and Parke, 1983).

Subsequently, an analysis of magnctic anomalies and other information has suggested the existence of 050° trending seafloor spreading magnetic anomalies (H.W. Menard, personal communications). Soundings compiled within about a two-degree square enclosing the site indicate the existence of ridges and troughs with a similar trend. However, a roughly N-S to NNW arcuate high-ridge feature is also well-delineated about 100 km to the east (Fig. 1).

Scant seismic reflection profiles from passage tracks of Conrad 17 and Eltanin 40, augmented by data from R.V. MELVILLE and D.V. GLOMAR CHALLENGER, indicate unusually thin sediments which are at least 0.05–0.10 sec thick in the vicinity of Hole 595B. Sediment thicknesses are difficult to determine accurately, however, due to the ubiquitous occurrence of a very strong, presumably intra-sediment, reflector concordant with the sea bed which obscures the sediment-basement reflection. Shipboard Scientific Party (this volume) measured seismic velocities of 1.46–1.54 km/sec^{-1} on the cores of brown pelagic clay from Site 595.

The sediment was 70-m thick in holes 595A and 595B. Cretaceous radiolarians were found at a depth of approximately 40 m, but, due to the nature of the sediments, the recovery of fossils from greater depths was poor. The sediment-basement contact was not recovered and palaeontological ages for this horizon are simply not available. An analysis of sea-floor spreading magnetic anomalies near the site indicates a crustal age considerably older than the Cretaceous quiet zone and within the Mesozoic magnetic anomaly sequence (H.W. Menard, personal communication). An earlier analysis of local magnetic anomalies placed the site at anomaly M-29 with an age of 157 Ma on the scale of Cande et al. (1978), although the interpretation is very tentative. The crust is, nevertheless, some of the oldest yet sampled in the Pacific Ocean and may be as old as late Jurassic.

The Experiment

The objectives of the seismic refraction experiment were to investigate the crust and upper mantle structure of old lithos here and to determine, by a pattern of radiating lines centered on the borehole, the direction and extent of upper mantle anisotropy. The experiment was constrained by the rate of progress of the MSS trials. Loss of time due to equipment malfunction allowed the shipboard recording of just two orthogonal refraction lines. The first, line 4 (including some fill-in shots of line 5) extended about 150 km SW of the hole. The second, line 5, was a split profile 50-km long to the SE and 260-km long to the NW (Fig. 1).

The seismic signals were detected by the borehole instrumentation package (BIP) of the MSS, a 10.5-m long, 0.2-m diameter cylinder. This was emplaced at the bottom of Hole 595B which had been drilled to a depth of 124 m beneath the seafloor and 56 m into layer 2. Due to unforeseen technical problems, the BIP was not clamped to the wall rock. In view of the rigidity of the basalt at the bottom of the hole and the large mass (1.2 tons) of the BIP resting on a small area (up to 0.03 m^2) at its base, it is estimated that at frequencies of under 10 Hz the BIP followed the vertical motion of the wall-rock without distortion (Sutton et al., 1981; White, 1983). The sensors were

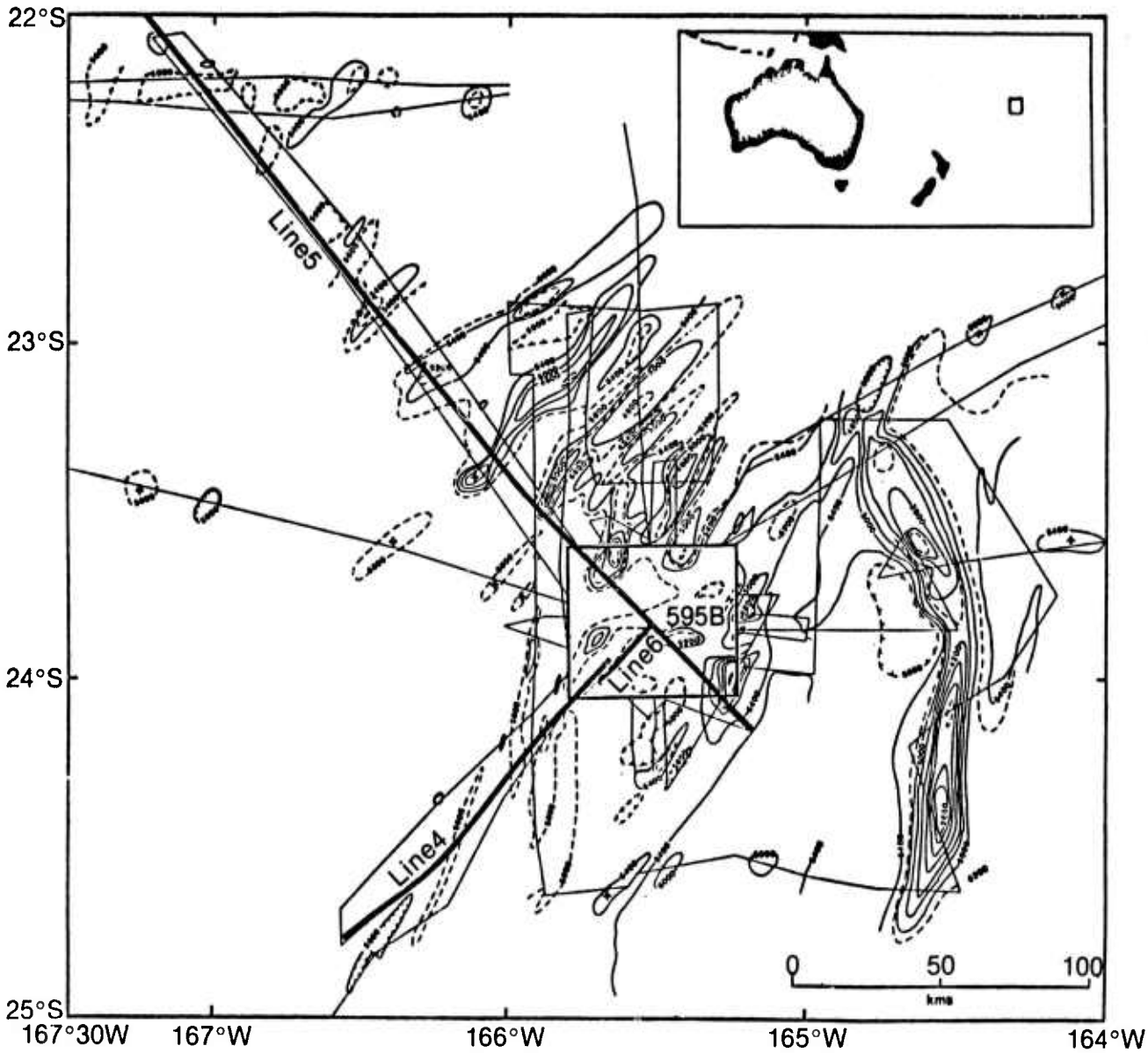


Figure 1. *Bathymetry and locations of Profiles 4 and 5 around Site 595 in the Southwest Pacific Basin (see inset). Fine lines denote available sounding tracks; tracks were too dense to be shown clearly within the box. Contour interval 400 m (solid lines) or 200 m (dashed lines).*

three orthogonal broadband Teledyne Geotech Inc. S750 accelerometers with one sensor vertical. There was no device to orientate the horizontal sensors.

After bandpass filtering (Fig. 2) the signals were digitized and passed up an electromechanical cable to GLOMAR CHALLENGER where they were recorded at 40 samples/sec/channel. Due to the appearance of strong instrumental noise on one of the horizontal seismometers shortly after emplacement, data from only the vertical and from one horizontal seismometer were available for analysts (data from just the vertical seismometer are presented here).

A near-surface hydrophone was also deployed from GLOMAR CHALLENGER at a depth of 10 m to record the relatively high-frequency water-waves from the explosions. This was necessary for the accurate determination of shot-to-receiver ranges.

Timing was with respect to a local clock on each ship which was checked regularly against radio time-signals from station WWVH.

Data Reduction

A sound-velocity depth profile (Table 1) was constructed on the basis of temperature and salinity observations, made during the experiment down to 1000 m and from observations made 500 km away by Stommel et al., (1973) to 5400 m in June–July 1967, using the equation of Clay and Medwin (1977). This profile was used to calculate shot-to-borehole ranges from the water-wave travel times of mainly bottom reflected phases detected by the near surface hydrophone. These ranges included a correction for the offset of GLOMAR CHALLENGER from the borehole using the precise (±15 m) measurements provided by the ship's dynamic positioning system. Ranges calculated by this method were consistent within ±80 m with ranges based on water-waves detected by the OBS hydrophones. At ranges in excess of about 90 km the signals at the surface hydrophone were too weak. Instead, the arrival-time on the vertical seismometer of a probably tube-wave, generated by the arrival of the water-wave at the top of hole, was used after correction for an estimated downhole propagation time of 0.09 sec.

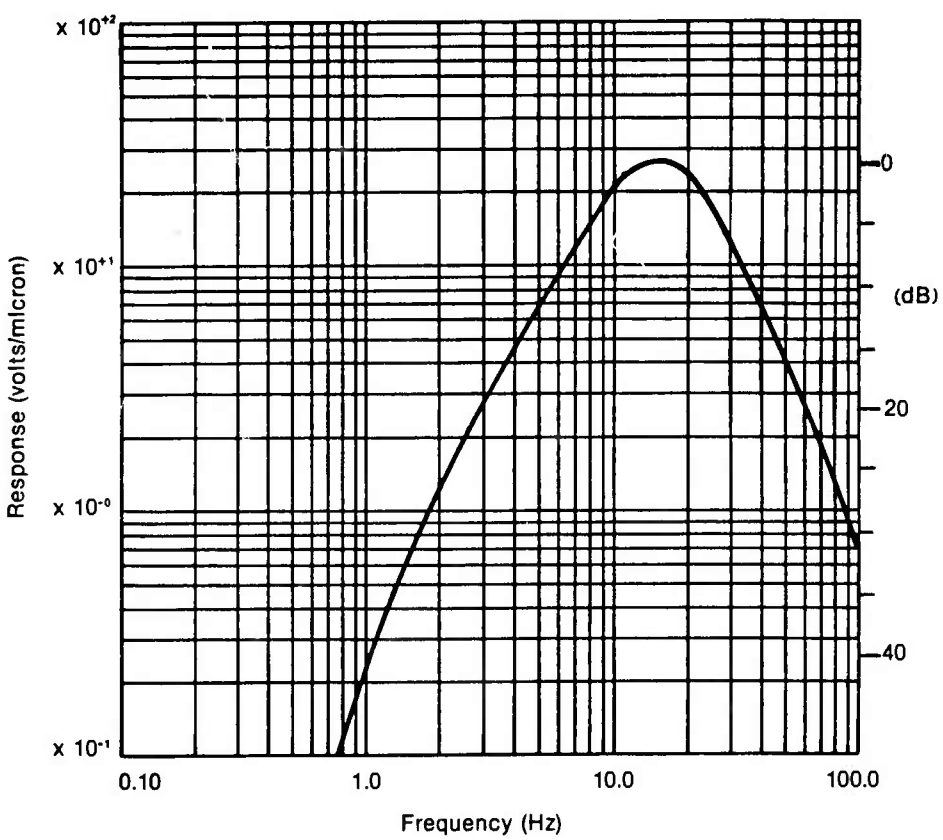


Figure 2. Displacement response of the short-period channels of the MSS.

Table 1. Sound speed/depth model.

Depth (m)	Sound speed (m s^{-1})
0	1535.5
380	1513.0
630	1488.7
1000	1484.3
1500	1484.3
3910	1519.6
6000	1553.1

To minimize the scatter in arrival times of several tenths of a second caused by the varying water-depth under the shots (Fig. 3) the water-path corrections used by Spudich and Orcutt (1980), and described in detail by Purdy (1982) were applied. This modifies travel-times and ranges to those applicable to a source situated at the point of entry into the sea-bed of the ray setting off from each actual shot. A horizontal phase-velocity/range function must be known or assumed with this method and this was determined from a cubic spline fitted to all the time/distance data for each line segment. The tightness of fit of the spline was chosen subjectively to the smoothest which seemed to fit the general trends in the data. Most time and distance corrections were about 3.9 sec and 1.3 km respectively. The appreciable decrease in travel-time scatter achievable by this technique is shown in Figure 3.

Nevertheless, even after applying the water-path corrections a systematic correlation between travel-times and the depths of the ray-entry point is apparent. For each line the depth residual with respect to the mean along-profile depth and the residual of the water-path-corrected travel times, from a second spline fitted to the time-distance data, were plotted. Least-squares linear regression on a compilation of all such depth and time residuals gave highly-significant (more than 99%) correlation coefficients of -0.41 and -0.47 for crustal and mantle arrivals respectively. The associated regression coefficients, which are called dt/dh, were -0.11 and -0.18 km^{-1} respectively. These values fall within the ranges of -0.09 to -0.11 and -0.15 to -0.19 sec km^{-1} found by White and Purdy (1983) for a larger data set of lower crustal and upper mantle arrivals, respectively. White and Whitmarsh (in press) determined dt/dh values of -0.10 and -0.14 sec km^{-1} for the upper and lower crust respectively.

The significance of the correlation coefficients and the consistency between dt/dh values from three different data

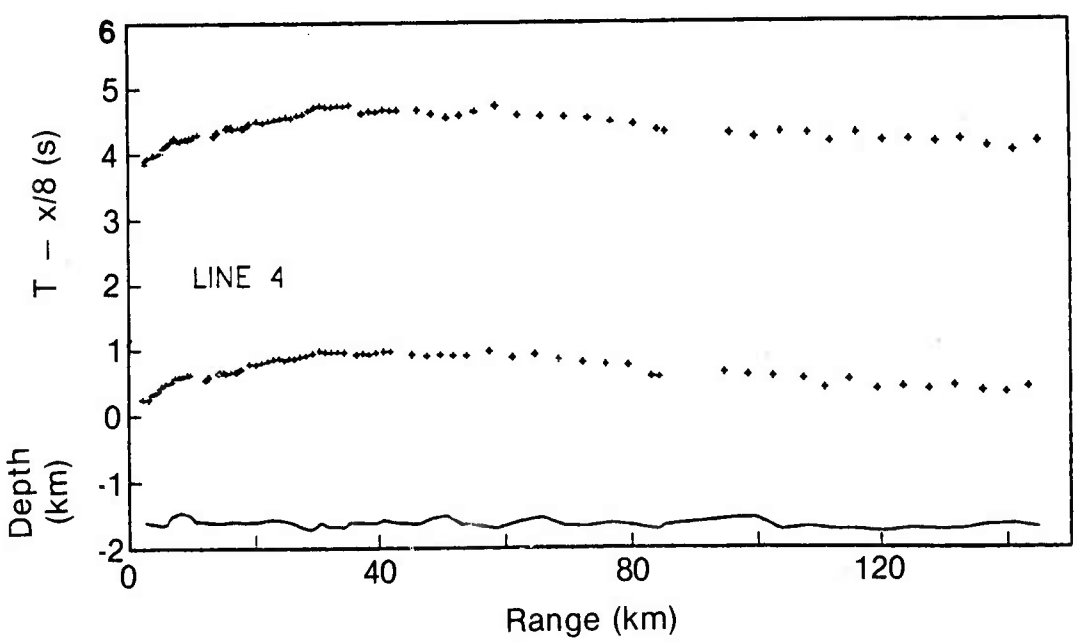


Figure 3 (a). First arrival picks (reduced to 8 km sec^{-1}) before and after application of the water-path and dt/dh correction (upper and lower curves, respectively) plotted above bathymetry along each profile (Line 4).

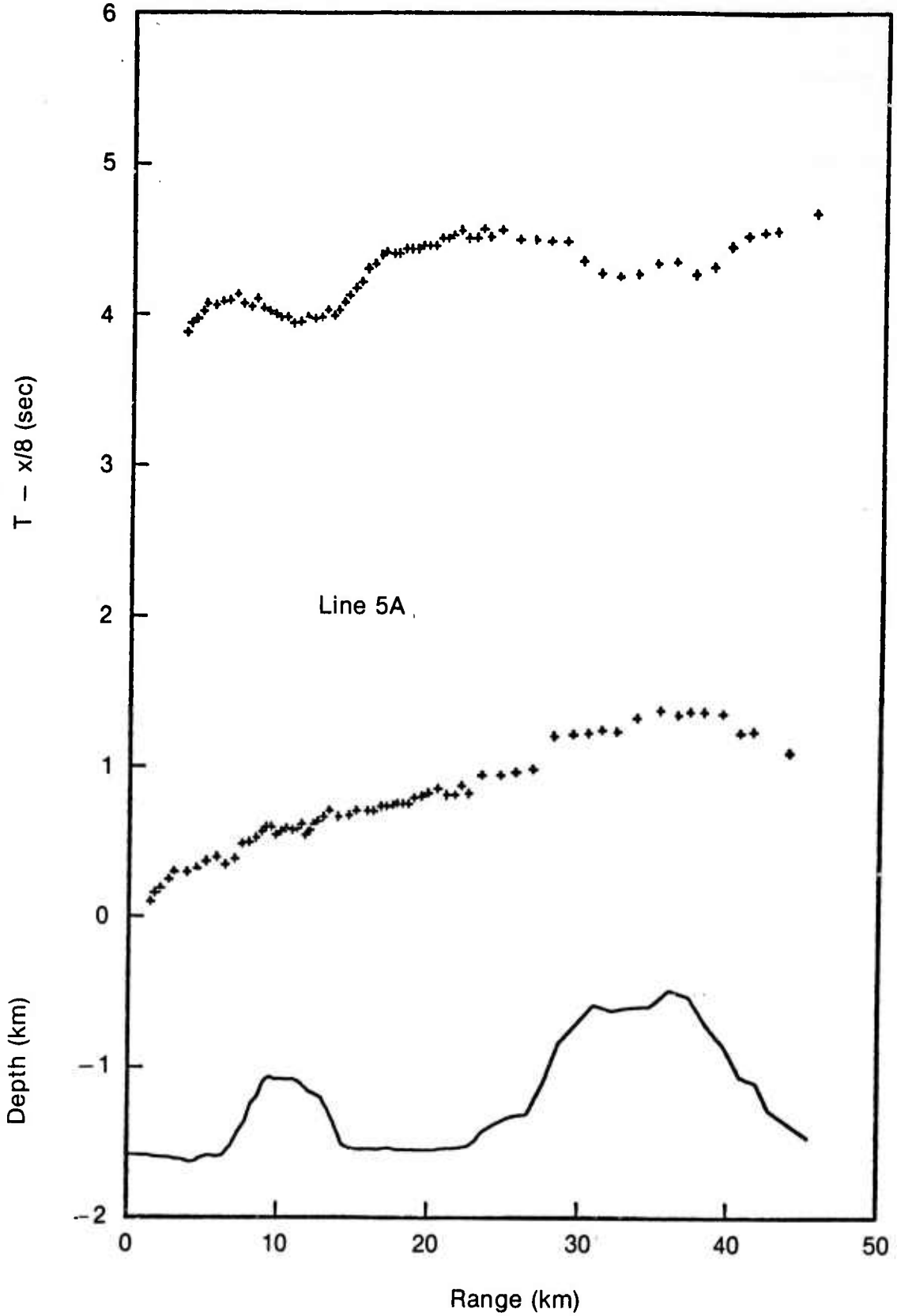


Figure 3 (b). First arrival picks (reduced to 8 km $^{sec\cdot 1}$) before and after application of the water-path and dt/dh corrections (upper and lower curves, respectively) plotted above bathymetry along each profile (Line 5).

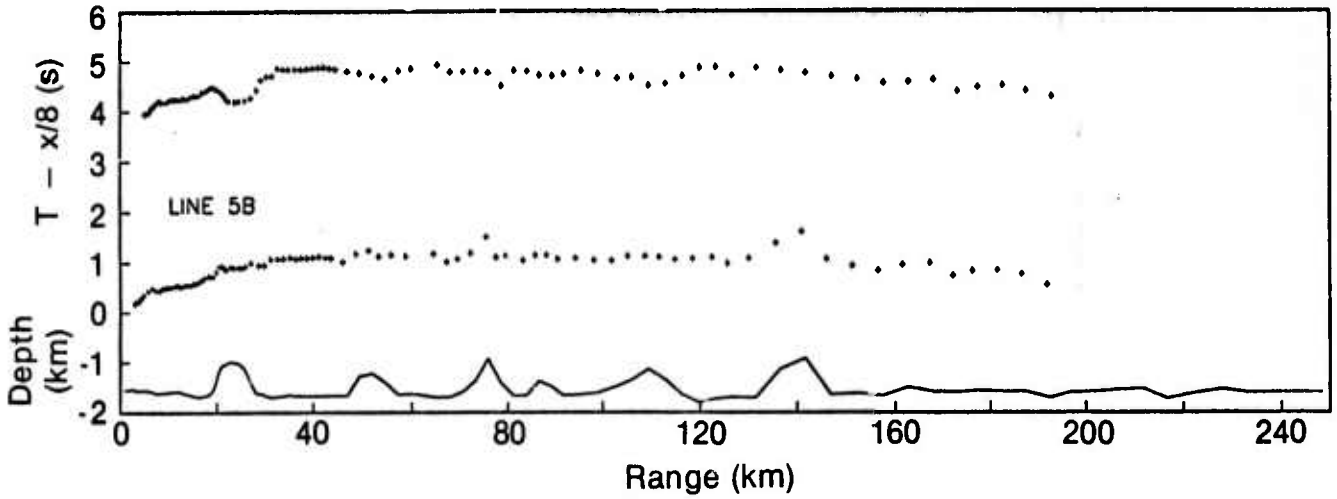


Figure 3 (c). First arrival picks (reduced to 8 km sec^{-1}) before and after application of the water-path and dt/dh corrections (upper and lower curves, respectively) plotted above bathymetry along each profile (Line 5b).

sets indicates a genuine systematic relationship. White and Purdy (1983), on the basis of ray-tracing experiments, believed the relationship was caused by deeper and deeper isovelocity surfaces becoming approximately planar. Therefore, a second correlation, equivalent to the appropriate regression coefficient was applied to the travel-times to remove the linear correlation between time and bathymetry, so as to obtain the smoothest possible set of time/distance data prior to the application of tau-p analysis. This correction involved no adjustment of distance since it is assumed, over a given distance range, that the regression coefficient is independent of distance. The datum chosen to apply the dt/dh correction was 5740 m, the depth of the BIP. It was further assumed that 75 m of 1.5 km sec^{-1} sediment lay under all shot points (there were no reflection profiles along the shooting tracks) and a small time correction was applied to remove the effect of this layer.

Finally, record sections of the three profile segments were plotted using ranges and time adjusted by the above procedures (Fig. 4). There are differences and similarities between the three observed record-sections. The profile 4 section has an excellent signal-noise ratio and many first arrival onsets can be picked to within ±0.05 sec or better even beyond 100 km. Weak lower crust arrivals between 20 and 30 km are followed by strong Moho reflections. At greater ranges there are unusual strong low-frequency secondary arrivals to just beyond 130 km which crudely fall on a 6.8 km sec^{-1} slope but in detail segments with

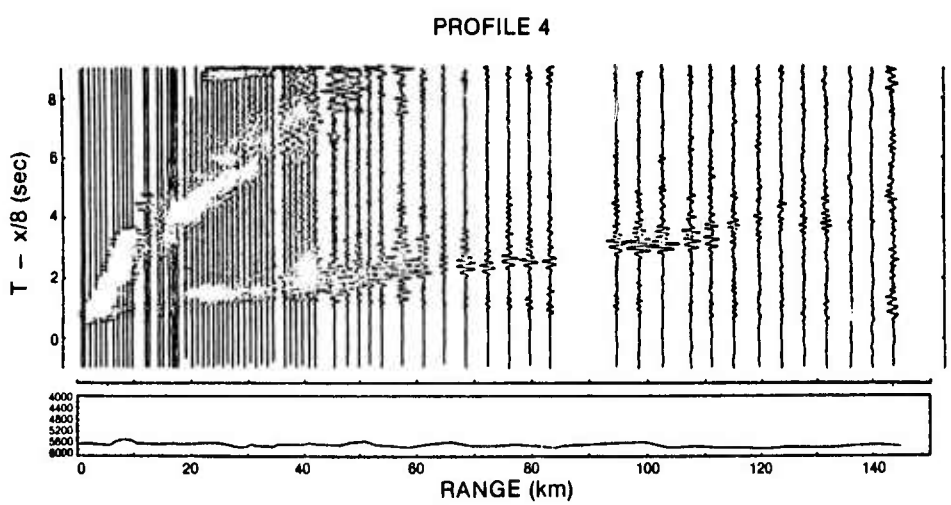


Figure 4 (a). Unfiltered record-sections (reduced to 8 km sec^{-1}) after application of the water-path and dt/dh corrections. Selected traces are from a short-period vertical seismometer (Line 4).

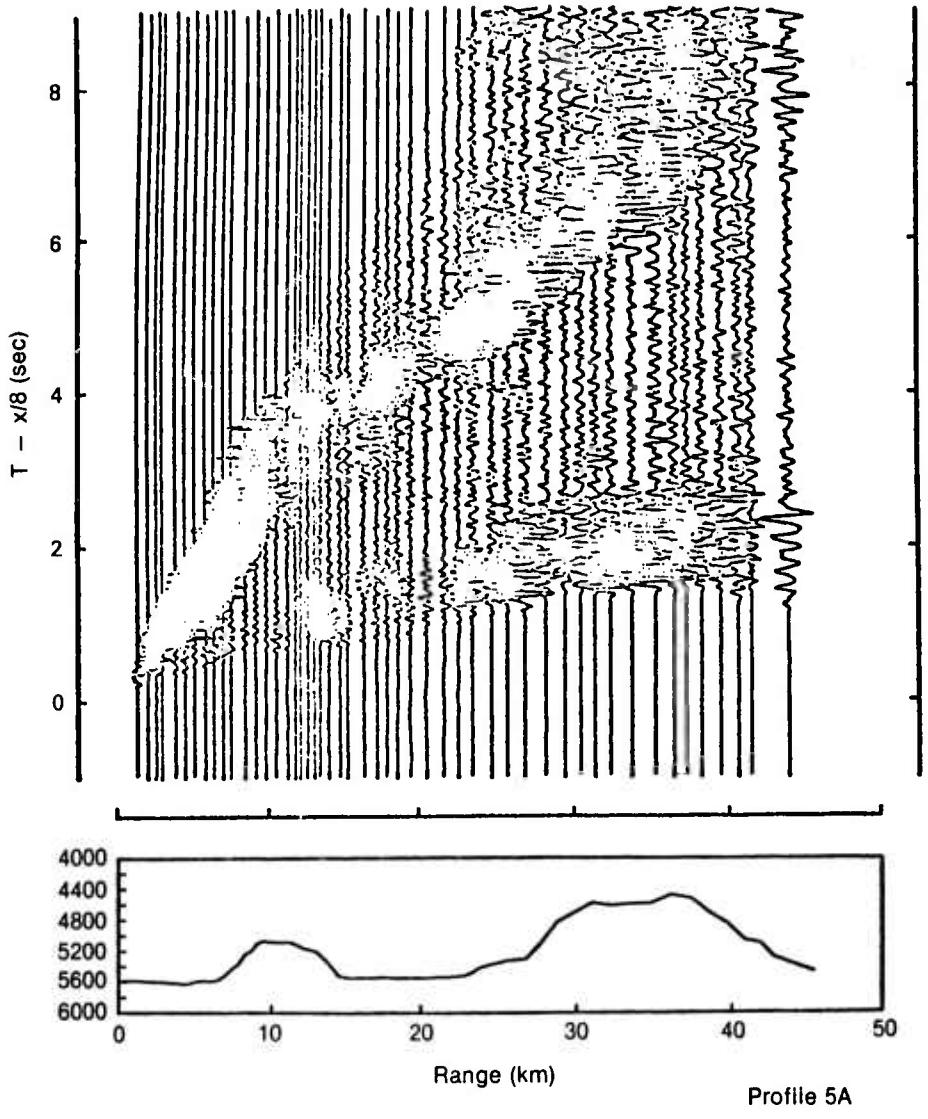


Figure 4 (b). Unfiltered record-sections (reduced to 8 km $^{sec-1}$) after application of the water-path and dt/dh corrections. Selected traces are from a short-period vertical seismometer (Line 5a).

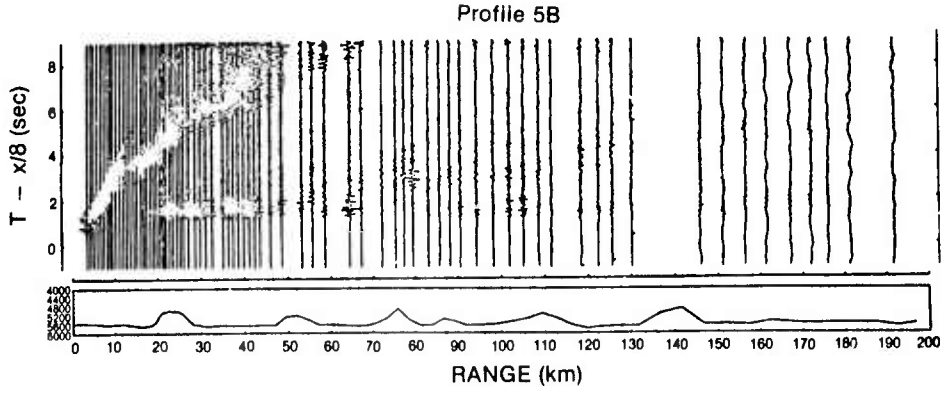


Figure 4 (c). Unfiltered record-sections (reduced to 8 km $^{sec-1}$) after application of the water-path and dt/dh corrections. Selected traces are from a short-period vertical seismometer (Line 5b).

phase velocities as high as 7.2 km sec^{-1} can be distinguished. The mantle first arrivals maintain a fairly constant amplitude but exhibit quite marked variations in high-frequency content (compare 40–65 km with 68–84 km).

Profile 5 was shot over a rougher sea-floor than Profile 4 and the effects of focusing and defocusing near sea-floor elevations manifest themselves as rapid trace-to-trace amplitude changes (e.g., on Section 5A, 17–13 km and beyond 24 km; on Section 5B 19–27 km, 110–111 km). The signal:noise ratio is again excellent out to about 150 km. Most arrivals could be picked to ±0.04 sec or better. Between 150 and 260 km and Section 5B first arrivals become increasingly hard to pick and for the last 70 km of the profile cannot be picked with any confidence. This was due in part to an increased noise level caused by a series of earthquakes probably originating in the Tonga-Kermadec Trench region. Again, weak lower crustal first arrivals are evident. Unlike Profile 4, strong low-frequency secondary arrivals are not seen between 40 and 130 km. The crust-mantle triplication is also less clear on Sections 5A and 5B. The mantle first arrivals exhibit trace-to-trace variations in high frequency content similar to Section 4 but they seem to be less systematic.

The above features will be accounted for eventually when full wave-form modeling of the observed record-sections has been completed.

Compilation of the corrected first-arrival travel-times from both profiles (Fig. 5) shows that all times out to 28 km fall within a narrow ±0.07 sec band suggesting only limited lateral variation in structure in all but the lower-most crust. Conversely, the upper mantle intercept time of Profile 4 is about 0.4 sec smaller than that of Profile 5; such a large difference suggests a thinner crust. Lastly, the increasingly earlier mantle arrivals seen as range increases along Profile 4 suggest higher velocity upper-most mantle material under that profile.

For the initial analysis of the data, a joint (x-p and tau-p) linear extremal inversion, based on travel-times, was carried out in order to obtain bounds outside which no velocity/depth model should lie (Orcutt, 1980). This procedure

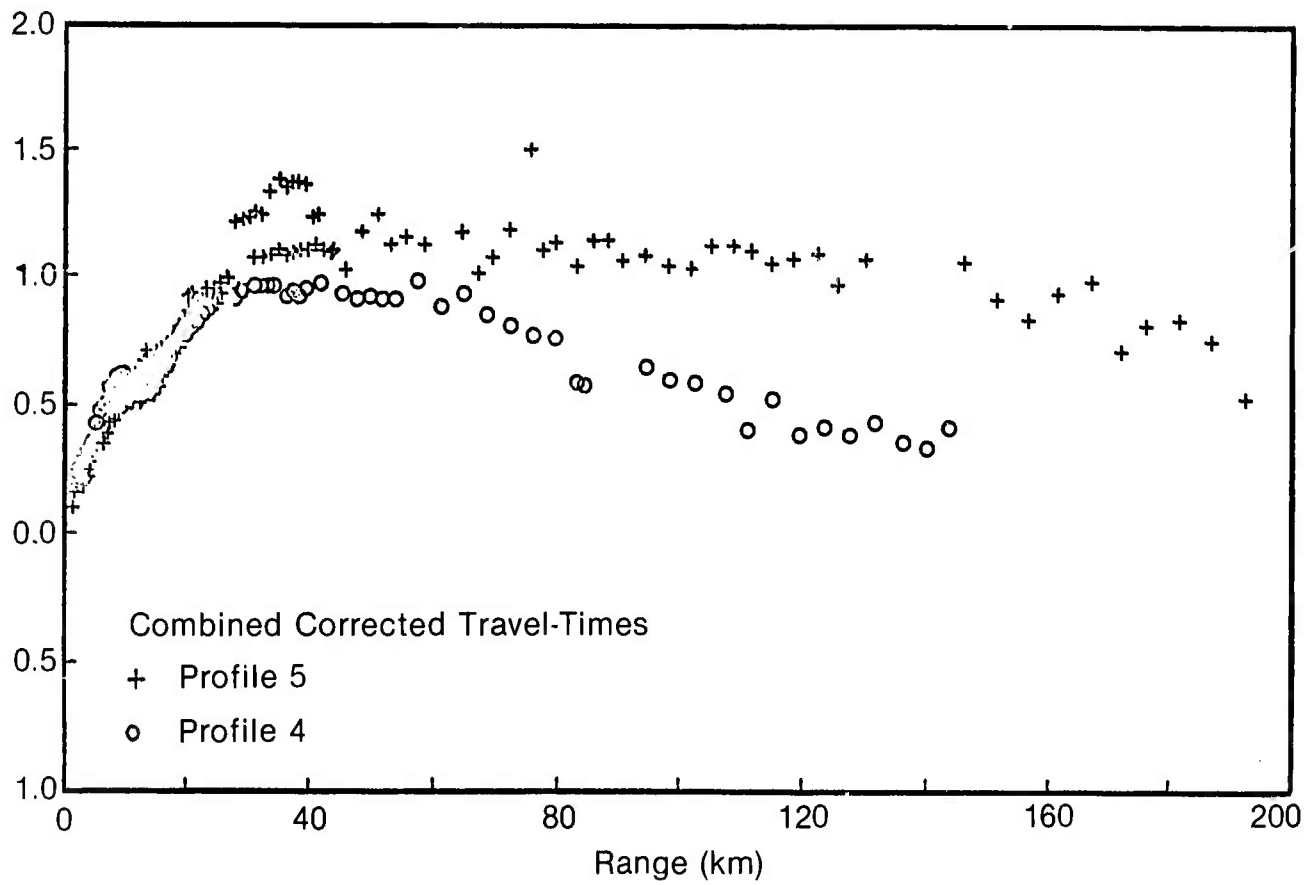


Figure 5. Combined first arrival picks (reduced to 8 km sec^{-1}) from lines 4 and 5 to illustrate the differences in upper mantle arrival times.

assumes a laterally homogeneous earth. Spudich and Orcutt (1980) discussed the disproportionately large effect of a small number of bad observations on the calculated bounds. As explained earlier, considerable care was taken to correct the observed (X,T) points not only for the varying water-path but also for the well-established correlation of travel-time residuals and depth residuals. Application of the dt/dh correction, where dh is relative to a horizontal datum has the effect of "flattening" the sea-bed. Any remaining scatter in arrival times must represent the effect of non-horizontal (undulating) isovelocity surfaces, real lateral velocity variations or observational errors (including poorly-known bathymetry and sediment thickness under the shots).

Stephen and Harding (1983) have noted that borehole observations give rise to an inflexion in the travel-time curve the inverse slope of which correponds to the velocity at the receiver. However, this inflexion point is expected to occur at ranges of less than 3 km (about 1 km corrected range) for the MSS observations. The few points apparently affected by this phenomenon were excluded from the inversion. Shot spacing was not sufficiently small to accurately predict the velocity at the BIP. Most measurements during Leg 91 on basalt cores gave velocities in the range of 4.4 to 5.2 km sec^{-1} (Shipboard Scientific Party, this volume).

The joint extremal inversion proceeded in steps. The first stage was to assign an uncertainty (typically in the range $\pm 0.01 - \pm 0.04$ sec) to each arrival-time pick. Upper and lower bounds to the arrival times were then picked in time, distance (T,X) space by selecting a small number of straight lines arranged to form the smallest possible envelope enclosing all the data (the x-p functions). The corresponding tau-p points (one for each straight line in (T,X) space) then formed the input to the initial joint extremal inversion. This inversion disregarded clear evidence for triplications and therefore gave bounds which varied smoothly with depth (Fig. 6a). In reality, there is a clear triplication in the record-sections due to the crust-mantle transition. The existence of such a triplication was introduced as a further constraint in the inversion procedure, firstly, by estimating the (T,X) bounds on the lower-crust/mantle cross-over point and then by introducing, in addition, estimated bounds on the location of the Moho reflection/upper mantle refraction cusp. The appropriate critical distance cannot be easily identified on record sections (Cerveny et al., 1977) and an overestimate by several kilometers was probably made. Smaller errors in the location of triplication cusps will also exist on record sections where the water-path correction has been applied to the traces. These errors (typically 0.24 km, 0.05 sec for the mantle critical point) are due to using a ray-parameter appropriate not to the cusp but to the nearby first arrivals. Thus the introduction of the cross-over constraint tightened the extremal bounds substantially (Fig. 6b); only a slight improvement was achieved by also using the cusp constraint due to the uncertainties in locating it (Fig. 6c).

The combined results of the extremal inversions are given in Figure 7. The bounds provide only quite broad constraints on possible velocity/depth models in spite of the carefully corrected travel-times due to the scatter in these times. Inspection of Figure 3 reveals that the most scattered travel-times along Profile 5 are associated with highs in the bathymetric profiles. The combination of the shooting track not being always directed precisely away from the MSS and rapid unknown depth changes normal to this track probably made a significant contribution to

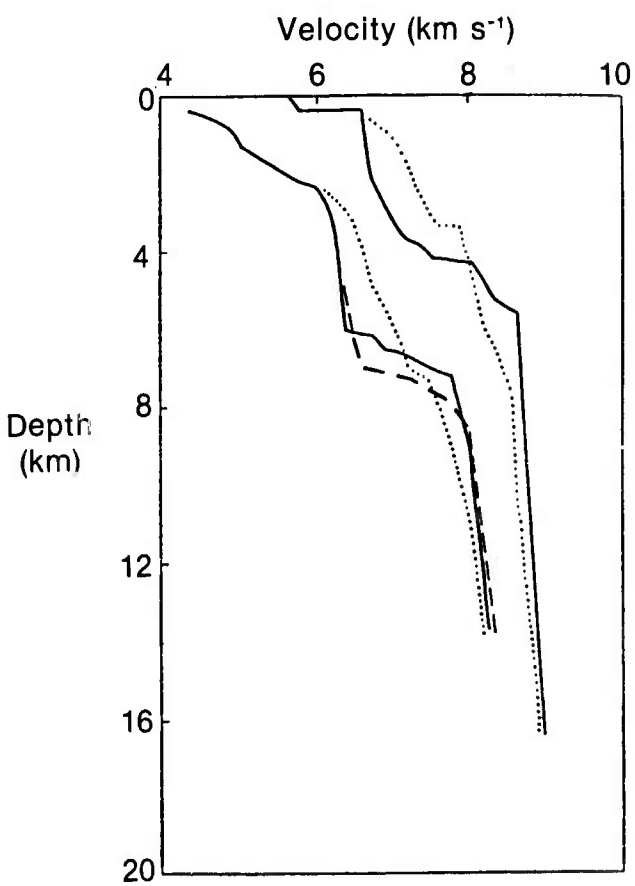


Figure 6. *Extremal bounds obtained from Line 4 based on (a) first arrival times alone (dotted line); (b) first arrival times plus an estimate of the lower crust/upper mantle cross-over point (dashed line, only shown where different from (c); as (b) plus an estimate of the mantle reflection/refraction cusp (solid line).*

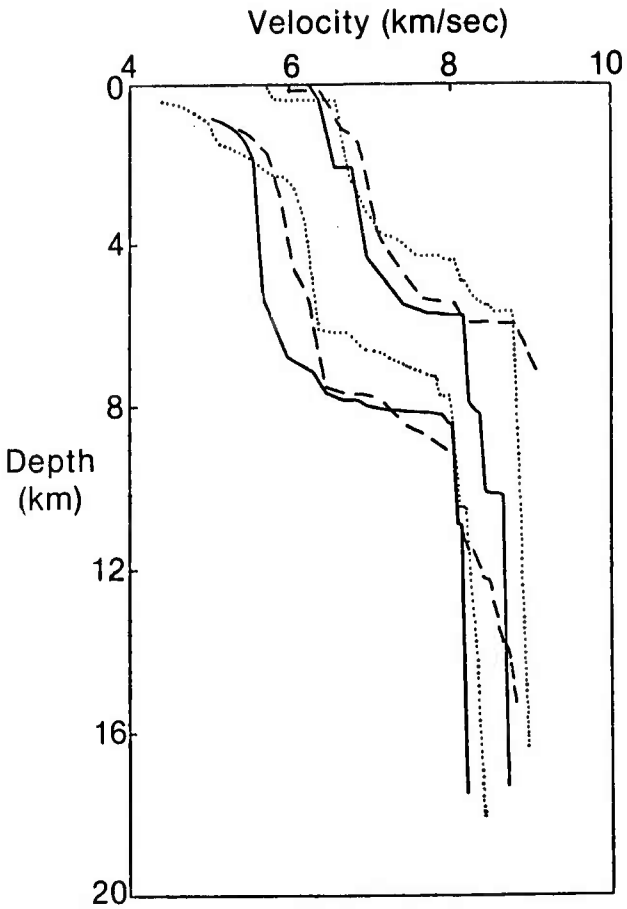


Figure 7. *The results of joint linear extremal tau-p analysis on Lines 4 (dashed line), 5a and 5b (continuous line).*

this scatter. It is notable that the velocity bounds for the main crustal layer of Profile 4, which experienced a total relief of only about 250 m , are significantly narrower than those of Profile 5 which experienced over four times as much relief.

In summary, Figure 7 indicates a normal oceanic crustal structure at Site 595; a 5.5- to 9-km thick crust overlies upper mantle material with a velocity of at least 8.0 km sec^{-1}. Greater resolution of the structure will only be achieved when synthetic seismogram modeling has been completed.

References

Cande, S.C., Larson, R.L., and La Brecque, J.L., 1978. Magnetic lineations in the Pacific Jurassic quiet zone. Earth Planet. *Sci. Letts.*, 41, 434-440.

Cerveny, V.I., Molotov, I.A., and Psencik, I., 1977. Ray method in seismology. *Univerzita Karolva, Praha,* 214 pp.

Clay, C.S. and Medwin, H., 1977. *Acoustical oceanography: principles and applications.* New York: John Wiley and Sons, 544 pp.

Dixon, T.H. and Parke, M.E., 1983. Bathymetry estimates in the southern oceans from Seaset altimetry. *Nature,* 304, 406-411.

Lewis, B.T.R. and McClain, J., 1977. Converted shear waves as seen by ocean-bottom seismometers and surface buoys. Bull. *Seismol. Soc. Amer.*, 67, 1291-1302.

Orcutt, J.A., 1980. Joint linear, extremal inversion of seismic kinematic data. *J. Geophys. Res.*, 85, 2649-2660.

Purdy, G.M., 1982. The correction for the travel time effects of sea-floor topography in the interpretation of marine seismic data. *J. Geophys. Res.*, 87, 8389-8396.

Sandwell, D.T., 1984. A detailed view of the South Pacific geoid from satellite altimetry. *J. Geophys. Res.*, 89, 1089-1104.

Spudich, P. and Orcutt, J., 1980. Petrology and porosity of an oceanic crustal site: results from wave-form modeling of seismic refraction data. *J. Geophys. Res.*, 85, 1409-1433.

Stephen, R.A. and Harding, A.J., 1983. Travel-time analysis of borehole seismic data. *J. Geophys. Res.*, 88, 8289-8298.

Stommel, H., Stroup, E.D., Reid, J.L., and Warren, B.A., 1973. Transpacific hydrographic sections on Lats. 43°S and 28°SL the SCORPIO Expedition-I:Preface. *Deep Sea Res.*, 20, 1-7.

Sutton, G.H., Duennebier, F.K., and Iwatake, B., 1981. Coupling of ocean-bottom seismometers to soft bottom. *Mar. Geophys. Res.*, 5, 35-51.

Threhu, A.M. 1984. On the use of observed incident angles and azimuths to infer lateral velocity variations in the Orozco Transform Fault, *Geophys. J. Roy, Astro. Soc.*, in press.

White, J.E., 1983. Underground sound-application of seismic waves. *Elsevier.*

White, R.S., and Purdy, G.M., 1983. Crustal velocity structure on the flanks of the Mid-Atlantic Ridge at 24°N. *Geophys. J. Roy. Astro. Soc.*, 174.

White, R.S., and Whitmarsh, R.B., in press. An investigation of seismic anisotropy due to cracks in the upper crust at 45°N, Mid-Atlantic Ridge. *Geophys. J. Roy. Astro. Soc.*

Anisotropy in the Oceanic Lithosphere—Theory and Observations from the Ngendei Expedition

P. Shearer and J. Orcutt, Geological Research Division,
Scripps Institution of Oceanography, La Jolla, California

Summary

P-wave travel time data from a seismic refraction experiment on the 1983 Ngendei expedition to the South Pacific indicate anisotropy at two levels in the oceanic lithosphere. In the upper mantle, p-wave velocities vary between 8.0 and 8.5 km/sec with the fast direction at N30°E. Crustal anisotropy within layer 2c is characterized by azimuthal p-wave velocity differences of about 0.4 km/sec, with the fast direction at N120°E. The observed anisotropy is consistent with a model in which aligned olivine crystals cause anisotropy in the upper mantle and aligned cracks within the sheeted dikes of layer 2c cause anisotropy in the crust.

We examine a model of p-wave propagation from a point source in an isotropic layer above an anisotropic half-space and show that under these conditions anisotropy can cause seismic ray paths to deviate from the vertical plane connecting source and receiver. This deviation has a negligible effect on seismic travel times but must be taken into account in modeling p-wave polarization anomalies. P-wave polarization anomalies within the anisotropic half-space are the sum of the particle motion deviation from the ray path, and the ray path deviation from the source receiver azimuth, and are typically range dependent. Polarization anomalies will also occur in the overlying isotropic layer, purely as a result of the ray path deviation, with greater deviations at long ranges. A simple model of upper mantle anisotropy (6 km/sec crust above 8.0 to 8.6 km/sec anisotropic mantle) produces surface polarization anomalies of 1.5 to 3.5 degrees. We examine the implications of anisotropic ray path deviations on travel times and p-wave polarizations for the Ngendei data as well as some previous marine seismic refraction experiments.

Introduction

The physics of wave propagation in general anisotropic media has been understood for some time. Recently seismologists have been considering the added complexities of anisotropy and many theoretical studies have been done (see, for example, Geophys. J. R. Astro. Soc. 49, 76). Most of these studies deal with the forward problem; that is, given a complete set of elastic constants for a medium, these studies describe analytical and numerical methods for computing the seismic waves which can travel in the medium. Many exotic types of possible anisotropy have been investigated (see, for example, Crampin 1982) and interesting complications in wave propagation have been discussed.

Unfortunately, actual, reliable observations of seismic anisotropy are found much less frequently in the literature. Anisotropy, unless quite strong, is easily hidden by inadequate source-receiver distributions and lateral heterogeneities in the earth. Allowing general anisotropy in the earth introduces so many additional free parameters that inverting for these parameters is difficult.

Refraction seismology is one area in which successful observations of anisotropy have been made. Hess, Raitt, Shor, and others in the 1960s used travel-time data to establish p-wave anisotropy of the upper mantle in the Pacific (for example, Raitt et al. 1969). Travel-time data have also been used to measure upper mantle anisotropy on continents (Bamford 1977, 1979). More recently, studies of travel-times, p-wave polarizations, and shear wave splitting have led to hypotheses of marine crustal anisotropy (Stephen 1981; White and Whitmarsh, in press). These have been primarily observational studies which have not dealt with theoretical detail about the nature of anisotropic wave propagation.

This paper will present some results from the 1983 Ngendei expedition to the South Pacific. We find evidence for p-wave anisotropy at two distinct levels in the oceanic lithosphere. The observed anisotropy is consistent with models in which sheeted dike complexes are related to anisotropy in an upper crustal layer and aligned olivine crystals cause anisotropy in the upper mantle. The suggested original spreading direction for the Ngendei site (23.82°S, 165.53°W) is N30°E.

In addition, we examine the general problem of extracting anisotropic parameters from seismic refraction data. In particular, we will look at p-wave travel times and polarizations resulting from a point source within an isotropic layer above an anisotropic half-space, a model which is typical of that used for many seismic refraction experiments. We will show that under these conditions, anisotropy can cause seismic ray paths to deviate from the vertical plane connecting source and receiver. We will show that this deviation has a negligible effect on p-wave travel times, but a significant effect on p-wave polarizations. Finally, we will show some examples of possible anisotropy induced p-wave polarizations which might be observable by receivers either within the anisotropic material or on the isotropic layer above.

Heuristic Review of Anisotropic Wave Propagation

There are three important directions in the propagation of a seismic plane wave. The group velocity direction is the direction along which energy moves and corresponds to a seismic ray path. The phase velocity direction is perpendicular to the advancing wavefront. The

particle motion direction is the direction that particles actually move as the wave passes.

In a homogeneous, isotropic medium the group velocity and phase velocity directions coincide. For p-waves the particle motion is also along this direction and for s-waves the particle motion is orthogonal to this direction. The picture for p-waves emanating from a point source is almost trivial (Fig. 1). The wavefronts will be spheres centered about the source. Energy travels radially out from the source in a direction perpendicular to the wavefronts.

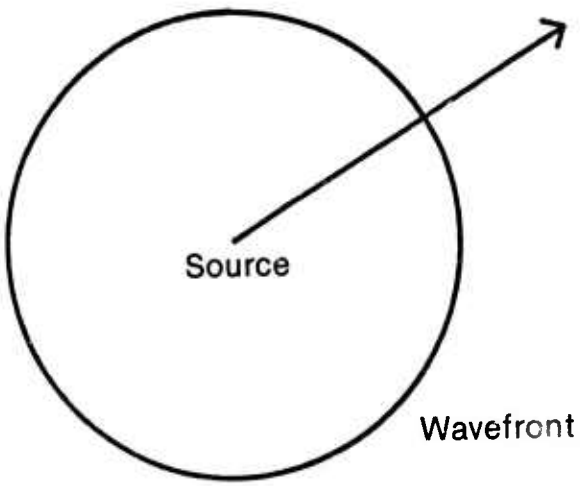


Figure 1. *Wavefront from point source in homogeneous, isotropic medium. Group velocity vector is also direction of phase velocity and particle motion for p-waves.*

For a homogeneous, anisotropic medium the situation is more complicated. In general, the group velocity, phase velocity, and particle motion directions will all be distinct, even for p-waves. In an anisotropic medium, the p-wave group velocity will vary with direction. Thus, wavefronts from a point source will not form spheres (see Fig. 2), and directions perpendicular to these wavefronts (the phase velocity direction) will not generally coincide with the line joining the source and the wavefront (the group velocity direction). Further, the p-wave particle motion direction will not generally coincide with either the group velocity or phase velocity directions.

This suggests a way to observe p-wave anisotropy by measuring differences between the source-receiver and particle motion directions. Crampin et al. (1982) examined this idea and found that the difference between the group velocity direction and particle motion direction is generally much smaller than the difference between the group velocity direction and phase velocity direction, and thus may be difficult to observe.

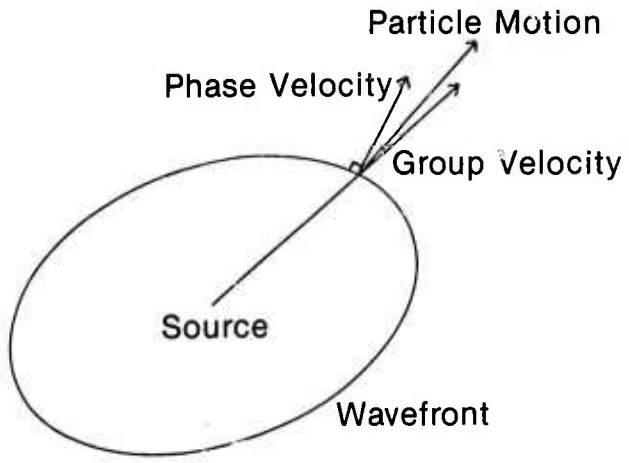


Figure 2. *Wavefront from point source in homogeneous, anisotropic medium. At a point on the wavefront, the group velocity vector, phase velocity vector, and particle motion vector all point in different directions.*

Following Crampin (1981) we may define the p-wave polarization anomaly as the difference between the observed p-wave particle motion and that which we would expect for purely isotropic media. In our example, the anomaly would be the angular difference between the source-receiver path (the expected particle motion direction for isotropic material) and the observed particle motion at the receiver.

Before leaving this example, it will be helpful to make several other observations. We are not allowed an arbitrary dependence of group velocity with direction since this angular dependence is a function of the elastic constants of the medium. There is no easy way to predict what the particle motion directions will be from the group velocities; in general we must derive both from the elastic constants. The ray paths define directions of energy transport which must obey Fermat's Principle; that is, the ray is a path in the group velocity field along which the travel time is stationary. This means that we could predict ray paths in any medium if we knew the group velocity throughout the medium as a function of position and direction.

Now consider a plane interface between an anisotropic medium and an isotropic medium. A source in the isotropic medium and a receiver in the anisotropic medium lie within a plane perpendicular to the interface (Fig 3). If both media were isotropic the ray path between the source and receiver would be a straight line lying in this plane. However, in our example the ray path will skew to one side as required by Fermat's Principle. The ray will want to "take advantage" of faster directions in the anisotropic medium in order to minimize its travel time. The ray path

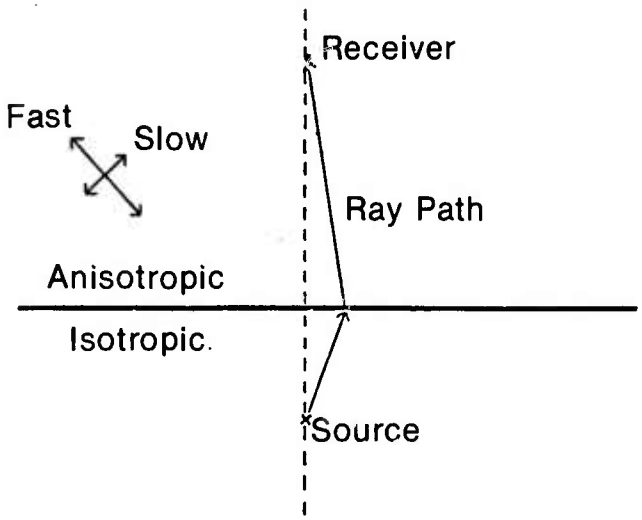


Figure 3. *Ray path between a source in an isotropic medium and a receiver in an anistropic medium. Both source and receiver are along a line perpendicular to the interface. The ray path skews to the side, so that the ray path within the anisotropic medium is rotated toward the fast direction.*

which is stationary with respect to travel time will in general not be a straight line between source and receiver.

In this case the p-wave polarization anomaly will be the sum of the deviation of the ray path from the source-receiver line and the deviation of the particle motion direction from the ray direction. Notice that now the polarization anomaly is not only a function of the anisotropic properties of the receiver medium and the ray azimuth, but also of the relative positions of the source and receiver and the velocity of the isotropic material. Also, if we imagine switching the positions of the source and receiver, we see that we could observe a polarization anomaly with a receiver in an isotropic medium, provided that the ray path goes at least partially through an anisotropic medium. We will consider this reciprocity later in the paper.

Finally, let us extend this example by considering head-waves propagating on an anisotropic half-space generated by a point source in a slower isotropic layer above (Fig. 4). We see that the ray path will generally skew to the side, out of the vertical plane connecting source and receiver, and will arrive at the receiver at an angle to the source-receiver azimuth. In this case we see that the group velocity direction within the anisotropic half-space is not generally the same as the shot-receiver azimuth.

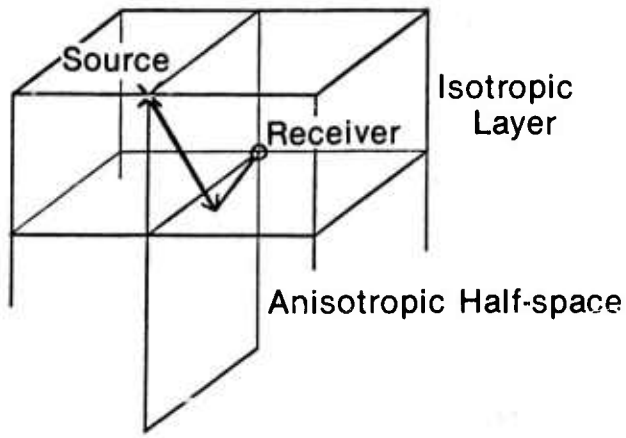


Figure 4. *Ray path for a head-wave traveling on an anisotropic half-space generated by a point source in an overlying isotropic layer. The ray path skews to the side, out of the vertical plane connecting source and receiver. The azimuth of the ray at the receiver will differ from the source-receiver azimuth.*

Again the observed p-wave polarization anomaly at the receiver will be the sum of the ray path deviation from the source-receiver azimuth and the particle motion deviation from the ray direction (we will only concern ourselves with the horizontal polarization anomaly). This polarization anomaly will be a function not only of the anisotropic half-space, but also of the velocity and thickness of the isotropic layer and the source-receiver range. In addition, the travel-time between source and receiver is not solely related to the group velocity of the anisotropic half-space along the source-receiver azimuth, but is also a function of the above-mentioned parameters.

Anisotropic Ray Tracing

Wave propagation in an anisotropic medium can be completely described if the 21 independent elements of the elastic tensor C_{ijkl} are known. If we consider a plane wave with unit directions of $\hat{\underline{s}}$ of slowness, we may write the eigen-value equation (Aki and Richards 1980):

$$M_{ip}u_p = \frac{\varrho}{|s|^2} u_i$$

where

$$M_{ik} = C_{ijkl}\hat{s}_j\hat{s}_l$$

$|s|$ = magnitude of $\underline{s}$ (slowness surface

$$\underline{s} = |\underline{s}|\,\hat{\underline{s}})$$

$\underline{u}$ = polarization vector (particle motion direction)

ϱ = density

In general there will be 3 values of $|\underline{s}|$ which will satisfy the equation and 3 orthogonal eigenvectors $\underline{u}$. In the case of an isotropic medium, there will be one eigenvalue for the p-wave and two degenerate eigenvalues for s-waves. By solving this eigenvalue problem, we can obtain phase velocities and polarization directions for any direction in slowness space that we require. In the general anisotropic case we will have 3 sheets in slowness space although we will consider only the p-wave surface in our analysis.

The ray direction (group velocity) is perpendicular to the slowness surface. As we discussed earlier for the general anisotropic case, the group velocity direction, phase velocity direction (slowness direction), and particle motion direction are all distinct, even for p-waves.

Now imagine a horizontal interface between an isotropic layer and an anisotropic layer with a planar p-wave traveling down from the top layer into the bottom layer. If we rotate the coordinate system such that the x_2 component of the phase velocity is zero, we can construct a diagram such as Figure 5. The generalization of Snell's law for anisotropic media is that the horizontal phase velocity S_1 is conserved (Aki and Richards 1980). For any point S_i on the upper slowness surface for the incident wave, we can find the appropriate point S_t on the lower slowness surface for the transmitted p-wave. Notice that in general the group velocity directions (rays) are not in the plane of the diagram (although the phase velocity directions must be) since they are perpendicular to the slowness surfaces.

If we wish to find the head wave which will travel in the S_1 direction, we simply find the point H_t on the lower slowness surface for which the group velocity vector (the perpendicular to the slowness surface) points in the x_1 direction. For general anisotropy this point will not lie on the S_1 axis. However, in all the examples we will deal with in this paper, the anisotropy will be symmetric about horizontal planes and, thus, will lie on the S_1 axis. The incident wave which will generate this head wave is given by H_i.

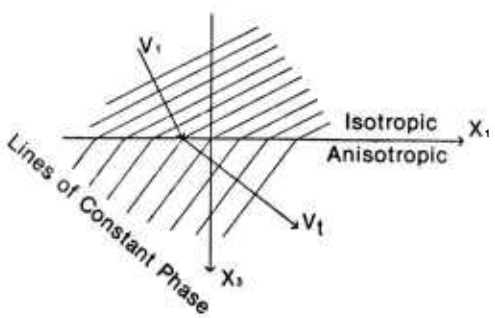


Figure 5(a). Plane p-wave striking an interface between an isotropic layer and an anisotropic layer. Vectors V_i and V_t do not represent rays, but are phase velocity vectors.

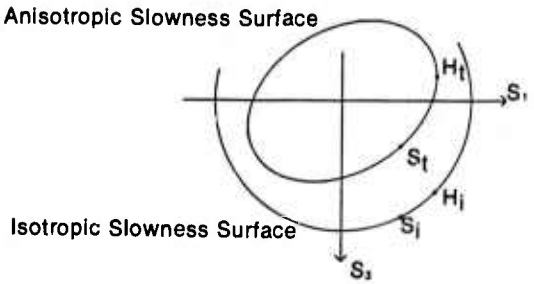


Figure 5(b). Slowness surface representation for p-waves of the isotropic and anisotropic layers. The outer, spherical slowness surface represents the isotropic layer. The inner slowness surface represents the anisotropic layer. Notice that in this example the anisotropic medium has smaller slowness in every direction, or in other words, is faster in every direction. S_i represents the downgoing incident p-wave. S_t represents the downgoing transmitted p-wave. The horizontal slowness S_1 is conserved. The head-wave which would propagate in the S_1 direction is given by H_t. H_i corresponds to the ncident wave which would generate the head-wave.

This is all the machinery we need in order to proceed with our forward modeling. We assume an isotropic layer velocity and values of C_{ijkl}/ϱ for the anisotropic half-space and we specify an azimuth for the ray leaving the source. This provides the horizontal phase direction which we use to find the appropriate point on the lower slowness surface for a head wave. We can now find the phase velocity direction in the upper layer and the group velocity direction and particle motion direction in the half-space. The phase velocity direction in the upper layer defines the ray parameter and azimuth of the ray in the isotropic layer, while the group velocity direction in the lower layer defines the ray azimuth in the anisotropic half-space.

In order to compute polarization anomalies for a given source and receiver, we specify a thickness for the isotropic layer and a source-receiver range. This allows us to calculate the source-receiver azimuth, which can then be compared to the ray azimuth and particle motion azimuth in the anisotropic medium.

Examples

Based on particle motion anomalies and S-wave splitting in a borehole seismic refraction experiment, Stephen (1981) modeled the oceanic crust as a highly anisotropic half-space with p-wave velocities varying from 4.0 to 5.5 km/sec with a 2θ dependence. He predicted particle motion deviations of up to 6 degrees with this model.

Using Stephen's values for $\Gamma_{ijkl} = C_{ijkl}/\varrho$ for an anisotropic half-space with hexagonal symmetry ($\Gamma_{1111} = 30.25$, $\Gamma_{2222} = 16.00$, $\Gamma_{1212} = 8.50$, $\Gamma_{1122} = 10.00$, $\Gamma_{1313} = 5.00$ km^{2}sec^{-2}), a water thickness of 5.5 km, and water sound velocity of 1.5 km/sec, we modeled the appropriate ray paths and particle motions. The results are shown schematically in Figure 6; these diagrams demonstrate many of the features that we have discussed. At the interface, the rays turn toward the fast direction in the anisotropic medium. The difference between ray azimuths and shot-receiver azimuths will be maximized at short ranges and will approach zero at long ranges.

Stephen calculated the particle motion deviation from the ray path (group velocity direction) for his model. In comparing these deviations directly with his data, Stephen made the implicit assumption that the ray path deviations from the source-receiver plane are small. However, we will show in this paper that the ray path deviation is significant and must be taken into account at these nearby ranges of 3 to 12 km. Figure 7 summarizes the expected polarization anomalies at these ranges. The ray path deviations are opposite in sign to the particle motion deviations and are larger in magnitude at ranges closer than about 8 km. Summing the ray path deviations and the particle motion deviations, we see that the expected polarization anomalies are very range dependent with maximum anomalies of -8 degrees at 3 km to $+2.5$ degrees at 12 km. Along lines of constant azimuth, the polarization anomalies change sign—at about 8 km they essentially vanish.

It is difficult to reconcile these predicted values with the data, which show maximum anomalies of $+15$ to $+20°$ (although with large error bars). The large magnitude of the polarization anomalies in the data and their apparent lack of range dependence suggest that it will be difficult to fit the anomalies with any reasonable anisotropy model. One possible alternative explanation is miscalibrated gains in the two horizontal channels of the seismometer, which would cause an apparent 2θ dependence in polarization anomalies. This is an effect which White and Whitmarsh (in press) noticed in their data. Nevertheless, the S-wave splitting that Stephen observes cannot be explained in this way and remains evidence for anisotropy.

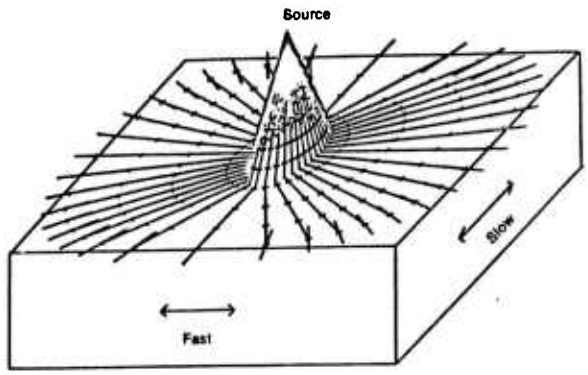


Figure 6(a). Schematic representation of ray paths for the Stephen anisotropy model. Near vertical lines leaving the source correspond to ray paths within the ocean. Horizontal lines correspond to head-wave ray paths on the surface of the anisotropic half-space. The rays shown are at increments of 10 degrees in azimuth leaving the source. Tic marks on the rays occur at intervals of 0.5 second. Black lines at the end of the rays represent particle motion directions for each ray path shown in the anisotropic half-space.

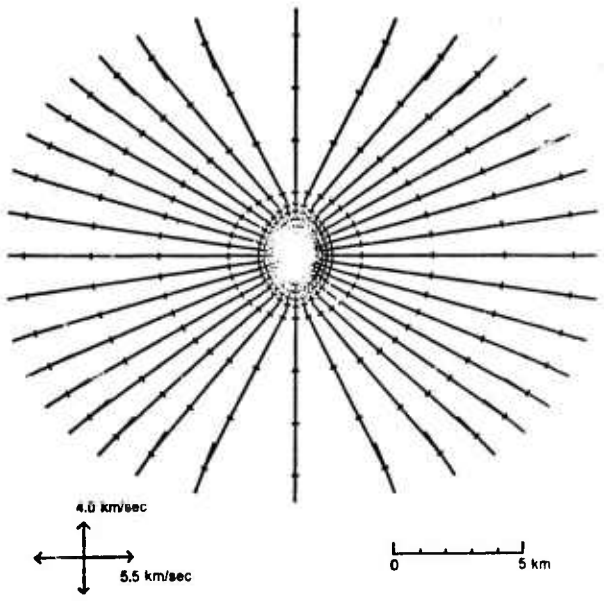


Figure 6(b). Map view of Figure 6a as seen from a point directly above the source. Ray paths turn toward the fast direction in the anisotropic half-space.

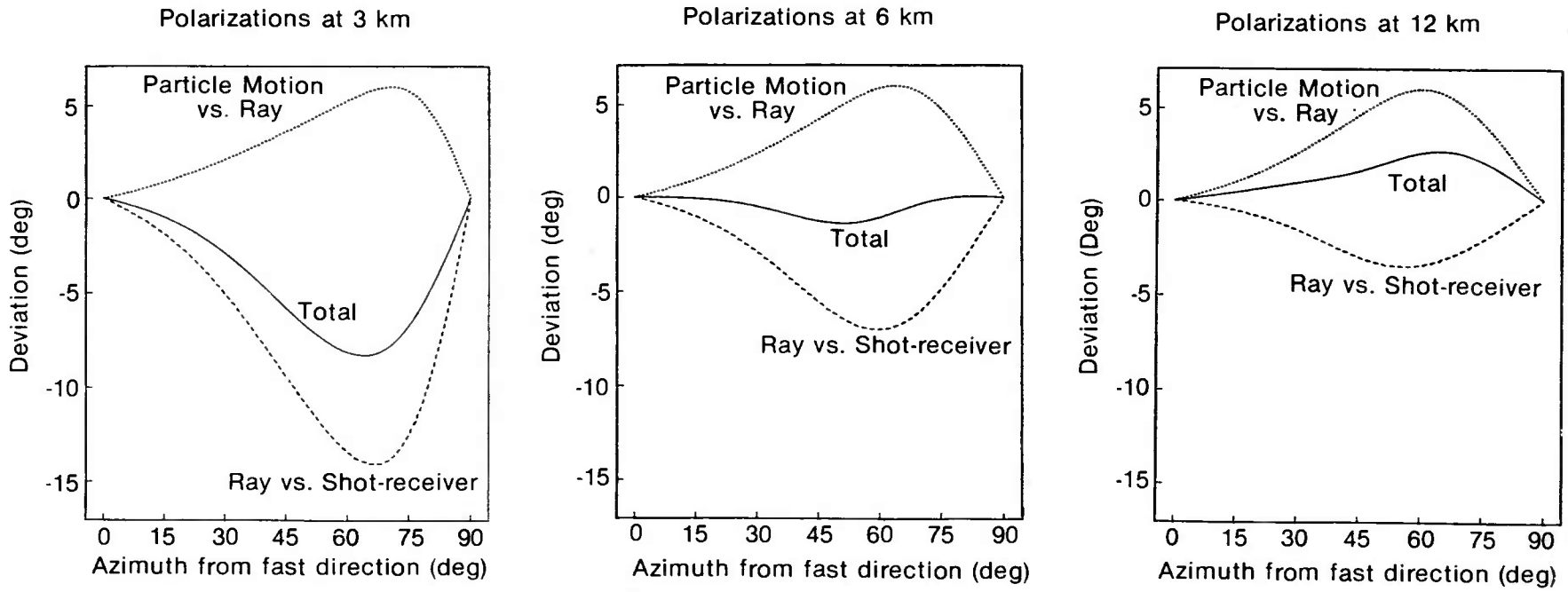


Figure 7. *Polarization anomalies for the Stephen model at shot receiver ranges of (a) 3 km, (b), 6 km, (c) 12 km. These show the ray deviation from the shot-receiver azimuth, the particle motion deviation from the ray, and the total (observable) deviation—the particle motion deviation from the shot-receiver azimuth. Positive deviations represent deviations away from the fast direction in the anisotropic half-space.*

The procedure we have described gives us the ray path for rays leaving the source at specified angles. An iterative scheme can be used to find the appropriate ray path to a specified receiver position and to then calculate the source-receiver travel time. We used this procedure to calculate travel-time curves for lines running radially away from the source. Figure 8 shows the results for the Stephen anisotropy model. As one would expect, the slopes of the travel-time curves asymptotically approach the group velocity in the direction of the line. However, even at close ranges, the travel-time curves deviate only slightly from straight lines. This is remarkable, considering how large the anisotropy is in the Stephen model (4 to 5.5 km/sec), and indicates that the travel-time perturbations due to ray perturbations are truly a second order effect. This is a result of Fermat's principle—to first order, travel times are unaffected by ray path deviations.

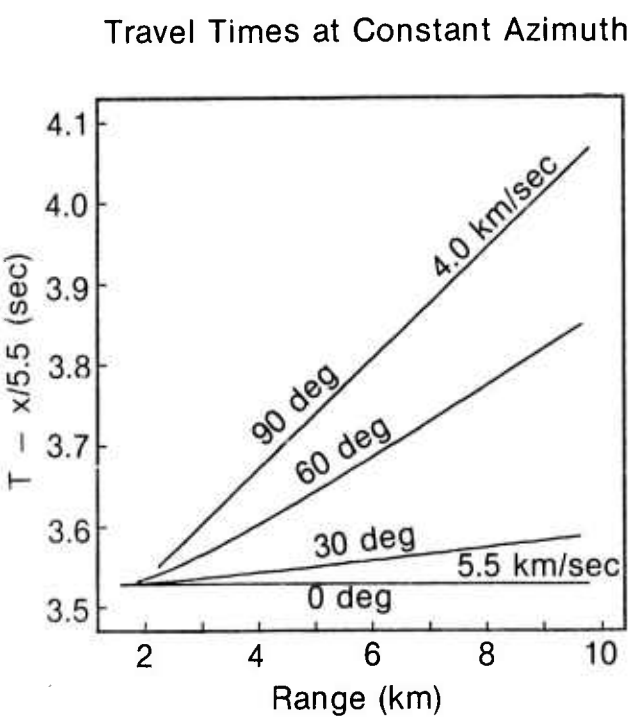


Figure 8. *Travel time for the Stephen anisotropy model along lines at various angles from the fast direction in the anisotropy. Curves start at the closest range at which head waves are generated. Travel times have been reduced at 5.5 km/sec, the velocity of the fast direction in the anisotropic medium. Travel-time curves at azimuths of 30 and 60 degrees are slightly curved, while travel-time curves at 0 and 90 degrees (corresponding to anisotropic symmetry axes) are straight.*

Using realistic data, it is difficult enough to observe differences in velocity with direction (i.e., noting the different slopes and positions of the lines in Fig. 8); it would be almost impossible to distinguish the slight curvature of the travel-time curves associated with the ray path deviations.

The classical travel-time studies of upper mantle anisotropy in the Pacific (for example, Raitt et al. 1969) assumed the group velocity was associated with a straight path between the source and receiver. In this upper mantle case the anisotropy (8 of 8.6 km/sec) is smaller than the Stephen model anisotropy and the ranges (40 to 100 km) are greater, which argues that this assumption was entirely justified.

In an OBS seismic refraction experiment in the Atlantic, White and Whitmarsh (in press) found particle motion deviations from the shot-receiver azimuth of 5 to 8 degrees and velocity variations of up to 0.4 km/sec, both with a 4θ dependence. They compare these results with model predictions for velocity and polarization anomalies as a function of azimuth for distributions of thin parallel cracks in an isotropic solid (Crampin 1978; Crampin et al. 1982). These modeled polarizations are the particle motion deviations from the ray azimuth, which, as Crampin et al. (1982) correctly note, are applicable for an anisotropic half-space containing both source and receiver.

However, in this case the source is not within an anisotropic half-space, but is in an overlying isotropic layer (the ocean). Thus, as we have seen, it is incorrect to assume that the ray direction is equivalent to the source-receiver azimuth. For the simple example of an isotropic layer over an anisotropic half-space, the observed polarization anomaly will be the sum of the particle motion deviation from the ray direction and the ray deviation from the source-receiver azimuth. Since White and Whitmarsh (in press) did not publish a specific anisotropy model for their data, we did not calculate how large the ray deviation contribution to the polarization anomalies would be. However, as we have seen, the polarization anomalies will be range dependent.

One apparent limitation to p-wave polarization studies of anisotropy is that the deviation of the particle motion from the ray path can only be measured by a seismometer within the anisotropic medium. In most places in the earth (i.e., inside!) such a direct measurement will be impossible. However, the anisotropy-induced deviation of the ray path from the source-receiver azimuth can be measured by receivers in an overlying isotropic layer (see Fig. 9). In this case we see that the deviation will be opposite in direction to the deviation within the anisotropic layer. Our procedure for calculating head wave ray paths in an

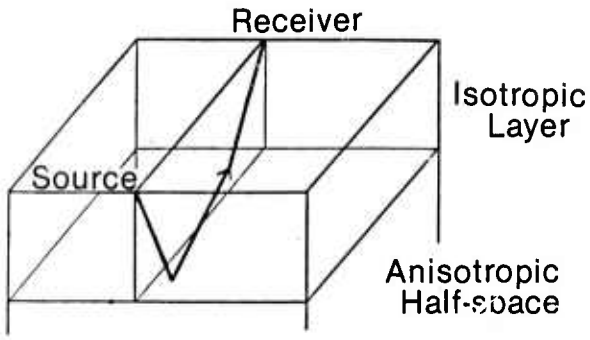


Figure 9. *Ray path for a source and receiver on an isotropic layer above an anisotropic half-space. The ray path is skewed, and the ray at the receiver will be at an angle to the vertical plane connecting source and receiver.*

anisotropic layer can easily be modified to account for this situation by noting the symmetry between the ray entering the anisotropic layer and the ray leaving the anisotropic layer. In this case we need not bother calculating particle motion directions, since they are not measurable in the anisotropic layer and are coincident with the ray path in the isotropic layer.

P-wave anisotropy in the upper mantle has been widely observed. We chose to model p-wave polarization anomalies that might be observable on the surface of the crust for two simple cases - oceanic and continental. We used a 2θ model of p-wave anisotropy with velocities varying from 8.0 to 8.6 km/sec. The exact shape of the group velocity versus azimuth curve will determine how large the ray path deviations will be, so we approached this problem in two ways.

First, we scaled the Stephen anisotropy model discussed earlier (but leaving out the 4θ part) so that it would produce the appropriate group velocity maxima and minima. This gave us values for Γ_{ijkl} (Γ_{1111} = 73.96, Γ_{2222} = 64.00, Γ_{1212} = 21.716, Γ_{1122} = 23.53, Γ_{1313} = 13.57 km^{2}sec^{-2}) which we could directly use to calculate ray paths. Second, we approximated the group velocity function as

$$U^2 = 68.98 + 4.98 \cos 2\theta$$

following Backus (1965) and again not including 4θ terms. Using this function for the group velocity we used an iterative procedure to find the least time ray path between source and receiver.

Figure 10 shows a comparison between the group velocity function determined by the exact model and the

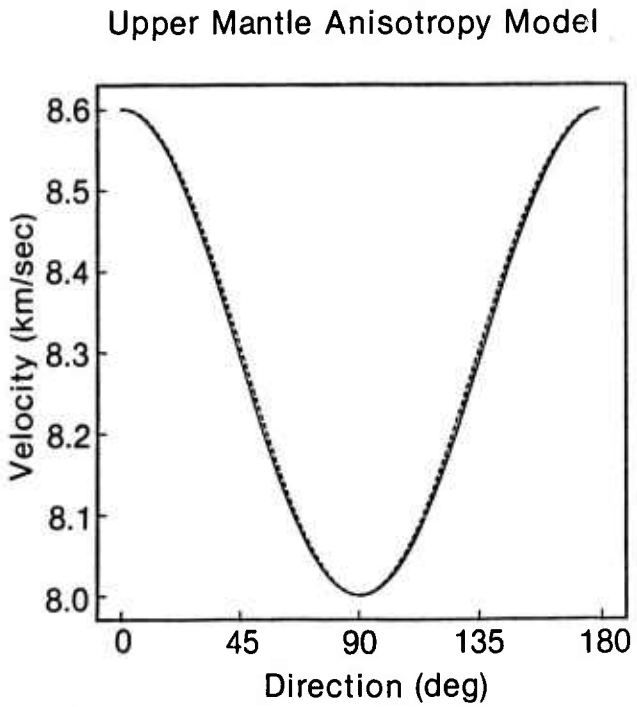


Figure 10. *Solid line is the group velocity function for a specific model of upper mantle anisotropy (Γ_{1111} = 73.96, Γ_{2222} = 64.00, Γ_{1212} = 21.716, Γ_{1122} = 25.55, Γ_{1313} = 13.57 km^{2}sec^{-2}). Dashed line is the calculated group velocity curve using the Backus approximation applied to this model (v^2 = 68.98 + 4.98 cos 2θ).*

approximation. The curves are slightly different and, thus, we should not expect identical results for our calculated polarization anomalies.

Figure 11 shows the polarization anomalies expected for a typical continental situation with source and receiver atop a 30-km-thick layer of 6 km/sec crust. The anomalies are range dependent with larger anomalies at longer ranges. Note that this range dependence is opposite to that predicted for ray path deviations within the anisotropic half-space. The anomalies range from 1.5° at 100 km to 3.5° at 500 km. The angular deviation is away from the fast direction of anisotropy, again opposite to the ray path deviations within the anisotropic medium, which are toward the fast direction. Note also that the least time algorithm gives nearly the same result as the exact calculation based on the Stephen type model. This is encouraging since the methods used to calculate the anomalies were completely different.

Figure 12 shows the polarization anomalies expected for a typical oceanic situation, with 6 km of 1.5-km/sec water above 6 km of 6-km/sec crust above an anisotropic upper

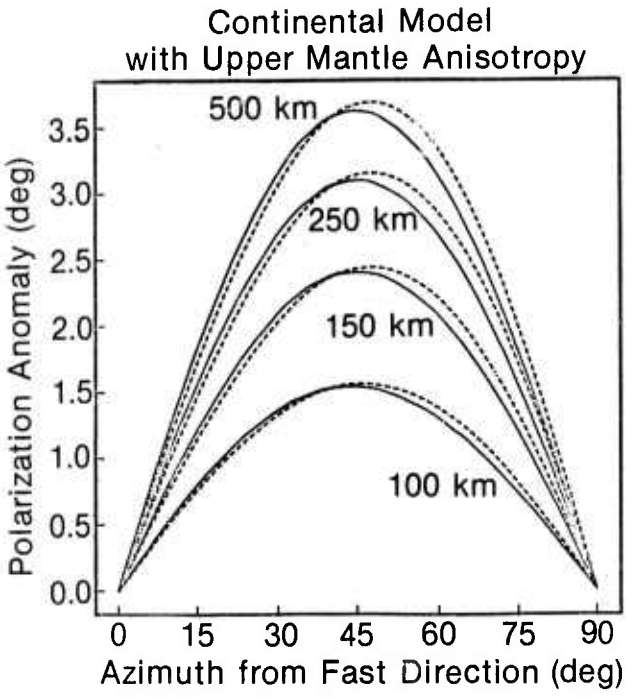


Figure 11. Calculated polarization anomalies for a continental model with 30 km of 6 km/sec crust above an anisotropic upper mantle with a 2θ velocity variation from 8.0 to 8.6 m/sec. Solid lines were calculated from the slowness surfaces for the exact model. Dashed lines were calculated using a least time algorithm on an approximate group velocity function.

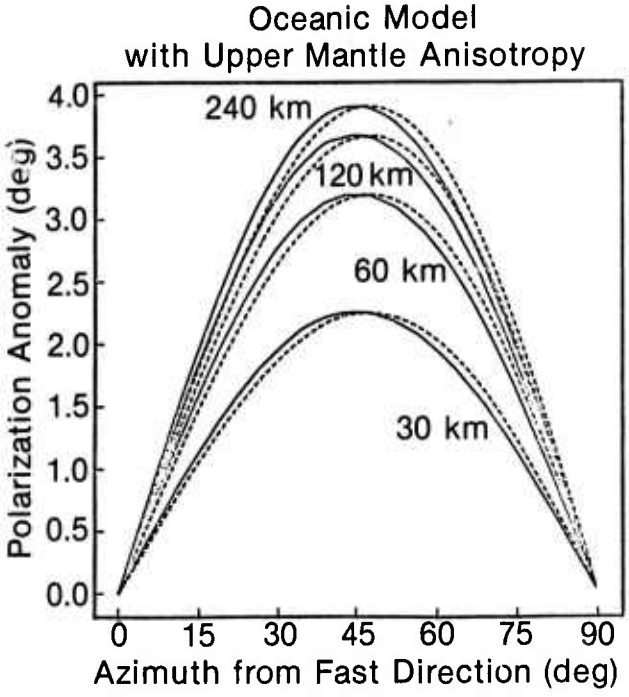


Figure 12. Calculated polarization anomalies for an oceanic model with 6 km of 1.5 km/sec water above 6 km of 6 km/sec crust above an anisotropic upper mantle. Source was assumed to be at surface of water; receiver was assumed to be at surface of crust. Anisotropy model calculations were done as in Figure 11.

mantle. The source is assumed to be on the surface of the water; the receiver on the surface of the crust. The polarization anomalies range from 2° at 30 km to 3.8° at 240 km. As we saw in the continental example, the two methods used to compute the anomalies give nearly the same answer.

Thus, we see that upper mantle p-wave anisotropy should cause small, but perhaps still observable, p-wave polarization anomalies on the surface of the crust. The amount of the polarization is a function of the range, crustal thickness and velocity, as well as the magnitude of the upper mantle anisotropy.

If we model the earth as a series of flat, homogeneous (but possibly anisotropic) layers, we see that an observation of a polarization anomaly on the surface does not necessarily indicate anisotropy in the surface layer, but simply that anisotropy must be present in at least one of the layers through which the ray passes. Since travel time variations and shear wave splitting also do not require surface anisotropy, the data presented by Stephen (1981) and by White and Whitmarsh (in press) do not directly require anisotropy within a surface layer.

In many cases the ray path deviation from the source-receiver azimuth will be greater in an overlying isotropic layer than it will be in the underlying anisotropic layer. For example, if we add a 1-km-thick, 3-km/sec isotropic layer to the top of the crust in the Stephen model, we would generate the polarization anomalies shown in Figure 13. These anomalies range from 5 degrees at 5 km to 14 degrees at 12 km. They are all at angles bending away from the fast direction of anisotropy.

In such a model, other evidence for anisotropy, such as travel time dependence upon azimuth and S-wave splitting would still be present. We do not mean to suggest that this model is the correct one, but only that models of this type should be considered. Large polarization anomalies (10 to 20 degrees) can be fit with models involving an isotropic layer above an anisotropic half-space with less anisotropy than would be necessary to generate the polarization anomalies with the anisotropic half-space

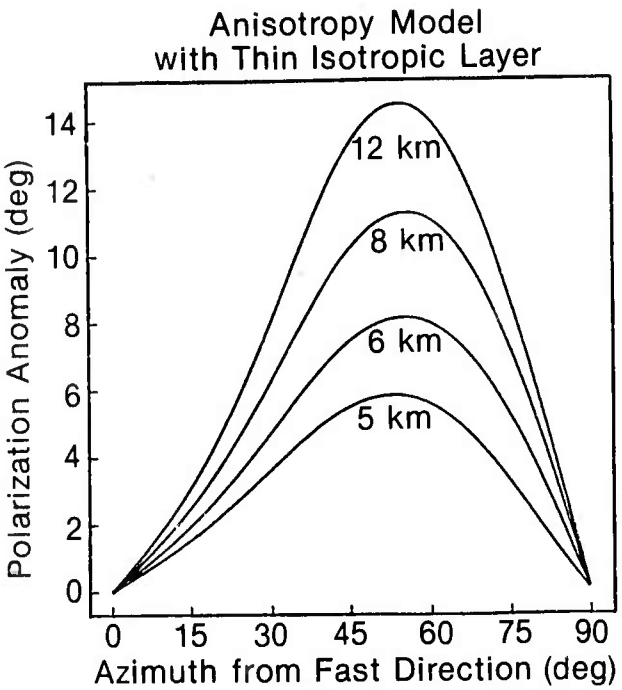


Figure 13. Calculated polarization anomalies for a model of the oceanic crust involving a 1-km thick, 3-km/sec isotropic layer above the Stephen model of an anisotropic half-space. Anomalies are shown at source-receiver ranges of 5, 6, 8, and 12 km. Positive anomalies represent deviations away from the fast direction in the anisotropic half-space.

alone. However, as in other ray theoretical approaches to seismic problems, we must be careful not to exceed the limits of the ray approach; our resolution will always be limited by the wavelengths involved. For example, it is clearly incorrect to generate huge polarization anomalies by adding a 10-m thick surface isotropic layer to our models, because seismic wavelengths in seismic refraction experiments are, at best, 150-m long (20 Hz at 3 km/sec).

Summary of Ray Deviation Effects

We have calculated the ray path deviation from the vertical source-receiver plane for a few simple examples involving a source on an isotropic layer above an anisotropic half-space. We found that in some cases this deviation is significant and should be taken into account when modeling polarization anomalies.

For a receiver on the anisotropic half-space the polarization anomaly will be the sum of the ray path deviation from the source-receiver azimuth and the particle motion deviation from the ray path. The ray path deviation will be in a direction toward the fast direction in the anisotropic medium, and will be range dependent, with the largest deviations at close ranges and deviations decreasing asymptotically to zero at infinite range.

For a receiver on the isotropic layer above the anisotropic half-space, the polarization anomaly will be the deviation of the ray path from the source-receiver azimuth and will be away from the fast direction in the anisotropic medium. The ray path deviation will increase with source-receiver range and asymptotically approach a finite limit at infinite range.

The polarization anomalies in both of these cases are, of course, dependent on the source-receiver azimuth and decrease to zero at azimuths aligned with either the fast or slow axes in the anisotropic medium. The deviation of the ray path from the vertical source-receiver plane also affects travel time calculations, but this is a second order effect which can be ignored in typical seismic refraction experiments.

The Ngendei Seismic Refraction Experiment

The 1983 Ngendei expedition to the southwest Pacific (Jordan et al. 1983; Orcutt et al. 1983) was at a site (23.82°S, 165.53°W) approximately 1000 km east of the Tonga Trench and 1500 km west-southwest of Tahiti (see Fig. 14). The oceanic lithosphere is estimated to be about 140 m.y. old at the site (Menard et al. 1983), one of the oldest areas in the Pacific. The Scripps research ship MELVILLE shot 4 split refraction profiles with azimuth spacing of 45 degrees and a circular line of 10-km radius (see Fig. 15). All of the lines were recorded by at least

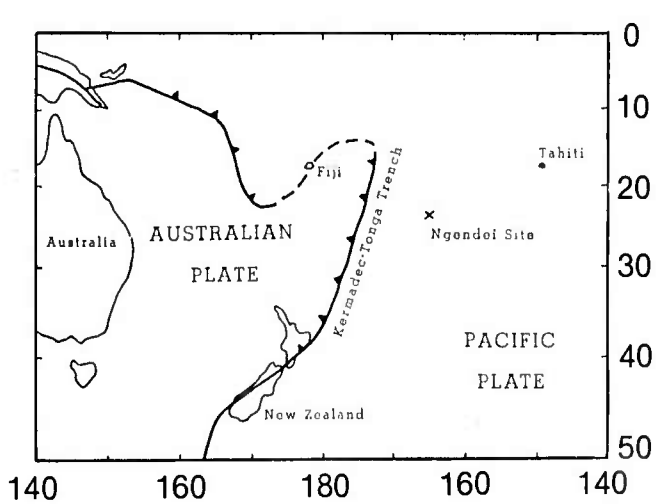


Figure 14. The Ngendei site (DSDP Hole 596) shown on a map of the South Pacific.

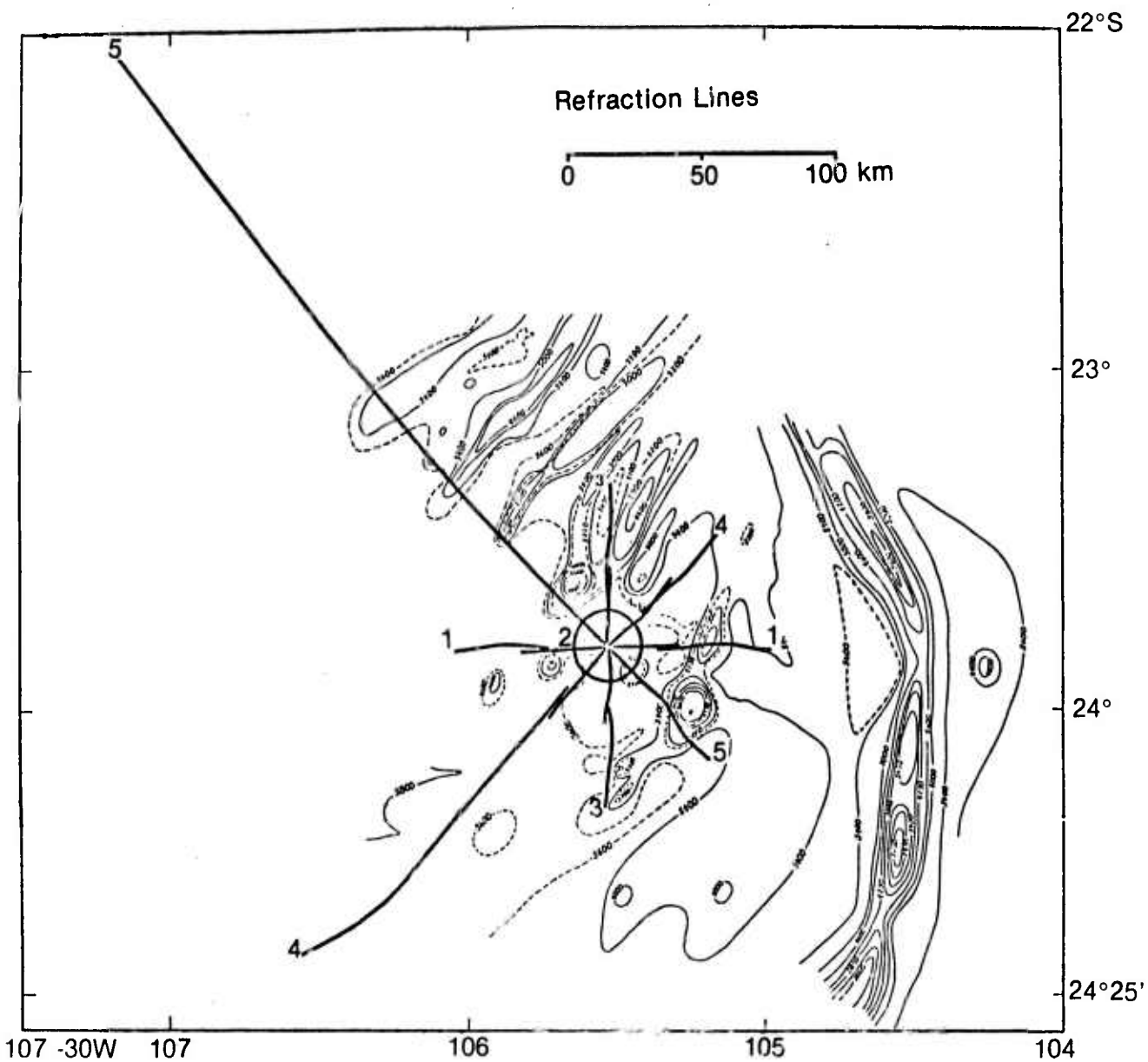


Figure 15. Four split refraction lines and a circular line of 10 km radius were shot at the Ngendei site. Water depth at the site is 5600 m.

two Scripps ocean bottom seismometers (OBSs) and two of the lines were recorded by a borehole seismometer, the Marine Seismic System (MSS).

Ranges were calculated and topographic corrections applied with standard techniques (Spudich and Orcutt 1980; White and Whitmarsh, in press). Figure 16 shows the reduced p-wave travel times for the entire OBS data set. The data are consistent with typical models of oceanic crustal velocity structure involving a steep velocity gradient in layer 2, a shallow velocity gradient in layer 3, and mantle velocities below the Moho.

In an earth consisting of horizontal isotropic layers, we would expect no systematic variations of travel time with azimuth. Figure 17(a) shows a comparison of travel times for shots along N–S azimuths vs. shots along E–W azimuths. Although there is considerable scatter in the data, some trends are apparent. Between about 5 and 15 km, the E–W arrivals come in before the N–S arrivals, while at ranges greater than 35 km, the N–S arrivals are first. Figure 17(b) shows a similar comparison of NE–SW arrivals vs. NW–SE arrivals. In this case the NW–SE arrivals are early at ranges of about 6 to 17 km, while the NE–SW arrivals are early at ranges greater than 35 km. These differences in p-wave travel times are indicative of anisotropy at two levels in the oceanic lithosphere. We can already see that the fast direction in the upper mantle anisotropy will be about N–NE while the fast direction in the crustal anisotropy will be about N–NW.

The borehole seismometer had much lower noise levels than the OBSs. Thus, it was possible to pick p-wave arrivals out to greater ranges. Figure 18 shows a comparison of MSS travel times for NW–SE vs. SW azimuths (the only lines the MSS recorded). At mantle ranges, the SW arrivals consistently come in ahead of the NW–SE arrivals, agreeing with the OBS data.

Figure 19 is a closeup of the OBS arrivals at close ranges. Out to about 4 km the N–S, NE–SW arrivals are roughly coincident with the E–W, NW–SE arrivals. Between about 4 and 6 km, the E–W, NW–SE arrivals come in increasingly early, and then maintain an approximately constant offset at ranges greater than 6 km. Since the slope of the travel-time curve is approximately flat at these ranges, the data can be reduced for a constant velocity in order to make a travel time vs. azimuth plot. Figure 20 shows such a plot for travel time picks between 7 and 11 km, reduced at 6.6 km/sec. The vertical alignments in the plot represent individual refraction lines, which were shot at approximately constant azimuth. Points between these

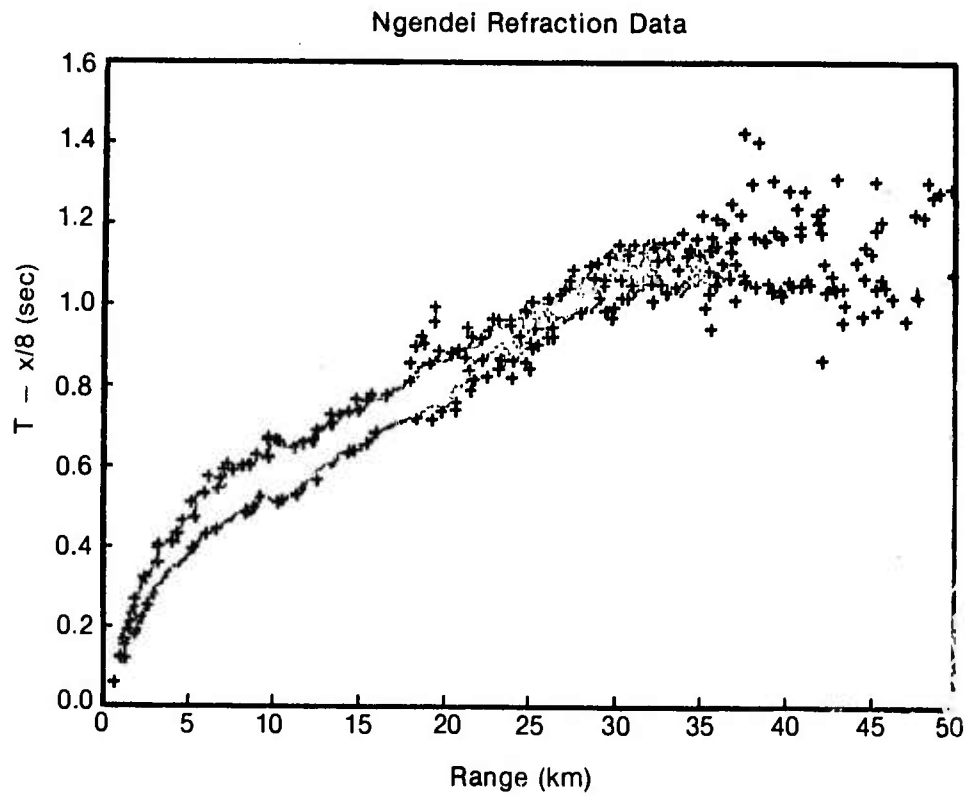


Figure 16. P-wave picks (totaling 1005) from the Ngendei refraction shooting. Topographic time and range corrections have been made and the travel-times reduced at 8 km/sec.

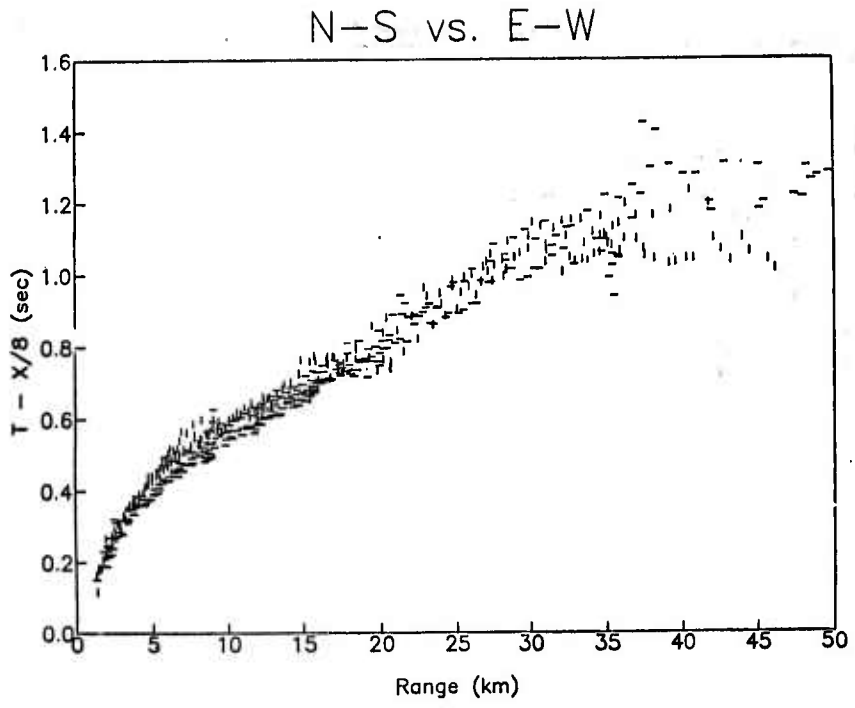


Figure 17(a). P-wave travel-times for shots at azimuths along a N–S line (shown as vertical bars) compared to shots at azimuths along an E–W line (shown as horizontal bars). Between about 5 and 15 km the E–W arrivals are early, while at ranges greater than 35 km, the N–S arrivals are early.

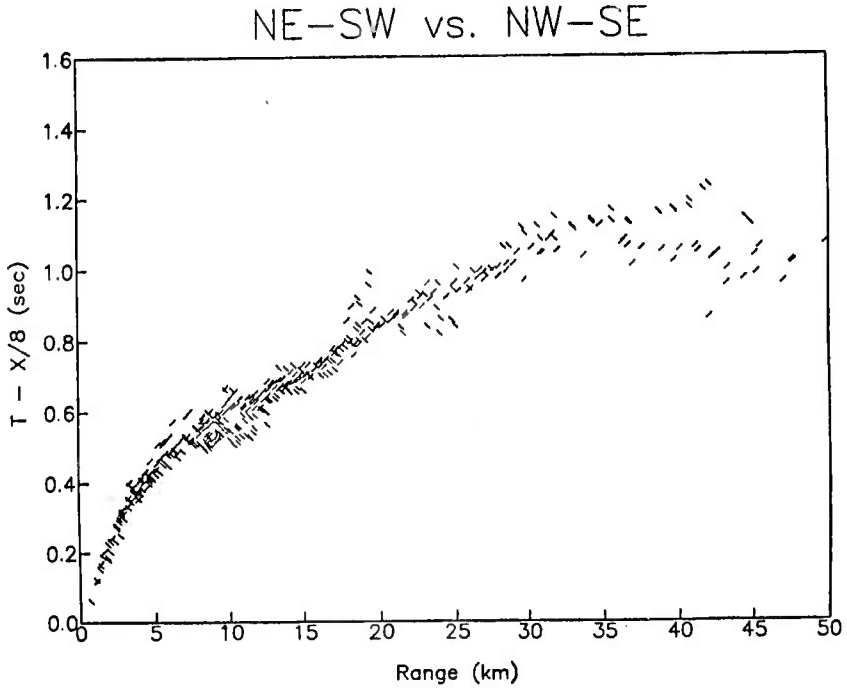


Figure 17(b). NE–SW shots (shown as diagonals to upper right) vs. NW–SE shots (shown as diagonals to lower right). NW–SE arrivals are early between about 6 and 17 km, while NE–SW arrivals are early at ranges greater than 35 km.

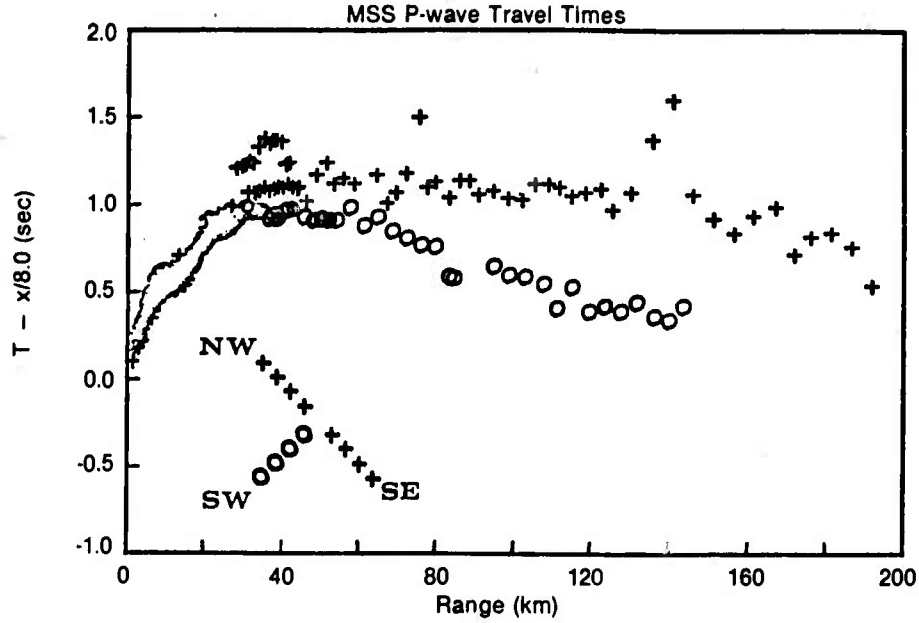


Figure 18. *P-wave travel-times as recorded by the MSS. Circles represent shots along a SW line, while crosses represent shots along a NW–SE line. Note the difference in upper mantle velocity.*

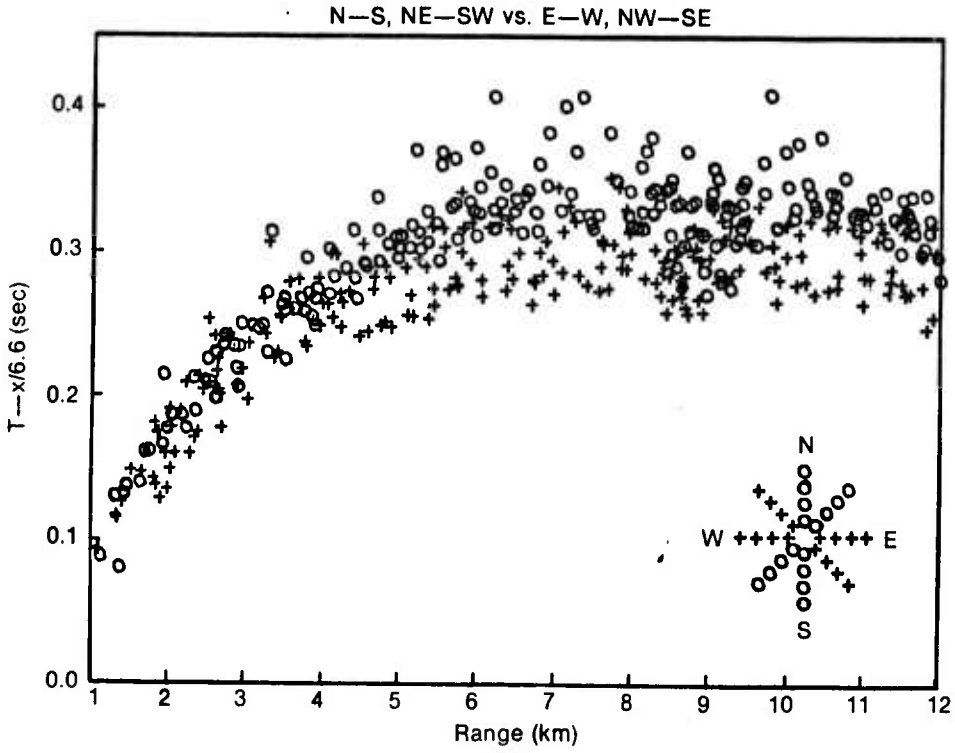


Figure 19. *A comparison of N–S, NE–SW arrivals (circles) with E–W, NW–SE arrivals (crosses) at ranges of 1 to 12 km. Arrivals from rays entering the sea floor at depths deeper than 5400 m have been eliminated because of scatter in the data and uncertainties in applying topographic corrections.*

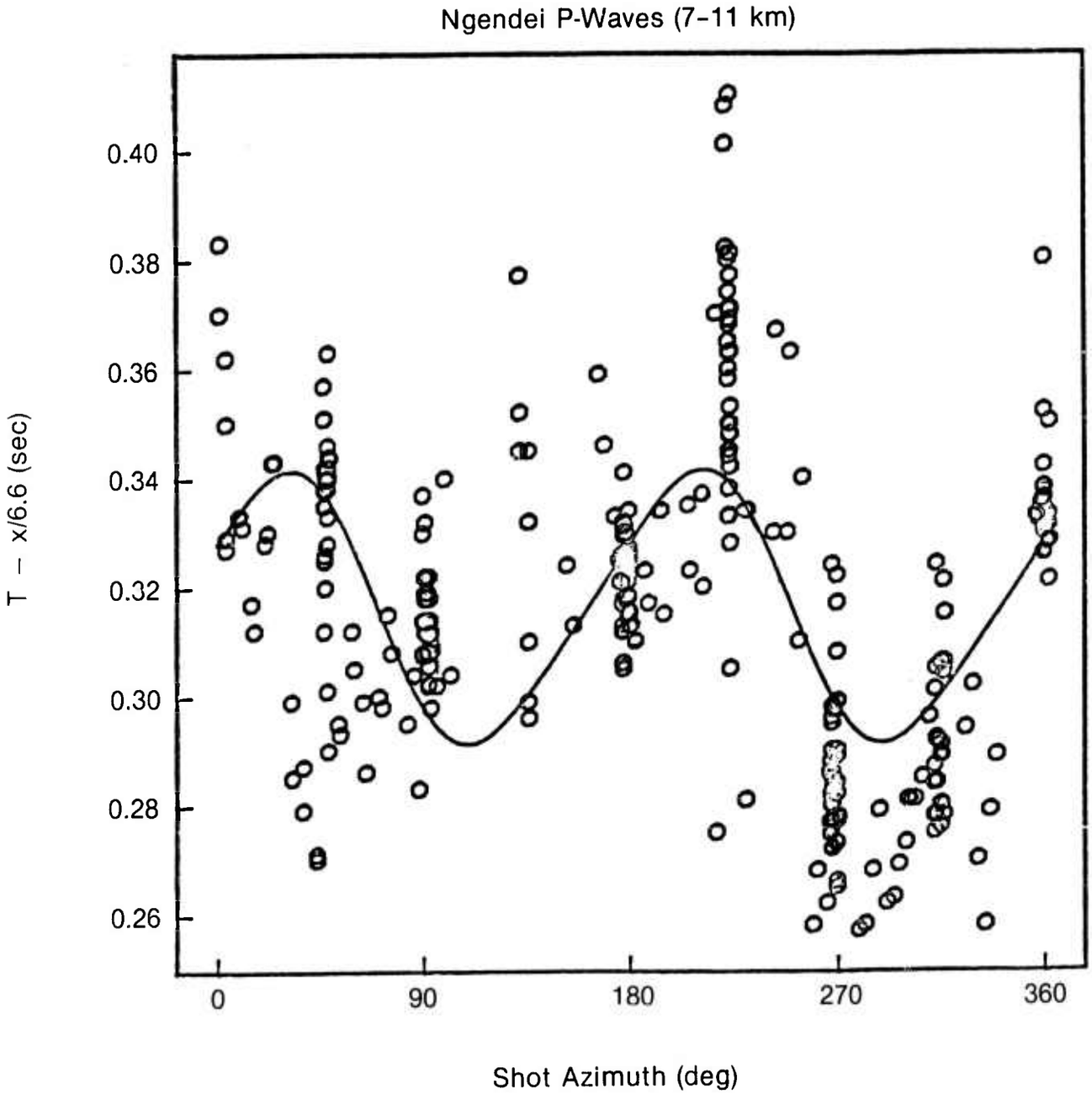


Figure 20. *Travel times vs. shot azimuth for shots at ranges of 7 to 11 km. All times have been reduced at 6.6 km/sec. Arrivals from rays entering the sea floor at depths shallower than 5400 m have been eliminated. Curve is least squares fit for a function of the form*

$$t = a_1 + a_2 \cos 2\theta + a_3 \sin 2\theta + a_4 \cos 4\theta + a_5 \sin 4\theta.$$

alignments represent data from the circular line. The data show considerable scatter, presumably representing lateral heterogeneities. However, some systematic azimuthal trends are apparent. Arrivals at azimuths of 0 to 45° (N–NE) and 180 to 225° (S–SW) are generally late, while arrivals at azimuths of 90 to 135° (E–SE) and 270 to 315° (W–NW) are generally early.

Backus (1965) derived an approximate expression for the velocity of p-waves traveling in a general weakly anisotropic medium

$$v^2 = a_1 + a_2 \cos 2\theta + a_3 \sin 2\theta + a_4 \cos 4\theta + a_5 \sin 4\theta$$

where

v = phase or group velocity of wave

θ = azimuth of wave propagation

As previously discussed, p-wave travel times are very insensitive to anisotropic ray deviation effects; thus, travel times at a particular azimuth are directly related to seismic group velocities at the same azimuth. To first order in the anisotropy, p-wave travel times which represent waves turning at approximately equal depths can be represented by a function of the form

$$t = a_1 + a_2 \cos 2\theta + a_3 \sin 2\theta + a_4 \cos 4\theta + a_5 \sin 4\theta$$

A curve of this type was fitted in a least squares sense to the travel-time data (see Fig. 20), reducing the variance of the data residuals (vs. residuals from the mean) by about 30%. The magnitude of the azimuthal travel-time differences is about 0.05 sec and the fast direction for the crustal anisotropy is N120°E.

It is difficult to assign confidence limits to a curve of this type since the leading alternative (non-anisotropic) explanation for the observed azimuthal variations is lateral heterogeneity. Because a hypothetical slow "blob" of crust will systematically affect many travel times, statistical confidence tests such as the f-test, which assume independence of the data, are not appropriate and would return unrealistically high confidence levels for the curve shown in Figure 20. We will simply say that anisotropy seems a simpler and less contrived explanation for the gross azimuthal trends in the data than lateral heterogeneity.

Figure 21 shows a similar plot for p-wave arrivals at mantle ranges, reduced at 8 km/sec. Although less data are available at these ranges, the anisotropy is quite clear. The curve shown is the least squares fit for a function of the form

$$t = a_1 + a_2 \cos 2\theta + a_3 \sin 2\theta$$

We did not include 4θ terms, which lead to wildly oscillatory fits (this is because the data are only present at approximate 45 degree increments, which can coincide with zero crossings in the 4θ terms). The curve reduced the variance of the data residuals by about 70%. The magnitude of the travel-time differences is about 0.3 sec while the inferred fast direction for the anisotropy is N30°E.

The travel-time data support anisotropy with a 2θ p-wave velocity dependence on azimuth at two levels in the oceanic lithosphere at the Ngendei site. The fast direction of the crustal anisotropy (N120°E) is orthogonal to the fast direction of upper mantle anisotropy (N30°E). The crustal anisotropy appears to occur at depths just above layer 3 of the oceanic crust.

Figure 22 shows a p-wave velocity profile of the oceanic lithosphere which satisfies the travel-time data. Such a model, while clearly not unique, demonstrates the features which are necessary to explain the azimuthal variations in travel times. A separate velocity profile is shown for each of two orthogonal azimuths. N30°E is approximately appropriate for the N–S and NE–SW lines, while N120°E is about right for the E–W and NW–SE lines. Figure 23 shows the travel-time curves for each model superimposed on the data for the associated refraction lines.

As can be seen in Figure 22, the two velocity models are identical in the uppermost crust, with velocities increasing from 4.3 km/sec at the surface to 5.2 km/sec at 0.75 km depth. This reflects the good agreement at all azimuths in the travel-time data at the closest ranges (see Fig. 19).

We model the crust between 0.75 km and 1.4 km with a velocity gradient also, but with a 0.4 km/sec offset between the two azimuths. The N30°E azimuth is slower, with velocities increasing from 5.4 km/sec at 0.75 km to 6.0 km/sec at 1.4 km. The N120°E azimuth is faster, with velocities increasing from 5.8 km/sec to 6.4 km/sec. The azimuthal differences in the velocity model reflect the azimuthal differences in slopes in the travel-time data between about 3 and 6 km (see Fig. 19).

The models are again identical between 1.4 and 7.4 km with velocities increasing from 6.6 to 7.5 km/sec. This

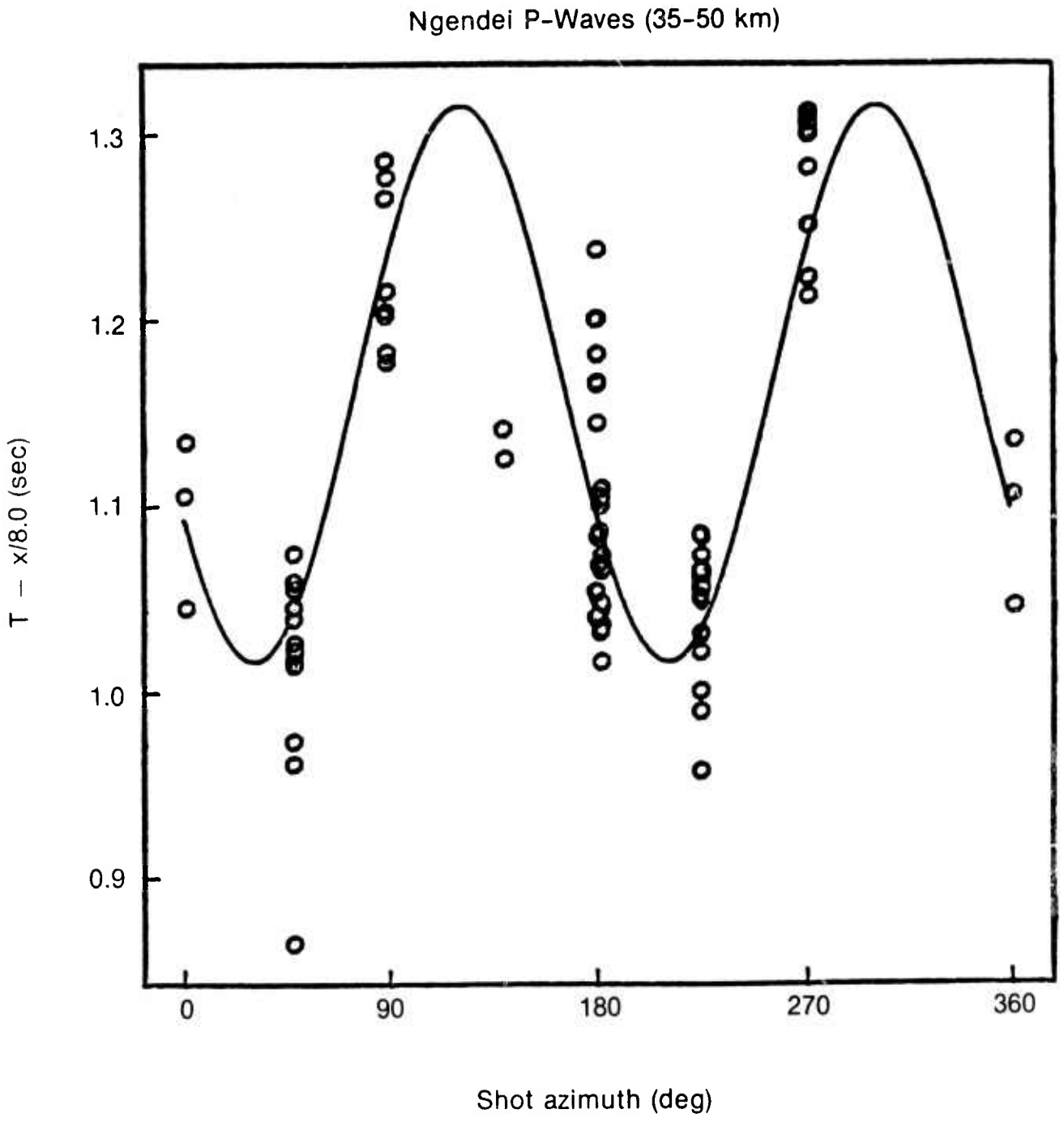


Figure 21. *Travel-time vs. shot azimuth for shots at ranges between 35 and 50 km. Times have been reduced at 8 km/sec. Arrivals from rays entering the sea floor at depths shallower than 5200 m have been eliminated. Curve is least squares fit for function of form*

$$t = a_1 + a_2 \cos 2\theta + a_3 \sin 2\theta$$

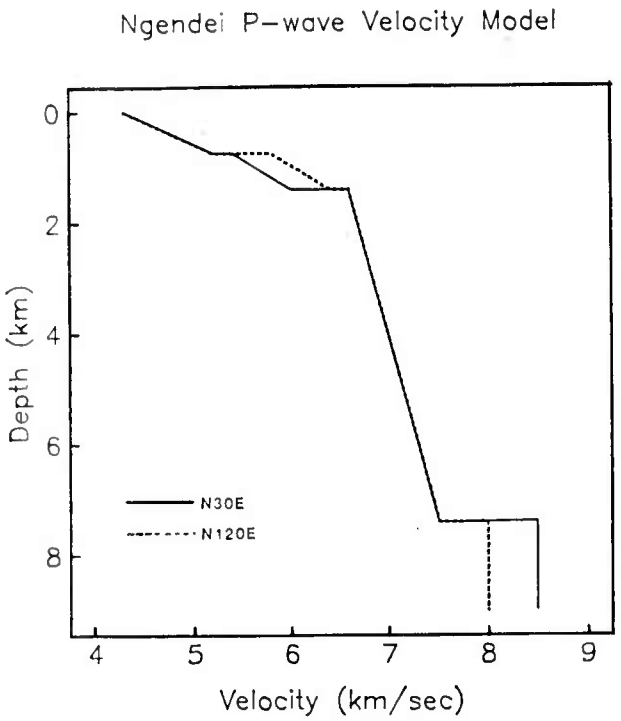


Figure 22. Anisotropic velocity vs. depth model which satisfies the Ngendei travel-time data. Solid line is velocity model at N30°E azimuth; dashed line is at N120°E azimuth.

shallow velocity gradient represents the relatively flat part of the travel-time data between about 7 and 30 km. The models again diverge at 7.4 km. The N30°E azimuth is faster with an upper mantle velocity of 8.5 km/sec. The N120°E azimuth is slower with an upper mantle velocity of 8.0 km/sec. This difference reflects the azimuthal difference in the travel-times at mantle ranges.

The travel-time curves based on this model (shown in Fig. 23) were calculated using a ray tracing program appropriate for an isotropic earth. In particular, it is assumed that the velocity at a given depth is not a function of ray parameter. This is not generally true within an anisotropic medium. However, for hexagonally symmetric anisotropy with a horizontal symmetry axis (which we will later claim is the most likely anisotropy model for both the crustal and upper mantle anisotropy) this type of ray tracing is approximately correct for rays near their turning points. We do not believe that using an anisotropic ray tracing program would result in significant changes to our model.

The gross shape of this velocity model agrees with previous models of the oceanic crust involving a steep velocity gradient in oceanic layer 2 and a shallow velocity gradient in layer 3 (Spudich and Orutt 1980). The non-uniqueness of inverting real travel-time data is well known, and we do not wish to place undue emphasis on this particular model, which was generated subjectively without the benefits of triplication constraints, amplitude modeling, or waveform analysis. However, we do think the model is useful because it demonstrates that a very simple velocity structure can explain the travel-time data. More sophisticated future models will differ from this model in detail, but presumably will share the more general characteristics.

These features include an isotropic velocity gradient in a surface layer, an anisotropic layer roughly corresponding to oceanic layer 2c, an isotropic layer corresponding to layer 3, and an anisotropic upper mantle. The upper mantle anisotropy is about 8.5 km/sec in the fast direction (N30°E) and about 8.0 km/sec in the slow direction. The absolute upper mantle anisotropic velocities are much better constrained (from the MSS data) than the crustal anisotropic velocities. The anisotropic velocity difference in the crustal layer is about 0.4 km/sec, with the fast direction approximately N120°E.

Ngendei Polarization Analysis

Only one of the two horizontal components of the MSS borehole seismometer was recorded, so unfortunately the MSS data are unsuitable for polarization studies. In addition, OBS Lynn and OBS Juan horizontal data are unusable. However, OBS Karen and OBS Suzy both recorded good horizontal data and all of the refraction shots were recorded by one of these two instruments. The OBS Pn arrivals are too weak for polarization analysis, so we will restrict our attention to the OBS crustal p-wave arrivals.

In order to obtain an idea of the size of the p-wave polarization anomalies that might occur at the Ngendei site, we simplified our crustal anisotropy model and considered a 0.75-km thick, 4.8-km/sec isotropic layer above a 5.7- to 6.1-km/sec anisotropic layer. We modeled the anisotropy as hexagonally symmetric with a 2θ azimuthal dependence ($\Gamma_{1111} = 37.21$, $\Gamma_{2222} = 32.49$, $\Gamma_{1212} = 10.97$, $\Gamma_{1122} = 12.91$, $\Gamma_{1313} = 6.86$ km^2 sec^{-2}). Figure 24 shows the resulting p-wave polarization anomalies for a receiver on the isotropic layer at ranges of 4 to 7 km (these ranges are not corrected to the sea floor). The polarization anomalies are purely a result of the ray path deviations discussed earlier and increase with range from the source. The maximum expected polarization anomaly at these ranges is about 2 degrees. We did not calculate polarization anomalies at ranges greater than 7 km because the initial p-wave arrivals at longer ranges represent rays turning beneath our anisotropic layer. These arrivals will exhibit polarization anomalies, but a more sophisticated ray tracing program is needed to calculate them.

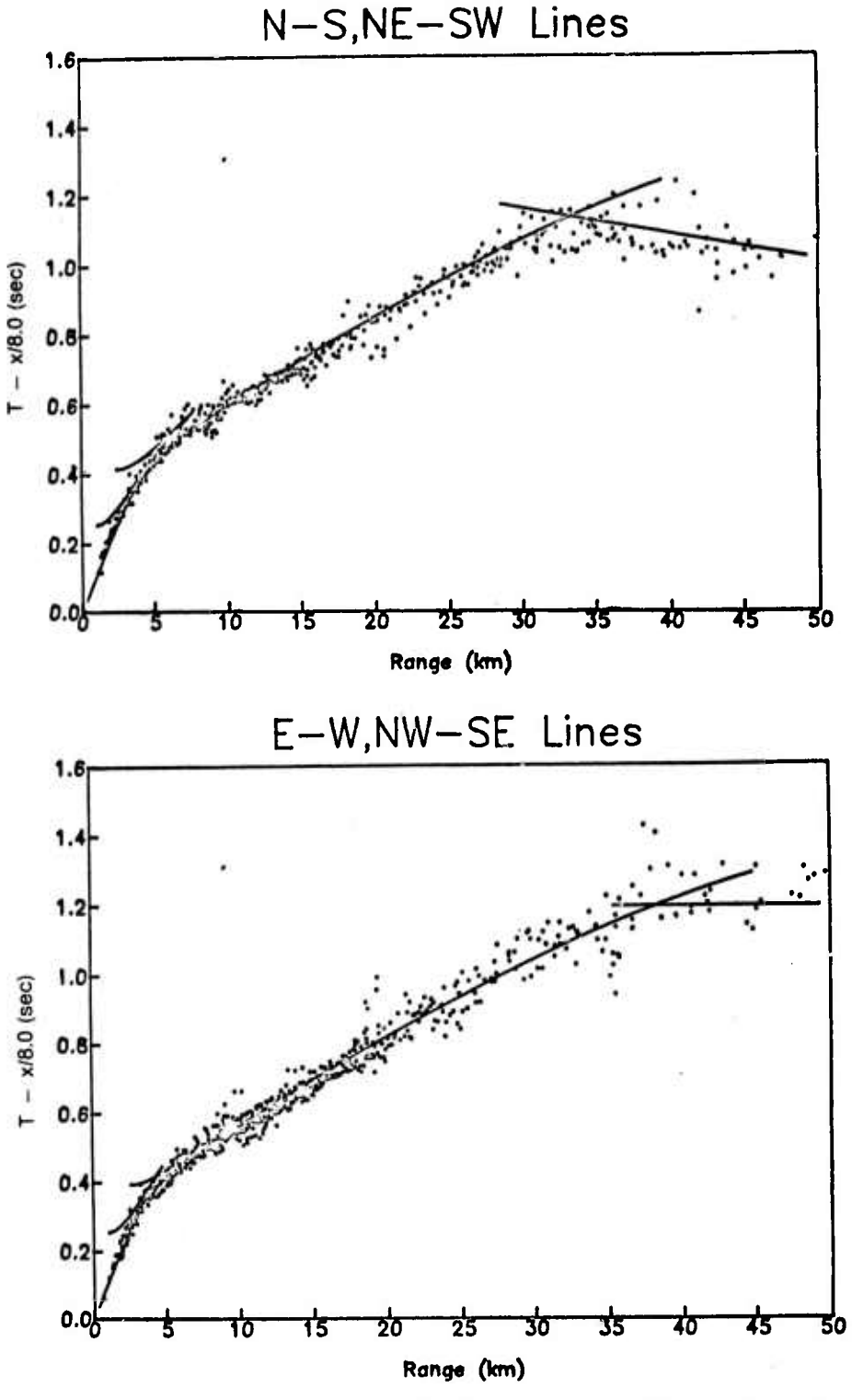


Figure 23. Travel-time curves calculated from model shown in Figure 22 superimposed on the data for
a. N–S, NE–SW azimuths
b. E–W, NW–SE azimuths

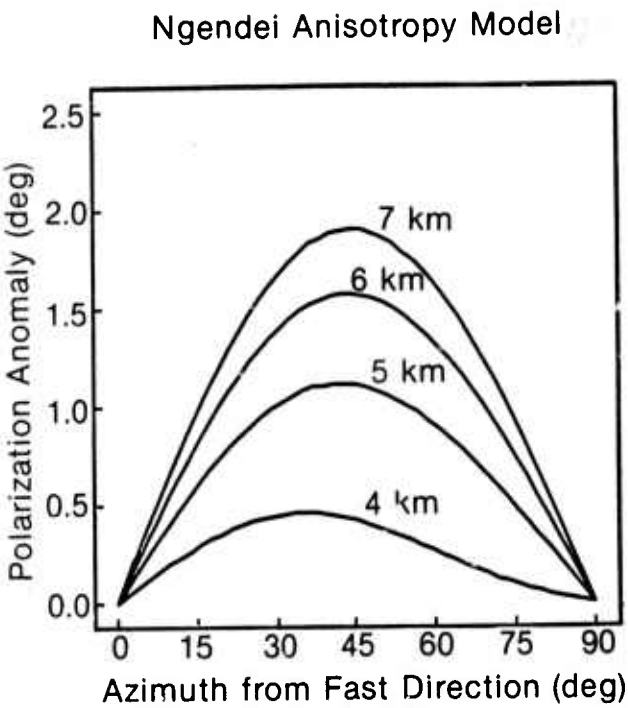


Figure 24. Predicted p-wave polarization anomalies for a simplified Ngendei model. Ranges are from source to receiver; equivalent ranges corrected to the sea floor are about 1.5 km closer. Positive anomalies represent deviations away from the fast direction in the anisotropy.

In order to compute p-wave polarization anomalies for the Ngendei OBS data we need to know the shot azimuth from the OBS, the absolute orientation of the OBS horizontal components, and the particle motion direction recorded by the OBS. The shot azimuths are the most easily computed. The CHALLENGER drill ship provided a fixed reference point to which sightings were made from the shooting ship. Since the OBS location was known relative to the CHALLENGER, these sightings, together with the OBS to shot ranges, allow the direct calculation of the OBS to shot azimuths. This approach is identical to the azimuth estimations used for the travel-time analysis and we estimate the uncertainty in the shot azimuths to be ± 2 degrees.

No direct measurement of the azimuths of the OBS horizontal components is possible since the OBS settles to the bottom at a random orientation. However, the orientation can be estimated from polarization analysis of the direct water waves recorded by the OBS. Since sound speed in the ocean is usually assumed to vary only in the vertical direction, the particle motion direction of the direct water wave at the OBS will be aligned with the shot azimuth. Thus, knowing the shot azimuth and the water wave polarization relative to the OBS horizontal components, we can calculate the absolute OBS horizontal orientation.

We used a method of polarization analysis from Kanasewich (1973) in which we form the covariance matrix between the horizontal channels. We assume that this matrix can be modeled as the sum of a directional signal and incoherent noise, and thus has the form

$$\begin{bmatrix} s^2 \cos^2\theta + n^2 & s^2 \sin\theta \cos\theta \\ s^2 \sin\theta \cos\theta & s^2 \sin^2\theta + n^2 \end{bmatrix}$$

where

θ = angle from OBS channel 2 to shot azimuth

s = amplitude of signal

n = amplitude of noise

This matrix has eigenvalues

$$\omega_1 = s^2 + n^2$$

$$\omega_2 = n^2$$

and eigenvectors

$$(\cos\theta, \sin\theta)^T$$

$$(-\sin\theta, \cos\theta)^T$$

We may also define a "rectilinearity" function

$$F(\omega_1,\omega_2) = 1 - \omega_2/\omega_1$$

which provides a measure of the degree of directionality of the signal. F varies between 0 and 1 with the endpoints respectively representing random noise and complete directionality.

In our water wave polarization analysis of the Ngendei OBS data, we windowed the horizontal time series for 0.1 sec after the initial water wave arrival. Many of the water wave arrivals were clipped and thus could not be used; however, the unclipped arrivals typically were very directional. Figure 25 shows the estimated channel 2 orientations for OBS Suzy and OBS Karen, based on unclipped water wave polarizations with $F \geq 0.95$.

The 182 water wave polarizations from OBS Karen (Fig. 25a) show considerable scatter, but there appear to

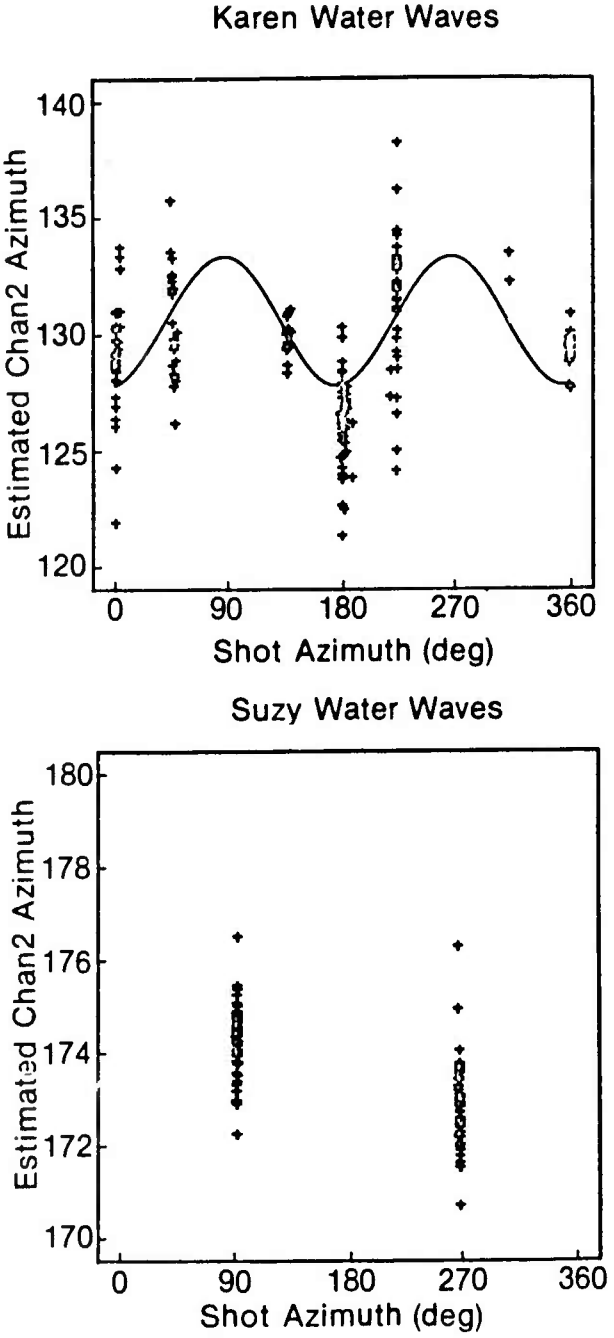


Figure 25. *(a) Estimated azimuth of channel 2 (first horizontal) for OBS Karen based on polarization analysis of unclipped direct water waves. The curve shown is the best least squares fit resulting from allowing the ratio of the gains of the two OBS horizontal components to vary. For the curve shown, the true channel 2 azimuth is 130.5 degrees and channel 3 (second horizontal) is 10% more sensitive than channel 2. (b) Estimated azimuth of channel 2 for OBS Suzy.*

be systematic variations of polarization direction as a function of shot azimuth. In p-wave polarization data, such variations might lead to hypotheses of anisotropy. However, in the case of water wave data, it is clear that there must be errors in either the calculated shot azimuths or the OBS horizontal response.

One possibility is that the horizontal gains of the OBS are slightly miscalibrated. This can lead to an apparent 2θ dependence in polarization anomalies (White and Whitmarsh, in press). In such a case we can express the relationship between the true channel 2 azimuth and the apparent channel 2 azimuth as

$$\tan(\phi' - \theta) = k \tan(\phi - \theta)$$

where

θ = shot azimuth

ϕ = channel 2 orientation

ϕ' = apparent channel 2 orientation

k = (channel 3 amplitude)/(channel 2 amplitude) for equal inputs

We solved for the unknowns k and ϕ using a non-linear least squares procedure. The curve shown in Figure 25a is the best fit for the OBS Karen water wave data (ϕ = 130.5 degrees, k = 1.10)—it reduces the variance of the data residuals (vs. residuals from the mean) by about 30%. However, systematic variations of a few degrees remain which are not explained by the differences in the horizontal gains.

These variations are also apparent in the 97 water wave polarizations from OBS Suzy (Fig. 25b). Since these polarization data are only available at shot azimuths separated by 180 degrees, we were unable to constrain the ratio of the horizontal gains. The mean channel 2 azimuth is 173.6 degrees, but there exists a slight difference between the polarizations at shot azimuths of 90 and 270 degrees.

The systematic polarization differences with shot azimuth for both OBS Suzy and OBS Karen are disturbing, since, ultimately, we want to use p-wave polarization data to look for anisotropic polarization anomalies. As we have seen, these anomalies are usually quite small—on the order of a few degrees. The water wave arrivals provide a null test of our ability to detect polarization anomalies, because direct water wave arrivals should not produce polarization anomalies. Since we do not have data

in common between OBS Suzy and OBS Karen, we cannot determine if the polarization differences that we observe are the result of inaccurate shot azimuths or variations in the OBS horizontal response.

The OBS p-wave arrivals were less directional than the water wave arrivals. We used the covariance matrix technique discussed earlier to determine polarizations for the first 0.2 sec of the p-wave arrival, including only those polarization directions with a F value greater than 0.80. We then calculated polarization anomalies based on the shot azimuths, channel 2 orientations, and the ratio of horizontal gains (we assumed k = 1.0 for OBS Suzy). These anomalies did not exhibit significant range dependence—anomalies for ranges between 1 and 12 km (ranges corrected to sea floor) are shown in Figure 26. The polarization anomalies are very scattered, with variations of roughly ±30 degrees.

The OBS Karen polarization anomalies appear randomly scattered while those from OBS Suzy have an apparent $\sin\theta$ azimuthal dependence. White and Whitmarsh (in press) noted a strong $\sin\theta$ term in their polarization data, which they ascribed to tilted horizontal seismometer components and/or dipping structures beneath the OBS. In our example, the lack of a similar variation in the OBS Karen data argues for the former explanation. The problem is complicated by the apparent difference between the OBS response to the direct water waves and the response to the p-waves. In addition, lateral heterogeneities in the crust can cause ray path deviations that will contribute scatter to the polarization data.

In any case, it is clear that anisotropic p-wave polarization anomalies of the magnitude predicted by the travel-time data (about 2 degrees) will be very difficult to observe with Ngendei OBS polarization data. We are studying this problem further to see what, if anything, can be learned about OBS response from p-wave and water wave polarization data, but we are not optimistic about use of OBS p-wave polarization data for observing anisotropy.

Interpretation of Ngendei Anisotropy

Magnetic and bathymetric data at the Ngendei site are currently insufficient to determine the original spreading direction (Menard, personal communication). Previous studies of Pacific upper mantle anisotropy have found that the fast direction in the upper mantle is parallel to the original spreading direction (see, for example, Raitt et al. 1969). Assuming that this is true at the Ngendei site, then

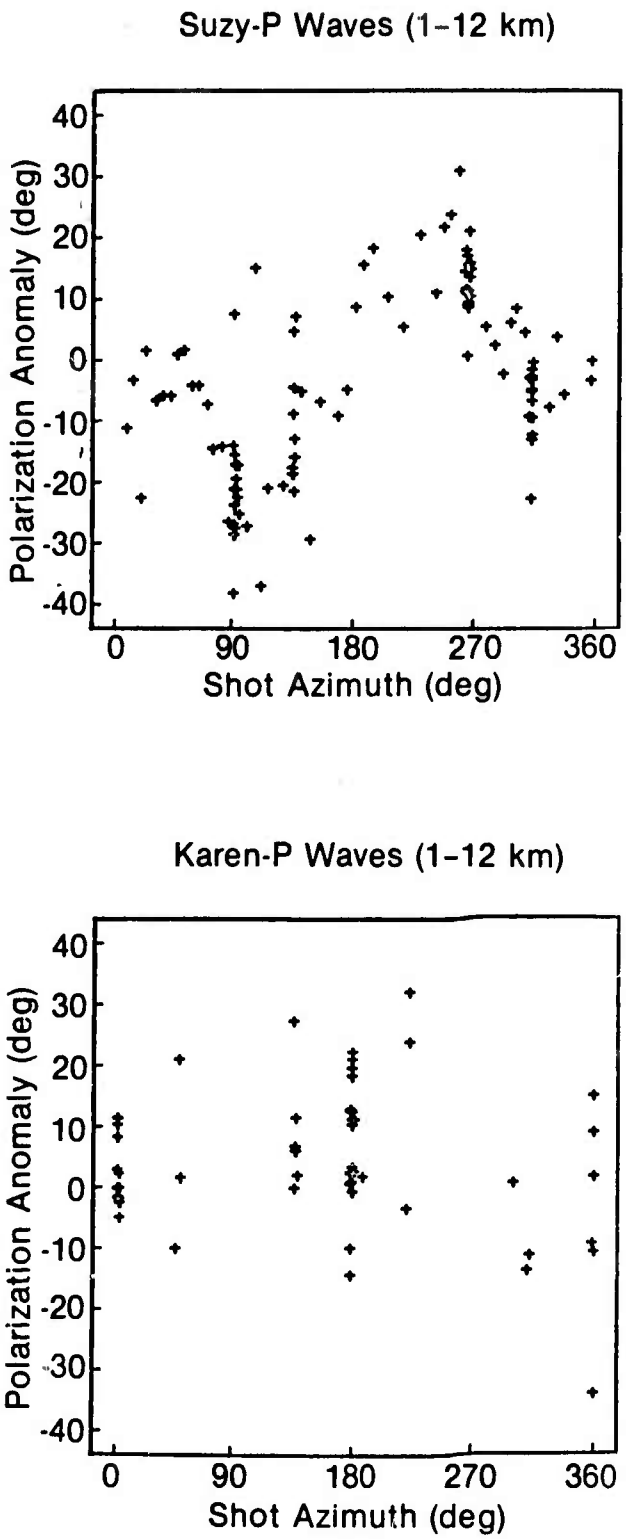


Figure 26. P-wave polarization anomalies for OBS a) Suzy and b) Karen at ranges (corrected to sea floor) of 1 to 12 km. Note the large scatter in the data.

the inferred fossil spreading direction is N30°E (of course with a 180 degree ambiguity). The fast direction in the crustal anisotropy is then perpendicular to this spreading direction.

Upper mantle anisotropy is usually explained by aligned olivine crystals (see, for example, Christensen 1984) which cause hexagonally symmetric anisotropy with a horizontal symmetry axis. Our observed upper mantle anisotropy (8.0 to 8.5 km/sec with a 2θ azimuthal dependence) is consistent with previous observations and undoubtedly results from the same cause.

The interpretation of our observed crustal anisotropy is not so straightforward. To our knowledge, while anisotropy has been hypothesized at the surface of the oceanic crust (Stephen 1981; White and Whitmarsh, in press) and in layer 3 (Christensen 1982; Christensen and Salisbury 1975) this is the first observation of layer 2c anisotropy.

Ophiolite models of the oceanic crust as well as recent drilling results (Anderson et al. 1982) indicate that layer 2c is composed of a sheeting dike complex. The dikes are approximately vertical and oriented parallel to the original spreading direction. Individual dikes are typically 0.5 to 2 m thick with a single chilled margin which is fine grained and glassy compared to the central part of the dikes. Laboratory velocity measurements of oriented cores 1.2 to 2.5 cm in diameter from ophiolite sheeted dike complexes have not indicated any velocity anisotropy (Salisbury and Christensen 1978; Christensen and Smewing 1981).

We wish to explain our observed layer 2c anisotropy in terms of a physical model based on what is known about the oceanic crust. For simplicity of calculation, we model the anisotropic crustal layer as a homogeneous section in which the p-wave velocity varies with azimuth from 5.7 to 6.1 km/sec. Thus, we seek to explain an anisotropic velocity variation of 5.9 ± 0.2 km/sec (about a 7% total difference) in which the fast direction is parallel to the sheeted dikes in layer 2c. Clearly, these figures are approximate but anisotropy of roughly this magnitude will be necessary to fit the travel-time data. One possible source for anisotropy is preferred crystal orientation in a material. However, if this was present in oceanic sheeted dikes, it seems probable that it would be observable in ophiolites. The lack of observed crystal alignments or velocity anisotropy in samples from ophiolite sheeted dikes (Salisbury and Christensen 1978; Christensen and Smewing 1981) suggests that preferred crystal orientation is not responsible for our observed layer 2c anisotropy.

Another possible type of anisotropy is thin, alternating layers of isotropic material of different velocities. At wavelengths long compared to the layer spacing, this results in effective anisotropy with an axis of hexagonal symmetry perpendicular to the layers. This is called periodic thin-layered (PTL) anisotropy and relationships between layer parameters and the effective anisotropic elastics constants have been theoretically derived (see, for example, Backus 1962) and experimentally tested (Melia and Carlson 1984). If the isotropic layers are vertical, then p-waves travelling within a horizontal plane will typically exhibit a 2θ azimuthal velocity dependence, with the fast direction parallel to the layers.

Since our observed anisotropy is 2θ dependent with the fast direction parallel to the sheeting dikes within layer 2c, PTS anisotropy would seem to be a good candidate to explain our observations. Certainly the dikes are much thinner than typical wavelengths in seismic refraction experiments. The difficulty with this explanation is that although the observed anisotropy and that predicted from modeling a sheeted dike complex agree very well in phase, they don't agree in amplitude. With PTL anisotropy, very large velocity differences in the isotropic velocities between layers are necessary to generate even small azimuthal velocity variations at large wavelengths. Realistic models of oceanic sheeted dike complexes do not include such large velocity variations.

For example, we might generously assume that chilled dike margins impose 10% of the volume of the sheeted dikes, and have a p-wave velocity 0.3 km/sec slower than the central part of the dikes (Salisbury, personal communication). Modeling the sheeted dike complex as alternating layers of 1 unit thick, 5.7 km/sec chilled margin material and 9 unit thick, 6.0 km/sec central dike material, and assuming a Poisson's ratio of 0.29 (p-wave result is very insensitive to choice of Poisson's ratio) we calculate an anisotropic p-wave velocity variation of 5.970 to 5.968 km/sec, or about 0.03%. This is over 200 times smaller than the 7% velocity anisotropy that we are trying to explain. Clearly, isotropic velocity variations within the sheeted dike complex itself are inadequate to account for the observed anisotropy.

PTL anisotropy is largest when the alternating layers have equal thickness (Backus 1962); thus, we can generate more anisotropy than in the chilled margin example if we consider the possibility of velocity differences between individual dikes of equal thickness. Velocity measurements of sheeted dike complexes in ophiolites typically show scatter of about 0.2 km/sec. If we assume that these variations are largely the result of velocity differences between

dikes, and create a model of a sheeted dike complex consisting of alternating layers of 5.7-km/sec and 6.1-km/sec material, we calculate anisotropic p-wave velocity variations of 5.901 to 5.890 km/sec. This velocity anisotropy of about 0.19% is over 35 times smaller than our observed 7% anisotropy. Clearly, isotropic velocity variations within the sheeted dike complex itself are inadequate to account for the observed anisotropy.

Another possibility is PTL anisotropy in a transition zone between layers 2b and 2c. In this region individual dikes might intrude into the lower velocity overlying basalt. This could provide a greater velocity difference between layers than the previous examples. If we assume that this transition zone consists of alternating vertical layers of 4.7-km/sec and 5.9-km/sec material, we could generate p-wave anisotropy of 5.20 to 5.31 km/sec (about 2%). This is still too small to explain our observed 7% anisotropy. Further, this transition zone would be restricted to the top of layer 2c and would be relatively thin. A borehole section into layer 2c near the Costa Rica Rift indicated a transition zone of about 200-m thickness (Anderson et al. 1982). Thus, anisotropy within the transition zone alone would need to be much greater than the 7% anisotropy previously discussed (based on modeling anisotropy throughout layer 2c) in order to explain the offset in the travel-times.

Thus, we must conclude that PTL anisotropy is not a viable explanation for our observed layer 2c anisotropy. The probable velocity contrasts between layers within the sheeted dike complex are simply too small to generate anisotropy of the required magnitude.

Another possible cause for anisotropy is preferred crack orientation, which some authors (Stephen 1981; White and Whitmarsh, in press) have suggested is responsible for generating marine crustal anisotropy. Randomly placed cracks of similar orientation can generate hexagonally symmetric anisotropy in an otherwise isotropic medium. Large porosities are not required to generate substantial anisotropy. Anderson et al. (1974) studied oriented, disc shaped, ellipsoidal, fluid filled zones within an isotropic matrix, and, using a method developed by Eshelby (1957), calculated anisotropic seismic velocities as a function of the velocities and porosity of the matrix, the parameters of the ellipsoids, and the bulk modulus of the fluid. These calculations indicated substantial p-wave anisotropy even for porosities as low as 1%.

For example, granite containing aligned ellipsoidal cracks (aspect ratio of 20) filled with sea water (bulk modulus of 20 kbar) with a crack density corresponding to 1% porosity will have a p-wave velocity anisotropy of 5.85 to 6.50 km/sec, or about 10% (Fig. 1, Anderson et al. 1974). The velocities have a 2θ dependence upon direction with the slow direction along the symmetry axis of the ellipsoidal disks. If the cracks are dry, the amplitude of the anisotropy is slightly greater. Porosities within layer 2c have been measured at 1 to 3% with very little fracture porosity (Becker et al. 1982). These porosities, although quite low, do not exclude the possibility of crack anisotropy of this type.

Garbin and Knopoff (1973, 1975) examined the case of oriented circular cracks of effectively zero thickness. This can be considered as the limit of the Anderson et al. calculations for ellipsoids of infinite aspect ratio. Anisotropy based on cracks of this type does not require any porosity at all in the host matrix. Garbin and Knopoff considered two different boundary conditions at the cracks. In one, corresponding to the fluid filled case, they assumed that the normal compressional component of stress is continuous and the normal shear component of stress vanishes at the crack boundary. In the other, corresponding to the dry crack case, all components of the normal stress vanish at the boundary.

Crampin (1978) used the Garbin and Knopoff results to calculate seismic velocities as a function of direction for materials with various crack densities. Again, p-wave velocity anisotropy can be substantial. For example, an isotropic matrix with p-wave velocity of 5.8 km/sec and a crack density $\epsilon = 0.1$ ($\epsilon = Na/V$, number N of cracks of radius a in volume V) will have p-wave velocities varying from about 4.6 to 5.8 km/sec for dry cracks and from about 5.6 to 5.8 km/sec for saturated cracks (Fig. 1a, 2a, Crampin 1978). For the dry crack example, the p-wave velocities are 2θ dependent with fast directions aligned with the cracks and the slow direction normal to the cracks. For saturated cracks, the velocities are 4θ dependent with fast directions both normal to and aligned with the cracks, and slow directions at 45 degrees to the crack normal.

This 4θ velocity dependence seems surprising, at least to the authors, but is a necessary consequence of the Garbin and Knopoff boundary conditions for saturated cracks of effectively zero thickness. Since normal stresses and displacements are continuous across the liquid filled cracks, the cracks can only make their presence felt when there is shear across them. Compressional waves traveling both orthogonal and parallel to the cracks will not generate any shear stress across the cracks and will be unaffected by them. This is why the p-wave velocities are identical for these waves. However, p-waves traveling at angles between 0 and 90 degrees from the crack normal will generate shear across the cracks and will be slowed

These unusual boundary conditions give rise to the 4θ velocity dependence with velocity maxima both normal to and aligned with the cracks.

Our observed layer 2c p-wave anisotropy has a 2θ velocity dependence, so we can eliminate the possibility of saturated cracks of the Garbin and Knopoff type. It seems probable that any cracks in layer 2c will be wet. This conclusion is supported by the good agreement of in situ porosity measurements in layer 2c from DSDP Hole 504B and the shipboard measurements of porosity (Becker et al. 1982). The in situ measurements are based on electrical resistivity within the rock and assume a sea water pore fluid, while the shipboard observations directly measure the fluid content of the rock. These measurements do not exclude the possibility of additional dry porosity, but the measured porosity must be wet. Assuming that all the porosity is fluid filled, we can eliminate the dry crack models from further consideration.

The Anderson et al. (1974) model of fluid filled cracks is the most reasonable model which can explain our observed crustal anisotropy. It requires the presence of cracks throughout layer 2c, oriented parallel to the sheeted dikes. Such cracks could have formed from tensional stress associated with the initial cooling of the dikes. The lack of observable anisotropy in oriented cores from ophiolite sheeted dikes indicates that these cracks may be cemented during ophiolite emplacement, or that they may be on too large a scale to affect velocities within a small core sample.

Observing Anisotropy with Seismic Refraction Experiments

We have discussed two ways in which p-wave anisotropy might be observed in typical seismic refraction experiments. These methods involve the measurement of azimuthal differences in travel-times and p-wave polarization anomalies. In most situations, we believe that travel-time analysis provides a more robust, less ambiguous, and more convenient way of measuring anisotropy than polarization analysis.

Seismic ray paths can be perturbed both by anisotropy and by lateral heterogeneities. To first order, p-wave travel-times are insensitive to these ray path perturbations, but p-wave polarization anomalies are directly affected. Travel-times can be measured with a single seismometer, while polarization measurements require either a small array of seismometers or horizontal components. In practice, this has limited marine polarization measurements to the sea floor, using either an OBS or borehole seismometer. In these circumstances, orienting the horizontal channels and calibrating gains is difficult. While approximate horizontal orientation and calibration can be derived from direct water wave arrivals at an OBS, no such procedure is available for borehole seismometers. This is a significant problem, since even a small difference in gain between the horizontal channels will lead to large apparent 2θ polarization anomalies. OBS polarization observations also suffer from unknown effects of OBS to sea floor coupling, which can lead to strange results in horizontal observations (Shearer and Orcutt 1982; Sutton et al. 1984). Taking all this into consideration, it is not surprising that the Ngendei p-wave polarization observations were unable to confirm the crustal anisotropy which was clearly resolved in the travel-time data. We believe that this will generally be true—seismic travel-times will measure anisotropy more clearly than polarization analysis.

Adequate azimuthal coverage is very important for both travel-time and polarization analysis. At a minimum, data should be available at increments of 45 degrees (even closer if 4θ anisotropy is suspected) and lines should be reversed in order to minimize the effects of dipping structures. For example, the 2θ dependent, 4.0 to 5.5 km/sec anisotropy hypothesized by Stephen (1981) for the upper oceanic crust should easily be observable in seismic travel-times. Unfortunately, the two orthogonal lines which were shot at this site are 45 degrees from the symmetry axis of the anisotropy, and thus cannot help constrain the magnitude of the anisotropy (each line indicated surface p-wave velocities of 5.0 ± 0.25 km/sec). Closer azimuthal spacing of refraction lines would eliminate problems of this type.

Summary

Observations of anisotropy are becoming increasingly important in seismology because of the directional information that they provide. Deep anisotropy is probably related to processes of mantle convection, while shallow anisotropy likely results from surface tectonics. Oceanic observations are particularly significant because they can be directly compared with plate tectonics models.

The 1983 Ngendei expedition to the South Pacific detected anisotropy both in the upper mantle and within an upper crustal layer. The upper mantle anisotropy agrees with previous observations and suggests that the original spreading direction at the Ngendei site was N30° E. The crustal anisotropy appears to be related to sheeted dike complexes within layer 2c, and is most likely caused by oriented cracks. No anisotropy was detected at the surface of the crust or within layer 3.

These observations are based on p-wave travel-time analysis, which can be used directly to measure anisotropy. P-wave polarization analysis has the potential to detect anisotropy, but care should be used in interpreting polarization anomalies. Anisotropic ray path deviations contribute significantly to polarization anomalies within anisotropic media, and can also cause polarization anomalies on overlying isotropic media. Polarization anomalies are typically range-dependent, and the nature of this range dependence can provide constraints on the depth and magnitude of anisotropy.

References

Aki, K. and Richards, P., 1980. *Quantitative seismology, theory and methods*, W. H. Freeman.

Anderson, R.N., Honnorez, J., Becker, K., Adamson, A.C., Alt, J.C., Emmermann, R., Kempton, P.D., Kinoshita, H., Laverne, C., Mottl, M.J. and Newmark, R. L., 1982. DSDP Hole 504B, the first reference section over 1 km through Layer 2 of the oceanic crust, *Nature*, 300, 589–594.

Anderson, D.L., Minster, B. and Cole, D., 1974. The effect of oriented cracks on seismic velocities, *J. Geophys. Res.*, 79, 4011–4015.

Backus, G.E., 1962. Long-wave elastic anisotropy produced by horizontal layering, *J. Geophys. Res.*, 67, 4427–4440.

Backus, G.E., 1965. Possible forms of seismic anisotropy of the uppermost mantle under oceans, *J. Geophys. Res.*, 70, 3429–3439.

Bamford, D., 1977. Pn velocity anisotropy in a continental upper mantle, *Geophys. J.R. Astro. Soc.*, 49, 29–48.

Bamford, D., Jentsch, M. and Prodehl, C., 1979. Pn anisotropy studies in northern Britain, and in the eastern and western United States, *Geophys. J.R Astro. Soc.*, 57, 397–429.

Becker, K., Von Herzen, R.P., Francis, T.J.G., Anderson, R.N., Honnorez, J., Adamson, A.C., Alt, J.C., Emmermann, R., Kempton, P.D., Kinoshita, H. Laverne, C., Mottl, M.J. and Newark, R.L., 1982. In situ electrical resistivity and bulk porosity of the oceanic crust Costa Rica Rift, *Nature*, 300, 594–598.

Christensen, N.I., 1972. Seismic anisotropy in the lower oceanic crust, *Nature*, 237, 450–451.

Christensen, N.I., 1984. The magnitude, symmetry and origin of upper mantle anisotropy based on fabric analysis of ultramafic tectonites, *Geophys. J.R. Astro. Soc*, 76, 89–111.

Christensen, N.I. and Salisbury, M.H., 1975. Structure and constitution of the lower oceanic crust, *R. Geophy. Space Phys.*, 13, 57–86.

Christensen, N.I. and Smewing, J.D., 1981. Geology and seismic structure of the northern section of the Oman Ophiolite, *J. Geophys. Res.*, 86, 2545–2555.

Crampin, S., 1978. Seismic-wave propagation through a cracked solid: polarization as a possible dilatancy diagnostic, *Geophys. J.R. Astro. Soc.*, 53, 467–496.

Crampin, S., 1981. A review of wave motion in anisotropic and cracked elastic-media, *Wave Motion*, 3, 343–391.

Crampin, S., 1982. Comments on "possible forms of anisotropy of the uppermost mantle under oceans" by George E. Backus, *J. Geophys. Res.*, 87, 4636–4640.

Crampin, S., Stephen, R.A. and McGonigle, R., 1982. The polarization of p-waves in anisotropic media, *Geophys. J.R. Astro. Soc.*, 68, 477–485.

Eshelby, J.D., 1957. The determination of the elastic field of an ellipsoidal inclusion and related problems, *Proc. Roy, Soc. Ser. A*, 241, 376–396.

Garbin, H.D. and Knopoff, L., 1973. The compressional modulus of a material permeated by a random distribution of circular cracks, *Q. appl. Math.*, 30, 453–464.

Garbin, H.D. and Knopoff, L., 1975. The shear modulus of a material permeated by a random distribution of circular cracks, *Q. appl. Math.*, 33, 296–300.

Garbin, H.D. and Knopoff, L., 1975. Elastic moduli of a medium with liquid filled cracks, *Q. appl. Math.*, 33, 301–303.

Jordan, T.H., Orcutt, J.A., Menard, H.W. and Natland, J., 1983. Ngendei seismic experiment: tele-seismic and noise studies, *EOS*, 64, 269.

Kanasewich, E.R., 1973. *Time series analysis in geophysics*, University of Alberta Press, pp 364.

Melia, P.J. and Carlson, R.L., 1984. An experimental test of p-wave anisotropy in stratified media, *Geophysics*, 49, 374–378.

Menard, H.W., Jordan, T.H., Natland, J.H. and Orutt, J.A., 1983. Tectonic evolution of the southwestern tropical Pacific basin, *EOS*, 64, 315.

Orcutt, J.A., Jordan, T.H., Menard, H.W. and Natland J., 1983. Ngendei seismic experiment: refraction and reflection studies, *EOS*, 64, 269.

Pallister, J.S., 1981. Structure of the sheeted dike complex of the Samail Ophiolite near Ibra, Oman, *J. Geophys. Res.*, 86, 2661–2672.

Raitt, R.W., Shor, G.G., Francis, T.J.G. and Morris, G.B., 1969. Anisotropy of the Pacific upper mantle, *J. Geophys. Res.*, 74, 3095–3109.

Salisbury, M.H. and Christensen, N.I., 1978. The seismic velocity structure of a traverse through the Bay of Islands Ophiolite complex, Newfoundland, an exposure of oceanic crust and upper mantle, *J. Geophys. Res.*, 83, 805–817.

Shearer, P. and Orcutt, J., 1982. Use of horizontal component data from ocean bottom seismographs, *EOS*, 63, 1025.

Spudich, P. and Orcutt, J., 1980. A new look at the seismic velocity structure of the oceanic crust, *Rev. Geophys. Space Phys.*, 18, 627–645.

Spudich, P. and Orcutt, J., 1980. Petrology and porosity of an oceanic crustal site: Results from wave form modeling of seismic refraction data, *J. Geophys. Res.*, 85, 1409–1433.

Stephen, R., 1981. Seismic anisotropy observed in upper oceanic crust, *Geophy. Res. Lett.*, 8, 865–868.

Sutton, G.H., Duennebier, F.K., Iwatake, B., Tuthill, J.D., Lewis, B.T.R. and Ewing, J., 1984. An overview and general results of the Lopez Island Experiment, *Mar. Geophys. Res.*, 5, 3–34.

White, R.S. and Whitmarsh, R.B. in press. An investigation of seismic anisotropy due to cracks in the upper oceanic crust at 45N, Mid-Atlantic Ridge, *Geophys. J.R. Astro. Soc.*, in press.

III. Project status

A. Background

The MSS program was a DARPA-sponsored plan for developing, installing, and operating a broadband, triaxial, ocean-bottom borehole seismometer station similar in capabilities to the land-based Seismic Research Observatories. The basic objective of the MSS program was to develop a large package of sensitive seismic instruments that would be implanted in a subocean-bottom borehole. The BIP would be deployed into the basalt layer of the ocean subfloor in water depths as great as 20,000 ft. The necessary deployment and support equipment would be developed concurrently with the BIP.

Whereas developing the BIP and its associated equipment was a function of the MSS team, the program relied on the NSF-sponsored Deep Sea Drilling Project and the D/V GLOMAR CHALLENGER for drilling boreholes and equipment deployment (see Appendix A for a brief description of the GLOMAR CHALLENGER). Deep boreholes were to be drilled through the sediments and into the basalt layer and cased to the top of the basalt layer, using existing DSDP technology. Procedures required for lowering a large instrument package external to the drill pipe were devised because previous DSDP borehole deployments were through the pipe bore (ID 4.25 inches). A reentry subassembly carrying the BIP would be used to stab into a reentry cone previously installed in the borehole (Configuration I).

The MSS experiments were not scheduled as a unique program for priority support by the DSDP. Instead, the MSS deployments were injected into the existing DSDP schedule, which resulted in finite block times or timeframes wherein MSS installations could be performed as part of a regular DSDP cruise. The tight, inflexible schedule, as well as the organizations involved, resulted in a formidable task with regard to overall project coordination.

Because the GLOMAR CHALLENGER might not be available for all MSS borehole deployments, the need for an alternate borehole reentry technique was identified. Therefore, near-term plans called for a deepwater-cable-guided reentry technique that would use a ship-of-opportunity (Configuration II).

Although the NSF deep-sea drilling team had repeatedly demonstrated deep-sea drilling and borehole reentry techniques, the MSS program introduced uncertainties with regard to deep-ocean reentry impacts with a sensitive instrument package, controlled lowering of the package within a borehole, and the potential for entanglement of the instrument package electromechanical cable and the drill string. Accordingly, the initial MSS operation was planned as an at-sea test to

- demonstrate deep-ocean borehole emplacement of a large instrument package external to the drill string,
- define handling and reentry shock levels imposed on the BIP,
- examine the potential for cable/drill pipe entanglement,
- determine whether the sensor state-of-health monitoring function can perform within design limits in a borehole environment,
- compare borehole seismometer signals and noise levels with similar signals recorded on conventional ocean bottom seismometers.

The overall MSS deployment program included the following major operational elements.

- MSS-81: An at-sea test using an existing mid-Atlantic DSDP borehole to demonstrate the feasibility of BIP deployment using the drill string reentry technique (Configuration I), and to determine the basic capabilities of the seismic sensor when deployed in a deep ocean borehole (March 1981).
- MSS-82: A Configuration I deployment in the Northwest Pacific for emplacement of a BIP, along with ocean-bottom support equipment, and emplacement of an ocean subbottom seismometer (August 1982).
- MSS-83: A Configuration I deployment in the South Pacific, along with ocean-bottom support equipment in early 1983.

NORDA, a field activity of the Chief of Naval Research, directed the MSS program. Global Marine Development, Inc. was the engineering contractor. Site preparation and deployment using the GLOMAR CHALLENGER were functions of the DSDP. The downhole instruments were designed and built by Teledyne Geotech, Inc. Other developments, contributing studies, and evaluations were performed by a number of organizations, including Gould, Inc., Raytheon and Sierra Geophysics, Inc. Representatives from NORDA, Global Marine Development, Teledyne Geotech, and Gould embarked in the GLOMAR CHALLENGER and participated in each MSS deployment.

B. Progress to date

1. MSS-81

In March 1981, the feasibility of borehole installation of large instruments carried in a package external to the drill string was successfully demonstrated. The instrumentation package was deployed into an existing 2178-ft borehole at a sea depth of 14,708 ft in the North Atlantic (DSDP site 395A). No major problems were encountered in drill string deployment, reentry, and subsequent recovery of the BIP. Equipment handling and deployment procedures were verified, and the BIP recorded high-quality seismic data. A limited data sample was obtained from one OBS. Primary operations support was provided by the GLOMAR CHALLENGER. Additional support was provided by the USNS LYNCH.

2. MSS-82

The MSS-82 operation, conducted in August–September 1982, was unsuccessful. Due to a combination of drilling equipment failures and adverse weather, the GLOMAR CHALLENGER was not able to establish a cased borehole in the Northwest Pacific area (DSDP site 581). Unsuccessful attempts were made to set casing in each of two boreholes. A Hawaii Institute of Geophysics ocean subbottom seismometer (OSS) was successfully deployed through the drill-pipe bore in a third, uncased, nonreenterable borehole. Based on MSS-81 experience, several MSS equipment designs and modifications were developed for the MSS-82 operation. Neither the modified equipment nor a BPP unit and its associated recovery and reinstallation system were evaluated. The participating support ship was the USNS DESTEIGUER.

3. MSS-83

The MSS-83 operation was conducted successfully at a site in the South Pacific (DSDP site 595). In January–February 1983, the GLOMAR CHALLENGER drilled and cased a reentry borehole in about 18,500 ft of water. The BIP was deployed and 5 days of seismic testing were accomplished. Subsequently a BPP and its associated installation, recovery, and reinstallation mooring system were deployed. During March 1983, the R/V MELVILLE, the participating support ship, returned to the site, recovered the BPP, and deployed a dummy BPP.

IV. Operations

A. MSS-81 operations

1. Summary

In March 1981, vertical seismometers in a large instrument package carried external to the drill string were deployed in an existing borehole near the mid-Atlantic Ridge at 22°45.34′N, 46°04.90′W. Deployment and recovery operations support was provided by the D/V GLOMAR CHALLENGER. Additional support was provided by the USNS LYNCH. The sea depth at the deployment site was 14,708 ft; original borehole depth was 2178 ft, 1873 ft of which were in basement rock. This instrument package emplacement was intended as a test of the procedures and equipment to be used during the 1982 emplacement of a semipermanent seismometer station in the North Pacific seafloor. Scientific and engineering goals of the at-sea test, in addition to gaining experience for future installations, were to

- demonstrate the capability for deep-ocean borehole emplacement of a large instrument package carried external to the drill string,
- define reentry and handling shock levels imposed on the BIP,
- determine the effects of surface and bottom currents on cable/drill pipe entanglement,
- establish whether the sensor state-of-health monitoring function can perform within design limits in a borehole environment,
- compare borehole seismometer signals and noise levels with similar signals recorded on conventional OBS records.

The MSS equipment was installed on GLOMAR CHALLENGER in San Juan, Puerto Rico. Once on site, the ship's position was held dynamically by four hull-mounted thrusters while the BIP was suspended from the drill string and lowered into the borehole. A reentry cone installed during original drilling of the borehole was used to guide the BIP into the hole, where it was lowered approximately 2000 ft below the sea floor into the basalt layer. The LYNCH deployed an OBS array and conducted a shooting program with shots that varied from 1.1 to 264.6 lb at ranges of 6–40 miles. Excellent seismic data,

including two small earthquakes, were recorded while the BIP was in the borehole. Deployment, reentry, and recovery of the BIP were achieved in 74 hrs 45 min without significant difficulties. The success of this complex operation, which involved using new equipment and untried procedures, was attributed to the experience of the GLOMAR CHALLENGER crew and the planning efforts of NORDA, Global Marine, Teledyne Geotech, and DSDP personnel.

This section covers deployment equipment design, at-sea operational procedures, test data and evaluation, mobilization and demobilization, and planning factors for MSS-81. A final report for the operation was prepared by Wallerstedt [5]. Since the MSS-81 deployment was performed as one of several experiments conducted during the DSDP Leg 78B operation, extensive details on the MSS operation and other related projects are presented in the DSDP Initial Reports [3].

2. Reentry site

DSDP site 395A (Leg 78B) was drilled during DSDP Leg 45 in December 1975–January 1976. The site is at 22°45.34′N, 46°04.90′W on the west flank of the mid-Atlantic Ridge, a complex geological area. Topography in the vicinity of the site is characterized by high relief (7884–15,092-ft water depths), and northeastward-trending lineations. Earlier studies (1974) indicated that sediments are present only in isolated ponds that occupy topographic depressions. Site 395A is at the foot of a 4265-ft scarp near the edge of one of the thickest sediment ponds. Water depth at the site is 14,708 ft. The hole was drilled to a 2178-ft depth below the sea floor and was cased to basement rock at a 367-ft depth. Cavings blocked the lower 180 ft of the hole, which left a total depth of 1998 ft open and in good condition.

Figure 1 is the site location. A sketch of the DSDP reentry cone, which was left attached to the borehole casing, is shown in Figure 2.

3. Downhole instrument system

3.1 System description

The MSS-81 instrumentation consisted of two subsystems, the BIP and the shipboard test console (STC). The STC provided power to the BIP, performed data recording and monitoring, and displayed selected data plus real-time BIP state-of-health information. DC power and data flow between the BIP and STC were via an armored EM cable. The EM cable also served as both deployment and recovery line for the BIP.

3.2 Functional description of the BIP

The BIP, Teledyne Geotech Model 53100, was an assemblage of acceleration, seismic, temperature, pressure and state-of-health sensors, along with associated signal conditioning and control electronics. The BIP was 28.5 ft long, with an outer diameter of 8 inches. With the instrumentation enclosed and with an external ballast weight attached, the BIP weighed 3300 lb.

Two sets of three-component orthogonal sensors provided acceleration ranges of 50-g or 100-g peak. Two Teledyne Geotech Model S-750 short-period, vertical, piezoelectric-type seismometers were programmed for staggered voltage gains to achieve a dynamic range of about 144 dB and an overlap of about 30 dB between adjacent channels.

Four temperature sensors were provided, each with a range of 0–100° C. Nine BIP state-of-health monitors were provided to monitor its condition and to assist in system fault analysis.

The data output from all sensor and state-of-health channels was input as analog signals to a pulse-code-modulated (PCM) encoder that time division multiplexed and digitized the data, and then formatted and output the data as a 54-kHz PCM digital data stream with appended synchronization data.

A detailed description of the BIP and its components is provided in Part V, Instrumentation.

3.3 Functional description of the STC

The STC was primarily an assembly of off-the-shelf components mounted in an 8- x 12- x 8-ft environment controlled van. Major functional items included a line receiver, a tape recorder, decommutators, a time code generator, strip chart recorders, a teletypewriter, a patch panel, a power supply, and uninterruptable power systems.

Raw PCM data with a time signal was recorded on magnetic tape. Data could be selectively recorded in a total of 7 passes and 14 tracks with 3.5 hrs of 50-kHz digital data per pass.

A detailed description of the STC and its component parts is presented in Part V, Instrumentation.

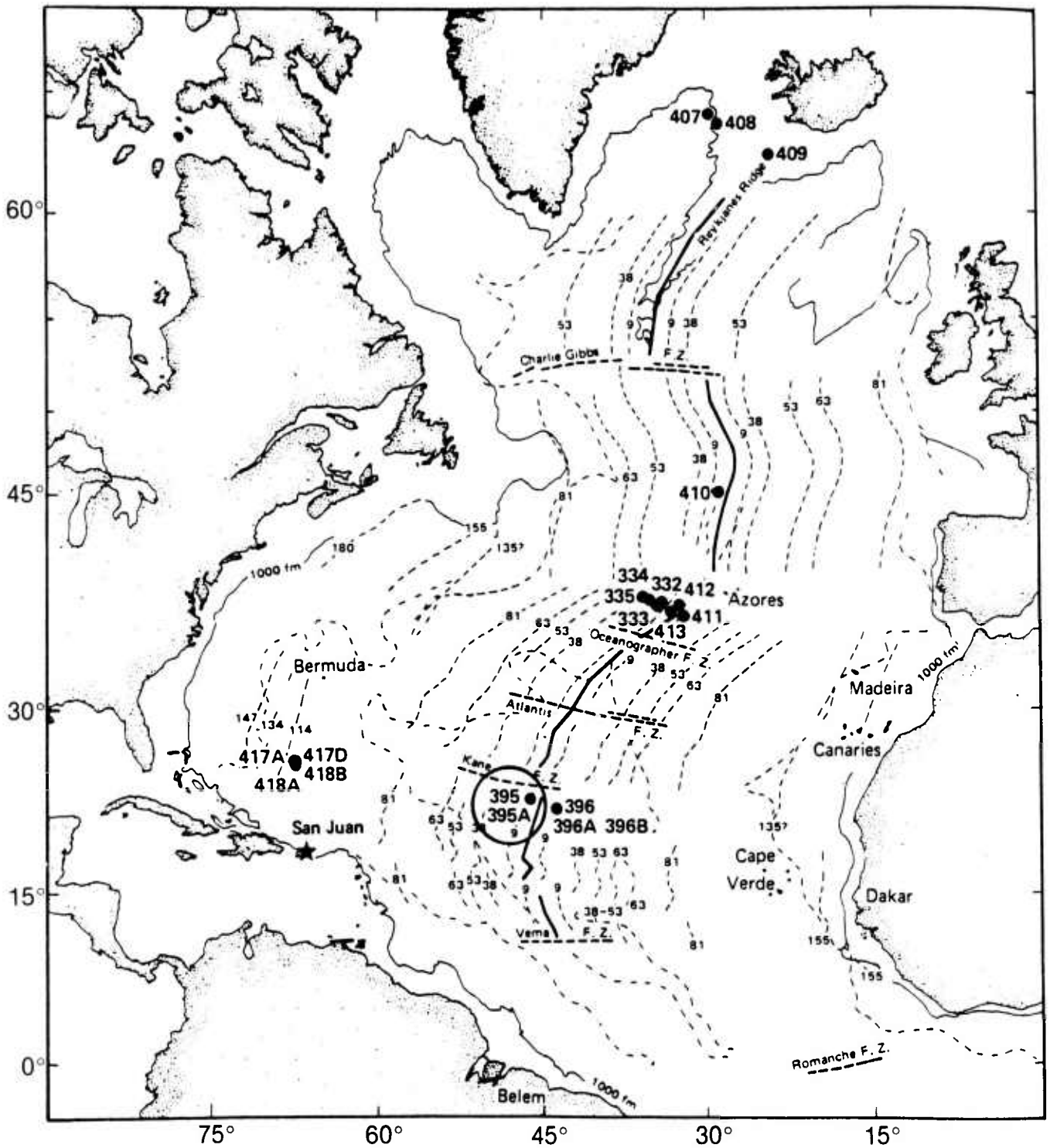


Figure 1. Location of MSS-81 site (DSDP site 395A, Leg 78B).

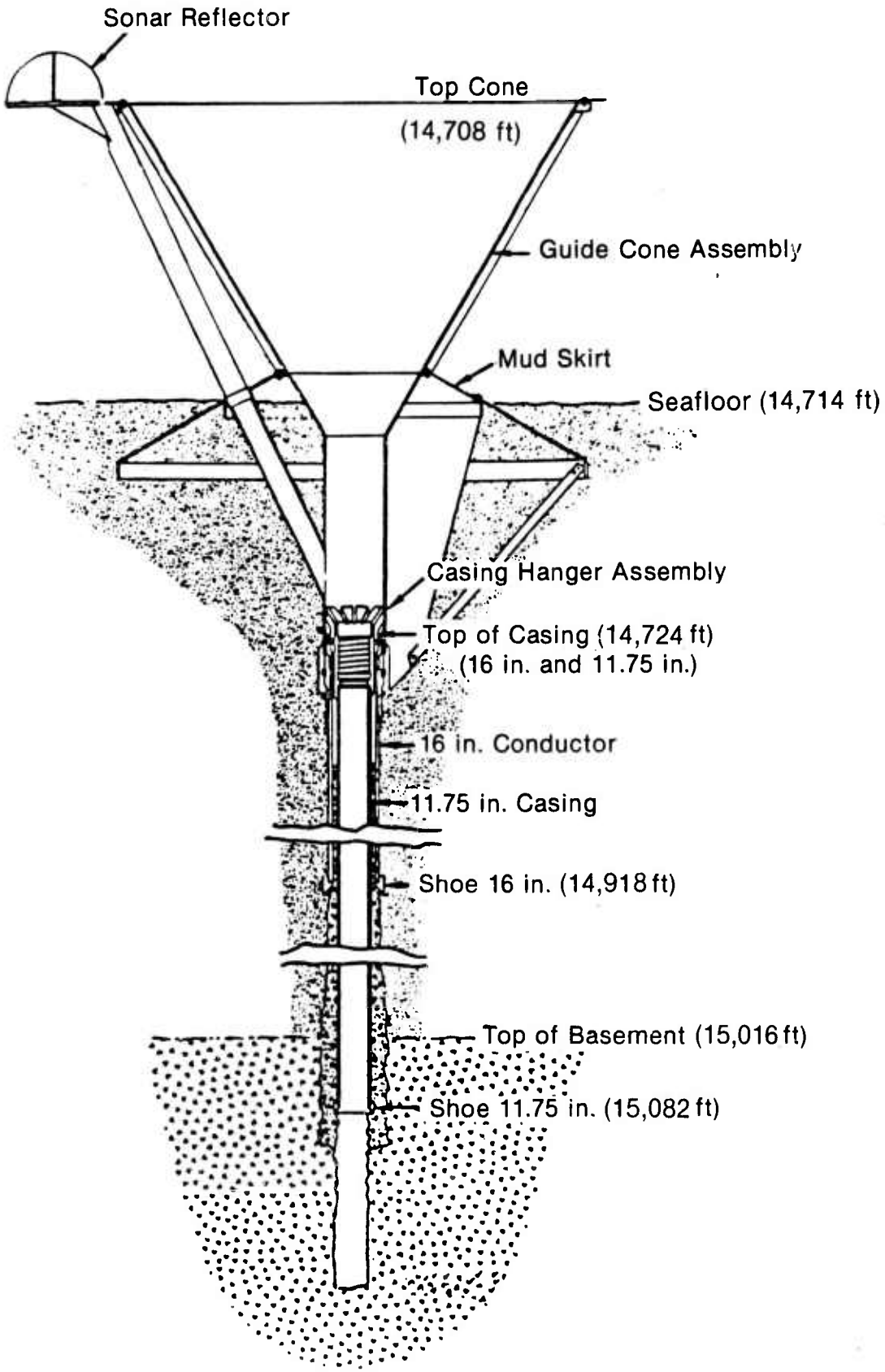


Figure 2. DSDP/MSS reentry cone.

4. Deployment equipment

4.1 General description

The MSS-81 at-sea test deployment equipment was divided into shipboard and subsea categories. The shipboard equipment included a dual traction drum EM cable winch, an over-the-side A-frame with a single-cylinder heave compensator, a large swiveled sheave, and an idler sheave. The subsea equipment consisted of a reentry subassembly and a specially designed coaxial EM cable.

4.2 Shipboard equipment

A new Pengo single-traction wheel winch was procured as the EM winch. However, this device proved unsatisfactory and a Pengo dual traction wheel winch was obtained from U.S. Navy stock and refurbished for the MSS-81 deployment. The winch was mounted to a welded deck foundation aboard the drill ship.

The 28,000-lb test A-frame projected about 15 ft over the side and 8 ft above the main deck. The A-frame was attached to a central heave compensator, which had a stroke of about 6 ft and was rated at 64,000 lb.

The 48-inch sheave was supported at the outboard end of the A-frame by a tension type Martin Decker load cell transducer. The idler sheave was positioned adjacent to and outboard of the EM cable winch.

The shipboard equipment was mounted on the port side main deck of the GLOMAR CHALLENGER. Detailed descriptions of this equipment are presented in Part VI, Deployment Equipment.

4.3 Subsea equipment

Reentry subassembly design: During previous borehole seismometer experiments aboard the GLOMAR CHALLENGER, the seismometer was lowered through the drill string. Because of the BIP's large diameter, a means for lowering the instrument to the sea floor in a carriage external to the drill pipe was necessary so that the pipe would be left clear for the passage of reentry tools. Once the reentry cone had been located and reentered, the BIP could be hydraulically shunted in line with the drill pipe and lowered into the borehole. The reentry subassembly was developed to accommodate these requirements while attached to the lower end of the drill string. The reentry subassembly was made up of a carriage control sub, BIP carriage housing, BIP carriage, reentry tool stinger, and a hydraulic plug/sonar adapter (see Section VI, Fig. 19). The reentry sub included a shock mounting for the BIP for borehole entry impact. Primary functions of the reentry sub were to

- carry the BIP during drill string deployment;
- support and position the sonar reentry tool to locate the reentry cone;
- stab into the reentry cone with BIP accelerations not exceeding 10 g;
- release the BIP, allowing it to be lowered into the borehole;
- allow the EM cable to run into the borehole;
- release the EM cable after the reentry sub was pulled out of the reentry cone.

Several design constraints for the reentry sub were imposed by the existing shipboard equipment and methods to be used, and material availability versus time constraints in a tight fabrication schedule. Limitations were:

- The reentry sub must pass through the rotary drill table of the GLOMAR CHALLENGER, which limited the outer diameter to 31 inches.
- The reentry sub must stab into the reentry cone and casing. The cone base had an inner diameter of 24 inches and the casing had an inner diameter of 11 inches.
- Steels of various strengths and other materials had to be readily available, and be of qualities that would not become brittle or undergo other alterations at the seafloor temperature and pressure.

Reentry sub fabrication: The reentry sub consisted mainly of weldments made from steel plate, pipe, and shapes. Several alloys were used to provide the various required strength levels. The reentry sub weight was about 16,600 lb (the BIP weight was about 3300 lb). The maximum outer diameter was 30.5 inches and the overall assembly length was 67.67 ft. Details of the reentry subassembly design, functions and instrumentation are presented in Part VI, Deployment Equipment.

Electromechanical cable: The 30,000-ft EM cable center element was a No. 16 AWG stranded 18/0.0234-inch SBC with a nylon center filament. Enclosing the wire were right-hand lay and left-hand lay armored,

torque-balanced wire mesh. The outside covering was a 0.040-inch wall Hytrel sheath with an outer diameter of 0.692 inch. The cable breaking strength was about 21,000 lb. The EM cable and the Pengo cable winch were installed as a unit. See Part VI, Deployment Equipment, for a detailed description of the EM cable.

5. Operations summary

The initial deep-ocean seafloor deployment test (MSS-81) commenced at 0200, March 27, 1981. The sea state and weather were favorable. Procedures for performing the at-sea test were developed by Global Marine Development [6]; however, the sequence of procedures to assemble the BIP carriage and insert the BIP were partially modified. The operational sequences actually performed follow.

The EM cable was keelhauled and tied off at the moonpool work platform. The stinger was run through the rotary table and landed on the slips. The carriage control sub was made up to the reentry housing carriage, and the attachment nuts were welded while on the ship's casing rack. The reentry subassembly was placed on traveling blocks and was lowered and aligned to the reentry stinger flange, bolted, and the nuts welded. The total assembly was deployed through the rotary table and hung off on drill collar slips and safety clamps. Four Baash-Ross bumper subs (8.25-inch outer diameter, 1800 lb each, 5-ft stroke) were made up to the carriage control sub and torqued to API specifications. The total reentry assembly was then suspended on traveling blocks and snubbed about 3 ft above and on the forward side of the rotary table while the drill collar slips were removed. The EM cable was rigged through a sheave hanging from the derrick by a tugger line.

The BIP was moved to the catwalk, the EM cable connected, and systems checks completed. The carriage assembly was lifted until its top was about 3 ft above the rotary table. The BIP was then lifted until the load could be taken by the EM cable. At this point, carriage shear pins and hydraulic lines were installed from the moonpool work platform, and the entire reentry assembly was lowered about 20 ft and snubbed with tugger and cat lines.

The bight of the EM cable was removed from the sheave, passed through the rotary, and secured to the lower work platform. The assembly was lowered and hung on the slips. One 30-ft drill collar (7.25-inch outer diameter, 3000 lb) was made up to the bumper sub, and the assembly was lowered and landed on slips. One stand of drill pipe was then made up above the drill collar.

With the slot in the BIP carriage assembly facing the A-frame sheave, orientation marks were scribed on the rotary table and the tool joint for reference during deployment. The drill pipe was lowered 30 ft, and the EM cable was passed through the piccolo base and released. The EM cable was kept taut but tension was not set during the first 1180 ft of deployment to prevent entanglement with the drill pipe. At 1180 ft depth, footage counters were set, weight indicators were checked, recorders were started, and the heave compensator was raised to midstroke. EM cable tension was set at 500 lb at a depth of 2017 ft and increased to 3000 lb at a depth of 2947 ft. Cable tension continued to be increased during pipe deployment up to a maximum of 7200 lb at a total depth of 14,724 ft. The time required for lowering the reentry sub to within 10 ft of the reentry cone was 17 hr.

Scanning for the reentry cone commenced at 1900. There was some concern about entanglement with the 15-ft tethers (for passive reflectors and hollow glass balls) attached to the reentry cone; however, these devices were not observed with the sonar tool. They may have been ripped off during earlier drilling operations. Once the reentry sub was positioned over the cone, the drill string was lowered to allow the reentry sub to drop about 57 ft into the reentry cone. Starting from a position about 7 ft above the cone, the reentry sub was stabbed for a distance of about 24 ft at a rate of 6 ft/sec and then lowered an additional 33 ft at a rate of 1-2 ft/sec. Reentry was made at 2357, March 27. About 5 hr were then required to recover the sonar tool and prepare for BIP deployment.

A major concern at this time was EM cable entanglement with the drill string. Cable tension was set at 7000 lb to carry about half the weight of the BIP and to allow the instrument to fall a short distance when the carriage pins were sheared. Hydraulic pressure was brought up to 2500 psi with the cement pump to sever the shear pins and shift the BIP into position for deployment into the borehole. Accelerometer outputs indicated that the BIP had shifted into position for lowering; however, the EM cable remained stationary. After a few moments the winch began paying out cable, confirming BIP release. Accelerations were recorded as the BIP was lowered to the bottom of the borehole (1998 ft subbottom).

The BIP was raised about 1000 ft above the bottom of the borehole while the ship moved about 200 ft up-current. The reentry subassembly was raised and suspended 63 ft above the cone. Hydraulic pressure (cement pump) was brought up to 3400 psi to release the EM cable gate. Initially, there was no indication that the gate seal had ruptured. Twenty strands of drill pipe were

carefully recovered with no evidence of cable entanglement. The BIP was again lowered to the bottom of the borehole. The drill string and reentry assembly were retrieved and returned to storage. The ship drifted about 3330 ft downwind while paying out 2000 ft of EM cable on the sea floor to evaluate ship-generated noise. Before the shooting program started, an additional 2400 ft of EM cable was payed out to help isolate the BIP.

An array of four triaxial OBSs was positioned by the LYNCH during BIP deployment. Seismic experiments commenced at 2300 on March 28. The LYNCH fired 113 shots at ranges of 0–40 miles from the site (shot lines passed directly over the site). Explosive weights varied from 1.1 to 264.6 lb. Excellent seismic data was obtained by the BIP. A variety of malfunctions prevented OBS data acquisition except for the vertical component of a single instrument located about 5000 ft west of the borehole. Approximately 26 hr of data, including two small earthquakes, were recorded while the BIP was in the borehole.

To initiate BIP recovery, the slack cable was taken up from the sea floor and a 3000-lb tension was applied as the ship moved back over the reentry cone. An attempt to retrieve the BIP with an 8500-lb overpull was unsuccessful. The BIP accelerometer indicated little, if any, movement. It was suspected that the cable was fouled by a sonar reflector on the reentry cone. The ship was moved 200 ft to the east, the cable slacked about 33 ft, and tension reapplied. The winch commenced taking in cable, confirming that the BIP was free of the bottom. BIP recovery was then completed without incident. The MSS-81 experiment was completed at 0445, March 30, with 100% of its objectives achieved. The time required from start to finish was 74 hr 45 min.

6. Test data evaluation, BIP impact forces, and EM cable dynamics

6.1 BIP impact forces

The seismometers incorporated in the BIP could withstand a maximum dynamic impact load of 10 g. To determine the impact load that these instruments were likely to incur during a normal reentry and borehole deployment, the initial test BIP was equipped with continuously recording triaxial accelerometers. The three accelerometers were aligned on orthogonal axes parallel to those of the three-component seismic sensor subsystem to be installed in the MSS-82 seismometer. A sharp horizontal shock followed immediately by a sharp vertical shock during the reentry phase were the impacts of major concern during system design.

During the overall BIP deployments, a variety of impacts was recorded during shipboard handling, lowering, and borehole reentry. The most severe forces occurred during initial reentry; however, these forces were concentrated at the bottom of the reentry sub stinger, about 30 ft below the carriage housing. An analysis of accelerometer outputs is presented below for each phase of BIP deployment.

Loading: Random impacts occurred throughout this 15-min phase. The maximum shock was 4.2 g on the X-axis when the BIP struck the rig floor.

Lowering of reentry sub: Mild vertical accelerations were recorded when pipe was added to the drill string. As the drill string length was extended, the shocks were increasingly attenuated.

Reentry: The initial stab of about 25 ft was estimated at 6 ft/sec and the last 33 ft estimated at 1-2 ft/sec. The major impact with the reentry cone was about 6 g. Greater shocks could be anticipated in rougher weather.

Standby in cone: Impacts with the cone apparently occurred due to ship and drill string motion while the assembly was standing by in the cone. Vertical accelerations of about 2 g and horizontal accelerations of about 5 g occurred.

BIP release: Accelerations of about 5 g on the horizontal axis were induced when the BIP carriage shifted laterally to the release position. Smaller accelerations registered on the vertical axis.

Lowering the BIP down hole: Shocks from 1 to 4 g were probably caused by the BIP striking rock ledges and rebounding.

Landing the BIP: Large vertical accelerations were expected when the BIP made contact with the bottom of the borehole. The peak vertical shock was less than 3 g, probably because of bits, tools, and other items at the bottom of the hole. However, horizontal accelerations were higher than expected, indicating that the BIP shifted horizontally as it reached the bottom. The peak horizontal shock was 4 g, while other axes showed shocks of about 1 to 2 g.

The reentry accelerations were less than expected, while other deployment accelerations were higher than expected but within the allowable range. Improved BIP shock isolation was considered necessary for more severe weather conditions. A study of reentry impacts associated with the last stage of BIP deployment was developed by Gershunov and Daoud [7].

6.2 EM cable dynamics

Possible entanglement of the EM cable with the drill string had been a major concern since inception of the MSS program. Proper cable tension was considered necessary to avoid entanglement during deployment. An extensive study was conducted in early 1981 to determine the maximum tensioning characteristics of the cable and to examine the probability of entanglement (see Appendix B). The study examined static loading due to ocean current and cable weight, and dynamic loading due to ship roll, pitch, and heave motion. Among other factors, the study endeavored to predict cable tension in all sources of loading, to describe the deflected shape of the cable for any deployed length, and to develop criteria for the tensioning system. The study findings included the following.

- The upper limits of total tension in the cable for a 20,000-ft water depth due to all sources of excitation were (no tensioning system)

  15,720 lb for 4-ft significant wave height,

  16,825 lb for 6-ft significant wave height,

  17,930 lb for 8-ft significant wave height.

- In near-surface conditions, entanglement of the cable with thrusters and screws cannot occur.

- Possible interference between the drill pipe and cable after BIP release may occur only in cases of no ship offset.

- Bottom current causes significant bottom separation between the cable and drill pipe.

- Other offset and current conditions do not indicate a tendency for interference between the drill pipe and the cable after BIP release.

- A current velocity of 0.25 knots is large enough to avoid entanglement between the drill pipe and cable after BIP release if the ship is maneuvered upstream.

- To avoid kink formation in the cable and snap loading, maximum controlled tension at the upper end should be about 10% more than the weight of the released length of cable.

Data derived from a hydraulic load cell gauge and analog recorder records during MSS-81 operations indicated general conformance with cable tensioning characteristics estimated by the study. The indicated static and dynamic cable loads were well within the ranges predicted by the analysis with no unusual reactions noted.

7. Mobilization and demobilization

Mobilization and demobilization for the at-sea test was a major operation due to foreign site locations and the amount of equipment required. The GLOMAR CHALLENGER schedule and varying equipment availability required continuous replanning of mobilization tasks. The At-Sea Test Mobilization Plan for MSS-81 was developed by Global Marine Development [8].

Mobilization was accomplished at the Puerto Rico Marine Terminal and Drydocks in San Juan. Most MSS equipment was shipped to San Juan by truck and trailer barge while some structural units (A-frame, equipment foundations) were fabricated at the shipyard. Clearing MSS equipment through Puerto Rico customs was a continuous, time-consuming problem, although no fees were charged. A major problem was the temporary loss of a BIP by the trucking firm. The BIP was eventually shipped via air, but major damage occurred during shipment and the BIP was rendered inoperative for MSS-81. Equipment removal was accomplished in Las Palmas, Canary Islands. Shipment back to the U.S. was very slow (2 months) and expensive.

8. Test evaluations and recommendations

Plans for seismic data analysis included comparing BIP and OBS data for signal and noise levels and crustal velocity resolution. Unfortunately, only the vertical component of a single OBS was functional. None of the OBS data was usable for travel-time inversion. However, a noise comparison between BIP and OBS data was possible. The noise levels detected by the BIP were 10-30 dB lower than those recorded by the OBS. The BIP data quality was generally excellent. The only important limitation was that the system frequency response was limited to below 10 Hz. (See Part II, Data Reports, for details on MSS-81 data.)

The MSS-81 operation successfully demonstrated the feasibility of emplacing large instrument packages in deep-sea drill holes. The value of such installations was demonstrated by acquiring a unique set of seismic refraction data during a two-ship seismic refraction experiment with shooting done by the USNS LYNCH.

The operation went smoothly despite the number of untried procedures involved. EM cable entanglement with the drill pipe was not encountered. Reentry was achieved

without difficulty, and the BIP and its cable were successfully released from the drill string/bottom hole assembly. The only potentially serious problem was partial closing of the reentry stinger cable release slot. The stinger tube bent about 5 degrees, which reduced the slot by 0.375 inch at the stinger flange; however, the remaining clearance was adequate for cable exit. Accelerations measured by the BIP during several phases of the deployment reached about 6 g. This acceleration was well within the design limit of 10 g, but pursuing methods to reduce these accelerations was considered advisable. Although the MSS-81 operation left little doubt that BIPs could be successfully deployed, it was noted that weather and sea conditions were ideal during this deployment. Rougher seas would make the operation much more difficult. For example, recovery of the reentry sonar tool and emplacement of an Otis/Baker "fishing" tool between reentry and BIP release required about 5 hr—a very long period for a rough weather reentry.

Accurate determination of static and dynamic EM cable loading was difficult because cable tension was not directly monitored. A direct readout of cable tension is considered desirable.

The EM cable winch operated satisfactorily; however, the communications system was noisy due to the unmuffled diesel engine on the winch. An improved communication system and reduced engine noise are considered desirable.

The Otis/Baker "fishing" tool operated incorrectly. The Baker plug stuck in the control carriage sub and caused the Otis release pin to shear, which resulted in an unsuccessful fishing operation and a slow, "wet" drill string recovery.

Relatively high shock loads were experienced during shipboard handling and release of the BIP. Shipboard handling could be more severe in the North Pacific. The BIP should always be handled within a shock-mounted canister.

The following recommendations were made by Global Marine Development [5] to reduce operational time, to limit BIP handling shocks, and to improve deployment reliability.

- Use a design that leaves the stinger in the borehole and does not require a cable release slot. (An alternative would be to strengthen the stinger assembly.)
- Provide full peripheral seating of reentry sub into reentry cone.
- Adapt dynaline-type, in-line cable tension/cable counter equipment. Provide damped gauge readout plus a two-track analog recorder for cable tension.
- Design a BIP carriage with a built-in shock isolator unit to be used as a BIP shipping container and later fitted into the reentry carriage on the rig floor.
- Reduce lateral shock to BIP by modifying offset shear pin release technique.
- Add an azimuth capability to sonar reentry tool (DSDP equipment).

B. MSS-82 operations

1. Summary

The MSS-82 operation was unsuccessful due to a combination of drilling equipment failures and adverse weather. After two attempts to prepare a borehole for BIP emplacement failed, the effort was abandoned because of an approaching typhoon.

The MSS-82 project was scheduled as a 30-day special operation with the GLOMAR CHALLENGER. Planned activities included drilling a reentry borehole to a depth of about 1500 ft at a Northwest Pacific site for emplacement of a Configuration I BIP. A Hawaii Institute of Geophysics ocean subbottom seismometer (OSS) was to be deployed in a second borehole. A support ship, the USNS DESTEIGUER, was scheduled to survey the area and deploy an array of 10 OBSs at the site. After the BIP was in place, the DESTEIGUER was programmed for 3.5 and 12.0 kHz bathymetry surveys and seismic surveys using the 30 kJ sparker as well as slant range explosive testing of the seismic sensors. The OSS, a small seismic instrument that is lowered through the drill string into an uncased borehole, was to be used in conjunction with the OBS array to confirm BIP data. After 5 days of real-time testing, a BPP and its associated recovery system were to be connected to the BIP via the EM cable, deployed, and left in place for on-site data recording. The OBS array, the OSS, and the BPP were to be recovered in 60 days. The BIP and EM cable, attached to a dummy BPP, were to be left at the site for further use, if initial results warranted.

The primary objectives of the MSS-81 operation were to determine the feasibility of BIP emplacement in, and recovery from, an existing borehole using the drill string technique and to evaluate the basic capabilities of the seismic sensor when deployed in a deep-ocean borehole. MSS-82, however, included the following objectives:

- Further demonstrate seismic capabilities of a BIP deployed in a deepwater borehole;
- Obtain Northwest Pacific subseabed seismic data;
- Demonstrate deepwater deployment of a BPP using an Installation, Recovery and Reinstallation (IRR) system;
- Verify a Data Acquisition and Recording System (DARS) seabed recording instrumentation capability;
- Demonstrate IRR installation and recovery techniques;
- Deploy and recover a Hawaii Institute of Geophysics OSS for hole-to-hole comparisons with the BIP;
- Deploy and recover 10 OBSs for comparisons with the BIP and for recording explosive refraction data and earthquakes.

After equipment mobilization and installation in Hakodate, Japan, the GLOMAR CHALLENGER departed for the designated site on August 20, 1982. Site operations began on August 24. Equipment failure dictated an attempt to drill a second borehole; however, because of the inability to release the casing string, the second borehole was abandoned prior to completion. After returning to the site on September 8 following the passage of Typhoon Gordon, the remaining time on-station was devoted only to implanting the Hawaii Institute of Geophysics equipment.

The contractor's final report for the MSS-82 operation was developed by Wallerstedt [9]. This section describes MSS-82 operations, the deployment equipment design, and mobilization/demobilization activities.

2. Reentry site

The Northwest Pacific site (DSDP Leg #88, site 581) is located at 43°55.6′N, 159°47.7′E. Site 581 lies just north of the Hokkaido Fracture Zone. This site was selected because of its proximity to the seismicity associated with the subduction zone off the Kuriles, and the need for better discrimination between earthquakes and man-made events in this area. The site has a water depth of 18,045 ft and a siliceous-calcareous sediment thickness of 1148 ft. A borehole depth of about 1476 ft was planned. Figure 3 shows the location of the site.

The borehole was planned for a depth that would penetrate about 160 ft into the basalt layer. A 16-inch diameter, 200-ft conductor casing would be installed in the upper unconsolidated sediments. The central borehole would be cased to about 1130 ft with 11.75 inch casing. The basalt portion would not be cased. The reentry cone was a standard DSDP cone with casing hanger. The upper cone area was 15 ft in diameter and 20 ft high (Fig. 2).

3. Downhole instrument system

3.1 System description

The MSS-82 instrumentation consisted of four subsystems, the BIP, the STC, the BPP, and the Test Equipment Rack (TER). The BIP-STC functions were essentially as described for the MSS-81 operation, with the EM cable providing DC power and data flow between the BIP and STC. The BPP was a new concept for supplying power to the BIP and recording BIP output after removing the STC from the system. The TER provided a means for shipboard interfacing with the BPP for troubleshooting and verifying systems performance prior to BPP deployment. After the GLOMAR CHALLENGER (and the STC/TER) departed, the EM cable would continue to provide power and data flow between the BIP and BPP. After BPP deployment, a deep-ocean installation, recovery, and reinstallation system (IRR) was the only means for recovering BPP, BIP, and MSS data.

Although the OSS was not a component of the MSS system, it was included in the MSS-82 deployment plan for comparisons between the OSS and the BIP, and between the OSS and other seafloor seismometers (OBSs). This unit is small enough to pass through the drill pipe and can be emplaced in a single bit hole. The MSS-82 OSS transmitted eight channels of digital data (three seismic, two tilt, one temperature, one hole diameter, and one engineering) via an armored cable for recording either on the ship or in a recording package anchored near the sea floor. The recording package contained a power supply, electronics, and five analog cassette recorders to record seismic data continuously for up to 75 days on three tracks, and low-rate digital data and time on a fourth track. A brief description of the OSS system is presented in Appendix C.

3.2 Functional description of the BIP

The basic BIP was as designed for MSS-81; however, several modifications primarily associated with installation of an isolation link were incorporated. Among other changes, the overall length of the BIP was increased from 28.5 ft to 34.5 ft. Three borehole locking devices, or pawls, were installed. These devices extended to a maximum radius of 5.5 inches in the borehole whenever BIP cable

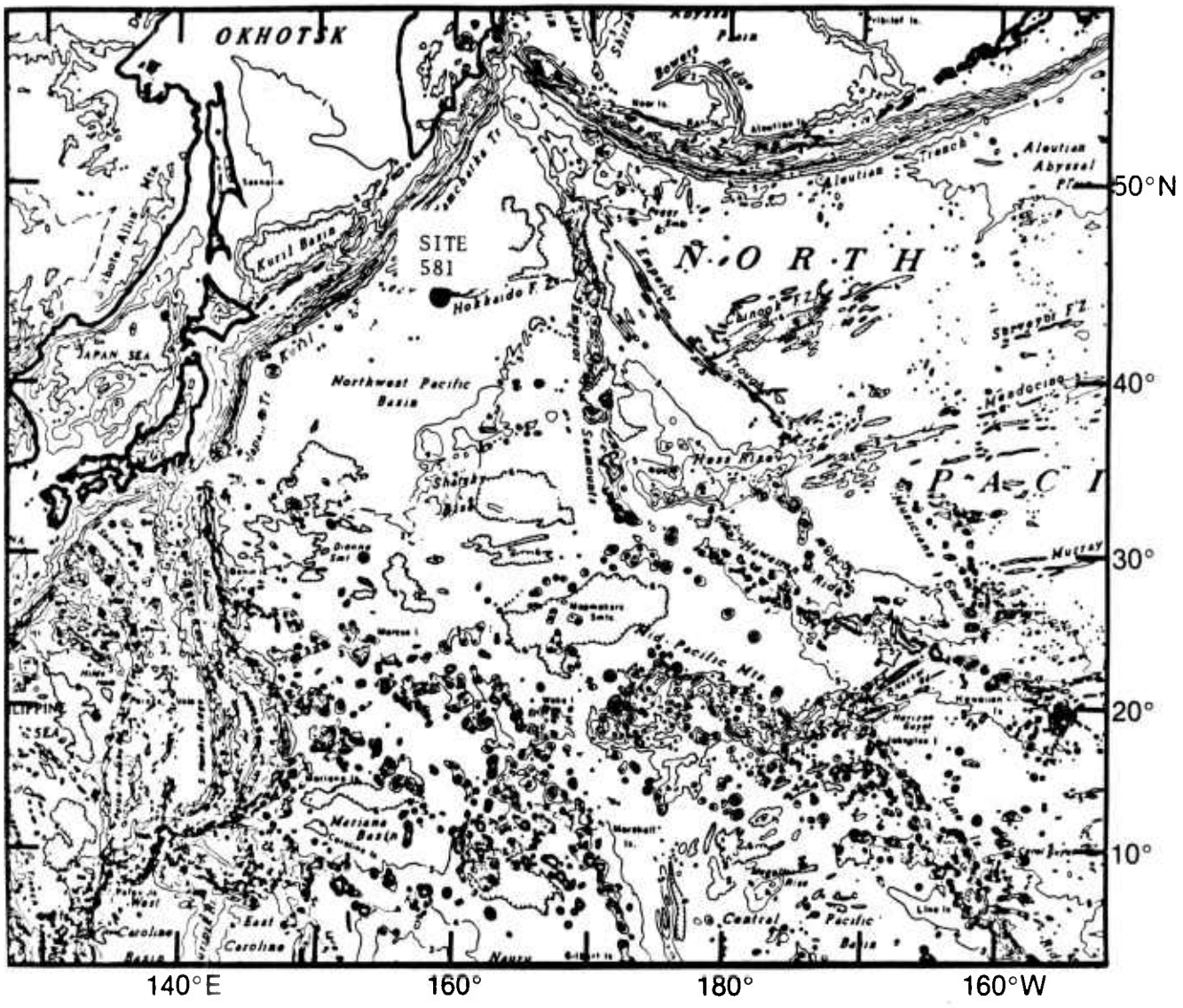


Figure 3. Location of MSS-82 site (DSDP site 581).

tension was below 1500 lb, thus coupling the BIP to the surrounding rock. BIP weight was about 3300 lb. See Part V, Instrumentation, for additional details on the BIP.

3.3 Functional description of the STC

STC functions and components remained as defined for MSS-81 operations. See Part V, Instrumentation, for information on the STC.

3.4 Functional description of the BPP

Basically, the BPP was comprised of three OBS-type aluminum spheres incorporated into a package 8- x 8- x 7-ft high. The 40.5-inch diameter spheres were rated for 20,000-ft depth capability. Two of the spheres contained silver zinc batteries and served as a power source, while the third sphere housed a DARS. The BPP weighed about 10,000 lb dry (4500 lb wet). The BPP was designed to serve as the sole source of power for the BIP and for recording all BIP data subsequent to disconnecting the STC. The data becomes available after recovery of the BPP with the IRR system. See Part V, Instrumentation, for a more detailed description of the BPP.

3.5 Functional description of the TER

The TER consisted of seven principal assemblies, a state-of-health communications receiver, a shipboard recording unit, a microprocessor control unit, a test interface unit, a strip chart recorder, a data input assembly, and a power supply. The TER interfaced with the DARS to test, troubleshoot, and verify system performance prior to BPP deployment. The TER also provided a way for interfacing with the BIP through the EM cable, for recording DARS data, and for monitoring system state-of-health during deployment. A detailed description of the TER is presented in Part V, Instrumentation.

4. Deployment equipment

4.1 General description

The MSS-82 at-sea test deployment equipment, as in MSS-81, was divided into two categories: shipboard and subsea. The shipboard equipment consisted of a dual-traction-drum EM cable winch, an over-the-side A-frame with a single cylinder heave compensator, an idler sheave, a large swiveled sheave, a work platform, and an IRR mooring line storage box. The subsea equipment included a reentry subassembly; an EM cable and an assortment of lines, buoys, and transponders; and an anchor for deploying the IRR system.

4.2 Shipboard equipment

The basic MSS-82 shipboard equipment was similar to that used for MSS-81; however, several design changes were made to improve handling, reduce stress, or shorten downhole operational periods.

The MSS-81 dual-traction-drum EM cable winch was refurbished at the Pengo factory and used again for MSS-82.

The A-frame for MSS-82 was a newly fabricated structure designed for greater loads anticipated during deployment and recovery of the BPP.

The heave compensator was modified by adding an 11-gal accumulator bottle. The new "dual accumulator," single-cylinder heave compensator offered improved overall operational response.

The idler sheave was modified by adding a "strain-sert" pin and "load-all" indicator. The modified idler sheave also included a Martin-Decker load cell.

A portable work platform was suspended from the bulwark 4 ft above the main deck in the vicinity of the EM cable winch.

An 8- x 8- x 20-ft steel container for storing the IRR mooring lines was installed on the starboard side main deck, athwart ship from the EM cable winch.

Three brackets were installed on the port side of the casing rack for stowing the BIP carriage housing.

The shipboard equipment, with the exception of the IRR line storage box, was mounted on the port side main deck of the GLOMAR CHALLENGER between the derrick subbase and the casing support rack. See Part VI, Deployment Equipment, for additional details on the shipboard equipment.

4.3 Subsea equipment

Reentry subassembly: Both the design constraints imposed on the reentry sub and its functions remained the same as those defined for MSS-81. As a result of MSS-81 experiences and changes in the MSS-82 BIP (Configuration I), several modifications were incorporated in the MSS-82 reentry subassembly. These changes included internal functional improvements, as well as an increase in overall length. See Part VI, Deployment Equipment, for reentry sub modifications.

The modified reentry subassembly dimensions were approximately 16 x 27 inches x 73 ft. The weight of the reentry sub plus BIP was about 24,000 lb. Part VI, Deployment Equipment, provides design details on the reentry subassembly.

EM cable: The MSS-81 EM cable was used for the MSS-82 operation. Approximately 30,000 ft of cable were programmed. See Part VI, Deployment Equipment, for a description of the EM cable.

IRR system: The IRR system consisted of a 21,500-ft riser line, a 10,000-ft grapnel line, 18,000 ft of anchor line, a 1500-ft isolation cable, a 300-ft strain relief cable, "A" and "B" crown buoys plus release transponders, and a 2000-lb clump anchor. The IRR system, when deployed, resembled a trapezoidal array (see Section VI, Fig. 21). One end was fixed to the bottom by the anchor, and the other end was fixed to the BPP (which was fixed to the BIP by the EM cable). An assembly of buoys supported the 10,000-ft grapnel line, which was suspended horizontally at a depth of about 4000 ft. Release and tracking transponders were fixed between the anchor and the buoy assembly. In the event the acoustic release failed and prevented surfacing of the buoy array, the grapnel line could be grapnelled for BPP recovery. The 300-ft strain relief cable was provided to temporarily support the EM cable when recovering the BPP, and the 1500-ft steel isolation cable was used to isolate the BPP from mooring loads.

A detailed description of the IRR system is presented in Part VI, Deployment Equipment.

5. Operations summary

Operational procedures for the MSS-82 deployment were defined by Global Marine Development [10].

The GLOMAR CHALLENGER arrived at the designated site on August 24, and began preparations for the MSS-82 deployment. Bathymetry lines (run off an automati station-keeping beacon to check the bottom for laying the IRR system) indicated an average water depth of about 18,000 ft. Due to marginal weather, further operations were delayed until 0600, August 25.

A reentry cone and casing assembly were run in to the sea floor and DSDP Hole 581A was spudded in early on August 26. Drill pipe measurements indicated a water depth of 17,979 ft. The hole was washed and drilled through 1181 ft of sediments where basalt was encountered. Considerable torquing occurred while coring 49 ft into basalt. When preparing the hole for the 11.75-inch casing, the drill pipe broke immediately above the bottom hole assembly, leaving the entire assembly in the hole. Fishing for the bottom hole assembly would have been complicated and time consuming. Since on-station time was limited, a decision was made to drill a new hole.

The GLOMAR CHALLENGER was moved clear of Hole 581A. A new reentry cone and casing assembly was run to the sea floor at 1615, August 29, for Hole 581B. Because Hole 581B was located less than 1000 ft from Hole 581A, a decision was made to save time by eliminating the drilling of a pilot hole to determine the amount of 16-inch casing required. Lateral variability of the sediments was such that the 16-inch casing could not be fully washed into the bottom. As a result, the reentry cone remained 56 ft above the mudline. Release from the cone was accomplished with considerable difficulty, but the drill string was retrieved. The spline of the lowermost bumper sub was found to be bent in the extended position.

Despite the reentry cone's precarious perch, a reentry was made, and the hole was drilled through the sediments to a basalt formation at a depth of 1183 ft below the sea floor. After coring through 54 ft of basalt, the bit was pulled from the hole to pick up 1183 ft of 11.75-inch casing. The cone was reentered with the 11.75-inch casing string, which was cemented in position; however, the casing could not be released because of an apparent casing hanger malfunction. An approaching typhoon dictated cessation of the operation. The drill string was severed at the first joint above the top bumper sub, the drill pipe was retrieved, and the ship departed the area.

The ship returned to the site on September 8 and commenced drilling hole 581C. The hole was drilled through 1165 ft of sediments and cored 20 ft into basalt. The Hawaii Institute of Geophysics OSS was successfully deployed through the drill pipe into the basalt layer. The DESTEIGUER deployed an array of 10 OBSs and then conducted an extensive shooting program. Shots ranging in size from 0.5 to 1800 lb were fired at distances ranging from normal incidence to 124 miles. Excellent borehole data was obtained for comparison with the seafloor OBS units. After completing the OSS/OBS experiment, the GLOMAR CHALLENGER departed the area on September 14.

6. Test data evaluation (equipment)

6.1 Studies and analyses

Because the combination of weather and DSDP drilling failures precluded MSS-82 operations, no equipment

evaluations were conducted. However, several engineering analyses of MSS-82 components were performed prior to the August–September effort. The following reports and computer programs were prepared.

- Reentry impact stress analysis of modified reentry subassembly [11]: The analysis showed that the modified reentry sub will withstand the applied impact loads and that all stresses during the impact are within the elastic limit of the structure.

- Drill pipe stress analysis [12]: Drill pipe stresses during deployment and installation of the BIP into the reentry cone were analyzed. Recommendations were made relative to the bottom assembly, ship heading, and ship offset during reentry.

- EM cable stress analysis [13]: The report evaluates the most probable tensions to be expected in the EM cable while it is attached to the lower end of the drill string. The study concluded that the BIP could be safely deployed in 12-ft seas. Recommended tension at the lower end of the EM cable was established.

- Stress analysis of the IRR deployment at the NW Pacific Site [14]: The report analyzed potential critical problems during IRR deployment. It concluded that the IRR system can be safely deployed in a 12-ft significant wave random sea. A-frame and crane maximum loads and limits on crane boom angles were determined.

- MSS-82 NW Pacific site environmental data [15]: The report presented predominant significant wave height and direction, as well as wind velocity and direction for the MSS-82 deployment.

- CABNAP (Cable Natural Period): This Global Marine Development computer program computes the first three longitudinal natural periods of a cable that is fixed at one end and has a concentrated mass at the other end.

- CABCON (Cable Configuration): This Global Marine Development computer program computes deflected shapes of cable systems due to current forces. The program was developed for MSS-82 to determine ship offset from any point, or mass package along the cable, knowing cable upper-end tension, current forces, and cable lengths and properties.

6.2 Drilling equipment

Although the GLOMAR CHALLENGER drilling equipment was not considered MSS equipment per se, on-station analyses of equipment failures encountered during MSS-82 operations were made.

With regard to the drill pipe failure in the first borehole attempt, visual inspection indicated that the quality of the pipe, although new, was questionable. In addition, it was determined late in the fabrication process that the new drill string was understrength. The methods used by the drilling crew were considered appropriate.

During the second borehole attempt, chert was encountered. Sticking of casing or tools in chert is a common problem in seawater, and a special drilling mud may be appropriate. Furthermore, it was possible that the hole bridged, preventing the casing from seating at the bottom. This factor and others apparently caused the casing to be lifted a short distance by hydraulic action during cementing. Inability to rotate the drill pipe out of the casing hanger was attributed to failure of the snap ring to engage in the housing. Since no splines were built into the slip joints, the drill pipe merely rotated and did not release within the slip joint.

Some drilling equipment modifications had been incorporated beforehand, based on MSS-81 experiences. The Otis/Baker "fishing" tool did not operate correctly during MSS-81. In addition the MSS-81 configuration required two or more wire line trips to recover the sonar tool and prepare for the BIP release. During MSS-82, a slightly modified Baker RD-2 Equalizing Valve was used in place of the Otis/Baker tool, thus requiring only one wire line trip.

7. Mobilization and demobilization

Prior to the MSS-82 mission, the GLOMAR CHALLENGER was scheduled for a 2 day port call in Hakodate, Japan, for receiving and installing MSS equipment. Extensive planning and coordination were required to assure timely logistics staging, assembly of equipment, fabrication and installation of the MSS equipment, and dockside testing within the short time available.

A field site in Hakodate was established about 45 days prior to the CHALLENGER's port call. Close control of all materials at the U.S. shipping points was required. The principal movers of the MSS equipment were the U.S. Military Sealift Command and the U.S. Military Airlift Command.

The primary West Coast staging site for Military Sealift Command shipments was the Naval Civil Engineering Laboratory at Port Hueneme, California. All equipment programmed for Military Sealift Command shipment was

trucked to the Port Hueneme trans-shipment point. Two BIPs, the STC, the BPP and console, the reentry recorder, and various electronic equipment were shipped via Military Airlift Command or by commercial air to Japan. Global Marine tracked all equipment from the point of debarkation in Japan to its destination in Hakodate.

Detailed plans were prepared for installing the equipment aboard the GLOMAR CHALLENGER and dockside testing of same. These installations included the STC van, EM cable winch, A-frame and components, heave compensator, fairlead sheaves, and IRR mooring line box. An extensive number of assorted MSS support equipment and spare parts were loaded aboard during these major component installations.

Following the MSS-82 deployment, the GLOMAR CHALLENGER returned to Yokohama, Japan, for demobilization and restoration to its original configuration. The EM cable winch, IRR handling gear, EM cable tie-off equipment, A-frame with sheaves and fairleads, heave compensator, IRR mooring line box, and miscellaneous tools and equipment were stored in Japan. Other equipment was returned to the United States. Global Marine developed the integrated logistics plan for MSS-82 [16].

8. Test evaluations and recommendations

Although the MSS-82 venture was abandoned, it was a valuable learning experience. Several logistical, organizational, and design weaknesses were addressed that would have been identified only in an actual deployment scenario. It was also apparent that inserting the MSS operation into an already fully obligated DSDP schedule served to decrease the odds of success. The schedule and the supply of critical hardware allowed only minimal setbacks. An expedition dedicated primarily to MSS deployment would probably have succeeded.

Despite failure of the MSS-82 operation, it was concluded that a deep-water borehole can be drilled at the Northwest Pacific site (No. 581). The 1981 at-sea test had already demonstrated the feasibility of deploying and recovering a large instrument package into an encased ocean-bottom borehole. Furthermore, MSS-81 operations verified that potential problems with controlled reentry, impact forces, cable entanglement, and release and lowering of the BIP into a borehole can be resolved. Although adding the BPP and its associated IRR system would complicate the operation and extend the time on-station, no major difficulties were foreseen.

As a result of MSS-82 equipment failures and technical problems, the following recommendations pertinent to deep-sea drilling operations were made [9]:

- assure use of quality drill string,
- use a motion compensator on the drill string,
- use special muds for coring in chert formations,
- cement the hole if bridging occurs,
- modify casing slip joints by building in splines or antirotation lugs,
- use about 6500 ft of 5.5-inch drill pipe to provide additional strength in upper sections of drill string.

Based on MSS-82 experiences, as well as MSS-81 operations and separate technical studies, the following recommendations were made for additional MSS operations [9].

- Continue efforts as planned for the MSS-83 demonstration at the proposed South Pacific site using the drill string deployment technique (Configuration I).
- Negotiate with the NSF for emplacing a borehole at the Northwest Pacific Site No. 581.
- Establish a working group to oversee development of a cable reentry deployment concept as an alternative to the drill string reentry technique.
- Conduct conceptual design, analyses, and tests to accomplish cable reentry (Configuration II) during MSS-83.

C. MSS-83 Operations

1. Summary

The MSS-83 operation was conducted January–February 1983. The GLOMAR CHALLENGER served as the primary support ship. Additional support was provided by the R/V MELVILLE of the Scripps Institution of Oceanography. A Configuration I BIP was deployed gently into a cased reentry borehole at a South Pacific site. Twenty-two days were required for the GLOMAR CHALLENGER to prepare the borehole, to implant the BIP, and to deploy the BPP/IRR system. Five days of real-time seismic recording and testing with the BIP were conducted prior to deploying the BPP and its associated IRR

system. Meanwhile, the MELVILLE deployed an OBS array and conducted a shooting program for monitoring by both the BIP and the OBSs during the 5-day recording period. MELVILLE then retrieved the OBSs, recovered their data, and redeployed them for recording in conjunction with the longer term BIP/BPP deployment phase. Forty-three days after the initial 5-day test period, MELVILLE returned to the site and recovered the OBSs and the BPP.

The operation objectives were the same as those defined for MSS-82, but the deployment site was shifted to the South Pacific to conform to GLOMAR CHALLENGER's schedule. The Hawaii Institute of Geophysics borehole instrument (OSS) was not included in MSS-83. The following additional scientific objectives, pertinent to the particular site, were included.

- Determine the seismic-velocity structure of the crust and upper mantle in old, fast-moving crust.
- Study seismicity in the vicinity of the Tonga Trench for a period of about 50 days.

Mobilization and demobilization for the GLOMAR CHALLENGER were accomplished in Wellington, New Zealand, and Papeete, Tahiti. Mobilization and demobilization for the MELVILLE involved port calls in Honolulu, Papeete, and San Diego.

The 18,471-ft implantation of the reentry cone and casing at the MSS-83 site was the deepest that had been made (at that time). Despite a number of technical and equipment problems, the overall deployment operation was successful. The capability for installing a large instrument package within deep-ocean boreholes was further demonstrated. Equipment designs and operating techniques were demonstrated and evaluated, including the newly developed BPP and IRR system. MSS-83 also demonstrated that several areas of technological concern could be accommodated; namely, seismic instrument impact loads, drill string characteristics, EM cable dynamics, and EM cable/drill string entanglement.

The final report for the MSS-83 operation was developed by Wallerstedt [17]. This section describes the design of deployment equipment, at-sea operational procedures, test data and evaluation, and planning factors for MSS-83.

2. Reentry site

The designated site was 24°03′S, 165°30′W (DSDP Leg 91, Site 595B), about 932 miles west-southwest of Tahiti (Fig. 4). Water depth at the site was 18,417 ft. The site was chosen to provide both regional and teleseismic information from the Tonga subduction zone, which is one of the most tectonically active areas in the world, and is particularly noted for numerous deep-focus events.

3. Downhole instrument system

3.1 System description

The MSS-83 downhole instrument system was the same as that programmed for MSS-82. The BIP, STC, TER, and BPP were the primary system components.

3.2 Functional description

The concepts and functions of the BIP, STC, BPP, and TER remained as defined for the MSS-82 deployment. See Part V, Instrumentation, for descriptions of these subsystems.

4. Deployment equipment

The MSS-83 at-sea test deployment equipment was defined in shipboard and subsea categories, as in previous MSS operations. Several modifications and some additions were made to the various MSS shipboard and subsea equipment units as a result of MSS-81 evaluations, and in response to expanded objectives. These changes were made in preparation for the MSS-82 at-sea test. However, MSS-82 deployment failure precluded further equipment evaluation. Accordingly, the MSS-83 shipboard and subsea equipment configurations were the same as those defined for MSS-82.

The MSS-83 shipboard equipment included a dual-traction-drum EM cable winch, an over-the-side A-frame with a single cylinder heave compensator, an idler sheave, a large swiveled sheave, a work platform, and a storage container for the IRR system mooring lines. The subsea equipment consisted of a reentry subassembly; an EM cable; an assortment of lines, buoys, and transponders; and an anchor for the IRR system. See Part VI, Deployment Equipment, for descriptions of the shipboard and subsea deployment equipment.

5. Operations summary

Detailed instructions and guidance used for deploying the BIP, the BPP, and its associated IRR system, and operating procedures for the various MSS systems and equipment were provided by Global Marine Development [18].

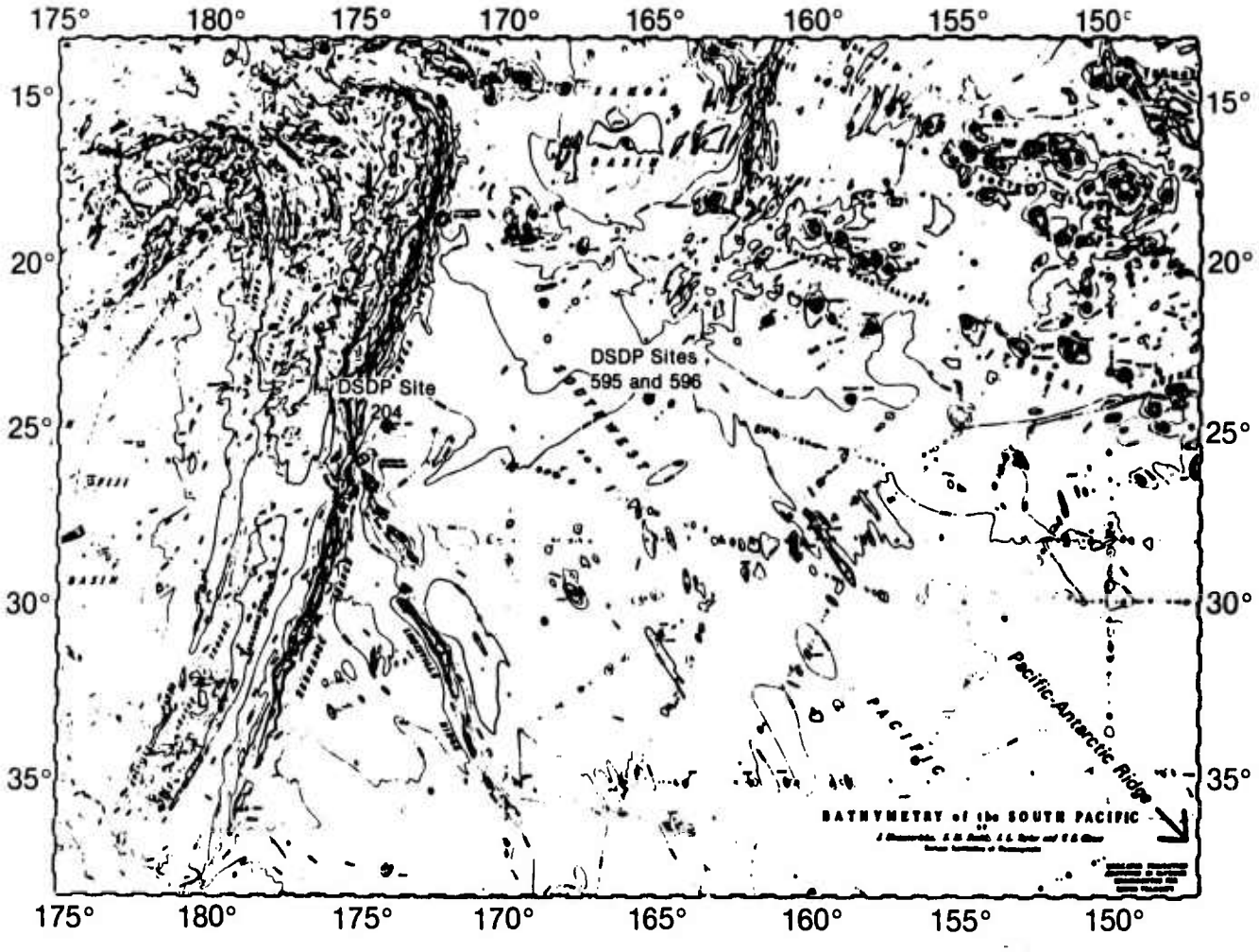


Figure 4. Location of MSS-83 site (DSDP Sites 595 and 596) in the southwest Pacific Ocean. Also shown is the location of DSDP site 204.

5.1 BIP deployment

The R/V MELVILLE arrived at the designated site about 30 hr prior to GLOMAR CHALLENGER and proceeded with a survey for an optimum drill site. Site 595 was identified on January 21. Water depth was set at 18,417 ft. A pilot hole test encountered a firm stratum at 108 ft below the sea floor. This soft sediment layer was considered too thin to support the reentry cone assembly or for lateral support for the bottom hole assembly when drilling in hard material. To find thicker sediments, the ship was offset 1500 ft east and 50 ft north where the water depth was 18,468 ft (Hole 595A). The pilot hole encountered extremely soft sediment that had a hard layer at 118 ft below the sea floor. (A sediment layer of 328 ft was considered necessary for safe and efficient drilling operations.) The hole was cored 105 ft through the hard stratum, and igneous rock was encountered at 230 ft below the sea floor. Coring in igneous rocks (acoustic basement) continued to a depth of 290 ft.

Because MELVILLE's surveys failed to identify a more favorable drilling site in the area, a decision was made to remain at site 595. A reentry cone with an abbreviated 16-inch casing string (three joints) was assembled and run in. Hole 595B was spudded in at 0524, January 25 in water depth of 18,471 ft. Igneous rock was encountered at 223 ft below the sea floor. The hole was cored to a 267-ft depth, and preparations were made for setting 11.75 inch casing. The casing string was lowered and stabbed into the reentry cone at 1244, January 27. The casing was latched in and cemented without difficulty. A reentry for further coring in hard basalt was made at 0623, January 29. An intensely fractured area of basalt was encountered from 344–377 ft. Hole-cleaning problems occurred at greater depths because of the fractured interval. Because there was a possibility of the drill string becoming stuck, coring was terminated at a depth of 406 ft below the sea floor.

Assembly of the reentry subassembly and testing and installation of the BIP required 11 hr. About half of this time was required for minor but time-consuming, mechanical problems. Lowering of the reentry subassembly was halted after six stands of pipe were run because of BIP electrical signal losses. The malfunction was a serious problem. Water had entered the EM cable through a damaged section in the uppermost cable isolator area of the BIP. The EM cable was reterminated to the spare BIP, and the experimental cable motion isolator mechanism was sacrificed in the process. Although the BIP would not be clamped to the walls of the borehole, it was felt that instrument mass would provide sufficient coupling. Repairs required 2.5 days; however, an additional delay of 17 hr ensued because of wind and swell conditions. Continued lowering of the reentry sub was again interrupted for 5 hr for repairs to the EM cable winch. The reentry sub reached reentry depth at 0830, February 5.

Several problems were encountered with the sonar reentry tool. The tool failed on the rig floor test. The tool was disassembled and the conductors in the logging cable head were reworked. The sonar tool failed again as it started down the drill pipe. More wires were found broken in the cable head. The wires were again reheaded and the spring centralizer of the sinker bar assembly was modified. Sonar function was normal on the the third lowering, after a 9-hour delay. A smooth, gentle reentry was made at 2128, February 5.

The sonar tool was recovered and a Baker equalizing valve was positioned at the top of the reentry subassembly. Pressure via the mud pump was raised to 2500 psi, which caused the shear pins to sever and move the BIP into the release position. A sudden weight gain was noted on the EM cable as the BIP was released into the stinger. The BIP was lowered into the borehole and came to rest about 66 ft above the bottom. The exact depth of the BIP could not be determined; however, all concerned were satisfied that the BIP was emplaced in igneous rock in the uncased portion of the hole.

The drill pipe was pressured to 3700 psi for EM cable gate release. The reentry sub was pulled clear of the reentry cone. The cable weight indicator showed no effect of the pipe movement, which confirmed separation of the reentry sub and the EM cable. The ensuing drill string recovery was uneventful until the reentry sub came into view. The stinger was missing. All 10 attachment bolts remained hanging in the BIP carriage base flange. All bolts showed similar tension failures in the threaded portion.

The MELVILLE had previously deployed an array of six OBSs in the vicinity of borehole 595B for a combined BIP/OBS experiment. After the BIP was in place, the GLOMAR CHALLENGER held her position while recording a series of refraction shots by the MELVILLE. The EM cable was then slowly payed out as the ship was offset to the northeast until 2789 ft of cable remained on the winch. The BIP was monitored continuously for 5 days.

Periods of coordinated refraction shooting by the MELVILLE were alternated with long intervals of passive recording of teleseismic events. MELVILLE shot five refraction profiles; shots varied in size from 1–300 lb. Delays in installing the BIP prevented the shooting program

activation until the shooting schedule was more than half completed. The BIP recorded 3 series of shots comprising 2 unreversed refraction profiles and 348 shots. In addition to the large amount of high-quality explosion data, 64 earthquakes were recorded. At the conclusion of the 5-day data gathering period, the MELVILLE recovered the OBSs, acquired their data, and redeployed the OBS array in preparation for the longer period of passive recording with the deployed BPP.

5.2 BPP/IRR system deployment

Several problems were encountered in preparing the BPP for deployment. Faulty DARS tape recorders and formatted tapes were replaced. One battery cell was replaced and a pin hole leak in one battery sphere was repaired. The BPP/IRR system deployment operation commenced at 1300, February 10. The EM cable was payed out and fixed to the ship structure while the winch was prepared for the IRR phase. When the EM cable was made up to the BPP, it was discovered that some of the vital BIP functions could not be recorded or interfaced with the BPP. Troubleshooting placed the malfunction in the interfacing circuitry within the BIP. Apparently, a failure in the BIP data transceiver resulted in losing mid-period vertical data channel and status/control communications between the BIP and the BPP. Since remedial action would require recovering (and redeploying) the BIP, a decision was made to continue the deployment with the system not fully operational.

The EM cable weight was first passed to the BPP, then the entire BPP cable weight was passed to the IRR isolation cable on the winch. The BPP was lowered into the water at 1400, February 11. After paying out cable for a few minutes, the operation was halted for 3 hrs for repairs to the winch. When the 1500-ft isolation cable had been payed out, a controlled drift was resumed as the riser leg was deployed. The BPP made a soft landing at a depth of 18,414 ft. Both position and depth were verified. Apparently, the riser leg was nearly 3280 ft longer than specified. Pay-out of the riser leg continued, with frequent stops for winch repairs, until the 10,000-ft grapnel line was reached. The "A" crown buoys were then attached and as pay-out of the grapnel leg continued the ship moved out of range of a positioning beacon. The ship's drift rate was semiautomatically controlled by monitoring tension on the line. When the "B" crown buoys were launched at the anchor end of the grapnel line, a 16-kHz beacon was dropped to fix the position of the anchor leg acoustic release. The beacon failed within minutes and was replaced by a 13.5-kHz unit. The acoustic release link was deployed and deployment of the 18,000-ft anchor line began. The 13.5-kHz beacon signal became unusable about 1 hr after launch. Teamwork of the pilot house and winch personnel, together with favorable sea conditions, permitted completion of the IRR system deployment without loss of control. The end of the anchor line was removed from the winch and attached to the anchor. When slow drift of the ship produced the proper tension in the IRR, the anchor was released at 0858, February 12. The last "B" crown buoy submerged at 0948. Interrogation of a transponder attached to the anchor line acoustic release verified a successful deployment.

The GLOMAR CHALLENGER returned to the BPP area for placing an acoustic transponder navigation transducer on each side of the BPP. These devices were to be used by the MELVILLE for BPP recovery. This task proved to be both difficult and time consuming. A transponder of the BPP was to be used as a reference for positioning other transponders; however, ship's noise made communications with the BPP transponder impossible. Using semiautomatic positioning on a distant, intermittent beacon, transponders were finally placed about 9022 ft on each side of the BPP on true bearings of 017° and 251°. The operation was completed at 1700, February 12. The positions of the various deployed IRR components are depicted in Figure 5. See Part VI, Deployment Equipment, for a description of the IRR system.

5.3 BPP/IRR system recovery

Instructions for recovery and reinstallation of the BPP/IRR system were developed by Global Marine Development [19].

The MELVILLE returned to the MSS-83 site in late March 1983. Her initial time on site was devoted to recovering the OBS array and surveying the acoustical transponder navigation array. IRR/BPP recovery commenced about 0430, March 23. Upon actuation of the anchor leg acoustic release, the grapnel leg floated to the surface. Only one of the two parallel acoustic releases functioned. The grapnel line was captured, fed into the cable winch via a sheave, and retrieved in about 2 hrs. The "B" and "A" crown buoys and flashers were recovered.

The riser line was separated from the grapnel line and threaded through the idler sheave, and the first 4921 ft were recovered. The MELVILLE was positioned over the BPP, and the riser leg tension was increased to 2500 lb. About 984 ft of line was then brought aboard, which increased the tension to about 7400 lb. At this stage, the riser leg cable was stretched about 6% of its total length. No BPP lift-off was noted on the Martin Decker gauge or line tension recorder. The riser leg was continually brought in with gradually increasing tension due to the

MSS COMPONENT LOCATIONS

– Hole 595 B	23 – 49.34S (good) 165 – 31.61W
– Point "A" (16 KHz beacon)	23 – 49.35S 165 – 31.85W
– Point "B"	23 – 49.39S 165 – 31.54W
– Point "Z"	23 – 48.83S (good) 165 – 32.23W
– 13.5 KHz beacon (not shown)	23 – 48.30S 165 – 33.03W
– Point "Y"	23 – 48.81S (good) 165 – 32.35W
– BPP	23 – 48.08S 165 – 33.27W
– "A" crown buoy	23 – 46.00S (est) 165 – 35.22W
– "B" crown buoy	23 – 45.00S (est) 165 – 36.55W
– Anchor drop point	23 – 42.40S (est) 165 – 39.90W
ATNAV transponders	
.X-1	23 – 49.38S 165 – 31.61W
.X-2	23 – 48.60S (est) 165 – 34.95W
.X-3	23 – 46.58S (est)
.Dual release	See "B" crown buoy
.BPP X-ponder	See BPP

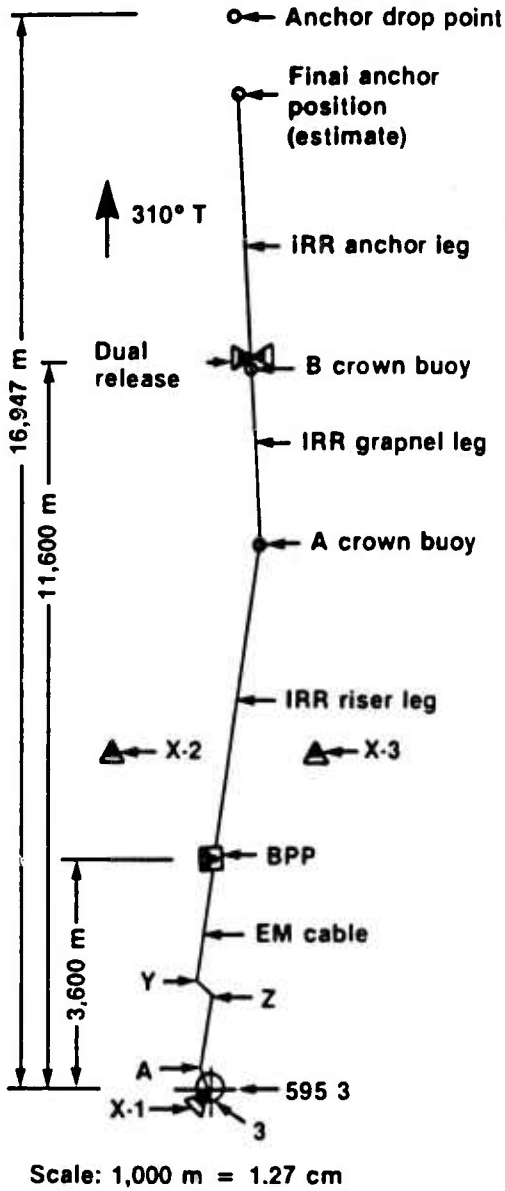


Figure 5. A sketch of the positions of deployed IRR system components, MSS-83.

EM cable weight increase. The connector to the isolation cable link was brought aboard at 1850 and was led through the winch. Line tension was 12,000 lb. With the wire cable secured, the isolation cable link was cut from the riser leg and dead-ended to the winch. The operation was secured at 2300; the BPP was suspended about 1500 ft below the ship, and the winch bore a majority of the cable load. Major cable oscillatory loads of ±4000 lb, due to ship motion, were noted on the Martin Decker gauge and line tension recorder.

The operation was resumed at 0730, March 24. The remainder of the isolation cable link was recovered and the BPP surfaced with an indicated load of 11,000 lb. The strain relief cable was attached to the ship's traveling winch cable, freeing the BPP from the EM cable load. The BPP was then hoisted clear of the water and lowered to a sled aboard the ship. As the BPP was lifted clear of the water, it experienced several impacts with the ship's hull. Initial visual inspection of the BPP showed numerous signs of damage and one of the spheres flooded after about 40 hr on the sea floor. The EM cable was disconnected from the BPP and linked to on-deck recording devices. The BIP was found to be still operational. The BIP was put through a calibration sequence, and about 7 hr of real-time data were recorded.

5.4 Dummy BPP/IRR system deployment

Deployment of a dummy BPP commenced early on March 25. Operations were halted when the EM cable was found to be broken near the water surface. The failure occurred due to torque imposed by twisting of the strain relief cable. A short length of the cable was retrieved, and a section of about 100 ft was trimmed off to remove any water damage. After resealing the mechanical and electrical terminations to the dummy BPP, deployment was resumed at 1900. The cable load was transferred to the dummy BPP and actual lowering commenced at 2240. This phase of the operation was complicated by twisting of the loaded strain relief cable and by the short payout length allowed by the ship's trawling winch cable.

The MELVILLE was unable to establish a position near the original BPP site because of subsea navigation problems. At 0040, March 26, the dummy BPP was set down at a position about 4920 ft short of the intended site. Payout of the riser line continued until transition to the grapnel line was accomplished. The "A" crown buoy group was attached, and the grapnel line was payed out as the ship transited to the position for deploying the "B" crown buoy group. The "B" crown buoys were installed and the new anchor leg, without release transponders, was fixed to the end of the 10,000-ft grapnel line. The 18,000-ft anchor line was payed out as the ship slowly transited toward the anchor launch position. Tension on the anchor line was maintained for about 2 hr until the line curvature straightened out. The clump anchor was launched at 0801 with a line pull of about 1000 lb. The "B" crown buoys submerged at 0915.

6. Test data evaluation (equipment)

6.1 Major areas of concern

The five areas of major technological concern with regard to the MSS program were instrument package deployment loads, drill string characteristics, EM cable dynamics, cable entanglement, and borehole emplacement. Based on MSS-83 evaluations, as well as on MSS-81 and MSS-82 experience, it was concluded that the equipment and techniques developed and employed during the program can generally accommodate these areas of concern. Some areas—in particular, drill string characteristics—should be further analyzed for future MSS operations.

Deployment loads: Possible damage to sensitive BIP instruments during handling or reentry was an area of major concern. A 10-g impact limitation was established for all conditions. Special procedures were established to reduce inadvertent handling shocks. Using a cantilevered stinger and BIP shock isolation supports (reentry subassembly modifications incorporated after MSS-81) provided adequate isolation for reentry impacts. The maximum shock loading observed during shipboard BIP handling was 6.5 g. The maximum reentry shock level was about 5 g. Since an even greater degree of shock isolation can be achieved, adherence to the 10-g impact limitation should not be a problem for future deployments.

The issues of reentry trajectory after initial contact with the reentry cone and the resultant bending movement distribution along the lower reentry assembly and transition areas were not completely defined. The localized bending stresses at the end of the stinger were considered acceptable.

Drill string/MSS deployment assembly characteristics: Throughout the MSS project, concern continued over specific response of the drill string when coupled to the MSS bottom deployment assembly. The drill pipe string had been longitudinally modeled by the DSDP team; however, this data had not been correlated with actual data. In addition, a detailed computerized analysis of the drill string lateral dynamic characteristics had not been performed. In-depth analyses of the upper section of the

drill string, the lower transition area, and the stinger-housing interconnection were considered a requirement for future deployments.

The upper drill string area was probably not critical with respect to MSS operations, although high axial loads plus bending forces could exist. An improved definition of the combined stress forces should be established.

The lower transition area was considered a critical section because of the change in stiffness in the transition from drill pipe to bumper subs through the drill collars to the housing assembly. This area was acted on by complex oscillatory and static lateral bending movements. This area was also the weakest of the lower drill string.

Two failures occurred in the stinger-housing interconnection area. The first failure, during MSS-81, resulted in partial closure of the EM cable release slot. This area was redesigned to increase local stiffness. During MSS-83 the 10 interconnection high-strength bolts for the stinger failed. Evaluation inferred that these bolts failed in tension, probably due to excessive bending. The failure apparently occurred during the recovery process. Overtorquing or tack-welding embrittlement may have contributed to the failure. Fatigue fractures were not apparent.

It is important that the drill string/bottom hole assembly interrelationships be fully understood prior to future operations. The varying sections of the drill string, including the reentry cone, should be defined and coupling modes established. Critical resonance areas should be identified. The question of how to treat damping should be resolved. The stinger-housing interconnection could be easily strengthened; however, this might shift a critical loading to the relatively weaker lower transition area. Thus, the uncertainties associated with static and dynamic responses of the drill string define a requirement for a detailed modeling of the drill string assembly.

EM cable dynamics: There was considerable uncertainty during early phases of the MSS program concerning dynamic characteristics of very long, tensioned EM cables. The tension levels were predicted fairly accurately by the axial cable analysis, and no unusual problems were noted. No excessive characteristics were noted at suspected resonance areas, which indicated reasonable damping effects. Lateral analysis correlations were not attempted.

Cable entanglement: Possible entanglement of the drill string and EM cable was an area of major concern. Early analysis (Appendix B) indicated that entanglement would occur only under light or slack cable tension conditions. Therefore, a minimum cable tension objective of 500 lb was established. Tension levels for deep deployments were critical due to cable strength limitations. Precautions were taken to maintain cable orientation down-current from the drill string. Backup procedures were established for recovery in the event of entanglement. Cable entanglement did not occur during MSS operations, although there were some momentary slack conditions. It was concluded that

- cable entanglement is possible but the risk is small;
- maintaining high tension throughout the cable significantly limits the possibility of entanglement;
- cable weight restricts the possibility of entanglement over most of its length;
- unfavorable currents can contribute to entanglement but are a secondary effect.

Borehole emplacement: MSS experience and extensive DSDP experience suggest that deep-water borehole emplacements at 20,000 ft and borehole depths of 1000 ft will present no unresolvable problems. More time should be allocated for areas of storms or high currents. In all cases, detailed information on the objective site is a necessity. The MSS-82 operation failed primarily because of drilling equipment malfunctions accentuated by inadequate time allowed, adverse weather, a marginal drill string, and difficult sediment conditions. Despite these adverse factors, achievement of the borehole emplacement was quite close when the operation was terminated because of drilling equipment losses.

6.2 MSS equipment malfunctions

Several malfunctions occurred with the various instrumentation systems and shipboard and subsea equipment. A number of minor mechanical problems occurred; however, these problems did not exceed what might be expected in such an environment. The more significant problems (less the reentry subassembly stinger failure) are discussed in the following paragraphs.

BIP: During the initial phase of the deployment attempt, a damaged cable in the cable isolator section of the BIP was discovered. This mechanical damage permitted water to enter the cable. The cable was reheaded, and the cable isolator was modified to remove the cause of cable damage. This work required removing the clamping pawls. Thus, the BIP was coupled to the borehole only by its own mass. Several BIP abnormal operating characteristics were identified during initial deployment efforts through sensor channel calibrations and preliminary data analysis:

- Short-period north sensor channel noise was approximately 12 dB greater than short-period vertical or east sensor channels.

- Short-period and mid-period north (common sensor) sensor calibrations deviated from the calibration norm.

- All mid-period calibrations indicated excessive deviations from the calibration norm.

- Apparent data transmission unit failure caused the loss of the mid-period vertical data channel and the status/command data channel (associated with BPP/DARS operation only).

- Interfering frequencies caused the primary short-period vertical channel to be excessively noisy (BPP/DARS operation only).

The OBSs appeared to perform flawlessly during the MSS-83 experiment.

BPP: The failure of the power cable jacket on sphere number 1 started a chain of events that resulted in a loss of power to the DARS sphere. The system failed after about 44 hr 18 min of operation. Tape cartridges 1, 2, and 3 recorded varying amounts of data for a total data record of 40 hr 16 min 25 sec. About 40 hr of the data recorded were valid, usable data. The details of the BPP failure and damage incurred, as well as an analysis of the BPP failure and recommendations for BPP system improvements, are provided by Gould [20] and Lawn [24].

EM cable winch: The winch malfunctioned during early BIP deployment attempts. About 5 hr were required for repairs. Repairs to the winch were again required during BPP deployment. Subsequently, frequent repairs were required during deployment of the IRR system riser leg (after positioning the BPP). In addition, the accuracy of the winch cable length read-out was questionable.

The EM cable winch roller sheave-strainsert transducer location was not adequate. An independent load measurement system is considered desirable.

IRR system characteristics: Uncertainties in the line length, stretch, and buoyancy characteristics contributed to an apparent long riser line deployment length. This deficiency was attributed to a combined error in initial line length measurement (riser line was found to be about 3280 ft longer than specified) and excessive EA (line modulus) stretch. The wet weight buoyancy factor appeared to be higher than originally projected. Touchdown of the BPP was achieved with approximately 17,500 ft of riser line deployed.

IRR system strain relief cable: Torque imposed by twisting of the strain relief cable resulted in a break in the EM cable. (The EM cable between the BPP and the strain relief cable twisted and severed when the EM cable weight was imposed on the strain relief cable.) The twisting of the loaded strain relief cable was aggravated by the short payout length of the MELVILLE's trawling winch cable. A torque-balanced wire cable with swivels on each end is considered necessary. In addition, the strain relief cable should be contained within an enclosure on the BPP.

6.3 Support equipment problems

Some problems were encountered with regard to DSDP equipment, ship's navigation, or other support equipment.

Sonar reentry tool: Several difficulties were encountered with the sonar reentry tool (standard DSDP equipment) during reentry with the reentry subassembly. Normal sonar functions were achieved on the third lowering attempt. (Sonar tool malfunctions also occurred during DSDP drilling activities prior to the MSS reentry attempts.)

Beacons, transducers: A 16-kHz beacon (navigation aid), which was dropped during IRR system deployment, failed shortly after launch. A second 13.5-kHz beacon became unusable about 1 hr after launch. During recovery of the IRR/BPP, only one of the parallel anchor release transducers functioned.

Navigation: The GLOMAR CHALLENGER's dynamic positioning system was essentially trouble-free during the entire operation. However, a number of acoustic devices were employed for data telemetering, navigation, bottom-finding, and other purposes. The effectiveness of these instruments was either greatly diminished or nil because the signals were degraded by the dynamic positioning system or because they could not be heard. The attenuation caused by the great water depth, together with the noise of the CHALLENGER's machinery and six propellers, often resulted in an unacceptably low signal-to-noise ratio. The MELVILLE also encountered subsea navigation problems when deploying the BPP/IRR. Improved surface navigation is considered necessary for IRR system cable pay-in/payout, and for anchor launch. Future planning for similar deep-water operations from noisy platforms should not rely heavily on acoustic transmissions.

7. Mobilization and demobilization

MSS-83 mobilization/demobilization involved coordinating the various requirements of the two support ships, GLOMAR CHALLENGER and MELVILLE, at several remote Pacific ports.

7.1 GLOMAR CHALLENGER

MSS equipment for the GLOMAR CHALLENGER was mobilized in Wellington, New Zealand. Some MSS-82 equipment was transported from Japan to Wellington via Military Sealift Command. Gould, Teledyne-Geotech, and NORDA equipment was air freighted via Military Airlift Command from Norton Air Force Base, California, to Christchurch, New Zealand. The equipment was then trucked to Wellington. After loading, installation, and dockside check-out of all MSS equipment, the GLOMAR CHALLENGER departed Wellington for the MSS-83 site on January 16.

Demobilization of the GLOMAR CHALLENGER was accomplished in Papeete, Tahiti, on February 20. All MSS equipment was removed from the ship. Equipment that would be required by MELVILLE for BPP-IRR deployment operations was placed in temporary storage. Other equipment that would not be required by MELVILLE (A-frame, BIP carriage, etc.) was returned to NORDA via ocean freight.

7.2 R/V MELVILLE

Mobilization/demobilization of the MELVILLE included several phases and extensive logistics. The MELVILLE initially made a port call in Honolulu, where a new winch, fairlead sheave foundation, BPP sled, grapnel hook, dummy BPP, and other miscellaneous equipment were either fabricated or loaded aboard. These equipment units were transported to Tahiti and placed in storage until required by the MELVILLE for BPP/IRR operations. Following the port call at Papeete, Tahiti, the MELVILLE proceeded to the MSS-83 site.

Upon completion of the BIP and BPP/IRR deployments, MELVILLE (and GLOMAR CHALLENGER) returned to Tahiti to mobilize for BPP/IRR recovery operations. Mobilization for the BPP/IRR operation commenced immediately following removal of MSS equipment from the GLOMAR CHALLENGER. An extensive assortment of equipment for transfer to or installation aboard the MELVILLE included

- refurbished EM cable winch,
- subsurface navigation equipment,
- installation of winch, wire rope box, idler sheave,
- grapnel hook,
- spare IRR anchor,
- spare buoys,
- DARS control console rack,
- Geotech BIP console rack,
- Martin Decker load cell.

Preinstallation checkout of the MSS equipment was hampered by a severe typhoon. Loading of MSS equipment aboard the MELVILLE was completed on March 16.

Demobilization of the MELVILLE was accomplished in two phases. All data equipment was off-loaded in Tahiti and shipped via air freight to Gould and Teledyne-Geotech for immediate processing. Other MSS equipment that would interfere with MELVILLE's en route operations was removed and shipped via ocean freight to Long Beach, California. Final transportation to NORDA was via truck. Upon MELVILLE's arrival in San Diego, the remaining MSS equipment, EM cable winch and spares, transponders, sheaves, navigation equipment, tools, etc., were off-loaded and shipped to NORDA. The Pengo EM cable winch was returned to Navy stock in Puerto Rico.

The plans for MSS-83 mobilization [21] and demobilization [22] were provided by Global Marine Development.

8. Test evaluation and recommendations

Although some BIP malfunctions occurred and the BPP functioned for only 40 hr rather than 45 days, preliminary examinations of the scientific data obtained indicated that the experiment was highly successful with regard to data objectives. The BIP rested unclamped at the bottom of the borehole; however, about 3280 ft of EM cable payed out on the ocean floor in the vicinity of the borehole apparently was effective in isolating the BIP from cable motions. Particularly clean, uncluttered BIP seismograms were obtained. A large amount of high-quality explosion data was recorded by the BIP, and even more voluminous data was recorded by the OBSs. The seismic data, which included 64 earthquakes, was particularly noteworthy. Some of these earthquakes appeared to have epicenters between 99 and 112 miles from the site. No epicenters have previously been reported in this region.

an engineering demonstration of the feasibility of ...oying a marine seismic station, the MSS-83 experiment was very successful, with the exception of the cable failure on the BPP. Based on MSS-83 achievements, as well as on MSS-81 and MSS-82 experience, MSS demonstrated that a capability exists for installing large seismometers or other delicate instrument packages within deep-ocean boreholes drilled into the basalt basement. Installation sites in water depths of 20,000 ft with borehole depths of 2000 ft are made possible by using the GLOMAR CHALLENGER drill string technique, with due consideration given to weather and ocean currents. Future MSS deployments could be accomplished using the basic equipment stored by NORDA and other MSS progra... participants.

The MSS concept required a dynamically positioned drillship to emplace a borehole and to deploy the packaged seismic instrument. Once a borehole was emplaced, various instrument configurations could be deployed and recovered. A cable reentry deployment technique (cable guided fly-in), as opposed to the drill string technique, would offer more flexibility for subsequent deployments. The basic elements of such technology are available.

The questions of MSS program feasibility were considered resolved; however, certain technical and conceptual areas should be further evaluated. It is recommended that the following technical areas be further explored:

- lateral response of unsupported drill string to drilling and deployment functions,
- accurate measurement of static and dynamic drill string loads,
- measurements of EM cable loads and payout lengths,
- improved reentry control,
- subsea positioning accuracy.

Planning for future MSS deployments should address acoustic noise potentials of the support ships from the standpoints of both instrument recorded noise and interference with subsea navigation systems.

To obviate the need for a dynamically positioned drillship for subsequent borehole reentries, it is also recommended that a cable-guided reentry fly-in development program be initiated.

V. Instrumentation

A. Borehole instrument package

The BIP, Teledyne Geotech Model 53100, was an assembly of acceleration, seismic, temperature, pressure, and state-of-health sensors and associated signal conditioning and control electronics. A design criterion for the BIP was easy deployment, which meant interfacing with current DSDP borehole reentry techniques. The BIP had to be small enough to pass through an 11-inch (inner diameter) casing while en route to its ultimate destination, an open hole in competent basement rock. Design specifications required that the BIP be a very high-reliability instrument with an operational life of 5 years. Other requirements included the capability to sense seismic earth motions along vertical and horizontal axes. Each axis had three frequency bands: 0.01–0.1 Hz (long period), 0.01–1.0 Hz (midperiod), and 0.2–20 Hz (short period). Long period sensors were never installed. In addition to a command and control capability, the BIP was required to sense and output secondary data, which included earth tilt, ambient temperature, and state of health. Operating power was supplied externally. The critical BIP (MSS-81) was 28.5 ft in length; the outer diameter was 8 inches. Basically, it was a pressure vessel with an enclosed instrumentation section and a ballast weight section. The total weight was 3300 lb. Figure 6 shows the mechanical layout of BIP components and subassemblies.

The BIP accelerometers consisted of two sets of three-component orthogonal sensors, each component output preconditioned by a charge amplifier and an antialiasing filter. Acceleration ranges were 50-g peak for all channels except the 2Z axis channel, which had a 100-g peak.

The seismic sensor system contained two Teledyne Geotech Model S-750 short-period, vertical axis, piezoelectric-type seismometers and associated frequency filters. Each seismometer drove two frequency filters. The voltage gains were staggered to provide a total dynamic range of about 144 dB, with an overlap of about 30 dB between adjacent channels. Figure 7 shows the dynamic gain-ranging format used. Figure 8 is a normalized seismic channel frequency response curve.

Four temperature sensors, each with a range of 0–100° C, were provided to monitor instrumental temperatures at various locations within the BIP. Sensors were attached to the DC-to-DC converter, to the mid-portion and bottom of the electronics stack, and near the

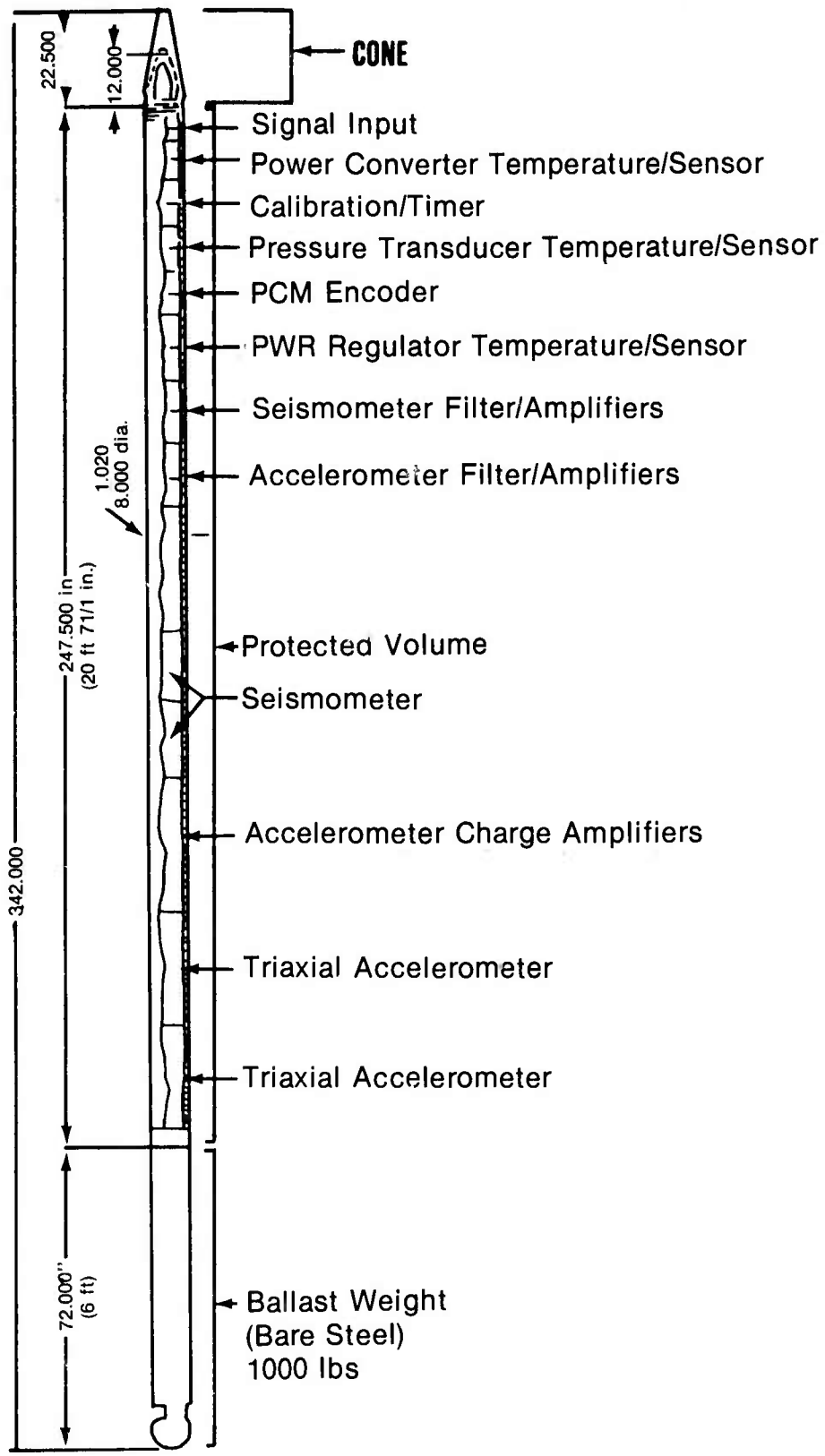


Figure 6. MSS-81 BIP physical layout illustrating components and locations of subassemblies (space is retained for long-period seismometers to be added).

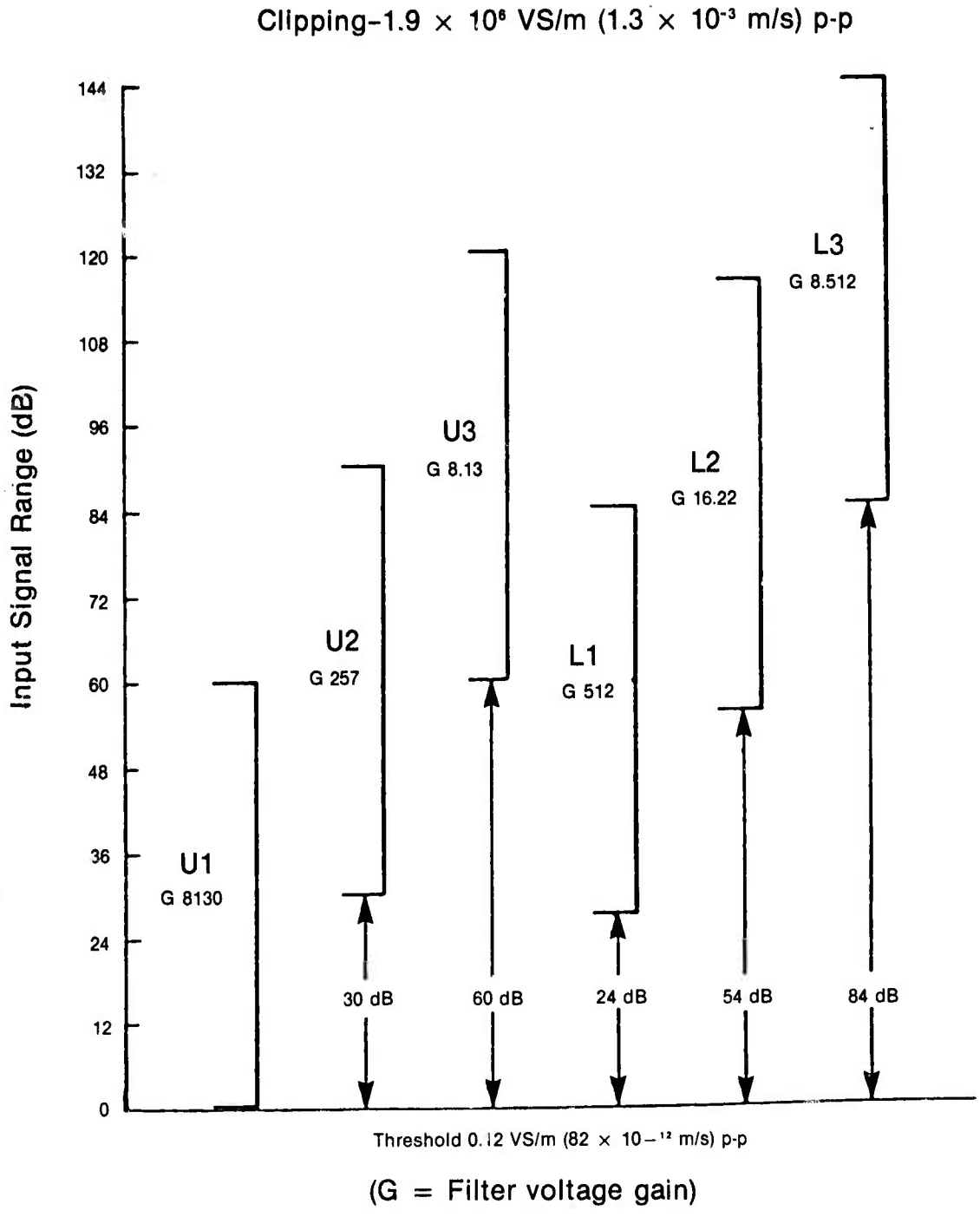


Figure 7. Dynamic gain ranging format used for BIP. L and U designations refer to lower and upper seismometer positions in the BIP.

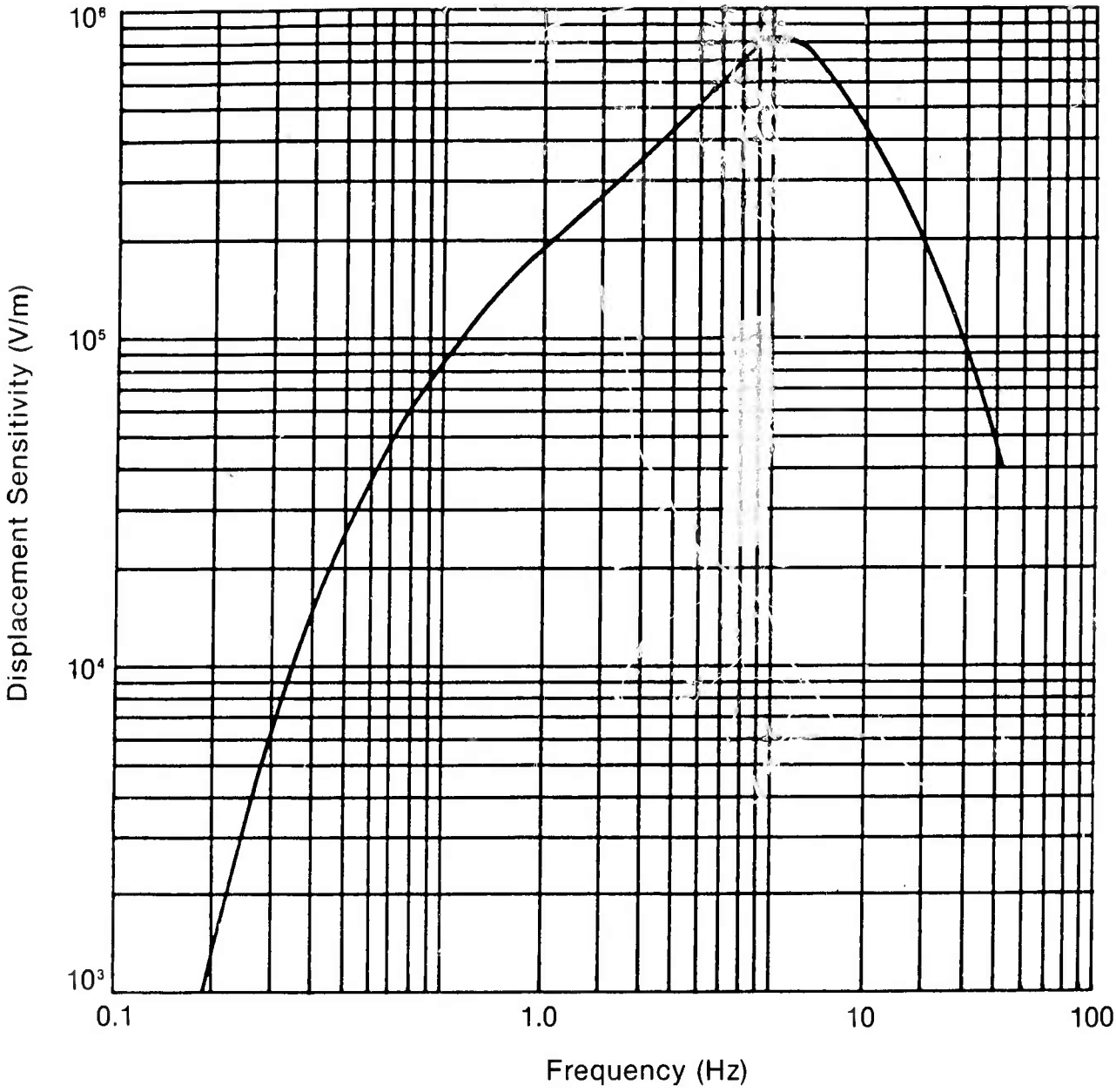


Figure 8. BIP normalized seismic channel frequency response curve.

bottom of the seismometer package. The lower sensor also provided a long-term record of borehole temperature.

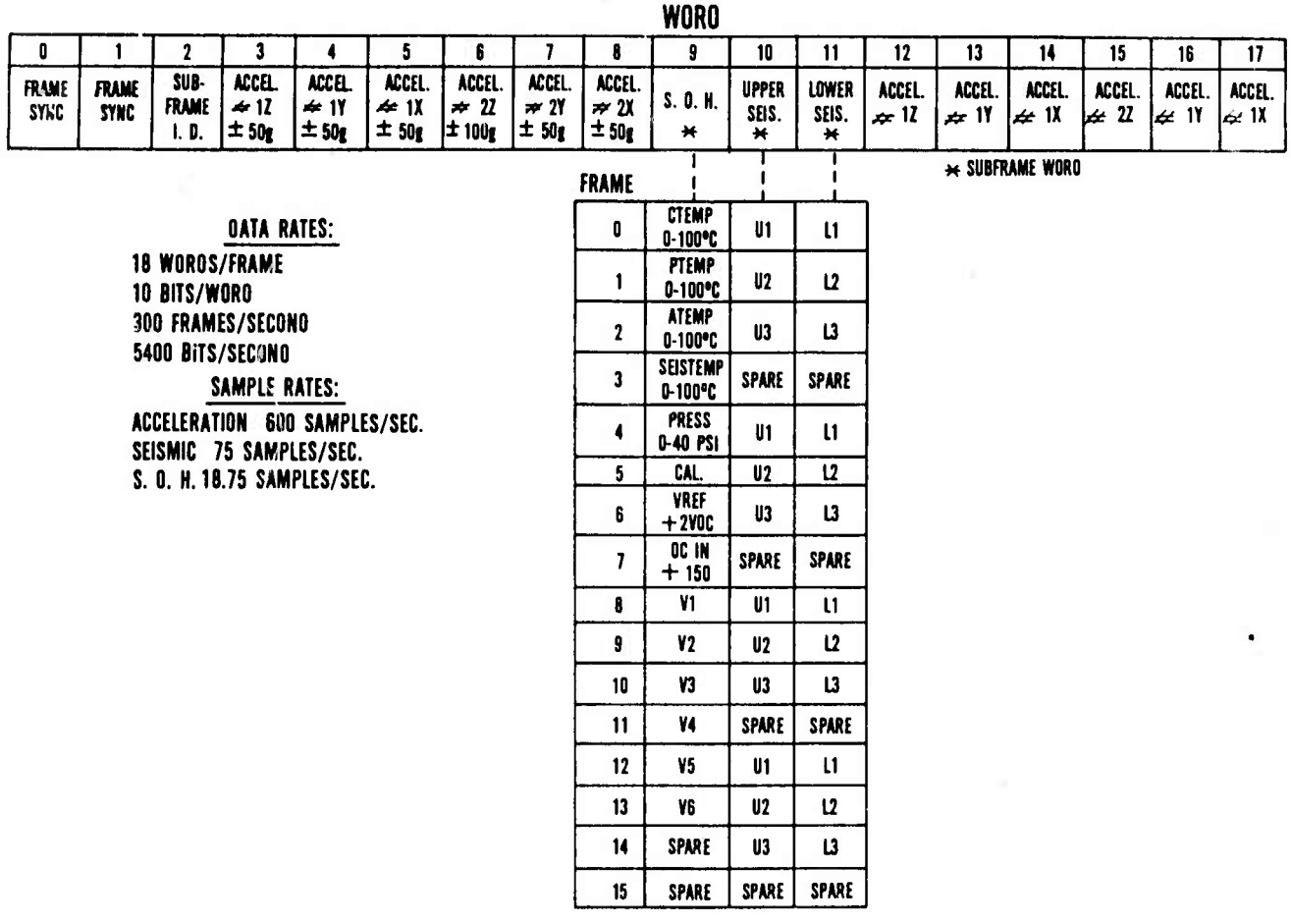
A pressure sensor with an output range of 0–40 psia was located in the electronics stack to measure BIP internal pressure. The BIP was evacuated and backfilled with helium to 16 psia during final assembly.

State-of-health monitors were provided to monitor internal conditions and assist in system fault analysis. The state-of-health devices were voltage monitors for the accelerometer filter and charge amplifier power supplies, for the seismometer filters, for two bipolar (±12 V) supplies for the two S-750 seismometers, for the temperature sensor bridge reference voltage, for the 150 VDC input voltage, and a negative (when active) monitor of the seismic channel calibration circuit output.

The data output from all sensor and state-of-health channels was input as analog signals to a pulse-code-modulated encoder that time-division multiplexed and digitized the data, and then formatted and output the data as a 54-kHz PCM digital data stream with appended synchronization data. Three levels of subcommutation were used to achieve the desired sampling rates. The PCM data format is shown in Figure 9.

The output of the PCM encoder was preconditioned by a PCM amplifier for transmission via the EM cable. This circuit also separated the high voltage DC component in the cable providing BIP power (150 VDC). A DC-to-DC converter module provided the various voltages required by the subassemblies. The outputs of the PCM encoder were further conditioned via outboard current-limited series regulators, which isolated the converter from external subassembly failure and minimized the risk of catastrophic system failures due to minor module failures.

After completing the MSS-81 deployment, the MSS equipment family was expanded to include a BPP. As a



WORD

0	1	2	3	4	5	6	7	8	9	10	11	12	13	14	15	16	17
FRAME SYNC	FRAME SYNC	SUB-FRAME I. D.	ACCEL. ⇙ 1Z ± 50g	ACCEL. ⇙ 1Y ± 50g	ACCEL. ⇙ 1X ± 50g	ACCEL. ⇗ 2Z ± 100g	ACCEL. ⇗ 2Y ± 50g	ACCEL. ⇗ 2X ± 50g	S. O. H. *	UPPER SEIS. *	LOWER SEIS. *	ACCEL. ⇗ 1Z	ACCEL. ⇗ 1Y	ACCEL. ⇙ 1X	ACCEL. ⇙ 2Z	ACCEL. ⇙ 1Y	ACCEL. ⇙ 1X

* SUBFRAME WORD

DATA RATES:

18 WORDS/FRAME
10 BITS/WORD
300 FRAMES/SECOND
5400 BITS/SECOND

SAMPLE RATES:

ACCELERATION 600 SAMPLES/SEC.
SEISMIC 75 SAMPLES/SEC.
S. O. H. 18.75 SAMPLES/SEC.

FRAME			
0	CTEMP 0-100°C	U1	L1
1	PTEMP 0-100°C	U2	L2
2	ATEMP 0-100°C	U3	L3
3	SEISTEMP 0-100°C	SPARE	SPARE
4	PRESS 0-40 PSI	U1	L1
5	CAL.	U2	L2
6	VREF +2VDC	U3	L3
7	DC IN + 150	SPARE	SPARE
8	V1	U1	L1
9	V2	U2	L2
10	V3	U3	L3
11	V4	SPARE	SPARE
12	V5	U1	L1
13	V6	U2	L2
14	SPARE	U3	L3
15	SPARE	SPARE	SPARE

Figure 9. MSS PCM data format.

part of this system modification, the BIP communications package was revised. A Data Transceiver Unit (DTU) within the BIP pressure vessel served as a seismic signal digitizer and a communications interface between the BIP electronics and the EM cable. The DTU contained seven Enhanced Delta Modulation Encoders (EDME), four short-period and three midperiod EDMEs. Data from the EDMEs were transmitted via a low-power Frequency Modulated/Frequency Shift Key (FM/FSK) telemetry system over the EM cable. The DTU used the FM/FSK communications technique for transmitting BIP status (state-of-health) and seven data channels. The DTU board types, as shown in Figure 10, included

- Switching Power Supply (SPS) Regulators: Decoupled DC power from the shielding of the EM cable for electronics within each bay.

- BIP status/state of health: Provided the functions of BIP state-of-health transmission and EDME calibration generation with 10-sec time-out control. BIP four-byte status messages were transmitted asynchronously at 300 baud with 16-bit CRC protection. The BIP command channel was used for control of DTU electronic and BIP sensor calibrations.

- EDME Encoders/FSK Transmitters: Seven EDME channels were provided for encoding the MP-Z, MP-N, and MP-E analog channels at 1.024 kbytes/sec with the SP-Z, SP-N, SP-E, and backup SP-Z analog channels at 10.24 kbytes/sec. A unique FSK frequency pair was assigned to each channel.

- EDME Telemetry Clock Receiver: A clock signal, synchronous with the system clock was provided. This signal was used to provide the 8.192/81.92 kbytes clock rates to the EDMEs and to supply a 81.92 kHz clock to the BIP calibration generation circuits.

The BIP structure was upgraded after the MSS-81 deployment. The electronics and sensors were housed as before in a 20-ft long x 8-inch outer diameter pressure vessel. A cable isolator was added to the upper section, extending the overall length from 28.5 to 34.63 ft. The cable isolator was designed to lock the EM cable termination into the uncased borehole while providing a slacking mechanism to mechanically decouple the EM cable from the sensor/electronic package. The cable electrical conductors passed through the center of the isolator, transferring very little of the vibrations incurred by the EM cable after system deployment. The upgraded BIP was also equipped with clamping pawls that extended to a radius of 5.5 inches in the borehole whenever cable tension dropped below 1500 lb, thus coupling the BIP with the surrounding rock. The lower 1.5 ft of the mechanical package provided a slotted keyway to lock the BIP into the carriage assembly during deployment.

Figure 11 is a diagram for the initial at-sea test BIP. The development specifications and interface definitions for the final BIP were prepared by Teledyne Geotech [23].

B. Shipboard test console

The STC was an assembly of primarily off-the-shelf commercial data recorders, a data decoder, a timer, and a microprocessor-based controller mounted in standard relay racks in an 8- x 12- x 8-ft environmentally controlled equipment van. Major functional items of the STC are listed:

- line receiver (special procurement)

- tape recorders (2), Ampex, Model PR-2230

- decommutators (2), Aydin Vector, Model PLD-400; Conic D-Pad III

- time code generator/translator, Datum, Model 9300–100

- strip chart recorders (3), Hewlett Packard, Model 7404, 4 channel

- teletypewriter, Texas Instruments, Model KSR 743

- patch panel (special procurement)

- power supply (4), Kepco, Model OPS 100–1m

- uninterruptable power systems (UPS) (2), Topaz, Model 82102-12 with battery modules Model 2566-2.

PCM data was received from the BIP via the receiver, preconditioned, then applied in parallel to each of two magnetic tape recorders (analog 14-track) and to each of two data decommutators. Raw PCM data and an Inter-Range Instrumentation Group Format B (IRIG B) time signal were recorded on selected magnetic tape(s) on even and odd channels, respectively. Through the use of a "switch back" mode and a modification allowing the activation or deactivation of selected tracks, data was recorded in seven passes. Each pass, at 3.75 in/sec, would accommodate 3.5 hr of 50 kHz digital data.

The data decommutators allowed real-time monitoring of data and BIP state of health. A Conic D-Pad III used a CRT

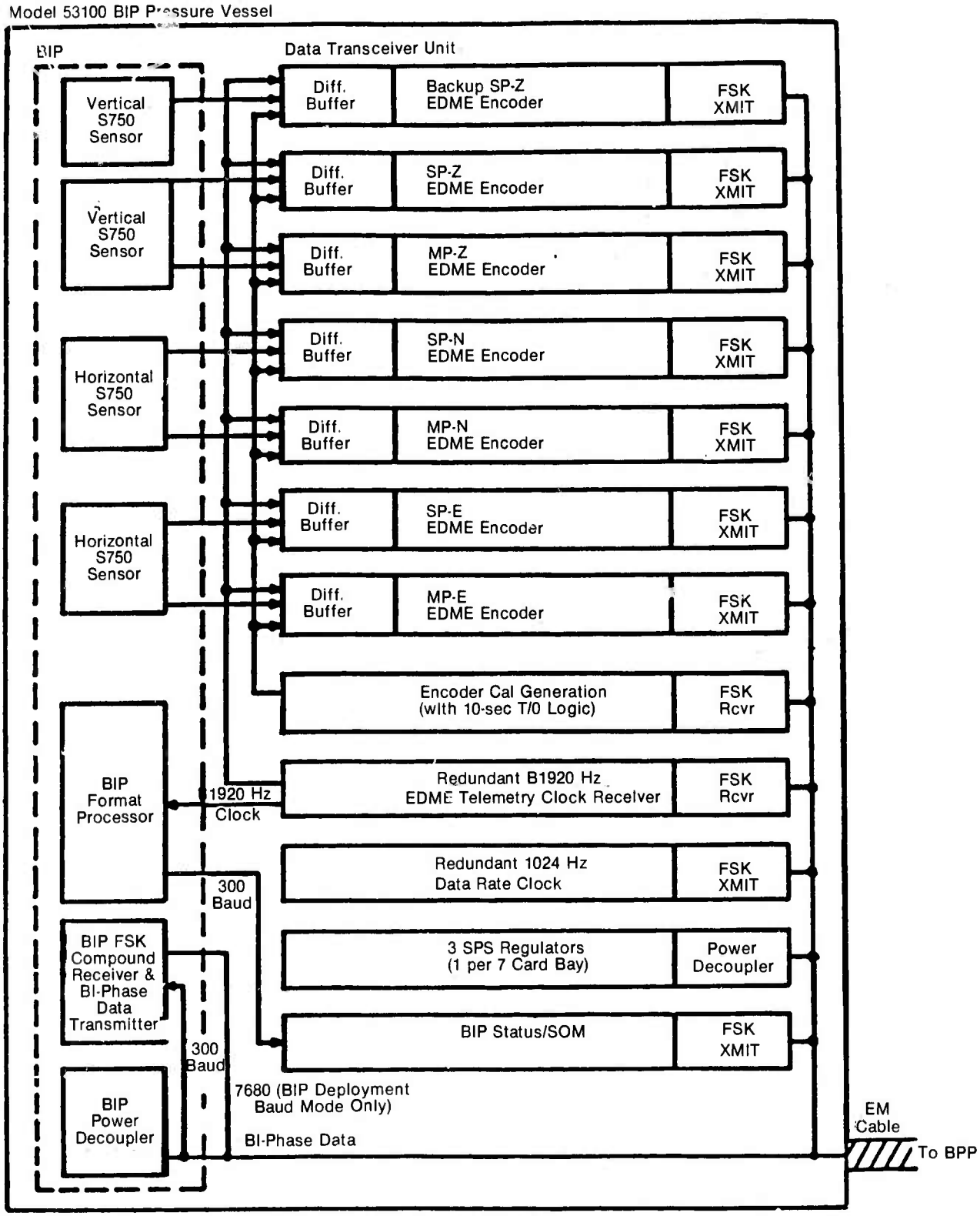


Figure 10. BIP data transceiver unit.

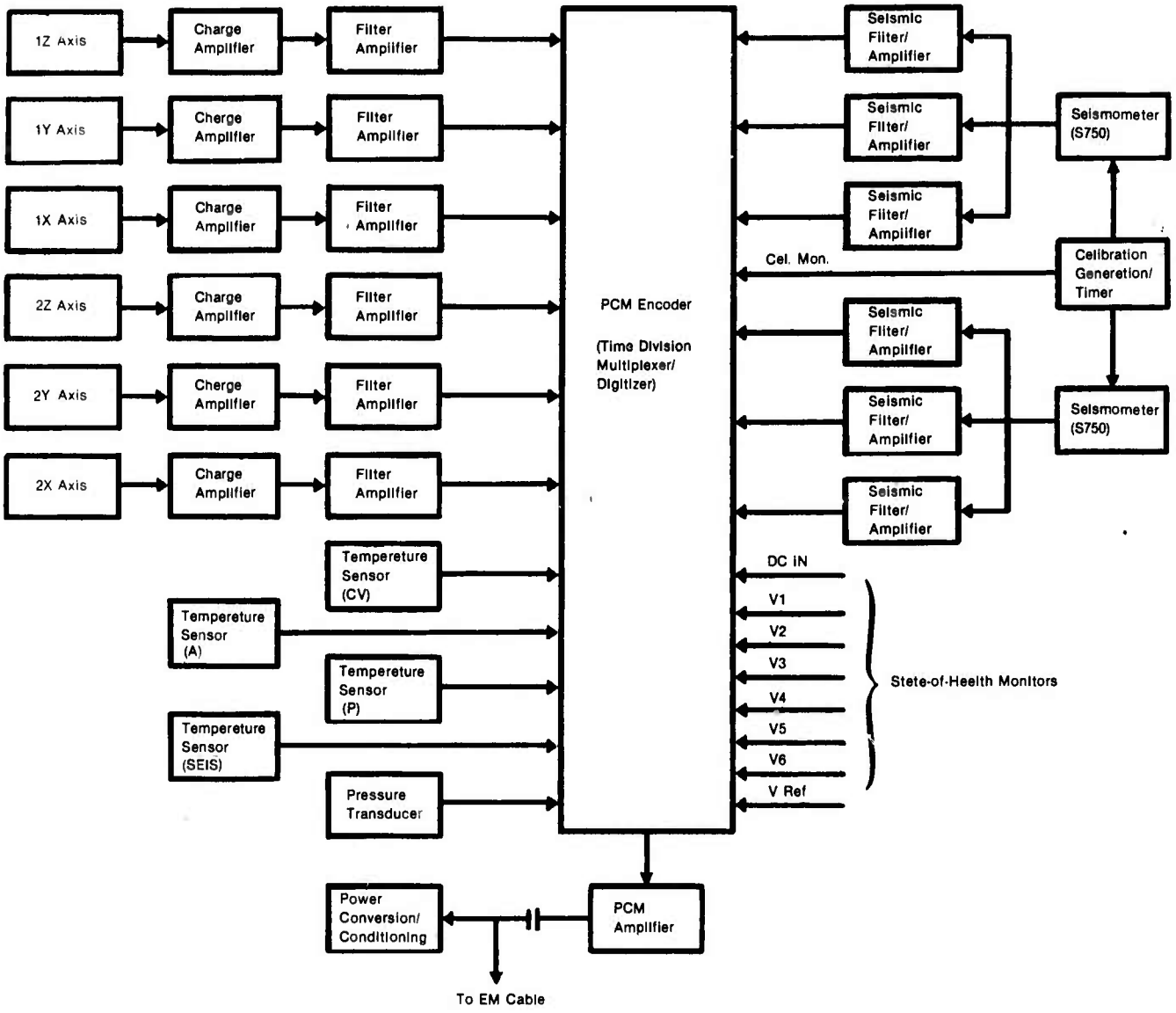


Figure 11. MSS-81 BIP functional block diagram.

display and 12 user programmable digital-to-analog (D/A) output ports to display BIP and state-of-health data. Hard-copy outputs of cathode ray tube displays were available. All D/A output ports were hardwired to the patch panel where they could be patched to any of 12 strip chart channels. The decommutator device was limited to 12 programmed D/A ports and 1 front panel D/A port, the input of which was selectable.

The three analog strip chart recorders permitted recording up to 12 channels of real-time or playback analog data. Each recorder had an additional edge-marker pen for use as a time or event marker. Time codes were normally applied to the input of this channel.

The BIP power supply system consisted of redundant sets of DC power supplies in series, providing 150 VDC @ 300 mA maximum. Back-up power could be selected via a front panel switch.

The STC technical system power was supplied by two uninterruptable power systems to isolate the system from ship's power surges. A reserve of 19 min of stable power was available in the event of loss of ship's AC power.

Figure 12 shows diagrams of both of the STC and the BIP. All power transmission and data flow between the STC and the BIP were via the EM cable.

The 9000-lb, watertight STC was mounted on 4- x 4-inch steel skids, which were welded to the port side main deck of the GLOMAR CHALLENGER.

C. Bottom processing package

The MSS-82 operation defined a requirement for a seismic signal analog-to-digital subsystem and a means for transmitting multiple data channels from the BIP to a DARS over a coaxial cable. The basic function of the DARS for MSS-82 was to provide a continuous recording of hydroacoustic, seismic, and BIP state-of-health data. The DARS, along with its power system and hydroacoustic

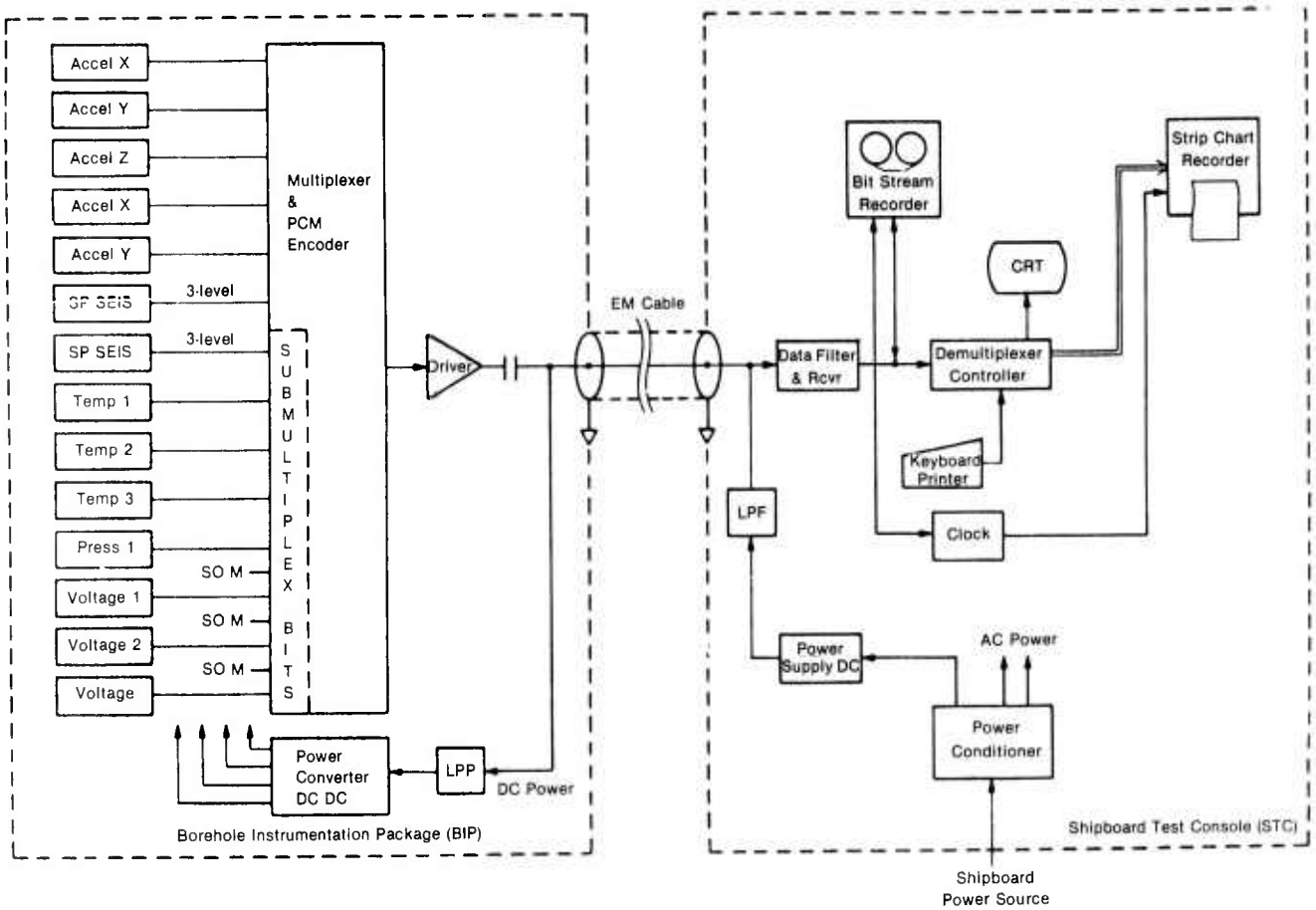


Figure 12. Functional block diagram of the STC (right) and the BIP (left). The EM cable connecting the two instrument subsystems was about 30,000 ft long. (SOH = state of health; 3-level indicates 3 gain bands for the recording.)

sensor system, was incorporated in a single package designed to rest on the seafloor, i.e., the BPP.

The BPP was about 8 x 8 x 7 ft high. It was comprised of three OBS-type aluminum spheres, each 40.5 inches in diameter. The 7078 aluminum spheres were designed for a 20,000-ft depth capability. A 12-inch mud skirt was designed to stabilize the BPP in the ocean-bottom sediments. The BPP weighed about 10,000 lb dry and 4500 lb wet. The EM cable terminated near the bottom of the package on a pivoted arm. Figure 13 shows the BPP configuration.

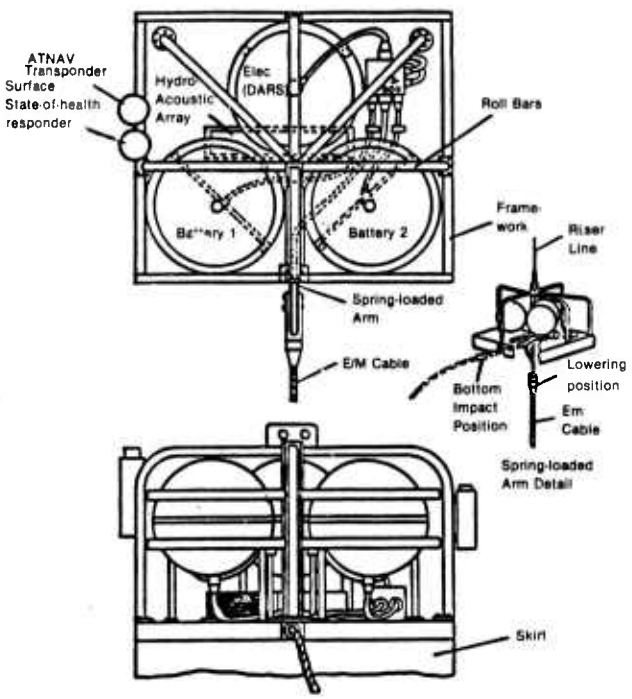


Figure 13. BPP configuration.

The DARS electronic package was housed in one of the aluminum spheres. Silver zinc batteries were installed in the other two spheres. The two battery spheres comprised the power system for supporting both the DARS and the BIP. Power transmission and the flow of data between the BIP and the DARS were via the EM cable. Basically, the BPP functional components comprised five subsystems:

- A hydroacoustic sensor system that would operate in parallel with the BIP and allow correlation of seismic events recorded through both mediums;
- A power system that would support system operations for up to 45 days, with output voltages of −12 V, 0 V, +5 V, +12 V, and +51 V;
- data input assembly (DIA);
- data storage controller (DSC);
- data storage assembly (DSA) (the DIA, DSC, and the DSA comprised the DARS).

Other DARS major assemblies were

- state-of-health sensors and surface communicator,
- HCD-75/controller/formatter (2),
- HDC-75 tape drives (20) and cartridges (20).

The DIA performed several functions in providing a communications interface between the BIP and the DSC. An FSK demodulator was provided for each of the seven data channels from the BIP, with an FSK modem provided for the BIP command/status channel. Two multichannel finite impulse response filters were incorporated to decimate, bandpass limit, and convert the serial bit stream output of the delta modulators into 24-bit, 2 samples per second (s/sec) complement integers. The midperiod, finite impulse response (FIR) filter output was 4 s/sec for each of the three midperiod data channels. The short-period FIR filter output was 40 s/sec for each of the three short-period data channels and the hydroacoustic channel. An 8-bit A/D converter and a 32-channel analog multiplexer provided means for acquiring and monitoring system state-of-health. Sixteen state-of-health inputs were monitored. BIP state-of-health/status was transmitted to the DIA via separate FSK communications channels. Time synchronization of the real-time clock was accomplished at the time of deployment. An EG&G Sealink model 321 responder was used to communicate DARS state-of-health during BPP deployment. The final function of the DIA was to acquire and buffer seismic, hydroacoustic, and state-of-health/status data one second at a time and to transfer this buffer to the DSC.

The primary functions of the DSC were to acquire the one-second buffers from the DIA, to reformat and buffer the data prior to recording, and to provide for control/interface with the DSA. The DSC contained two 64-kbyte random access memory boards. This 128 kbytes of buffer memory was used to store the one-second data buffers from the DIA prior to recording. In addition, the DSC performed command and control functions with the DSA.

The DSA consisted of two controller/formatters and twenty 3M model HCD-75 tape drives. The 3M HCD-75 tape drives utilized a 600-ft, 1/4-inch formatted digital cartridge. Each cartridge consisted of 16 tracks, 4096 blocks

per track, 1224 bytes per block, for a total of 65,536 blocks or 67.1 million bytes of data storage. Two redundant 3M HCD-75 controller/formatters were capable of addressing any of the 20 tape drives. The block transfer rate was about 58.5 msec per block (1024 byte transfer at 17.5 kbytes/sec). Typical write time was 8 sec for the 128 kbytes buffer memory. Dependent upon data format, there were 38.2, 75.7 or 112.3 hr of data per cartridge.

The hydroacoustic assembly was located on the BPP sled between the DARS and battery spheres (see Fig. 13). The hydroacoustic assembly consisted of four hydrophones, one sensor mount, one pressure vessel connector, one preamplifier, enhanced delta modulation encoder and calibration signal generation electronics, power regulator, sensor package termination, a cable between the sensor and pressure vessel, and pressure vessel termination. Power supply and calibration control were provided from the DARS electronics, and the hydroacoustic analog signal and calibration signal generation were provided from the hydroacoustic sensor electronics.

The BPP/DARS/BIP primary power was provided by two silver-zinc batteries. Each battery was made of 25 PML 2500 cells, connected in series for a minimum capacity of 2500 ampere-hours, at a nominal 38.75 voltage load. The two batteries were connected in parallel for a total minimum capacity of 5000 ampere-hours. With the exception of the state-of-health communicator, which had its own battery power supply, and +12 V batteries that supplied surge relay power to the HCD-75 tape drives, all BPP and BIP power was supplied by the two silver-zinc batteries.

A TER was provided for checking out the various BPP components, as well as BIP interface, prior to deployment.

A diagram of the DARS/BPP components is shown in Figure 14. The design requirements and specifications for the DARS and the DARS/BIP interface were developed by Gould [20] and Lawn [24].

Once the BPP was deployed, the DARS could not communicate with the outside world during the period of the

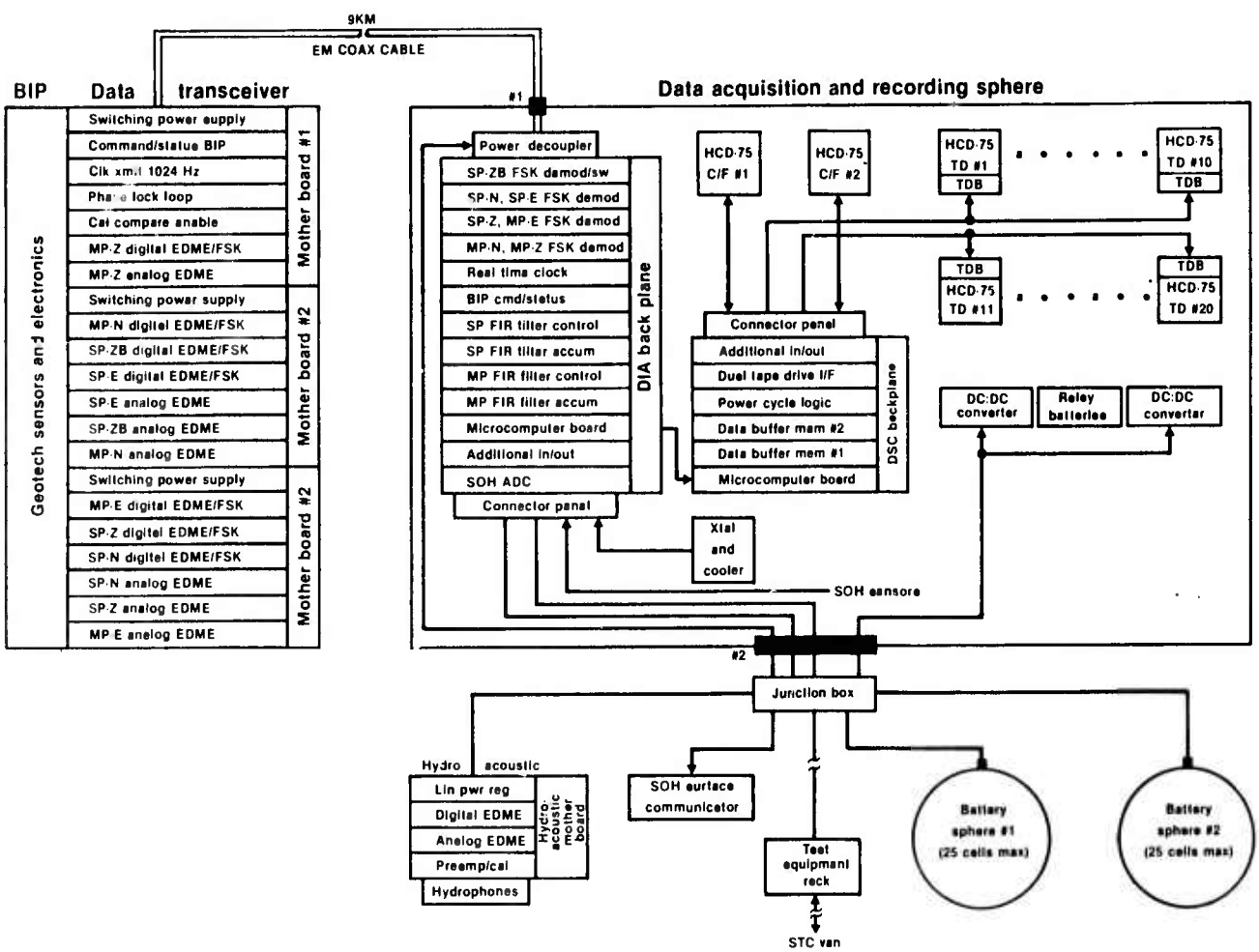


Figure 14. Diagram of BPP and DARS components.

MSS mission. All digitized seismic, hydroacoustic, and state-of-health data was stored within the DARS on high capacity cartridge tapes. A complex IRR system was developed for recovering the BPP (see Part VI, Deployment Equipment).

Gould, Inc., Defense Electronics Division, under the technical direction of NORDA, developed the DARS, the hydroacoustic sensor assembly, the power system, supporting mechanical structures, and test equipment and software required to determine system performance and to acquire shipboard data. Gould also fabricated the BPP sled, using aluminum spheres provided by NORDA.

Detailed descriptions of the BPP and its subsystems, system performance tests and test results, results of the MSS-82 and MSS-83 deployments, and recommended improvements are provided by Gould [20]. Appendix D lists a limited number of drawings applicable to the BPP.

D. Test equipment rack

The TER, fabricated by Gould, Inc., emulated most of the BPP functions. The TER provided a means for interfacing with the DARS unit of the BPP to test, troubleshoot, and verify system performance prior to deployment of the BPP. The TER also provided a means for directly interfacing with the BIP via the EM cable, recording data acquired by the DARS, and monitoring system state-of-health during deployment. The TER consisted of the following assemblies:

- state-of-health communications receiver,
- shipboard recording unit,
- microprocessor control unit,
- test interface unit,
- strip chart recorder,
- data input assembly,
- power supply.

Figure 15 is an overview of the interfaces and functions performed by the TER. The control assemblies of the TER were the test interface unit and the microprocessor control unit. The test interface unit provided a means for

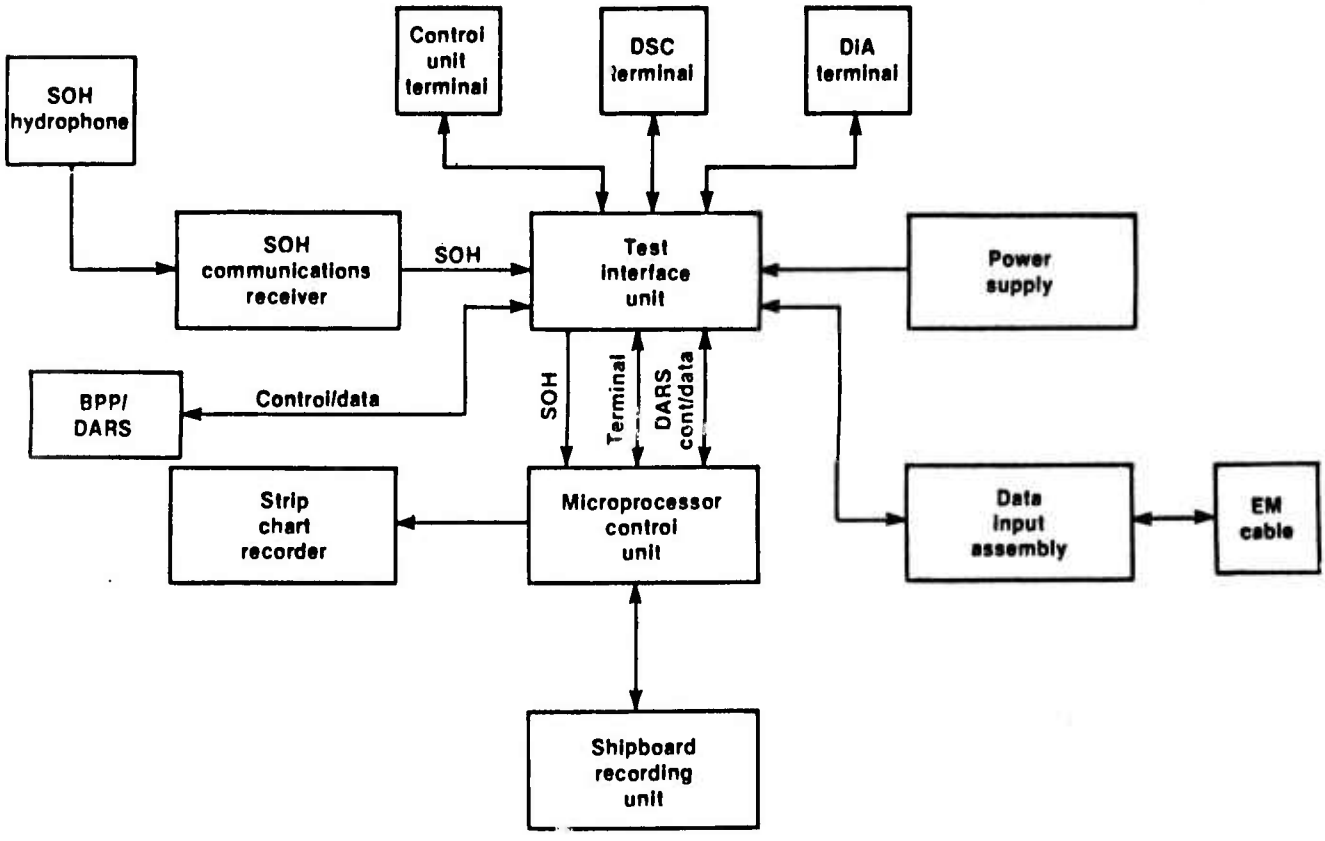


Figure 15. Test equipment rack block diagram.

interfacing the various peripheral units, as well as the BPP, with the microprocessor control unit. The test interface unit could interface with the DARS either through the BPP junction box, or directly when the DARS was removed from its sphere. The test interface unit also provided an interface between the state-of-health communications receiver and the microprocessor control unit, such that during the deployment of the BPP, the system status transmitted by the state-of-health responder was received by the state-of-health communications receiver, digitized by the test interface unit, processed by the microprocessor control unit, and displayed on the control unit terminal. The DIA, which was identical to the unit in the DARS, also interfaced with the microprocessor control unit through the test interface unit. System time synchronization was performed by the test interface unit.

The microprocessor control unit provided a means to perform the shipboard recording function (emulating the DARS data storage control unit), processed and displayed system state-of-health during deployment, postprocessed data from tapes, and provided real-time displays of single channels of data. The shipboard recording unit, consisting of two HCD-75 tape drives and one HCD-75 controller/formatter, performed real-time data recording when the BIP was in the borehole and the BPP was still aboard the ship. The unit could also process previously recorded data. The DIA, a duplicate of the DARS unit but with the state-of-health/ADC board removed, interfaced the TER to the BIP prior to deployment. The TER power supply provided power to the data input assembly or the DARS in place of the batteries during shipboard checkout of the system.

The TER, the BPP, and the STC were used in three modes of operation: BIP deployment/installation mode, the dual recording mode, and the operational mode. During the BIP deployment and installation, the TER and STC were connected to the EM cable to provide power to the BIP by the TER, exercise command and control of BIP functions by the STC, acquire BIP status and data by the STC during BIP deployment, and verify BIP sensors and electronics through the STC after BIP installation.

In the dual recording mode, as data was recorded on board ship, the BPP was interfaced to the EM cable as well as the STC. The TER was connected to the BPP to acquire data from the DARS. In this mode, power was provided by the TER, command and control of the BIP was performed by the STC, BIP status and state-of-health were acquired by both the TER and STC, seven channels of seismic data were acquired and recorded by both the TER and STC, and calibrations were initiated by the STC.

In the operational mode, the BPP was connected directly to the EM cable and the STC was removed from the circuit. The TER was connected to the BPP to initialize the DARS and to synchronize and set system time. The TER was then disconnected and the BPP deployed. The functions performed by the BPP and the TER were to provide system power by the batteries, monitor system status by the TER via an acoustic link during deployment, and initialize tape drives and data recording.

E. Ocean bottom seismometer

The OBS was included in all MSS deployment plans for comparing borehole seismometer signals and noise levels with similar signals recorded on the conventional OBS. The MSS-81 experiment included four OBSs dropped by seismologists from the University of Texas. These seismometers were 10 Hz, Mark L6 geophones. Each OBS was programmed to record 40 s/sec of digital data with a sampling interval of 8.352 msec during refraction shots.

OBSs from the Scripps Institution of Oceanography were used for the MSS-83 deployment. These OBSs were self-contained, digital instruments that recorded a vertical component, two orthogonal horizontal components, and a hydrophone. Data was digitized at 128 s/sec with approximately 13 sec of data stored in memory before tape recorder activation. The OBS frequency response used during MSS-83 is shown in Figure 16.

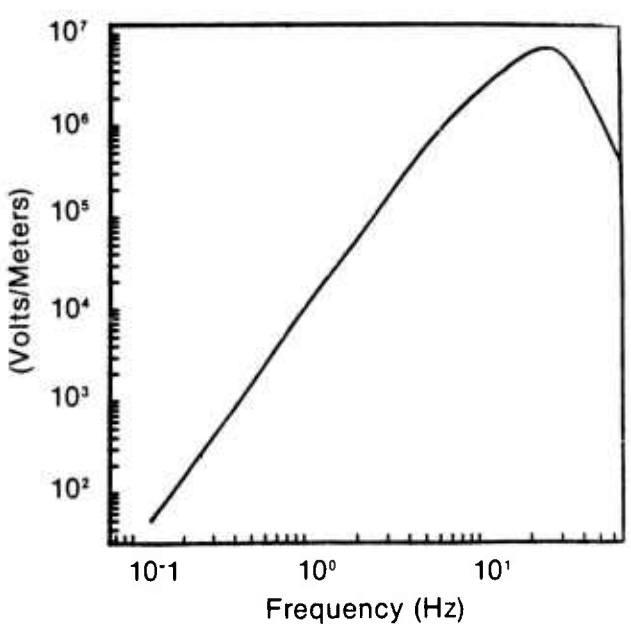


Figure 16. OBS frequency response.

VI. Deployment equipment

A. Shipboard equipment

The principal MSS shipboard equipment units were a dual-traction-drum EM cable winch, an over-the-side A-frame with a large swiveled sheave and a centrally mounted heave compensator, an idler sheave, a work platform, and a box for storing IRR system mooring lines. A large assortment of miscellaneous equipment was required for each deployment. Figure 17 shows the general layout of MSS equipment aboard the GLOMAR CHALLENGER. Drawings of the equipment layout aboard the GLOMAR CHALLENGER are included in Appendix D. A list of other drawings applicable to MSS shipboard equipment is also presented in Appendix D.

1. EM cable winch

The Pengo diesel-powered, dual-traction wheel winch was obtained from Navy stock and refurbished during MSS-81. The winch assembly, mounted on a steel tubing frame, was 110 inches high, 91 inches wide, and 232 inches long. The winch weighed about 38,000 lb when loaded with cable.

The winch would accommodate 30,000 ft of 0.692-inch coaxial cable and could be rigged for 2-inch wire rope, 1.5-inch and 0.875-inch polyester braided line (IRR system mooring line). The winch provided power takeup and payout, including variable constant cable tensioning up to 15,000 lb and a maximum line pull of 20,000 lb. A variable cable speed payout of up to 20 ft/sec was available.

The winch assembly was mounted on an 8-inch I-beam foundation that was welded directly to the port side main deck of the GLOMAR CHALLENGER (see Fig. 17). Figure 18 is a sketch of the installed winch.

2. A-frame

The initial A-frame (MSS-81) was a simply designed structure that was mounted on two pinned inboard pedestals at frames 134 and 142 on the port side main deck. The MSS-81 A-frame was fabricated and installed

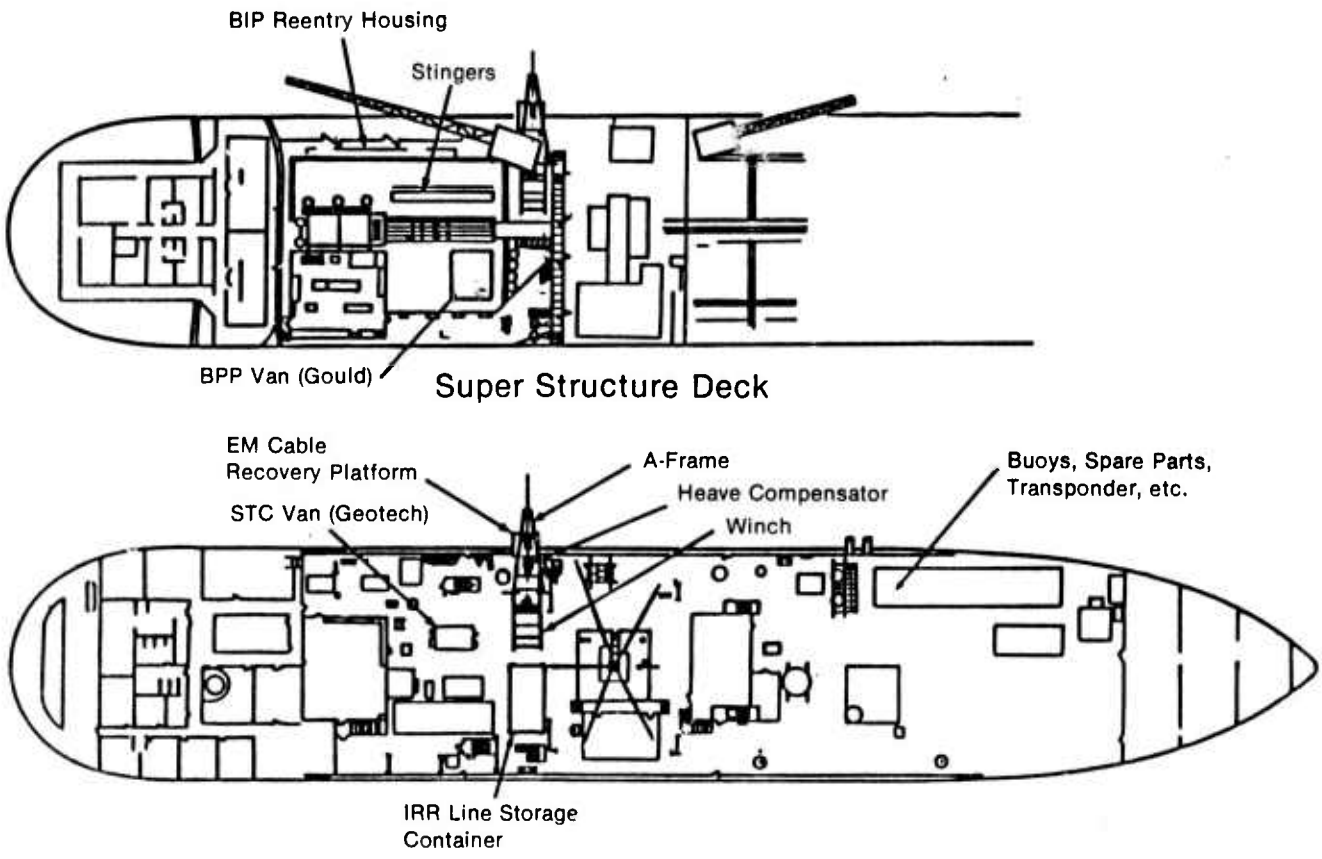


Figure 17. General layout of MSS equipment aboard the GLOMAR CHALLENGER.

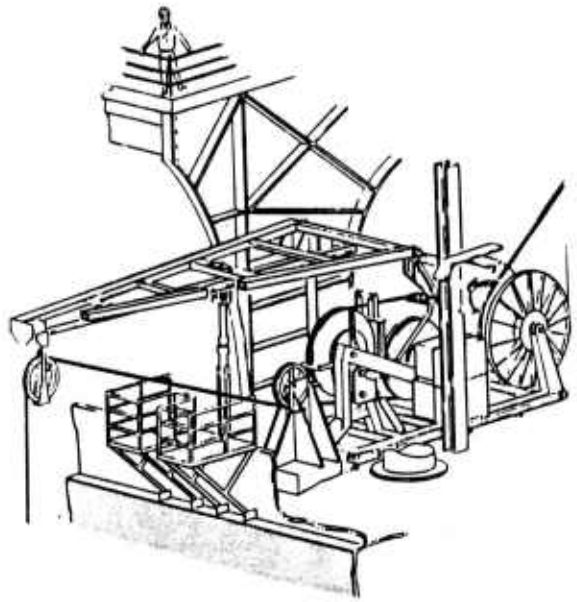


Figure 18. General layout of the EM cable winch, idler sheave, A-frame, sheave, and heave compensator aboard the GLOMAR CHALLENGER.

at Puerto Rico Drydock and Marine Terminals Shipyard. The A-frame projected above the deck about 8 ft and overhung the side about 15 ft. The A-frame was rated at and tested to 28,000 lb. A 48-inch sheave was supported at the outboard end by a tension type Martin Decker load cell transducer. The load cell could be read out at either a large gauge dial or a digital recorder mounted at the heave compensator console.

For MSS-82/83, the A-frame was a newly fabricated structure that had been strengthened for greater loads anticipated during BPP deployment and recovery operations. The removable 28-ft, cantilevered A-frame extended about 18 ft over the ship's port side (Fig. 18). The 48-inch swivel sheave was remounted on an I-beam trolley that could be moved inboard by a jacking screw, which was manually driven by a chain wheel through a 10-ton Duff-Norton jactuator. The gear ratio of the jactuator was selected so that the trolley could be stopped at any selected position without a special securing mechanism.

3. Heave compensator

The heave compensator was fabricated from a refurbished air/oil guideline tensioner and mounted in the center of the A-frame (Fig. 18). The system included a single 11-gal accumulator, 4 standard size nitrogen bottles, a gas-oil reservoir, and a control manifold console. Following the MSS-81 deployment a second 11-gal accumulator bottle was added to the system to improve overall operational response. Figure 18 shows a partial sketch of the installed heave compensator.

The heave compensator maintained constant tension on the EM cable by taking up or paying out cable through the rise and fall of the A-frame in accordance with vessel motion due to sea action. Tension was maintained on the line through A-frame movement, which was generated by nitrogen gas pressure in the compensator cylinder. When upward movement of the ship caused an increase in tension, the cylinder retracted (thus increasing the free length of cable) and maintained the selected line tension. The reverse movement tended to decrease line tension and allowed the cylinder to extend (thus shortening the free length of cable) so that constant tension was maintained.

The pressure in the tensioner cylinder determined the tension achieved. The two 11-gal accumulator bottles served to limit the range of pressure variation in the tensioner cylinder as the cylinder position changed. The volume of these two pressure vessels determined the tension variation from the movement of the cylinder. A gas-oil reservoir was mounted on the tensioner and connected to the cylinder. Oil filled the rod end of the cylinder and partially filled the reservoir, which had a low-pressure air charge. This feature provided continuous lubrication, system damping, and safety control by means of a restrictor in the line. In the event of a cable failure, the cylinder extended to its full stroke but at a controlled velocity, thus preventing any damage to the tensioner or adjacent equipment. Complete control of the heave compensator was accomplished at a centralized control panel.

4. Idler sheave

The idler sheave (U.S. Navy equipment) was fixed to the deck immediately outboard of the EM cable winch assembly (Fig. 18). Its function was to align the EM cable off the A-frame sheave with the winch traction wheel. After MSS-81 the idler sheave was modified by adding a strain-sert pin and load-all indicator. The indicator was calibrated to provide a direct reading of tension in the EM cable. The redesigned idler sheave also included a Martin-Decker load cell (relocated from the A-frame sheave). However, it was determined that this load cell functioned better in its original position between the end of the A-frame and the swivel sheave.

5. Work platform

A portable work platform was suspended from the bulwark 4 ft above the main deck in the vicinity of the

EM cable and the A-frame (Fig. 17). The platform was used for changing out the swivel sheave (suspended from the A-frame trolley) and for securing the EM cable during load transfers required for BPP deployment.

6. IRR system mooring line box

Lines for the IRR mooring system were stored in an 8- x 8- x 20-ft steel container. The container was fixed to the main deck, starboard side, in line with and athwart ship from the EM cable winch (Fig. 17). The container foundation was designed to accommodate deck camber and to permit water to flow under the container.

7. Miscellaneous equipment

A rather extensive array of special tools, fittings, and miscellaneous handling equipment was required for each MSS deployment. Included in this category were such items as fishing tools, handling slings for the BIP and reentry sub, sheaves, Baker special tools, test equipment, etc.

B. Subsea equipment

The subsea equipment consisted of a reentry subassembly; a specially designed coaxial EM cable; and an assortment of lines, buoys, transponders, and an anchor comprising the IRR mooring system.

1. Reentry subassembly

The primary purpose of the reentry subassembly was to deliver a working BIP (i.e., attached to the EM cable) into the top of a borehole. Design constraints required that the reentry sub weight be approximately the same as that of the normal downhole assemblies. Other constraints required that the reentry sub be compatible with the drilling equipment and geometry of the GLOMAR CHALLENGER. The components or subassemblies of the reentry sub were the carriage control sub, the BIP carriage housing, the BIP carriage, the stinger housing, and the stinger (Fig. 19). The transition to the drill string was provided by an assortment of bumper subs and lightweight drill collars. The overall length of the MSS-81 reentry sub was 67.6 ft. The outer dimensions of the 35.96-ft BIP carriage housing were 16 x 27.25 inches. The reentry sub weighed about 16,600 lb. Several alloys were used in fabricating the reentry subassembly to achieve the required strength levels.

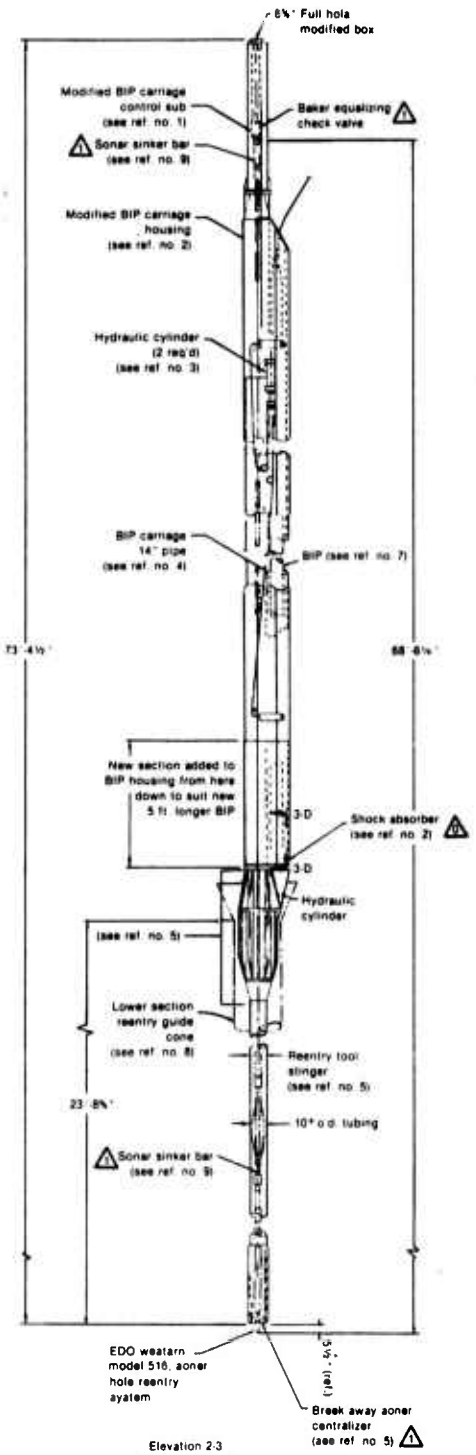


Figure 19. Reentry subassembly configuration illustrating components or subassemblies.

- The control sub was made of A1S1 4140; yield strength was 100,000 psi.

- The carriage housing was 16-inch, schedule 40 pipe of API-5LX, grade X-52, split lengthwise, with a 0.5- x 11.25-inch plate, made of ASTM A-131 with a yield strength of 51,000 psi, inserted.

- The carriage tube was 14-inch, schedule 40 pipe, ASTM A-53 grade B.

- The stinger tube was made from A1S1 WDOM tubing with a 60,000-psi yield strength.

- The stinger tip was made of ASTM-543 CL1 forged steel; yield strength was 85,000 psi.

- The hydraulic plug/sonar adapter was made of A1S1 4140; yield strength was 100,000 psi.

- The shock ring elastomers were Buna-N and natural rubber.

The reentry control sub was 7.5-ft long, heavy wall, high-strength cylinder designed to mate with a Baker internal packer plug. With the plug in place, saltwater hydraulic pressure could be applied to actuate BIP transfer cylinders. The reentry control sub was also designed to support a special Edo reentry sonar tool.

The BIP carriage housing assembly was a welded structure that supported the internal movable BIP carriage. The carriage was carried off-center to provide passage for the sonar reentry tool. The BIP carriage was locked in place by four shear pins. Saltwater pressure applied to two hydraulic cylinders would cause the pins to shear and move the carriage laterally into the centerline release position. Within the carriage, the BIP was installed on shock mounts. The 24-ft stinger section, designed to guide into and seat at the reentry cone throat, was bolted to the housing section with eight high-strength bolts.

The sequential functions of the reentry sub were to provide a protective enclosure for the BIP during drill string deployment, support and position the sonar reentry tool for cone reentry, stab into the reentry cone with a BIP impact of less than 10 g, release the BIP for entry into the borehole, allow the EM cable to run into the borehole, and release the EM cable from the reentry sub.

Initial deployment procedures (MSS-81) called for a hydraulic plug/sonar adapter positioned at the lower end of the stinger and for the sonar tool to extend a few inches below the stinger. After locating the reentry cone and positioning the reentry sub, the stinger was stabbed into the cone. The hydraulic plug/sonar adapter was then raised to the control sub, where it served as a hydraulic packer. Pressure was applied to the reentry sub hydraulic system and caused the BIP to be moved into the centerline position above the borehole. The BIP was lowered into the borehole by paying out the EM cable, with the cable feeding through a slot in the carriage, carriage housing, and then through the stinger. The EM cable release cylinder, at the lower end of the BIP carriage, retained the cable inside the stinger until the stinger was clear of the reentry cone. Once the stinger was raised clear of the cone, hydraulic pressure was again applied to actuate the EM cable release gate, and the cable was freed from the reentry sub.

Subsequent to the MSS-81 deployment several modifications were made to the reentry subassembly. The stinger was redesigned to provide a better interface with the reentry cone and to improve the overall strength of the unit. The high-strength bolts attaching the stinger to the carriage housing were increased from 8 to 10. The bottom of the stinger was modified to accommodate a sonar centering breakaway plug. This plug was supported by shear pins capable of supporting the weight of the sonar tool, but would shear when the weight of the BIP was released.

The BIP carriage housing was lengthened by 5 ft to accommodate a longer BIP. The MSS 2/83 BIP was equipped with a cable decoupler and BIP centering device, which opens locking pawls when there is no load on the EM cable. A shock absorber lined with stainless steel was installed in the BIP carriage to restrain the pawls during the BIP carriage transfer operations.

The control sub was modified by permanently welding the hydraulic plug/sonar adapter in the control sub position. The centering function was then served by the sonar breakaway plug, or a centralizer spring.

The hydraulic plug/sonar adapter was modified to provide a shoulder support for a new Baker check valve. This valve closed the opening through the control sub when the saltwater hydraulic system was activated.

The sonar tool sinker bar assembly had an overall length of 69 ft, which included the sonar tool, a centering spring, three lengths of 2-inch schedule 80 steel pipe, and a support sub. When the support sub rested on the hydraulic plug/sonar adapter support shoulder, the sonar tool extended about 6 inches below the end of the stinger.

Two modifications were made to the BIP transfer system. Plugs with orifice holes were installed in the outlet ports of the BIP carriage transfer cylinders to provide more controlled travel of the cylinders after the pins sheared. In addition, a 1000 psi relief valve was installed at the EM cable release cylinder to provide a visual indication at the drill floor when pressure was applied to the EM cable release cylinder. The BIP carriage transfer cylinders operated at 2500 psi. After BIP transfer, the pressure was increased to 3000 psi, which caused a disc to rupture. The rupture permitted a saltwater hydraulic fluid flow to the EM cable release cylinder. When water reached the cylinder, a 1000 psi relief valve activated, which caused the system pressure to drop to 1000 psi. This sudden drop in system pressure was observed on the pressure gauge at the drill floor.

The overall length of the modified reentry subassembly was 73.5 ft. The weight, when loaded, was about 22,880 lb. A selection of drawings, as well as a list of other drawings of the reentry sub, is presented in Appendix D.

2. EM cable

The EM cable, developed by NORDA, was a submarine tow cable with a center element of No. 10 AWG stranded 18/0.234-inch SBC with nylon center filament wire. The wire was enclosed by left- and right-hand armored, torque-balanced mesh. The main characteristics of the EM cable are listed:

- Outside diameter 0.692 inch
- Length 30,000 ft
- Breaking strength 21,000 lb
- Design load 16,000 lb
- Dry weight per unit length 0.46 lb/ft
- Wet weight per unit length 0.29 lb/ft
- Longitudinal stiffness 2×10^6 lb

The cable length of about 30,000 ft allowed for ocean current, ship stationkeeping, and slacking off during data recording. Figure 20 shows the details of the cable structure. Studies of EM cable response due to currents and ship motion, and EM cable and drill pipe entanglement are presented in Appendix B.

3. IRR system

After BPP deployment, the IRR system provided the sole means for recovering MSS data and the borehole instrumentation (see BPP, Part V, Instrumentation). The IRR system was a completely submerged array, designed for high reliability by the Naval Civil Engineering Laboratory, Port Hueneme, California. Primary design criteria included:

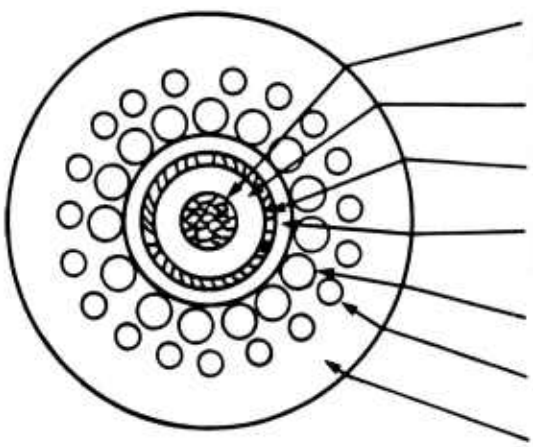
- assurance of structural integrity, with emphasis on static and dynamic loads;
- isolation of BPP from IRR system tensions and vibrations (a "soft" cable system);
- high recovery probability (redundant recovery procedures);
- high probability of successful operations through simplified procedures and component parts.

The following performance factors were considered critical for successful operations:

- shape of the installed array,
- behavior of the array in various failure modes,
- capability to free-fall the anchor while maintaining acceptable loads and final configuration,
- capability to activate acoustic release and surface some part of the array.

The IRR system, when deployed, resembled a trapezoidal array. One end of the array was fixed to the ocean bottom by a 2000-lb clump anchor. An 18,000 ft, 0.875-inch power braid (anchor leg) extended from the anchor to a parallel set of release and tracking transponders. A 10,000 ft, 0.875-inch power braid (grapnel leg) extended between the release/tracking transponders and a 26,500 ft, 1.75-inch power braid (riser leg). The grapnel leg was partially suspended in a horizontal mode about 4000 ft below the ocean surface by an assortment of buoys and flashers. The 21,500-ft riser leg was connected at its lower end to a 1500-ft length of 1.125 inch steel cable that was fixed to the BPP. This 1500-ft cable served as an isolation link for the BPP; its weight provided a reaction to the static and dynamic tensions produced in the mooring

The BIP Em cable is a submarine tow cable consisting of (10) #10 AWG coax with an overall double-caged armored and Hytrel jacket.



#10 AWG, stranded, 18/.0234″ SBC. with a nylon center filament. O.D. = .117″.

LDPE, nom wall = .081″. O.D. = .279″.

Braid return, #33 AWG SAC, O.D., = .307″.

LDPE, .050″ wall. O.D. = .407″ (compressed O.D. = .397″).

16/.059″ GXIPS, RHL. O.D. = .513″.

18/.049″ GXIPS, LHL. O.D. = .611″.

Hytrel sheath, .040″ wall. O.D. = .692″.

Characteristics

• Electrical:	Nom conductor DC resistance @ 20°C:	@ 10 AWG:	1.08 ohms/K ft.
		Coax return braid:	1.40 ohms/K ft.
	Voltage rating:		2,500 Volts rms
	Characteristic impedance:		40 ohms (ref)
	Attenuation at 500 KC:		1.4 dB/K ft.
• Mechanical:	Filled shield:		Templube blkng compound.
	Break strength:		21,000#
	Weight in air:		462 #/K ft.
	Weight in water (SG = 1.027)		295 #/K ft.
	Torque balanced design		

Figure 20. EM cable components and characteristics.

system. A 300-ft length of 0.625-inch (strain relief) cable was connected to the BPP and the EM cable to temporarily support the EM cable while recovering the BPP.

The static shape of the array was defined by the assortment of buoys (17-inch diameter glass spheres). The positioning of the buoys controlled the shape of the array, since the cables were close to neutrally buoyant. The buoys served to lift a portion of the array to the surface after the acoustic release was activated. The buoys and flasher/reflectors also provided visual references for locating the grapnel leg on the surface. In the event of acoustic release failure, the horizontal portion of the array would be grapnelled.

Figure 21 is a sketch of the IRR system, and Table 1 is a list of IRR system components and approximate weights. IRR system performance analysis was provided by the Western Instrument Corporation [25]. A stress analysis of the system was performed by Global Marine [14]. Procedures for IRR deployment [18], as well as for the recovery and redeployment of the system, were developed by Global Marine [19]. Drawings for the IRR system arrangement are included in Appendix D.

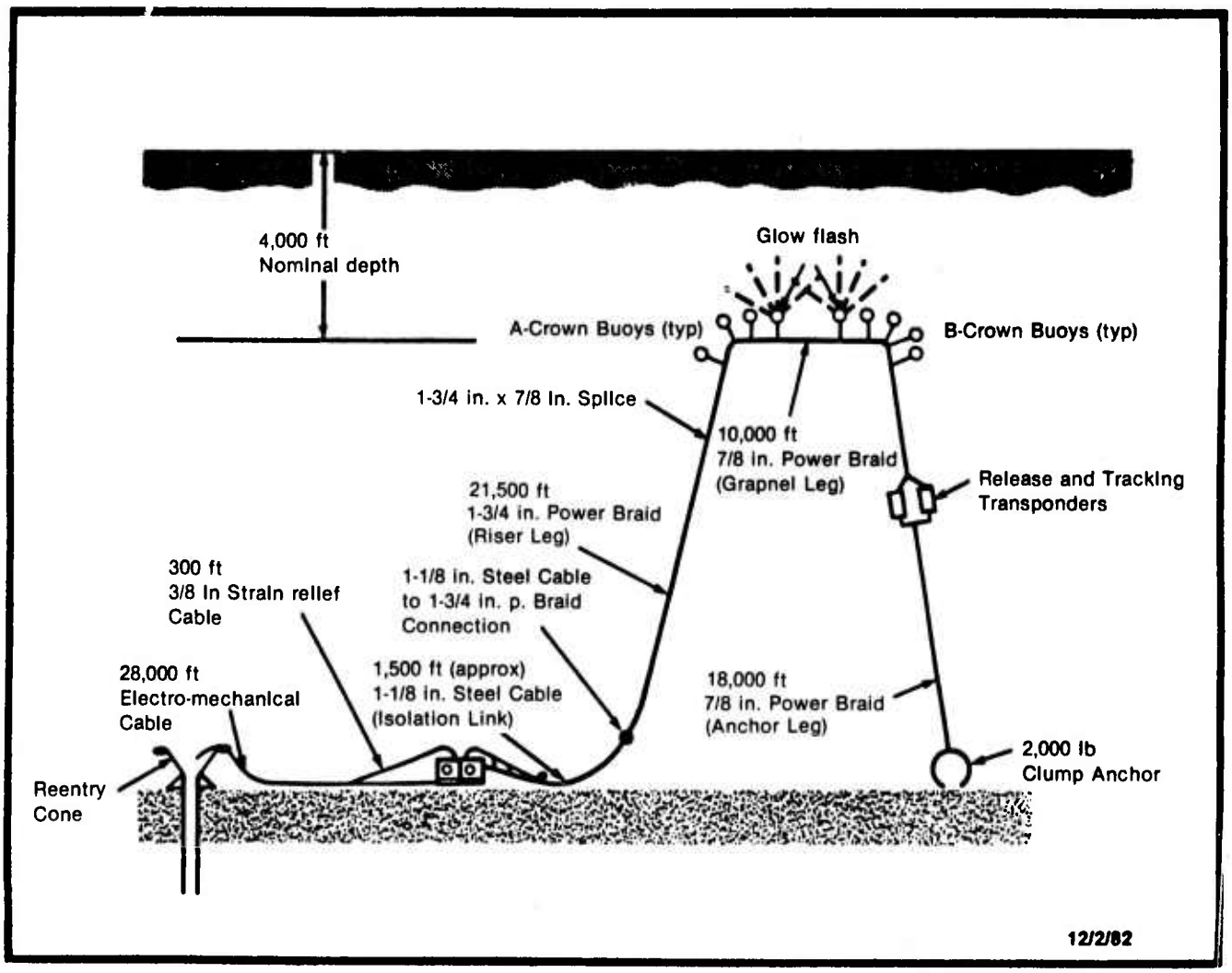


Figure 21. Deployed configuration of the BPP IRR.

Table 1. List of IRR system components and approximate weights.

Item	Weight (Pounds) Dry	Wet	Remarks
BPP	9,600	4,900	8 x 8 x 7 ft sled
Swivel (BPP)	35	30	—
Wire cable	3,195	2,812	1500 ft, 1.5-inch wire rope
Strain relief cable	200	176	300 ft, 0.625-inch wire rope
Lifting line	16,985	-645	21,500 ft 1.75-inch polyester braid
A-crown buoy	368	-408	8, 17-inch diameter glass sphere buoys with hard hats
A-flasher/reflector	15	-4	1, with hard hat
A-buoy pendant	11	8	5, 15 ft lengths of 0.5-inch polyester braid
B-crown buoys	460	-510	10, 17-inch diameter glass sphere buoys with hard hats
B-flasher/reflector	15	-4	1, with hard hat
B-buoy pendants	13	10	6, 15-ft lengths of 0.5-inch polyester braid
Grapnel line	1,970	-79	10,000 ft, 0.5-inch polyester braid
Dual acoustic release	30	20	—
Anchor line	3,546	-720	18,000 ft, 0.5-inch polyester braid
Swivel (anchor clump)	5	4	—
Chain and shackles	30	27	10 ft, 0.5-inch chain
Clump anchor	2,000	1,600	Steel ball
Connections (lift line)	25	20	—
Miscellaneous hardware	50	44	Bolts, nuts, thimbles, etc.

VII. MSS Program cost summary

A. Overall MSS program costs

The initial MSS program plan was divided into six phases:

- Phase I: Feasibility studies (1980)
- Phase II: Design, mobilization planning (1980)
- Phase III: Procurement, design, MSS-81 at-sea tests (late 1980-late 1981)
- Phase IV: MSS-82 mobilization and operations (late 1981-late 1982)
- Phase V: MSS-83, "Fly-In" (Configuration II) development operations (late 1982-late 1983)
- Phase VI: Configuration II mobilization and operations (late 1983-late 1984)

The program sponsor accepted the first four phases and later supported MSS-83 when the MSS-82 effort was aborted. The overall estimated costs of the MSS program for Phases I through V are shown in Table 2.

B. Deployment costs

The costs for the three MSS deployment operations are shown in Tables 3 through 5.

Table 2. MSS deployment program costs projection.*

Activity	I Jan-Jun 1980	II Jun-Sep 1980	III Oct-Sep 1980-81	IV Oct-Dec 1981-82	V Dec-Mar 1982-84	Total
Engineering	$59,000	120,200	71,700	287,200	—	538,100
Testing	—	17,200	1,160,100	99,100	—	1,276,400
Planning	15,400	15,100	37,100	84,100	—	151,700
Program Management	11,200	35,700	108,800	148,700	106,900	411,300
1982 Deployment	—	—	—	762,400	—	762,400
1983 Deployment	—	—	—	103,300	582,500	685,800
Advanced Studies	—	—	—	—	65,700	65,700
Totals	$85,600	188,200	1,377,700	1,484,800	755,100	3,891,400

*Figures displayed represent the broad categories listed. They are not intended to portray the negotiated contract or total actual cost to the Government by detailed work breakdown structure.

Table 3. Costs for the MSS-81 deployment, March 1981.*

Activity	Costs ($)
At-Sea-Test Equipment Design	345,300
At-Sea-Test Equipment Procurement	369,300
At-Sea-Test Planning	21,800
At-Sea-Test Integration	86,400
At-Sea-Test Mobilization and Demobilization	265,100
Operations	83,100
Shore Testing	84,700
Evaluation	35,800
Total	1,291,500

Notes: 1. Excludes GLOMAR CHALLENGER costs
2. Excludes program management costs

Table 4. Costs for the MSS-82 deployment, August-September 1982.*

Activity	Costs ($)
Configuration I Design including IRR	287,200
Configuration I Procurement including IRR	242,900
Operation Planning	84,100
Equipment Test	99,100
Mobilization and Demobilization	286,800
Operations	95,200
Integration	137,500
Total	1,232,800

Notes: 1. Excludes GLOMAR CHALLENGER costs
2. Excludes program management costs
3. Includes IRR system

*Figures displayed represent the broad categories listed. They are not intended to portray the negotiated contract or total actual cost to the Government by detailed work breakdown structures.

Table 5. Costs for the MSS-83 deployment, January-February 1983.*

Activity	Costs ($)
Deployment Mobilization/Demobilization	393,600
Deployment Operations	88,700
Recovery Mobilization/Demobilization	120,600
Recovery Operations	59,800
Evaluation and Reports	88,100
Total	750,800

Notes: 1. Excludes GLOMAR CHALLENGER costs
2. Excludes program management costs

*Figures displayed represent the broad categories listed. They are not intended to portray the negotiated contract or total actual cost to the Government by detailed work breakdown structures.

VIII. Extension of MSS technology

A. Current status

MSS deployments in 1981, 1982, and 1983 demonstrated both the feasibility of implanting seismic instruments in deep-ocean boreholes and the capabilities of such installations for acquiring high-quality seismic data. Techniques for transmitting borehole seismic data to a shore processing facility were not demonstrated; however, this capability has been extensively addressed in conceptual modes and appears to be feasible. Existing DSDP technology, as well as new equipment and technology developed during the MSS program, could accommodate either a continued MSS development program or the establishment of operational ocean-bottom borehole seismic stations served by BPPs for acquiring and storing data.

Initial deep-ocean borehole emplacement and subsequent BIP deployment should require about 20 days on site, including limited contingency time. About 30 days should be allowed for severe weather sites. Most operations can be conducted in sea state 5 conditions or less. However, the reentry cone keelhauling and casing liner reentry should be undertaken in less than sea state 4 conditions.

The MSS equipment, comprised of major components (e.g., the BIP, the reentry subassembly), spare units, and an imposing array of support items and materials, was returned to cognizant custodians upon termination of the MSS program. A final MSS program logistics report [26] includes lists of the MSS equipment and its custodians.

The MSS equipment stored by NORDA and other organizations [26] could, with certain augmentation, refurbishment or replacement, support a reactivated MSS program. Obviously, a well-planned and coordinated effort would be required to retrieve and restore the necessary equipment and execute an MSS deployment.

Certain planning aspects must be tailored to the specific borehole site; however, the basic planning factors and procedures for conducting an MSS deployment are available via the supporting documents developed for MSS-83. The following is a synopsis of those documents.

MSS 83 deployment operational procedures [18]: This document provides instructions for equipment checkout and operation and extends through all phases of an MSS deployment, including initial deployment of the BPP and its associated IRR system. Contingency plans/guidance are included for the most probable equipment failures or malfunctions, and adverse weather. Safety factors and operational limits pertinent to specific phases of a deployment are also included.

MSS 83 IRR recovery & redeployment operational procedures [19]: Step-by-step procedures are provided for recovering a previously deployed BPP and IRR system and their redeployment.

Mobilization and demobilization [21,22,26]: Any MSS site would probably involve a remote ocean area and calls at remote ports. Since mobilization/demobilization requirements are dictated to a large degree by the MSS site, as well as by unique circumstances defined by the time frame and the supporting ships, MSS-83 planning in this respect would not be entirely applicable to a future MSS deployment. However, MSS-83 mobilization/demobilization plans would be of interest to the planners of an MSS-type deployment. These plans are described in References 21, 22, and 26. (Ref. 26 summarizes the logistics requirements for all three MSS deployments.)

While these documents offer definitive guidelines for an MSS deployment, the following elements should be considered for a difficult, deep-water site emplacement:

- detailed plans, including accommodation of potential problems pertinent to designated site;
- adequate time for weather and emergencies;
- full-strength drill pipe string, possibly oversized upper sections;
- cement or heavy mud in highly fractured formations;
- extensive pretest of subsea equipment;
- improved load, penetration, and torque measurement instrumentation.

1. Studies and analyses

A number of studies and analyses were conducted to support the MSS program. These efforts provided a basis for decisions with regard to developing equipment, technology and procedures, as well as for decisions relative to program direction and implementation. Appendix E lists studies and analyses in addition to those discussed in this report that would be of particular interest to a future MSS program.

B. Future operational aspects of the MSS program

The MSS program served to demonstrate new concepts and current technologies with regard to subocean-bottom seismic stations and to identify conceptual approaches to various aspects of the MSS.

1. Alternate reentry concepts

All MSS operations through the 1983 deployment depended on the GLOMAR CHALLENGER for boreholes and BIP implantment. Alternate reentry techniques were considered appropriate, since a dynamically positioned drillship might not be available or, in fact, desirable for future deployments. In addition, an alternate reentry method might provide access to numerous existing DSDP boreholes, if such access becomes desirable.

Two basic alternate approaches for reentry were investigated. These approaches were the use of a guideline-type system and a remotely controlled "fly-in" system. Several options and configurations were evaluated for each of these concepts [27,28]. The "fly-in-on-a-cable" (cable reentry) concept offered the greatest potential for reentry into a borehole with a large seismic instrument package [29]. The basic approach to developing the cable reentry capability was to develop the simplest deployment system. This approach would basically rely on surface-ship maneuvering and incorporating existing automatic station-keeping positioning equipment, plus deployment package sonar ranging or long-base positioning equipment. A simple platform thruster pulse augmentation might be necessary to reduce deployment time.

A scenario for a cable reentry deployment involves a U.S. Navy AGOR or equivalent ship recovering the DARS/BPP/BIP system via the IRR system and EM cable. Subsequently, the cable reentry vehicle would be lowered with the BIP on a special cable. By maneuvering the ship, the cable reentry platform would be positioned over the reentry cone and guided into the cone. After BIP release the reentry platform would be retrieved and the BPP/IRR system redeployed.

Table 6 lists the preliminary general requirements for a cable reentry deployment. The concept requires that these capabilities be integrated into a relatively lightweight, easy-to-handle configuration. In addition, the reentry platform deployment actions would have to be accomplished without entangling the EM cable and the platform support cable.

Table 6. Preliminary general requirements for a cable reentry deployment.

Stow and handle 30,000 ft of EM cable, 25,000 ft of deployment cable, and 20,000 ft of mooring line
Vessel with automatic station-keeping (ASK) capability
Thruster augmentation for surface vessel
Sonar ranging or long baseline platform position reference system
Directional stability for reentry platform
Borehole reentry capability
Isolation of seismometer from impact shock
Subsea release mechanism and control
Cable disentanglement procedure
Motion compensation evaluation
Cementing capability evaluation

Figure 22 shows a conceptual type platform that would meet the preliminary requirements. The platform would be similar in size to the MSS reentry subassembly; however, BIP offset would not be required. The total package (BIP included) would weigh between 8000 and 26,000 lb. Although the concept uses a separate cable to support, control, and recover the platform, it may be possible to use an expendable cable and platform.

A possible developmental test program leading to an operational cable reentry platform is shown in Table 7. This program would use MSS capabilities and equipment to the maximum extent. Despite the apparent feasibility of a deep-water cable reentry deployment, actual data would be needed to verify maneuvering capabilities, platform/cable response characteristics, and drag characteristics. A dynamic three-dimensional computer program would eventually be required to establish the complex interactions between ship motion, current conditions, and platform hydrodynamic responses.

2. Alternate drillships

Resuming the MSS program at its current level of development would require using GLOMAR CHALLENGER or a vessel of similar capabilities. In the event GLOMAR CHALLENGER could not be made

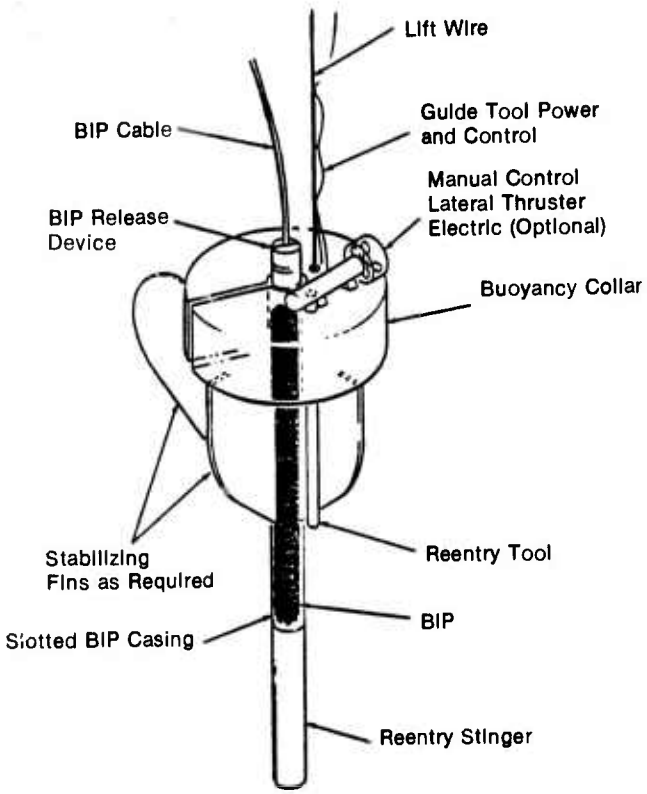


Figure 22. Conceptual MSS fly-in platform.

Table 7. Program for a cable reentry platform development.

Conceptual analysis of maneuvering characteristics
Preliminary design of deployment platform and cable handling system
Model testing of deployment platform
Shallow water (1,000-2,000 ft) reentry test of mockup
Deep-water test of mockup
Final design of deployment system
Procurement and test of deployment system
Mobilization of deployment system
Field operation

available, various alternate dynamic-positioned drillships could be used (Tables 8 and 9). Almost all of these ships have more extensive equipment and more advanced capabilities than the GLOMAR CHALLENGER. All of these ships could be used for MSS deployments; however, substantial predeployment activities would be required to prepare them for MSS operations. Predeployment actions would include procurement of a high-strength drill string (for deep water) and special auxiliary pipe equipment, adaptation of shipboard handling equipment, specialized crew training, and shallow-water tests for working out specific details.

The charter vessel cost of the listed drillships will vary considerably, depending on ship age, length of charter, site hazards, etc. A typical projected short-term rate for an older vessel could be between $30,000 and $60,000/day, while rates for newer vessels could be in the $70,000–$100,000/day range. Fuel, supplies, field office support, mobilization and demobilization are additional costs. Table 10 shows estimates of some typical costs for single or multiple borehole emplacements and instrument deployments. Overall deployment costs (1983 dollars) were estimated to be on the order of $6 million for a single deep-ocean site and $38 million for six to eight worldwide sites accomplished within a one-year period.

3. Deep-ocean seismometers

Since the start of the MSS program, a number of technological advances have occurred that serve to enhance the state of the art in earthquake detection and data collection. Accordingly, several improvements or advancements to the MSS BIP should be considered prior to further experimentation or deployments with this system.

BIP power supply system: A commercially available power supply was selected so that tight project schedules could be met. Although these units performed satisfactorily, they do not have the power efficiency ratings desirable for a system operating from a primary power source other than a commercial or similar AC power line. Future MSS plans should consider a new and improved BIP power supply design.

Long-period (0.01–0.1 Hz) data channels and sensors: The BIP provided this coverage, but a less than optimum sensor was used. The BIP was developed with a design goal of future improved capability in this passband. Improved instruments are now available (see Models 36000 and 44000, Table 11) and could be incorporated in the existing BIP.

Table 8. U.S. Flag drilling ships.

Vessel Name & Owner	Dimensions (ft)	DP System	Drilling Depth/ Water Depth (ft)	Derrick Capacity (lbs)
SEDCO 472 (Sedco)	470 × 70 × 32	Honeywell (ASK)	6,000/25,000	1,000,000
GLOMAR PACIFIC (Global Marine)	452 × 72 × 35	Delco	2,000/25,000	1,300,000*
GLOMAR ATLANTIC (Global Marine)	452 × 72 × 35	Delco	2,000/25,000	1,300,000*
GLOMAR CHALLENGER (Global Marine)	400 × 65 × 26.75	Delco	2,500/25,000	750,000

*approximate

Table 9. Foreign-built U.S.-owned drilling ships or submersibles.

Vessel Name & Owner	Dimensions (ft)	DP System	Drilling Depth/ Water Depth (ft)	Derrick Capacity (lbs)
SEDCO 445 (Sedco)	445 × 70 × 32	Honeywell (ASK)	3,000/20,000	1,000,000
SEDCO/BP471 (Overseas Drilling, Inc.)	470 × 70 × 32	Honeywell (ASK)	6,000/20,000	1,000,000
DISCOVERER SEVEN SEAS (Sonat Offshore Drilling, Inc.)	534 × 80 × 32	Honeywell (ASK)	6,000/18,000	1,300,000
DISCOVERER 534 (Sonat Offshore Drilling, Inc.)	534 × 80 × 32	Honeywell (ASK)	3,000/20,000	
BEN OCEAN LANCER (ODECO/BP)	450 × 77 × 41	Honeywell (ASK)	3,000/20,000	
SEDCO 709 (Semi) (Marine Drilling)	295 × 245 × 113	Honeywell (ASK)	6,000/25,000	1,100,000
SEDCO 710 (Semi) (Sedpex, Inc.)	295 × 249	—	5,000/25,000	
HENRY GOODRICH (Semi) (Sunat)	316 × 246	—	10,000/30,000	
(SEMI)* (ODECO/BNOC)	390 × 231	—	1,500/25,000	1,400,000

*under construction 1984

Table 10. MSS operations cost projections.

Sites	1 (30-dey Charter) ($M) Shellow Weter	8-12 (9-monlh Cherter) ($M) Deep Weter	1 (40-dey Cherter) ($M) Deep Weter
Deployed Equipment, Inc. Development	0.50	5.40	1.30
Drillship	0.80	14.80	2.80
Operetions Support	0.12	2.10	0.38
Mobilization/ Demobilizetion	0.12	1.20	0.17
Drill String & Hendling Equipment	0.21	3.2	0.35
Recovery	0.06	1.2	0.08
Engineering	0.10	1.5	0.25
Contingency	0.19	3.3	0.48
Totels	2.10	37.5	5.81

Table 11. Potential Teledyne Geotech seismometer package configurations.

Instrument Package	Diameter/ Length of Pressure Case	No. of Sensors	Response	Bandwidth	Comments
531000/ 36000	8 inches 33 ft	Up to 6 3 primary 3 secondary or 3 primary 2 vertical backup	Primary 1 x 10^6 V per m/sec^2 secondary 200 V per m/sec^2	Primary 0-20 Hz secondary 0.01-100 Hz	Built-in backup sensors. Single deployment package. Technology and hardware exlst. Reentry of hole necessary.
531000/ 44000	8 inches 33 ft	Up to 6 3 primary 3 secondary or 3 primary 2 vertical backup	Primary 2 x 10^4 V per m/sec^2 secondary 200 V per m/sec^2	Primary 0-25 Hz secondary 0.01-100Hz	—
44000	4.25 inches/ Two 12-ft packages separated by 1000-ft maximum	3 primary only	2 x 10^4 V per m/sec^2	0-25 Hz	Two 12-ft packages 1000-ft separation maximum. Deployed through drill string (ID 4.5 Inches or greater)
Multiple S-750 Verticals	4.25 inches/ One 12-ft, One 6-ft, or One 8-ft, 1000-ft suspension maximum. One 6-ft sensor separated by 1000-ft maximum	Up to 6 verticals only	200 V per m/sec^2 typlcal acceleration 3 x 10^4 V per m/sec typical velocity	0.01-100 Hz	Vertical only. Single or dual packages. Deployed through drill string.
Multiple S-500 Verticals	3.75 inches/ 2 packages One 14-ft signal processor	Up to 6 verticals	500 V/g typical acceleration 450 V per m/sec typical velocity	1.0-160 Hz	Vertical only. Disposable sensor package. Deployed through drill string.

Extended (high frequency) short-period data passband: The BIP sensor channel designs were modeled after land-based seismic surveillance systems and applicable optimization (flat acceleration versus flat velocity responses) features were incorporated. Observing seismic phenomena at frequencies beyond 20 Hz may be justified. But to do so, existing filter designs must be extended and higher data sampling rates achieved with minimal impact on other designs and features of the BIP.

24-bit A/D conversion: Technology advancements have produced digitizers with greater range and lower threshold. The EDME, developed by Gould, Inc., is an example. Teledyne Geotech has developed a single-board, 24-bit digitizer with comparable capabilities.

Cable isolator: Cable decoupling techniques were deemed critical to induced noise-free operation of the BIP. Although an EM cable isolator-seismometer coupler device was developed for the MSS, it was not used. Future MSS efforts should include additional testing and modification, if required, of the existing EM cable isolator. In addition to isolating cable motion, the locking pawls served to center the BIP and couple it securely to the walls of the hole. Although the BIP's mass couples the seismometers to surrounding rocks better than comparable instruments, additional coupling capability is desirable.

EM cable and electrical connector: The EM cable and connecting devices performed satisfactorily; however, there was some concern about the cable-BIP termination interface. The material used (LDPE) offered desirable insulation features, but serious problems were encountered when attempting to provide a bond to the electrical connecting device and achieve the necessary environmental integrity at MSS operating depths. Additional research in this area would be appropriate.

Horizontal sensor orientation: The nature of the BIP deployment made orientation of the device nearly impossible. Reliance was placed on known, man-made, or natural events for determining orientation of the horizontal sensor sensitive axes. These techniques allow orientation determination accuracy of about $\pm 5°$. Future MSS efforts should consider solutions to this problem.

A variety of existing seismometers other than the BIP could potentially be used for deep-ocean borehole installations. Table 11 presents an assortment of Teledyne-Geotech seismometers that have been under development or are in use for various U.S. seismic programs. The MSS program used the large (8-inch outer diameter in pressure case) instrument, which must be delivered external to the drill string. However, smaller-sized packages can be more easily deployed directly through the drill string. This operation eliminates the reentry borehole and allows direct, single trip, hole coring and package deployment activities. This concept is constrained by an instrument with lesser capabilities (as compared to the larger BIP) and is limited to relatively shallow basalt borehole penetrations. Instrument retrieval would probably be eliminated by wall collapse in the uncased borehole. In addition, the EM cable would have to be stripped from the drill string during recovery and terminated on deck under less than optimum conditions for a leak-proof seal.

In addition to the seismometers shown in Table 11, the Hawaii Institute of Geophysics OSS, which has a 3.8-inch outer diameter, has been successfully deployed through the 5-inch DSDP drill string. The OSS consists of a borehole package, recording package, and recovery system. The borehole package is an 8.2-ft pressurized container, which encloses a three-geophone seismometer, auxiliary sensors, signal electronics, multiplex, A/D converter, telemetry, and power conditioning electronics (see Appendix C).

The general considerations applicable to the two existing modes of borehole seismometer deployment are summarized in Table 12.

Table 12. Seismometer deployment concept considerations.

Through the drill string
Package diameter constrained by drill string inner diameter
Only one drill string trip required
Minimal extra handling equipment
EM cable must be stripped out of drill string
Recovery of instruments may not be possible
Possible limit to penetration depth in basalt
Drill string reentry
Multiple drill string trips and reentries required
No practical package limits up to about 24 inches diameter
Special subsea and shipboard handling equipment
Recovery of borehole package possible
Possible redeployment of new instrument into borehole
Cased or uncased borehole can be provided

4. Drill string characteristics

Within the foreseeable future, only a small range of drill string configurations can be considered for 20,000-ft deep-ocean operations. The size range between 5 and 6.625 inches is based on the available American Petroleum Institute drill pipe sections. Smaller drill pipe sections cannot support the necessary weight or drilling functions. Larger diameter drill pipe is specially made with strengthened tool joints and would probably require substantially upgraded shipboard handling capabilities.

Several considerations are involved in selecting a specific drill string configuration. When the drilling is to be accomplished through ocean drilling and emplacement applications, the system's resonance and damping characteristics are critical, even under moderate weather conditions. Table 13 indicates the basic capabilities of four different drill strings at three total depths.

Most dynamically positioned drillships can accommodate 4,- 5-, or 5.5-inch pipe drill strings although pipes up to 9 inches in diameter are available. A 6.625-inch drill string would probably require modifications to the ship's pipe racks, derrick pipe handling and power drilling systems. Most of the drillships listed in Tables 8 and 9 would probably have sufficient derrick loading capabilities for handling larger pipe.

The MSS program deployment operations indicated a need for drill string heave compensation for operations at the greatest water depths. Some type of heave compensation is definitely required when weather conditions are severe. Active or passive heave compensation systems can be used; however, the active system is preferred.

Table 13. MSS drill string comparison.

	4 inch	5 inch	5.5 Inch	6.625 inch
DRILL STRING				
Inner diameter (inch)	3.?	4.25*	4.50*	5.0
Joint outer diameter (Inch)	4.5	7.5	7.5	8.0
I (inch^4)	6.5	14.3	21.6	32.4
Dry wt. (lb/ft)	15.6	19.50	24.7	25.2
Load capacity (lb)**	514,000	712,000	895,000	881,000
Torque capacity (lb)**	36,320	64,210	88,240	110,090
Drill power capacity (ft/lb) (120 rpm)	86	151	192	240
Mud velocity (ft/sec) (500 gpm)	18.5	11.3	11.3	8.1
BHA weight (lb)	40,000	50,000	60,000	90,000
Topside DS weight (lb)	25,000	30,000	35,000	40,000
TYPICAL HOOK LOADS				
2,000 ft (lb)	98,000	115,000	135,000	175,000
10,000 ft (lb)	208,000	250,000	305,000	350,000
20,000 ft (lb)	341,000	425,000	525,000	575,000

*Special tool joint
**High-strength S-135 drill string

Accurate pipe string load measurements are particularly important. Such measurements should be recorded in both static and dynamic modes. Deep-ocean drilling will frequently involve operations near the stress limits of the drill pipe, in particular, when all combined loadings are considered. Such load data should be correlated with computerized load evaluations, taking into account both axial and lateral dynamic effects.

5. MSS data transmission systems

Early concepts of the MSS station addressed three basic components: the encapsulated seismic sensor system; a data handling system that would collect sensor outputs, assemble same, and prepare them for transmission; and a data transmission system that would relay the data to a shore-processing facility.

The initial concept for the MSS program included eventual development of a near real-time telemetry link for transmitting data. If desirable, a site-to-shore submarine cable would be installed and integrated with the MSS station. The alternative would be to operate via a surface-to-shore satellite telemetry link.

Two analyses were performed from 1979 to 1980 for determining the feasibility of an MSS data transmission system and for defining characteristics, requirements, and capabilities of such a system.

5.1 Communications methods

A Gould, Inc., study [30] addressed possible communications methods for transmitting data from an ocean-based MSS platform to a continental U.S. data processing center. The following factors were defined as minimum acceptable characteristics for such a communications system to meet MSS requirements.

- ability to store seismic, hydroacoustic, and secondary sensor data for up to 90 days.
- ability to transfer all data to a secondary storage medium for input to a land-based data processing center.
- ability to receive and update timing information.
- ability to receive and respond to system parameter updates.

UHF satellite communications was identified as the most viable means for telemetering MSS data between an ocean-based telemetry platform and a shore-based processing facility. Three UHF satellite systems, FLTSAT, MARISAT and GOES, were believed to be viable data links for the MSS.

No commercially available UHF transceivers for FLTSAT or MARISAT satisfied the requirements of the ocean-based portion of the MSS; however, the U.S. Navy had two transceivers capable of communicating with these satellites. A number of transceivers were available for communications with GOES; one transceiver was specifically designed for buoy application.

Analysis of the three subject satellite systems indicated that either could fulfill data retrieval requirements of the MSS. A major advantage of FLTSAT and MARISAT was the ability to retrieve all data from an MSS ocean-based system on a daily basis; however, it would have been necessary to design, build, and test a real-time dedicated command and data acquisition hardware/software system for MSS deployment. GOES offered several advantages, including the ability to use existing command and data acquisition, and data collection systems. A notable disadvantage of GOES was the selective daily retrieval of sensor data (all sensor data would be retained within the ocean-based subsystem and could be retrieved periodically by passing ships).

While both FLTSAT and MARISAT offered significant capabilities, it was determined that FLTSAT was not a good candidate system because operational access to the system could not be assured. It was concluded that either MARISAT or GOES could fulfill the communications requirements of the MSS, and either system should be available for use. MARISAT offers a wideband data link capability, but a demanding development program would be required and it would be expensive to operate. GOES offers a low data rate, which would require using a diary and data compression techniques. On the other hand, GOES is a proven system and relatively simple and inexpensive to implement.

5.2 Data transmission subsystem

An MSS communications link feasibility study by Raytheon [31] developed a set of specifications and requirements that would serve as the basis for detailed data transmission system designs. The recommended system included a self-righting, discus-type buoy and a mooring line/data link made up of five sections. The system is briefly described in the following paragraphs.

The self-righting minidiscus buoy was about 6.5 ft in diameter, weighed 1764 lb (including a 500-lb payload).

and was about 8.2 ft high, including the antenna. The mooring line/data link system consisted of a 98-ft tapered attachment hose, a 644-ft surface buoy line with seven small floats attached, a subsurface flotation system consisting of nine spheres connected by chains, a 15,000-ft upper tautline and a 1970-ft lower tautline. The system was tethered to a 37,000-lb anchor. Figure 23 shows a sketch of the mooring system.

This concept included a satellite telemetry link with FLTSAT, based on the assumption that access priorities could be negotiated with the Navy. Lithium batteries would provide power for the transceiver.

The MSS program was terminated prior to development of a data transmission system. Resuming the MSS program would require an early decision with regard to a means for transmitting seismic data to a shore facility. Prior studies and analyses should provide adequate guidance for proceeding with satellite telemetry system development. Decision factors regarding a site-to-shore submarine cable remain to be determined.

6. Projected MSS development tests

New applications of MSS technology are possible. In any new application, single-site development testing would probably be initially required to verify sensor-specific capabilities and to establish associated data hardware and software requirements. Borehole instruments measuring up to 8 inches in diameter have been successfully demonstrated. Instruments up to 24 inches in diameter may be considered potential candidates for such deployment. Both shallow-water sites (to 2000 ft) and deepwater sites (20,000 ft) may be programmed as required. The deepwater test would be a much more expensive endeavor than a shallow-depth project (by a factor of 2 to 3). The following paragraphs discuss the various parameters applicable to shallow- and deepwater MSS tests.

6.1 Shallow-water test

The detailed seismic characteristics and instrumentation requirements for a shallow-water borehole-emplaced seismic system have not been defined. A shallow-water borehole test could be easily accomplished at a number of U.S. offshore sites. A dynamically positioned drillship would be desirable but not required for water depths approaching 2000 ft. (Most drillships carry adequate mooring equipment for holding positions over a site for short periods during good weather.) A high-strength drill string would not be mandatory. The site should be at least 10 miles offshore to reduce shore and surf noise.

Instrument emplacement through either a reentry borehole or a through-the-pipe deployment can be considered; however, a permanent test station site would require a reentry encased borehole. Either approach involves numerous considerations. A decision on the seismometer deployment mode would have to be based on the projected use of the site and the capabilities of the instruments to be used.

The data recording capability would be a major consideration for any MSS test. The basic requirements are established by the data format, range, sensitivity level, number of tracks and time period objectives. Several available recording packages can be adapted to this type of application. A basic problem regarding these recording systems will be where the package should be installed, particularly for extended periods. Table 14 presents some options for shallow-water test recording package installations. All options should fall within the same general cost range; however, a requirement for a hard-line tieup with a nearby (up to 5 miles) platform or structure would significantly escalate the cost of any option. Although each of the listed recording options have an area(s) of specific concern, each can be readily accomplished using only a deployment vessel.

The project required to provide the necessary subsea equipment, deploy that equipment, and record the data would not be extensive. The estimated cost elements (1983 dollars) of such a project are summarized in Table 15.

In terms of a general scenario for a shallow-water test site project, the first tasks would be to select the borehole and recording package configurations, and the EM cable. Pressure vessel packaging of the various subsea components would be required. Meanwhile, a deployment engineering and planning effort would be conducted. An appropriate drillship and mobilization port would be selected. Procurement of long lead-time items (i.e., EM cable, reentry cone, reentry sonar, etc.) would be initiated. Refurbishing existing MSS equipment would also be accomplished as required. All various project equipment and elements would be received and assembled at the mobilization port. After the mechanical and electrical interfaces were checked out, a dockside test would be conducted that would simulate, as feasible, the at-sea operations.

After the dockside tests are completed, the ship would proceed to the selected site and install a deepwater moor. A pilot core would be taken in preparation for the initial reentry cone/conductor casing installation. The borehole would then be drilled to depth and cased as required.

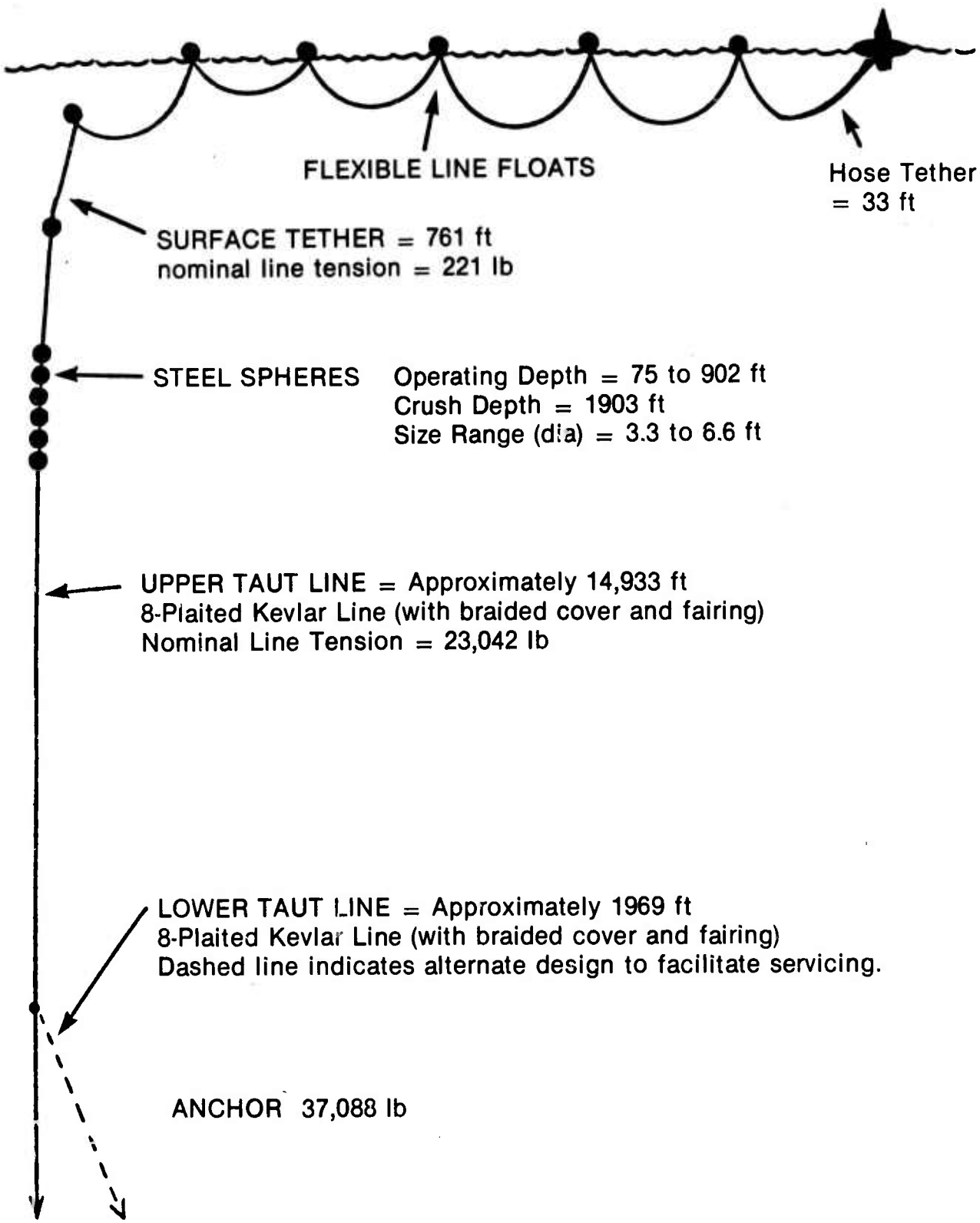


Figure 23. Mooring configuration for MSS satellite telemetry buoy.

Table 14. Shallow-water test recording package installation options.

Type Package Pressure Vessel	Mooring/ Retrieval System	Deployment Functions	Recovery Functions	Available Units	Data Format	Remarks
Seabed, moderate wall	Possibly riser line	Lower package to seabed, controlled freefall	Release transponder with float	HIG OSS	Analog tape	Long term (60 days)
		Lower package from ship	Package riser or grapnel line lift	BPP	Digital tape	Long term (45 days)
Subsurface buoy, light wall	Anchor cable possibly riser line	Lower package from ship	Release transponder	HIG OSS*	Analog tape	
			Riser or grapnel line lift	OBS* BPP*	Digital tape	Short term (2 to 4 days)
Surface buoy, light wall	Anchor line	Deploy over side	Pickup buoy	HIG OSS* OBS* BPP*	Tape	Susceptible to damage or theft
Standby ship (no pressure vessel)	Anchor or DP	Cable terminated at ship	Not applicable	Many	Real-time and/or tape	Emergency release required, noise on ship
Platform (no pressure vessel)	No	Deploy cable to platform	Not applicable	Many	Real-time and/or tape	Noise on platform Site near platform
Shore station (no pressure vessel)	No	Deploy cable to shore	Not applicable	Many	Real-time and/or tape	Distance from shore

*Could be configured surface or subsurface for buoy installation

Table 15. Shallow-water (2000 ft) test cost projection.

Borehole Package Procurement and Integration	$ 300,000
Recording Package Procurement and Integration	200,000
EM Cable/Winch Procurement	60,000
Deployment Engineering & Planning	100,000
Deployment Equipment Refurbishment	90,000
Ship Charter (30 days)	800,000
Test Equipment (Shipboard)	60,000
Mobilization and Conversion	80,000
Demobilization	40,000
Recovery Vessel Charter (15 days)	60,000
Operations Support	120,000
Miscellaneous and Contingency	190,000
	$2,100,000

Notes: 1. Ship charter is a commercial, dynamically positioned drillship.
2. A 30-day in situ recording capability is provided.
3. Does not include instrumentation development, data evaluation, or management cost.

Several reentries could be required for a deep borehole. Following emplacement of the borehole instrument package, four or five days of real time recording may be performed. The recording package or hardline interconnection would then be deployed with associated recovery equipment. The drilling vessel would return for demobilization. A small workboat-type vessel would eventually be chartered to recover the recording package and the borehole package, if required.

The overall project would require from 9 to 12 months, provided the borehole instrument could be developed within the initial 6 months. The drillship charter should include about 30 days to cover mobilization, transit, 10 days of onsite operations, and demobilization.

6.2 Deepwater test

Planning factors for the deepwater test are similar in many respects to the shallow-water project. The deepwater test is, of course, much more complicated, more expensive, and requires a considerably longer period for overall integration and deployment.

A deepwater test could be accomplished at a number of U.S. offshore sites. As in the shallow-water test, the site probably should be at least 10 miles offshore to reduce shore and surf noise. A dynamically positioned drillship and a high-strength drill string would be required. The projected use of the site and the size of the selected instruments would dictate the use of either a reentry borehole or a through-the-pipe deployment. An encased reentry borehole would be required for a permanent, reusable test site. The depth of the site, seabed geologic structure, and applicable weather/environmental factors are of prime importance in planning the project. The drill string is probably the limiting element with regard to shipboard handling requirements.

The data format, range sensitivity level, number of tracks, and time period objectives define the requirements for a data recording capability. Only a few existing recording packages can be adapted to the deepwater application unless a shallow subsurface buoy is used. Consequently, the decision on where to position the recording package becomes a matter of prime importance. Table 16 presents some possible options for recording packages. All these options fall within the same general cost range and can be accomplished using only the deployment vessel.

The EM cable would also be a critical element, particularly if sophisticated, sensitive data recording is desired. Torque-balanced, long-length, high-strength, low-impedance, deepwater EM cable is available in very limited quantities and is very expensive.

The overall effort required to provide the necessary subsea equipment, deploy that equipment, and record data is rather extensive. An estimate of the costs of major elements of such a project is presented in Table 17. These estimates address a permanent 1000-ft reentry borehole at a water depth of 15,000 ft. A 30-day in situ recording capability is assumed.

A general scenario for the deepwater test would first address specific or unique equipment requirements, borehole and recording package requirements, and identification of a dynamically positioned drillship and a mobilization base. An overall project plan would be developed to cover the planning efforts, equipment development and procurement requirements, time tables and operating factors and responsibilities. Procurement of long lead time items and refurbishment of any existing MSS equipment would be initiated at an early date.

Table 16. Deepwater test recording package installation options.

Type Package Pressure Vessel	Mooring/ Retrieval System	Deployment Functions	Recovery Functions	Available Units	Data Format	Remarks
Seabed, heavy wall	Extensive anchor and riser line	Lower package to seabed	Release transponder with package float	HIG OSS	Analog tape	60-day recording period
			Riser or grapnel line lift	BPP	Digital tape	45-day recording period
Subsurface buoy, moderate	Anchor cable possibly riser line	Lower package or controlled freefall	Riser or grapnel line lift	HIG OSS*	Analog tape	60-day recording period
				OBS*	Digital tape	2- to 4-day recording period
		Lower package	Release transponder	BPP*	Digital tape	45-day recording period
Surface buoy, light wall	Anchor cable	Deploy over the side	Pickup buoy	Many	Tape	Susceptible to damage, loss or theft
Seabed (hard line), heavy wall	Riser line	Lower package to seabed	Riser or grapnel line lift	HIG OSS BPP	Real-time	Very long EM cable interconnection

*Could be configured for surface or subsurface buoy installation.

All elements, equipment, and components would be received and assembled at the mobilization port. All equipment would undergo complete mechanical and electrical checkout. Dockside tests that simulate at-sea operations would be conducted as feasible. A shallow-water checkout/training evolution should be considered after evaluating the crew's experience and the equipment complexity.

Upon arrival at the site, the drillship would position a subsea beacon and proceed with borehole preparation. A pilot core would be taken in preparation for installing the reentry cone and conductor casing. The borehole would then be drilled out and cased as required. Several reentries should be anticipated. After deploying the borehole package, 4 to 5 days of real-time recording will probably be required. The drillship would then deploy the recording package and its associated recovery equipment, and return to port for demobilization. A medium-sized oceanographic research vessel or a large workboat would be chartered for recovering the recording package and borehole package.

The overall integration and deployment would require from 18 to 24 months, provided the borehole instrument could be developed within the initial 12 months. A drillship charter of about 40 days should cover mobilization, transit, 20 days of onsite operations, and demobilization.

7. Deepwater operational program

A series of deepwater operational MSS sites could be installed by using the deployment and emplacement techniques previously discussed. The major decision areas of such a program are

- specific site parameters,
- instrumentation package characteristics and capabilities,
- weather and environmental conditions,
- communications network.

Table 17. Deepwater test cost estimate.

Borehole Package Procurement and Integration	$ 500,000
Recording Package Procurement and Integration	400,000
EM Cable/Winch Procurement	150,000
Deployment Engineering and planning	250,000
Deployment Equipment Refurbishment	120,000
Ship Charter (40 days)	2,800,000
Test Equipment (Shipboard)	80,000
Mobilization and Conversion	120,000
Demobilization	50,000
Recovery Vessel Charter (15 days)	80,000
Operations Support	380,000
IRR Mooring/Subsea Buoy	200,000
Miscellaneous and Contingency	480,000
	$5,610,000

Notes: 1. Estimates are based on a 15,000-ft water depth and use of a commercial drillship.
2. Overall estimate does not include costs of Instrumentation development, data evaluation, and management.
3. 1983 dollars.

Table 18. Cost estimate for a multiple-site operational deployment program.

Instrument Package Development and Hardware	$6,500,000
Communications/Data Recording Development and Hardware	3,900,000
Deployment System Engineering	1,500,000
Shallow-water Checkout	600,000
Deployment Hardware Procurement	3,200,000
Ship Charter (9 months)	14,600,000
Mobilization	700,000
Operations, Fuel & Supplies	1,500,000
Demobilization	500,000
Recovery/Maintenance Support (1 year)	1,200,000
Miscellaneous & Contingency	3,300,000
	$37,500,000

Notes: 1. Costs include a commercial, dynamically positioned drillship.
2. Costs represent rough estimates of an 8-12 site, deep-ocean deployment program.
3. 1983 dollars.

The MSS development program has demonstrated that the first three areas can be accommodated. The communications network represents a significant unknown, particularly if rapid data feedback is required. The communications network could take the form of a recoverable recording package, a hard link to existing subsea circuits, satellite communications, a long-wave radio system, or acoustic data transmission. Pop-up buoy systems could be used for the radio communications approaches. Each of the foregoing networks represents a possible option; however, technical difficulties can be anticipated in each case.

For this discussion, a program for 8–12 deepwater sites across the Atlantic and Pacific Oceans has been projected. The principal costs of such a program are shown in Table 18.

The overall deployment program for 8–12 stations would probably require about 30 months, provided the sensors and instrumentation only required packaging into a deep-water configuration. Actual at-sea operations could be accomplished in about 9 months if the projected MSS sites are relatively near to each other. Figure 24 depicts a possible schedule for the subject program.

The initial actions in a scenario for a multiple site MSS program (Fig. 24) would be developing the borehole instrument package and the data recording package with its supporting hardware and subsystems. A comprehensive evaluation of all projected sites would be undertaken, and a preliminary schedule would be developed that takes

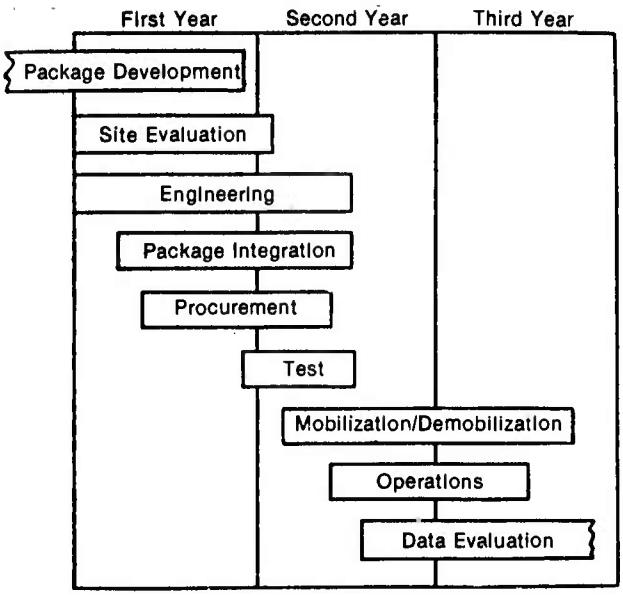


Figure 24. Projected multiple MSS site deployment schedule.

into account difficult sites and probable weather conditions. A preliminary operations plan would then be prepared. This plan would establish specific vessel and support equipment requirements.

Upon selection of a deployment ship, the detailed design of subsea and specialized shipboard handling equipment would be accomplished. Procurement action on major long leadtime items (i.e., winches, drill pipe, etc.) would be initiated. A preliminary mobilization and logistics support plan would be prepared. A comprehensive set of procedures would be defined for ground tests of equipment and shallow-water demonstrations. A base or port of operations would also be established.

Conversion of the drillship, including installation of special shipboard handling equipment, would take place at or near the selected port of operations. Final development, checkout, and functional testing would also be accomplished during this period. Dockside testing of various integrated equipment systems would be performed as appropriate. After all developmental and shore test checkouts were accomplished, a shallow-water demonstration would be performed to indoctrinate personnel and to verify procedures, equipment capabilities, and data transmittal techniques. This demonstration would require about 1 month. Some utilization of breadboard-type hardware/software may be required in the initial phase of the shallow-water demonstration.

The deployment schedule should be broken down into Atlantic and Pacific legs. Each leg would encompass from 4 to 6 months. Refueling, resupply, and crew changes would be scheduled at intervals of 6–8 weeks and would be accomplished in foreign ports as necessary. At least one trip through the Panama Canal would be required.

Operations at each site would require an average of 20 days for borehole emplacement, instrument deployment, and realtime recording. Some stations could require up to 30 days for severe weather holds. The major expendables for the program, other than specialized equipment, fuel, food, etc., would include casing, reentry cones, and cement (Table 18).

The demobilization phase of the overall MSS site installation program would be completed with the reconversion of the drilling vessel. All program-procured shipboard handling equipment would be retained and stored, as directed.

IX. Conclusions

Overall, the MSS project was successful. The tight, inflexible schedule, among other constraints, tended to preclude adequate testing of instrumentation designs prior to deployment. Additional system testing would have been appropriate to determine optimum system gains, thresholds, resolution, seismic coupling, and to identify possible spurious modes that may appear due to internal mechanical structure designs.

Very few advancements to the state of the art in seismic instrumentation were made during the project. However, the knowledge gained in the deployment, operation, and recovery of fragile, sophisticated systems in a deep-ocean environment is extremely significant. A sizable data base was amassed, which will allow scientists to better understand the earth's structure and will permit comparison of ocean borehole seismic installations with other types of seismic surveillance techniques.

The MSS project demonstrated the feasibility of establishing a seismic station in the ocean subbottom at water depths approaching 20,000 ft. Such a seismic station can be installed using existing technology and equipment. However, techniques or equipment for transmitting seismic data from the MSS site to a shore facility have not been demonstrated. MSS-associated studies indicate that automated transmission of seismic data to a shore facility is feasible; however, such a transmission system would require a well-defined research and development effort.

The MSS experiments also demonstrated the capability of MSS instruments to record man-made events and

earthquakes at teleseismic and regional distances in the deep ocean environment. In addition to a capability for monitoring man-made and natural seismicity over long periods of time, an MSS site or a series of MSS sites would substantially contribute to geological knowledge of the earth. MSS sites would complement or contribute to the on-going studies of the Ocean Margin Drilling Project.

The following specific conclusions may be drawn from the MSS project.

- The technology now exists for placing and releasing large instrument packages in deep-ocean boreholes using a single deployment vessel.
- The MSS/DSDP system that was used is adequate for deployments in water depths to about 20,000 ft.
- The diameter of borehole instrument packages is not restricted to the inside diameter of the drill string.
- Instrument cables may be run outside the drill string without entanglement.
- Boreholes may be emplaced and then reoccupied years later for instrument package insertion, or they may be drilled and cased as part of a deployment operation.
- Instrument packages may be recovered from a borehole without using a drill string.
- Large, heavy seafloor recording installations, i.e., the BPP, may be deployed and recovered by vessels equipped with appropriate winch and navigation systems.
- Shipboard dynamic positioning capabilities, although desirable, are not mandatory for the installation of large seafloor instruments.
- The IRR system design provides sufficient strength, flexibility, and redundancy to ensure recovery without precise navigation or placement of navigation aids.
- Extensive sets of noise, explosion, and earthquake data were collected by the BIP during the 1981 and 1983 MSS experiments.
- Seismic data collected by the BIP are generally superior to OBS data.
- Signal-to-noise ratios recorded by the BIP are superior to those of the OBS due to improved sensor coupling and isolation of sensors from environmental noise.
- Long-term, unattended collection of high-quality seismic data is feasible by means of recoverable recording packages with renewable power sources.
- A future MSS program should address data transmission systems as an area of priority. Depending on access to drill ships, alternate reentry techniques may also be an area of priority.

X. Recommendations

The experiences and achievements of the MSS program, in terms of deployment equipment, seismic instrument packages, and acquired data, should be examined with a view toward identifying and substantiating requirements for a marine seismic system (or systems) from both the scientific and military applications standpoints.

In the event of a renewed or refocussed MSS program, the following actions and considerations are also recommended.

- The MSS program developments should be used as a basis or starting point for identifying improvements and technological advancements applicable to existing designs and implementations of the MSS program before further experimentation or deployments.
- If at all feasible, MSS deployments or experiments should be accorded a priority schedule or dedicated support ships and equipment, rather than incorporation into an existing, related deployment program such as the Ocean Margin Drilling Program.
- All new equipment and instrumentation designs should be adequately tested and qualified prior to deployment. System testing requirements should be identified and incorporated in program schedules.
- Early program planning should address MSS data transmission systems and establish a subprogram for development of same, as appropriate. A parallel action may be required for an alternate reentry technique, depending on drillship availability.

XI. References

1. Green, J.A. and P. Fleischer, *Environmental Report of the Northwest Pacific for the Marine Seismic System*, Naval Ocean Research and Development Activity, NSTL, Mississippi, NORDA Technical Report 31, 1980.

2. Bolt, B.A., *Nuclear Explosives and Earthquakes, The Parted Veil*, Univ. of California, Berkeley, California, W.H. Freeman and Company, San Francisco, p. 108-140, 1974.

3. Hyndman, R.D., Salisbury, M.H., et al., *Initial Reports of the Deep Sea Drilling Project*, Volume 78B, Washington, D.C. (U.S. Govt. Printing Office), 1984.

4. Duennebier, F.K., Stephen, R., Menard, H.W., Natland, J.H., et al., *Initial Reports of the Deep Sea Drilling Project*, Volume 88/91. Washington, D.C. (U.S. Govt. Printing Office), (in preparation).

5. Wallerstedt, R.L., *Marine Seismic System At-Sea Test Deployment Operation*, Final Report for Period March 1981, Report No. 006-007, prepared for NORDA by Global Marine Development, Inc., Irvine, California, 1981.

6. Global Marine Development, Inc., *Marine Seismic System At-Sea Test Operational Procedures*, Revision 2, Report No. 006-003, prepared for NORDA by Global Marine Development, Inc., Irvine, California, 1981.

7. Gershunov, E. and N. Daoud, *Marine Seismic System Reentry Impact*, Revision 2, Report No. 001–001, prepared for NORDA by Global Marine Development, Inc., Irvine, California, 1980.

8. Global Marine Development, Inc., *At-Sea Test Mobilization Plan*, Revision 1, Report No. 001–004, prepared for NORDA by Global Marine Development, Inc., Irvine, California, 1980.

9. Wallerstedt, R.L., *Marine Seismic System Deployment*, Phase IV Final Report, 1 Oct. 1981-30 Sept. 1982, Revision A, Report No. MSSA02-SYS-R003, prepared for NORDA by Global Marine Development, Inc., Irvine, California, 1982.

10. Global Marine Development, Inc., *Marine Seismic System MSS '82 Deployment Operational Procedures*, Revision 1, Report No. MSSA02-SYS-P002, prepared for NORDA by Global Marine Development, Inc., Irvine, California, 1982.

11. Gershunov, E. and D. Davies, *Reentry Impact Stress Analysis of Modified Reentry Sub Assembly*, Report No. MSSA02-STR-R001, prepared for NORDA by Global Marine Development, Inc., Irvine, California, 1981.

12. Gershunov, E. and D. Davies, *Drill Pipe Stress Analysis*, Report No. MSSA02-STR-R003, prepared for NORDA by Global Marine Development, Inc., Irvine, California, 1982.

13. Gershunov, E. and N. Daoud, *Marine Seismic System EM Cable Static and Dynamic Response Due to Current and Glomar Challenger Motion*, Revision 1, Report No. 006-002, prepared for NORDA by Global Marine Development, Inc., Irvine, California, 1980.

14. Global Marine Development, Inc., *Stress Analysis of the IRR Deployment at the Northwest Pacific Site*, Report No. MSSA02-STR-R005, prepared for NORDA by Global Marine Development, Inc., Irvine, California, 1982.

15. Global Marine Development, Inc., *MSS '82 Northwest Pacific Site Environmental Data*, Revision 1, Report No. MSSA02-SYS-R001, prepared for NORDA by Global Marine Development, Inc., Irvine, California, 1982.

16. Global Marine Development, Inc., *Integrated Logistics Plan for Mobilization, MSS '82*, Report No. MSSA02-SYS-P003, prepared for NORDA by Global Marine Development, Inc., Irvine, California, 1982.

17. Wallerstedt, R.L., *Phase V Marine Seismic System Deployment Final Report*, Report No. MSSA04-SYS-R001, prepared for NORDA by Global Marine Development, Inc., Irvine, California, 1984.

18. Global Marine Development, Inc., *Marine Seismic System MSS '83 Deployment Operational Procedures*, Report No. MSSA04-SYS-P002, prepared for NORDA by Global Marine Development, Inc., Irvine, California, 1982.

19. Global Marine Development, Inc., *Marine Seismic System MSS '83 IRR Recovery and Redeployment*

Operational Procedures, Report No. MSSA04-SYS-P005, prepared for NORDA by Global Marine Development, Inc., Irvine, California, 1983.

20. Gould, Inc., *Marine Seismic System Development, Deployment and Recovery*, Final Report, prepared for NORDA by Gould, Inc., Glen Burnie, Maryland, 1985.

21. Global Marine Development, Inc., *Marine Seismic System MSS '83 Deployment Mobilization Plan*, Report No. MSSA04-SYS-P003, prepared for NORDA by Global Marine Development, Inc., Irvine, California, 1982.

22. Global Marine Development, Inc., *Integrated Logistics Plan for Demobilization MSS '83*, Report No. MSSA04-SYS-P006, prepared for NORDA by Global Marine Development, Inc., Irvine, California, 1983.

23. Teledyne Geotech, *Prime Item Product Specification for the Model 53100 Borehole Instrumentation Package (BIP)*, prepared for NORDA by Teledyne Geotech, Garland, Texas, 1984.

24. Lawn, J.R., *Marine Seismic System/1982 System Design Disclosure*, Revision C, Document No. 81-0015, prepared for NORDA by Gould, Inc., Glen Burnie, Maryland, 1981.

25. Western Instrument Corp., *Design and Analysis of the Marine Seismic System Installation, Recovery, and Reinstallation System*, prepared for Civil Engineering Laboratory, Naval Construction Battalion Center, Port Hueneme, California, by Western Instrument Corporation Offshore Engineering, Oxnard, California, 1982.

26. Wallerstedt, R.L., *Marine Seismic System (MSS) Deployment System Final Logistics Report*, Report No. MSSA04-SYS-P007, prepared for NORDA by Global Marine Development, Inc., Irvine, California, 1983.

27. Wallerstedt, R.L., *Marine Seismic System Deployment, Phase II*, Report No. 001-005, prepared for NORDA by Global Marine Development, Inc., Irvine, California, 1981.

28. Wallerstedt, R.L., *Marine Seismic System Deployment, Phase III*, Report No. MSSA01-001, prepared for NORDA by Global Marine Development, Inc., Irvine, California, 1982.

29. Wallerstedt, R.L., *Marine Seismic System Deployment Final Report, Phase IV*, Revision A, Report No. MSSA02-SYS-R003, prepared for NORDA by Global Marine Development, Inc., Irvine, California, 1982.

30. Gould, Inc., *Marine Seismic System Satellite Telemetry Study*, prepared for NORDA by Gould, Inc., Glen Burnie, Maryland, 1980.

31. Raytheon, *Marine Earthquake Monitoring System Communications Link Feasibility Study*, prepared for NORDA by Raytheon Ocean Systems Co., Portsmouth, Rhode Island, 1980.

Bibliography

Aspel, R.J., R.K. Wyss, G.R. Mellman, and R.S. Hart (1983). *Three Dimensional Wave Propagation Using Boundary Integral Equation Techniques.* Report No. SG1-R-83.083. Prepared for NORDA by Sierra Geophysics, Redmond, Washington.

Beardwood, J. and P.Pollock (1978). *Seismological and Implementation Considerations Concerning Near Zone Network Performance in the Detection, Location, and Identification of Underground Nuclear Explosions.* Prepared for AFTAC by Gould, Inc., Glen Burnie, Maryland.

Butler, R. (1979). *An Amplitude Study of Russian Nuclear Events for WWSSN Stations in the United States.* Report No. SG1-R-79-001. Prepared for DARPA by Sierra Geophysics, Inc., Arcadia, California.

Butler, R. and R.S. Hart (1979). *Summary of Current Research on Seismic Waveform Analysis of Underground Nuclear Explosions.* Report No. SG1-R-79-004. Prepared for DARPA by Sierra Geophysics, Inc., Arcadia, California.

Chmilewski, M. and D. Ricketts (1982). *Marine Seismic System Data Tape Format Description Document.* Report No. 82-0094. Prepared for NORDA by Gould, Inc. Glen Burnie, Maryland.

Fleischer, P. (1980). *Weather and Currents in the Vicinity of 23°N, 46°W, North Atlantic Ocean.* Naval Ocean Research and Development Activity, NSTL, Mississippi. NORDA Technical Note 47.

Gershunov, E. and J. Gompers (1980). *Marine Seismic System Static and Dynamic Behavior of the Drill Pipe During the Reentry Sub Installation.* Report No. 001-002

(Appendix F to Global Marine Development Inc. Report No. 001-005 of 9 Jan 1981). Prepared for NORDA by Global Marine Development, Inc., Irvine, California.

Global Marine Development, Inc. (1980). *Marine Seismic System Deployment Feasibility Study, Phase I.* Report No. 04114-001. Prepared for Gould, Inc., by Global Marine Development, Inc., Irvine, California.

Green, J.A. and S.D. Trowell (1981). *Data Report for Oceanography/Geophysical Surveys in the Northwest Pacific (46-47°N, 159-161°E), USNS SILAS BENT, 2-3 Aug 1980.* Naval Ocean Research and Development Activity, NSTL, Mississippi. NORDA Technical Note 81.

Hadley, D.M. and R.S. Hart (1979). *Seismic Studies of the Nevada Test Site.* Report No. SG1-R-79-003. Prepared for DARPA by Sierra Geophysics, Inc., Arcadia, California.

Hart, R.S. and S.K. Kaufman (1980). *Seismic Propagation in the Kurile/Kamchatka Region.* Report No. SG1-R-80-022. Prepared for NORDA by Sierra Geophysics, Inc., Arcadia, California.

Matthews, J.E. (1980). *An Approach to the Quantitative Study of Sea Floor Topography.* Naval Ocean Research and Development Activity, NSTL, Mississippi, NORDA Technical Note 47.

Samowitz, I.R., and D.M. Hadley (1981). *Seismic Studies of Regional Path Properties of Eurasia.* Report No. SG1-R-81-044. Prepared for DARPA by Sierra Geophysics, Inc., Redmond, Washington.

Scripps Institution of Oceanography (1983). *Deep Sea Drilling Project, Preliminary Scientific Report Operations Resume, Leg 91.* Prepared for the National Science Foundation (for Initial Reports of the Deep Sea Drilling Project, Volume 88/91, in preparation) by Scripps Institution of Oceanography, La Jolla, California.

Scripps Institution of Oceanography (1984). *Deep Sea Drilling Project, Preliminary Scientific Report—Initial Core Descriptions, Leg 88/91.* Prepared for the National Science Foundation (for Initial Reports of the Deep Sea Drilling Project, Vol. 88/91, in preparation) by Scripps Institution of Oceanography, La Jolla, California.

Appendix A. Description of the D/V GLOMAR CHALLENGER

The D/V GLOMAR CHALLENGER (Fig. A-1) is a dynamically positioned drillship operated by the Global Marine Drilling Company under the direction of Scripps Institution of Oceanography, University of California, San Diego. The ship is capable of drilling in water depths up to 20,000 ft and can penetrate about 2500 ft into the sea floor. She was launched in March 1968, and after completion and outfitting, commenced drilling operations in August 1968.

The GLOMAR CHALLENGER has a length of 400 ft, a beam of 65 ft, a draft of 20 ft, and displaces 10,500 long tons. She is powered by twin screws, each driven by three 750 hp electric motors. Maximum speed is 12.5 knots. Four tunnel thrusters are provided for lateral positioning. A total of 13 AC and DC diesel generators provide basic power.

The drilling equipment is dominated by a 142-ft, 750,000-lb derrick. Approximately 38,000 ft of special S-135 5-inch drill pipe is carried, plus associated drill collars, bumper subs, swivels, etc., A passive action heave compensator can be used in the drill string with some difficulty. Two 5000 psi mud pumps are available. A 50-ton and a 15-ton crane are provided for deck loads.

An early version, Delco-type automatic station keeping (ASK) system is used to maintain position relative to a single ocean-floor-mounted transponder. The ship's thrusters are directed automatically to maintain the desired position. Stationkeeping in deep water can normally be achieved within ± 10 ft of a selected position within an offset distance of about 3000 ft from the beacon. A summary of the ship's capabilities and performance data is presented in Table A-1.

The ship has accommodations for 74 marine, drilling, and scientific personnel. Typical deployments (legs) last about 2 months, at which time a complete crew changeover is accomplished.

The GLOMAR CHALLENGER was removed from active service in November 1983, but the ship still retains the basic capability to perform MSS-type, deep-ocean deployments. The probable outcome for the ship is major conversion for another use, or disposal as scrap.

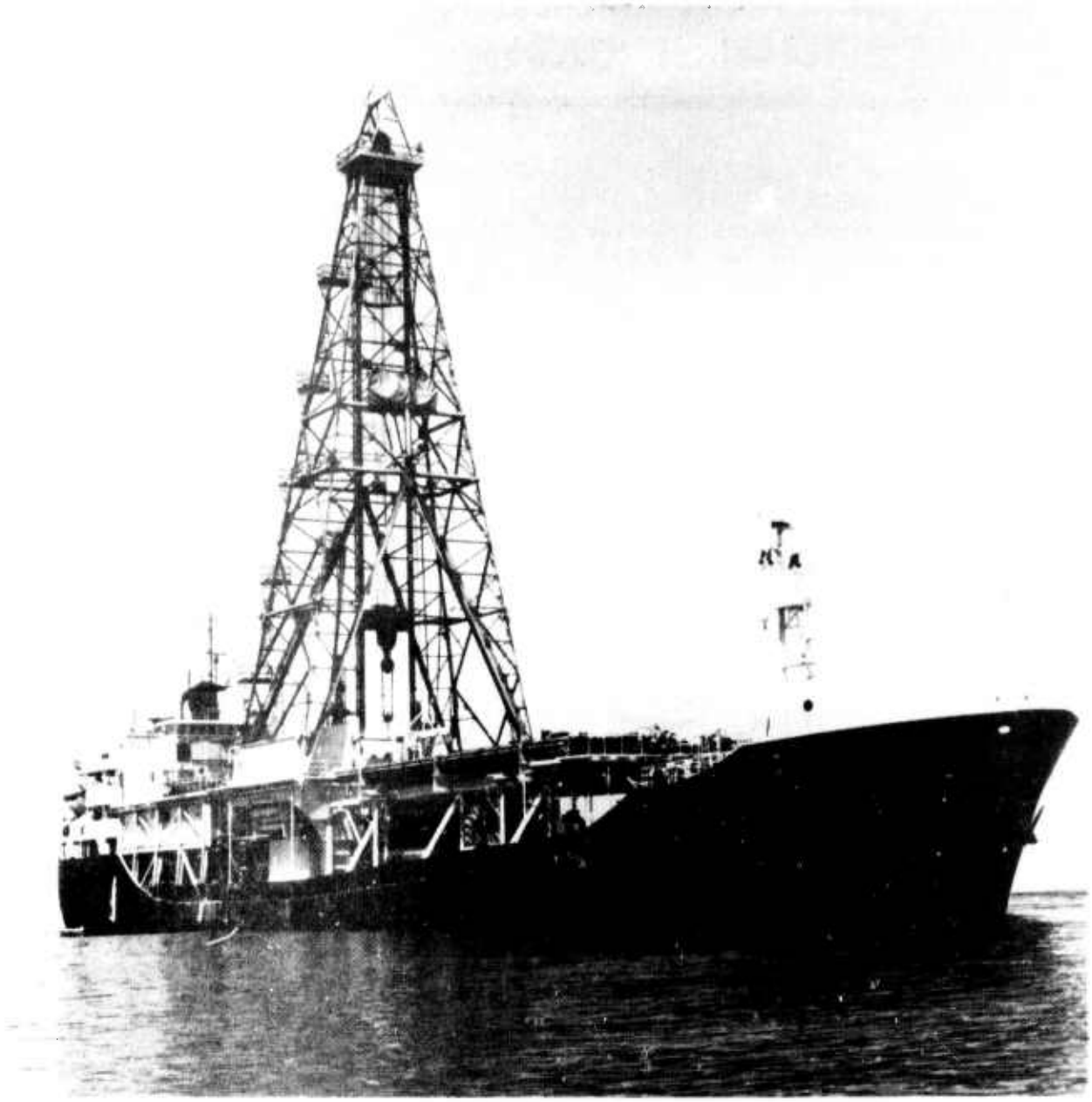


Figure A 1. Photograph of the drillship ***GLOMAR CHALLENGER***

Table A-1. Ship's capabilities and performance data

Length, Beam, Draft:	Length: 400 ft Beam: 65 ft 2 in. Draft: 9 ft 2 in. (light ship)
Displacement:	4,470 L.T. (light ship)
Centerwell:	22 x 24 ft
Propulsion:	Diesel electric, twin screw, driven by GE752 RI electric motors
Ground Tackle:	Three 111,000-lb anchors with 900 ft 2-in. anchor chain
Anchor Winches:	American Hoist and Derrick Company 2-0.06-in. galvanized wire, diesel driven
Cranes:	1—Marine 500, 50 ton, diesel 1—15 ton, diesel
Auxiliary Pumps:	Fuel, salt water, fresh water
Compressed Air System:	1—3.2 cfm 100-psi air compressor 2—358 125-psi air compressors with after coolers 1—22 cfm 100-psi emergency air compressor
Water Distillation Unit:	2—Aqua Chem
Radio:	Northwest Instruments Model NW-38 radio-telephone and RCA type CRM CIC radio-telegraph
Radar:	2—Decca Model RM 914
Fathometer:	EDO Model 185
RDF Unit:	Bendix Model ADF-100
Intercom System:	Sound powered telephone system
Welding Machine:	2—Lincoln 300 amp electric-driven
Reserve Mud:	2490 barrels
Drilling Water:	4769 barrels
Bulk Mud:	12,300 cu ft
Bulk Cement:	N/A
Riser Tensioning:	None
Sack Material Storage:	12,000 sacks
Fuel:	16,568 barrels
Potable Water:	1019.2 barrels
Derrick:	142 x 61 x 38 ft special design galvanized with 750,000 lb hookload capacity, API rating
Drawworks:	National type, 1625 DE, with Elmagco type eddy current brake; driven by 2 GE 752 RI electric motors, with 1.5-in. drilling line and 26,000 ft 0.5-in. wire line
Rotary Table:	Power swivel
Mud Pumps:	2—National type, N-1300 duplex power slush pumps driven by dual GE 752, 800 HP each
Mud Mixing Pump:	2—Mission 6 x 8R centrifugals, 75 HP each
Traveling Block:	National, 500-ton capacity with special guide rail rollers
Swivel:	National type N-1324, 335 ton National type NSF-650, 450 ton
Air Tuggers:	8—2,000-lb capacity 4—4,000-lb capacity 2—5,000-lb capacity
Rotary Hose:	3.5 in. x 65 ft
Crown Block:	National 760-H, 500-ton capacity
Master Bushing:	None
Drill Pipe:	5-in. drill pipe, Grade S-135, 19.5 lb/ft, Range 2
Drill Collars:	8.25 in. OD x 30 ft 7.25 in. OD x 30 ft
Logging Unit:	None
BOP Control System:	None
BOP Stack:	None

Appendix B. Marine Seismic System EM Cable Static and Dynamic Response Due to Current and GLOMAR CHALLENGER Motions

The subject study was prepared by E. Gershunov for Global Marine Development, Inc., as a part of planning and preparations for MSS-81. A summary of the study was included in Chapter 10 of Volume 78B of the DSDP initial reports [3], The latter summary is reprinted in this appendix.

RPT-006-002
Revision 1
2 February 1981

MARINE SEISMIC SYSTEM EM CABLE STATIC AND DYNAMIC RESPONSE DUE TO CURRENT AND"GLOMAR CHALLENGER" MOTION (JOB 00006, TASK 333000)

27 OCTOBER 1980

Prepared by
Dr. E. Gershunov

Approved by
Y. Ozudogru, Manager,
Structural, Naval Architecture

Checked by:
Dr. N. Daoud
S. Wetmore
Vice-President, Engineering

APPENDIX

Static and Dynamic Response of a Suspended Cable Due to Current and Ship Motions[1]

In order to examine the probability of the drill pipe and the cable entangling, an extensive study was made by E. Gershunov to estimate the tension in the cable and the deflected shape of the cable due to currents and ship motion (Fig. 1), and to specify requirements for a tensioning system. It was felt that understanding and controlling these factors would aid in reducing the impact accelerations experienced during deployment and in reducing the probability of cable–drill pipe entanglement.

During the test in Hole 395A, the lower end of the cable was secured to the lower end of the drill pipe, and the upper portion of the cable was controlled by a ship-mounted constant tension winch. The weights, lengths, and tensions discussed here are applicable to the reentry of an existing borehole with seismometer package carried outside the drill string by an external cable. The cable is subjected to all of the motions induced in the pipe by ship roll, pitch, heave, and yaw plus additional stresses induced independently on the cross-sectional profile of the cable by currents in the water column.

The cable was assumed to be coaxial, hytrel-jacketed, spaced, armored, and torque balanced. It had a 17.6-mm O.D., a breaking strength of about 9500 kg, and a longitudinal stiffness of 4.85×10^6 kg. The dry and wet weights were 0.663 and 0.432 kg/m, respectively.

While it was not possible to describe all wave, sea, and current conditions likely to be imposed on the cable and pipe during deployment, average and limiting conditions served as useful guides. The surface conditions assumed for Site 395 included an average wave height of 1.1 m and an average wave period of 5 s. Seas in excess of 1.5 m were assumed to occur less than 20% of the time. Typical surface currents were 17 to 35 cm/s, while midwater depth currents were not expected to exceed 10 to 15 cm/s. Strong bottom currents were considered extremely unlikely.

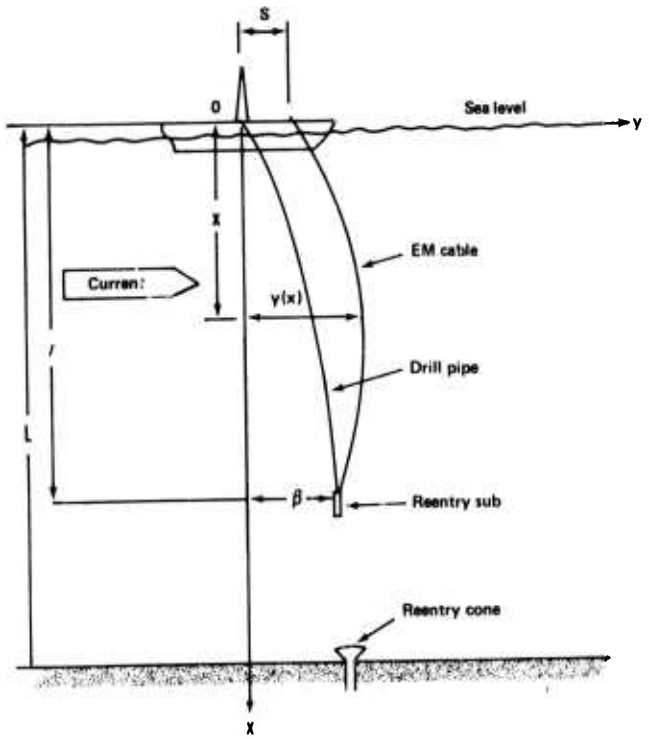


Figure 1. Drill pipe and cable configuration during reentry in the presence of a current. L = water depth, l = drill pipe length, x = point at which deflection is measured, s = initial offset between EM cable and drill pipe, y = deflection of cable, and β = deflection of drill pipe.

Results

Although the calculations made during the course of the study are too tedious to reproduce here, many of the conclusions reached have considerable bearing on any future deployment of heavy equipment by cable. The conclusions are thus summarized below as an aid to future investigators.

1. Tension in the cable is controlled primarily by its own weight, by current, by the roll, pitch, and heave of the ship, and the release of the reentry sub. Surge, sway, and yaw-generated tensions are small and may be neglected. Cable weight and current generate static tension; ship motion and the release of the reentry sub cause dynamic tensions in the cable.

2. The maximum static tension is dependent on cable length and current and occurs at the upper end of the cable. For the case of a 100-cm/s current at the surface and a linear decrease in velocity to a

[1] Summary of GMDI Report 006-002 by E. Gershunov for Global Marine Development, Inc., Newport Beach, CA 92663.

value of 0 cm/s at the bottom, the maximum tension is about 34 kg. The main contributor to static tension is the weight of the cable. Additional tension due to current is in the range of 10 to 20% of the tension caused by the weight of the cable. The minimum static tension occurs at the lower end of the cable where the tension is limited to about 450 to 680 kg to avoid entanglement.

3. Generally, the dynamic tension applied to the upper end of the cable causes changes not only in the elongation of the cable but in its deflected shape. A conservative evaluation of the upper limit of the dynamic tension is based on two assumptions: the dynamic tension transforms completely into strain energy in the cable and only causes elongation; and the lower end of the cable is attached to the reentry sub-drill pipe and is immovable for any given cable length.

4. The dynamic tension depends on the wave frequency, cable length, and velocity of strain propagation in the cable (3426 m/s). The maximum dynamic tension occurs at the lower end of the cable.

5. The first natural frequency of the cable in longitudinal oscillation ranges from 0.88 to 3.53 radians/s, which corresponds to a natural period of 1.8 to 7.1 s, depending on the length of the cable. The frequency and period of the second mode range between 2 to 11 radian/s and 0.6–2.4 s, respectively. The highest modes have periods of less than 2 s, which correspond to the very low energy end of the sea energy spectrum (Table 1).

6. If the magnitude of the dynamic tension in the cable is considered to range from 225 to 680 kg, then the magnitude of the dynamic tension applied to the upper end of the cable may be determined in accordance with Figure 2 for various wave frequencies and the first natural frequency of the cable. Figure 2 may be used to establish the tension transferred by the tensioning system to the cable.

7. The deflected shape of the cable was determined for a plane current profile (Fig. 3) and a spatial profile (Fig. 4). For comparison and evaluation of the possibility of cable-drill string entanglement, each figure contains the deflected shapes for both cable and drill pipe. These figures show that there is no reason to anticipate cable-drill pipe entanglement or cable wrapping for the conditions investigated if the current is sweeping the cable away from the pipe.

8. With the ship located 900 m downstream from the borehole, the slacked length of the cable is about 305 m and the tension at the borehole is estimated to range from 360 to 410 kg for a 50 cm/s surface current, a linear current profile, a water depth of 4493 m, and sea-state 5 conditions.

9. If the cable is captured by the reentry sub after the BIP is released, two cases are possible: the cable is locked in the reentry sub; or the cable is pulled through the reentry sub. If the cable is locked at the reentry sub, tension, as registered by the shipboard dynamometer, will have a tendency to decrease as the pipe is withdrawn. If the cable is pulled through the reentry sub, the observer will note an increase in tension as the BIP load is taken up by the cable but should see no additional tension.

Table 1. Circular frequency and period of the first (N = 0) and second (N = 1) longitudinal oscillation modes of the EM cable.

	Cable Length (ft.)	5000	10,000	15,000	20,000
N = 0	Frequency (radians/s)	3.53	1.77	1.17	0.88
	Period (s)	1.8	3.5	5.4	7.1
N = 1	Frequency (radians/s)	10.6	5.3	3.5	2.6
	Period (s)	0.6	1.6	1.8	2.4

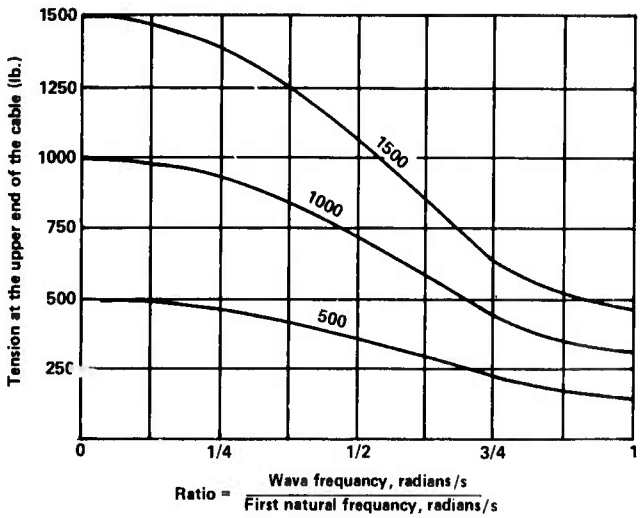


Figure 2. Dynamic tension at the upper end of the cable versus the ratio of the wave frequency to the first natural frequency of the cable for dynamic tensions of 500, 1000, and 1500 lb.

10. Possible interference between the drill pipe and the cable after the BIP has been released may occur only in cases with no ship offset. If the reentry sub is raised 20 m and the ship is moved 150 m up current at 12 to 15 cm/s in the presence of a 50-cm/s current, the pipe and cable will offset by about 125 m. Other offset and current conditions do not indicate a real tendency for interference between the drill pipe and the cable after the BIP release.

11. Bottom currents cause significant bottom separation between the cable and the drill pipe. The computed relative configuration of the drill pipe and cable show that the separation is even larger if shear currents are present than in the case of bottom currents alone.

12. If the ship maneuvers upstream at a speed of about 12 to 15 cm/s, the deflected shape of the drill pipe and the cable suggest enough separation to avoid entanglement.

13. If the length of the cable is equal to the water depth, ocean currents may cause additional substantial tension in the cable due to its elongation. This additional tension is uniformly distributed along the length of the cable.

14. To decrease the tension due to currents that may be considered undesirable when applied to the lower end of the cable, the total released cable length is recommended to be about 5 to 6% more than the depth of the water plus the borehole.

15. To avoid kink formation in the cable and snap loading, it is recommended that the maximum tension at the upper end be maintained at approximately 10% more than the weight of the released length of the cable. In this case, the maximum tension at the lower end of the cable is expected to be no more than 10% of the maximum tension applied to the upper end.

16. For sea state 5 conditions, a water depth of 6100 m, a 6400-m cable length, no ship offset, a linear current profile with a 100-cm/s current at the surface and a 0-cm/s current at the bottom, the maximum tension at the upper end of the cable will be about 7710 kg, and the maximum tension at the lower end 710 kg.

17. During Leg 78B, no snap loads appeared in the cable for any of the conditions tested and described.

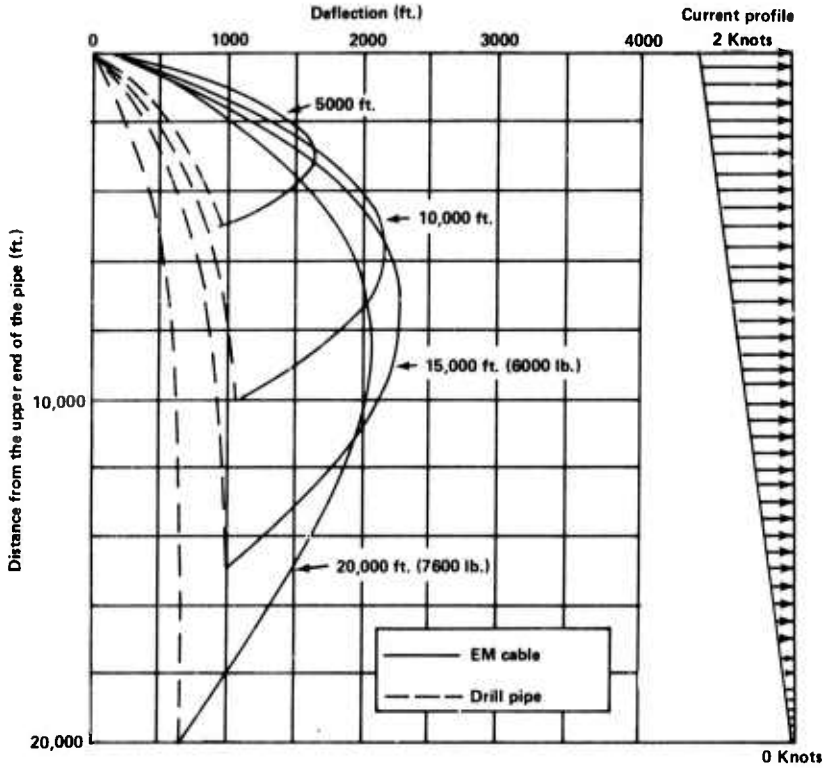


Figure 3. Deflections introduced in the cable and drill pipe by a 2-knot current, which decreases monotonically with depth.

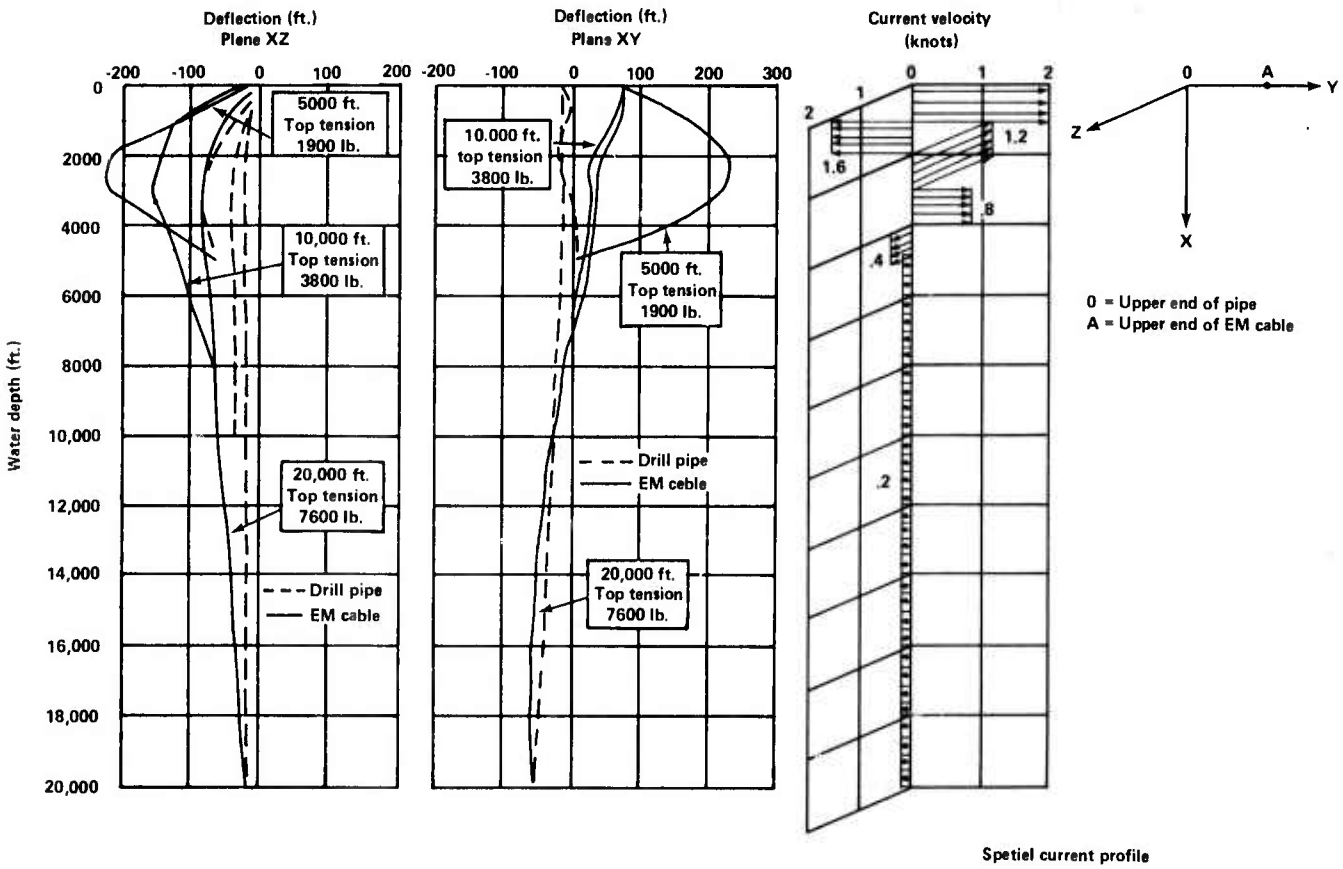


Figure 4. Deflected shape of cable and drill pipe due to a spatial current profile for 5000-, 10,000-, and 20,000-ft. water depths.

Appendix C. The Ocean Subbottom Seismometer

The following discussion of the ocean subbottom seismometer is a paper prepared by F.K. Duennebier and G. Blackinton of the Hawaii Institute of Geophysics. The paper is reprinted from the *Handbook of Geophysical Exploration at Sea,* 1983, with the permission of CRC Press, Inc., Boca Raton, Florida.

CRC

CRC PRESS, INC.
2000 Corporate Blvd., N.W.
Boca Raton, Fl.
33431

PERMISSION TO REPRINT IS GRANTED
BY CRC PRESS, INC.
CREDIT LINE REQUIRED: Reprinted with permission from (full book or journal reference). Copyright ~~The Chemical Rubber Co.~~, CRC Press, Inc., Boca Raton, FL

7-29-85
Date

Barbara Brownlee
Permissions

THE OCEAN SUBBOTTOM SEISMOMETER

F. K. Duennebier and G. Blackinton

INTRODUCTION

Since the beginning of the Deep Sea Drilling Project (DSDP) more than ten years ago, there has been interest in emplacing instruments in the holes and leaving them to monitor geophysical parameters, especially seismic, after the drilling ship has left the site. Until 1979, however, no serious attempt was made to achieve this goal because of conceptual problems in the emplacement and recovery of data. Briefly, the main problem is how to get the data out of the hole after the drilling ship leaves the site. During 1977, a series of meetings were held at DSDP to attack this problem and develop a system to be emplaced in a deep sea drill hole. Although the system conceived during these meetings was too ambitious for funding agencies to sponsor, many of the ideas bore fruit in the system subsequently developed at the Hawaii Institute of Geophysics.

The drilling schedule at the end of 1977 put the GLOMAR CHALLENGER in the Gulf of California in early 1979. Since a large seismic experiment (ROSE) was to take place then in the same area, an effort was made to have an instrument ready for emplacement at that time. National Science Foundation funding was obtained in April 1978 and the first system installed in February 1979. The system is explained in detail in this paper along with the method of emplacement and data recovery. We hope that the simplicity and versatility of the system will be apparent and that others will want to try their own sensors or recording devices in similar packages.

SYSTEM DESIGN

The ocean subbottom seismometer (OSS) system is divided into three main components: the borehole package, the recording package, and the recovery system (Figure 1). The borehole package obtains all of its power from the recording package and thus can remain in the hole indefinitely (Figure 2). The recording package supplies power to the borehole package and records data. The borehole package is connected to the recording package through 9 km of 7-conductor armored cable. The recording package is attached to the free end of the cable and can be pulled to the surface with the recovery rope to resupply the batteries and tapes. While on the surface, the end of the cable can be connected to a test box for real-time monitoring of the borehole package. All data are telemetered from the borehole package in digital form and seismic data are converted to analog form for recording. The recovery system includes the rope used in recovery of the recording package and the anchor-release system that holds it on the ocean floor.

Borehole Package

The borehole package contains all sensors, signal electronics, multiplexer, A to D converter, telemetry, and power conditioning electronics. The pressure case, which has an inner diameter of 65 mm, is housed in a modified density logging tool similar to those routinely used on the GLOMAR CHALLENGER. The tool was specially manufactured for this experiment by Gearhart-Owen, Inc. The maximum tool diameter (3 7/8 in.) is constrained by the inner diameter of the drill pipe (4 1/8 in.). A command can be sent down the cable to enable a spring to push the borehole package out of the

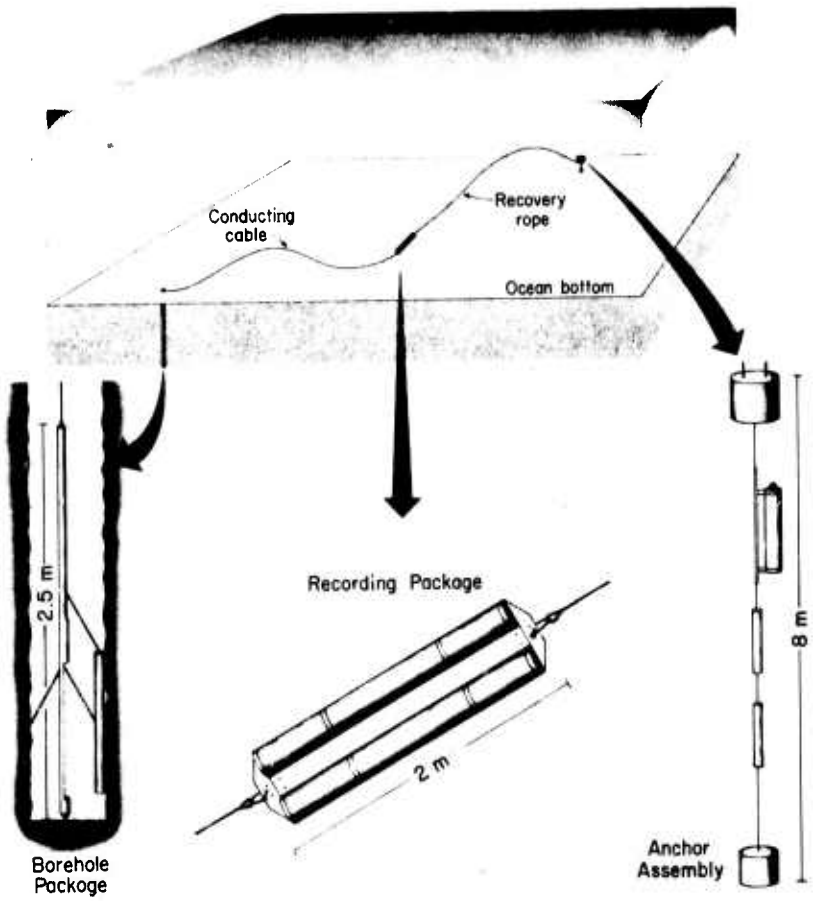


FIGURE 1. The ocean subbottom seismometer system. The borehole package is emplaced in a deep sea drill hole with power transferred to it, and data sent from it, through a conducting cable connected to a recording package. The recording package is attached to a floating rope that is in turn connected to a float-anchor assembly for recovery.

body of the tool and against the side of the hole (Figure 1), insuring good seismic coupling. The electronics in the borehole package are divided into modular units for ease in interchanging sections and for electrical isolation (Figure 3). Although many sensor configurations (up to 16 sensors) are possible, the present configuration has three short-period geophones, two bubble tilt meters, and temperature multiplexed into 16 data channels. The processing of the multiplexed data is discussed in the section on signal handling.

Three 4.5-Hz Geospace model HS-1 high temperature geophones are mounted orthogonally in a single block of aluminum (Figure 4) and secured with set screws. The corners of the two horizontal geophone cases were machined to fit into the cylindrical block. The tilt meters (Fredericks Model 7660) are aligned along the same axes as the horizontal geophones. They are functional over ± 0.2 rad with sensitivities after electronics of 0.3 V/mrad at the absolute tilt output and 30 V/mrad for signals between 1 and 50 sec periods at the differential tilt output. Although these sensitivities are not high enough to resolve tides or reasonable tectonic tilts, they are valuable in deciding the orientation and sensitivities of the geophones and the tilt of the package in the hole. Higher sensitivities are possible with lower-range bubble tilt meters[1] at the cost

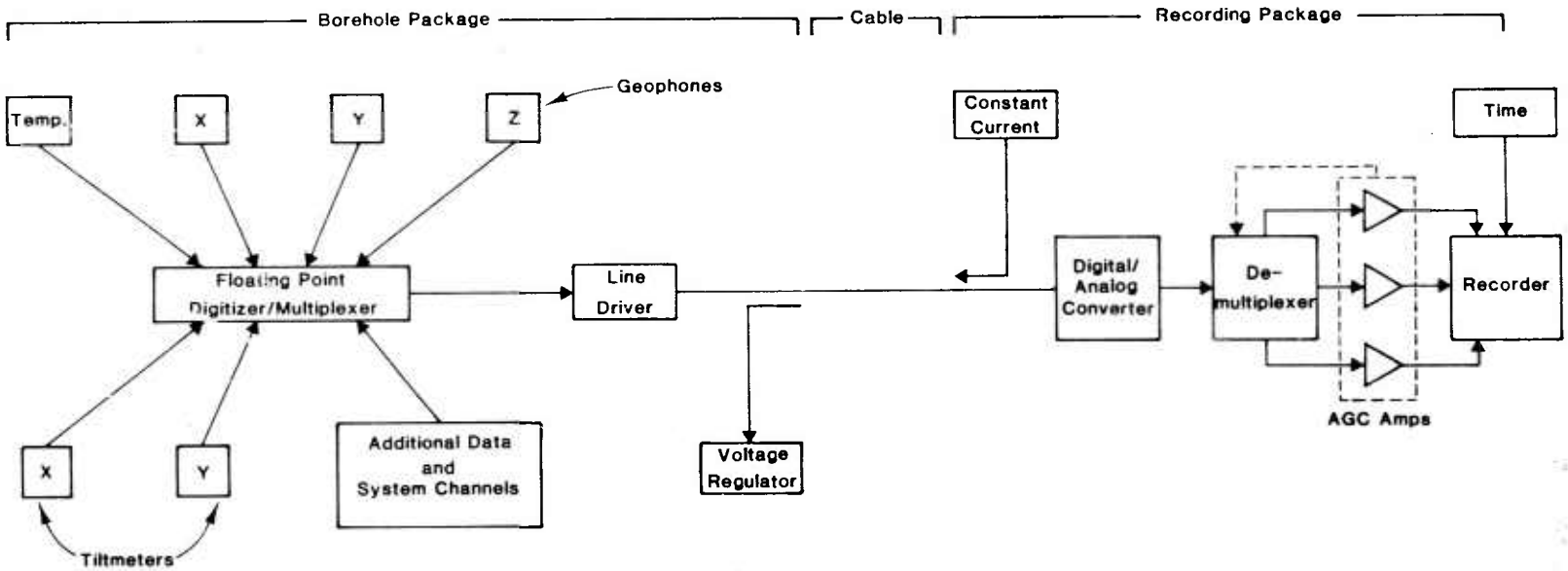
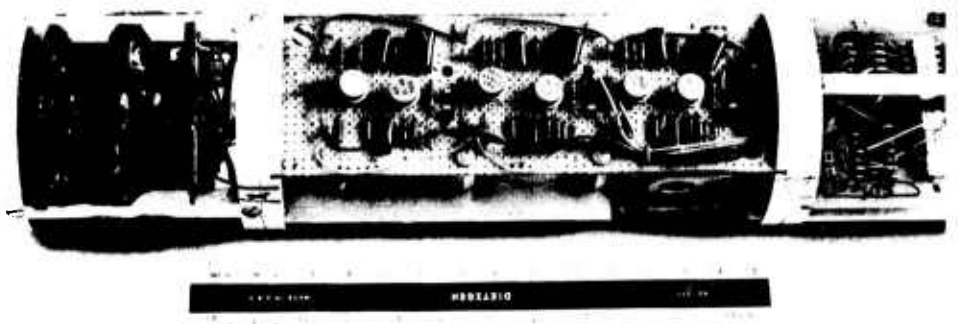
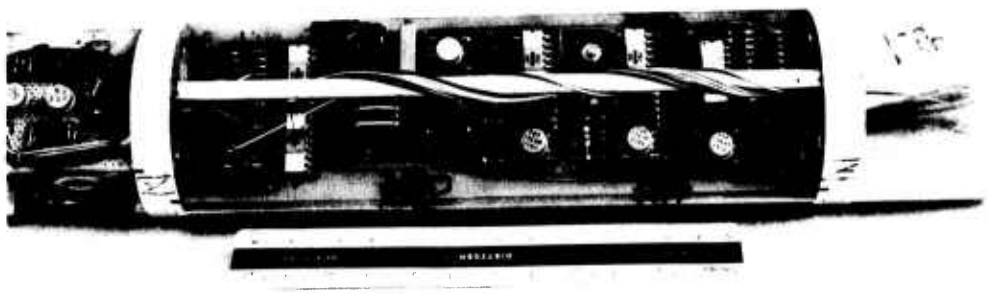


FIGURE 2. Block diagram of ocean subbottom seismometer system.



A



B

FIGURE 3. A and B. Borehole package electronics showing modular design for ease of replacement and modification.

of requiring high-precision mechanical leveling of the bubble. This was not practical in this first instrument although it is certainly possible in future designs. The thermal sensors are Analog Devices AD590, with a sensitivity of 1 m V/°C within the range from −55 to +150°C.

The resolution of the digitized signals from each of the sensors is between 0.8% and 0.2% of the absolute value of the sensor output. This is discussed in more detail in the section on the floating point analog to digital converter.

The package can easily accept other sensors that do not require significant power (less than 30 mW) and that can fit inside the pressure case. The sensors chosen for the package were standard off-the-shelf units and may not be the most sensitive or reliable sensors available. Now that the system is developed, more effort will be put into sensor optimization.

The 9 km of cable that connects the borehole package to the recording package is the single most expensive item in the system. Seven-conductor double armored Vector 7-J46RB cable was chosen for two reasons: DSDP uses this cable for the logging operations aboard the GLOMAR CHALLENGER and has the equipment and experience necessary to handle it and its connectors and splices, and the cable has the strength necessary to survive the wire stripping operation. Standard connectors manufactured by Gearhart-Owen used to connect the cable to the packages were filled and booted with a Devcon® potting compound rather than grease to minimize long-term leakage.

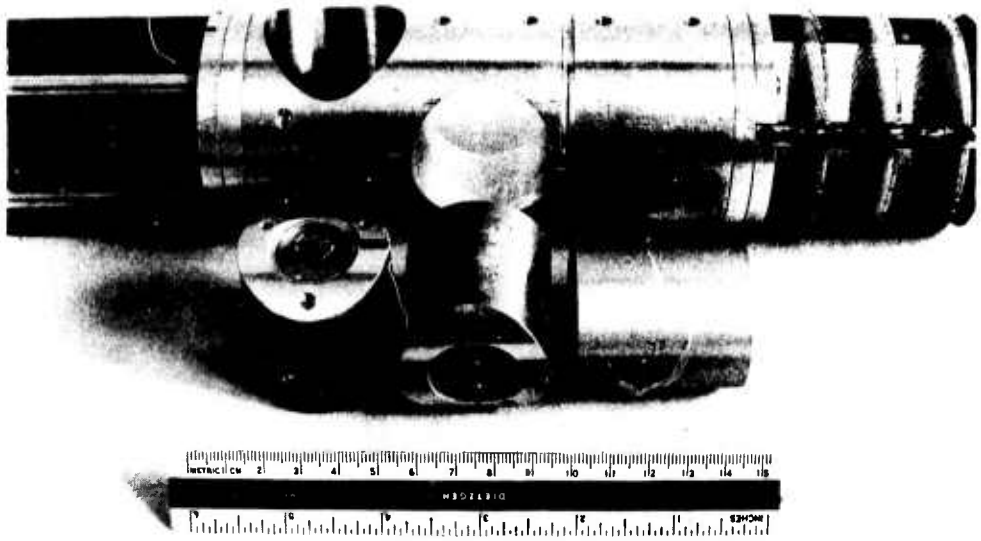


FIGURE 4. Geophones and geophone mounting block in the borehole package. No provision is made for leveling since the geophones will operate up to 5° from vertical and the package tilt can be measured from the tilt meters.

Data Recording/Power Units

Two units are used at the upper end of the cable: a test box to monitor data in real time and the recording package to record data unattended for long periods of time. Other data retrieval methods, such as buoys, digital packages, and satellite links are possible but have not yet been developed.

When the end of the wire is at the ocean surface all data are available in digital form. At this point, the user is free to decimate, compress, or otherwise choose the data he wishes to monitor while recording all data on tape for later analysis. The test box acts as a test set for system check out, a D-to-A unit for real-time monitoring, as a playback unit for playing back tapes of data that were recorded in real time, and as an interface to the computer for data processing. It also is capable of sending the command to extend and retract the borehole package from the tool. The data handling functions of the test box are discussed in the section on data processing.

The recording package pressure case consists of two aluminum tubes approximately 2 m in length (Figure 5). One side contains batteries to power the tool and the other contains electronics, tape recorders, and more batteries. Five cassette recorders (Figure 6) can be preset to start recording at individual times and speeds. Each is capable of recording four tracks of signals up to 20 Hz for 15 days or up to 100 Hz for 3 days. The batteries (standard D-cells) and electronics are amounted in aluminum frames for easy access and removal. Prior to launch a vacuum is pulled in both tubes. The internal pressure of each tube can be monitored through a bulkhead connector to detect pressure leaks.

Recovery System

The recovery rope attaches to the end of wire rope about 5 m above the recording package. This rope, 1¼ in. plaited polypropylene, has a length greater than 1.5 times the depth of water. Its buoyancy is such that the recording package never actually touches the ocean floor. Since the breaking strength of the rope is about 10 tons, the cable (breaking strength 8 tons) should break first if it snags on the bottom, insuring recovery of the recording package. A swivel at each end of the rope limits snarls.

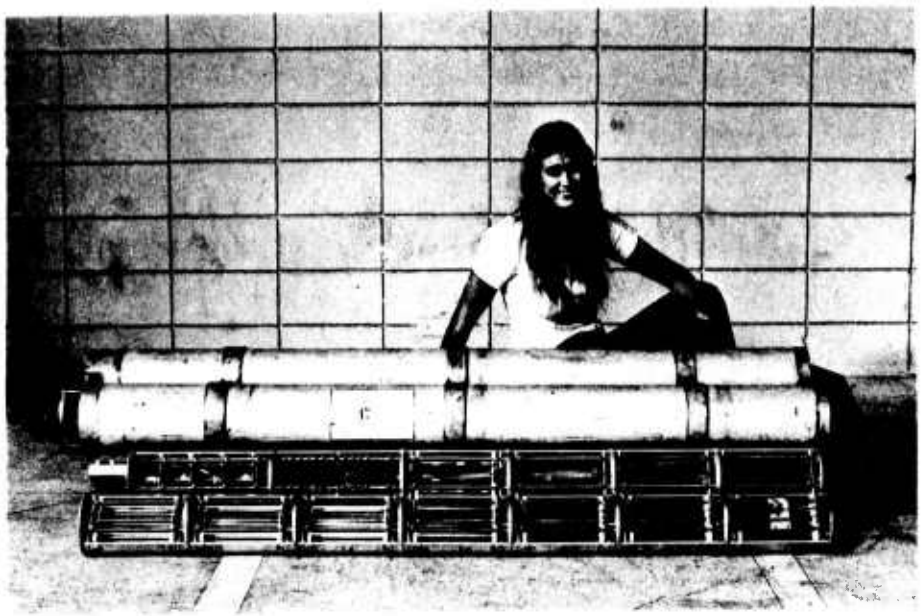


FIGURE 5. Recording package. Two aluminum tubes about 2 m in length contain batteries, electronics, and recorders for recording continuous data from the borehole for up to 75 days unattended.

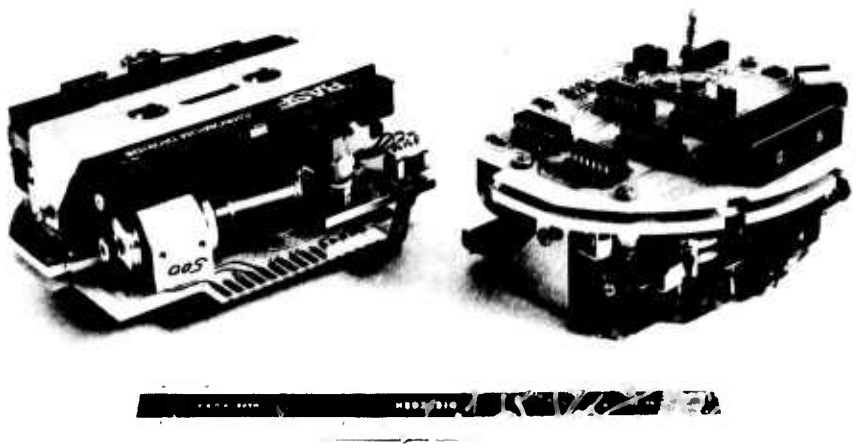


FIGURE 6. Cassette tape recorders. Analog geophone data are recorded on three tracks and time and digital data on the fourth. Each recorder is preset to turn on at a particular time and record continuously for up to 16 days.

The anchor assembly attaches at the free end of the rope (Figure 7). It holds the rope fixed on bottom with a lead anchor weight and a small Danforth® anchor. The rope can be connected to the anchor through three release devices, an acoustic transponding release and, if the recovery time is known, two timed releases, any one of which can release the anchor and allow the rope to float to the surface. The decision

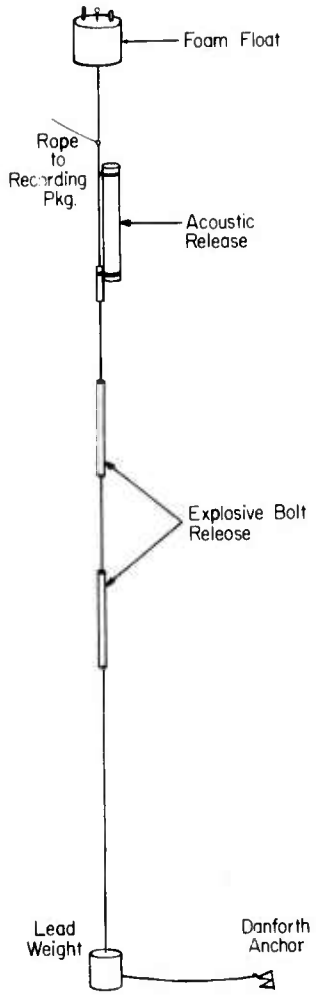


FIGURE 7. Float-anchor assembly. The anchor is released from the float and recovery rope either at a specific time (explosive bolt release) or on command (acoustic release), allowing the float and recovery rope to return to the surface.

to have no equipment on the ocean surface was made because of the risk to (and from) passing ships and susceptibility to damage in poor weather. It was judged considerably easier to design a reliable anchor system than a surface buoy that would survive for the required length of time.

The system was designed to be emplaced in the deep ocean by the GLOMAR CHALLENGER and recovered by an oceanographic research vessel. However, there is nothing to prevent its emplacement in a hole on land, in an offshore exploration well, or possibly in an existing hole in the deep ocean from a research ship.

SIGNAL HANDLING

Multiplexing and Digitizing

The 16 channels of data are sequentially sampled according to the hierarchical

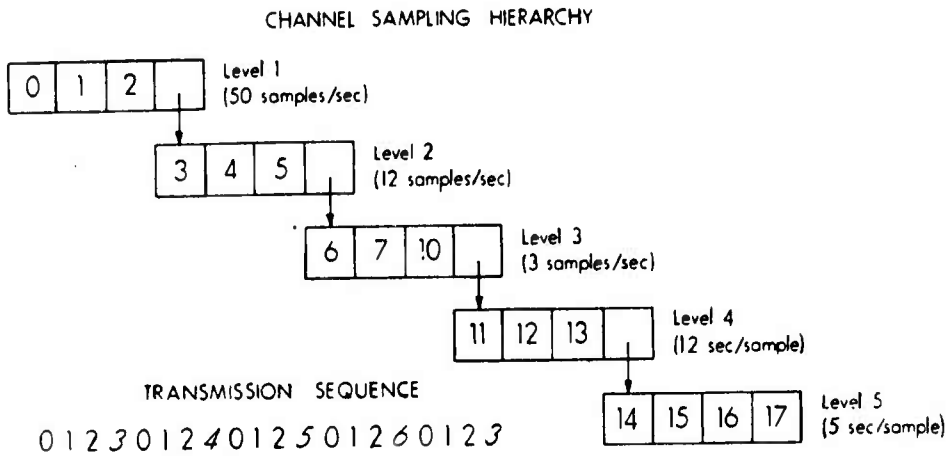


FIGURE 8. Channel sampling hierarchy: 16 channels are sampled at five different rates, from 50 samples/sec to 5 sec/sample.

scheme of Figure 8. The scheme is a modified four-channel scanning sequence with five steps. The fourth channel of each step is one channel of a lower step. The highest step channels are thus sampled 50 or 100 times per sec and those of the lowest step once every 5 or 2.5 sec. The signals that were connected to each channel in the first two instruments are described in Table 1. All signals are conditioned to vary between +2.5 and −2.5 V for digitizing.

As the signal on each channel is connected in turn to the digitizer it is converted into a 12-bit floating point digital number. The number has a 3-bit, base 4 exponent and a 9-bit mantissa (8 bits plus sign).[2] The ranges of the exponent and mantissa allow signals from ±0.6 μV to ±2.5V to be encoded — a dynamic range of 138 dB. This is equivalent to the dynamic range of a 23-bit linear converter. The 9-bit mantissa, however, limits the resolution of each digital representation to 0.2% at best. The base 4 exponent means that the resolution can be as poor as 0.8% of the value of the sample.

For most varying signals with zero average, a resolution better than 1% is sufficient. Few direct tape recordings of the signals will provide much better fidelity. A small signal superimposed on a large steady-state signal, however, may be severely distorted. The 1% resolution of the large signal may represent 10% or even 100% of the small signal. The ratio of signal to digitizing noise throughout the converted dynamic range is summarized in Figure 9.

Telemetry

The digital sample is sent serially to the recording package in the form of an 18-bit delay modulated word.[3] The 18 bit are 1 start bit, 4-bit channel number, 12-bit sample, and 1 stop bit (Figure 10). As each of the high-frequency channels is sampled 50 times per sec, 200 samples or 3200 bit are sent each second. In the recording package, the start and stop bits are sensed and each sample is converted from serial to parallel. A floating point digital-to-analog (FPD/A) converter reproduces the voltage sampled 10 msec earlier in the borehole package. Only three selected channels are demultiplexed and recorded in analog form on tape.

Recording

In the first instruments only the three geophone signals were analogized by the FPD/A. The FPD/A, however, does not reproduce exactly the sampled voltage. Rather,

Table 1
OSS CHANNEL ASSIGNMENTS

Channel (Octal)	Signal
0	Vertical geophone
1	Horizontal geophone (parallel)
2	Horizontal geophone (perpendicular)
3	Differential tilt (parallel)
4	Differential tilt (perpendicular)
5	Differential temperature
6	Absolute tilt (parallel)
7	Absolute tilt (perpendicular)
10	Triangle (system)
11	Absolute temperature
12	Excess current monitor (system)
13	Open (system)
14	+ 5V Monitor (system)
15	−5V Monitor (system)
16	Common (system)
17	Open (system)

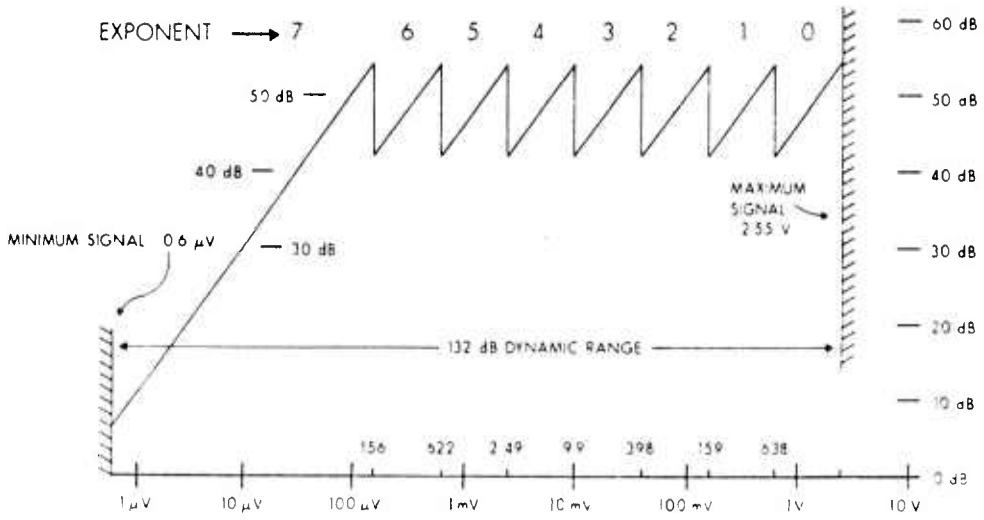


FIGURE 9. Signal amplitude vs. digital signal-to-noise ratio. A 12-bit floating point word with a 3-bit (base 4) exponent and a 9-bit mantissa is used. This is equivalent in total dynamic range to 132 dB with resolution of better than 1% of the signal amplitude.

automatic gain control (AGC) circuits remember the average value of the preceding samples from each channel being recorded. When one of those channels is again sent, the respective AGC instructs the FPD/A to decode the digital word as if its exponent represented a larger signal. The 132-dB dynamic range of the FPA/D process is thus compressed to fit the 40-dB dynamic range of the slow-speed analog tape recorders. The actual level of the signal is continuously recoverable since the AGC command to the FPD/A is allowed to change only at the start of each minute, and the command for each minute for each channel is coded into seconds 50 to 58 of the modified IRIG-H time code (Figure 11) recorded on the fourth data channel. The characteristics of the OSS AGC system are similar to the AGC system used in the HIG ocean bottom seismometers.

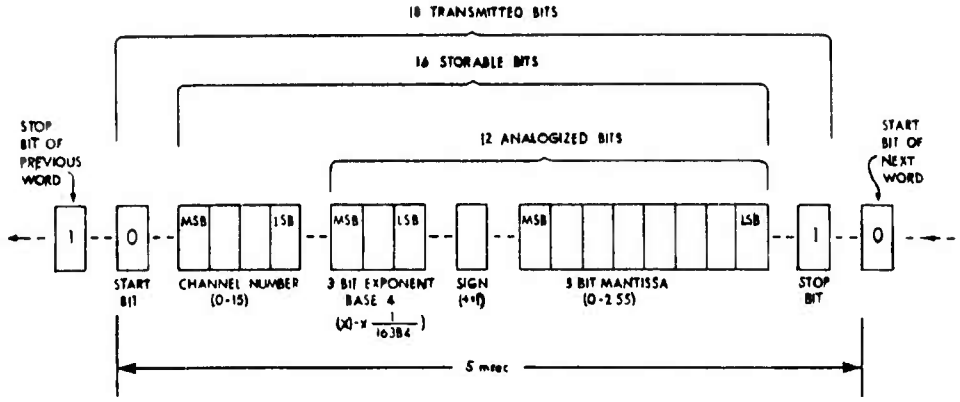


FIGURE 10. Transmission sequence. This sequence is sent up the wire at 200 samples/sec or 3200 bits/sec. The rate is limited by the power available to the system.

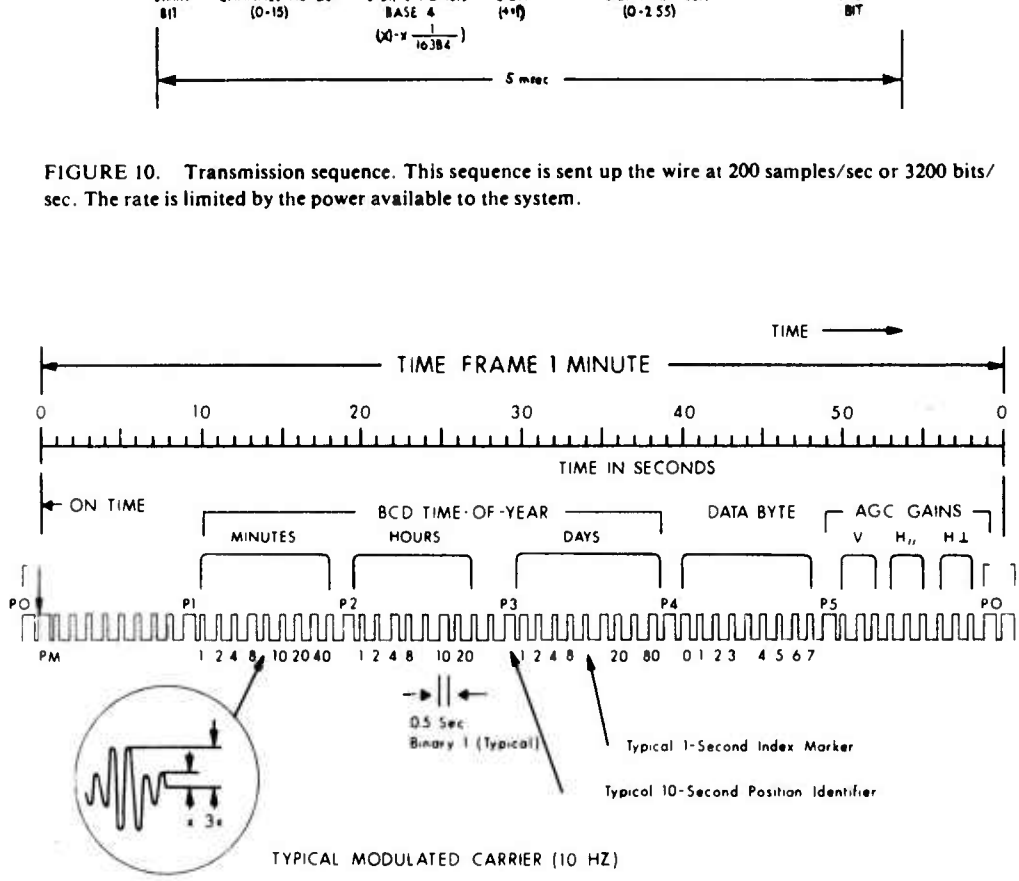


FIGURE 11. Time code. In addition to time, the code contains the recorded geophone gains and the digital data from the borehole package recorded at a rate of one sample/channel/32 min. On playback, the 10 Hz carrier is used in phase lock to control digitization rate.

The AGC system fixes the background level to be within the dynamic range of the tape. If the average level gets above −26dB or below −40 dB the level is allowed to change by 12 dB at the beginning of the next minute. In this way, a background noise signal is always above the tape noise and the smallest signals are always seen. The major disadvantage of this recording technique is that large signals will exceed the dynamic range of the tape and be clipped. For seismic signals, however, the times of the first arrivals are often more important than the amplitude. A sample of a signal showing the time code and a gain change is shown in Figure 12.

The recording package currently in use is designed for long-term unattended recording of continuous data. The recording medium is thus analog slow-speed magnetic

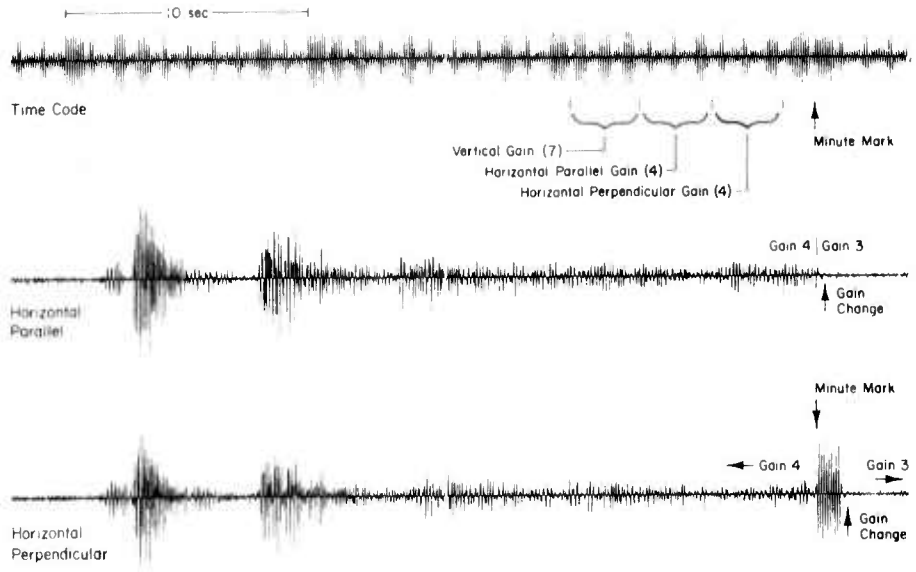


FIGURE 12. Automatic gain ranging. A large change in signal or background level causes the gain to change 12 dB at the next minute mark. The gain is recorded as part of the time code.

tape. Either a digital or an analog format can be used for recording long-term data. Digital recording retains the high quality and dynamic range of the FPA/D system but requires either a large physical volume for data storage or selective recording during specific times. Analog signals can be recorded continuously for long periods of time in small volumes but with reduced dynamic range. For this experiment, with interest in a considerable variety of seismic events from teleseismic earthquakes to small explosions, analog recording was judged more practical than digital recording. If more dynamic range was required, the present analog recording package could be replaced by a digital recording package. Although only the three geophones are recorded on the analog tape, each of the data channels from the borehole package is recorded in digital format on the fourth tape channel in an unused section of the time code. In this way, each channel is sampled once every 32 min. Although this rate is of little use for seismic signals, it has provided an excellent record of the thermal and tilt history of the package as well as other slowly varying parameters.

EMPLACEMENT

The most difficult problem in designing a downhole marine instrument system is the actual installation technique. As the system described here has been successfully emplaced in two DSDP holes, the technique used is discussed in detail.

The first problem is selection of a deployment site. While the site should ideally be chosen on the basis of the information desired, the necessity of using the drill ship restricts possible sites to those scheduled for drilling. In our case this was not a problem, since it is hard to imagine any site without sufficient merit to warrant long-term instrumentation. The site chosen should be known well in advance, as water depth will affect the amount of recovery rope needed, and predicted hole temperature could affect the sensors used.

Once the drilling is complete, the drill bit is dropped to allow normal logging of the

hole. Logging of holes to be instrumented is of great value since characteristics of the hole can be important in understanding the OSS signal. When the logging is completed, the OSS borehole package is attached to the logging cable, tested, and lowered to the bottom of the hole with the logging winch. When geophone channels are being monitored, it is obvious when the package reaches the bottom of the hole because package motion is detected by the geophones. The clamping arm is extended and the tilt meters are monitored to insure that the hole angle is not beyond the limit of the horizontal geophones (about 5°). The rate of change of hole temperature also can be monitored to insure that the equilibrium temperature will not exceed the design limits. When testing is complete, the clamping arm is retracted and the package lifted about 10 m from the bottom of the hole in preparation for pipe stripping. The telemetered signal from the OSS borehole package is continuously recorded on magnetic tape during the lowering and testing.

The most important procedure in the installation is removing the drilling pipe from around the logging cable while keeping the borehole package in the hole. To do this, the cable connecting the borehole package to the ship is clamped at the drill floor and tension transferred from the logging winch to the clamp. The cable is cut and terminated with a snap fitting that mates with the overshot on a lifting line. From the time the cable is cut until all pipe is stripped and the cable is rejoined, no data can be obtained from the borehole package.

The sand line on the CHALLENGER was used as the lifting line and connected through a swivel and the overshot to the logging cable. The swivel was found necessary to prevent twist developed by tension on the sand line (not torque balanced) from being passed through the cable to the borehole package. The tension is taken on the sand line and the overshot positioned just above the level of the rig floor as shown in Figure 13A. The pipe is lifted about 90 ft as usual until a joint is level with the overshot (now inside the pipe). The joint is broken, revealing the cable, overshot and mating snap fitting (13B). A fork is inserted in the cable snap fitting and tension is taken on the fork by lowering the sandline until the fork rests on the top of the remaining drill pipe. The overshot joint is broken and the lifted pipe stand is returned to the pipe rack (13C). The sand line is pulled out of the pipe stand, reconnected to the cable snap fitting, lifted, and the fork removed. The process is repeated until all pipe has been removed and only the cable connects the ship to the hole. Lifting pipe in this manner takes 20 to 30% longer than normal. It was feared that a large horizontal motion of the drill pipe as it cleared the mud line could shear the cable or that a gross movement of the ship away from the hole could pull the package from the hole. In the two installations so far, however, neither of these problems has occurred.

After the stripping, the hanging cable is reconnected to the cable remaining on the winch drum with a "torpedo" splice. Following the connection, signals can again be obtained from the borehole package with the test box. The package is lowered to the bottom of the hole while the signals from all 16 channels are carefully monitored. The clamping arm is extended and about 50 m of cable payed out to prevent ship motion from pulling on the clamped package. Again, the telemetered signal is recorded continuously. With the pipe stripped and the borehole package working properly, the ship is allowed to drift away from the hole while the remaining cable is payed out. Care must be taken to pay out cable at a specific rate. Ideally, the cable in the hole should not move. The cable out vs. distance from the hole can be calculated for a given weight in the hole, water depth, and cable weight. The calculated schedule is used during the pay-out operation. If the ship moves too far relative to the amount of the cable out, the package will be pulled up in the hole. If cable is payed out too soon, it will start to pile up in the hole or on the bottom and be more likely to break when pulled during recovery.

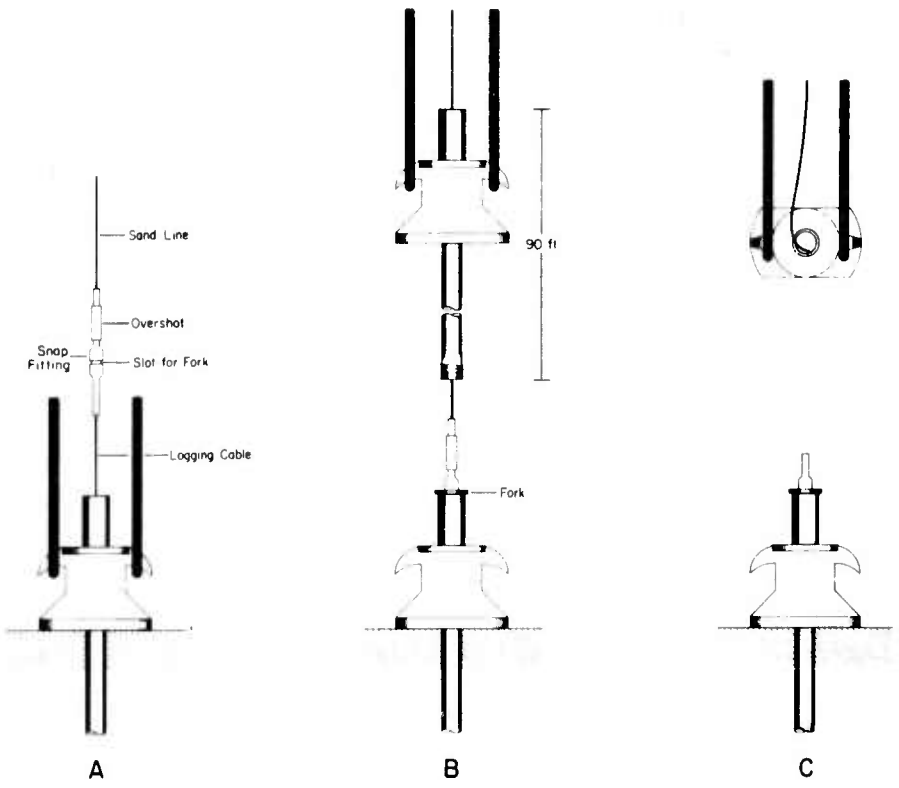


FIGURE 13. Pipe stripping. When the borehole package is in place, the drill pipe is stripped from around the cable as discussed in the text.

Near the end of the cable the ship is stopped. This is an excellent point in the operation for taking real-time data. During the second deployment, the CHALLENGER held this position for 12 hr while a second ship (R/V KANA KEOKI) shot refraction lines to the borehole package and to an array of ocean bottom seismometers. After real-time operations and testing, the wire is again clamped, headed with a new connector, passed to the side of the ship (keelhauled) and the borehole package fully tested. The recording package assembly is tested and connected to the cable. The time code from the recording package is recorded with WWV signals to calibrate the internal chronometer. The time code is checked to be sure that the telemetered signal is being decoded correctly. When the complete system has been checked, the recording package is lifted over the side and tension is taken on the recovery rope.

Once again the ship is allowed to drift and the rope payed out at a speed about equal to the ship speed over the bottom. On the GLOMAR CHALLENGER, rope tension was controlled at a tensioner (Figure 14) before passing to the spool of rope. Tension on the rope decreases as the wire is laid on the ocean bottom and the buoyancy of the rope supports the recording package. The end of the rope is attached to the anchor assembly. The ship moves slowly away to pull the anchor assembly away as far as possible from the recording package (Figure 1), and the anchor assembly is dropped overboard.

RECOVERY

To recover the recording package, the recovery ship locates itself with respect to the

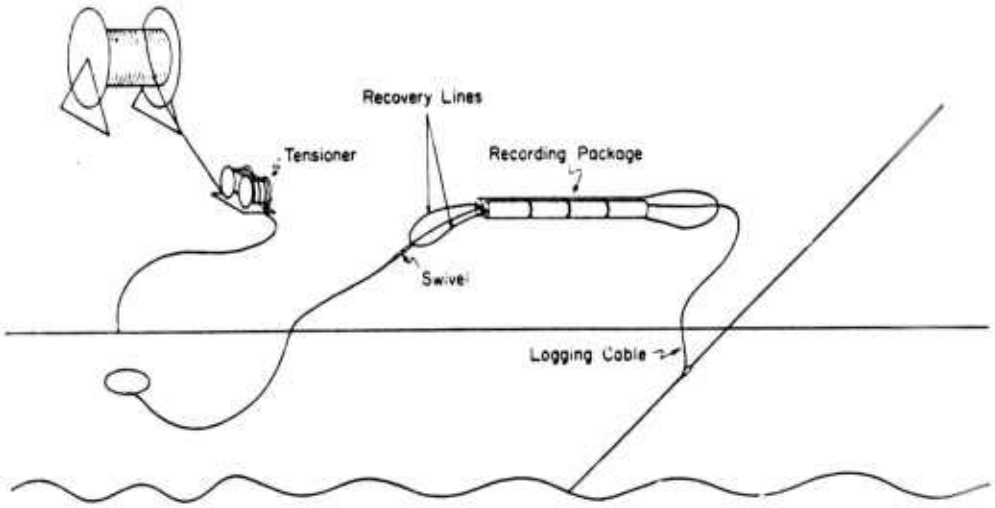


FIGURE 14. Deployment of recording package.

transponders on the anchor assembly and either waits for or commands the rope and float to release from the anchor. The time releases free the buoy and recovery rope from the bottom at a preset time. The transponder release can be commanded to return to the surface when the recovery ship is ready. If neither of the above works, the third recovery technique is grappling for the recovery rope (Figure 1). If the recovery rope cannot be located or is broken, the final resort is to drag for the cable lying between the hole and the recording package. The last two methods are undesirable for reasons of increasing danger to the OSS system and increasing time involved in recovery. Release can be detected by the change in travel time of the acoustic pulses from the recovery rope transponder to the ship. When the recovery buoy arrives at the surface it is located by sight and picked up. The 1¼ in. rope is threaded across a roller on the stern, through a tension measuring device, and around a hauler (Figure 15). The rope is drawn on board with the hauler and stored.

When the recording package is brought up to the ship the time code is immediately recorded for chronometer calibration purposes and the package is removed from the cable.

The borehole package (still in the hole) is tested by connecting the test box to the end of the cable. If the borehole package is working well, the recording package is tested, refurbished, and reinstalled by reversing the procedure outlined above. If the borehole package is not working well, an attempt is made to pull it from the hole and recover it.

CURRENT STATUS AND FUTURE PLANS

The system has been emplaced twice; in DSDP holes 482C and 494A. The first system (Downhole 1) was damaged during the stripping operation (probably because of the lack of a swivel in the sand line) and worked only in the real-time mode, but valuable temperature and seismic noise data were obtained.[5] The Downhole 1 borehole package was pulled from the hole after 42 days. The second system worked as planned except for electronic problems that caused the sensitivity of the seismic sensors to be considerably degraded. Refraction lines were shot to the system and to an OBS array around the hole while the data were recorded in real time. Several more lines were shot

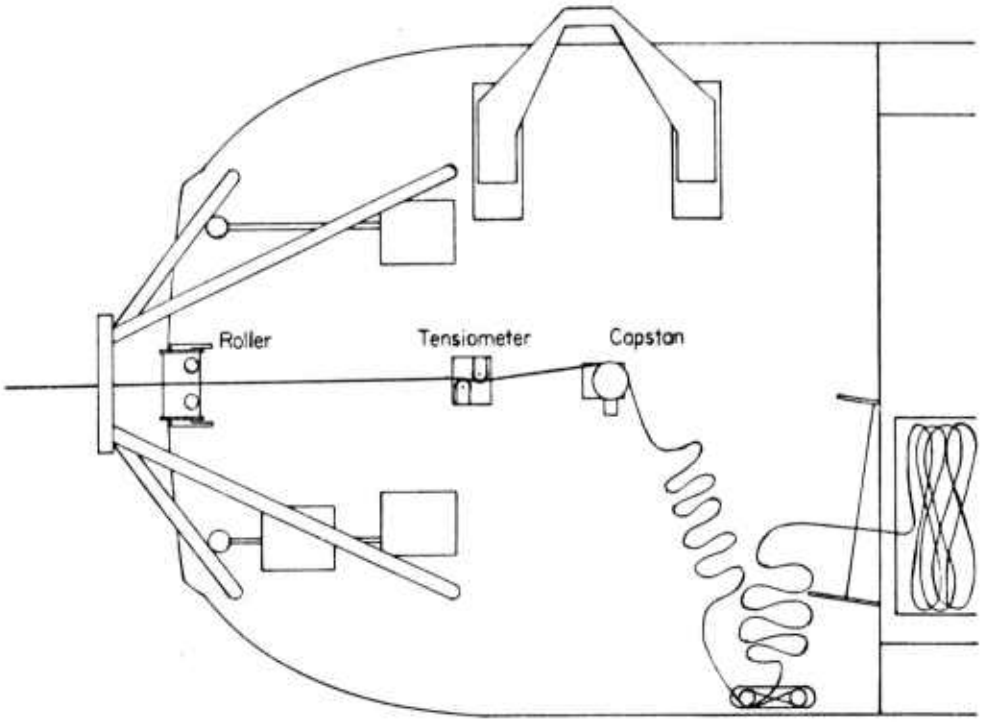


FIGURE 15. Recovery of recording package.

after the recording package was emplaced. The recording package was recovered, refurbished, and redeployed in June 1979, with no degradation noted in the system. Due to lack of suitable ships in the area, the system was not revisited again until May, 1980. By that time the transponding release at the anchor had failed and the recovery rope was grappled. Rather than hooking it, however, the grapple wire cut the rope close to the anchor. The rope floated to the surface and the recording package was recovered. Although the borehole package was still operating, an attempt to pull the borehole package from the hole failed when the wire parted.

Emplacement of the third system is now planned. This system will have considerably more sensitivity and will use 8 of the 16 channels to record and remove the DC levels from the other 8 channels. Nine vertical geophones will be wired in series and two geophones in each horizontal direction to yield more sensitivity. The rate at which data is sent up the wire will be controlled by the amount of power available with 100 samples per sec on the geophones when recording is done in real time and 50 samples per sec when batteries are used. Improvements in the analog tape system have increased the effective dynamic range to about 45 dB and guaranteed constant speed of operation to within a few percent.

CONCLUSIONS

The instrument system described in this paper can be used to obtain large amounts of high quality geophysical data from deep sea drill holes for long periods of time. Although the concept is still in its infancy, the principles of emplacement and recovery have been shown to work and easily fit into the framework of the deep sea drilling program.

ACKNOWLEDGMENTS

This paper has been critically reviewed by George Sutton, Don Hussong, Jerry Carter, and Rita Pujalet. This project would not have occurred without the encouragement and support of Charles Helsley, Director of Hawaii Institute of Geophysics. Several groups have contributed a great deal of help and expertise to this project. Our thanks to the personnel of the HIG Engineering Support Facility, the University of Hawaii Snug Harbor Marine Facility, the Deep Sea Drilling Project, the IPOD Downhole Measurements Panel, and the scientists and crew of the D/V GLOMAR CHALLENGER on Legs 65 and 67 for their aid in making this project a success. The funds for design, manufacture, and emplacement of Downhole 1 were supplied by NSF Grant OCE78-10772. The emplacement of Downhole 2 was funded by the Office of Naval Research. HIG Contribution No. 1138.

REFERENCES

1. Miller, W. F., Geller, R. J., and Stein, S., Use of a bubble tiltmeter as a horizontal seismometer, *Geophys. J. R. Astron. Soc.*, 54, 661, 1978.
2. Blackinton, J. G. and Odegard, M. E., An ocean bottom seismograph using digital telemetry and floating point conversion, *IEEE Trans. Geosci. Elect.*, GE-15(2), 74, 1977.
3. Bentley, V., Squeeze more data onto mag tape, *Electron. Design.*, 23(21), 76
4. Byrne, D. A., Blackinton, G., and Duennebier, F. K., Isolated sensor ocean bottom seismometers, in preparation.
5. Duennebier, F. and Blackinton, G., A manmade hot spring on the ocean floor, *Nature (London)*, 284, 338, 1980.

Appendix D. List of MSS Equipment Drawings (All were prepared by Global Marine Development, Inc.)

Shop level drawings of BIP/BPP and associated components were retained by Teledyne Geotech and Gould DED. Copies may be obtained through NORDA.

Drawing No.	Title
The following drawings are enclosed:	
MSSA04-SYS-D003, Rev. 1	MSS-83 GLOMAR CHALLENGER equipment installation arrangement (2 sheets)
MSSA04-SYS-D004, Rev. 0	MSS-83 IRR system arrangement and assembly (2 sheets)
MSSA02-MTL-D001, Rev. 1	MSS-82 modified BIP reentry sub with stinger control drawing
MSSA02-MTL-D002, Rev. 0	MSS-82 modified reentry assembly control drawing
MSSA02-MTL-D003	MSS-82 BIP carriage control sub detail and assembly
MSSA02-MTL-D006, Rev. 0	MSS-82 modified BIP carriage housing main assembly
MSSA02-MTL-D007, Rev. 1	MSS-82 modified BIP reentry subassembly
MSSA02-MTL-D011	MSS-82 sonar sinker bar assembly and details (2 sheets)
MSSA02-MTL-D012	MSS-82 reentry sub stinger assembly and details (2 sheets)
The following is a reference list of MSS drawings (includes drawings enclosed):	
MSSA02-MTL-D001, Rev. 1	MSS-82 modified BIP reentry sub with stinger control drawing
MSSA02-MTL-D002, Rev. 0	MSS-82 modified reentry assembly control drawing
MSSA02-MTL-D003, Rev. 0	MSS-82 BIP carriage control sub detail and assembly
MSSA02-MTL-D004, Rev. 1	MSS-82 modified BIP carriage housing assembly and details (sheets 1-2)
MSSA02 MTL-D006, Rev. 1	MSS-82 modified BIP carriage housing main assembly110/
MSSA02-MTL-D007, Rev. 1	MSS-82 modified BIP reentry sub assembly
MSSA02-MTL-D008, Rev. 0	MSS-82 hydraulic plug/sonar adapter modification
MSSA02-MTL-D009, Rev. 1	MSS-82 dummy sonar reentry tool
MSSA02-MTL-D010, Rev. 2	MSS-82 idler sheave support detail assembly

MSSA02-MTL-DO11, Rev. 1	MSS-82 sonar sinker bar assembly and details (sheets 1-2)
MSSA02-MTL-D012, Rev. 4	MSS-82 reentry sub stinger assembly and details (sheets 1-2)
MSSA02-MTL-D013, Rev. 0	MSS-82 Baker valve and sinker bar adapter modifications, details, and assembly
MSSA02-MTL-D014, Rev. 2	MSS-82 jacking screw details
MSSA02-MTL-D015, Rev. 1	MSS-82 EM cable termination on winch reel modification detail
MSSA02-MTL-D016, Rev. 3	MSS-82 hydraulic plug/sonar adapter modification
MSSA02-MTL-D017, Rev. 1	MSS-82 Baker equalizing check valve modification
MSSA02-MTL-D018, Rev. 1	MSS-82 GLOMAR CHALLENGER equipment installation arrangement (sheets 1-2)
MSSA02-MTL-D019, Rev. 2	MSS-82 A-frame details and assembly
MSSA02-MTL-D022, Rev. 0	MSS-82 EM cable winch layout of exhaust system
MSSA02-MTL-D023, Rev. 1	MSS-82 cable protectors and ring gauge assembly details
MSSA02-MTL-D024, Rev. 1	MSS-82 centering spring sonar sinker bar assembly
MSSA02-MTL-D025, Rev. 3	MSS-82 trolley and jacking screw detail layout
MSSA02-MTL-D026, Rev. A	MSS-82 test instrument installation
MSSA02-MTL-D027, Rev. A	MSS-82 layout of shock absorber for experimental test
MSSA02-MTL-D028, Rev. A	MSS-82 layout of sonar reentry tool and breakaway plug
MSSA02-MTL-D029, Rev. A	MSS-82 mock-up layout of narrow section of piccolo base
MSSA02-MTL-D030, Rev. 1	MSS-82 BIP housing support brackets
MSSA02-MTL-D031, Rev. 2	MSS-82 line storage container securing details
MSSA02-MTL-D032, Rev. 1	MSS-82 reentry guide cone installation layout
MSSA02-MTL-D033, Rev. A	Recovery tug equipment installation arrangement
MSSA02-MTL-D034, Rev. 1	IRR-custom two-plate connector and insulation details
MSSA02-MTL-DO35, Rev. A	BPP handling configuration layout
MSSA02-MTL-D036, Rev. A	Interference between A-frame and crane cab application of preformed dead end

MSSA02-MTL-D037, Rev. A	Layout of crane position at transfer of load from EM cable to BPP
MSSA02-MTL-D038, Rev. A	BPP connect up and launch position
MSSA02-MTL-D039, Rev. A	EM cable and BPP launch sequence
MSSA02-MTL-D040, Rev. A	Contingency plan for winch hydraulic system failure
MSSA02-MTL-D041, Rev. A	Contingency plan for winch brake system failure
MSSA02-MTL-D042, Rev. A	Reentry sub stinger recovery tool
MSSA02-MTL-D043, Rev. A	BPP platform
MSSA02-MTL-D044, Rev. A	A-frame and idler sheave assembly T-ATF (stern mount arrangement)
MSSA02-MTL-D045, Rev. A	BPP skid T-ATF (stern mount arrangement)
MSSA02-MTL-D046, Rev. A	Winch foundation T-ATF (stern mount arrangement) (sheets 1-2)
MSSA02-MTL-D047, Rev. A	Recovery platform T-ATF (stern mount arrangement) (sheets 1-2)
MSSA02-MTL-3048, Rev. A	Electrical installation T-ATF (stern mount arrangement)
MSSA02-MTL-3049, Rev. 2	GLOMAR CHALLENGER electrical installation (sheets 1-2)
MSSA02-MTL-3050, Rev. A	Equipment installation arrangement T-ATF (stern mount arrangement)
MSSA02-MTL-3051, Rev. A	A-frame foundation T-ATF (stern mount arrangement)
MSSA02-MTL-3052, Rev. A	Heave compensator foundation T-ATF (stern mount arrangement)
MSSA02-MTL-3053, Rev. A	A-frame modification T-ATF (stern mount arrangement)
MSSA02-MTL-3054, Rev. A	Idler sheave foundation T-ATF (stern mount arrangement)
MSSA02-MTL-3055, Rev. A	Elevated walkway T-ATF (stern mount arrangement)
MSSA02-MTL-3056, Rev. A	Testing arrangements
MSSA02-STR-D001, Rev. 1	EM cable recovery platform
MSSA02-SYS-D001, Rev. A	MSS-82 installation, recovery and reinstallation system control drawing
MSSA04-SYS-D001, Rev. 0	MSS-83 GLOMAR CHALLENGER electrical installation
MSSA04-SYS-D002, Rev. 0	MSS-83 winch and idler sheave foundation details
MSSA04-SYS-D003, Rev. 1	MSS-83 GLOMAR CHALLENGER equipment installation arrangement (sheets 1-2)

MSSA04-SYS-D004, Rev. 0	MSS-83 IRR system arrangement and assembly (sheets 1-2)
MSSA04-SYS-D005, Rev. 0	MSS-83 BPP skid detail assembly
MSSA04-SYS-D006, Rev. C	MSS-83 recovery installation arrangements (sheets 1-2)
MSSA04-SYS-D007, Rev, 0	MSS-83 winch line splitter detail (sheets 1-2)
MSSA04-SYS-D008, Rev. B	MSS-83 R/V MELVILLE recovery sequence layout (sheets 1-2)
MSSA04-SYS-D009, Rev. 0	MSS-83 dummy (BPP) bottom processing package details assembly
MSSA04-SYS-D010, Rev. A	MSS-83 dummy (BPP) bottom processing package arrangement

Appendix E. Additional Studies and Reports of Interest to a Future MSS Program

Ballard, J.A. (1978). *Marine Earthquake Monitoring System.* Prepared for ARPA by NORDA Ocean Programs Office, NSTL, Mississippi.

Ballard, J.A., Mulcahy, C.C., Wallerstedt, R.L., and Kiser, E.L., (1984). *The Borehole Seismic Experiment in Hole 395A: Engineering and Installation.* In Hyndman, R.D., Salisbury, M.H., et al., Init. Repts. DSDP, 78B: Washington (U.S. Gov. Printing Office), 743-757.

Boyd, J.D. (1982). *Ocean Current Effects on Marine Seismic Systems and Deployments.* NORDA (Technical Note 132), NSTL, Mississippi.

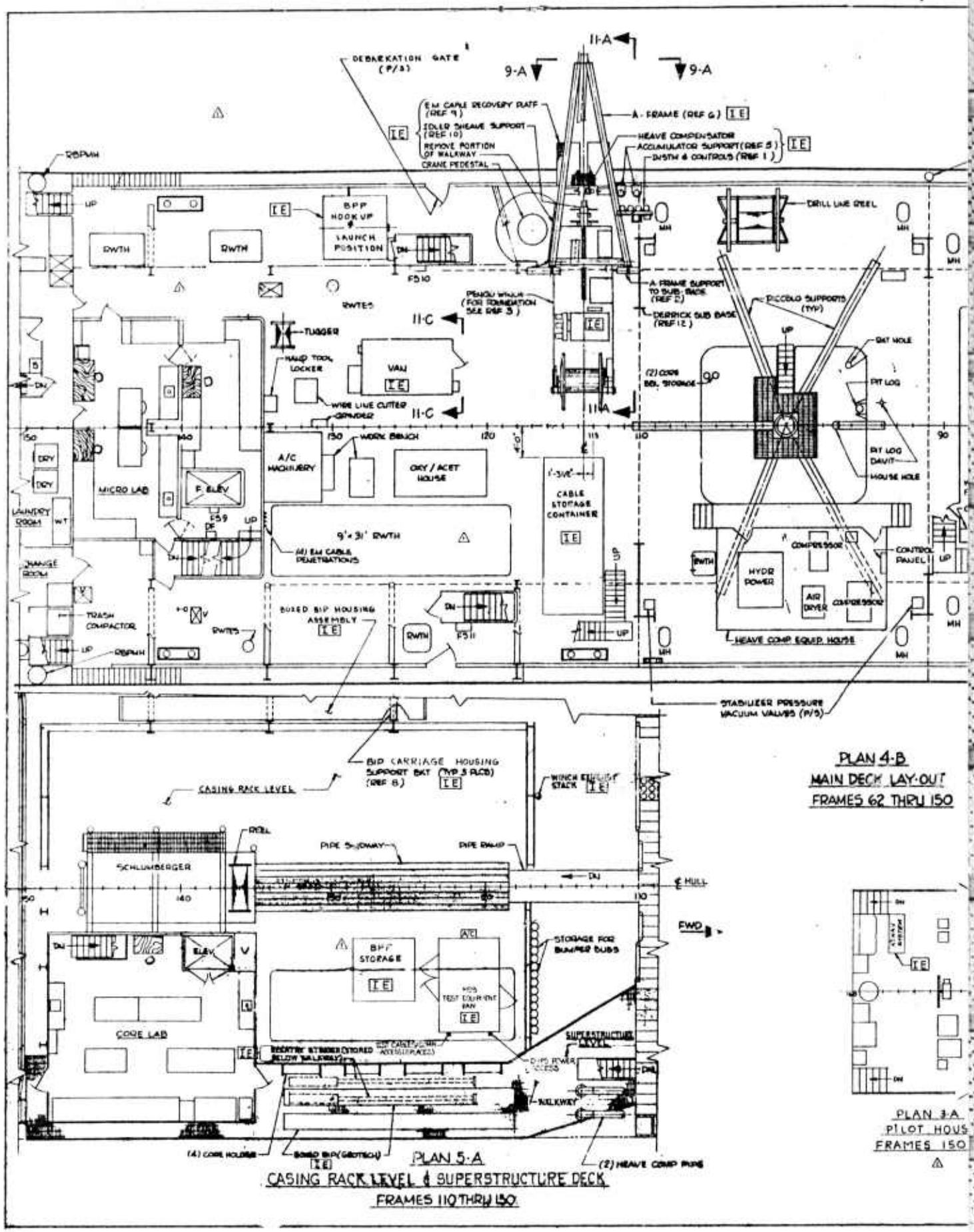
Foss, G.N. and Wallerstedt, R.L. (1984). *Operational Aspects of Borehole Deployment of a Marine Seismic System in Deep Water.* 16th Annual Ocean Technology Conference (OTC 4757), Houston, Texas. May 7–9.

Naval Ocean Research and Development Activity (1981). *Plan for Development of a Marine Seismic System for Detection and Discrimination of Earthquake and Underground Nuclear Explosions.* Prepared for ARPA/NMRO by NORDA, NSTL, Mississippi.

Scripps Institution of Oceanography (1982). *International Phase of Ocean Drilling, Leg 88 Scientific Prospectus, Downhole Seismometer Experiment, Kurile/Kamchatka Region.* Prepared for the National Science Foundation (for Initial Reports of the Deep Sea Drilling Project, Volume LXXXVIII (in preparation) by Scripps Institution of Oceanography, La Jolla, California.

Teledyne Geotech (1984). *Marine Seismic System Sensor Design and Development,* Technical Report 83–8, Final Report. Prepared for NORDA by Teledyne Geotech. Garland, Texas.

Wallerstedt, R.L. (1984). *Marine Seismic System Advanced Operations Evaluation.* Revision O, Report No. MSSA04-SYS-R003. Prepared for NORDA by Global Marine Development, Inc., Irvine, California.



PLAN 4-B
MAIN DECK LAY-OUT
FRAMES 62 THRU 150

PLAN 3-A
PILOT HOUSE
FRAMES 150

PLAN 5-A
CASING RACK LEVEL & SUPERSTRUCTURE DECK
FRAMES 110 THRU 150

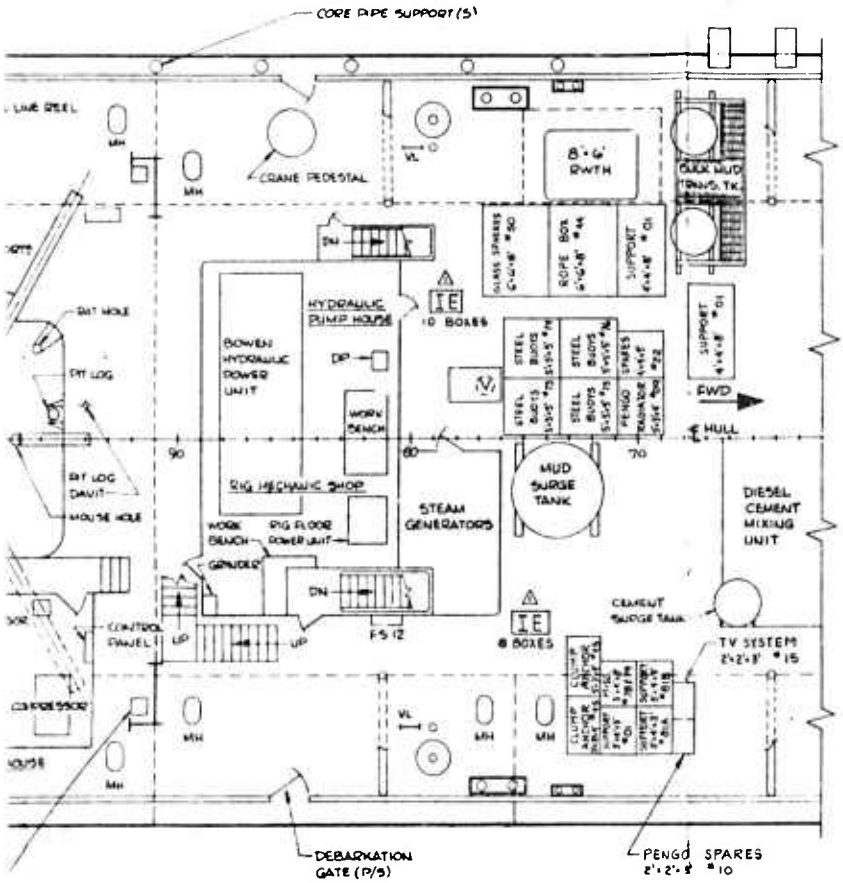
Reproduced from best available copy.

LIST OF MATERIALS

OWNER FURN.	ITEM	QTY	DESCRIPTION	MATERIAL OR DWG NO.

GENERAL NOTE:

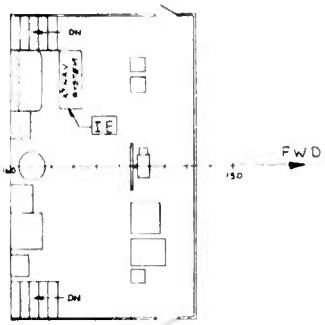
1. ALL EQUIPMENT LABELLED IE (INSTALLED EQUIPMENT) IS PART OF THIS INSTALLATION.



PLAN 4-B
IN DECK LAY-OUT
AMES 62 THRU 150

REFERENCE DRAWINGS:

1) GMDI DWG: E-001-A018 MARINE SEISMIC SYSTEM (MSS) HEAVE COMPENSATOR CONTROL BOARD, DETAILS & ASSEMBLY
2) GMDI DWG: E-001-A023 MARINE SEISMIC SYSTEM (MSS) A-FRAME SUPPORT TO SUB BASE DETAILS & ASSEMBLY
3) GMDI DWG: E-001-A025 MARINE SEISMIC SYSTEM (MSS) WINCH FOUNDATION DETAILS & ARRANGEMENT
4) GMDI DWG: E-001-A029 MARINE SEISMIC SYSTEM (MSS) HEAVE COMPENSATOR BRACKET MODIFICATION & DETAILS
5) GMDI DWG E-001-A030 MARINE SEISMIC SYSTEM (MSS) ACCUMULATOR SUPPORTS DETAILS & ASSEMBLY
6) GMDI DWG MSSA02-MTL-D019 MARINE SEISMIC SYSTEM (MSS-82) A-FRAME DETAILS & ASSEMBLY
7) GMDI DWG: MSSA02-MTL-D031 MARINE SEISMIC SYSTEM (MSS-82) IRR LIIIE STORAGE CONTAINER SECURING DETAILS
8) GMDI DWG MSSA02-MTL-D030 MARINE SEISMIC SYSTEM (MSS-82) BIP HOUSING SUPPORT BRACKET LAYOUT
9) GMDI DWG MSSA02-STR-D001 MARINE SEISMIC SYSTEM (MSS-82) EM CABLE RECOVERY PLATFORM
10) GMDI DWG: MSSA02-MTL-D010 MARINE SEISMIC SYSTEM (MSS-82) IDLER SHEAVE SUPPORT DETAIL ASSEMBLY
11) LEVINGSTON SHIPBUILDING CO. DWG: T-54-54-S15 CASING RACK LOCATION & DETAILS
12) LEVINGSTON SHIPBUILDING CO. DWG: T-54-54-S16 DERRICK SUB BASE DETAILS



PLAN 3A
PILOT HOUSE
FRAMES 150 THRU 160

NO	DATE	BY	DESCRIPTION	JOB AUTH	APPD
1	12/6/82	F.H.	FOLLOWING REVISIONS & ADDITIONS MADE PER DCN-001, PLAN 3A ADDED, CROWN BUOYS REMOVED ZONE G-D, BPP MOVED ZONE 5-A, ADDED 18 BOXES ZONE 2C.	01/5510	
ORIGINAL			DESIGN RELEASE	01/5510	

GLOBAL MARINE DEVELOPMENT INC.
Newport Beach, Calif

MARINE SEISMIC SYSTEM (MSS-83)
GLOMAR CHALLENGER
EQUIPMENT INSTALLATION ARRANGEMENT

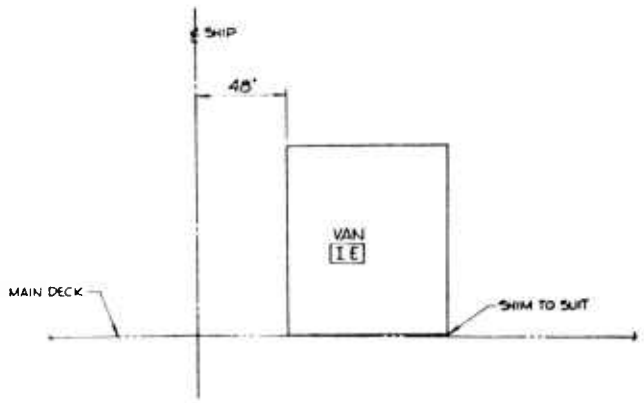
	APPROVED	CLASSIFIED OR REVIEWED	SEC. NO.	LETTER DATE	SEC. NO.
AAA					
U.S.C.G.					

DRN R. JONES
CHK F.H. 12-6-82
APPD
MFG ENG

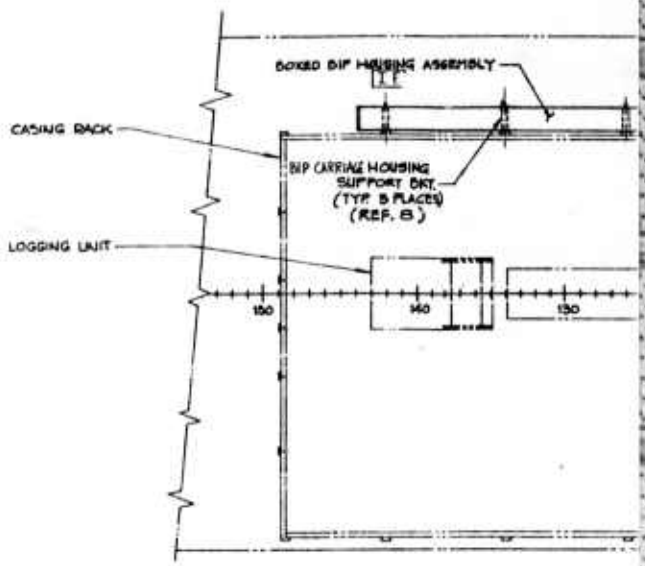
SCALE 3/16"=1'-0" & NOTED
TOLERANCE UNLESS OTHERWISE NOTED: FRACTION ± 1/16" ANGULAR ± 1° DECIMALS ± .030 MILLIMETER ± .800

SIZE E | DWG NO MSSA01-SYS-0003 | REV 1 | SHT 1

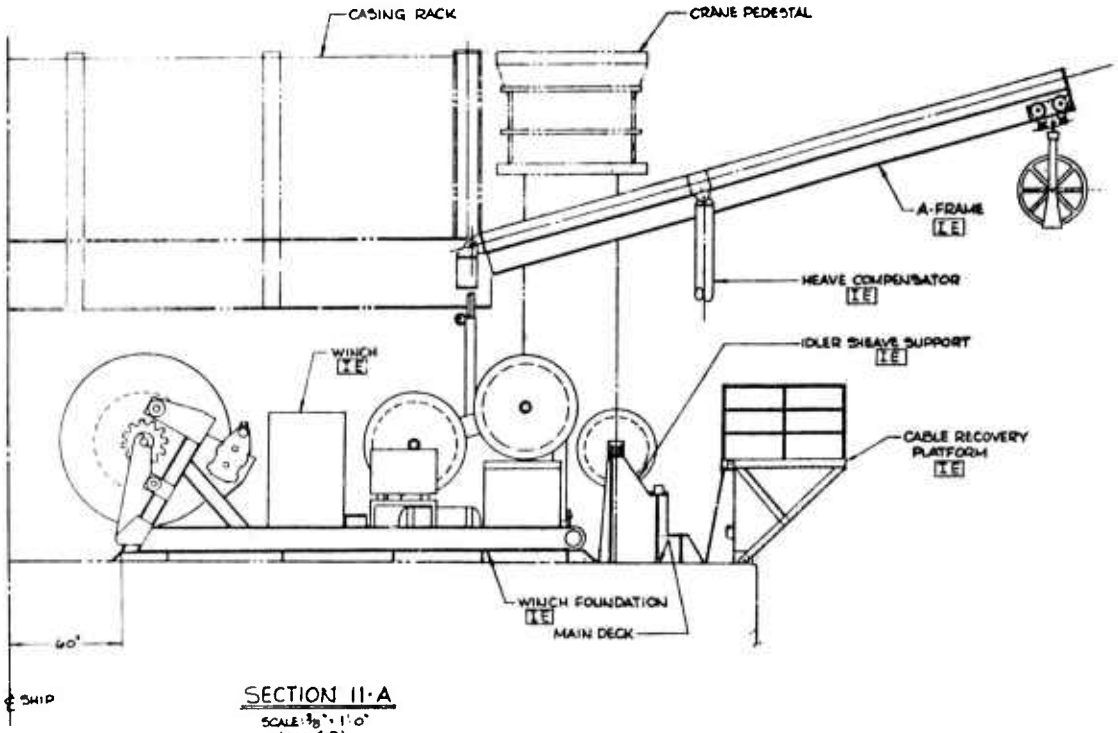
Reproduced from best available copy.



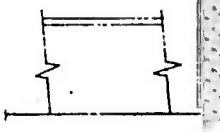
ELEVATION 11-C
SCALE: 3/8" = 1'-0"
(SEE 4-B)
(VIEW LOOKING AFT)



PLAN 9-C
RE-ENTRY TOOL & MISC EQPT ST
SCALE: 1/8" = 1'-0"



SECTION 11-A
SCALE: 3/8" = 1'-0"
(SEE 4-B)
(VIEW LOOKING AFT)

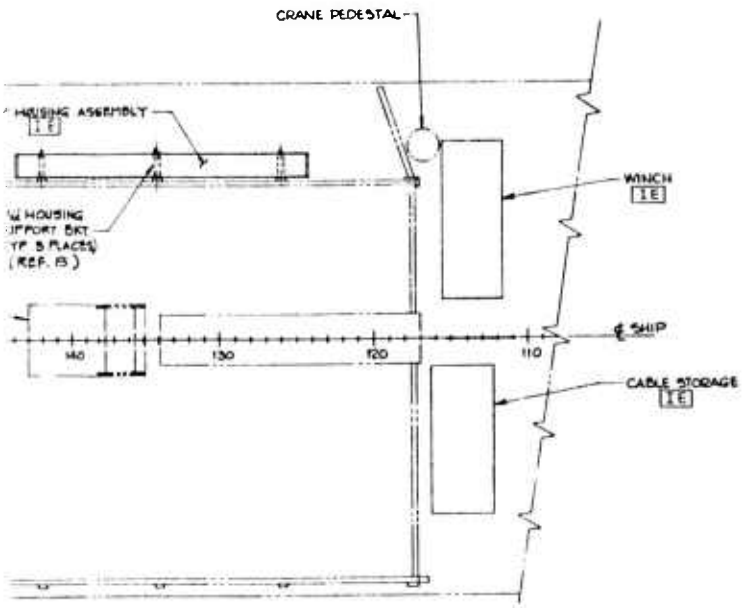


1092

Reproduced from best available copy.

LIST OF MATERIALS

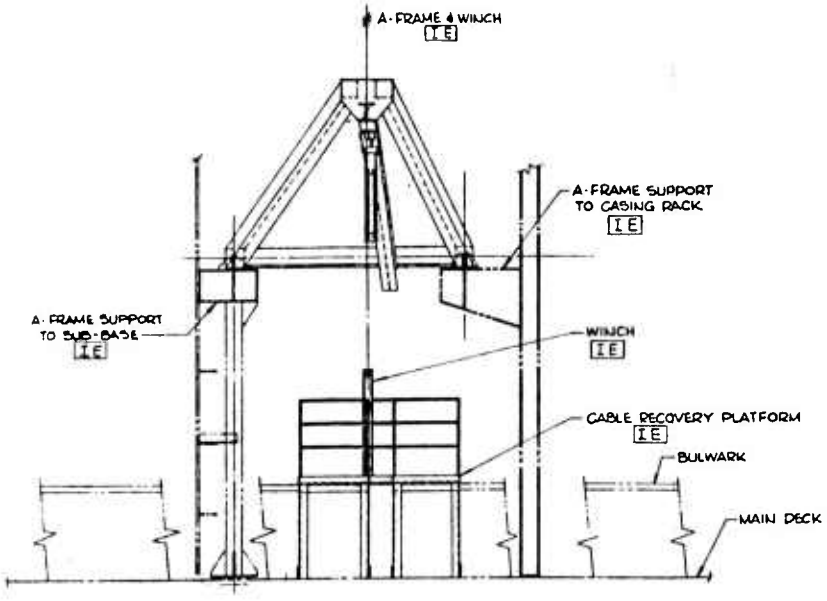
OWNER FURN.	ITEM	QTY	DESCRIPTION	MATERIAL OR DWG. NO.



PLAN 9-C

E-ENTRY TOOL & MISC EQPT STORAGE

SCALE ⅛"=1'-0"



ELEVATION 9-A

SCALE: ³/₁₆"=1'-0"
(SEE 4-B)
(VIEW LOOKING INBOARD)

SEE SHEET 1 FOR NOTES, REFERENCES AND ALTERATIONS

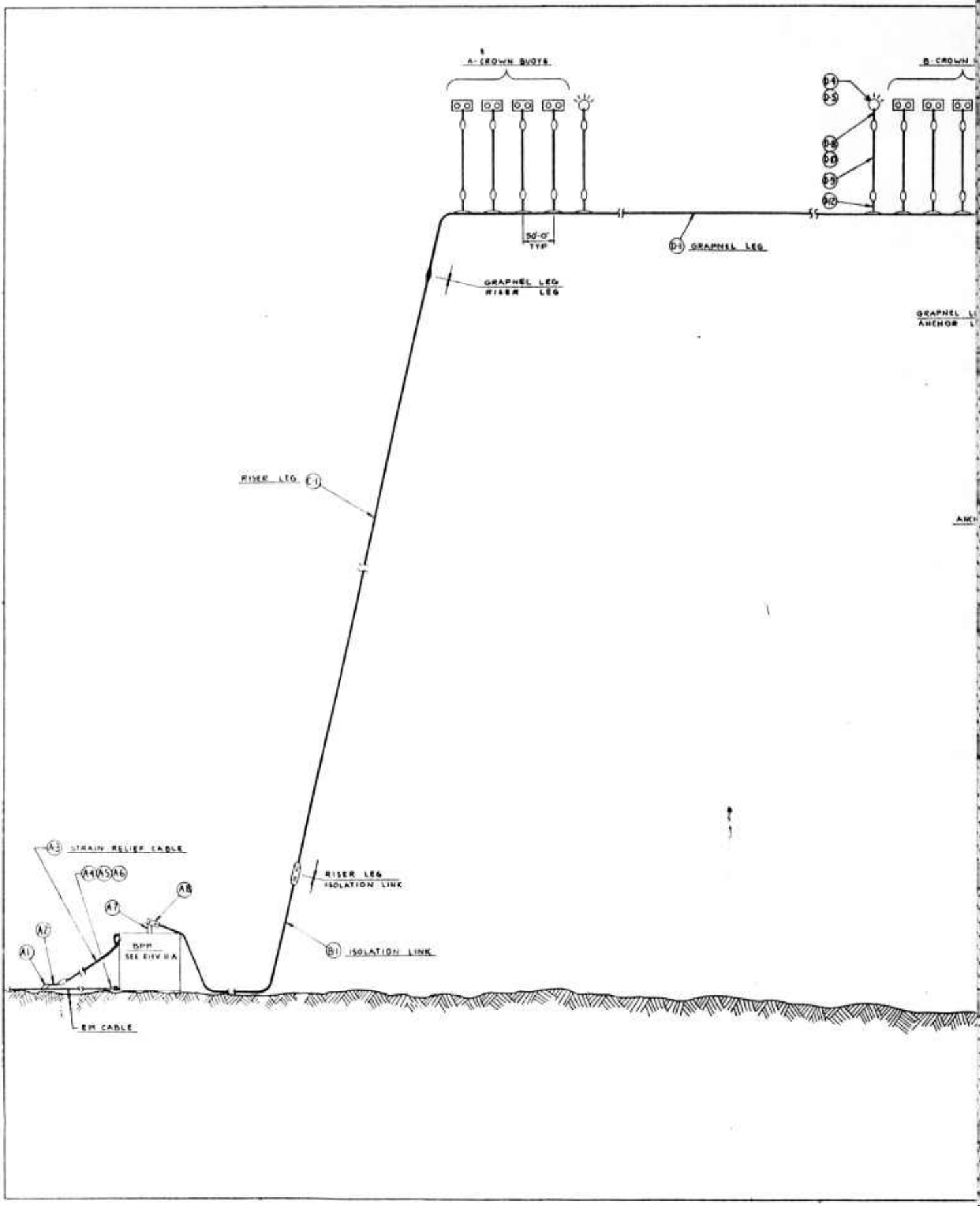
GLOBAL MARINE DEVELOPMENT INC.

MARINE SEISMIC SYSTEM (MSS-83)
GLOMAR CHALLENGER
EQUIPMENT INSTALLATION ARRANGEMENT

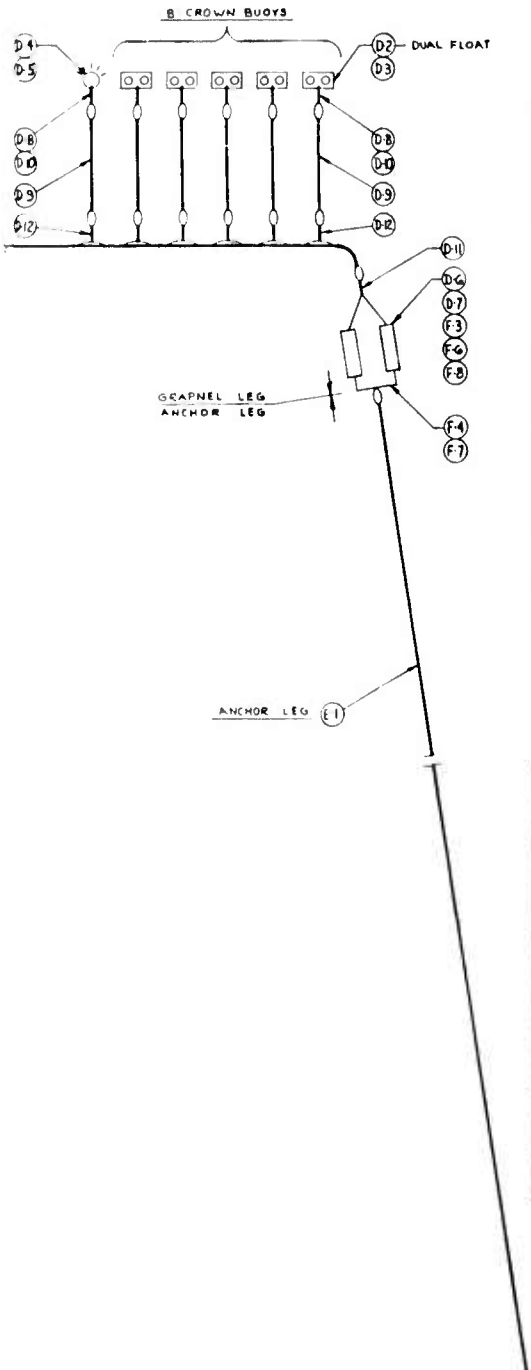
SCALE	SIZE	DWG NO	REV	SHT	ALT
NOTED	E	MSSA04-SYS-0003	41	2 of 2	1

292

Reproduced from best available copy.



Reproduced from best available copy



LIST OF MATERIALS

OWNER FURN.	ITEM	QTY	DESCRIPTION	MATERIAL OR SPEC NO.
	D-1 (CONT)		THE FIRST AT TWO HUNDRED (200) FEET FROM THE EN AND THE REMAINING SIX (6) AT FIFTY (50) FOOT INCREMENTS FROM THE FIRST. STARTING FROM THE LAST (1000) FOOT MARK ON ITEM C-1, MARK THE ROPE IN ONE THOUSAND (1000) FOOT INCREMENTS.	
	D-2	18	BENTHOS DEEP SEA OLP 65 SPHERE, MODEL 204D-17V.	
	D-3	18	BENTHOS RIBBED HARDHAT, MODEL 204HR-17.	
	D-4	2	BENTHOS GLOW FLASH WITH PRESSURE SWITCH OPTION MODEL 2145-PS.	
	D-5	2	BENTHOS STANDARD HARDHAT MODEL 204H-10, CUT AWAY TO PROVIDE CONNECTION POINT FOR ITEM D-4.	
	D-6	2	ATNAV TRANSPONDER MINIMUM DEPTH RATING 10,000 FEET.	
	D-7	1	DUAL RELEASE FRAMEWORK FOR ATNAV TRANSPONDER.	
	D-8	11	7/16"-14 UNC-2A x 2" SHOULDER EYE BOLTS, 304 SS.	
	D-9	11	SEVEN AND ONE HALF (7 1/2) FEET OF 1/2" SAMSON POWER BRAID WITH A STANDARD METAL ROPE THIMBLE AT EACH END.	
	D-10	11	5/8" BOLT TYPE ANCHOR SHACKLE, CROSBY G-2130.	
	D-11	1	3/4" BOLT TYPE ANCHOR SHACKLE, CROSBY G-2130.	
	D-12	11	5/8" SNAP SHACKLE 17-4 SS, MERRIMAN.	
	E-1	1	EIGHTEEN THOUSAND (18,000) FEET OF 7/8" SAMSON POWER BRAID (NYLON COVER/MULTI-FILAMENT POLYPROPYLENE CORE 8-IN-1 BRAIDED ROPE) WITH A STANDARD METAL ROPE THIMBLE AT BOTH ENDS. MARK THE LINE IN ONE THOUSAND (1000) FOOT INCREMENTS.	
	E-2	1	STEEL CLUMP ANCHOR WEIGHING (2000) LBS. (IN WATER WEIGHT).	
	E-3	1	3/4" BOLT TYPE ANCHOR SHACKLE, CROSBY G-2130.	
	F-3	2	RELEASE/TRANSPONDER MODEL 723A.	
	F-4	1	DUAL RELEASE MECHANISM FOR MODEL 723A RELEASE/TRANSPONDER.	
	F-5	2	LITHIUM BATTERY SET FOR MODEL 723A RELEASE/TRANSPONDER.	
	F-7	1	RELEASE LINK FOR MODEL 723A RELEASE/TRANSPONDER	
	F-8	2	HOOK ANODES FOR MODEL 723A RELEASE/TRANSPONDER	

LIST OF MATERIALS

OWNER FURN.	ITEM	QTY	DESCRIPTION	MATERIAL OR SPEC NO.
	A-1	4	PLP OR KELLEMS GRIP IN-LINE CONNECTION, 5/8" WIRE ROPE TO EM CABLE.	
	A-2	1	5/8" BOLT TYPE ANCHOR SHACKLE, CROSBY G-2130	
	A-3	1	TWO HUNDRED (200) FEET OF 5/8"-6x37 MONITOR IWRC WIRE ROPE WITH STANDARD WIRE ROPE THIMBLE BOTH ENDS.	
	A-4	1	PLP TERMINATION FOR EM CABLE. (SPECIFIED BY GEOTECH)	
	A-5	1	D.G. O'BRIEN CONNECTOR FOR EM CABLE. (SPECIFIED BY GEOTECH)	
	A-6	1	FULL PRESSURE DUMMY PLUG FOR ITEM A-5. (SPECIFIED BY GEOTECH).	
	A-7	1	MILLER SWIVEL MODEL GG TYPE 4 UW (15 TON) FOR SUBSEA APPLICATION.	
	A-8	1	CUSTOM TWO-PLATE CONNECTION BETWEEN ITEM A-7 AND ITEM B-1.	
	B-1	1	ONE THOUSAND FIVE HUNDRED (1500) FEET OF 1 1/8"-6x37 MONITOR IWRC WIRE ROPE, BOTH ENDS TERMINATED WITH HEAVY WIRE ROPE THIMBLES.	
	B-2	1	CUSTOM TWO-PLATE CONNECTION BETWEEN ITEM B-1 AND ITEM C-1.	
	C-1	1	TWENTY ONE THOUSAND FIVE HUNDRED (21,500) FEET OF 1 3/4" SAMSON POWER BRAID (NYLON COVER/MULTI-FILAMENT POLYPROPYLENE CORE 8-IN-1 BRAIDED ROPE) SPECIALLY BUILT WITH A SPECIFIC GRAVITY OF 0.99, WITH A STANDARD METAL ROPE THIMBLE AT ONE END AND A FULL STRENGTH TAPER SPLICE TO ITEM D-1 AT THE OTHER END. MARK THE LINE STARTING AT THE THIMBLE IN ONE THOUSAND (1000) FOOT INCREMENTS.	
	D-1	1	TEN THOUSAND (10,000) FEET OF 7/8" SAMSON POWER BRAID (NYLON COVER/MULTI-FILAMENT POLYPROPYLENE CORE 8-IN-1 BRAIDED ROPE) SPECIALLY BUILT WITH A SPECIFIC GRAVITY OF 0.99, WITH A FULL STRENGTH TAPER SPLICE TO ITEM C-1 AT ONE END AND A STANDARD METAL ROPE THIMBLE AT THE OTHER END. STARTING FROM THE SPLICE TO ITEM C-1, ADD SIX (6) STANDARD RUNNING EYE THIMBLES FIFTY (50) FEET APART. STARTING FROM THE FREE END, ADD SEVEN (7) STANDARD RUNNING EYE THIMBLES, (CONT.)	

NO.	DATE	BY	DESIGN RELEASE	ON/ESIO
0	12-1-82	JB		

GLOBAL MARINE DEVELOPMENT INC.
Newport Beach, Calif.

MARINE SEISMIC SYSTEM (MSS-83)
IRR SYSTEM
ARRANGEMENT & ASSEMBLY

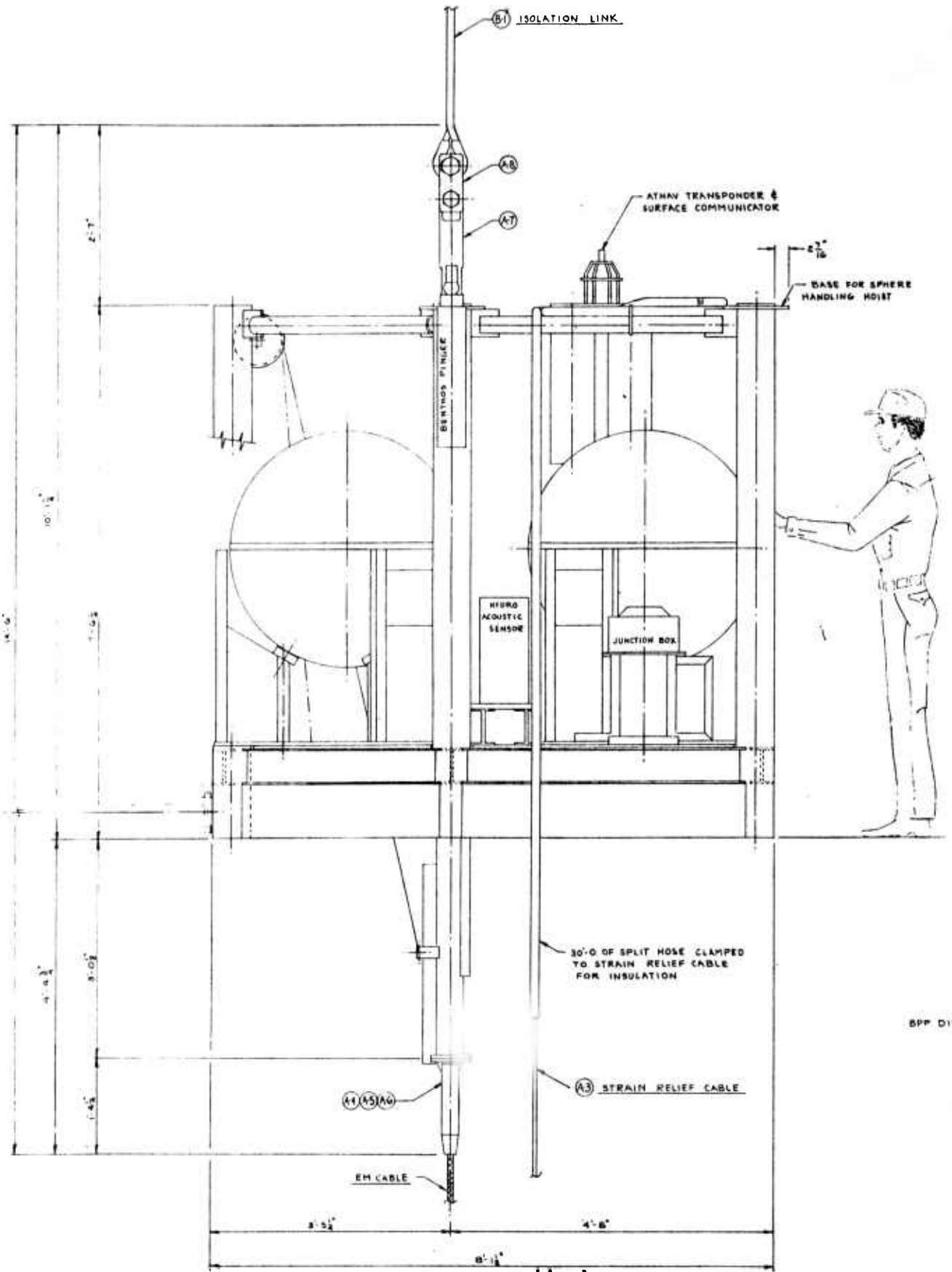
DRAWN	J.B.	12-1-82
ENGR.	W.B.	12-1-82
CHK.	P.N.	12-1-82
APPD.		
MFG.		

SCALE: NONE

SIZE: E | DWG. NO.: MSSA04-SYS-D004 | REV: 0 | SHT: 41 | 1/2

202

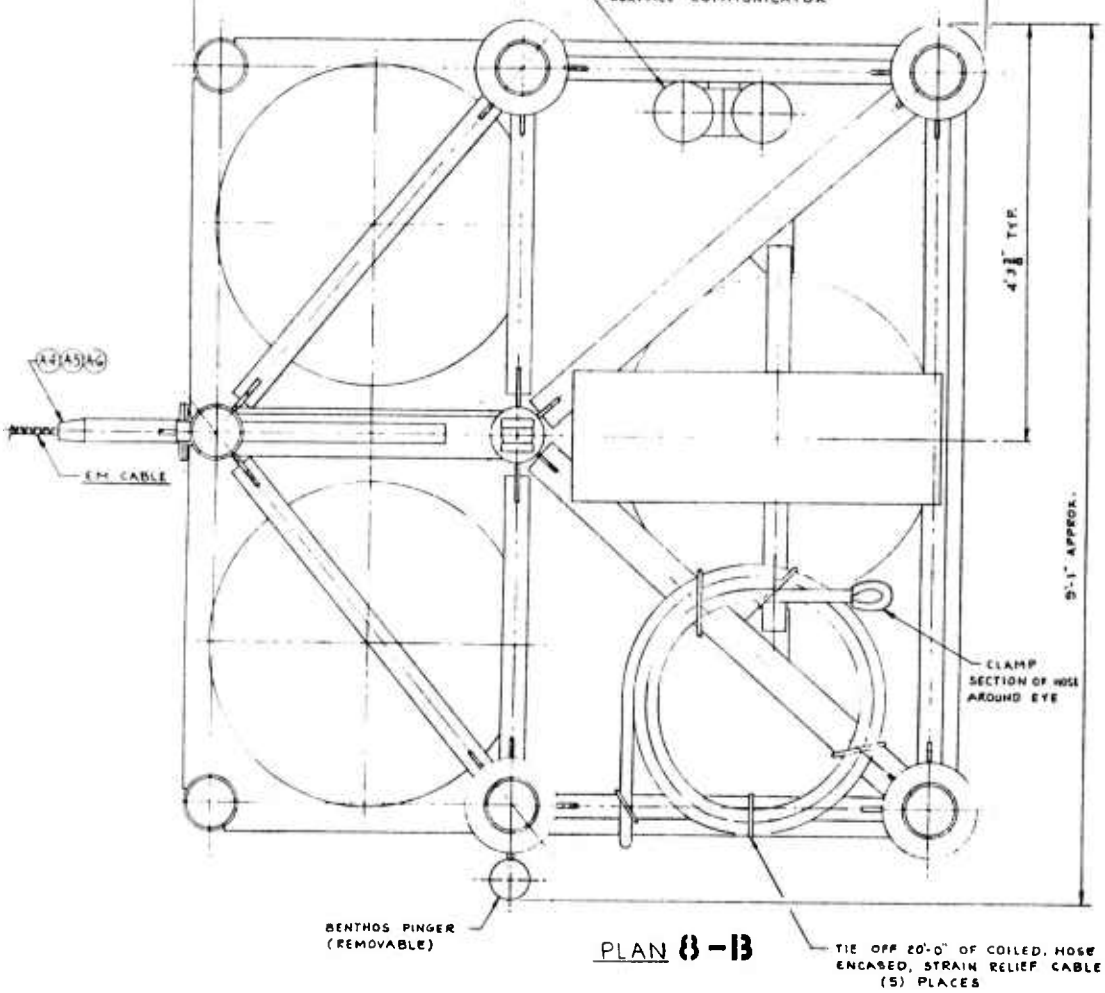
Reproduced from best available copy.



ELEVATION II-A

Reproduced from best available copy.

LIST OF MATERIALS				
OWNER'S PLANS	ITEM	QTY	DESCRIPTION	MATERIAL OR SPEC. NO.



PLAN B-B

BPP DIMS 8'-1 1/4" OAW x 8'-1 3/8" OAL

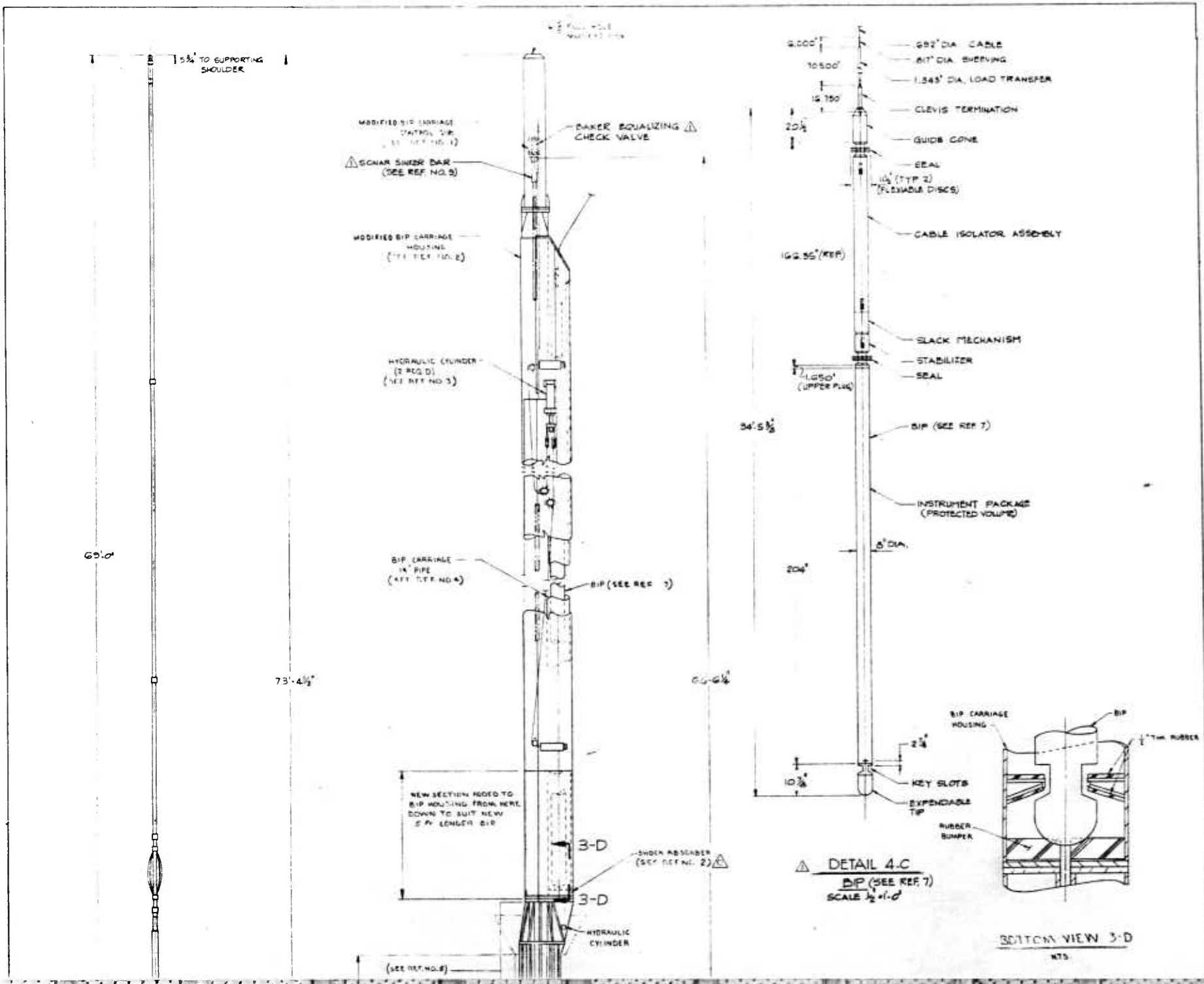
8'-3 11/16" OAW x 9'-1" OAL AT TOP

GLOBAL MARINE DEVELOPMENT INC.
Newport Beach, Calif

MARINE SEISMIC SYSTEM (MSS-83)
IRR SYSTEM
ARRANGEMENT & ASSEMBLY

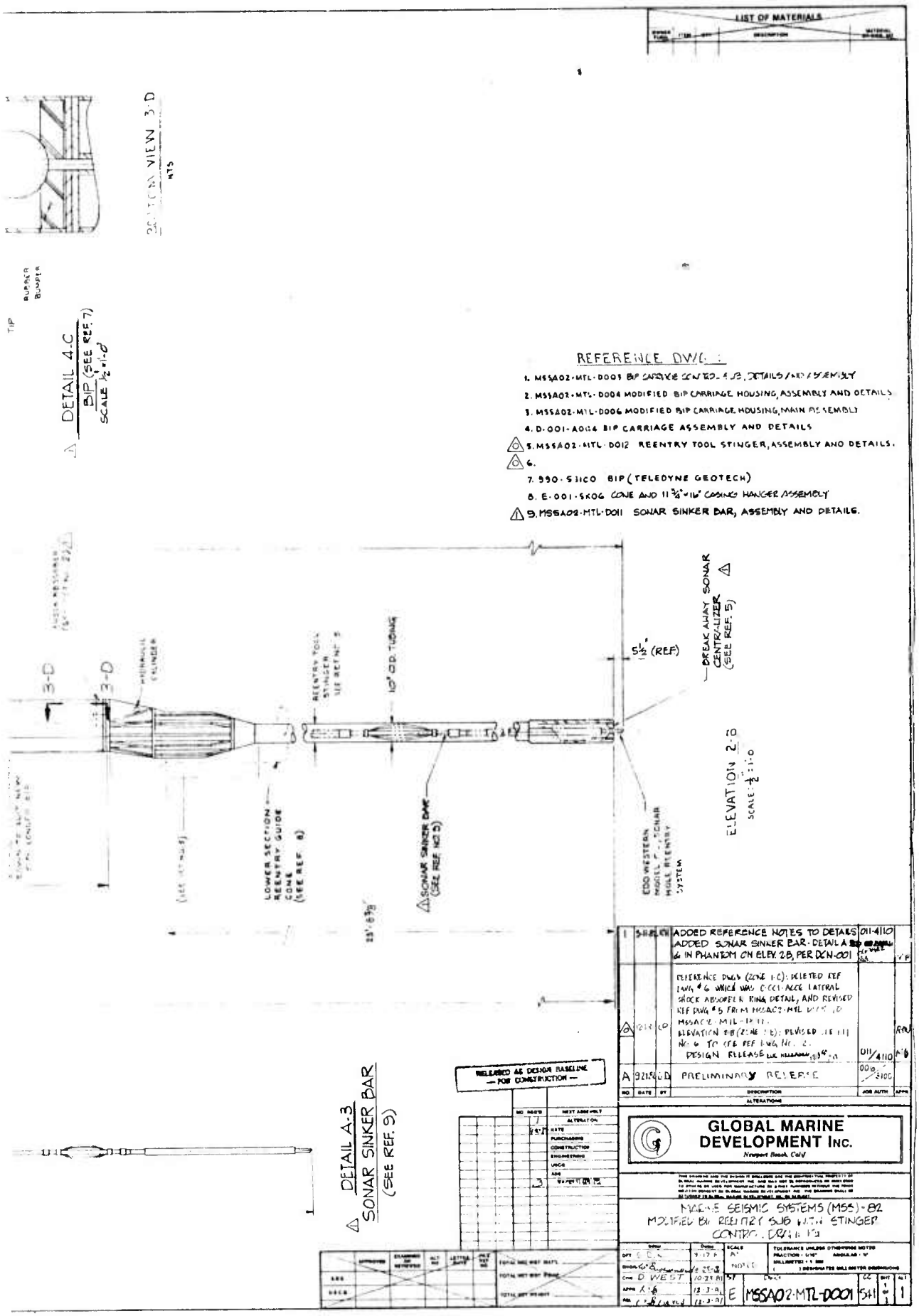
DFT R. TOPNESS	12-8-82	SCALE 1 1/2" = 1'-0"	TOLERANCE UNLESS OTHERWISE NOTED: FRACTION ± 1/16" ANGULAR ± 0° DECIMALS ± .1 ± .02 DIMENSIONS ARE MILLIMETER DIMENSIONS		
DES. W.B.	12-8-82				
CHK. F.M.	12-8-82				
APPD. W.B. for F.M.	12-9-82	SIZE E	DWG. NO. MSSA04-SYS-D004	REV 41	SHT 2/2
APPD.					ALT 0

Reproduced from best available copy.

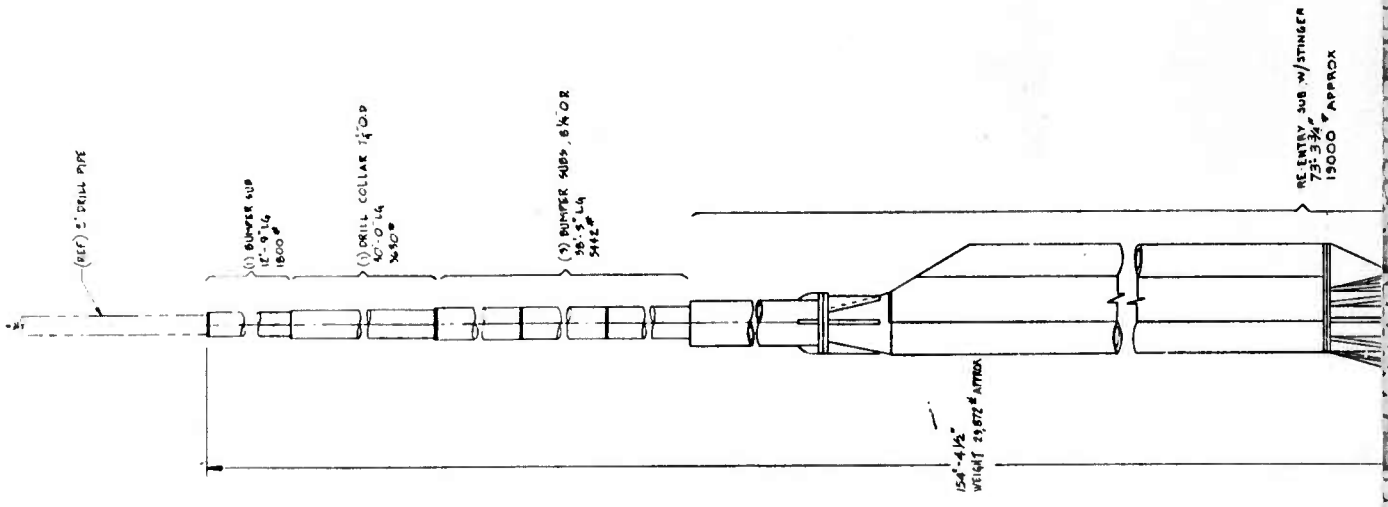


192

Reproduced from best available copy.



Reproduced from best available copy.

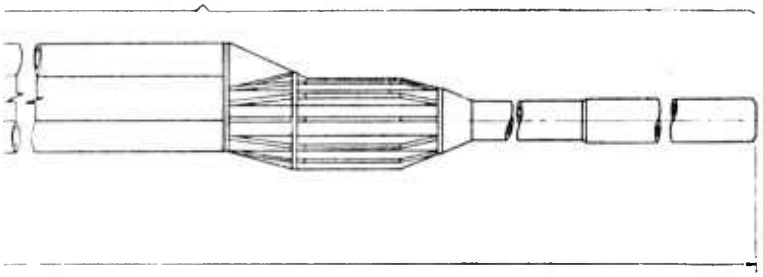


Reproduced from best available copy.

LIST OF MATERIALS

OWNER FURN.	ITEM	QTY	DESCRIPTION	MATERIAL OR DWG. NO.

RE ENTRY SUB W/STINGER
73-3¾"
19000 ♦ APPROX



ELEVATION 2-C
N.T.S

REFERENCE DRAWINGS:

1 E-001-A003 BIP CARRIAGE [illegible] SUB DETAILS ASS'Y.

2 E-001-A012 BIP CARRIAGE HOUSING ASSY & DETAILS.

3 M55A02-MTL-D004 MODIFIED BIP CARRIAGE HOUSING ASS'Y & DETAILS.

⚠4 M55A02-MTL-D012 REENTRY TOOL STINGER ASSY & DETAILS

NO.	DATE	BY	DESCRIPTION	JOB AUTH.	APPR
			ADDED "CONTROL DRAWING TO TITLE (ZONE 1-A). REFERENCE DWG #4 (ZONE 1-B) REVISED DWG # FROM M55A02-MTL-D005 TO M55A02-MTL-D012.		
0	12/18/81	CP	DESIGN RELEASE EOC RELEASED 1-19-82 EO	011/4110	
A	10/30/81	CD	PRELIMINARY RELEASE	006/3100	

RELEASED AS DESIGN BASELINE — FOR CONSTRUCTION —

GLOBAL MARINE DEVELOPMENT INC.
Newport Beach, Calif

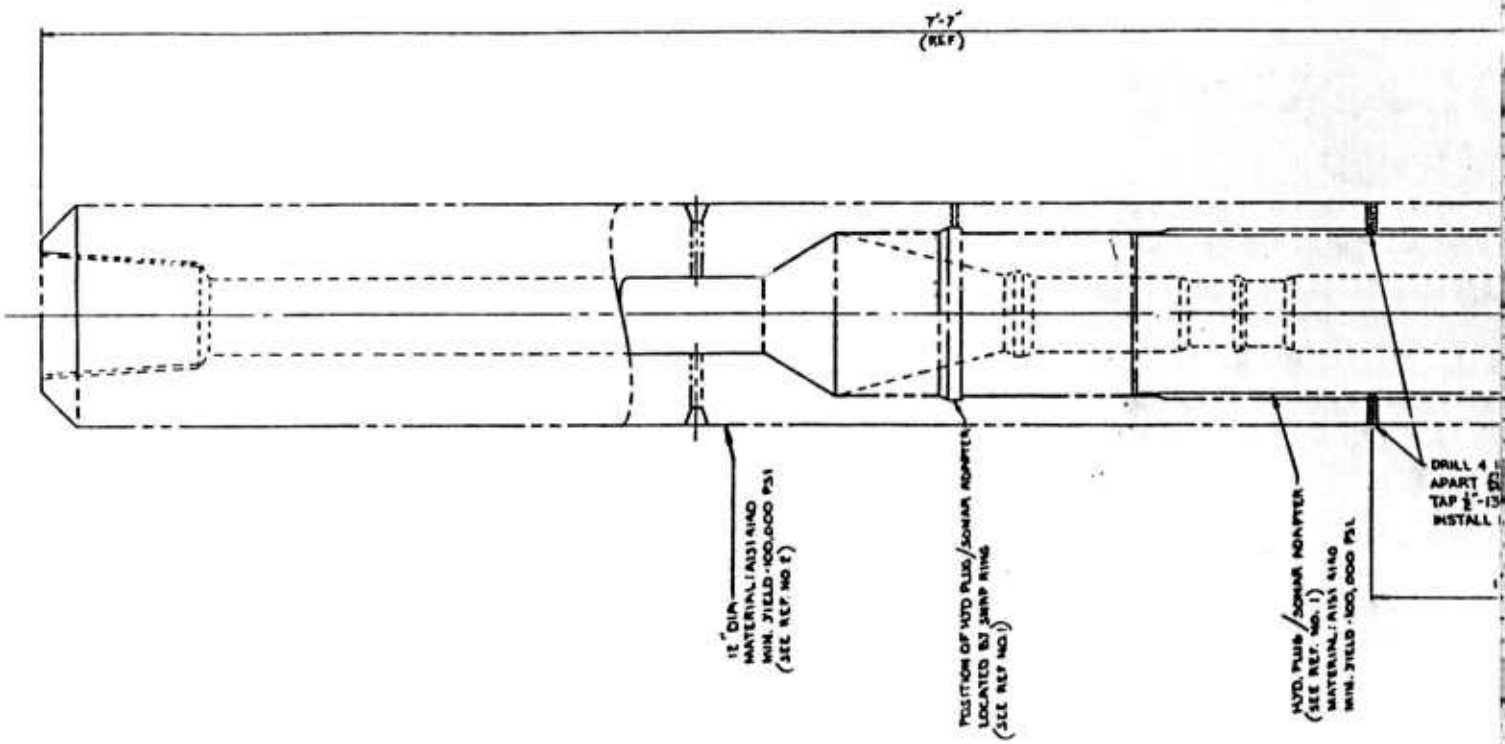
MARINE SEISMIC SYSTEM (MSS)-82
MODIFIED REENTRY
⚠ ASSEMBLY CONTROL DRAWING

DRAWN	DATE	SCALE	TOLERANCE UNLESS OTHERWISE NOTED
G. Dimmick	5-11-81	NONE	FRACTION ± 1/16" DECIMALS ± .X" ANGULAR ± 1°
CHK'D			
D. WEST	10-29-81		
APPD.			
MFG.			

SIZE	CODE	DWG NO.	REV	SHT	ALT
E	54841	M55A02-MTL-D002			

292

Reproduced from best available copy.



DETAIL 4-B

1 of 2

Reproduced from best available copy.

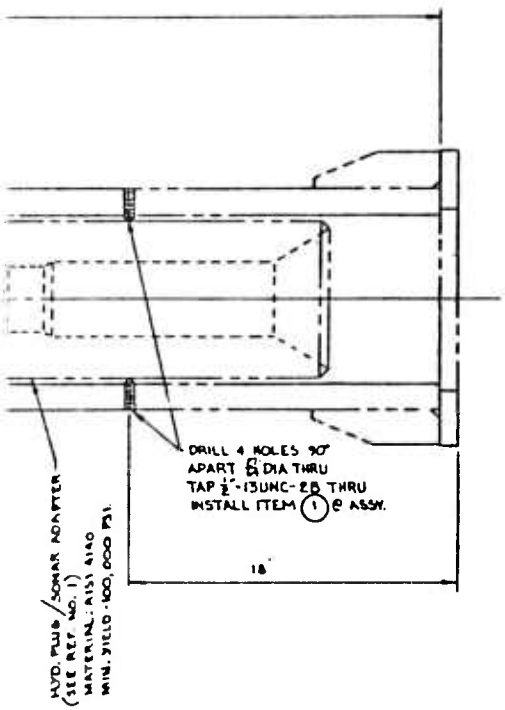
	1	4	½"-13 UNC-2A × 1¼" LG SET SCREW, ALLEN HEAD, SELF LOCKING	B.S.T.

GENERAL NOTES: (UNLESS OTHERWISE NOTED)

1. THE PURPOSE OF THIS DWG IS TO GIVE DETAILS FOR SECURING HYDR PLUG SONAR ADAPTER IN POSITION SEE REF. 2
2. THIS DWG IS MODIFIED AND WAS DEVELOPED FROM REF #2, ALT #1. ALL OTHER DIMENSIONS ARE SHOWN ON THAT DRAWING.
3. ONE ASSEMBLY TO BE REQUIRED AS SHOWN.

REFERENCE DWGS:

1. M5SA02-MTL-D008 — HYDRAULIC PLUG/SONAR ADAPTER MODIFICATION
2. E-001-A003 — (M5S) BIP CARRIAGE CONTROL SUB DETAILS AND ASSEMBLY



A	9-17-81	GD	PRELIMINARY RELEASE	004/5100
NO.	DATE	BY	DESCRIPTION	JOB NO. APPR.

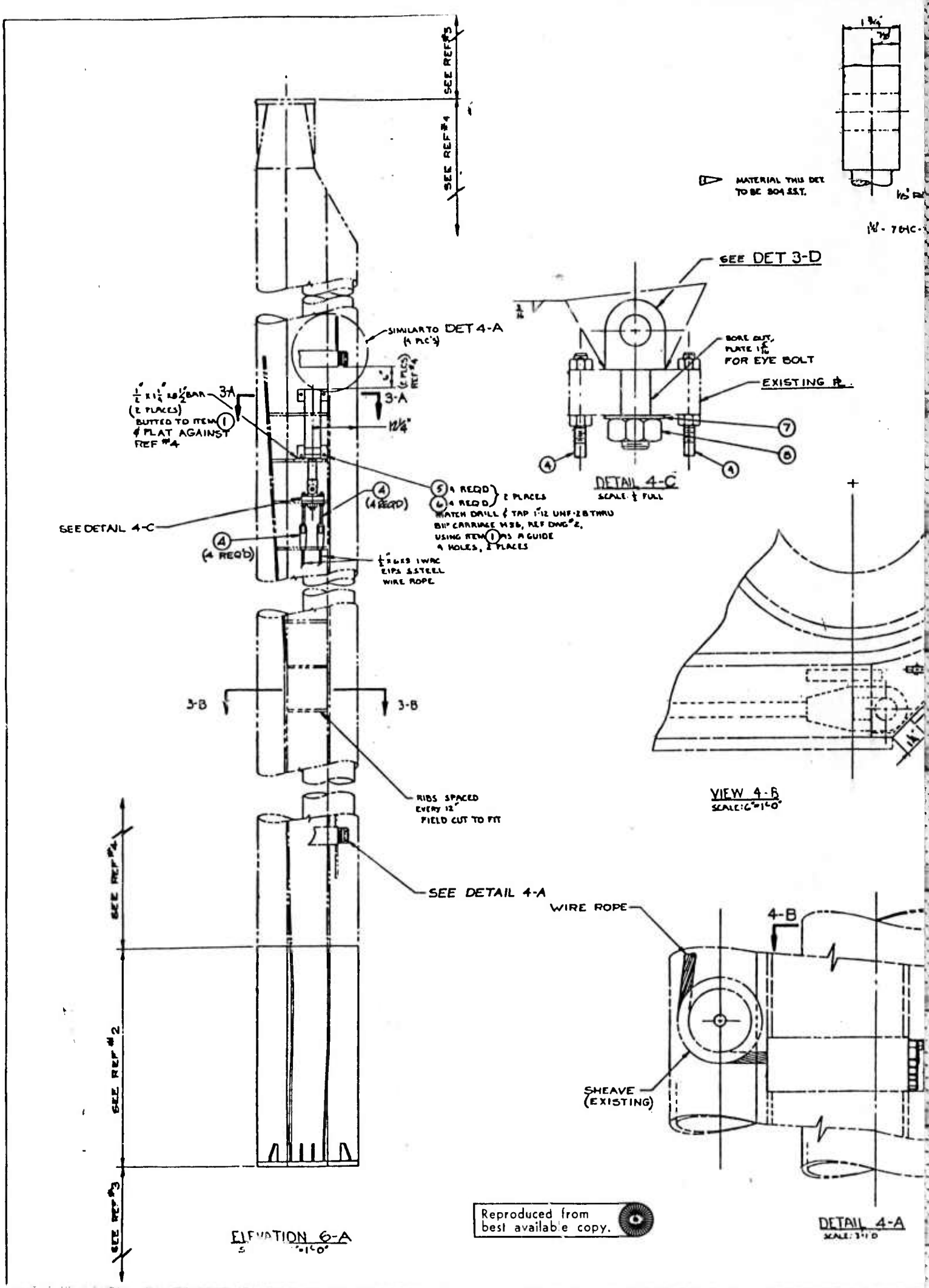
M5SA02 MTL-D001

GLOBAL MARINE DEVELOPMENT INC.
Newport Beach, Calif

MARINE SEISMIC SYSTEMS (M5S)-02
BIP CARRIAGE CONTROL SUB
DETAIL & ASSEMBLY [2]

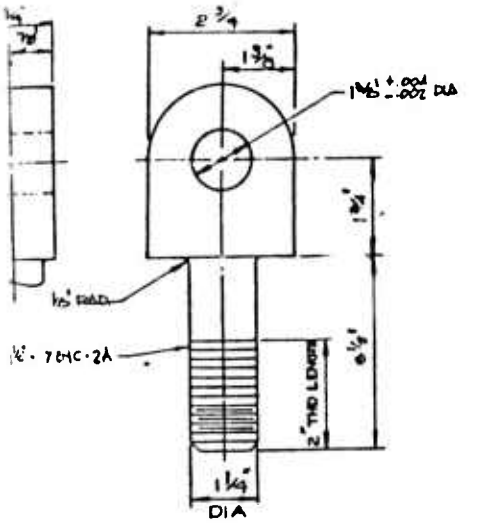
DES. & DRAWN	9-17-81	SCALE 3"/1'-0" & AS NOTED	TOLERANCES UNLESS OTHERWISE NOTED: FRACTIONS ± 1/64 ANGULAR ± 0° DECIMALS ± .01				
CHK'D							
APPD	D. WEST	10-23-81	SIZE E	CODE IDENT NO.	DWG NO. M5SA02-MTL-D003	REV. 541	SHT. 1 OF 2 A

Reproduced from best available copy.

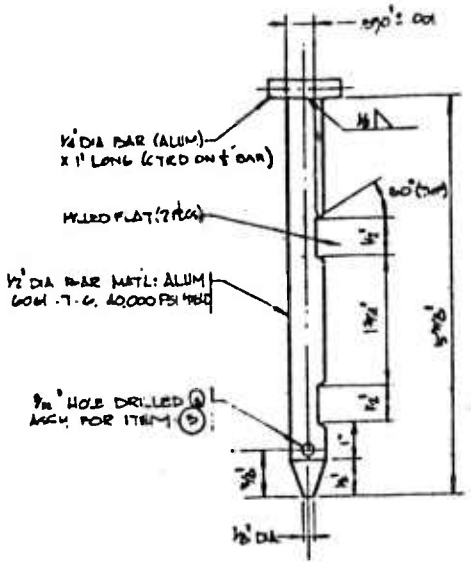


Reproduced from best available copy.

(1)

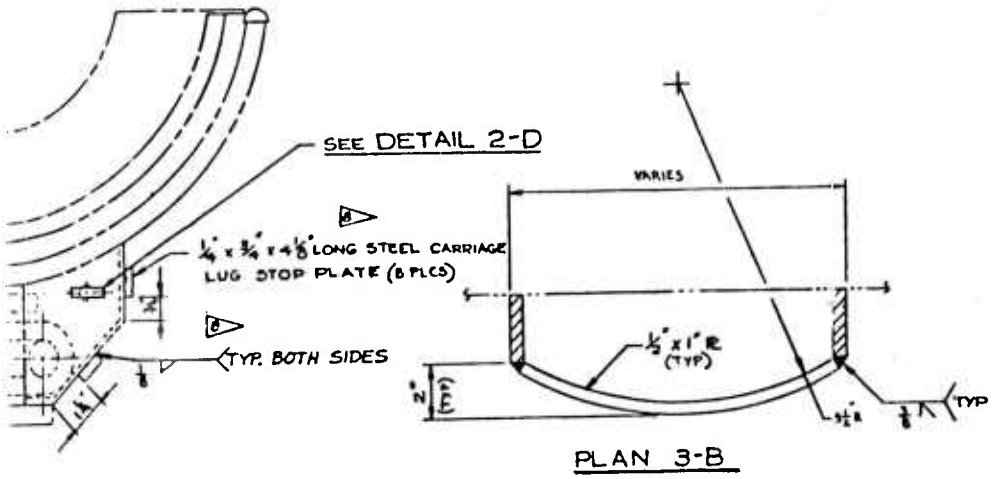


DETAIL 3-D
EYE BOLT (2 REQ'D)



DETAIL 2-D
SHEAR PIN
(16) REQ'D. INCLUDING SPARES
SCALE: FULL SIZE

ITEM NO.	SPEC	QTY	DESCRIPTION	REMARKS OR SPEC NO.
	1	2	4" BORE 12" STROKE SERIES "2H" HEAVY DUTY HYDRAULIC CYLINDER STYLE E (NFPA MS2) W/1½ DIA ROD CLEVIS ROD END 1½-12 THREAD W/DBA NUT CUSHIONED BLIND END WORKING PRESS 2500 PSI	PARKER HANNIFIN OR EQUAL ALL PARTS S.STEEL OR ONLY WHERE CORROSION RESISTANT
	2	12	⅝" LOCK WASHER	S.S.T.
	3	16	⅛" COTTER PIN 1½ LONG	S.S.T.
	4	4	BOLT ELEVATOR SOCKET FOR ½" DIA WIRE ROPE 8" SHANK W/4" THD LENGTH	P/N 737-S BALDWIN TITEHOLDER CORP OR EQUAL BEST
	5	8	WASHER LOCK-1" I.D. X ⅛ THK	S.S.T.
	6	8	BOLT HEX HD 1-12 UNF -2A X 1¾ LG	S.S.T.
	7	2	1¼" Ø FLAT WASHER	S.S.T.
	8	2	1¼"-7 UNC-2B NUT, HEAVY HEX	S.S.T.
	9	12	⅜"-16 UNC-2A BOLT 1¾ LG	S.S.T.
	10	12	⅜"-16 UNC-2B NUT, HEAVY HEX	S.S.T.



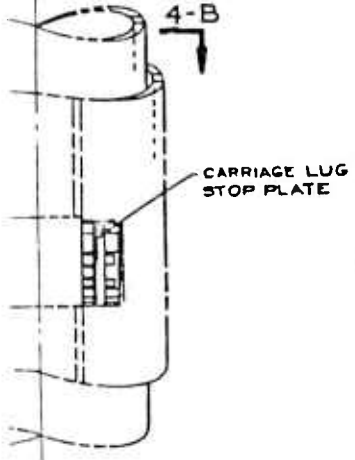
PLAN 3-B
SCALE: NONE

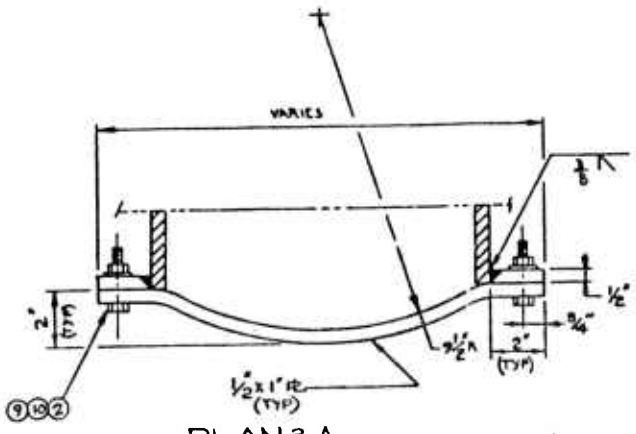
GENERAL NOTES: (UNLESS OTHERWISE NOTED)

1. ALL MATERIAL TO BE ASTM A-36 OR EQUAL EXCEPT WHERE OTHERWISE NOTED.
2. ALL WELDING TO BE IN ACCORDANCE WITH AWS DL1 STRUCTURAL WELDING CODE STEEL.
3. ALL MACHINE SURFACES TO BE 125
4. BREAK ALL SHARP EDGES AND REMOVE ALL BURRS.
5. PAINT IN ACCORDANCE WITH GMDI SPEC 001-002.
6. ALL WELDS THIS ASSEMBLY SHALL USE E 7018 ELECTRODE.
7. THIS DWG WAS DEVELOPED FROM DWG NO. E001-A008 ALT 2 AND ALL OTHER DIMENSIONS ARE SHOWN ON THAT DWG.
8. THESE CARRIAGE LUGS STOP PLATES ARE INSTALLED SO THAT WHEN BIP CARRIAGE LUGS ARE HARD UP AGAINST THEM THE SHEAR PIN HOLES WILL BE IN PERFECT ALIGNMENT.

REFERENCE DRAWINGS:

1. D-001-A004 BIP CARRIAGE ASSEMBLY AND DETAILS
2. MSS402-MTL-D004 MODIFIED BIP CARRIAGE HOUSING ASSY & DETAILS.
3. MSS402-MTL-D005 GANTRY TOOL STINGER ASSY (DETAILS
4. E-001-A005 BIP CARRIAGE HOUSING ASSEMBLY AND DETAILS.
5. MSS402-MTL-D003 BIP CARRIAGE CONTROL SUB DETAILS & ASSEMBLY
6. E-001-A008 BIP CARRIAGE HOUSING MAIN ASSEMBLY.





PLAN 3-A
(INSTALLED IN THE VICINITY OF THE ELEVATOR SOCKETS)
(3 REQ'D)
SCALE: NONE

REV	DATE	BY	DESCRIPTION	JOB DATA
A	10/16/80		PRELIMINARY RELEASE	006/300

GLOBAL MARINE DEVELOPMENT INC.
Newport Beach, Calif

MARINE SEISMIC SYSTEM (MSS)-B2
MODIFIED BIP CARRIAGE HOUSING
MAIN ASSEMBLY

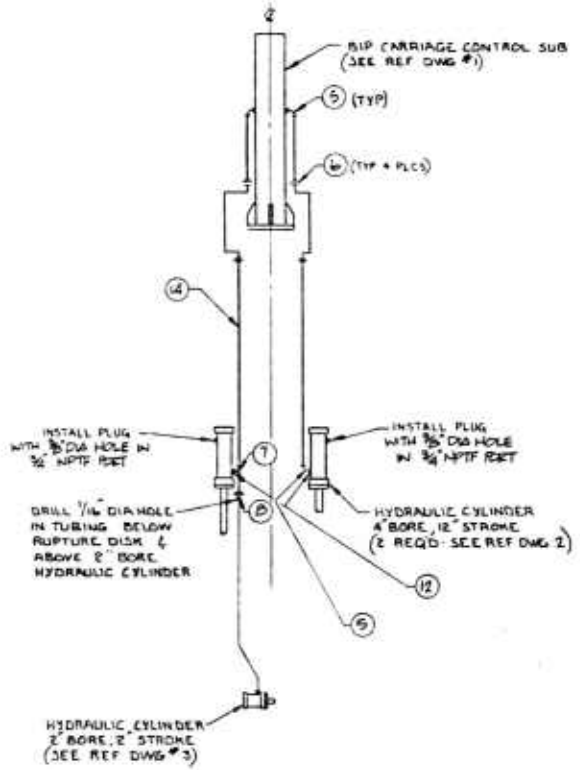
DRAWN D. WEST 10-23-80
SCALE 1/2" = 1'-0"
SIZE E
MSS402-MTL-D006
SHT 1 OF 1
REV A

MSS402-MTL-D001

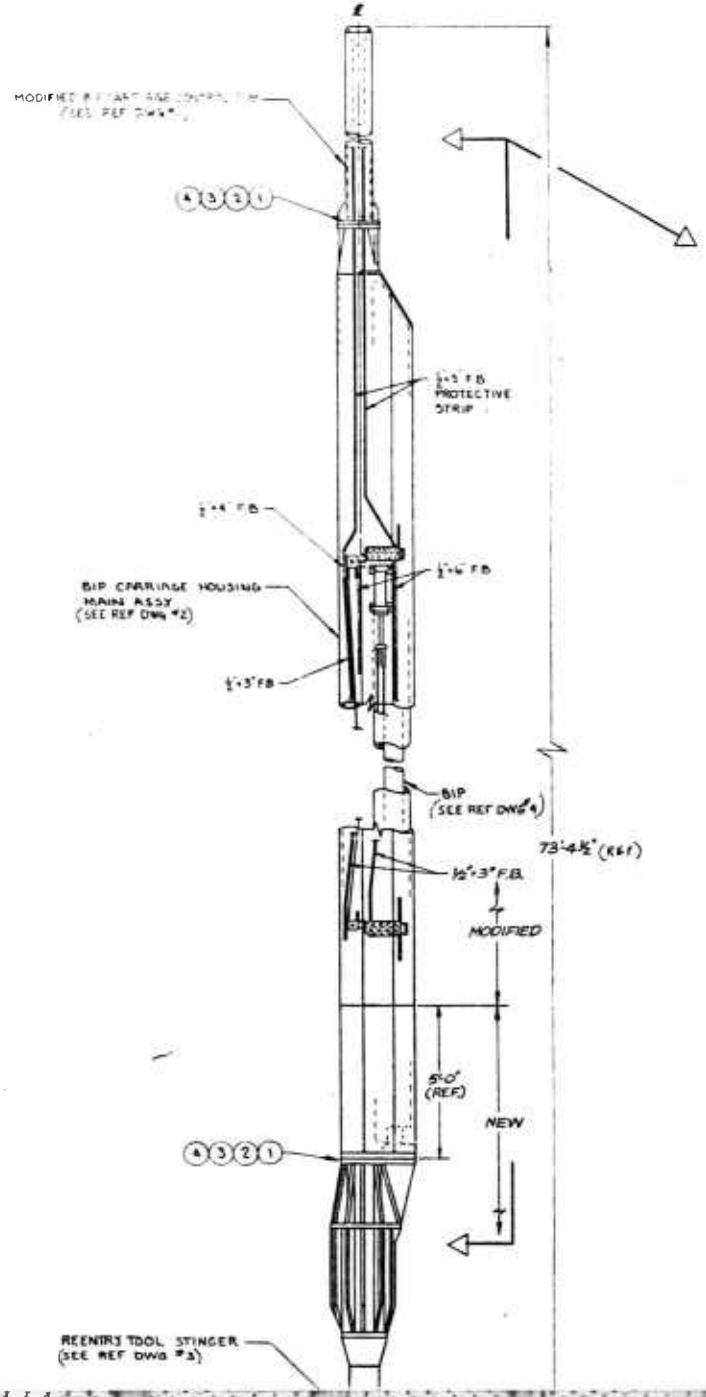
Reproduced from best available copy.

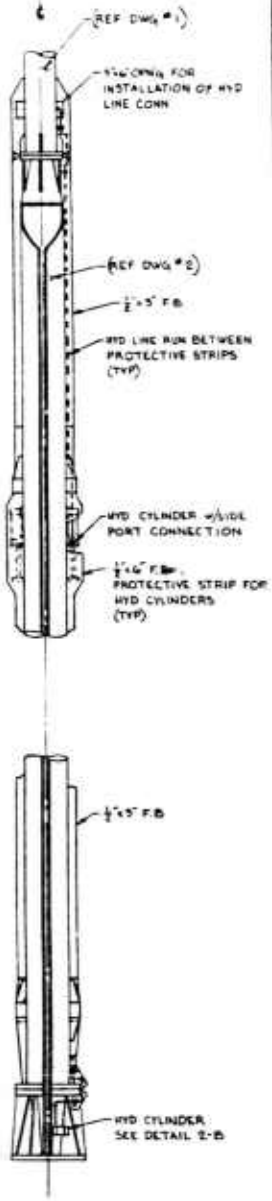
4-A
3 of 10

(2)

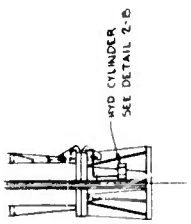


HYDRAULIC SCHEMATIC
N.T.S.



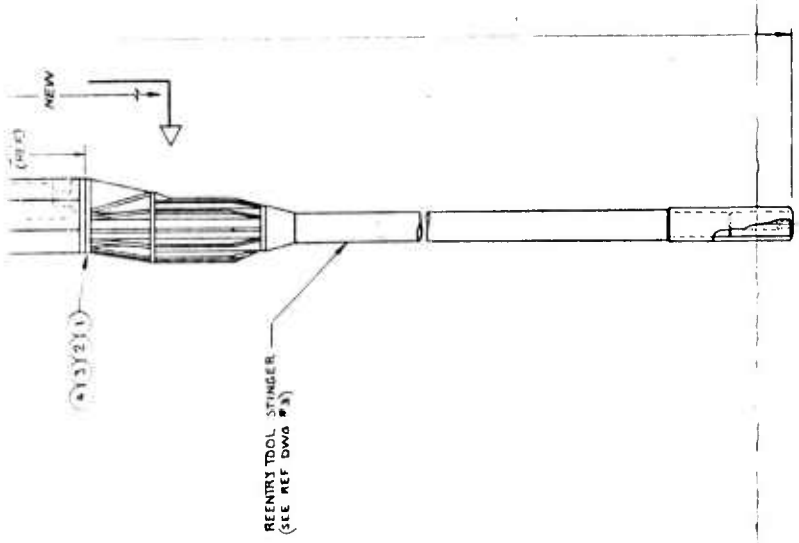


Reproduced from best available copy.

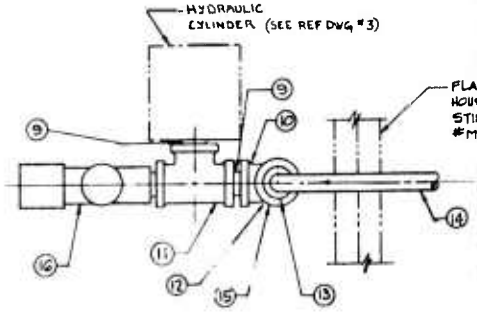


HYDRAULIC SCHEMATIC
N.T.S

HYDRAULIC CYLINDER
2 BORE, 2 STROKE
(SEE REF DWG #3)



ELEVATION 2-C
N.T.S



⚠ DETAIL 2-B
N.T.S

	ITEM	QTY	DESCRIPTION	MATERIAL OR SPEC NO
	1	24	7/8"-14UNF 2A X 3 3/4 LG CORROSION RESISTANT BOLT	ASTM A 325 TYPE 3
	2	24	7/8" PLAIN WASHER	SST
	3	24	7/8" LOCK WASHER	SST
	4	24	7/8"-14 UNF 2B CORROSION RESISTING NUT	ASTM A 325 TYPE 3
	5	2	8-8 FOTL MALE ELBOW (PARKER) WORKING PRESS 9500 PSI	SST
	6	4	8 HBTL UNION (PARKER) WORKING PRESS 9000 PSI	
	7	1	8-8-8BTL MALE BRANCH TEE WORKING PRESS 9500 PSI (PARKER)	
	8	1	1/2" NPTF UNION RUPTURE DISK, SOLID DISK SET AT 2800 PSI FIKE, CONTINENTAL OR EQ.	
	9	2	NIPPLE 1/2" NPTF x 1 1/2" LG, SCH 80 GALV, TBE, WORKING PRESS 9500 PSI	
⚠	10	1	1/2" NPTF 90° ELL - 9500 PSI	
⚠	11	1	1/2" NPTF TEE 9500 PSI	
⚠	12	3	3/4" NPTF - 1/2" NPTF BUSHING 9500 PSI	
	13	1	PARKER HANNIFIN CONNECTOR 8-12-FBTX, WORKING PRESS 9500 PSI	
⚠	14		1/2" X .065 SEAMLESS TUBING 18-8 TYPE 304	S.ST. ASTM A449 Y.P.
	15	1	1/2" NPTF INLINE CHECK VALVE CRACKING PRESS 71.4 PSI, MILLER MODEL C-3, WORKING PRESS 9500 PSI	S.S.T.
⚠	16	2	1/2" NPT RELIEF VALVE SET ABOUT 1000 PSI CIRCLE SEAL CONTROLS PART NO. 5159T-4M-1000 OR EQUAL	303 S.ST.

GENERAL NOTES: (UNLESS OTHERWISE NOTED)

1. ALL TUBE FITTINGS ARE JIC 37 1/2° FLAIR TYPE DESCRIPTION IS PER PARKER HANNIFIN'S CATALOG 4300, SEPT 1980, INDUSTRIAL TUBE FITTINGS.
2. HYDRAULIC TUBING RUN TO BE DETERMINED BY MANUFACTURE.
3. ⚠3 THIS DWG IS MODIFIED AND WAS DEVELOPED FROM DWG NO. E-001-A004 PLT 1
4. HYDRAULIC TUBING & WIRE ROPES ARE TO BE ROUTED WITHIN THE BOUNDRIES OF THE PROTECTIVE STRIPS AS SHOWN TO GIVE MAXIMUM PROTECTION FROM DAMAGE
5. VENT PORTS OF CYLINDERS ARE TO BE COVERED WITH ADHESIVE TAPE DURING ASSEMBLY AND AFTER TEST
6. ALL BOLTS TO BE TACK WELDED ON FINAL ASSEMBLY.
7. ALL HYDRAULIC PIPING SHALL BE ADEQUATELY STAYED & SUPPORTED
8. BEND RADIUS OF TUBING SHALL NOT BE LESS THAN 5 TIMES THE DIAMETER OF THE TUBING.

REFERENCE DWGS:

1. M55A02-MTL-D003 BIP CARRIAGE CONTROL SUB DETAILS & ASSEMBLY
2. M55A02-MTL-D006 MODIFIED H P CARR. NGE HOUSING, MAIN ASSEMBLY
3. ⚠3 M55A02-MTL-D012 REENTRY TOOL STINGER ASSEMBLY AND DETAILS

TELEDYNE GEOTECH DWGS

4. 990-53100 BIP

NO.	DATE	BY	DESCRIPTION	JOB AUTH.	APPD
			ALTERATIONS		
1	9-7-82	RH	ADDED ITEM 16 AND REVISED DETAIL 2-B, PER DCN 6011	6011-4210	
			REVISED ITEM 11, WAS 3500 PSI TO 9500 PSI ZONE 1-D		
			REVISED ITEM 14, REMOVED 1/2" WALL FROM DESCP CALLOUT & CHANGED MAT'L FROM SST TO SST ASTM A 450-79, ZONE 1-C.		
			REVISED REF DWG #'S FROM M55A02-MTL-D005 TO M55A02-MTL-D012, ZONE 1-B.		
			ADDED 3500 PSI TO ITEM 12 DESCRIPTION.		
0	12-1-81	CP	DESIGN RELEASE EDP RELEASED 1-31	011/4110	
A	10/2/81		PRELIMINARY RELEASE	006/3900	

RELEASED AS DESIGN BASELINE — FOR CONSTRUCTION —

GLOBAL MARINE DEVELOPMENT INC.
Newport Beach, Calif.

MARINE SEISMIC SYSTEM (MSS)-B2
MODIFIED BIP REENTRY SUB ASSEMBLY ⚠3

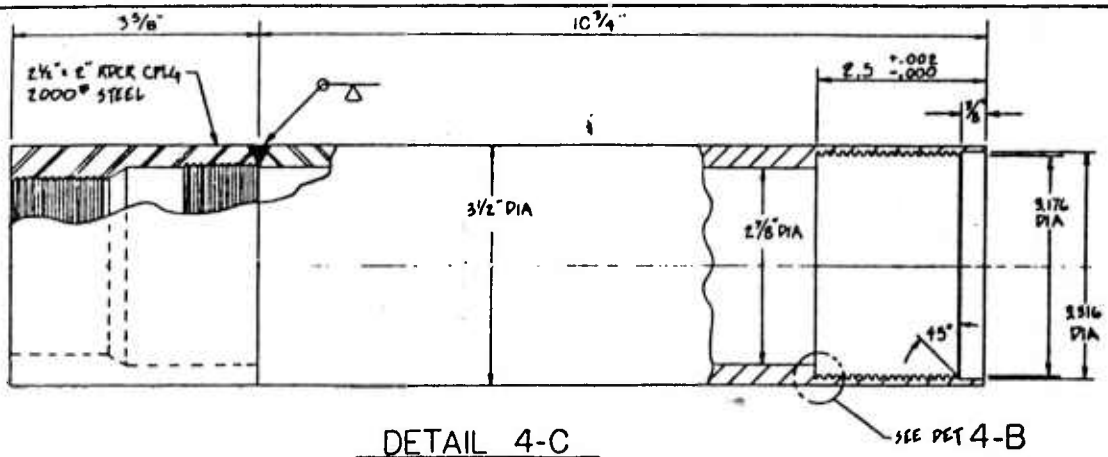
DRAWN G. Duncan	5-11-81	SCALE NOTED	
DESIGN [illegible]	5-12-81		
CHK. D. WEST	10-23-81	SIZE E	M55A02-MTL-D007
APPR. RSB	11-2-81		SHT 1
MGR. R&D C/A MGR	11-2-81		

TOTAL THIS SHEET, WT'L
TOTAL NET THIS SHEET
TOTAL NET WEIGHT

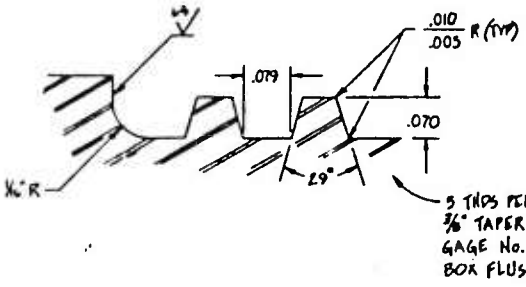
NO. REQ'D.	SHEET ASSEMBLY
1	
DATE	ALTERATIONS
	PURCHASING
	CONSTRUCTION
	ENGINEERING
	USCG
	ABS
3	[illegible]
1	SLATE

THIS DRAWING AND THE DESIGNS IT DISCLOSES ARE THE PROPRIETARY PROPERTY OF GLOBAL MARINE DEVELOPMENT INC. AND MAY NOT BE REPRODUCED OR USED FOR ANY PURPOSE WITHOUT THE WRITTEN CONSENT OF GLOBAL MARINE DEVELOPMENT INC. THE DRAWING SHALL BE RETURNED TO GLOBAL MARINE DEVELOPMENT INC. ON DEMAND.

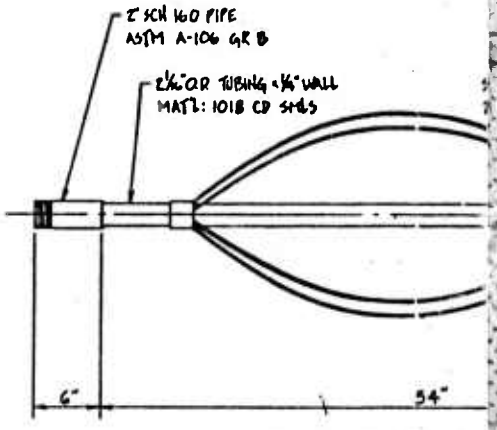
Reproduced from best available copy.



DETAIL 4-C
SONAR SINKER BAR COUPLING SUB
N.T.S.
(FROM VIEW 3-A)

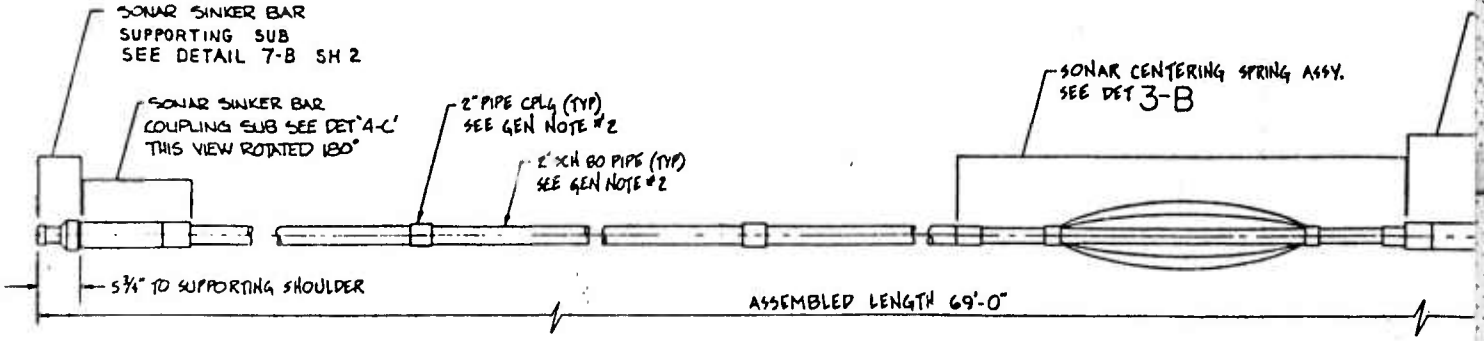


DETAIL 4-B
N.T.S.
(FROM VIEW 4-C)



SPRING CENTRALIZER B&W SERIES AE07 (BOW SPRING)
57" LONG MIN DIA 5 1/2": MAX DIA 12 1/8"

DETAIL 3-B
SONAR CENTERING SPRING
SCALE: 1 1/2" = 1'-0"
(FROM VIEW 3-A)



VIEW 3-A
SONAR AND SINKER BAR ASSEMBLY
N.T.S.

1092

Reproduced from best available copy.

LIST OF MATERIALS				
OWNER FURN.	ITEM	QTY.	DESCRIPTION	MATERIAL OR SPEC. NO.

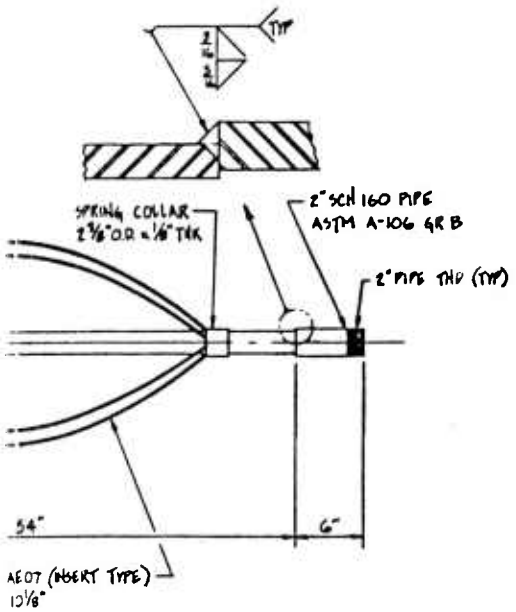
GENERAL NOTES:

1) FINISH 125 EXCEPT WHERE NOTED.

2) SUFFICIENT PIPE LENGTHS AND COUPLINGS SHALL BE SUPPLIED TO MAKE UP ASSEMBLED LENGTH.

3) THE FOLLOWING DIMENSIONAL TOLERANCES SUPERCEDE TOLERANCES NOTED IN TITLE BLOCK AND ARE TO BE USED ON THIS PART.
.X = .X ± .1
.XX = .XX ± .03
.XXX = .XXX ± .010

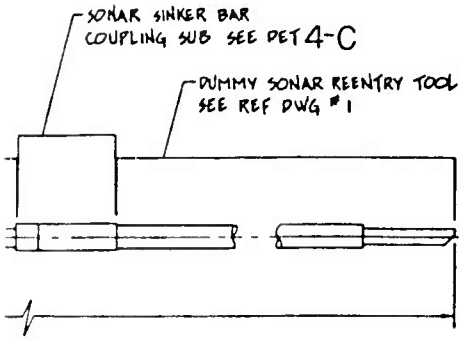
4) BREAK ALL SHARP CORNERS .063 UNLESS OTHERWISE NOTED.



3-B
SPRING ASSY
1" = 1'-0"
3-A1

REFERENCE DWG'S:

1. MSSA02-MTL-D009 MARINE SEISMIC SYSTEM (MSS-82)
DUMMY SONAR REENTRY TOOL



NO.	DATE	BY	DESCRIPTION	JOB AUTH.	APPR.
0	12-28-81	CJB	DESIGN RELEASE 1-26-82 EDC RELEASED	CM/4110	
			ALTERATIONS		

TOP ASSY
NEXT ASSEMBLY
ALTERATION
DATE
PURCHASING
CONSTRUCTION
ENGINEERING
MSOB
ABS

RELEASED AS DESIGN BASELINE
— FOR CONSTRUCTION —

	APPROVED	CHANGED OR REVISED	ALT. NO.	LETTER DATE	FILE REF. NO.
A.B.S.					
U.S.C.G.					

TOTAL NET SHOT. WT'L. _____
TOTAL NET SHOT. EQUIP. _____
TOTAL NET WEIGHT _____

GLOBAL MARINE DEVELOPMENT INC.
Newport Beach, Calif.

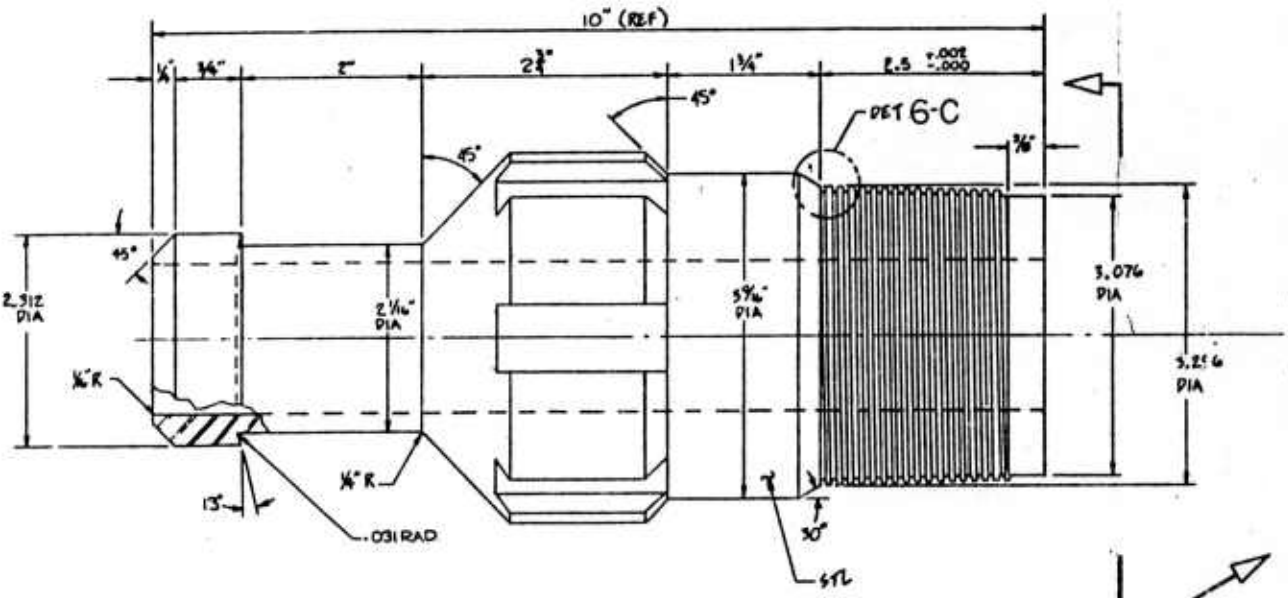
THIS DRAWING AND THE DESIGN IT DISCLOSES ARE THE CONFIDENTIAL PROPERTY OF GLOBAL MARINE DEVELOPMENT, INC. AND MAY NOT BE REPRODUCED OR USED EXCEPT FOR WORK DONE FOR GLOBAL MARINE DEVELOPMENT, INC. OR OTHERWISE FOR WHICH PERMISSION HAS BEEN GRANTED IN WRITING BY GLOBAL MARINE DEVELOPMENT, INC. THIS DRAWING SHALL BE RETURNED TO GLOBAL MARINE DEVELOPMENT, INC. ON REQUEST.

MARINE SEISMIC SYSTEM (MSS-82)
SONAR SINKER BAR
ASSEMBLY AND DETAILS

DFT. R. J BUDA	12-14-81	SCALE NOTED	TOLERANCE UNLESS OTHERWISE NOTED: FRACTION ± 1/16 ANGULAR ± 1° MACHINED ± 1/64 DECIMAL ± .1 3 DECIMAL PLACES ± .010		
DES. W. EU...	- - -				
CHK. P PALMER	12-23-81	DWG SIZE D	DWG. NO. MSSA02-MTL-D011	C.F.	ALT. 0
APPR.				SHT. 1 OF 2	
APPR.	28 Dec 81				

292

Reproduced from best available copy.



DETAIL 7-B

SONAR SINKER BAR SUPPORTING SUB

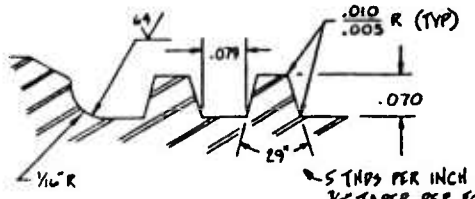
SCALE: FULL SIZE

1 REQ'D PER ASSY

MATERIAL: 4130 HT TR BHN 223-235
(FROM VIEW 3-A)

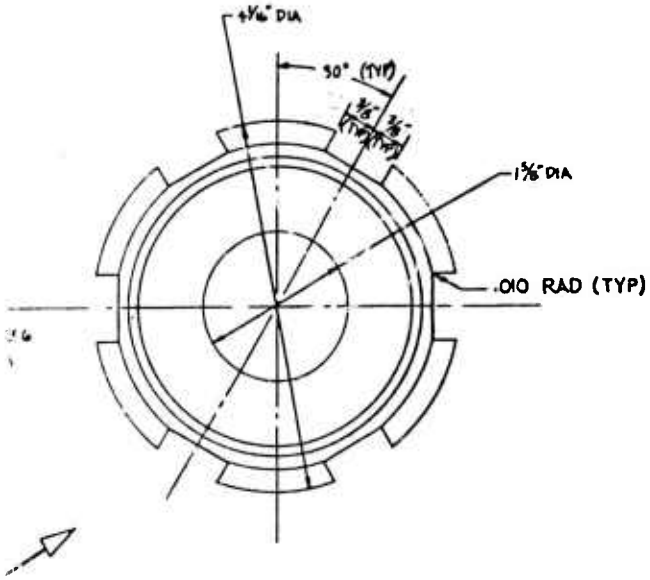
Reproduced from best available copy.

LIST OF MATERIALS				
OWNER FURN.	ITEM	QTY.	DESCRIPTION	MATERIAL OR DWG. NO.



5 THDS PER INCH
3/8" TAPER PER FOOT
GAGE No 65
PIN = S.L.O. .16" TO 1/4"
STAND-OFF (RING GAGE)

DETAIL 6-C
N.T.S
(FROM VIEW 7-B)



NO.	DATE	BY	DESCRIPTION	JOB AUTH.	APPR.
0	12-28-81	CJB	SEE SH 1 FOR NOTES AND ALTERATIONS ECC NOT PUBLISHED	011/4110	

ALTERATIONS

NO. NOTES	NEXT ASSEMBLY
	ALTERATION
	DATE
	PURCHASING
	CONSTRUCTION
	SHIPPING
	USED ON
	ADD

RELEASED AS DESIGN BASELINE
— FOR CONSTRUCTION —

	APPROVED	CHANGED OR REVISED	ALT. NO.	LETTER DATE	FILE NO.
ABS					
USCG					

TOTAL NET SHT. MATL. _____
TOTAL NET SHT. WORK _____
TOTAL NET WEIGHT _____

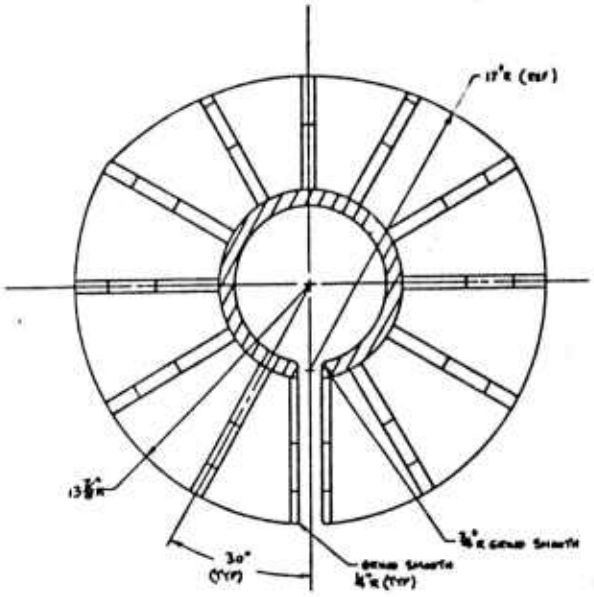
GLOBAL MARINE DEVELOPMENT INC.
Newport Beach, Calif.

THIS DRAWING AND THE DESIGN IT EMBODIES ARE THE CONFIDENTIAL PROPERTY OF GLOBAL MARINE DEVELOPMENT INC. AND MAY NOT BE REPRODUCED, PUBLISHED OR DISCLOSED TO OTHERS WITHOUT THE WRITTEN CONSENT OF GLOBAL MARINE DEVELOPMENT INC. THIS DRAWING SHALL BE RETURNED TO GLOBAL MARINE DEVELOPMENT INC. ON DEMAND.

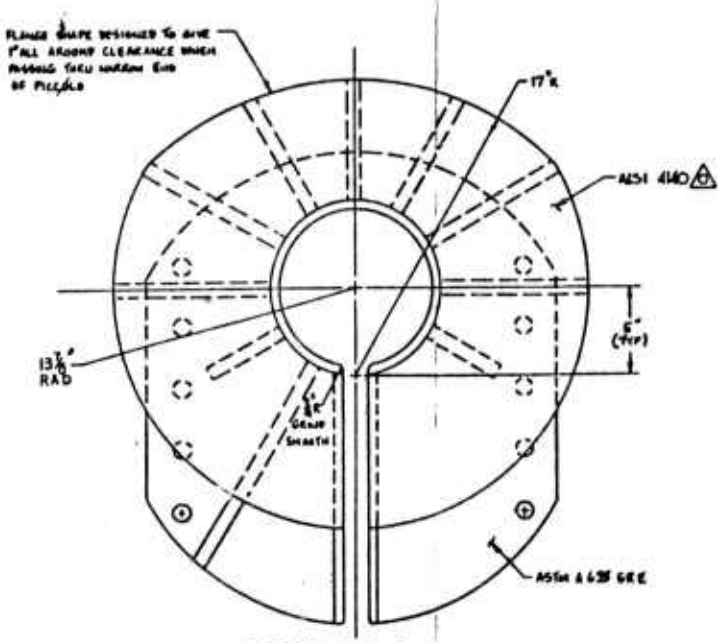
MARINE SEISMIC SYSTEM (MSS-82)
SONAR SINKER BAR
ASSEMBLY AND DETAILS

DSN. R. J BUDA	12-15-81	SCALE NOTED	TOLERANCE UNLESS OTHERWISE NOTED: FRACTION = ±1/16" ANGULAR = ±1° DECIMAL = ±.005
DWN. W. BUCHANAN	12-23-81		
CHK. P. PALMER PE	12-23-81		
APPR.			
ENG. Richard Hart	28 Dec 81	DWG SIZE D	DWG. NO. MSSA02-MTL-D011 C.C. 541 SHT 1 OF 1 REV 0

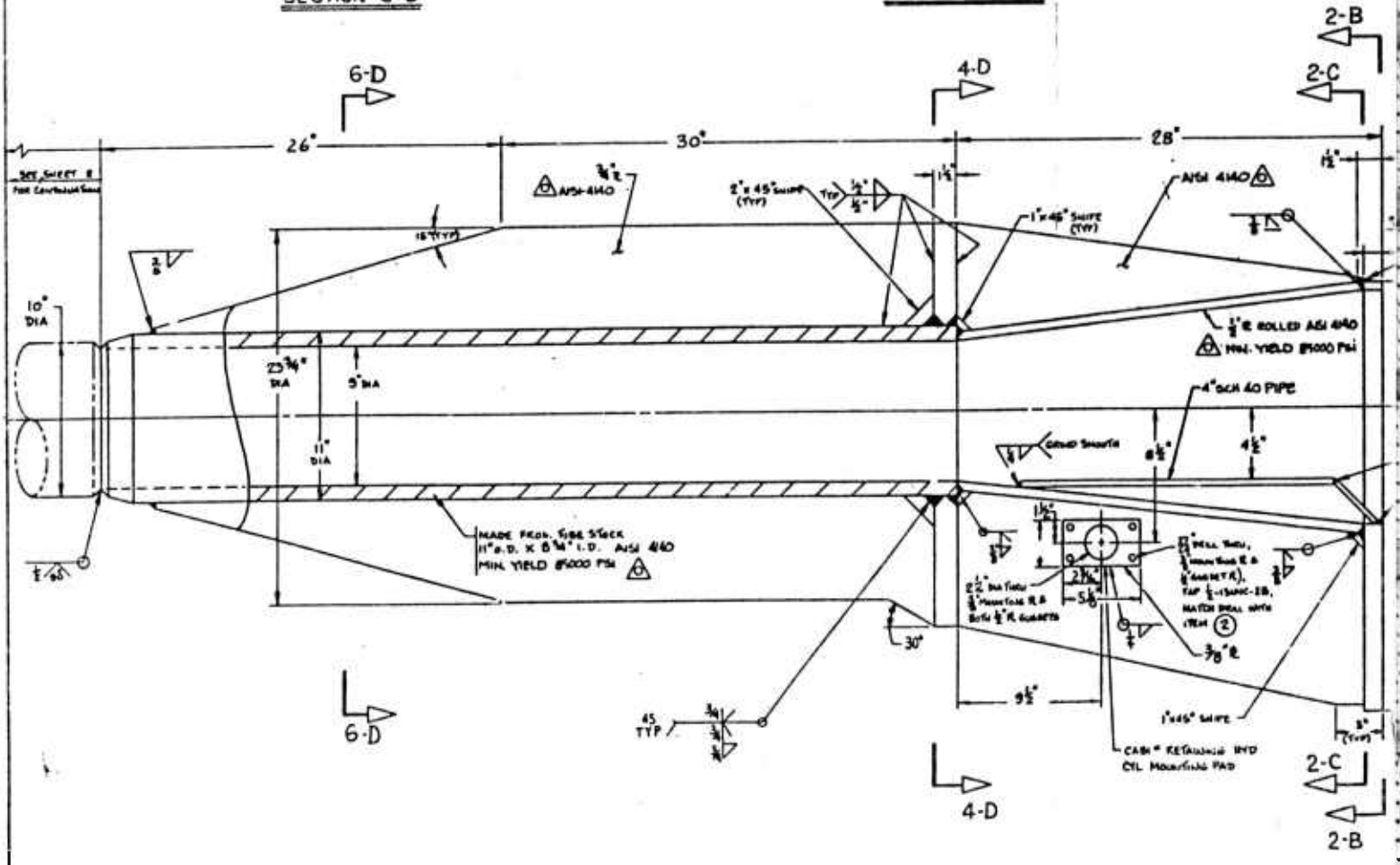
Reproduced from best available copy.



SECTION 6-D



SECTION 4-D



SECTION 5-B

Reproduced from best available copy.

LIST OF MATERIALS				
	ITEM	QTY		
	1		NOT USED	
A	2	1	HYD CYLINDER, 8" BORE 2" STROKE, 2500 PSI "B" HEAVY DUTY, STYLE 3 (100% ION) ROD AND END STYLE 3 [illegible]	[illegible]
	3	4	½-13 UNC-2A X 1¼" LG HEX HEAD BOLT	S.ST.
	4	4	½" LOCK WASHER	S.ST.
	5		NOT USED	
	6	4	5/32" DIA X 1" LONG PIN	1040 STL
	7	4	¼"-20 UNC-2A X ⅜" LG SOCKET HEAD FLAT POINT SET SCREW SELF LOCKING	S.ST.

AISI 4140 A

AISI 4140

AISI 4140

CABLE RETAINING HYD CYLINDER

GROUND SMOOTH ⅛" R (TYP)

½" R AISI 4140 A

30° (TYP 10 PLCS)

8" DIA THRU

⅜" R (TYP)

5" (TYP)

SECTION 2-C

GENERAL NOTES:

1. ALL WELDING IS TO BE IN ACCORDANCE WITH AWS D1.1-79 STRUCTURAL WELDING CODE - STEEL.
2. BREAK ALL SHARP EDGES AND REMOVE BURRS.
3. ALL MACHINE SURFACES TO BE 125
4. PAINT IN ACCORDANCE WITH GMDI. SPEC. 001-002
5. ALL WELDS THIS ASSEMBLY ARE TO BE WELDED WITH E 8018-C3 ELECTRODE AND PRE-HEAT @ 175°F
6. ALL INTERNAL DIAMETERS ARE TO BE CONCENTRIC TO WITHIN .003" OF AN INCH
7. AFTER TURNING SONAR PLUG, CUT INTO 4 SECTIONS, DRILL FOR LOCATING GUIDE PINS, INSTALL GUIDE PINS THEN PLACE ASSEMBLED PLUG IN STINGER AND ALIGN AS SHOWN IN SECTION B-C AFTER WHICH THE HOLES FOR SHEAR PINS ARE INSTALLED. THE MATERIAL REMOVED WHEN CUTTING INTO 4 SECTIONS SHOULD BE COMPENSATED FOR BY BRAZING HIGH SPOTS AND FILING.

REFERENCE DWG'S:

1. MSSA02-MTL-D004 MODIFIED TOP CARRIAGE HOUSING ASSEMBLY AND DETAILS

2-B

2-C

2-C

2-B

4140 A

1½" 1¾" AFTER MACHINING (PLG TO BE SQUARE WITH ℄ OF ASSEMBLY)

½" E ROLLED AISI 4140 MIN YIELD 85000 PSI

4" SCH 40 PIPE

4½"

⅜" R

15" DIA THRU

30° (TYP)

ASTM A-633 GR. E (NORMALIZED) 60 000# PSI MIN YIELD

GROUND SMOOTH ⅛" R (TYP)

1" DIA THRU (TYP 10 PLCS)

GROUND SMOOTH ⅛" R (TYP)

4 EA 3PCS @ 3½" ON CENTERS (TYP BOTH SIDES)

27¼"

1½"

10"

12"

24"

SEE REF DWG #1

VIEW 2-B

			LIST OF MATERIALS REV'D (ZONE 4-B, 5H 1) AND ED "ASA B89.3-3-1965 TO PARTS DESCRIPTION. REVISED MATERIAL SPECS IN SECTION 6-B (ZONE 4-B, 5H 1), SECTION 2-C (ZONE 8-C, 5H) AND SECTION 4-B (ZONE 4-D, 4H) FROM ASTM A572-677 TO AISI 4140 AND ADDED NOTE OF MIN YIELD OF 85000 PSI IN SECTION 5-B. DETAIL 100-A (ZONE 10-A, 5H 2 OF 2) CHANGED MATERIAL SPEC FROM ASTM A543 CL (H-B) TO AISI 4140.	
A	8181	CP	DESIGN RELEASE	04/4110
			PRELIMINARY RELEASE	04/4110

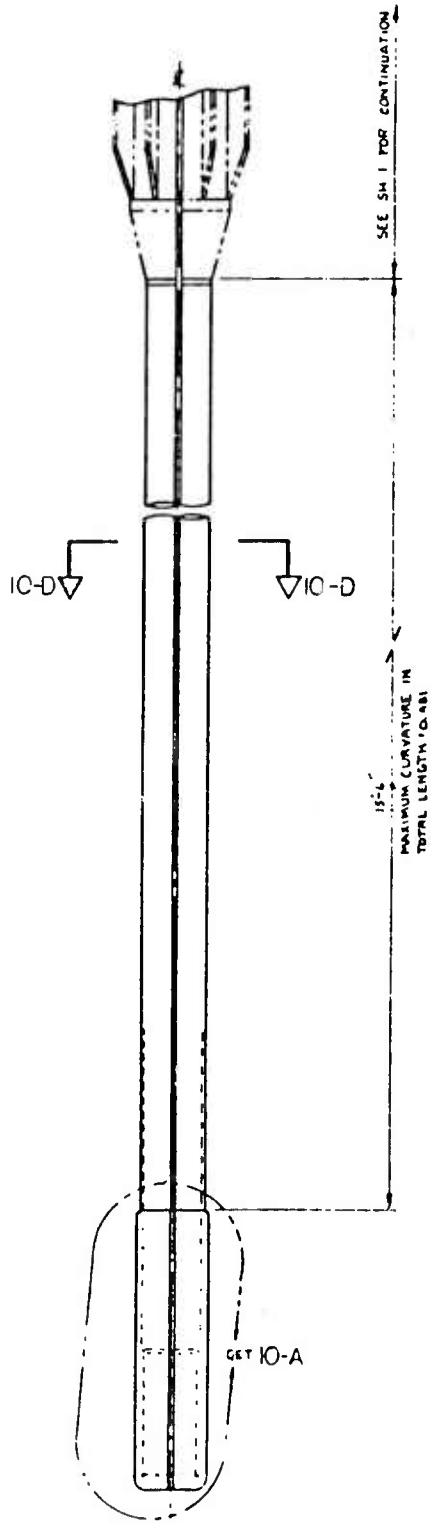
RELEASED AS DESIGN BASELINE — FOR CONSTRUCTION —

GLOBAL MARINE DEVELOPMENT INC.

MARINE SEISMIC SYSTEM (MSS)-82
REENTRY SUB STINGER
ASSEMBLY AND DETAILS

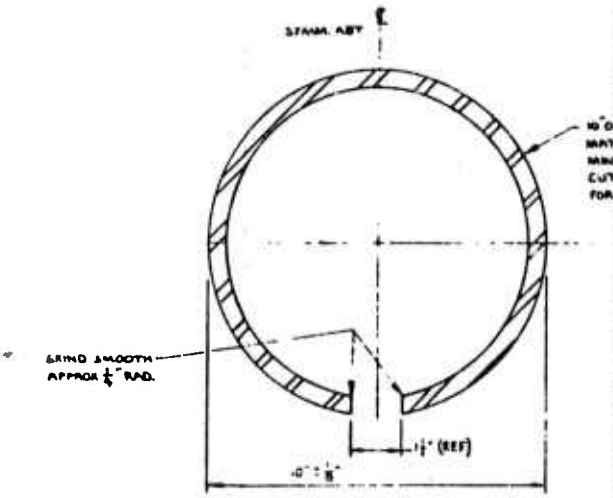
DRN W.B	8-8-2011	SCALE	3"=1'-0"		
DSGN W.B	11-6-881				
APP'D PALMER	11-8-81				
APP'D RGB	11-8-81	SIZE	DWG. NO.	CC	REV
APP'D [illegible]	11-8-81	E	MSSA02-MTL-0012	541	0

Reproduced from best available copy.



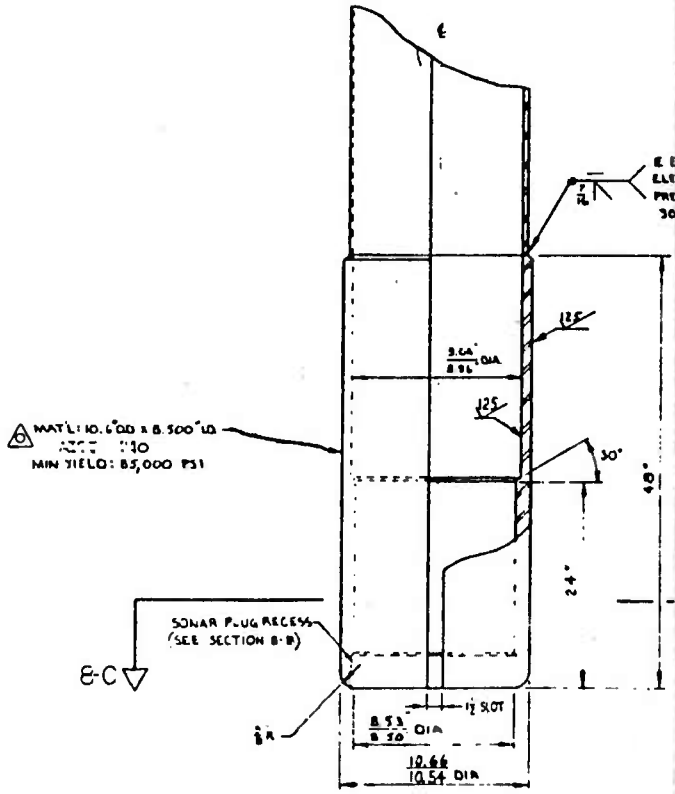
ELEVATION 12-A

SCALE 1"=1'-0"



SECTION 10-D

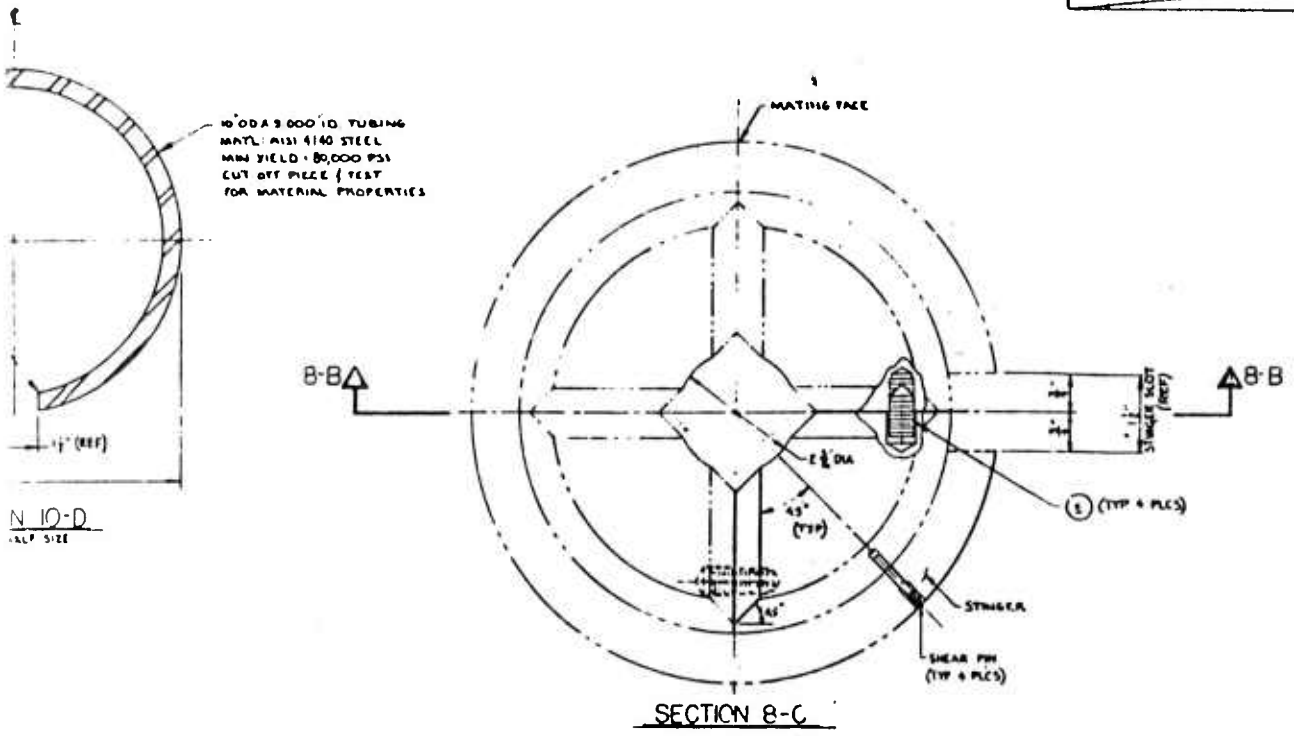
SCALE HALF SIZE



DETAIL 10-A

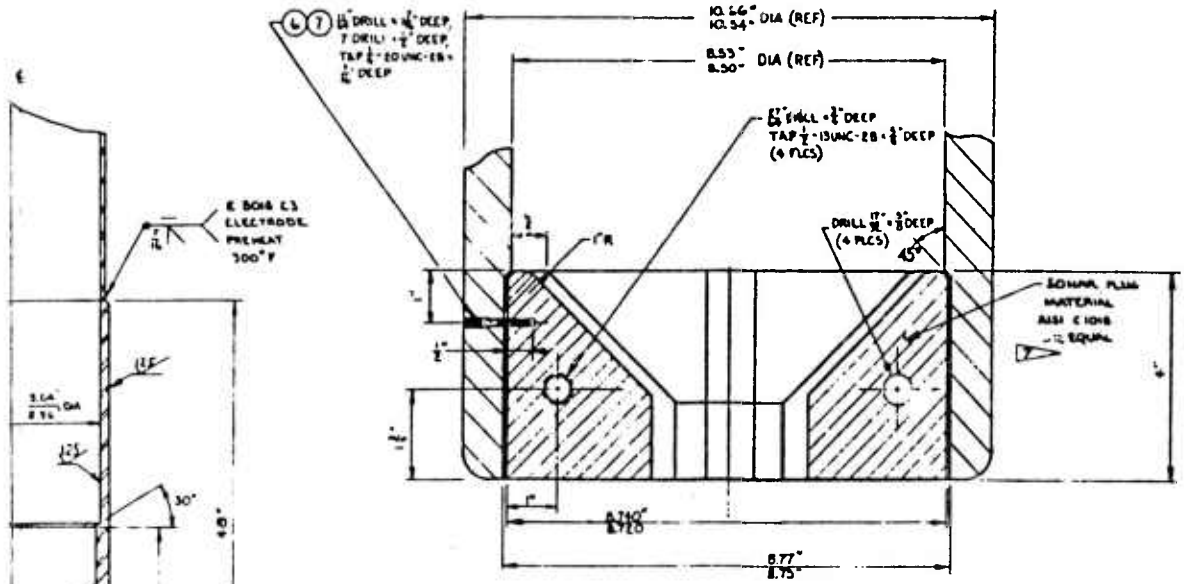
Reproduced from best available copy.

LIST OF MATERIALS



N 10-D

SECTION 8-C



SECTION 8-B
SONAR PLUG
SCALE 1/2" = 0'-1"

ALL 10-A

RELEASED AS DESIGN BASELINE — FOR CONSTRUCTION —

SEE SHEET 1

GLOBAL MARINE DEVELOPMENT INC.
Newport Beach, Calif.

MARINE SEISMIC SYSTEM (MSS)-82
RLENTRY TOOL STINGER
ASSEMBLY & DETAILS

DRAWN AS NOTED E MSSA02LMTL-0012 341

Reproduced from best available copy.

UNCLASSIFIED

SECURITY CLASSIFICATION OF THIS PAGE

AD-A162 539

REPORT DOCUMENTATION PAGE

1a. REPORT SECURITY CLASSIFICATION Unclassified	1b. RESTRICTIVE MARKINGS None
2a. SECURITY CLASSIFICATION AUTHORITY	3. DISTRIBUTION/AVAILABILITY OF REPORT Approved for public release; distribution is unlimited.
2b. DECLASSIFICATION/DOWNGRADING SCHEDULE	
4. PERFORMING ORGANIZATION REPORT NUMBER(S) NORDA Report 111	5. MONITORING ORGANIZATION REPORT NUMBER(S) NORDA Report 111
6. NAME OF PERFORMING ORGANIZATION Naval Ocean Research and Development Activity	7a. NAME OF MONITORING ORGANIZATION Naval Ocean Research and Development Activity
6c. ADDRESS (City, State, and ZIP Code) Ocean Science Directorate NSTL, Mississippi 39529–5004	7b. ADDRESS (City, State, and ZIP Code) Ocean Science Directorate NSTL, Mississippi 39529–5004
8a. NAME OF FUNDING SPONSORING ORGANIZATION DARPA/GSD 8b. OFFICE SYMBOL (If applicable)	9. PROCUREMENT INSTRUMENT IDENTIFICATION NUMBER
8c. ADDRESS (City, State, and ZIP Code) 1400 Wilson Blvd. Arlington VA 22209	10. SOURCE OF FUNDING NOS PROGRAM ELEMENT NO: 62714E; PROJECT NO; TASK NO; WORK UNIT NO
11. TIT E (Include Security Classification) Comprehensive Final Report for the Marine Seismic System Program	
12. PERSONAL AUTHOR(S) J. D. Ward* and J. A. Ballard	
13a. TYPE OF REPORT Final 13b. TIME COVERED From _____ To _____	14. DATE OF REPORT (Yr., Mo., Day) August 1985 15. PAGE COUNT 199
16. SUPPLEMENTARY NOTATION *Computer Sciences Corporation	
17. COSATI CODES FIELD / GROUP / SUB GR	18. SUBJECT TERMS (Continue on reverse if necessary and identify by block number) marine seismic system, borehole seismometer, engineering, ocean sub-bottom seismometer, Pacific intraplate seismicity

19. ABSTRACT (Continue on reverse if necessary and identify by block number)

From 1981 through 1983, the Defense Advanced Research Projects Agency funded the National Science Foundation to conduct three marine expeditions as part of a developmental program for a deep-ocean marine seismic station. Long-range plans called for installation of a seismic station at a site in the Northwest Pacific in 1982. A coalition of institutions, agencies, and private firms combined various aspects of marine technology for placing large seismic instrument packages in dedicated boreholes in the floor of the Atlantic and Pacific Oceans. The drillship GLOMAR CHALLENGER was used as the deployment vehicle for preparing boreholes and emplacing the seismometer in the borehole, and for positioning a companion ocean-floor data recording package.

During an expedition in the Atlantic Ocean in March 1981, a large instrument package was lowered, external to the drill string, and placed in a previously drilled borehole at a depth about 2000 ft below the ocean floor. Water depth at the site was 14,708 ft. The seismic instruments were monitored by shipboard recorders. Background noise levels were quite low, and refraction shooting by a second ship produced crisp, clean signals. The instrument package was recovered with a cable winch.

A full-scale Marine Seismic System installation was attempted near the Kurile Trench in the Northwest Pacific in August–September 1982. This expedition was plagued by drilling equipment failures and adverse

20. DISTRIBUTION/AVAILABILITY OF ABSTRACT UNCLASSIFIED/UNLIMITED ☐ SAME AS RPT ■ DTIC USERS ☐	21. ABSTRACT SECURITY CLASSIFICATION Unclassified
22a. NAME OF RESPONSIBLE INDIVIDUAL J A. Ballard	22b. TELEPHONE NUMBER (Include Area Code) (601) 688-4599 22c. OFFICE SYMBOL Code 360

DD FORM 1473, 83 APR EDITION OF 1 JAN 73 IS OBSOLETE

UNCLASSIFIED

SECURITY CLASSIFICATION OF THIS PAGE

weather and drill conditions. The cased reentry borehole, required for seismic instrument installation, was never completed. Seasonal weather deterioration, the GLOMAR CHALLENGER operating schedule, and logistical considerations forced abandonment of the operation. However, a simpler seismometer, owned by Hawaii Institute of Geophysics, not requiring a cased reentry borehole was installed and provided an outstanding data set.

Failure of the 1982 attempt led to a schedule for a priority test in the South Pacific in early 1983. The area selected was about 500 miles east of the Tonga Trench and is one of the most seismically active regions in the world. Water depth at the site was 18,417 ft. A seismic instrument package was implanted in igneous rock at about 340 ft below the sea floor. A large bottom-processing package for data formatting and recording was successfully deployed and later recovered. Although some technical and equipment problems were encountered, the operation was considered successful. An extensive set of noise, explosion, and earthquake data was collected by the borehole instrument package and an ocean-bottom seismometer array. Two-ship refraction experiments were carried out with explosion data recorded from distances up to 140 miles.

The Marine Seismic System program demonstrated that the technology exists to place large instrument packages, carried external to the drill string, in deep ocean boreholes using a single deployment vessel. Operating depths of 20,000 ft are feasible, with borehole depths to 2,000 ft below the ocean floor. Large, heavy, long-term data recording packages may be deployed on the sea floor and recovered by vessels with adequate winch and navigation systems. Seismic data collected by the Marine Seismic System are generally superior to ocean-bottom seismometer data. Signal/noise ratios of borehole instruments exceed those of ocean bottom seismometers by more than 15 dB in the 1–15 Hz frequency band.

Subsequent to the 1983 expedition, the Marine Seismic System program was terminated. The borehole instrument package and a dummy bottom processing package remain at the 1983 experiment site. No existing programs are presently deisgned for continued development of a permanent marine seismic station.